

# Investigating the Impact of Adaptive Façades on Energy Performance Using Simulation and Machine Learning



A thesis submitted in fulfilment of the requirements for the award  
of Doctor of Philosophy in Architecture

**Cardiff University**

Welsh school of architecture

BY

**Ammar Alammar**

November 2022

## Acknowledgment

---

I would like to express my most sincere thanks and immense gratitude to my main supervisor, Professor Wassim Jabi, for his valuable and supportive guidance, motivation, assistance, and extensive knowledge throughout my PhD journey, which has contributed to the enrichment of this dissertation and its successful completion. Also, I would like to express my sincere gratitude to my second supervisor, Dr. Simon Lannon, for his support, advice, and constructive comments on my research. And I deeply appreciate the help of Dr Vicki Stevenson, who provided helpful comments and precise feedback as an expert on building performance simulation. Thanks are also due to Dr Thomas Worthmann and Dr Satish Basavapatna Kumaraswamy for agreeing to examine my research and for taking the time to review this thesis.

I would like to thank all staff at the Welsh School of Architecture, Cardiff University, for their help during my study. Special thanks go to Katrina Lewis and Sarah Nicholas for their help during this journey. I would like also to thank my PhD colleagues, who have been part of the completion of this research, for their time, interest, and helpful comments.

My gratitude is also extended to the government of KSA and to King Saud University for giving me the opportunity to study for this PhD, and for their financial support throughout this period.



## Dedication

---

*I dedicate my humble effort to*

*the loving memory of my late father, Abdulrahman Alammar*

*my beloved Mom, Noura Alammar, for her love, support, and prayers, which enabled to work through various difficulties and challenges*

*my wonderful wife, Muneera Alqublan, for her love, patience, care, and great encouragement to achieve my dream and to overcome the difficulties, especially during COVID-19*

*my brothers and sisters, for supporting and encouraging me throughout my life*

*my sons, Abdulrahman and Nassir, for bringing moments of laughter and happiness to each day*

# Investigating the Impact of Adaptive Façades on Energy Performance Using Simulation and Machine Learning

## Abstract

---

Buildings consume approximately 40% of the world's primary energy, and half of this energy demand stems from space cooling and heating. To meet the targets of designing high performance buildings, intelligent solutions need to be integrated into the design process of buildings to achieve indoor environmental comfort and minimize energy consumption. In particular, the building façade plays a crucial role, as it acts as a separator element that can control the indoor environment and energy performance. This is even more important in buildings with extensive glazing systems particularly in harsh, hot climates. As stated in the literature, buildings are exposed to dynamic environmental factors that change continuously throughout the day and the year. Nonetheless, regardless of the climatic variations, building skins have been typically designed as static envelopes, which are limited in terms of their responsiveness to indoor or outdoor environmental conditions. In contrast, adaptive façades (AFs) are flexible regarding the adaptability of the system to climatic conditions enabling them to respond to short-term changes in the environment.

From an environmental viewpoint, it is essential to reduce the energy consumption of buildings and mitigate their environmental impacts. Numerous innovative building envelope technologies have been developed to improve indoor comfort and reduce the environmental impact of buildings during their life cycle. As stated in the literature, AFs can make a major and practical contribution to achieving the worldwide zero-energy building targets and sustainability of our cities. In practice, assessing the performance of AFs during the early stages of the design is still a challenging task due to their time-varying dynamic behaviour. Most current building performance tools (BPS) were originally developed to assess fixed façades where changes to the geometry of the façade are not taken into consideration during simulation. To that end, adaptive systems require a more complex workflow that can correctly predict their performance.

This research is intended to assist architects and façade specialists in two main aspects; firstly, an algorithmic framework was developed to predict the energy performance of AFs in the early design stages. The algorithmic workflow creates a link between plug-ins including the Ladybug and Honeybee tools, and Energy Plus for running the simulation with the built-in tool energy management system (EMS) to program a code to actuate the AF system in an

hourly time step. The workflow considers the time-varying dynamic behaviour of AFs based on different environmental parameters. The aim is to accurately evaluate the potential of AFs in the energy performance of an office tower. Secondly, by exploring the complexity and limitation of current tools, a novel method is proposed to assess the energy performance of AFs using machine learning (ML) techniques. Two different ML models, namely, an artificial neural network (ANN) and a Random Forest (RF), were developed to predict the energy performance of AFs in the early design stages in a significantly faster time compared to simulation. The surrogate models were trained, tested, and validated using the generated synthetic database by simulation (hourly cooling loads of AF and hourly solar radiation). During the training phase, a hyperparameters tuning procedure was carried out to select the most suitable surrogate model.

By comparing the static shading system with AFs in terms of energy consumption, the results confirmed that the AFs were more effective in terms of cooling load reduction compared to static façades where cooling loads were reduced by 34.6%. The findings also revealed that the control scenario that triggered both incident solar radiation and operative temperature in a closed loop mechanism performed better than other control scenarios. Regarding the surrogate models, this research found that ML techniques can predict the hourly cooling loads of AFs with a high level of accuracy in the range of 85% to 99%. In particular, the RF model showed a 17% improvement in  $R^2$  accuracy over the ANN model in predicting the hourly cooling loads of AFs.

## List of Publications

---

The following papers have been published based on the results of this research:

1. Alammar, A. and Jabi, W. 2022. [Predicting cooling energy demands of adaptive façades using artificial neural network](#). Presented at the 13<sup>th</sup> annual Symposium on Simulation for Architecture and Urban Design (SimAUD) with the Annual Modelling and Simulation Conference (ANNSIM), San Diego State University, San Diego, CA, USA, 18-20 July 20222022 Annual Modelling and Simulation Conference (ANNSIM). IEEE pp. 656-669., ([10.23919/ANNSIM55834.2022.9859413](#))
2. Alammar, A. and Jabi, W. 2022. Generation of a large synthetic database of office tower's energy demand using simulation. Presented at the 6<sup>th</sup> International Symposium Formal Methods in Architecture (6FMA), Escola Técnica Superior de Arquitectura - Universidade da Coruña (ETSA-UDC), A Coruña, Spain, May 24-27, 2022.
3. Alammar, A., Jabi, W. and Lannon, S. 2021. [Predicting incident solar radiation on building's envelope using machine learning](#). Presented at the 12<sup>th</sup> Symposium on Simulation for Architecture and Urban Design (SimAUD 2021), Virtual, 15-17 April 2021.

# Table of Content

---

|  |             |
|--|-------------|
| <b>Acknowledgment</b> .....  | <b>i</b>    |
| <b>Dedication</b> .....  | <b>ii</b>   |
| <b>Abstract</b> .....  | <b>iii</b>  |
| <b>List of Publications</b> .....  | <b>v</b>    |
| <b>Table of Content</b> .....  | <b>vi</b>   |
| <b>List of Figures</b> .....   | <b>xiii</b> |
| <b>List of Tables</b> .....  | <b>xx</b>   |
| <b>List of Abbreviations</b> .....   | <b>xxi</b>  |
| <b>CHAPTER ONE: INTRODUCTION AND OVERVIEW</b> .....  | <b>1</b>    |
| 1.1. Introduction .....  | 2           |
| 1.2. Research Background and Context .....   | 2           |
| 1.2.1. Static Façade .....   | 3           |
| 1.2.2. Adaptive Façade.....  | 4           |
| 1.2.3. Machine Learning .....  | 5           |
| 1.2.4. Energy Consumption of Buildings in Riyadh, Saudi Arabia .....   | 5           |
| 1.2.5. High Rise Office Buildings in Riyadh .....  | 9           |
| 1.2.6. Riyadh Location and Climatic Condition - Hot-Arid Regions.....  | 13          |
| 1.3. Research Aim and Objectives.....  | 15          |
| 1.4. Research Questions.....   | 16          |
| 1.5. An Overview of the Research Design .....  | 17          |
| Phase 1: Literature Review and Critical Analysis .....   | 17          |
| Phase 2: Data collection.....  | 17          |
| Phase 3: Data Analysis .....   | 18          |
| Phase 4: Development of Machine Learning (ML) Surrogate Models.....  | 18          |
| Phase 5: Incorporation of the Surrogate Models within a Computational Design Tool,<br>and Validation of the Results..... | 19          |
| 1.6. Structure of the Following Chapters .....   | 19          |
| 1.7. Chapter Summary .....   | 23          |
| <b>CHAPTER TWO: LITERATURE REVIEW</b> .....  | <b>24</b>   |
| 2.1. Introduction .....  | 25          |
| Part (A) Adaptive Building Envelope .....  | 25          |
| 2.2. Static to Adaptive Façade – Overview.....   | 25          |
| 2.2.1. Adaptive Façade History .....   | 28          |

|   |    |
|---|----|
| 2.2.2. Adaptive Façade Definition.....                              | 29 |
| 2.2.3. Adaptive Façades Terminologies .....                         | 30 |
| 2.2.3.1. Active Façades .....                                       | 30 |
| 2.2.3.2. Biomimetic or Bio-Inspired Façades.....                    | 31 |
| 2.2.3.3. Passive Façades .....                                      | 32 |
| 2.2.3.4. Kinetic Façades .....                                      | 33 |
| 2.2.3.5. Intelligent Façades.....                                   | 34 |
| 2.2.3.6. Interactive Façades.....                                   | 35 |
| 2.2.3.7. Movable Façades .....                                      | 36 |
| 2.2.3.8. Smart Façades .....  | 36 |
| 2.2.3.9. Responsive Façades.....                                    | 37 |
| 2.2.3.10. Switchable Façades .....                                  | 38 |
| 2.3. Classification of Adaptive Façades .....                       | 40 |
| 2.3.1. Physical Domains .....                                       | 41 |
| 2.3.2. Responsive Time Scale .....                                  | 41 |
| 2.3.3. Scales of Adaptation .....                                   | 42 |
| 2.3.4. External Factors .....                                       | 43 |
| 2.4. Automatic Control System .....                                 | 44 |
| 2.4.1. Open-Loop Control .....                                      | 45 |
| 2.4.2. Closed-Loop Control .....                                    | 47 |
| Part (B) Building Performance Simulation for Adaptive Façades.....  | 50 |
| 2.5. Building Performance Simulation for Adaptive Façades.....      | 50 |
| 2.5.1. Current Research for the BPS tools .....                     | 51 |
| 2.5.2. Discussion of Existing Studies .....                         | 52 |
| 2.6. Challenges for Performance Prediction of Adaptive Façades..... | 60 |
| 2.7. BPS Tools and their Ability to Simulate Time Changes .....     | 61 |
| 2.7.1. Parametric Tools .....                                       | 62 |
| 2.7.2. Grasshopper.....   | 63 |
| 2.7.3. Parametric Integrated Simulation Tools.....                  | 63 |
| 2.7.3.1 Honeybee .....  | 64 |
| 2.7.3.1. Ladybug .....  | 64 |
| Part (C) Machine Learning (ML) .....                                | 64 |
| 2.8. Machine Learning (ML) – Overview .....                         | 64 |
| 2.8.1. Supervised Learning (SL).....                                | 65 |
| 2.8.2. Unsupervised Learning (USL) .....                            | 66 |

|   |            |
|---|------------|
| 2.9. Surrogate Model for Building Performance .....   | 66         |
| 2.9.1. Data Pre-Processing .....  | 68         |
| 2.9.2. Model Training and hyperparameter tuning .....   | 69         |
| 2.9.3. Performance evaluation .....   | 69         |
| 2.9.4. Data Types .....   | 70         |
| 2.10. Artificial Neural Networks (ANN) - Overview .....   | 70         |
| 2.10.1. Fundamentals of Artificial Neural Networks .....  | 72         |
| 2.10.2. Neural Network Architecture .....   | 75         |
| 2.10.3. Activation Function .....   | 77         |
| 2.11. Decision Tree (DT) .....  | 78         |
| 2.12. Existing Studies .....  | 80         |
| 2.12.1. Neural Networks Studies .....   | 81         |
| 2.12.2. Decision Tree Studies .....   | 87         |
| 2.12.3. Discussion of the Review .....  | 88         |
| 2.13. Identified Gaps and Conclusions .....   | 99         |
| <b>CHAPTER THREE: RESEARCH DESIGN AND METHODOLOGY .....</b>   | <b>100</b> |
| 3.1. Introduction .....   | 101        |
| 3.2. Research Methodology and Methods .....   | 102        |
| 3.3. Choosing a Quantitative Approach .....   | 103        |
| 3.4. Research Design .....  | 104        |
| 3.5. Research Framework .....   | 104        |
| 3.5.1. Literature Review .....  | 105        |
| 3.5.2. Data Collection .....  | 106        |
| 3.5.2.1. Case studies .....   | 106        |
| 3.5.2.2. Data Collection Using Modelling and Simulation .....   | 107        |
| 3.5.3. Data Analysis .....  | 110        |
| 3.5.4. Development of Machine Learning Surrogate Models .....   | 110        |
| 3.5.5. Incorporation of the Surrogate Models within a Computational Design Tool, and<br>Validation of the Results ..... | 112        |
| 3.6. Chapter Summary .....  | 113        |
| <b>CHAPTER FOUR: SYNTHETIC DATABASE GENERATION USING SIMULATION APPROACH..</b>  | <b>115</b> |
| 4.1. Introduction .....   | 116        |
| 4.2. High-Rise Office Building Characteristics .....  | 117        |
| 4.3. Generation of Synthetic Database Based on Modelling and Simulation .....   | 128        |
| 4.4. Base Case and Adaptive Façade Modelling .....  | 130        |

|  |            |
|--|------------|
| 4.4.1. Modelling Stage .....   | 130        |
| 4.4.2. Typical Closed Office.....  | 131        |
| 4.4.3. Setting Up the Model Parametrically - Generative Parametric Tower.....  | 132        |
| 4.4.4. Climatic Analysis .....   | 135        |
| 4.4.5. Simulation Settings .....   | 137        |
| 4.5. Validation of the Base Model.....   | 138        |
| 4.6. Implementation of Adaptive Façade Shading System .....  | 142        |
| 4.7. Adaptive Façade Energy Simulation.....  | 145        |
| 4.8. Solar Radiation Analysis .....  | 147        |
| 4.8.1. Validation of Tool Accuracy .....   | 148        |
| 4.8.2. Solar Radiation Settings.....   | 151        |
| 4.8.3. Solar Analysis Input Parameters .....   | 154        |
| 4.8.4. Solar Radiation Database.....   | 157        |
| 4.9. Shade Factor Analysis.....  | 158        |
| 4.9.1. Shade Factor Methods.....   | 159        |
| 4.9.2. Shade Factor Settings .....   | 159        |
| 4.9.3. Shade Factor Database .....   | 161        |
| 4.10. Energy Simulation .....  | 163        |
| 4.10.1. Input Parameters.....  | 166        |
| 4.10.2. Construction Materials and Thermal Settings .....  | 169        |
| 4.10.3. Zone Loads .....   | 171        |
| 4.10.4. Automatic Control System.....  | 172        |
| 4.10.5. Simulation Challenges.....   | 178        |
| 4.10.6. Simulation Matrices.....   | 179        |
| 4.10.7. Energy Simulation Database .....   | 181        |
| 4.11. Chapter Summary .....  | 186        |
| <b>CHAPTER FIVE: SIMULATION RESULTS.....</b>   | <b>187</b> |
| 5.1. Introduction .....  | 188        |
| 5.2. Evaluation based on Engineering Parameters .....  | 188        |
| 5.3. Evaluation based on Shading System Type .....   | 192        |
| 5.4. Evaluation based on Control Scenarios.....  | 199        |
| 5.5. Evaluation based on Control Scenario (C4).....  | 205        |
| 5.6. Chapter Summary .....   | 216        |
| <b>CHAPTER SIX: DEVELOPMENT OF A SURROGATE MODEL FOR ADAPTIVE FAÇADE PERFORMANCE IN THE EARLY DESIGN STAGES.....</b> | <b>217</b> |



|   |     |
|---|-----|
| 6.1. Introduction .....                                       | 218 |
| 6.2. Solar Radiation Prediction Using Machine Learning .....  | 220 |
| 6.3. Data Pre-processing .....                                | 220 |
| 6.4. ANN Model Development .....                              | 221 |
| 6.4.1. Training Process .....                                 | 222 |
| 6.4.2. Data Splitting Procedure (Hold Out Validation).....    | 224 |
| 6.4.3. Optimization of Hyperparameters (Grid-Structure) ..... | 224 |
| 6.4.3.1. Architecture of the Neural Network .....             | 225 |
| 6.4.3.2. Learning Rate.....                                   | 227 |
| 6.4.3.3. Number of Epochs .....                               | 227 |
| 6.4.3.4. Batch Size.....                                      | 228 |
| 6.4.3.5. Results of Hyperparameters.....                      | 228 |
| 6.4.4. K-fold Cross Validation.....                           | 229 |
| 6.4.5. Optimization of Hyperparameters.....                   | 230 |
| 6.4.6. Testing the Architecture .....                         | 232 |
| 6.5. Random Forest Model Development.....                     | 232 |
| 6.5.1. Optimization of Hyperparameters.....                   | 233 |
| 6.5.1.1. Bootstrap.....                                       | 233 |
| 6.5.1.2. Minimal Cost-Complexity Pruning.....                 | 234 |
| 6.5.1.3. Number of Trees.....                                 | 234 |
| 6.5.2. K-fold Cross Validation.....                           | 235 |
| 6.5.3. Optimization of Hyper parameters.....                  | 235 |
| 6.6. Comparison of ANN and RF.....                            | 237 |
| 6.7. Cooling Loads Prediction Using Machine Learning .....    | 238 |
| 6.8. Data Pre-processing .....                                | 241 |
| 6.9. ANN Model Development .....                              | 241 |
| 6.9.1. Optimization of Hyperparameters (Grid-Structure) ..... | 244 |
| 6.9.1.1. Architecture of the Neural Network .....             | 244 |
| 6.9.1.2. Learning Rate.....                                   | 246 |
| 6.9.1.3. Batch Size.....                                      | 247 |
| 6.9.1.4. Number of Epochs .....                               | 248 |
| 6.9.1.5. Results for Hyperparameters .....                    | 248 |
| 6.9.2. Optimization of Hyperparameters.....                   | 251 |
| 6.9.3. Testing the Architecture .....                         | 252 |
| 6.10. Random Forest Model Development.....                    | 253 |

|  |            |
|--|------------|
| 6.10.1. K-Fold Cross Validation .....  | 253        |
| 6.10.2. Optimization of Hyperparameters.....   | 254        |
| 6.10.3. Results of Cooling Prediction using RF.....  | 254        |
| 6.11. 6.11 Experiment to Analyse Time Series Nature of the Data.....                                   | 256        |
| 6.11.1. Modelling Particularly the Time Series Inputs.....   | 256        |
| 6.11.1.1. Approach 1 (Time Differencing) .....   | 256        |
| 6.11.1.2. Approach 2 (Time Window) .....   | 256        |
| 6.11.2. Modelling the Time Series and Non-Time Series Inputs.....                                      | 257        |
| 6.11.3. Random Forest Model Development .....  | 257        |
| 6.11.4. K-Fold Cross Validation .....  | 257        |
| 6.11.5. Optimization of Hyperparameters.....   | 258        |
| 6.11.5.1. Experiment (1): Time Differencing Approach with only Time Series inputs .....                | 258        |
| 6.11.5.2. Experiment (2): Time Window Approach with Only Time Series Inputs...                         | 259        |
| 6.11.5.3. Experiment (3): Time Differencing Approach with Time Series and Time Non-Series Inputs. .... | 261        |
| 6.11.5.4. Experiment (4): Time Window Approach with Time Series and Time Non-Series Inputs .....       | 262        |
| 6.11.6. Comparative Analysis.....  | 264        |
| 6.12. Chapter Summary .....  | 265        |
| <b>CHAPTER SEVEN: DEPLOYMENT OF THE DEVELOPED SURROGATE MODELS .....</b>                               | <b>266</b> |
| 7.1. Introduction .....  | 267        |
| 7.2. Model Deployment .....  | 267        |
| 7.3. Solar Radiation (Predicated Design Scenarios vs. Simulated).....                                  | 271        |
| 7.4. Solar Radiation Prediction for New Design Scenario .....  | 272        |
| 7.5. Cooling Loads (Predicted Design Scenarios vs. Simulated).....                                     | 275        |
| 7.6. Cooling Loads Prediction for Different Cities .....   | 282        |
| 7.7. Chapter Summary .....   | 285        |
| <b>CHAPTER EIGHT: DISCUSSION AND CONCLUSION .....</b>  | <b>286</b> |
| 8.1. Introduction .....  | 287        |
| 8.2. Discussion of Research Findings.....  | 287        |
| 8.2.1. An Algorithmic Framework to Evaluate the Energy Performance of Adaptive Façades .....           | 287        |
| 8.2.2. The Impact of Adaptive Façades on Energy Performance in High Rise Office Buildings.....         | 288        |
| 8.2.3. Parametric Generative Database based on Simulation Approach .....                               | 291        |

|  |            |
|--|------------|
| 8.2.4. Machine Learning (ML) Models to Predict Energy Performance of Adaptive Façades..... | 292        |
| 8.2.5. Surrogate Model to Assist in Early Design Stages of AF for Decision Making ....     | 294        |
| 8.3. Achievement of the Research Objectives .....  | 295        |
| 8.4. Simulation Novelty and Surrogate Model Generalizability.....                          | 298        |
| 8.5. Contributions to the Body of Knowledge.....   | 300        |
| 8.6. Research Limitations .....  | 300        |
| 8.7. Recommendations and Future Work.....  | 301        |
| 8.8. Chapter Summary .....   | 302        |
| <b>REFERENCES.....</b>   | <b>303</b> |
| <b>APPENDIX .....</b>  | <b>325</b> |
| Appendix A: Validation .....   | 326        |
| Appendix B: High Rise Buildings (Case Studies).....  | 329        |
| Appendix C: Modelling and Simulation Workflow (Database Generation).....                   | 342        |
| Appendix D: Synthetic Database .....   | 362        |
| Appendix E: ML Surrogate Models Codes and Deployments.....                                 | 376        |

## List of Figures

---

|   |    |
|---|----|
| Figure 1.1: Building sector electricity consumption in KSA.....   | 6  |
| Figure 1.2: KSA typical daily electricity load curve during summer. ....  | 7  |
| Figure 1.3: KSA typical daily electricity load curve during winter. ....  | 7  |
| Figure 1.4: Monthly total KSA electricity consumption and average ambient temperature... ..                                 | 8  |
| Figure 1.5: High-rise buildings timeline in Riyadh .....  | 9  |
| Figure 1.6: First phase of constructed tall building’s structure in Riyadh.....   | 10 |
| Figure 1.7: Examples of the second phase of Riyadh's tall building development, followed the international style.....       | 11 |
| Figure 1.8: Examples of the third phase of tall buildings development implemented fixed shading systems. ....               | 12 |
| Figure 1.9: Examples of tall buildings constructed in the King Abdullah Financial District (KAFFD). ....                    | 12 |
| Figure 1.10: World map of Koppen-Geiger Climate Classification. ....  | 13 |
| Figure 1.11: Climate zones of KSA based on SRBEC classifications. ....  | 14 |
| Figure 1.12: Annual temperature profile for Riyadh city. ....   | 14 |
| Figure 1.13: Structure of the thesis.....   | 21 |
| Figure 1.14: Detailed structure of the thesis.....  | 22 |
| Figure 2.1: Timeline of kinetic architecture's history.....   | 29 |
| Figure 2.2: Examples of active façades the Children's Museum of Pittsburgh (left), and the ICT-Media building (right). .... | 31 |
| Figure 2.3: Examples of bio-mimetic façades, One Ocean Thematic Pavilion (left), and the BIQ House in Germany (right). .... | 32 |
| Figure 2.4: Example of passive façade, the Energybase building.....   | 33 |
| Figure 2.5: Example of kinetic façades, Al-Baher Towers. ....   | 34 |
| Figure 2.6: Example of an intelligent façade, the GSW Headquarters building in Germany. ....                                | 35 |
| Figure 2.7: Example of interactive façade, the GreenPix building. ....  | 35 |
| Figure 2.8: Example of movable façade, the EWE Arena in Hamburg. ....   | 36 |
| Figure 2.9: Example of smart façade, the Bloom Project. ....  | 37 |
| Figure 2.10: Example of a responsive façade, the Kiefer Technic Showroom. ....  | 37 |
| Figure 2.11: Relations between the various types of AFs .....   | 39 |
| Figure 2.12: Adaptive façade in terms of technologies and purpose.....  | 40 |
| Figure 2.13: All possible physical overlappings related to building envelopes. ....   | 41 |
| Figure 2.14: Schematic role of adaptive façade .....  | 43 |
| Figure 2.15: Open-loop control system.....  | 44 |
| Figure 2.16: Closed-loop control system.....  | 45 |
| Figure 2.17: Analysis of existing studies regarding simulation tools used to simulate AFs. ..                               | 53 |
| Figure 2.18: Analysis of current studies of AFs systems that used BPS tools. ....   | 56 |
| Figure 2.19: Types of machine learning .....  | 65 |
| Figure 2.20: Supervised machine learning process .....  | 66 |
| Figure 2.21: Stages to develop ML surrogate models.....   | 67 |
| Figure 2.22: Structural diagram of neuron.....  | 72 |
| Figure 2.23: Schematic diagram of two-layered architecture network .....  | 73 |

|  |     |
|--|-----|
| Figure 2.24: The primary steps to develop the ANN model.....   | 74  |
| Figure 2.25: ANN architecture with multiple hidden layers.....   | 75  |
| Figure 2.26: Gradient based to update the weights of the network.....  | 76  |
| Figure 2.27: The global minimum value on the error surface.....  | 77  |
| Figure 2.28: Two commonly employed activation functions.....   | 78  |
| Figure 2.29: Procedure for Decision tree development.....  | 79  |
| Figure 2.30: A decision tree showing how the decisions are made.....   | 80  |
| Figure 2.31: Analysis of the existing studies that used ANN or DT methods for building performance prediction.....   | 90  |
| Figure 3.1: Typical architectural design phases.....   | 101 |
| Figure 3.2: The basic characteristics of the three research approaches.....  | 102 |
| Figure 3.3: The overall research framework.....  | 105 |
| Figure 3.4: A diagram showing (Phase 4: Development of ML surrogate models), and (Phase 5: Incorporation of the surrogate model within a computational design tool)..... | 111 |
| Figure 3.5: The research framework.....  | 114 |
| Figure 4.1: Geographical map showing the locations of the selected high rise building cases.....   | 118 |
| Figure 4.2: High-rise office buildings: selected cases.....  | 119 |
| Figure 4.3: Office building types.....   | 120 |
| Figure 4.4: (A) Gross Floor Area (GFA), and (B) Net Lettable Area (NLA).....   | 121 |
| Figure 4.5: Graph showing the floor efficiency parameter of the analysed cases.....  | 121 |
| Figure 4.6: Lease span in the office tower zone.....   | 122 |
| Figure 4.7: Graph showing the average leasing depth.....   | 122 |
| Figure 4.8: Number of floors of the analysed office cases.....   | 123 |
| Figure 4.9: Graph showing the heights of high-rise office buildings in the studied context.....  | 124 |
| Figure 4.10: Most applied forms in high-rise buildings.....  | 125 |
| Figure 4.11: Existence of shading devices in current high-rise buildings in the studied region.....  | 126 |
| Figure 4.12: Correlation between time and the application of shading systems in high-rise buildings.....   | 127 |
| Figure 4.13: Schematic framework of the modeling and simulation phase, and the surrogate model development phase.....  | 129 |
| Figure 4.14: (Left) 3D parametric urban context, which varies in each simulation, and (Right) a detailed typical floor plan.....   | 131 |
| Figure 4.15: Single closed office space within the office tower facing main orientations... ..   | 131 |
| Figure 4.16: Scripting to create the office zone using Honeybee tools.....   | 132 |
| Figure 4.17: Parametric modelling and simulation tools used in the study.....  | 132 |
| Figure 4.18: Parametric modelling generation rules.....  | 134 |
| Figure 4.19: Scripting for setting up the geometry in a parametric way.....  | 135 |
| Figure 4.20: The location and borders of Saudi Arabia and the location of Riyadh.....  | 136 |
| Figure 4.21: The average annual daily solar radiation in KSA.....  | 136 |
| Figure 4.22: Dry bulb temperature (top), global horizontal radiation (middle), and direct solar radiation (bottom).....  | 137 |
| Figure 4.23: Annual energy consumption results of the examined building compared to base model.....  | 140 |

|  |     |
|--|-----|
| Figure 4.24: Annual cooling energy consumption of the examined cases compared to base model. ....  | 140 |
| Figure 4.25: Monthly energy consumption comparison between case study (F), which obtained from electricity bills and the simulated base case model. ....               | 141 |
| Figure 4.26: Different prototypes of an adaptive façade with different movement motions. ....  | 143 |
| Figure 4.27: Modelling process of the AF geometry. (A) Scaling movement, and (B) Folding movement, which shows the variation of adaptive façade shading states. ....   | 144 |
| Figure 4.28: Framework of the three conducted stages: modelling, simulation, and database recording. ....  | 146 |
| Figure 4.29: Annual solar radiation map of the world. ....   | 147 |
| Figure 4.30: Incident solar radiation on a west-facing wall, Riyadh. ....  | 148 |
| Figure 4.31: Temperature and solar radiation striking south-facing surface during (top) 20 June and (bottom) 20 December (Source: Touma and Ouahrani 2018). ....       | 149 |
| Figure 4.32: Solar radiation striking south-facing surface during (top) 20 June and (bottom) 20 December for the conducted study. ....                                 | 150 |
| Figure 4.33: Average monthly total incident solar radiation on four main orientations in Jeddah. ....  | 151 |
| Figure 4.34: Average monthly total incident solar radiation on four main orientations for the conducted study. ....  | 151 |
| Figure 4.35: Workflow used to conduct the solar radiation analysis. ....   | 153 |
| Figure 4.36: Scripting process used to conduct the solar radiation analysis in Grasshopper using the Ladybug tool. ....  | 153 |
| Figure 4.37: Fixed and dynamic model parameters. ....  | 154 |
| Figure 4.38: Sample of the solar radiation data generated automatically in the simulation process, which produced different SR results in each design situation. ....  | 155 |
| Figure 4.39: (A) Test point coordinates, (B) Radiation results based on each test point. ....  | 156 |
| Figure 4.40: Pre-processing of solar radiation results. ....   | 156 |
| Figure 4.41: An example of two different cases of solar radiation results within different orientations and based on the variation of building contexts and time. .... | 157 |
| Figure 4.42: Shade factor (SF) calculations. ....  | 159 |
| Figure 4.43: Workflow used to conduct the shade factor analysis. ....  | 160 |
| Figure 4.44: Scripting process to conduct the shade factor analysis in Grasshopper using the Ladybug tool. ....  | 161 |
| Figure 4.45: Shade factor calculation for some selected cases for two AF movements (scaling and folding). ....   | 163 |
| Figure 4.46: Closed office room with detailed constructions and location of sensor. ....   | 164 |
| Figure 4.47: Algorithmic workflow of the parametric modelling and simulation in Grasshopper environment. ....  | 165 |
| Figure 4.48: Scripting process using Colibri tool to iterate through design solutions. ....  | 169 |
| Figure 4.49: Construction parameters considered for this study. ....   | 170 |
| Figure 4.50: Artificial lighting – continuous dimming control. ....  | 172 |
| Figure 4.51: Energy management system (EMS) principles. ....   | 173 |
| Figure 4.52: Scripting process to create hourly shading states schedules in grasshopper using Honeybee tool. ....  | 175 |

|  |     |
|--|-----|
| Figure 4.53: EMS conditional (IF, ELSE-IF) statement to control the AF opening ratio based on a predefined threshold. ....   | 177 |
| Figure 4.54: Sample of the generated energy data, which vary based on each design solution. ....   | 183 |
| Figure 4.55: Sample of cases for hourly shading states in three selected hours (9:00 am, 12:00 pm, 15:00 pm).....  | 184 |
| Figure 4.56: Sample of cases for hourly shading states in three selected hours (9:00 am, 12:00 pm, 15:00 pm).....  | 185 |
| Figure 5.1: Simulation results of engineering parameters in terms of cooling loads within different orientations.....  | 190 |
| Figure 5.2: Solar heat gain results for 48 cases. ....   | 191 |
| Figure 5.3: Comparison of external shading systems for (Ext2_Glaz3) in terms of cooling loads and solar heat gain. ....  | 193 |
| Figure 5.4: Comparison of external shading systems for case (Ext2_Glaz3), in terms of cooling load reduction and solar heat gain reduction. ....   | 194 |
| Figure 5.5: Comparison of external shading systems for case (Ext0_Glaz0), in terms of cooling loads and solar heat gain.....   | 195 |
| Figure 5.6: Comparison of external shading systems for case (Ext0_Glaz0), in terms of cooling load reduction and solar heat gain reduction. ....   | 195 |
| Figure 5.7: Simulation results of fixed vertical shading in terms of cooling loads and solar heat gain within different orientations.....  | 197 |
| Figure 5.8: Simulation results of fixed horizontal shading in terms of cooling loads and solar heat gain within different orientations.....  | 197 |
| Figure 5.9: Simulation results of adaptive faced (scaling movement) in terms of cooling loads and solar heat gain within different orientations.....   | 198 |
| Figure 5.10: Simulation results of adaptive façade (folding movement) in terms of cooling loads and solar heat gain within different orientations. ....  | 198 |
| Figure 5.11: Comparison of control scenarios in terms of cooling and lighting loads within different orientations, case (ExtW2_Glaz3).....   | 201 |
| Figure 5.12: Simulation outputs for (C3) (south orientation), hourly direct solar radiation (top), and the hourly corresponding shading states (bottom). ....                                  | 201 |
| Figure 5.13: Simulation outputs for (C2) (west orientation), hourly transmitted solar radiation (top), and the hourly corresponding shading states (bottom).....                               | 202 |
| Figure 5.14: Simulation outputs for (C2) (south orientation), hourly transmitted solar radiation (top), and the hourly corresponding shading states (bottom).....                              | 202 |
| Figure 5.15: Comparison of control scenarios in terms of cooling and lighting loads within different orientations, case (ExtW1_Glaz2).....   | 203 |
| Figure 5.16: The interface webpage of Design Explorer allowing parallel coordinate chart. ....   | 206 |
| Figure 5.17: Web-based comparison of energy performance for control scenario (C4) showing optimum and worst cases for all orientations.....  | 208 |
| Figure 5.18: Simulation outputs for (C4), (west orientation): operative temperature (top), solar radiation (middle), and hourly variations of shading states based on SR and OT (bottom). .... | 209 |

|  |     |
|--|-----|
| Figure 5.19: Simulation outputs for (C4), east orientation): operative temperature (top), solar radiation (middle), and hourly variations of shading states based on SR and OT (bottom). .....   | 210 |
| Figure 5.20: Simulation outputs for (C4), (south orientation): operative temperature (top), solar radiation (middle), and hourly variations of shading states based on SR and OT (bottom). ..... | 210 |
| Figure 5.21: Simulation outputs for (C4), (north orientation): operative temperature (top), solar radiation (middle), and hourly variations of shading states based on SR and OT (bottom). ..... | 211 |
| Figure 5.22: Hourly transmitted solar radiation through window (south orientation), prior to implementing the AF shading (top), and after implementing the AF shading (bottom).....              | 212 |
| Figure 5.23: Hourly transmitted solar radiation through window (west orientation), prior to implementing the AF shading (top), and after implementing the AF shading (bottom).....               | 212 |
| Figure 5.24: Hourly transmitted solar radiation through window (north orientation), prior to implementing the AF shading (top), and after implementing the AF shading (bottom).....              | 212 |
| Figure 5.25: Hourly transmitted solar radiation through window (east orientation), prior to implementing the AF shading (top), and after implementing the AF shading (bottom).....               | 213 |
| Figure 5.26: Relation between shading states variations, and urban contexts and its impact on cooling loads for South orientation. ....  | 214 |
| Figure 5.27: Relation between variations in shading states, and urban contexts and their impact on cooling loads for west orientation.....   | 215 |
| Figure 6.1: Workflow used to develop the surrogate models.....   | 219 |
| Figure 6.2: Architecture of the ANN model.....   | 222 |
| Figure 6.3: ANN components. ....   | 223 |
| Figure 6.4: Tools used in the study to train and test both models. ....  | 223 |
| Figure 6.5: Hold out validation splitting procedure .....  | 224 |
| Figure 6.6: A comparison of all examined ANN models. ....  | 226 |
| Figure 6.7: Training and validation loss against epochs. ....  | 229 |
| Figure 6.8: The data split procedure. ....   | 230 |
| Figure 6.9: k-fold cross validation results for choosing the architecture.....   | 231 |
| Figure 6.10: The performance metric comparison of best performing model among one-, two-, three-, and four-layer networks .....  | 231 |
| Figure 6.11: The actual and predicted solar radiation values by ANN for a set of 25 coordinates. ....  | 232 |
| Figure 6.12: The modelling of RF (top), and how the decision is made in the decision tree algorithm (down). ....   | 233 |
| Figure 6.13: The performance metric visualization for the best model when the number of trees is considered. ....  | 236 |
| Figure 6.14: The result visualization of hyperparameter tuning in RF, CCP stands for the CCP alpha value chosen, and BS stands for bootstrap option. ....  | 236 |



|  |     |
|--|-----|
| Figure 6.15: The actual and predicted solar radiation values by RF for a set of 25 coordinates plotted as a heatmap. ....  | 237 |
| Figure 6.16: Sample of the data generated based on simulation. ....  | 238 |
| Figure 6.17: An artificial Neuron. ....  | 239 |
| Figure 6.18: Data flow overview.....   | 240 |
| Figure 6.19: Architecture of the ANN model.....  | 242 |
| Figure 6.20: ANN components. ....  | 243 |
| Figure 6.21: Results of sensitivity analysis on ANN architecture. ....   | 245 |
| Figure 6.22: RMSE, MAE and $R^2$ score of the best performing models among the one-, two-, three- and four-layer networks. ....  | 246 |
| Figure 6.23: RMSE, MAE and $R^2$ score for the learning rate.....  | 247 |
| Figure 6.24: RMSE, MAE and $R^2$ score for the batch size. ....  | 247 |
| Figure 6.25: RMSE, MAE, and $R^2$ score for the number of epochs.....  | 248 |
| Figure 6.26: Training and validation loss against epochs. ....   | 249 |
| Figure 6.27: Plot of actual and predicted values for 100 testing cases.....  | 250 |
| Figure 6.28: The data split procedure. ....  | 250 |
| Figure 6.29: K-fold cross validation results on choosing ANN architecture.....   | 252 |
| Figure 6.30: RMSE, MAE, and $R^2$ score of the best performing models among the one-, two-, three-, and four-layer networks ....   | 252 |
| Figure 6.31: Training and validation loss against epochs.....  | 253 |
| Figure 6.32: The result of cooling load prediction. The figure corresponds to the visualization of the results of hyperparameter tuning in RF (BS stands for bootstrap option). ....   | 254 |
| Figure 6.33: Performance metrics corresponding to the best performing models. ....   | 255 |
| Figure 6.34: The plot of the actual and predicted values for a set of 100 randomly chosen test points in the case of cooling load prediction.....  | 255 |
| Figure 6.35: The result of cooling load prediction in the time differencing approach with only time varying inputs. The figure corresponds to the visualisation of the results of hyperparameter tuning in RF (BS stands for bootstrap option). .... | 258 |
| Figure 6.36: Performance metrics corresponding to the best performing models. ....   | 259 |
| Figure 6.37: The plot of the actual and predicted values for third week of October in the case of hourly cooling load prediction (Experiment 1). ....  | 259 |
| Figure 6.38: The plot of the actual and predicted values for fourth week of October in the case of hourly cooling load prediction (Experiment 1). ....   | 259 |
| Figure 6.39: The result of cooling load prediction in the time window approach with only time varying inputs. The figure corresponds to the visualisation of the results of hyperparameter tuning in RF (BS stands for bootstrap option). ....       | 260 |
| Figure 6.40: Performance metrics corresponding to the best performing models. ....   | 260 |
| Figure 6.41: The plot of the actual and predicted values for third week of October in the case of hourly cooling load prediction (Experiment 2). ....  | 260 |
| Figure 6.42: The plot of the actual and predicted values for fourth week of October in the case of hourly cooling load prediction (Experiment 2). ....   | 260 |
| Figure 6.43: The result of cooling load prediction in the time window approach with only time varying inputs. The figure corresponds to the visualisation of the results of hyperparameter tuning in RF (BS stands for the bootstrap option). ....   | 261 |

|  |     |
|--|-----|
| Figure 6.44: Performance metrics corresponding to the best performing models. ....   | 262 |
| Figure 6.45: The plot of the actual and predicted values for third week of October in the case of cooling load prediction (Experiment 3). ....   | 262 |
| Figure 6.46: The plot of the actual and predicted values for fourth week of October in the case of cooling load prediction (Experiment 3). ....  | 262 |
| Figure 6.47: The result of the cooling load prediction in the time window approach with only time varying inputs. The figure corresponds to the visualisation of the results of hyperparameter tuning in RF (BS stands for bootstrap option). .... | 263 |
| Figure 6.48: Performance metrics corresponding to the best performing models. ....   | 263 |
| Figure 6.49: The plot of the actual and predicted values for third week of October in the case of cooling load prediction (Experiment 4). ....   | 263 |
| Figure 6.50: The plot of the actual and predicted values for fourth week of October in the case of cooling load prediction (Experiment 4). ....  | 263 |
| Figure 7.1: The loaded codes inside GH CPython to make predictions within Grasshopper. ....  | 268 |
| Figure 7.2: Inputs required to make predictions for solar radiation using the RF model. ....   | 268 |
| Figure 7.3: Inputs required to make predictions for cooling loads using the RF model. ....   | 269 |
| Figure 7.4: RF surrogate model workflow for predicting hourly solar radiation within Grasshopper. ....   | 270 |
| Figure 7.5: RF surrogate model workflow for predicting hourly cooling loads within Grasshopper. ....   | 270 |
| Figure 7.6: Workflow to conduct energy performance of AF shading system. ....  | 271 |
| Figure 7.7: New design scenario with several office towers. ....   | 273 |
| Figure 7.8: Workflow of the surrogate model in Grasshopper using GH-CPython to predict incident solar radiation on the building envelope for 150 design cases. ....  | 273 |
| Figure 7.9: Sample of the hourly solar radiation output of the 150 cases as predicted by the RF surrogate model. ....  | 274 |
| Figure 7.10: Comparison between simulated solar radiation results using Ladybug and the predicted results using the RF surrogate model for two random cases. ....  | 274 |
| Figure 7.11: Selection of inputs from the slider component. ....   | 275 |
| Figure 7.12: Selection of inputs from a panel component for three different design scenarios. ....   | 276 |
| Figure 7.13: The developed workflow to predict hourly cooling loads within the Grasshopper interface. ....   | 276 |
| Figure 7.14: Comparison between RF model predictions, ANN model predictions, and simulation predictions of hourly cooling loads for four months of the year (March, June, September, and December). ....   | 280 |
| Figure 7.15: Comparison between RF model predictions, ANN model predictions, and simulation predictions of hourly cooling loads for four months of the year (March, June, September, and December). ....   | 282 |
| Figure 7.16: Comparison between surrogate models' prediction and simulation prediction for Jeddah and Kuwait cities. ....  | 283 |
| Figure 7.17: Comparison between surrogate models' prediction and simulation prediction for Phoenix and Tucson cities. ....   | 284 |

## List of Tables

---

|  |     |
|--|-----|
| Table 2.1. Review of some existing studies in relation to automatic control systems.....   | 48  |
| Table 2.2. Current research of BPS of adaptive façades in literature.....  | 57  |
| Table 2.3. ANN and DT application techniques to building-energy-related areas. ....  | 91  |
| Table 3.1: Research objectives and methods .....   | 113 |
| Table 4.1. Summary of the examined parameters. ....  | 127 |
| Table 4.2. The annual energy consumption of the examined buildings.....  | 139 |
| Table 4.3. Fixed simulation parameters.....  | 168 |
| Table 4.4. Dynamic simulation parameters .....   | 169 |
| Table 4.5. Characteristics of materials used in the simulation.....  | 171 |
| Table 4.6. Control scenario parameters. ....   | 174 |
| Table 4.7. Dynamic simulation matrix for base case model. ....   | 179 |
| Table 4.8. Dynamic simulation matrix for fixed shading system. ....  | 180 |
| Table 4.9. Dynamic simulation matrix for adaptive façade shading system. ....  | 180 |
| Table 5.1. The simulation results for cooling loads, the orange row representing the optimal-case scenario and the yellow row representing the worst-case scenario. .... | 191 |
| Table 5.2. Total number of hours spent in each shading state for some specific cases in different orientations and urban contexts.....                                   | 215 |
| Table 6.1. The input data used for the machine learning modelling.....   | 221 |
| Table 6.2. The different number of layers experimented in the study. ....  | 225 |
| Table 6.3. Different values of learning rate. ....   | 227 |
| Table 6.4. Variations of the number of epochs. ....  | 228 |
| Table 6.5. Different batch sizes used in the analysis. ....  | 228 |
| Table 6.6. Architecture optimization of ANN by k-fold cross validation. ....   | 231 |
| Table 6.7. Experiments using bootstrap. ....   | 234 |
| Table 6.8. Experiments using various hyperparameters of $\alpha$ . ....  | 234 |
| Table 6.9. Experiments using different number of trees.....  | 235 |
| Table 6.10. The k-fold cross validation results for RF. ....   | 236 |
| Table 6.11. Performance comparison of ANN and RF for solar radiation data. ....  | 237 |
| Table 6.12. The input data used for the ANN modelling .....  | 239 |
| Table 6.13. Experiments using different ANN architecture.....  | 244 |
| Table 6.14. Experiment using different values of learning rate.....  | 246 |
| Table 6.15. Experiment using different batch size.....   | 247 |
| Table 6.16 Experiment using different number of epochs. ....   | 248 |
| Table 6.17. Training and validation loss against epochs.....   | 249 |
| Table 6.18. Results of hyperparameter tuning for ANN architecture .....  | 251 |
| Table 6.19. Performance comparison of ANN and RF for cooling loads data.....   | 255 |
| Table 6.20. Performance comparison of the four conducted experiments. ....   | 264 |
| Table 7.1. Performance comparison of ANN and RF for cooling load data. ....  | 275 |
| Table 7.2. The specifications of the examined cases.....   | 277 |
| Table 7.3. Input parameters of the examined four cities. ....  | 282 |

## List of Abbreviations

---

|        |   |
|--------|---|
| IEA    | International Energy Agency   |
| AF     | Adaptive Façade   |
| NZB    | Net Zero Buildings  |
| AFs    | Adaptive Façades  |
| AF     | Adaptive Façade   |
| KSA    | Kingdom of Saudi Arabia   |
| GCC    | Gulf Cooperation Council  |
| MOMRA  | Ministry of Municipal and Rural Affairs                                       |
| HVAC   | Lighting and Heating, Ventilation, and Air-Conditioning                       |
| SEC    | Saudi Electric Company  |
| KACST  | King Abdulaziz City for Science and Technology                                |
| SEEC   | Saudi Energy Efficiency Centre  |
| SBC    | Saudi Building Code   |
| CTBUH  | Council on Tall Buildings and Urban Habitat                                   |
| KAFD   | King Abdullah Financial District  |
| BPS    | Building Performance Simulation   |
| EMS    | Energy Management System  |
| CABS   | Climate Adaptive Building Shell   |
| SVM    | Shape Variable Mashrabiya   |
| AKE    | Acclimated Kinetic Envelope   |
| DSF    | Double Skin Facade  |
| PCM    | Phase Change Memory   |
| IAQ    | Indoor Air Quality  |
| sDA    | Spatial Daylight Autonomy   |
| ASE    | Annual Sunlight Exposure  |
| TC     | Thermochromic Glazing Systems   |
| PVC    | Photovoltaic-Chromic Glazing Systems  |
| SI     | Solar Irradiance  |
| CFS    | Complex Fenestration Systems  |
| EUI    | Energy Use Intensity  |
| ERL    | EnergyPlus Runtime Language   |
| EPW    | Weather File  |
| AI     | Artificial Intelligence   |
| ML     | Machine Learning  |
| ANN    | Artificial Neural Network   |
| DT     | Decision Tree   |
| RF     | Random Forest   |
| SL     | Supervised Learning   |
| SM     | Surrogate Model   |
| BMS    | Building Management Systems   |
| ASHRAE | The American Society of Heating, Refrigerating and Air-Conditioning Engineers |

|                |   |
|----------------|---|
| MLP            | Multilayer Layer perceptions            |
| BP             | Backpropagation                         |
| EMM            | Energy Model Machine                    |
| CBR            | Case Based Reasoning                    |
| MLFFNN         | Multi-Layer Feed Forward Neural Network |
| GRNN           | Generalized Regression Neural Network   |
| SVM            | Support Vector Machine                  |
| SR             | Solar Radiation                         |
| SF             | Shade Factor                            |
| OT             | Operative Temperature                   |
| GFA            | Gross Floor Area                        |
| NLA            | Net Leasable Area                       |
| WWR            | Window-Wall Ratio                       |
| U-Value        | Thermal Transmittance                   |
| VLT            | Visual Transmittance                    |
| SHGF           | Solar Heat Gain Coefficient             |
| SC             | Shading Coefficient                     |
| CL             | Cooling Loads                           |
| HCL            | Hourly Cooling Loads                    |
| RMSE           | Root Mean Square Error                  |
| MAE            | Mean Absolute Error                     |
| R <sup>2</sup> | Coefficient of Determination            |
| ReLU           | Rectified Linear Unit                   |

## **CHAPTER ONE**

### **INTRODUCTION AND OVERVIEW**

## **CHAPTER 1: INTRODUCTION AND OVERVIEW**

---

### **1.1. Introduction**

This chapter presents a background of the research, states the research problem, explains the significance of the study, identifies the aim and objectives of the study, outlines the research questions, indicates the scope, and focus of the research, presents an overview of the methodology and research design, and lastly, concludes by exhibiting an outline of the thesis structure and a summary of this chapter.

### **1.2. Research Background and Context**

According to the International Energy Agency (IEA), energy consumption by buildings is increasing significantly, and buildings account for 40% of the global energy. Furthermore, IEA reported that energy demand is estimated to increase by 30% by 2035 (Building and Codes 2013). Other studies have stated that the building sector consumes more energy compared to other sectors, such as the industry and transportation sectors (Shakouri and Banihashemi 2012; Alyami and Omer 2021). Therefore, various countries have formed new regulations to achieve net zero buildings (NZB) and reduce greenhouse emissions. As an example of this, the Saudi government established the Saudi Green Initiative, which aims to achieve NZB by 2040 in new constructed buildings. In addition, the Saudi policies emphasise the significance of energy efficient buildings and the issue of climate change. These above-mentioned goals can be achieved using effective measurements to reduce buildings' energy consumption and maximize indoor environmental quality in buildings.

To meet the current targets of designing high performance buildings with the future of nearly ZEB, there is a need to continue the advances made in the design, technology, and materials of buildings. Integrating intelligent solutions into the design process of buildings can achieve the indoor environmental comfort of the building occupants and minimize energy consumption (Ochoa and Capeluto 2008). The building envelope plays an important role in achieving this target; it acts as a separator element between the indoor and outdoor environments of a building and is a crucial factor that determines the quality of indoor conditions (Sadineni et al. 2011). Furthermore, the building envelope not only defines the aesthetic appearance of buildings but also performs several functions such as safety, privacy, and protection from outdoor conditions. Additionally, it connects the building's occupants with the outdoor world allowing them access to daylight, air, and views while controlling the energy exchange (Loonen 2018). Since buildings with extensive glazing systems are the dominant type of envelopes found in most high-rise and mid-rise office buildings particularly

## **CHAPTER 1: INTRODUCTION AND OVERVIEW**

in harsh, hot climates, it is vital to install shading systems on such buildings to prevent the penetration of direct sunlight and solar radiation into the internal spaces. The intensive solar radiation has an impact on increasing the cooling energy loads required to achieve human comfort in these office spaces.

As stated in the literature, a building's skin or façade is a key factor in determining the comfort and energy consumption of the building. This is because buildings are exposed to dynamic environmental factors, such as solar radiation, temperature, and wind, and these outdoor conditions change continuously throughout the day and the year. Regardless of the outdoor climate, which changes constantly, a building's skin has been typically designed as a static envelope. However, fixed or static shading devices are limited in terms of their responsiveness to indoor or outdoor environmental conditions. Thus, this leads to less performance once these systems have been installed especially if changes over time are required (Tabadkani et al. 2021a). In addition, studies have shown that static façades are no longer favourable and have limitations in terms of attaining the desired energy efficiency, adequate daylighting, and control flexibility (Al-Masrani and Al-Obaidi 2019). On the other hand, adaptive façades (AFs) are effective in responding to the variable climatic conditions. These AFs have unique features or behaviours that repeatedly and reversibly change over time and respond to changing performance requirements aiming to improve the building performance (Loonen et al. 2014b). To that end, numerous studies have been conducted regarding substituting the static envelope with an adaptive one to achieve greater efficiency and performance by exploiting the dynamic environment.

To successfully develop AF systems, it is crucial to assess their benefits and performance during the early stages of the design. However, the lack of a suitable method and appropriate tools makes it challenging for architects and engineers to evaluate AFs' performance (Favoino et al. 2016; Loonen et al. 2017). Most of BPS tools are often characterised as complex digital modelling and not user-friendly (Loonen et al. 2017). Therefore, numerous studies have primarily focused on the development of AF technologies that are only able to alter their physiological features. In contrast, view studies have examined the geometrical variations of AFs in response to environmental conditions (Kuru 2020).

### **1.2.1. Static Façade**

The application of external shading devices refers to the installation of shade elements on the exterior part of the window. The design of fixed external shading devices has to prevent solar radiation from penetrating through the shading. However, these fixed devices cannot



## **CHAPTER 1: INTRODUCTION AND OVERVIEW**

change to react to the direction of the sun. In addition, a static shade device's effectiveness is influenced by its orientation, the sun's position in the sky, and the device's features. The success of fixed shading devices requires that they be designed and positioned in such a way that, while preventing solar penetration, they do not adversely affect the internal luminance throughout the year.

Based on the literature, fixed or static shade systems have a limited ability to respond to interior or exterior environmental variables over the course of a day or season, which may lead to poor performance if the operational requirements change over time. In addition, researchers have demonstrated that static façades are no longer advantageous and have constraints in achieving the appropriate energy efficiency, suitable daylighting, and control flexibility (Al-Masrani and Al-Obaidi 2019). Armstrong states that the traditional static approach to the design of façades is not the most effective approach for responding to the varying environmental conditions (Armstrong 2012). Hence, the new developed adaptive architectural envelope can replace the traditional approach since it can respond to different environmental conditions.

External static shade systems are utilised for both solar radiation control and energy saving. However, these shading systems might prevent daylight, resulting in the need to use artificial light and prohibiting the healthy winter solar radiation. Therefore, it is crucial to utilise the appropriate type of shade device at the correct time and place.

### **1.2.2. Adaptive Façade**

The methodologies for creating high-performance second skins and the measures required to ensure that environmental factors and energy-efficiency techniques are incorporated into the envelope design process are the most crucial elements. As a result, building façades serve as more than merely a physical barrier between interior and exterior environments; they are also building elements that can dynamically adapt to the internal and external environment of a building to create a comfortable environment while drastically reducing energy consumption. However, a high degree of integration is required to accomplish these design goals, which should be considered at the beginning of the design process. Due to technological improvements, designers can now utilise responsive and adaptable building envelopes as opposed to static and conventional ones. It has been demonstrated that these external adaptive envelopes can serve a unique purpose in the design of high-performance buildings and offer considerable potential for improving the energy efficiency of buildings.

## **CHAPTER 1: INTRODUCTION AND OVERVIEW**

The components of an adaptive shading system can be moved and can operate according to an algorithm. The term "adaptive shading system" can be used to describe applications for intelligent façades, which have been shown to improve occupant comfort by allowing them to interact based on both interior and exterior environments (Sheikh and Asghar 2019).

### **1.2.3. Machine Learning**

To achieve a sustainable built environment, building performance must be addressed in the early phases of design. Hence, the design process becomes more complex than ever before. To manage this complexity, architects and designers have to have an overview of the whole building performance. Machine learning (ML) provides a solution to this challenge, with advantages such as fast prediction and simplified parameter structures that are well-suited for the early stages of design. In a Design Space Exploration process, this enables designers and engineers to rapidly tweak concepts and assess the performance of the building.

The ML method has the potential to evaluate building performance more effectively than traditional simulation. Numerous studies have investigated ML-based prediction models to forecast the energy consumption of buildings. For example, the ML models utilised in building energy prediction employ artificial neural networks (ANNs) (Wu et al., 2007) and the decision tree (DT) (Yu et al. 2010; Killian and Kozek, 2016). Among ML methods, Random Forest (RF) is an ML technique that is easy to train and is effective at dealing with high-dimensional data and solving difficult problems (Zhu et al., 2020). The performance of this technique is consistent and accurate due to the fact that it builds several DTs and combines them to produce output.

### **1.2.4. Energy Consumption of Buildings in Riyadh, Saudi Arabia**

The rapid increase in energy consumption by the building sector, along with the issue of CO<sub>2</sub> emissions, has driven the Kingdom of Saudi Arabia's (KSA) government to implement new, stricter construction regulations in its building codes and standards. Moreover, the Saudi Vision 2030, which was launched in 2016, with the primary objective of reducing the reliance on oil and so diversifying the economy, has also addressed the issue of energy consumption in buildings in order to meet the government's environmental and economic goals (Almushaikah and Almasri 2021). The Kingdom of Saudi Arabia (KSA) is the leading country among the Gulf Cooperation Council (GCC) region in terms of the quantity and scale of construction projects (Asif 2016). According to the Ministry of Municipal and Rural Affairs

## CHAPTER 1: INTRODUCTION AND OVERVIEW

(MOMRA), approximately 90% of all building permits issued in 2015 were for commercial and residential buildings (Alrashed and Asif 2012).

According to Krarti et al. (2017), the building sector consumes a significant amount of energy in KSA with a growth of roughly 10% annually and accounting for 76% of overall electricity consumption in the country Figure (1.1). Additionally, the IEA reported in 2018 that KSA's electrical energy consumption per capita had increased significantly. According to the IEA, energy consumption increased from 7.2 MWh in 2006 to 10.2 MWh in 2018, a 41.7 percent increase over this period (Almushaikh and Almasri 2021). Buildings in KSA are characterized by excessive electrical consumption, whether for HVAC systems, artificial lighting, equipment, or other devices, resulting in a high degree of consumption (Asif 2016). For example, in Riyadh, the major energy consumption is mainly consumed due to the use of air conditioning systems to cool interior spaces during the summer months (Alrashed and Asif 2014).

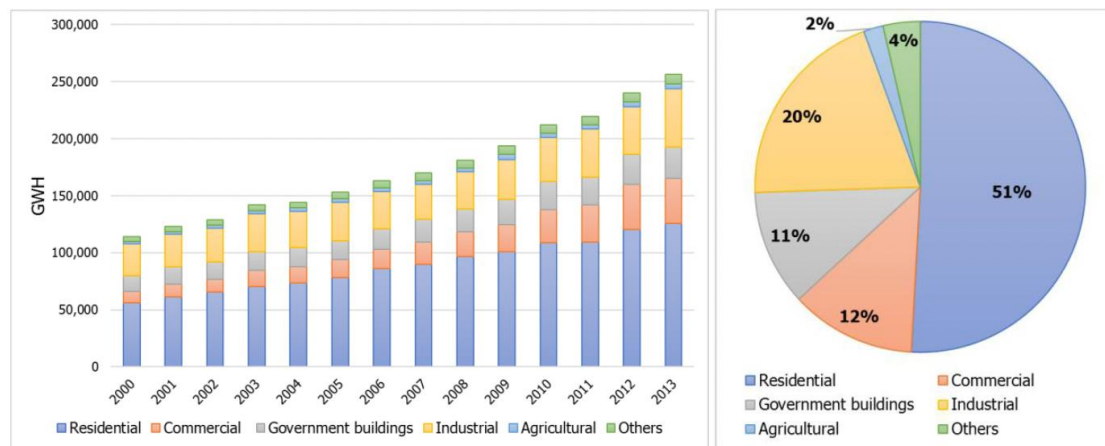


Figure 1.1: Building sector electricity consumption in KSA (SEC, 2013).

Figures (1.2) and (1.3) show the typical daily electricity load curve in KSA during the summer and winter seasons, respectively. KSA's peak demand for electricity typically occurs between 12:00 and 17:00 in the summer (from May to October). Looking at the two figures, the summer and winter demand at 13:00 pm on weekdays is 52 GW and 26.5 GW, respectively, while weekend demand is 56 GW and 28 GW, respectively. During the hottest months of the year, HVAC systems require huge amounts of power to maintain the temperature at a comfortable level (Alshahrani and Boait 2019). It can also be seen from these two figures that air conditioning is used throughout the day and night during the warmer months (Alshahrani 2018). Alshahrani stated that this increased demand for cooling loads in buildings is a result of the city's severe daytime temperatures and limited rainfall, which are also observed in other desert climates (Alshahrani 2018).

## CHAPTER 1: INTRODUCTION AND OVERVIEW

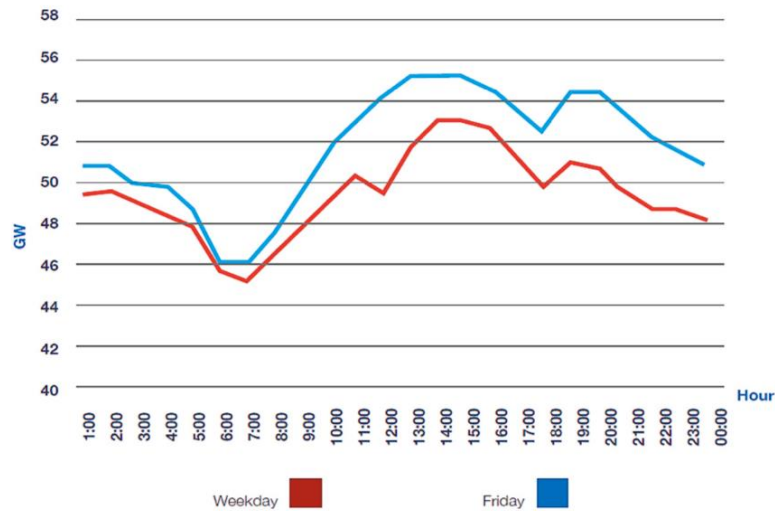


Figure 1.2: KSA typical daily electricity load curve during summer (Alshahrani and Boait 2019).

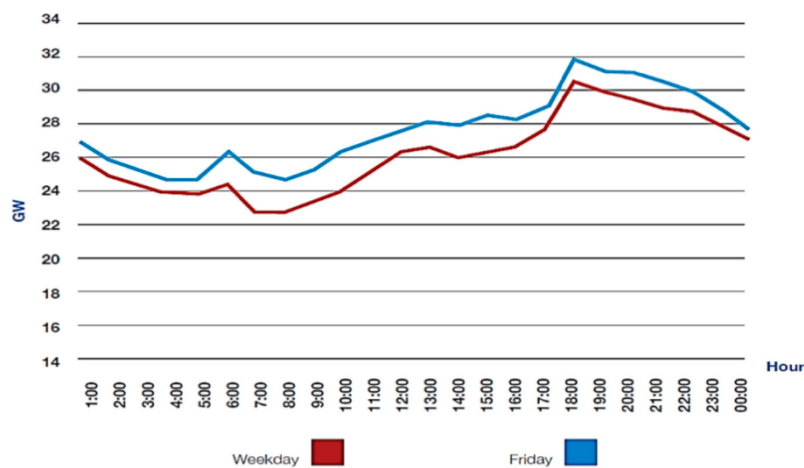
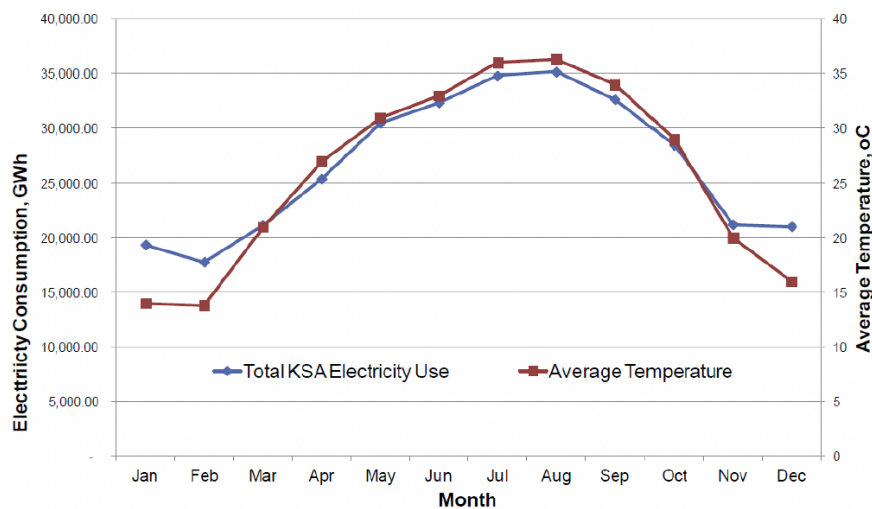


Figure 1.3: KSA typical daily electricity load curve during winter (Alshahrani and Boait 2019).

In addition, the Saudi Electric Company (SEC) reported in 2017 that electricity usage nearly doubles in Riyadh during the hot summer season is highly dependent on the daily temperature profile. Figure (1.4) is based on data collected in 2014, which shows how monthly total electricity usage in KSA closely follows average ambient temperatures. The significant association between electricity usage and ambient temperature indicates the serious importance of air conditioning during the summer months, when electrical demand is more than double that of the winter (Albogami and Boukhanouf 2019). Furthermore, in 1993, KSA recorded an energy consumption of 4422 KWh per capita, and this amount increased by almost double within two decades, reaching to 8757 KWh per capita in 2013, and 9347 KWh per capita by 2016 (Al Harbi and Csala 2019). This increase in energy consumption per capita indicates the size of the current issue and emphasizes the critical importance of implementing a strategy to reduce the excessive energy consumption,

## **CHAPTER 1: INTRODUCTION AND OVERVIEW**

particularly by buildings. Ghabra 2019, stated that most high-rise buildings in the GCC region are constructed without any concern for the local climate. Instead, they rely on mechanical active systems to mitigate the effects of undesirable climatic conditions, making them significant contributors to high energy consumption. Moreover, the number of high-rise offices, which are among the buildings with the highest energy consumption, has been rapidly growing in popularity, particularly in dense urban areas (Sauerbruch et al. 2011).



*Figure 1.4: Monthly total KSA electricity consumption and average ambient temperature (Albogami and Boukhanouf 2019).*

As a response to the government's goal of energy efficiency, several national sectors and innovative programs have been initiated in a plan to reduce the excessive use of energy in the Saudi building sector. For example, at King Abdulaziz City for Science and Technology (KACST), the National Energy Efficiency Program (NEEP) was formed to assist research activities, address environmental challenges, and make recommendations to help the government achieve its aim of rational energy consumption patterns. Moreover, KSA's government established the Saudi Energy Efficiency Centre (SEEC) in 2010 to encourage energy efficiency across all sectors, with a major focus on the building sector. SEEC's primary objective is to decrease energy use through audits, load control, regulation, and education (Karti et al. 2017). The lack of thermal insulation is one of the most serious deficiencies in the country's building stock, affecting over 70% of current buildings (SEEC 2015). Therefore, in 2014, SEEC collaborated with SBC to make thermal insulation an obligatory requirement for all new buildings in KSA.

From the previous discussion, it is clear that buildings in Riyadh consumes an enormous amount of energy as a result of its extreme hot climate conditions and the excessive heat gain from solar radiation, which requires the use of cooling systems to meet human comfort requirements in interior spaces. In addition, the lack of consideration of the building

## CHAPTER 1: INTRODUCTION AND OVERVIEW

envelope in the design and of the importance of thermal insulation has contributed to increasing energy consumption by buildings. Thus, it is essential to minimize the energy consumption of buildings by implementing energy conservation measures and designing energy efficient buildings. Office building designs should be responsive and adaptable to changing climates, and architects should develop intelligent design solutions that reduce energy consumption for cooling, heating, and lighting in such buildings.

### **1.2.5. High Rise Office Buildings in Riyadh**

High-rise buildings are one of the main elements of the urban fabric of most cities, and the number of these tall buildings is increasing globally to provide solutions for the growing demand for office space and accommodation and the rapid migration toward cities. (Hadi et al. 2014; van Soomeren et al. 2016). However, the energy consumption of such buildings is enormous. Riyadh, the case study city, has been transformed over the past five decades from a small-enclosed town into a modern urban advanced city (from 9 km<sup>2</sup> in 1917 to 1,798 km<sup>2</sup>). In recent years, the government has placed a greater emphasis on the construction of tall office buildings in Riyadh as a means of attracting business, investors, entrepreneurs, and small-to-medium-sized enterprises to relocate and launch branches in the city. These high-rise structures will contribute to the city's development, create a pleasant image, and promote a sense of power. Currently, Riyadh is considered the second city in the Middle East based on the number of developed high-rise buildings (Asif 2016). Figure (1.5) shows a timeline of the number of tall buildings constructed in Riyadh between 1980 and 2022 (CTBUH 2017).

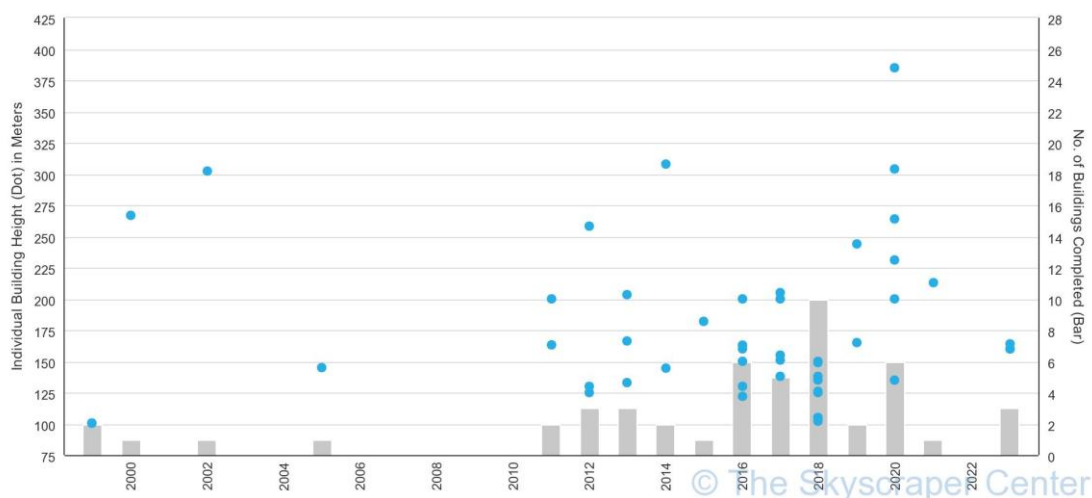


Figure 1.5: High-rise buildings timeline in Riyadh (The Global Tall Building Database of the CTBUH).

## **CHAPTER 1: INTRODUCTION AND OVERVIEW**

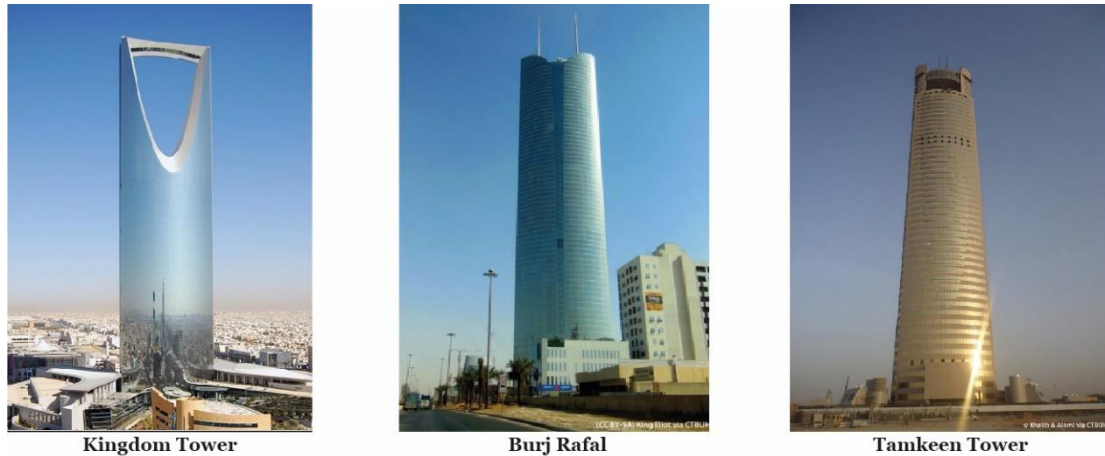
An observational analysis of the timeline of Riyadh's tall buildings reveals three distinct historical phases, in which evident changes were seen to the design of the building façade. The earliest examples of tall structures date from the early 1980s through to the early 1990s, most notably during the second oil boom, which is associated with the 1980s price surge. In 1984, Al Atta'Awuneya Tower was completed, and at 101 metres high is considered the first tall building in the region (CTBUH 2017). In the first phase, tall buildings are designed with mostly a solid form toward the west and south elevations, and small punched windows are used to control and block the harsh climate conditions. In addition, the design of tall buildings during this phase was more considerate of the region's climate and culture, but connectivity to the outdoors and views to the outside are lacking. However, throughout this period, only a few towers were constructed. Figure (1.6) shows some examples of the tall buildings constructed between the 1980s and 1999.



*Figure 1.6: First phase of constructed tall building's structure in Riyadh.*

The second phase of Riyadh's tall building development saw the construction of tall buildings in the "international design style", which is characterized by a fully glazed envelope and unornamented façade. This style depends heavily on extensive mechanical air conditioning and artificial lighting to meet the human need for indoor comfort (Heiselberg 2007). Elkhatieb (2016) argued that the international glazing envelope creates a unified style that can be seen similarly in different cities worldwide, neglecting the variations of the local climatic conditions and cultural requirements of each city independently. In addition, the author stated that this approach was criticized by many architects, as the building envelope loses its role as a climatic mediator that can promote human comfort and reduce energy demands. Figure (1.7) shows examples of some tall office buildings in Riyadh, which adopted the design principles of the fully glazed western style.





*Figure 1.7: Examples of the second phase of Riyadh's tall building development, followed the international style.*

In the third phase of tall building development, architects and designers paid more attention to designing tall buildings that are sustainable and energy efficient and that provide comfort for the occupants. The façade design appears to be the primary environmental strategy in these buildings, whether through the use of shading systems, orientation consideration, and responsive transparency and opacity in glazed façades, or through double skin façade technologies (Ghabra 2019). During this phase, architects designed tall office buildings with an emphasis on the building skin, with the goal of creating an external shelter that protects the occupants from the outdoor climate. Thus, various shading strategies, such as louvres, overhangs, blinds, and solar screens, were developed as a building skin, and these shading systems achieved a reasonable level of performance given the technology and materials available at the time (Mohamed 2015). As an example, Alfaisaliah Tower, designed by Norman Foster architects, was one of the first office building in Riyadh that incorporated overhang shading systems on its building envelope to block the intense solar radiation from penetrating into the interior environment. From 2000 to the present, different fixed shading strategies have been applied on the building façade of high-rise office buildings by many architects as shown in Figure (1.8). However, these shading systems were installed as a static skin with fixed thermophysical and optical properties and without considering variations in the outdoor environment (Loonen et al. 2010; Konstantoglou and Tsangrassoulis 2016).



## **CHAPTER 1: INTRODUCTION AND OVERVIEW**



Olaya Tower



Al Faisaliah Center



Al Majdoul Tower

*Figure 1.8: Examples of the third phase of tall buildings development implemented fixed shading systems.*

Internationally, the concept of a dynamic building envelope has emerged as an effective alternative to the static shading system. This adaptive skin is a more suitable shading system because it can adapt to the outdoor variations and so achieve high performance buildings. This concept is beneficial in hot climate areas where excessive solar heat gain results in high energy consumption during the summer. Although the adaptive system functions more effectively in a hot climate region, such a system has not yet been applied on the building skins of high-rise office buildings in Riyadh. Hence, this study focuses on AF shading systems for high-rise office buildings to explore the energy-saving potential of these shading systems. Recently, the King Abdullah Financial District (KAJD) was constructed in Riyadh as a way to promote sustainable, environmentally friendly buildings and to reflect the global awareness of energy efficiency within buildings. The KAJD district included a number of Grade A office towers with the objective of establishing the district as a regional and global financial hub Figure (1.9). Different tall buildings within this urban complex were designed according to the green building standards and regulations.



Public Investment Fund Tower



Parcel 3.04 Tower



Samba Bank HQ Tower

*Figure 1.9: Examples of tall buildings constructed in the King Abdullah Financial District (KAJD).*

**1.2.6. Riyadh Location and Climatic Condition - Hot-Arid Regions**

Geographically, KSA is situated in the southwest of Asia with a large area of desert, and lies between 24° N, and 45° E above the equator. It is the largest country in the Middle East, with a surface size of approximately 2.5 million square kilometres. According to the Koeppen-Geiger Climate Classification, KSA in general is classified as a single climate zone known as hot arid climate region (BWh) Figure (1.10). However, for more precision, the Saudi Building Council (SBC) separates KSA into three zones due to the country's varied climates Figure (1.11) (Alardhi et al. 2020). Climate zone 1 is the most prevalent hot, dry climate zone in Saudi Arabia. Riyadh is the capital, which located in the central part of the country (climate zone 1), at an elevation of 600 metres above sea level. Riyadh city experiences a hot desert environment for most of the time between May and October, with an average rainfall of 100 millimetres, whereas the remaining months create a milder season. Thus, Riyadh has two main climatic seasons that can be distinguished: summer and winter.

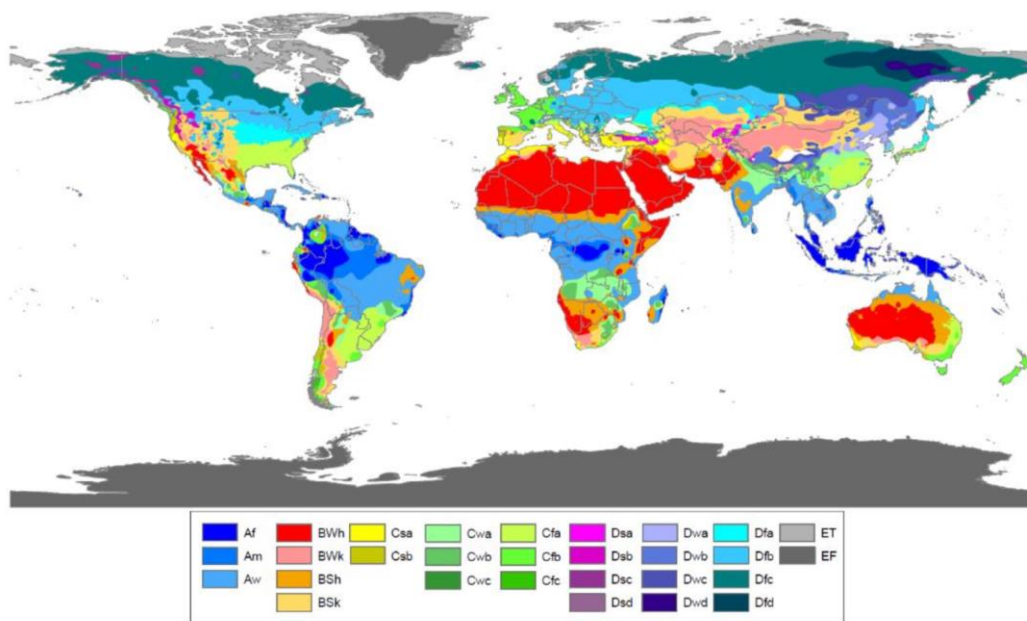


Figure 1.10: World map of Koppen-Geiger Climate Classification (Peel et al., 2007).

**CHAPTER 1: INTRODUCTION AND OVERVIEW**

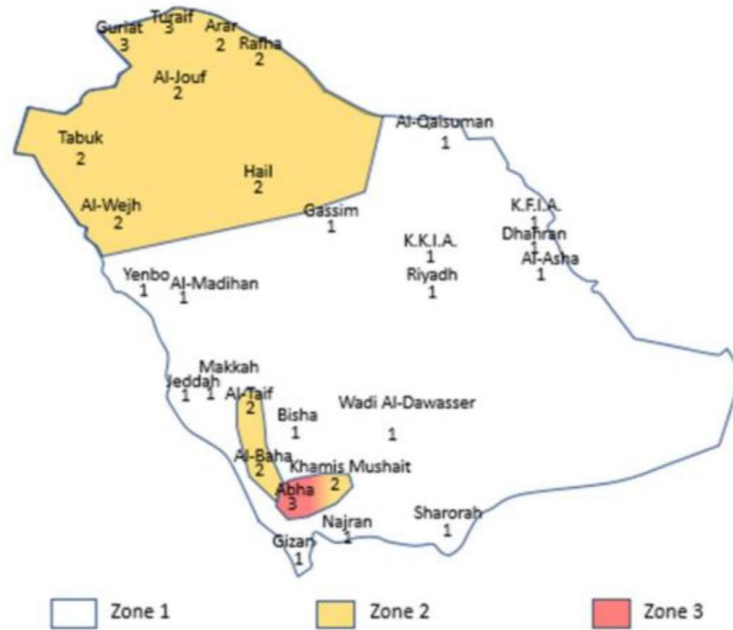


Figure 1.11: Climate zones of KSA based on SRBEC classifications (SBCNC, 2018).

In general, during the summer, the average temperature may exceed 45°C, while ambient temperatures may reach 50°C. In addition, the summer mean maximum and minimum temperatures range between 27.3 and 37.1°C and 16 and 26°C, respectively Figure (1.12) (Alyami and Omer 2021). The extreme high temperature during the summer season requires architects to find solutions for maintaining a suitable thermal comfort for a building’s occupants. In winter, the mean maximum and minimum temperatures are 21 – 29°C and 8 – 13°C, respectively.

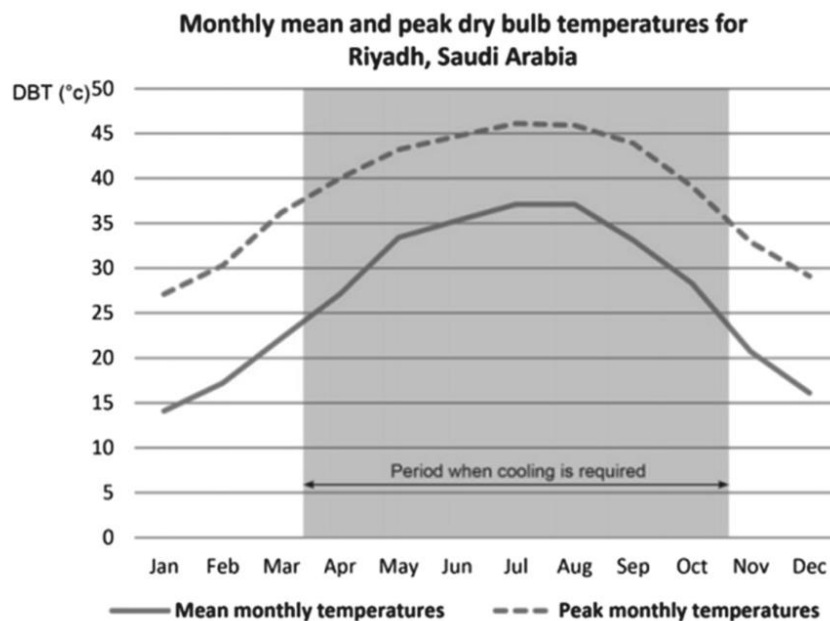


Figure 1.12: Annual temperature profile for Riyadh city (Alyami and Omer 2021).

## **CHAPTER 1: INTRODUCTION AND OVERVIEW**

Riyadh is recognised as a leading city and financial hub in the Middle East due to its strategic location and stable economy. In recent years, the government has paid immense attention and provided significant incentives for the construction of high-rise buildings in Riyadh, as such buildings will contribute to the city's development and economy, as well as creating a pleasant image. In terms of already constructed high-rise buildings, Riyadh is currently the second-largest city in the Middle East following Dubai (Asif, 2016).

The provision of offices is an increasing trend in the Riyadh construction market. The Riyadh Plan suggested that the city's central district would require additional office space between 2015 and 2030. According to Frank (2018), the demand for office space in Riyadh has increased since SA implemented a policy demanding that the regional headquarters of foreign companies be located in the country's capital (Knight Frank, 2018). Frank states that office occupancy level in Riyadh had reached 98% due to an unprecedented demand for office space. By the end of 2023, the total stock of office space in Riyadh was anticipated to reach approximately 5.11 million sqm GLA. Therefore, to meet the demand for new office space, the construction of high-rise office buildings is encouraged and supported. Most high-rise office buildings are currently air-conditioned. The objectives are to provide occupants with a higher degree of comfort, create more productive settings, and increase the rental value of floor spaces.

Another crucial factor in the installation of such systems in buildings is concern about the influence of excessive solar heat gain on energy consumption. Moreover, it is anticipated that Riyadh's temperatures will rise as a result of climate change. This will result in warmer summers with an increase in the number of days that are extremely hot and a decrease in the number of days that are cold. The above conditions indicate that the use of mechanical ventilation will increase in Riyadh. However, although adaptive systems are more successful in regions with hot temperatures, high-rise office buildings in Riyadh have not yet been installed with such systems. Consequently, the adaptive shade system can be beneficial to Riyadh and other cities that in regions with hot temperatures and high energy usage during the summer due to excessive solar heat gain.

### **1.3. Research Aim and Objectives**

The aim of this study is to investigate the potential of AF shading systems for reducing the energy consumption in high-rise office buildings in hot climates. Moreover, it seeks to examine the potential of using machine learning (ML) techniques as an alternative method to predict the energy performance of AFs in the early stages of the design.

The research objectives are as follows:

## **CHAPTER 1: INTRODUCTION AND OVERVIEW**

### ***Objective 1. Investigate the impact of adaptive façades on energy performance.***

- Survey the literature to explore adaptive façade shading systems.
- Survey the literature to assess building performance simulation tools (BPS) for predicting the performance of AFs.

### ***Objective 2. Develop an algorithmic workflow to evaluate the energy performance of AF shading system.***

- Conduct simulation to investigate the influence of adaptive façades on energy performance (cooling loads).
- Compare the performance of adaptive façade shading systems with external static shading in terms of reducing cooling loads.
- Integrate an automatic control system to actuate the AFs based on environmental parameters.

### ***Objective 3. Generate a synthetic database of AF cooling energy loads of offices to train and test the surrogate models.***

- Use parametric tools and simulation to parametrically generate various design alternatives.

### ***Objective 4. Develop machine learning models to predict energy performance of AF in the early stage of the design.***

- Employ ANN and RF surrogate models to predict the energy performance (cooling loads) of adaptive façades.
- Validate and compare both ANN and RF for energy predictions in the early stages of the design for adaptive façades.

### ***Objective 5. Establish a workflow that incorporates the surrogate model within a computational design tool to assist in early-stage design-decision making.***

## **1.4. Research Questions**

Research questions are used to frame the structure of the research to gain a deeper understanding of the research issues. Robson and McCartan (2011) stated that research questions are used to define the structure of research to uncover new knowledge. Thus, research questions were used to guide the discovery of new knowledge in the research area. This study seeks to answer the following main research questions in accordance with the stated aim and objectives:

## **CHAPTER 1: INTRODUCTION AND OVERVIEW**

1. **Can** adaptive façades improve the energy efficiency in high-rise office buildings in hot climate?
2. **Can** current BPS tools meet the challenges of simulating adaptive façades?
3. **What** are the needed workflows to model and simulate the energy performance of adaptive façades?
4. **What** machine-learning models can be used to accurately predict the energy performance of adaptive façades?

### **1.5. An Overview of the Research Design**

The development of applicable AFs for the goal of improving the energy consumption in high-rise office buildings needs smart and advanced approaches. The research method was divided into five phases to achieve the research objectives. These phases are literature review, data collection, data analysis, development of the surrogate models, validation of the results, and testing of the surrogate models. To accomplish the research objectives, various data collection and analysis methodologies and techniques were reviewed. This study adapted a quantitative approach to data collection to achieve the research objectives.

#### **Phase 1: Literature Review and Critical Analysis**

The literature review was the first phase of the research to explore the impact of AF shading systems on the energy performance in buildings and its applications. In addition, it aimed to review the current studies of AFs regarding AF system type, adaptability of the system, performance, and tools used to simulate the AFs. It also examined the challenges and difficulties of current BPS tools to assess AFs during early stage of the design. Moreover, it reviewed the literature in ML techniques and their potential use for building performance predictions.

#### **Phase 2: Data collection**

The data collection was the second phase of the research to achieve the research objectives. It included two main activities: data collection from case studies, and data collection using a modelling and simulation approach. This phase included the following steps:

#### ***Case Studies***

Different high-rise office buildings were selected in the study area as case studies to inform the prototype physics (design factors) of the modelling and simulation stage. The architectural drawings were collected and analysed for all the selected cases numerically to

## **CHAPTER 1: INTRODUCTION AND OVERVIEW**

define the existing typical office building and the design characteristics of high-rise office buildings. Thus, the developed prototype could be representative of a real case study of an office building.

### ***Data Collection using Modelling and Simulation***

The data collection used a simulation approach, which involved two main activities: (1) development of a comprehensive framework for evaluating the performance of AFs during the early stages of the design, and (2) generation of a synthetic database of hourly cooling loads of AFs and hourly solar radiation to develop the ML surrogate models due to the absence of real data. To achieve this, the study conducted the simulations using an algorithmic workflow that links between different plug-in tools in the computational design tool (Grasshopper) to facilitate the parametric generation and simulation of adaptive systems. Ladybug and Honeybee plug-ins were used, which were linked to EnergyPlus and Radiance to calculate energy loads and solar radiation. In addition, these tools were linked to EnergyPlus with its built-in tool, Energy Management System (EMS) to program a code to actuate the AF system hourly based on indoor and outdoor environmental conditions.

### **Phase 3: Data Analysis**

The data analysis was the third phase of the research to analyse the simulation results and compare the different external shading systems. This phase evaluated the engineering parameters, such as exterior wall and glazing types in terms of cooling loads and solar heat gain. Moreover, external shading system and adaptive systems were compared in terms of cooling load reduction and solar heat gain reduction. This phase also compared the different environmental control scenarios of AFs in terms of cooling and lighting loads in relation to different parameters, such as office orientation, building contexts, and shading state hourly variations.

### **Phase 4: Development of Machine Learning (ML) Surrogate Models**

This phase aimed to develop an ML surrogate model that can predict the performance of AFs in the early stages of the design. This phase included the processing and translation of the collected database generated using simulation in phase (2) to develop the ML surrogate models. The collected hourly cooling loads (HCL) database and hourly solar radiation (HSR) database were used to construct, train, and validate different ML algorithms, artificial neural networks (ANN), and random forest (RF). To develop the surrogate models, three major

## **CHAPTER 1: INTRODUCTION AND OVERVIEW**

steps were carried out: data pre-processing, model training, testing, hyper-parameter optimization, and model validation.

### **Phase 5: Incorporation of the Surrogate Models within a Computational Design Tool, and Validation of the Results.**

This phase sought to develop a framework of the trained surrogate models within the Grasshopper interface to predict the cooling loads of AFs and to assist with the decision making for design. This phase also evaluated the developed surrogate models in terms of prediction accuracy, time efficiency, and their generalisation prediction capability. The results of the models were compared with simulation results to validate the models. In addition, in this phase, the surrogate model was tested in terms of its applicability in predicting other similar hot-climate cities.

## **1.6. Structure of the Following Chapters**

The research is arranged into eight chapters, starting with this introductory chapter (Chapter One) as shown in Figure (1.13) and (Figure 1.14). The content of each chapter is presented below:

**Chapter Two: Literature Review:** This chapter is divided into three parts. Part (A) presents a general overview of the design of AFs, their history, similar terms used by scholars, and the performance classifications of AFs. It also presents the current studies of AFs, and their influences on buildings' energy consumption. Part (B) presents a discussion of current studies to provide an overview of what has been published in the field of AFs and their performance evaluation. It also explores the challenges and difficulties designers face in predicting the performance of an AF shading system using the existing BPS tools. Part (C) reviews the studies that employed ML techniques to predict the energy performance. It also presents the fundamentals and steps employed to develop surrogate models.

**Chapter Three: Research Design and Methodology:** This chapter starts by presenting different theoretical paradigms and research approaches. It also provides a comprehensive description of the selected research methodology, and the different phases, methods, and techniques that are adopted to answer the research questions.

**Chapter Four: Synthetic Database Generation using Simulation Approach:** This chapter is divided into two parts: Part (A) analyses the collected case studies for the extraction of the design characteristics of high-rise office buildings. Part (B) presents the modelling and simulation framework conducted to simulate the energy performance of AFs. The framework integrates the automatic control system to actuate the AFs based on different



## **CHAPTER 1: INTRODUCTION AND OVERVIEW**

environmental control scenarios. Moreover, it presents the collected synthetic database of the hourly solar radiation, the hourly shade factor, and the hourly cooling loads of AFs.

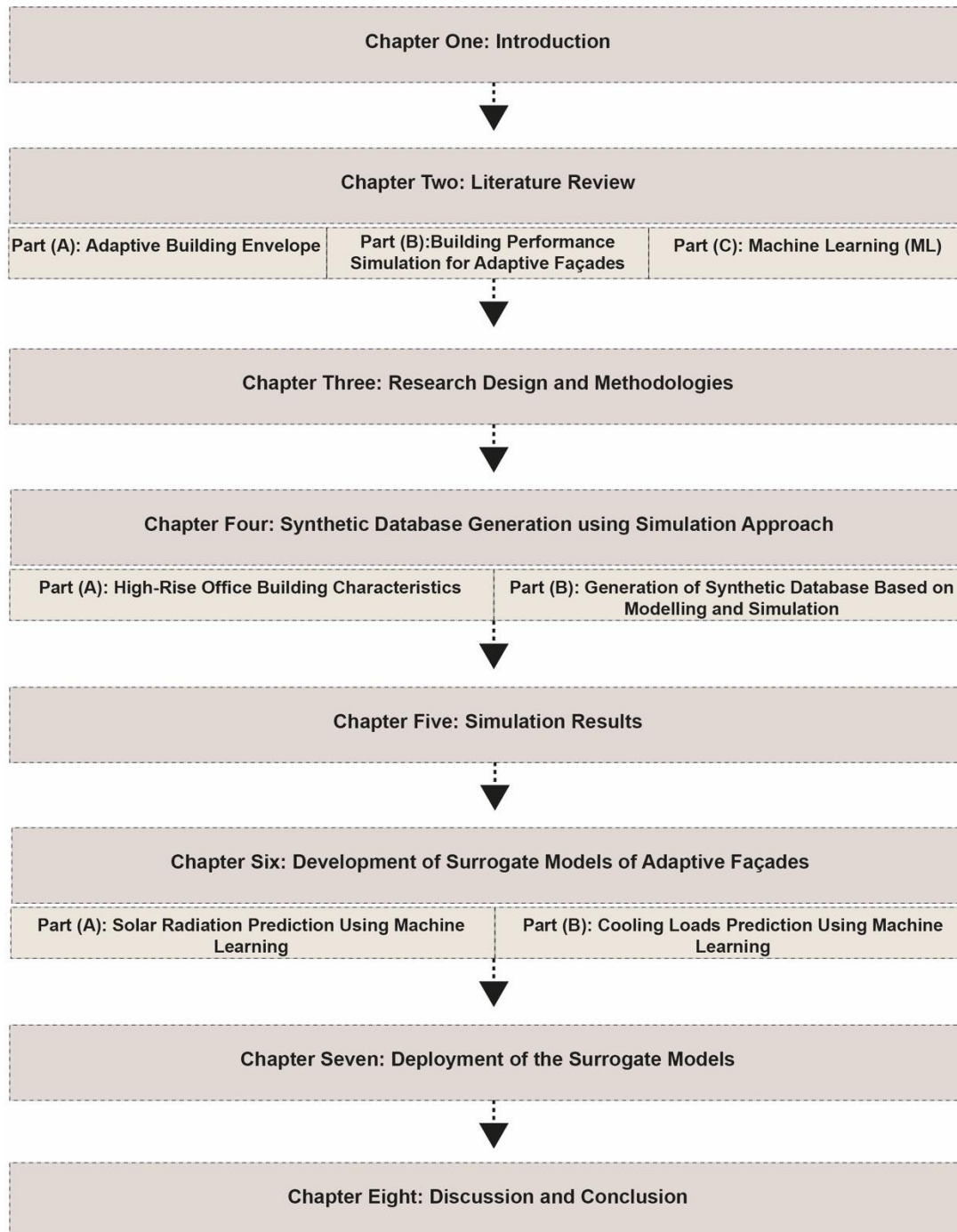
**Chapter Five: Simulation Results:** This chapter analyses the results of the simulations presented in (Chapter Four). In addition, this chapter evaluates the engineering parameters of the building envelope, different external fixed and adaptive shading systems, and different automatic control scenarios of AFs. The results were evaluated in terms of cooling loads and solar heat gain.

**Chapter Six: Development of Surrogate Models for Adaptive Façades in the Early Stages of the Design:** This chapter include two parts: Part (A) presents the development of ANN and RF surrogate models to predict the hourly solar radiation in the early design stages. Part (B) presents the development of ANN and RF surrogate models to predict the energy performance (hourly cooling loads) of AFs in early design stages. Moreover, this chapter presents the data pre-processing, model training, testing, hyper-parameter optimisation, and model validation for both ANN and RF models. It also makes a comparison between ANN and RF surrogate models in terms of prediction accuracy. Lastly, it examines the time series nature of the data using different time series modelling approaches.

**Chapter Seven: Deployment of the Developed Surrogates Models:** This chapter presents the results obtained from the developed surrogate model and compares them with the simulation results. In addition, it evaluates the surrogate models in terms of prediction accuracy, time efficiency, and its generalisation prediction capability. It also presents the workflow to predict the hourly cooling loads of AFs within a computational design tool.

**Chapter Eight: Discussion and Conclusion:** This chapter discusses the research findings from the previous chapters. In addition, it summarises the achieved research objectives, the contributions to the body of knowledge, the limitations, the recommendations, and the suggestions for future research.

## **CHAPTER 1: INTRODUCTION AND OVERVIEW**



*Figure 1.13: Structure of the thesis.*

## CHAPTER 1: INTRODUCTION AND OVERVIEW

| Thesis Structure  |  |   |
|---|--|---|
| <b>Chapter One: Introduction and Overview</b>   |  |   |
| <ul style="list-style-type: none"> <li>- Research Context and Background</li> <li>- Research Aim, Objectives, and Research questions</li> <li>- Scope and Focus</li> <li>- Research Design and Methodology</li> </ul>   |  |   |
| <b>Chapter Two: Literature Review</b>   |  |   |
| Part (A): Adaptive Building Envelope  | Part(B): Building performance simulation for adaptive façades  | Part (C) Machine Learning   |
| <ul style="list-style-type: none"> <li>- Static to Adaptive Façade</li> <li>- Adaptive Façade History</li> <li>- Adaptive Façade Definition</li> <li>- Adaptive Façade Similar Terminology</li> <li>- Performance classification of adaptive facades</li> <li>- Automatic Control System</li> <li>- Responsive Time Scale</li> <li>- Scale of Adaptation</li> <li>- External Factors</li> </ul> | <ul style="list-style-type: none"> <li>- Current research for the BPS of adaptive facades</li> <li>- Discussion of Existing Studies</li> <li>- Challenges for performance prediction of AFs</li> <li>- BPS tools</li> <li>- Parametric Tools</li> <li>- Parametric Integrated Simulation Tools</li> </ul>                                      | <ul style="list-style-type: none"> <li>- Supervised Learning</li> <li>- Unsupervised Learning</li> <li>- Surrogate Model for Building Performance</li> <li>- Data Pre-processing</li> <li>- Model Training and Hyperparameter tuning</li> <li>- Performance Evaluation</li> <li>- Data Types</li> <li>- Artificial Neural Network</li> <li>- Decision Tree/Random Forest</li> </ul> |
| <b>Chapter Three: Research Design and Methodology</b>   |  |   |
| <ul style="list-style-type: none"> <li>- Research Paradigms and Research Models</li> <li>- Research Methodology, Methods and Research Design</li> <li>- Research Framework</li> </ul>   |  |   |
| <b>Chapter Four: Synthetic Database Generations Using Simulation Approach</b>   |  |   |
| Part (A): High-Rise Office Building Characteristics   | Part (B): Generation of Synthetic Database Based on Modelling and Simulation   |   |
| <ul style="list-style-type: none"> <li>- Cases Studies Data Collection</li> <li>- Characteristics of high-Rise office Buildings</li> <li>- Data Analysis</li> <li>- Floor Efficiency</li> <li>- Leasing Depth</li> <li>- Number of Floors</li> <li>- Building Heights</li> <li>- Building Geometry and Shading System</li> </ul>  | <ul style="list-style-type: none"> <li>- Modelling (Base Case and Adaptive Façade Modelling)</li> <li>- Climatic Analysis</li> <li>- Validation of the Model</li> <li>- Solar Radiation Analysis</li> <li>- Shade Factor Analysis</li> <li>- Energy Simulation</li> <li>- Automatic Control System</li> <li>- Database Preparations</li> </ul> |   |
| <b>Chapter Five: Simulation Results</b>   |  |   |
| <ul style="list-style-type: none"> <li>- Analysis of the Simulation Results</li> </ul>  |  |   |
| <b>Chapter Six: Development of Surrogate Models of Adaptive Façades</b>   |  |   |
| Part (A): Solar Radiation Prediction Using Machine Learning   | Part (B): Cooling Loads Prediction Using Machine Learning  |   |
| <ul style="list-style-type: none"> <li>- Artificial Neural Network Development</li> <li>- Random Forest Development</li> <li>- Data Pre-procession</li> <li>- Model Training and Testing</li> <li>- Hyperparameters Tuning</li> <li>- Model Validation</li> </ul>   | <ul style="list-style-type: none"> <li>- Artificial Neural Network Development</li> <li>- Random Forest Development</li> <li>- Data Pre-procession</li> <li>- Model Training, Testing</li> <li>- Hyperparameters Tuning</li> <li>- Model Validation</li> </ul>   |   |
| <b>Chapter Seven: Deployment of the Surrogate Models</b>  |  |   |
| <ul style="list-style-type: none"> <li>- Results Validation, and Testing the Models with New Design Scenarios</li> <li>- Models Prediction Accuracy</li> <li>- Time Efficiency</li> <li>- Generalizability of the Models</li> </ul>   |  |   |
| <b>Chapter Eight: Discussion and Conclusion</b>   |  |   |
| <ul style="list-style-type: none"> <li>- Discussion of Research Findings</li> <li>- Achievement of Research Objectives</li> <li>- Contributions to the Body of Knowledge</li> <li>- Research Limitations, Recommendations and Future Work</li> </ul>  |  |   |

Figure 1.14: Detailed structure of the thesis.

## **1.7. Chapter Summary**

This chapter has provided an overview introduction and a general background of the research. It described the problem of the study and the justifications for this investigation, the research aims and objectives, and the research questions, and gave an overview of the adopted methodology. It concluded by presenting a summary of the outline of the thesis.

## **CHAPTER TWO**

### **LITERATURE REVIEW**

## **CHAPTER 2: LITERATURE REVIEW**

### **2.1. Introduction**

This chapter presents a detailed examination of adaptive façade (AF) shading systems through a comprehensive literature review. It also reviews the effect of AFs on energy savings and on the performance evaluation process. This chapter also presents the existing AF studies and looks at different factors including the AF system type, the adaptability of the system, the performance, and the influences of AFs on buildings' energy consumption. In addition, it presents the challenges and difficulties designers face in predicting the performance of an AF shading system using the current BPS tools. Lastly, the chapter reviews machine learning (ML) techniques and their potential use for building performance predictions. It also discusses the relevant studies that employed ANN and DT approaches.

### **Part (A) Adaptive Building Envelope**

#### **2.2. Static to Adaptive Façade – Overview**

The advances in architectural envelopes have changed the design approach from static and conventional envelopes to adaptive and responsive ones that aim to improve the performance of the building. Traditionally, conventional control systems are mainly installed on windows and doors, using inexpensive and easy-to-operate manual shading or shading devices, such as louvres, blinds, and sunshades. These shading devices are installed to control solar gain and prevent heat loss (Leatherbarrow and Mostafavi 2005). However, in this approach, the building envelope acts not as a barrier but as a medium (López et al. 2017). Therefore, the static conventional approach in the design of façades is not the optimum solution to adapt to the changing climatic conditions (Armstrong 2012). Thus, the recent emerging adaptive architectural envelope can replace the conventional approach due to its capability of responding to different environmental conditions and of providing buildings that perform well.

The development of more adaptive building envelopes has received growing attention from both researchers and practitioners in recent years (Ritter 2007; Schumacher et al. 2010; Johnsen and Winther 2015; Tabadkani et al. 2018; Tabadkani et al. 2019a). These external adaptive envelopes have shown immense potential in improving building energy performance and can play a new role in high performance building design in general. Loonen et al. (2013) defined an AF as a climate adaptive building shell (CABS), which has the ability to change its features or configuration over time in response to changing weather conditions

## **CHAPTER 2: LITERATURE REVIEW**

and comfort preferences (Loonen et al. 2013). The authors presented an overview and analysis of CABS in terms of their design, research, and development. The review looked at 44 CABS case studies and highlighted the motivations of CABS applications, their technologies, and their characteristic features. The research suggested that the concept of CABS is not yet mature because of the lack of literature regarding post-occupancy evaluations and operational performance (Loonen et al. 2013).

Similarly, Aelenei et al. (2016) aimed to categorise AFs according to three main groups: materials, components, and systems. The study conducted a simple data analysis of some existing adaptive building envelopes, assessing the external factors associated with the need for AFs. The analysis examined 130 case studies of existing adaptive building envelopes, which revealed interesting findings regarding the need to apply AFs in buildings. The study looked at all the external factors (solar radiation, outdoor temperature and humidity, wind and precipitation, and noise) that influence human comfort needs. The authors found that the most common external factors associated with AFs are solar radiation and temperature. These two factors are known to be most influential on thermal and visual comfort and on energy performance (Aelenei et al. 2016). In another study, Velasco et al. (2015) presented an overview of the current state of computationally controlled dynamic façades and an analysis of the most contemporary projects that have applied dynamic systems. The study considered two main factors, namely, movement and control for the classification of high-performance kinetic façades. The authors classified the movement of the analysed case studies into two main groups: (1) mechanical based, which includes rotation, translation, and hybrid modes, and (2) material-deformation based, which includes the factors that may cause deformation (temperature, humidity, or electricity). The control factor divided the case studies into local and central (Velasco et al. 2015).

Nguyen and Aiello (2013) promoted the application of adaptable buildings to optimise energy consumption, while Ghaffarianhoseini et al. (2016) concluded that intelligent façades can contribute to reducing energy and responding to indoor and outdoor environments. Pan and Jeng (2010) highlighted the importance of AFs and explained that buildings with interactive systems use less energy and offer better space flexibility.

Recently, Loonen (2018) discerned that development of the new AF systems is taking two main directions: (1) kinetic components with actuation based on mechanical systems, and (2) responsive smart materials with the capability of changing their physical behaviour according to the climatic conditions (Loonen 2018). This also includes the biomimetic design approach, where design and elastic materials are integrated together for the development

## **CHAPTER 2: LITERATURE REVIEW**

of new AFs, such as the bio-inspired kinetic GFRP façade for the thematic pavilion of EXPO 2012 in Yeosu. The advancement of materials in science laboratories has helped in the application of scalable solutions with this second direction (Bastiaansen et al. 2013; Loonen et al. 2014).

Giovannini et al. (2015) developed the Shape Variable Mashrabiya (SVM) shading system for an office building in Abu Dhabi. The authors applied the shading in two different orientations - east and west façade - to analyse the effect of the SVM shading system on reducing the annual energy demand. Several scenarios were performed to determine the most effective configurations utilising DIVA-for-Rhino and EnergyPlus. Sun angles were used to control the movement of the perforated shields. The results revealed the immense potential of an AF shading system on both daylighting and energy saving. When compared to a reflective glazed non-shaded façade, the system reduced the total energy consumption by up to 27% while reducing the cooling demand by 17.2% when compared to a low-E double-glazed façade with adjustable Venetian blinds.

A recent study by Bui et al. (2020) proposed a computational optimisation method to minimise the energy consumption of buildings based on the AF design that can adapt to the dynamic variation of outdoor climatic conditions. Two case studies were designed, namely, a typical single office room and a medium-sized office building, to validate their approach. Researchers utilised three different software programs for energy evaluation: EnergyPlus; Eppy as a Python toolkit; and a modified firefly algorithm as an optimisation tool. Their results concluded that an AF system can reduce energy consumption in the first and second cases by 14.9–29.0% and 14.2–22.3% respectively when compared to static façades.

Another study by Shi et al. (2020) investigated the effect of different motions of AF on energy and daylight performance. A parametric simulation approach was implemented to optimise the AF in a closed office room located on the middle floor (50 m) of a high-rise tower. A total of 75 cases were evaluated and compared to determine the optimum cases for balance between energy and daylighting. Based on the results, it was found that the implementation of AF can reduce energy consumption by 14–24% compared to the base case model (Shi et al. 2020).

From the literature, it is clear that AF systems have a significant impact on the total energy consumption of buildings. In addition, we noticed that predicting the energy performance of buildings with an AF system in the early stages of the design is highly complex, and challenging.



### **2.2.1. Adaptive Façade History**

A variety of AF systems have emerged gradually over the last 50 years. The history of kinetic or adaptive design can be classified into seven periods, beginning with early concepts and sketches, and concluding with today's high-tech AF systems. The timeline depicted in Figure (2.1) corresponds to the chronological order of each period, which will be discussed in detail in this section. One of the earliest examples of kinetic architecture was designed as sketches by Thomas Gaynor in 1908 for an unbuilt Rotary villa (Nashaat and Waseef 2018). Then, in 1916, Le Corbusier developed the 'le Mur neutralisant', using stone and glass in a circuit of two membranes to maintain the temperature in Moscow at 18 degrees (Nady 2017).

The “active” or “adaptive” design approach started to emerge in 1930, when Le Corbusier introduced a concept design of the universal house for all climates: “Only one house for all countries, the house of exact breathing”. However, this design proposal was not built as a real project because at that time, the technology to do so was lacking, which restricted the implementation of such a futuristic idea (López et al. 2017). Following that, in 1935, Angelo Invernizzi constructed Villa Girasole, a dynamic villa that revolved along three circular rails and followed the sun's path allowing the house to be completely revolving (Nashaat and Waseef 2018). In 1960, Yona Friedman challenged architects' ability to control the life of their building's occupants and presented a town plan in which a town could be constructed with adaptable architecture, allowing residents to adapt their spaces according to their requirements.

Later, in Expo Montreal 1967, Richard Fuller implemented a dynamic skin for the façade of the US Pavilion. The skin was made of translucent acrylic sheets and a steel structure and was controlled by computer, aiming to create a comfortable environment for visitors (Sharaidin et al. 2012). Then, in 1970, William and Clark described kinetic architecture as “a field of architecture in which building components or whole buildings have the capability of adapting to change through kinetics in reversible, deformable, incremental and mobile modes” (William and Clark 1970). In the book, “Kinetic architecture” a number of subjects were discussed including systemic knowledge and the fundamentals of kinetic architecture, as well as active control devices. Next, in 1975, Negroponte (1975) introduced the ‘responsive environment’ as a concept that is capable of playing an active role. Next, Mike Davies proposed “the polyvalent wall”, an envelope system that consists of one layer that controls several functions (Davies 1981). Later, in 1987, a major revolution in kinetic architecture was introduced by Jean Nouvel “the Arab Institute in Paris” in 1987, which is

## CHAPTER 2: LITERATURE REVIEW

considered one of the first and best-known examples of a building to implement an active façade system using a mechanical control system.

The twenty-first century marked a major turning point in the evolution of kinetic architecture. For example, in 2011, Brisbane Airport's parking garage installed a dynamic wall comprising 250,000 wind-sensitive metal panels. Additionally, the Mercedes-Benz stadium in Atlanta features a unique retractable roof that opens diagonally like a camera aperture (Park 2016). Another well-known example of an AF system is the Al Bahar tower in Abu Dhabi, where a reinterpretation of Arabic-Islamic patterns was performed using actuator-controlled triangular panels that open and close in reaction to the sun's movement. In addition, there are other well-known examples of AF systems, such as switchable glazing (Ruben et al. 2010), dynamic insulation (Kimber et al. 2014) or façade systems with phase-change materials (Favoino et al. 2014a). Nevertheless, the number of AFs applied in buildings is still limited (Loonen et al. 2013).

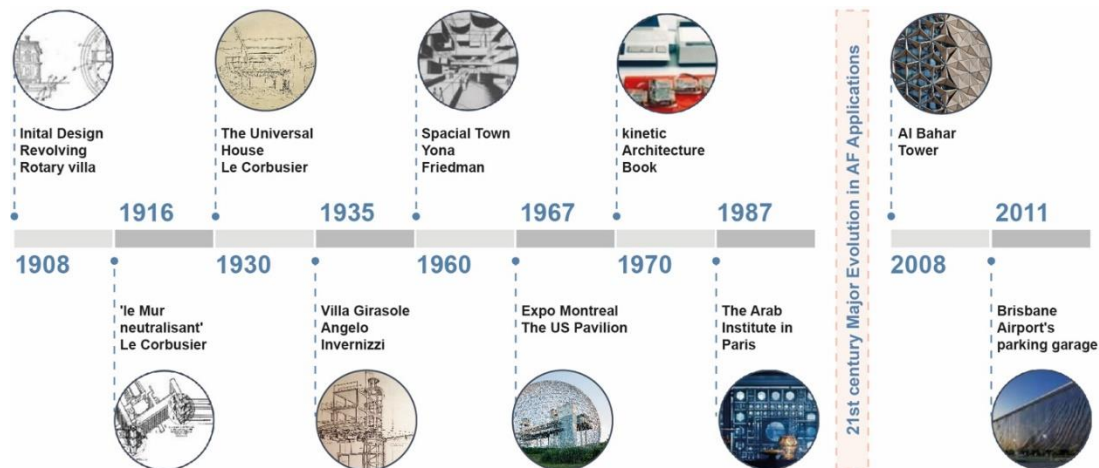


Figure 2.1: Timeline of kinetic architecture's history (Nashaat and Waseef 2018).

### 2.2.2. Adaptive Façade Definition

There are multiple definitions in the literature that describe the adaptive building envelope, such as climate adaptive building shell (CABS) by Loonen (2010) and de Boer et al. (2011), acclimated kinetic envelope (AKE) by Wang et al. (2012), adaptive skin by Hasselaar (2006), intelligent skin by Wigginton and Harris (2002), or adaptive building skins by Grosso and Basso (2013). All of these terms have been defined and compared in Fiorito et al. (2016) work "Shape morphing solar shadings: A review" (2015). AFs are "building envelopes that are able to adapt to changing boundary conditions in the form of short-term weather fluctuations, diurnal cycles, or seasonal patterns. Such façades have the ability to respond to, or benefit from, changes in outside climatic conditions and dynamic occupant requirements" (Attia et al. 2018).

## **CHAPTER 2: LITERATURE REVIEW**

Loonen et al. (2015) stated,

“Adaptive façades consist of multifunctional highly adaptive systems, where the physical separator between the interior and exterior environment is able to change its functions, features or behaviour over time in response to transient performance requirements and boundary conditions, with the aim of improving the overall building performance. (Loonen et al. 2015)”.

Moreover, these adaptive envelope systems have the advantage of saving energy by adapting to prevailing environmental conditions and assisting human level comfort internally by responding to people’s needs and preferences (Loonen et al. 2013).

Tabadkani et al. (2021b) reviewed several terms of AFs found in the literature, indicating that scientific research on AFs is progressing toward creative design solutions through the integration of mechanical and automated actuators, materials, and information technology systems. As Tabadkani et al. (2021) stated, numerous scholars utilise similar terminology for AFs, such as "dynamic," "active," "kinetic," "intelligent," "switchable," "responsive," "interactive," "movable," "smart," "biomimetic," and "plant-inspired", which causes confusion in the field of building façades. As a result, it is difficult to categorise existing types of AFs because each kind may overlap with another group.

### **2.2.3. Adaptive Façades Terminologies**

#### **2.2.3.1. Active Façades**

Active façade technology incorporates active features rather than complex electronics, allowing envelopes to self-adjust in reaction to internal and exterior conditions, providing comfort while conserving energy without requiring human interaction. In this type of system, the goal does not involve controlling the interior environment. An example of an active façade system is the façade of the Children's Museum of Pittsburgh; it is a façade that responds to wind vibration, creating a dynamic visual effect that changes the feel of the indoor areas of the building Figure (2.2, left). Another example of an active façade is the ICT-Media building, which features air cushions made of ethylene tetrafluoroethylene (ETFE) that respond by inflating or deflating to block up to 85% of UV rays and heat, hence contributing to the reduction of building energy use Figure (2.2, right) (Tabadkani et al. 2021a).



*Figure 2.2: Examples of active façades the Children's Museum of Pittsburgh (left), and the ICT-Media building (right).*

### **2.2.3.2. Biomimetic or Bio-Inspired Façades**

The term “bio-inspired façade” implies a type of AF where biomimetic approaches are followed in the design generation process. Both building envelopes and organisms share the similar function of withstanding external environmental challenges. The terms “biomimicry” and “biomimetics” originally came from the Greek words “bios”, meaning “life”, and “mimesis”, meaning “to imitate” (López et al. 2017). Julian Vincent defined it as “the abstraction of good design from nature” (Vincent 2009). In biomimetics, solutions are derived through mimicking principles found in nature, their mechanisms, and their strategies. There are different approaches and classifications to implementing the strategies found in nature to the design of adaptive building envelopes. However, in general, researchers and practitioners have two main approaches to biomimetic design: a top-down approach (Speck et al. 2006), or a challenge to biology (Baumeister 2012), and a bottom-up approach (Speck et al. 2006), or biology to design (Baumeister 2012). In their work, Badarnah and Kadri (2015) indicated that the first approach seeks a specific solution found in nature for a particular issue. On the other hand, Vattam et al. (2009) called it a problem-based direct approach, where in the initial process, a design problem or human needs are identified in order to find an answer through looking at other organisms or ecosystems that have solved a similar problem (Vattam et al. 2009). This approach is more commonly used by designers because it is a more direct method (ElDin et al. 2016). El Ahmar (2011) stated that designers using this approach could obtain potential design solutions from nature without the need to understand the scientific side of it or even for collaboration with biologists or ecologists. Schleicher et al. (2011) and Badarnah (2017) implemented the problem-driven

## **CHAPTER 2: LITERATURE REVIEW**

approach in their work to seek a particular solution in nature for the design of an adaptive building envelope Figure (2.3, left).

The second approach is the bottom-up or solution-based approach (Vattam et al. 2007). In this approach, the overall observation of behaviour, function, and other characteristics in nature is translated into the design and products (Aziz and El Sheriff 2016). Therefore, this direction relies on having previous scientific knowledge and understanding of biological research rather than of human design issues. An example that applied the solution-based approach is the BIQ House in Germany Figure (2.3, right).



*Figure 2.3: Examples of bio-mimetic façades, One Ocean Thematic Pavilion (left), and the BIQ House in Germany (right).*

### **2.2.3.3. Passive Façades**

Passive AFs are those equipped with technology systems that do not require power, controls, or maintenance, and can even be considered self-maintaining. These types of façades are formed from a range of passive architectural design solutions whose primary purpose is to respond to climatic variations acting as a weather-protective layer on the exterior of a structure, hence improving the building's overall comfort level. This means that instead of using intelligent components, passive façades are the result of several 'passive design methods,' with their thermophysical properties defined by operational procedures, such as window-opening schedules. The most common examples of passive façades are as follows: double-skin façades, wood-based responsive building skins, opaque ventilated façades, glass surfaces with silk, light-directing systems, and Trombe walls. Numerous examples of passive façades exist in practice, such as the passive façade design in the Energybase building, with its stepped façade that serves as both a solar generator and a sunshield Figure (2.4) (Tabadkani et al. 2021a).





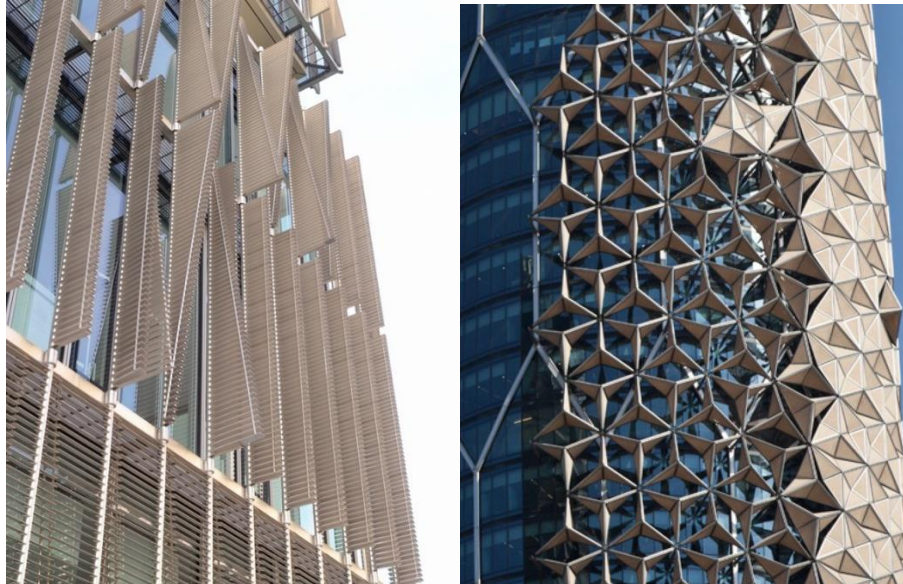
*Figure 2.4: Example of passive façade, the Energybase building.*

### **2.2.3.4. Kinetic Façades**

The field of kinetics focuses on the relationship between motion and its underlying causes, particularly the laws of motion controlling forces and masses (Lienhard 2015). When designing kinetic façade envelopes, complex mechanical systems are employed to operate the components in a variety of motions, such as sliding, expanding, folding, or reshaping, to ensure the system's changing geometry and mobility (Loonen et al. 2010). In general, these envelopes have to be adaptable to a wide variety of boundary conditions, such as temperature, location, and functional needs. To maintain the kinematic, an actuation force is required to generate the movement. Numerous examples have been developed using this approach, including the Helio Trace, a hypothetical prototype window by SOM in which the perforated aluminium surfaces operate in two distinct layers in response to the sun's movement throughout the day. Four vertical triangular folding shade surfaces cover each window. The Q1 Headquarters Building in Germany is another example of a kinetic envelope; the system functions as a sunshade device composed of 400,000 triangular, square, and trapezoid-shaped metal pieces. All these elements operate automatically with the assistance of 1,280 electric motors to open and close the sunshade, effectively blocking off glare and heat gain (Böke et al. 2020) Figure (2.5, left). A further example is Al-Baher Towers, which applied 1,049 hexagonal panels creating a folding and unfolding movement in response to the outdoor conditions and regulating daylight and glare in the interior environment. The kinetic elements are programmed to change into three states: completely

## **CHAPTER 2: LITERATURE REVIEW**

closed, mid-open, and fully open (Ahmed et al. 2016a) Figure (2.5, right). All kinetic façades share a common feature, specifically, their ability to respond to external environmental stimuli, which is a driving force for their conversion to responsive façades (Tabadkani et al. 2021a).



*Figure 2.5: Example of kinetic façades, Al-Baher Towers.*

### **2.2.3.5. Intelligent Façades**

Intelligent façades integrate two components into their system: human control and automation. This enables them to react dynamically to environmental conditions by optimising their usage patterns independently or cumulatively using predictive models with limited user interaction. The three fundamental functions of intelligent systems have been recognised as perception, reasoning, and action, which have the capability of learning and responding in time (Romano et al. 2018). According to Wigginton and Harris (2002), an intelligent façade should be able to self-adjust via a process called 'instinctive autonomic adjustment' (Wigginton and Harris 2002), thereby optimising the building's systems in terms of temperature, energy balance, and human comfort, and frequently through the use of predictive models. As an example, two intelligence parameters contribute to the improvement of comfort in the GSW Headquarters building in Germany: natural ventilation provided by a thermal flue within the Double Skin Facade (DSF) and automatic ventilation management with manual override via a wall-mounted zone controller. It features double-skin-coloured panels on the west façade of the building that create a cavity assisting in the control of solar heat gain and natural lighting Figure (2.6).



*Figure 2.6: Example of an intelligent façade, the GSW Headquarters building in Germany.*

### **2.2.3.6. Interactive Façades**

The term interactive is more frequently used regarding computer-enabled artworks, installations, and other situations that allow active public participation than it is in reference to building envelopes. Interactive façades can be constructed with sensors, microprocessors, or building management systems and require human engagement to initiate a response. However, despite the existence of adaptive elements within the building, these types of façades do not have the potential to influence internal comfort (Haeusler 2009). GreenPix has an interactive media wall which comprises 2,292 RGB LED light dots as a monitor screen and is used to display dynamic content. The building's skin communicates with the interior spaces and the external public space through custom software, turning the façade into an interactive entertainment and engagement experience Figure (2.7).



*Figure 2.7: Example of interactive façade, the GreenPix building.*



### **2.2.3.7. Movable Façades**

Using movable systems, moveable façades incorporate technological systems that can respond rapidly to changing environmental circumstances and location via movable systems, such as detecting the position of the sun to provide renewable energy. Thus, this typology's objectives include the regulation of the indoor environment, the enhancement of user comfort, and the reduction of energy use in new or existing structures (Schumacher et al. 2010). There are several examples of photovoltaics (PVs) being installed on building façades. An example of a massive-scale installation is the EWE Arena in Hamburg, Germany; the structure comprises 200m<sup>2</sup> PV panels that can be rotated 200 degrees around the perimeter of the envelope, generating approximately 27MWh each year Figure (2.8).



*Figure 2.8: Example of movable façade, the EWE Arena in Hamburg.*

### **2.2.3.8. Smart Façades**

The term smart has been most frequently used in relation to materials and surfaces in the design disciplines. For a system to be considered as "smart," it must incorporate technological capabilities, be responsive to specific environmental conditions, and operate through changes in internal physical properties or external exchanges. Additionally, smart systems can be used efficiently in conjunction with other types of façades, such as responsive or intelligent façades, due to their inherent settings (Tabadkani et al. 2021a). In addition to Aerogel, a synthetic low-density translucent material used in window glazing, phase-changing materials such as micro-encapsulated wax, salt hydrates, thermochromic polymer films, and building integrated PVs are all examples of smart materials utilised in high-performance building skins to achieve greater energy efficiency and comfort in buildings (Addington and Schodek 2005). In terms of application, the Bloom Project is an example of a smart responsive system. It utilises thermo-bimetal shape memory alloys that

## **CHAPTER 2: LITERATURE REVIEW**

expand and contract in response to both temperature variations and direct solar radiation to manage daylight, provide air ventilation and act as a sun shading system Figure (2.9).



*Figure 2.9: Example of smart façade, the Bloom Project.*

### **2.2.3.9. Responsive Façades**

The primary purpose of a responsive façade is to adapt to both human needs and environmental changes. As with kinetic or intelligent façades, responsive systems are characterised by sensors, actuators, and controlling devices that enable the façade's configuration to be changed based on a programmed performance, but the key difference between the two is the responsive system's ability to respond to user input (Tabadkani et al. 2021a). As a result, responsive façades are restricted to those that require a user action to perform an activity in order to respond by modifying the material properties or mechanical behaviour of the building envelope (Tabadkani et al. 2021a). The Kiefer Technic Showroom is an example of a responsive façade that allows for user engagement. This responsive façade, which is composed of perforated aluminium panels that are controlled centrally by light sensors, enhances the indoor climate based on outside circumstances while also allowing users to override the automatic control as necessary Figure (2.10).



*Figure 2.10: Example of a responsive façade, the Kiefer Technic Showroom.*

### **2.2.3.10. Switchable Façades**

A switchable façade is a transparent façade that is composed of 'smart adaptive materials' and can change the energy and light flow. Control can be either active or passive, depending on whether the control is responding to building automation and occupant inputs or to inputs from the local environment. Electrochromic or thermochromic glazing systems that can be switched between transparent and opaque states using smart materials such as Phase Change Memory (PCM) are a common example of such façades (Sadek and Mahrous 2018)

Based on the examined cases, the façade typologies may overlap, and a given example may relate to more than one type as shown in Figure (2.11). For instance, a switchable façade can be a part of a smart façade since it uses smart materials, and it can be a part of a moveable façade that uses kinetic properties to generate energy. In addition, interactive façades permit input from the user, but only as an encouragement for physical changes and not to control their comfort (Tabadkani et al. 2021a). Consequently, the classification of an AF into one of the abovementioned typologies is feasible only on a case-by-case basis, taking into account the AF adaptation mechanism, its environmental condition, and the user interaction. This classification enhanced clarity regarding AF terminologies, allowing researchers to categorise their proposed prototype according to a particular category of AFs.

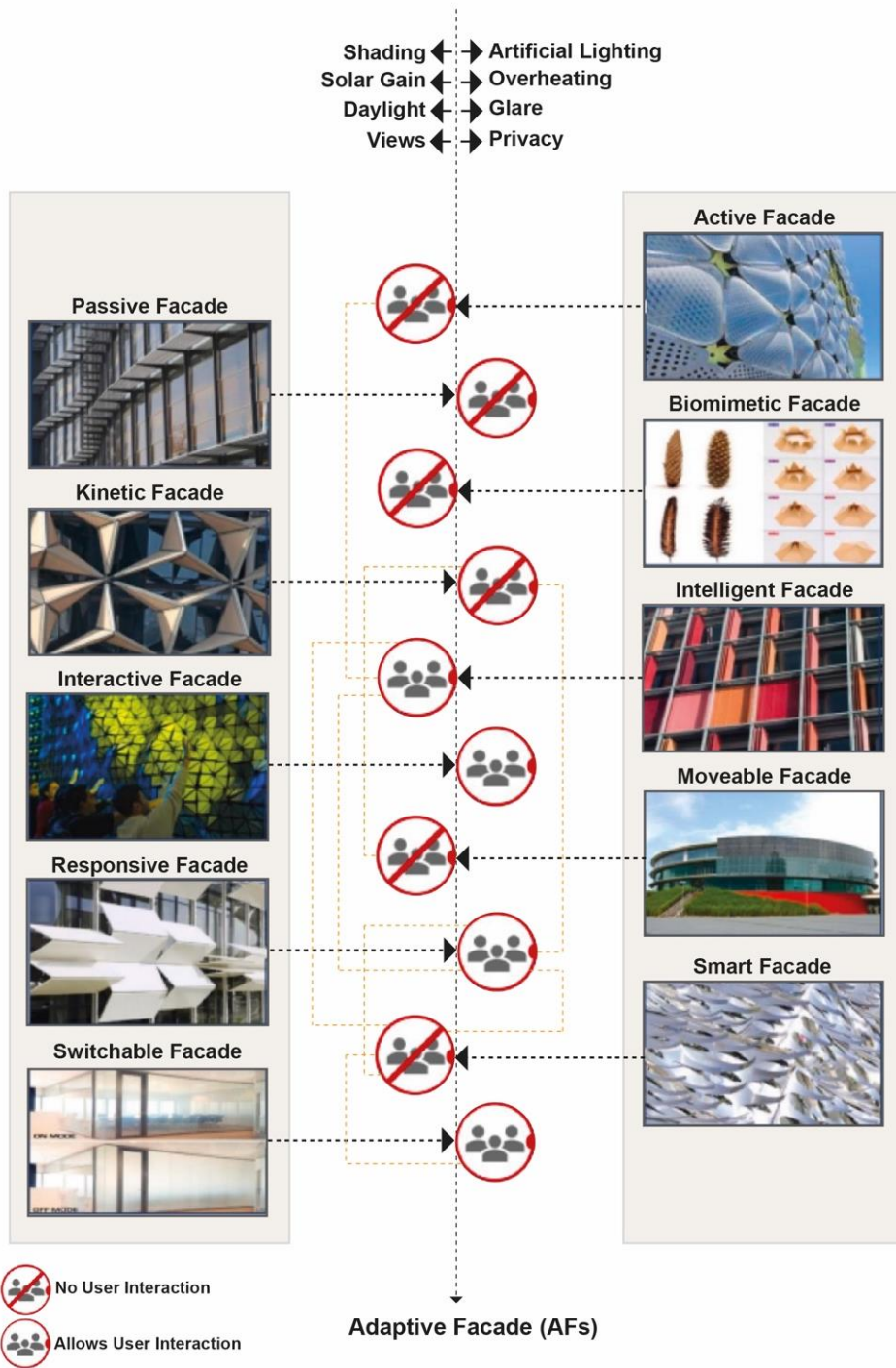


Figure 2.11: Relations between the various types of AFs (adapted from Tabadkani et al. (2021)).

### 2.3. Classification of Adaptive Façades

Several researchers in the field of AFs have helped to classify AFs into sub-groups with shared characteristics. In addition, many review papers have been published on the different categories of AFs, such as adaptive glazing, phase-change materials, solar façades, and daylighting systems (Loonen et al. 2015). In the work carried out by the scientific plan of COST Action TU 1403, researchers looked at the complexity of AF systems and the multiple variables that affect the performance of building envelopes. Then, they categorised AFs in terms of technologies and purpose, as seen in Figure (2.12) (Aelenei et al. 2016). The first column represents the purpose of the AF, which is to achieve thermal comfort, energy performance, indoor air quality (IAQ), and visual and acoustic performance. The classifications approach to AFs helps in detecting patterns, defining unexplored ideas, and increasing the knowledge of this multidisciplinary field (Attia et al. 2015). In their work on AF networks (COST Action), they classified the case studies of AFs into three main groups: façade systems, materials, and components.

| Purpose               | Responsive Function | Operation               | Components         | Response Time  | Spatial Scale     | Visibility | Degree of Adaptability |
|-----------------------|---------------------|-------------------------|--------------------|----------------|-------------------|------------|------------------------|
| Thermal Comfort       | Prevent             | Intrinsic               | Shading            | Seconds        | Building Material | No         | Intrinsic              |
| Energy Performance    |                     |                         | Insulation         | Minutes        | Facade Element    |            |                        |
| IAQ                   | Reject              | Extrinsic               | Switchable Glazing | Hours          | Wall              | Low        | Extrinsic              |
| Visual Performance    | Modulate            |                         | PCM                | Day            | Window            |            |                        |
| Acoustice Performance | Collect             |                         | Solar Tubes        | Seasons        | Roof              |            |                        |
| Control               |                     | Integrated Solar System | Years              | Whole Building | High              |            |                        |

Figure 2.12: Adaptive façade in terms of technologies and purpose (adapted from Aelenei et al. 2016).

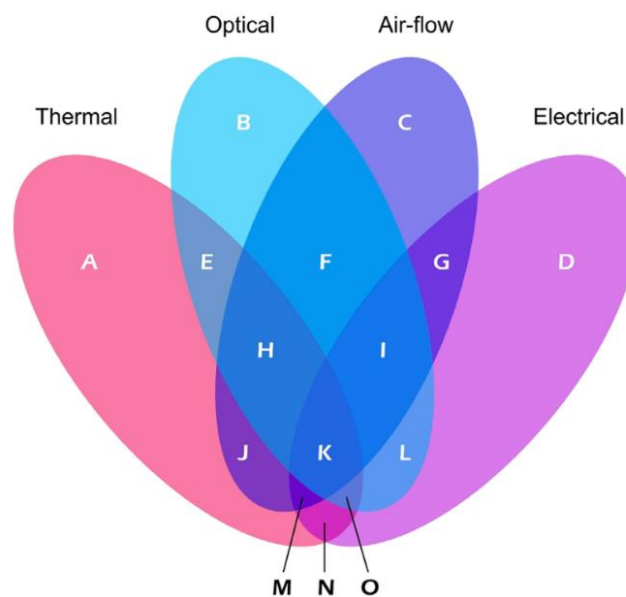
According to the study "Design for façade adaptability: Towards a unified and systematic characterization," three stages were considered to form a coherent and systematic performance classification system for AFs: The first stage is related to the collection of ambient data such as interior and exterior climate conditions and occupancy patterns, while the second phase determines the controlling strategies using computational tools. Choosing an effective control system for the AF system is critical for the building's overall performance and operation. Control systems can be subdivided into two types in practice: extrinsic control systems and intrinsic control systems. The final stage is related to physical domains,



responsive time scales, adaptation scales, and spatial scales (Loonen et al. 2015). The following sections discuss both stage two and stage three in more detail.

### **2.3.1. Physical Domains**

There are four primary physical interactions between the building envelope and the surrounding environment (thermal, optical, airflow, and electrical), which allow for a variety of reaction activities, such as preventing, rejecting, modulating, collecting, and admitting. In the domain of adaptable building skin systems, each system responds and interacts in a distinct way, depending on the adaptiveness objective of the system (Loonen et al. 2017). Figure (2.13) shows the various intersections among the four domains, representing all possible combinations of physical interactions between adaptive systems and the climate. With regard to the thermal domain, adaptation alters the energy balance of the building through conduction, convection, radiation, and thermal energy storage, while in the case of the optical domain, adaptive behaviour has an impact on the visual experience of the building's occupants by altering the transparency surfaces of the building skins. For the airflow domain, the adaptive behaviour of the façade is affected by the direction and speed of the wind.



*Figure 2.13: All possible physical overlappings related to building envelopes.*

### **2.3.2. Responsive Time Scale**

Throughout a building's life cycle, it is vulnerable to a wide range of environmental influences that frequently occur at a variety of time scales, ranging from seconds to the entire life of the building; however, the rate of adaptation is dependent on the technology utilised or the designer's preference. As a result, Loonen et al. (2013) divided the time scale

## **CHAPTER 2: LITERATURE REVIEW**

of an adaptable envelope into four distinct time scales: minutes, hours, diurnal, and seasonal time scales (Loonen et al. 2013).

- a. **Seconds:** The smallest fluctuations that occur frequently in nature, such as sudden shifts of wind direction and speed as well as an interactive façade that responds to the needs of its users in short time intervals.
- b. **Minutes:** Some of the factors that represent this time constraint are daylight availability and cloud cover; both variations are measured in minutes. Most thermo-optical adaptive skins change their transparency on a minute-by-minute basis.
- c. **Hours:** The sun's angular motion in the sky is an ongoing process that occurs throughout the day. However, AFs that follow the path of the sun frequently adapt on an hourly basis. In addition, variances in air temperature, both interior and exterior, and solar radiation can suitably be discretised in hourly values, which are classified in this category.
- d. **Diurnal:** The building's occupants typically follow daily 'working hours', so AFs can take advantage of this by exploiting this regular 24-hour pattern.
- e. **Seasonal:** The adaptive envelope adjusts in this case to the seasonal variations (winter, spring, summer, and autumn), which impose widely varying boundary conditions.

### **2.3.3. Scales of Adaptation**

According to Loonen et al. (2013), the scale of adaptation can be modified at either the macro or micro scales, depending on whether the adaptation mechanism is based on the configuration of the adaptable skin or on changes in material properties, although a mix of the two classes is also possible. The following section discusses both scales in greater detail.

- a. **Macro scale:** In the case of the macro scale, the adaptation is achieved through changes in the configuration of the façade at the macro level, and the motion and transformation of its components can be easily observed, such as folding, expanding, sliding, rolling, rotating, stretching, and inflating. This category includes 'kinetic', 'active', 'movable', 'responsive', and 'biomimetic' façades, which are all examples of façades that modify their configuration on a macro level. Typically, these forms of adaptable envelopes are referred to as 'kinetic envelopes,' implying the presence of some form of observer motion. The macro-level concept can come with different forms and transformation patterns, such as the mechanically operated Venetian blinds or the folding and unfolding panels of Al Bahar Tower (Oborn 2013).

## CHAPTER 2: LITERATURE REVIEW

- b. **Micro scale:** This form of adaptation occurs as a result of changes to the material's internal structure. When a material transitions between phases, such as from liquid to solid or from gas to liquid, the arrangement or structure of its molecules changes; as a result, the material's properties change, and the material behaves differently. Adaptability is demonstrated in this context by changes in the thermophysical properties or opaque optical features, as well as through the energy exchange across forms, all of which are commonly found in 'switchable', 'media', and 'smart' façades (Al-Masrani and Al-Obaidi 2019).

### 2.3.4. External Factors

Building envelopes are exposed to different external factors that are highly dynamic and change continuously throughout the day and season, which can influence humans' comfort levels. Aelenei et al. (2016) examined six external factors that may have a significant influence on occupants. The study focused its analysis only on the need for adaptability driven by external factors because of the complexity of adaptability needs in buildings. The authors considered the following external factors for the analysis: solar radiation, outdoor temperature, wind, humidity, precipitation, and noise. The purpose of an AF is to respond to these external factors and provide occupants with an acceptable internal environment for achieving thermal comfort, energy performance, IAQ, acoustic performance, visual performance, and durability, as shown in Figure (2.14) (Aelenei et al. 2016).

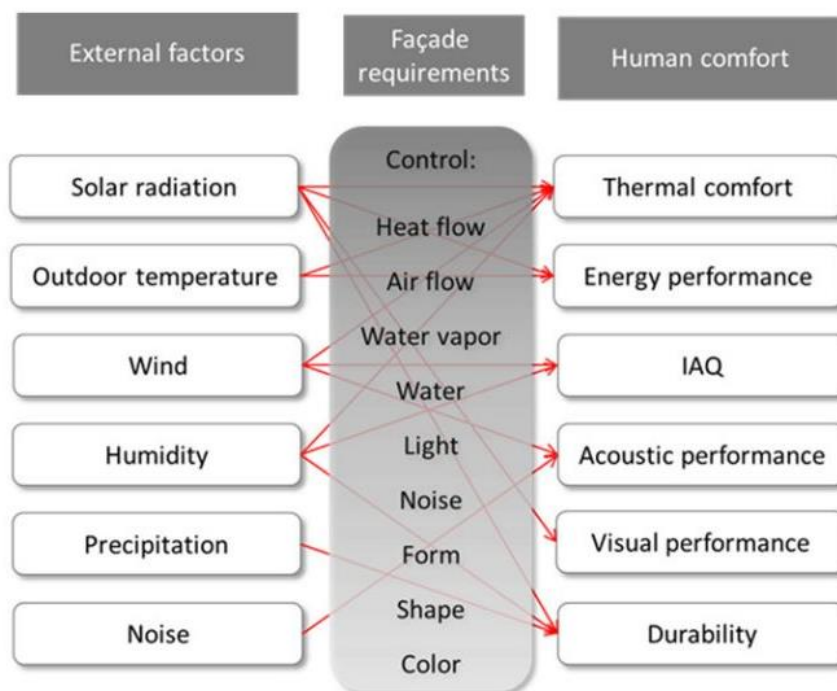
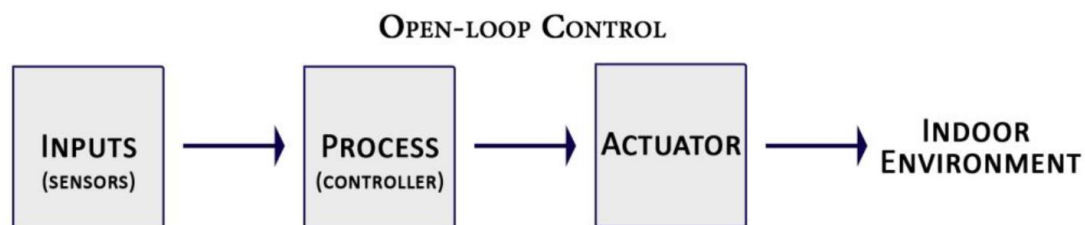


Figure 2.14: Schematic role of adaptive façade (adapted from Aelenei et al. 2016).



## **2.4. Automatic Control System**

Defining an effective control system is the key factor for achieving a high performance AF system (Tabadkani et al. 2021a). Based on the literature, there are two different types of control strategies for automated shading systems: (1) intrinsic and (2) extrinsic control strategies (Loonen et al. 2013). The adaptive mechanism for both control systems is triggered in an automatic way by environmental stimuli, such as solar radiation, relative humidity, surface temperature, etc. Intrinsic control is based on internal self-adjustment control systems like smart materials (e.g., thermochromic, photochromic, and PCMs), and it is actuated based on the variation of its internal energy. This type of control does not allow users to interact with the system or to integrate external inputs; therefore, the activation of actuators occurs directly without using a feedback loop. It is also known as a ‘direct’, ‘passive’, or ‘open-loop’ (feedforward) control system, as environmental inputs are transformed automatically into actions regardless of whether an external decision-making component is used Figure (2.15) (Tabadkani et al. 2020a). An advantage of using intrinsic rather than extrinsic control is that the system has low maintenance costs, and it does not consume fuel or electricity to change the façade configuration for each state transition.



*Figure 2.15: Open-loop control system.*

On the other hand, extrinsic control or active control is based on actuators, sensors, and processors (controllers) to operate the AF shading system. This type of control can accept a feedback signal through using an external decision-making component, and users can interfere with its algorithm Figure (2.16). Therefore, the level of complexity and the operation costs are higher than for an intrinsic control system, but the degree of façade adaptation is more advanced. This kind of control is also called ‘active’ or ‘closed-loop’ control, as the system compares the actual output (action) with the desired state (set-point) and uses them as a feedback signal for reducing the variation error (Bishop 1998). The structure of a closed-loop system consists of three main elements: sensors, processors

(controllers), and actuators. In this research, the terms ‘open-loop’ and ‘closed-loop’ are used to avoid using different terms interchangeably.

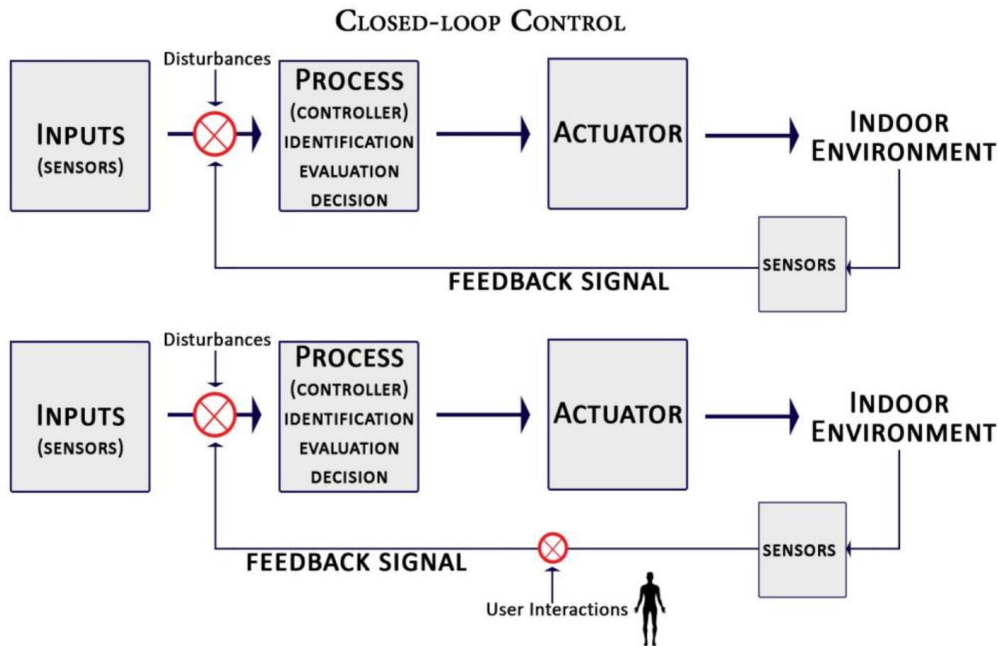


Figure 2.16: Closed-loop control system.

Closed-loop is the most advanced system and most suitable control for dynamic operation because it has the ability to reject unavoidable external disturbances (Al-Masrani and Al-Obaidi 2019). Bishop (1998) defined disturbances as any “unwanted input signal that affects the output signal”. In the operation stage, all control systems are prone to disturbances, which can enter the loop in two main forms: (1) actual data, such as noise and load measurement, and (2) virtual data from various resources, such as changing the desired set-points (Al-Masrani and Al-Obaidi 2019). Consequently, to deal with these unwanted inputs that affect the desired output, the adaptation of a feedback control system is the optimum, where errors are fixed constantly by the controller. Table (2.1) presents some existing studies that implemented an automatic control examining the control system type, the control sensors, the activation thresholds, the method used, and the simulation tools.

### 2.4.1. Open-Loop Control

In this control system, the controller is actuated solely by the exterior conditions through the installed outdoor sensors with predefined setpoints; therefore, the indoor environment does not affect the system performance (Mukherjee et al. 2010). Moreover, Jain and Garg stated that this kind of control system does not have the sensitivity to change based on user preferences or indoor conditions since the feedback loop is absent, but it can utilise a network of internal sensors to share information (Jain and Garg 2018). The most common

## **CHAPTER 2: LITERATURE REVIEW**

example of an open-loop control system found in the literature is the cut-off angle for blinds, which considers the sun's position to adjust the angle of the blind based on blocking direct sunlight (Tabadkani et al. 2020a).

Several researchers have implemented an open-loop system to actuate shading systems automatically. A study by Bustamante et al. (2017) presented different open-loop control strategies for shading devices to simultaneously control solar heat gain to achieve low energy usage and visual comfort. In this article, two external shading devices were evaluated, namely, perforated louvres and Venetian blinds, in terms of energy consumption, spatial daylight autonomy (sDA), and annual sunlight exposure (ASE). The control logic of the slat angle is based on the maximum incident solar irradiance on the glazed surface of an office space. The authors found that perforated louvres are lower than Venetian blinds in terms of saving energy because of the high solar gain and daylighting transmittance that can penetrate through the perforations into the indoor space (Bustamante et al. 2017). Another study explored the use of roller shades with different solar radiation setpoints (high, medium, and low) as a control strategy for automatic shade (open-loop) control coupled with automatic dimming lighting control. A private office zone was simulated using different climate zones, that is, a cooling-dominated climate and heating-dominated climate, to address the energy saving in each zone. They concluded that a high solar control setpoint achieved the maximum energy saving in the Houston climate, which is a cooling-dominated zone. In addition, the integration of a roller shade control system with electric lighting control could save up to 36% in hot zones and up to 11% in cold zones (Wankanapon and Mistrick 2011).

Another study by Touma and Ouahrani (2017) investigated three different scenarios in Qatar with Venetian blinds: no control, cut-off control, and both cut-off control and daylighting control on both south and north-oriented office rooms. According to the results, adopting open-loop control for the third option reduced the total energy by 37.8% and 26.1% respectively. Kim et al. (2015) implemented a complex kinetic façade, and the control logic is based on the incidence angle of the sun that defined the opening ratio of each panel individually with decentralised behaviour. The comparison between the fixed shading and the kinetic façade was done in terms of energy consumption. Researchers found that a smaller opening ratio consumes less energy; however, daylighting performance was not considered. The focus was limited to the difference between the energy consumption and the opening ratio without the consideration of daylighting, which will result in an increase in the usage of electric lighting.

### **2.4.2. Closed-Loop Control**

Olbina and Hu (2012) implemented feedback (closed-loop split-controlled blinds) to improve daylighting and thermal performance in a hot climate zone. In this study, three different automatic Venetian blind systems (conventional, split predicted, and split optimum) were analysed to identify which of these systems is more effective in accomplishing two objectives: energy saving and daylighting performance. The use of split-blinds control (predicated and optimum) achieved an energy saving of up to 37% and increased indoor illuminance when compared to conventional blinds (Olbina and Hu 2012).

Evola et al. (2017) aimed to adapt a suitable automatic shading device that would improve human comfort and reduce energy needs for cooling while limiting indoor overheating. In this article, the researchers evaluated a series of shading-system solutions, such as internal venetian blind, external roller blind, and solar control film, for a highly glazed office building in Italy. An automatic control system was integrated with a predefined threshold, which closes when "solar irradiance on the window surface exceeds  $200 \text{ W/m}^2$  and the zone air temperature is equal to or higher than  $26 \text{ }^\circ\text{C}$ " (Evola et al. 2017). Their results concluded that none of the studied shading systems show the same effectiveness. The external roller shade and solar film could reduce the indoor temperature significantly when internal temperature and solar radiation are combined as setpoint inputs for the control logic (Evola et al. 2017).

**CHAPTER 2: LITERATURE REVIEW**

Table 2.1. Review of some existing studies in relation to automatic control systems

| ID | Study                          | Studied Location     | Climate       | Shading Type   | Office Type | Automatic Control Strategy |   |   |   | Design Criteria     | Simulation Tools                  | Approach                 |
|----|--------------------------------|----------------------|---------------|--|-------------|----------------------------|---|---|---|---------------------|-----------------------------------|--------------------------|
|    |                                |                      |               |  |             | Control Type               | Control Sensors                           | Activation Threshold  | Action  |                     |                                   |                          |
| 1  | (Evola et al. 2017)            | Italy                | Hot           | Internal Venetian blind, external roller blind, solar control film | S           | FF                         | Global irradiance, and indoor temperature | >200 [W/m <sup>2</sup> ]<br>=> 26 °C  | The shade closes when solar radiation is >200 W/m <sup>2</sup> , and the operative temperature is =>26 °C   | Energy, daylighting | EnergyPlus                        | Simulation               |
| 2  | (Wankanapon and Mistrick 2011) | Houston, Minneapolis | Multi climate | Roller shades  | P           | FF                         | Solar radiation                           | Low - 95 W/m <sup>2</sup> ,<br>Medium -189 W/m <sup>2</sup> High - 400 W/m <sup>2</sup>                           | Shades are lowered considering different incident solar radiation setpoints.  | Energy              | EnergyPlus                        | Simulation               |
| 3  | (Touma and Ouahrani 2017)      | Qatar                | Hot           | Venetian blinds  | S           | FF                         | Solar radiation                           | >524W/m <sup>2</sup>  | When solar radiation on the surface was higher than 524W/m <sup>2</sup>   | Energy, DGI         | EnergyPlus                        | Simulation, experimental |
| 4  | (Bustamante et al. 2017)       | USA, Canada, Chile   | Multi climate | Exterior Venetian blinds, exterior perforated louvers              | S           | FF                         | Global irradiance                         | Between 530 W/m <sup>2</sup> and 610 W/m <sup>2</sup> , and Between 290 W/m <sup>2</sup> and 350 W/m <sup>2</sup> | “Threshold varied between 530 W/m <sup>2</sup> and 610 W/m <sup>2</sup> for Venetian blinds and varied between 290 W/m <sup>2</sup> and 350 W/m <sup>2</sup> for the louvres” | EUI, sDA, ASE       | EnergyPlus, Radiance, mkSchedule  | Simulation               |
| 5  | (Eltaweel and Su 2017b)        | Egypt                | Hot           | Venetian blinds  | P           | FF                         | Sun position                              | -   | -   | Energy, daylighting | EnergyPlus, Honeybee, and Ladybug | Simulation               |
| 7  | (Nielsen et al. 2011a)         | Denmark              | Temperate     | Venetian blinds  | P           | F                          | Indoor air temperature                    | >24°  | “Blinds turn to low if indoor air temperature is over 24° or the glare exceeds”   | Energy, daylight    | iDbuild                           | Simulation               |
| 8  | (Wienold et al. 2011)          | Rome, Frankfurt      | Multi climate | Venetian blinds  | P           | F                          | Global irradiance                         | >100 [W/m <sup>2</sup> ]<br>>150 [W/m <sup>2</sup> ]<br>>200 [W/m <sup>2</sup> ]                                  | Venetian blind is lowered and set to their cut-off angle  | Energy, daylight    | ESPr                              | Simulation               |
| 9  | (Skarning et al. 2017)         | Rome, Copenhagen     | Multi climate | Roller shade   | P           | F                          | Solar radiation, and outdoor temperature  | > 300 W/m <sup>2</sup><br>> 18 °C   | “The shade closes when a certain value of 18° C outdoor air temperature and 300 w/m <sup>2</sup> solar irradiation exceeds”   | Energy, daylight    | EnergyPlus                        | Simulation               |

**CHAPTER 2: LITERATURE REVIEW**

| ID | Study                    | Studied Location             | Climate       | Shading Type                                       | Office Type | Automatic Control Strategy |  |                          |   | Design Criteria                            | Simulation Tools              | Approach     |
|----|--------------------------|------------------------------|---------------|--|-------------|----------------------------|--|--------------------------|---|--|-------------------------------|--------------|
|    |                          |                              |               |  |             | Control Type               | Control Sensors                        | Activation Threshold     | Action  |  |                               |              |
| 10 | (Ahmed et al. 2016b)     | Egypt                        | Hot           | Folded panels                                      | P           | F                          | Indoor temperature                     | -                        | Indoor air temperature 28 °C  | Thermal Energy (cooling)                   | Grasshopper                   | Experimental |
| 11 | (Atzeri et al. 2014)     | Rome                         | Hot           | Roller shade                                       | S           | FF                         | Global irradiance                      | >150 [W/m <sup>2</sup> ] | Roller shade is lowered.  | Energy, daylight                           | EnergyPlus                    | Simulation   |
| 12 | (Atzeri et al. 2013)     | Italy                        | Hot           | Exterior Venetian blinds and roller shade Exterior | S           | FF                         | Glare index, global irradiance         | -                        | -   | Energy, DGI                                | EnergyPlus                    | Simulation   |
| 13 | (Shen et al. 2014)       | Baltimore, London, Abu-Dhabi | Multi climate | Venetian blinds                                    | S           | F                          | Sun position, and vertical illuminance | -                        | -   | Energy daylight                            | EnergyPlus, BCVTB, Matlab     | Simulation   |
| 14 | (Atzeri et al. 2018)     | Italy                        | Hot           | Roller shades                                      | S           | F                          | Solar position, workplace illuminance  | 2000 lx                  | -   | Energy daylight                            | EnergyPlus, Matlab            | Simulation   |
| 15 | (Hoffmann et al. 2016)   | Burbank, Oakland             | Multi climate | Roller shades                                      | S           | FF                         | Glare index                            | DGP ≥0.38 or DGI ≥24     | -   | Energy daylight                            | Radiance, EnergyPlus, EMS     | Simulation   |
| 16 | (Olbina and Hu 2012)     | Florida, USA                 | Hot           | Automated blinds                                   | S           | F                          | Task illuminance                       | <2000 lx                 | Close the blinds  | Energy daylight                            | EnergyPlus                    | Simulation   |
| 17 | (Kim et al. 2015)        | UAE/Abu Dhabi                | Hot-arid      | Origami  | S           | FF                         | Sun position                           | -                        | “Incidence sun angle 0°–90° of a given surface drives three states: closed, partially and fully open” | Energy (cooling loads)                     | Dynamo/Revit/eQUEST           | Simulation   |
| 18 | (Giovannini et al. 2015) | UAE/ Abu Dhabi               | Hot-arid      | SVM  | P           | FF                         | Sun position                           | -                        | The shading system is varied based on sun position  | Daylight energy (lighting /cooling) Hammad | DIVA- Grasshopper /EnergyPlus | Simulation   |

P: Private office

S: Shared office

F: Feed forward control

FF: Feedback control

## **Part (B) Building Performance Simulation for Adaptive Façades**

### **2.5. Building Performance Simulation for Adaptive Façades**

The development of AF systems requires evaluation of their benefits and performance during the early stages of the design. The AF concept has become the primary focus of many recent researchers (Elzeyadi 2017; Hosseini et al. 2019a; Tabadkani et al. 2019; Böke et al. 2020; Bui et al. 2020; Panya et al. 2020; Shi et al. 2020). Therefore, it is critical to develop an effective approach to predicting their performance in the early in the design process and to evaluate their applicability, which can be accomplished through building performance simulation (BPS), especially when resources such as money and time are limited (Hensen and Lamberts 2011). Computer simulation based on mathematical models has demonstrated its effectiveness through its capacity to simulate and predict the real-world performance of buildings. BPS is a design assistance tool that is commonly used in the field of building engineering. It is used, for example, to evaluate a building's overall performance, such as its total primary energy consumption and indoor environmental quality, among other things. BPS has the potential to contribute to the decarbonisation of the built environment; however, simulating the performance of AFs with BPS is challenging.

Integrating modelling and simulation into the design process enables designers to gain a better understanding of the critical relationship between the design and performance aspects of adaptive building envelopes, hence, contributing to the increased application of AF in the building construction industry (Loonen et al. 2017). BPS is also able to compare various materials, systems, and controls quantitatively, as well as performance metrics such as primary energy consumption, total cooling loads, comfort or discomfort indices, indoor air quality, and whole life value indicators. However, this study focuses on the total cooling loads of AF systems in office buildings.

There is consensus in the literature that evaluating AF performance is often complex due to a lack of research and methods and the limited tools available to the designers and engineers (Favoino et al. 2016; Loonen et al. 2017). Numerous studies have been carried out focusing primarily on the development of AF technologies that are capable of changing only their physiological properties in order to quantify their energy and environmental performance, such as switchable, thermochromic (TC), and photovoltaic-chromic (PVC) glazing systems (Loonen et al. 2014c; Favoino et al. 2016; Sadek and Mahrous 2018; Giovannini et al. 2019). On the contrary, limited cases were found in the literature that

examine the geometry-changing behaviour of AF that adapts to outdoor climatic conditions using computational methods (Kuru 2020).

### **2.5.1. Current Research for the BPS tools**

The lack of available tools is a significant factor in limiting the studies on AF performance prediction. Loonen et al. (2017) mentioned that a majority of software packages are often described as complicated digital modelling and not user-friendly (Loonen et al. 2017). In addition, most existing tools lack the capability to simulate AFs within their built-in objects, apart from a few software programs that target specific types of technologies, such as TC glazing technology. However, these systems experience only physiological changes, making it extremely difficult to integrate a variety of variables that change in response to time (Sheikh and Asghar 2019).

When compared to conventional façades, AFs are unique in their ability to adapt to changing environmental conditions throughout time. The term "motion" in the context of AFs refers to a system that dynamically modifies its properties over time, which is crucial for evaluating the performance of AFs. In a static state, only a limited number of configurations can be investigated for pre-defined points in time, such as a "compact schedule", which can be used to determine the state of the system at various times of the day throughout the course of a year. In this case, the program is incapable of determining the optimal system configuration based on environmental variables.

Certain software systems enable the parallel simulation of multiple dynamic states linked to environmental variables. For instance, EnergyPlus includes tools for modelling and simulating moveable insulation and TC glazing technologies; however, these tools are restricted to modelling movable insulation and TC glazing systems. Additionally, this software incorporates an Energy Management System (EMS) that enables the use of 'if statements' and programmable controls, referred to as customisable objects (Kuru et al. 2021). With the integration of these features, it is feasible to simulate the dynamic states of AFs. However, EnergyPlus is a complicated software package, and modelling geometric changes of AFs is a challenging and time-consuming process (Kuru et al. 2021). To address the geometric modelling challenge, some researchers have integrated parametric modelling tools, such as Grasshopper and Dynamo with EMS add-ons to simulate the geometric changes associated with AFs. Nonetheless, there is no straightforward method for designers to assess the performance of AFs.

The simplification approach is one of the methods followed by some researchers, where the AF is simulated by dividing the simulation run into different short periods according to time,



## **CHAPTER 2: LITERATURE REVIEW**

seasons, weeks, or months, with the application of varied building properties on each division (Loonen et al. 2011; Favoino et al. 2014b; Kasinalis et al. 2014). However, this approach is limited to façade systems with long adaptation cycles and not to systems where the façade varies based on each second, minute, or hour. Moreover, this method does not take into account that the end of each simulation should be different from the following simulation in terms of the outdoor conditions, such as surface temperature, indoor temperature etc. (Loonen et al. 2017). Therefore, physical changes of the system and the consideration of time in varying behaviour is necessary in delivering a performed AF system. As an example of the physiological changes of adaptive systems, Favoino et al. (2016) developed an adaptive 'PVC switchable glazing' system, which can modify its material properties over time in response to changes in solar irradiance (SI) levels. In addition, the researchers conducted multi-objective optimisation, an algorithmic technique for determining the optimal option from a pool of variables. The study simulates the energy performance of a switchable glazing system in a variety of climates using EnergyPlus and its integrated EMS tool to model the changing physiological behaviour of the switchable glazing.

### **2.5.2. Discussion of Existing Studies**

This section reviews some of the current BPS studies of AF systems to provide an overview of what has been published in the field of AFs; however, it is not a comprehensive review Table (2.2). The studies are analysed and categorised to gather information about the current state of use of BPS tools on AFs. The examined studies are divided into three major categories: (1) AF system type, including whether the system is conventional or non-conventional, building type, and climate; (2) adaptability; and (3) performance. The adaptability and performance groups include the following parameters: adaptive typology, the state and type of change it generates, the behaviour changes generated by the system, whether geometrical or material-based, the timeframe of adaptability and its various configurations, the evaluation methods used, the control strategy, the control sensors, the physical domain of the performance evaluation, and the design objective of the system.

Based on the reviewed studies, it was found out that most researchers used parametric tools in conjunction with EnergyPlus, Daysim and Radiance to model and simulate the geometrical changes. However, none of these studies have properly examined the automatic control system during the simulation Figure (2.17). Apart from modelling and simulating adaptive smart material systems, the researchers employed non-parametric tools to simulate the complex movements of AFs due to the difficulty of modelling adaptive geometrical changes

## CHAPTER 2: LITERATURE REVIEW

based on a sequence of time-varying steps that correspond to different climatic conditions. Although parametric tools, such as Grasshopper, Honeybee, and Ladybug, allow users to incorporate add-ons as EMS for controlling AFs with predefined control logic, no studies used EMS as a control strategy system to automate the non-conventional AF systems due to the complexity and the interface limitation of current PBS. On the other hand, most studies implemented the control strategy system using EMS for conventional dynamic façades such as Venetian blinds, roller shades, dynamic blinds, louvres, etc. that has a basic movements characteristic. In these systems, the adaptive behaviour is not complex, and modelling and simulating the systems is embedded in most BPS software packages. For instance, EnergyPlus can simulate conventional window shade controls, such as Venetian blinds, utilising either a fixed schedule for cut-off or slat angles approach. EnergyPlus is the most widely used tool for evaluating the thermal and daylighting performance of conventional façades as well as more unconventional shading systems, such as complex fenestration systems (CFS) (Kirimtat et al. 2016).

| Adaptive Façade Performance         |                     |              |              |                         |          |        |
|-------------------------------------|---------------------|--------------|--------------|-------------------------|----------|--------|
| Adaptive Façade Type                | Conventional Façade |              |              | Non-Conventional Façade |          |        |
| Control System                      | Feed-Forward        | Feedback     | Feed-Forward | Feed-Forward            | Feedback |        |
| No. of System                       | 8                   | 4            | 4            | 4                       | 0        |        |
| Type of BPS Software                | Parametric Tools    |              |              | Non-Parametric Tools    |          |        |
| BPS Tool                            | Grasshopper/Rhino   | Dynamo/Revit | TRNSYS       | EnergyPlus              | IES-VR   | IDbild |
| Plugin built in                     | Ladybug/Honeybee    | DIVA         |              | EMS                     |          |        |
| No. of System/<br>Geometrical Based | 8                   | 5            | 3            | 2                       | 4        | 2      |
| No. of System/<br>Materials Based   | 1                   | 0            | 1            | 0                       | 3        | 0      |

Figure 2.17: Analysis of existing studies regarding simulation tools used to simulate AFs.

As examples of dynamic conventional façades, Yun et al. (2014) developed a motorised Venetian blinds (conventional façade) in an office space in South Korean to investigate the impact of the system on energy and visual comfort. EnergyPlus and Diva-for-Rhino were used to evaluate various lighting and shade control strategies, each of which was actuated by an illuminance level threshold monitored by two indoor and outdoor sensors. Another

## **CHAPTER 2: LITERATURE REVIEW**

study conducted by Konstantoglou et al. (2013) studied seven different control strategies to automate a dynamic louvre (conventional façade) in an office room in Greece. EnergyPlus was used to evaluate the system's overall energy consumption for lighting, cooling, and heating with hourly and annual adjustments of the slat angles. A control logic and illuminance level threshold strategy were defined to maximise daylighting, block glare, and connect to the outdoor environment while reducing energy by 25% compared to static shading systems.

Hammad and Abu-Hijleh (2010) examined the effect of dynamic louvers on the lighting and heating, ventilation, and air-conditioning (HVAC) energy consumption of an office space in Abu Dhabi with the goal of achieving the lowest possible energy consumption. The Integrated Environmental Solutions (IES) simulation tool was used to model and evaluate a variety of slat angles. Tzempelikos and Athienitis (2007) developed a dynamic conventional roller shade for an office space in Montreal, Canada with the aim of reducing lighting and cooling energy using simulation. The shading device is controlled by incident solar radiation on windows.

In addition, Tabadkani et al. (2020) proposed an innovative control system for assessing the annual energy demands of AF which considers the dynamic behaviour of the shading system with a basic movements on an hourly basis. The authors employed the Honeybee tool, which was linked to the EnergyPlus engine as the most-used tool for AF modelling together with the EMS, which allows users to define a control logic based on one sensor or multiple sensors and to actuate the slat angle on hourly time steps based on the predefined control scheme (Crawley 2007). In this research, two different methods were conducted to translate the hourly slat angle into fractions: (1) SF calculations and (2) solar transmittance schedule.

Another study by Kim et al. (2015) compared the cooling energy consumption of complex kinetic shading (origami) with basic fixed shading in office spaces in Abu Dhabi. Modelling was carried out using Revit and Dynamo, and energy simulation was calculated using the eQUEST software after simplifying the kinetic façade. The authors implemented an open control system that was activated by the incidence angle between the sun's direction vector and the normal vector of a surface, which defined the opening ratio of each panel individually. They discovered that the smaller openings consumed less energy but did not take daylighting performance into consideration. The methods that were followed is complex due to the use of different tools within different environment.

Pesenti et al. (2015) developed a non-conventional shading system for office buildings to meet human comfort requirements while reducing energy consumption for cooling, heating,

## **CHAPTER 2: LITERATURE REVIEW**

and artificial lighting. The study assessed the following visual comfort parameters – Useful Daylight Illuminance (UDI), Daylight Autonomy (DA), and Daylight Glare Probability (DGP) – as well as the Total Energy Consumption (TE). To adapt to outdoor solar conditions, a design strategy was followed that combined origami pattern techniques with the usage of shape memory alloys (SMA) as micro-actuators. The Ron Resch Origami pattern was chosen for the study because of its flexibility when reacting in a variety of directions. Moreover, a comparison of several origami patterns was tested in terms of no shading against complete shading. The analysis was conducted using the parametric tools Grasshopper, Honeybee, and Ladybug in conjunction with EnergyPlus to examine various shading system modifications. However, a control system wasn't considered properly for energy calculations during the simulation. They observed that increasing the amount of shaded space resulted in an improved energy performance.

Kuru et al. (2021) proposed a simulation approach for modelling and simulating a complex origami-inspired biomimetic AF that changes its form and physiology simultaneously through photovoltaic (PVC) glazing and spring-activated openings. The framework of their methodology included generating configurations, calculating performance descriptors, linking performance descriptors to environmental variables, and evaluating the environmental performance of multifunctional Bio-ABS (Kuru et al. 2021). Additionally, they examined the difficulties related to predicting the performance of AF systems using the current available tools. Two control logics were implemented: the SMA springs generate movement in response to variations in the material's surface temperature, while the PVC glazing generates opacity changes in response to changes in the SI levels. The control system was programmed to adapt to the defined surrounding climatic conditions using EnergyPlus and its built-in feature EMS for the PVC glazing system. The authors concluded that when compared to conventional façades, Bio-ABS improve building performance, "reaching 37.1% for 90% acceptability limits and 18% for 80% acceptability limits for adaptive thermal comfort".

In the case of adaptive smart materials such as PVC glazing, as mentioned earlier, several researchers have successfully developed this technology as an adaptive skin for buildings that changes its material properties, such as U-value and  $T_{vis}$ , in response to climatic data using current PBS tools. This review included a few studies on smart adaptive materials, as this thesis focuses on AFs that modify their geometry in response to changing environmental circumstances over time through the employment of an appropriate control strategy system.

## CHAPTER 2: LITERATURE REVIEW

Based on current studies, 48% of developed AF models did not implement an automatic control system. An automatic system was applied mostly with conventional façades; 39% of studies used a feedforward control system, while 13% used a feedback control system to automate the façade. The analysis also showed that most studies simulated the AFs based on hourly timeframe changes Figure (2.18).

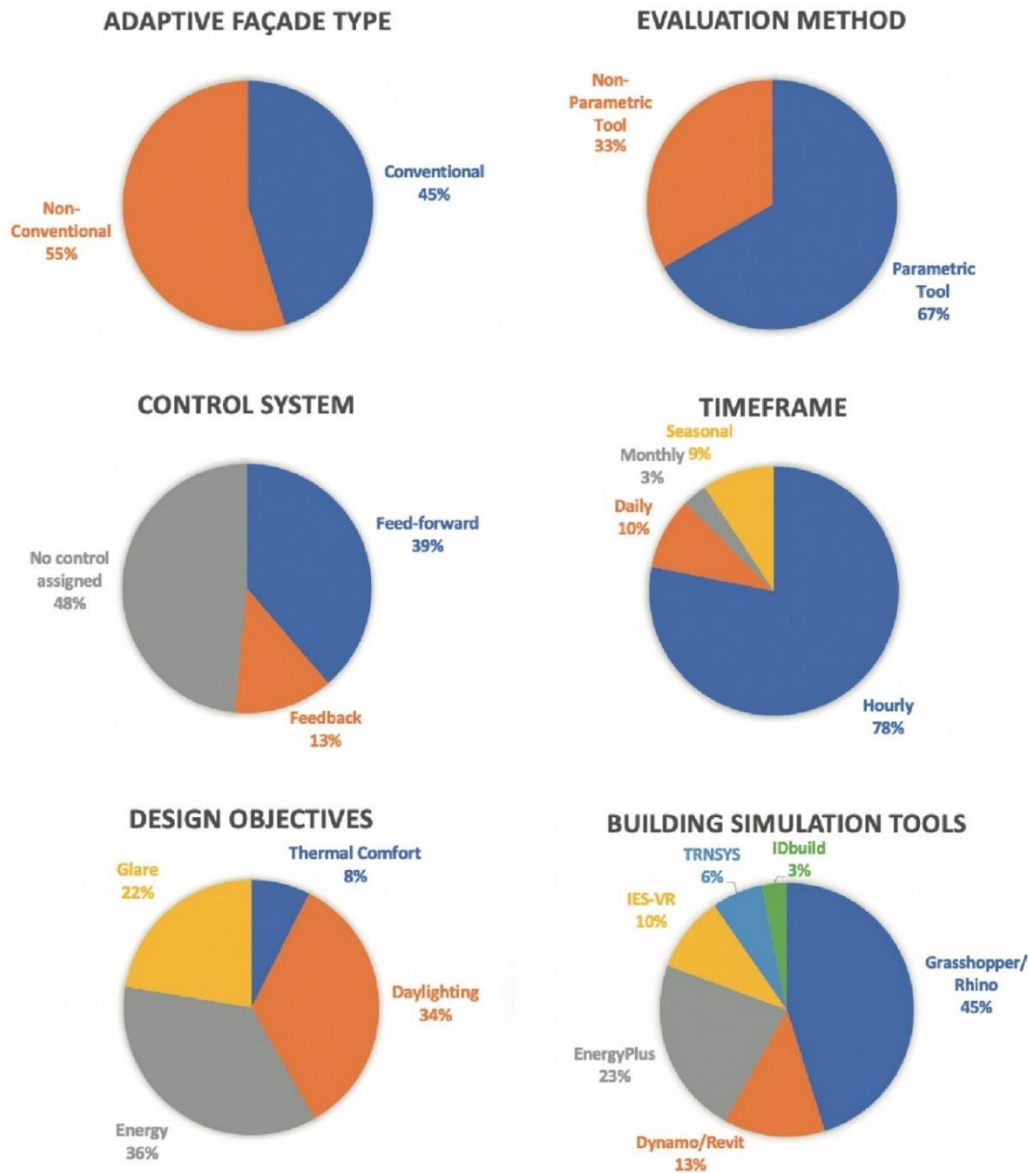


Figure 2.18: Analysis of current studies of AFs systems that used BPS tools.

## CHAPTER 2: LITERATURE REVIEW

Table 2.2. Current research of BPS of adaptive façades in literature.

| Adaptive Façade |                                   |  |   |                    |               |                  | Adaptability      |         |        |                    |                 |           | Performance    |  |                  |   |                   |             |        |       |          |
|-----------------|-----------------------------------|--|---|--------------------|---------------|------------------|-------------------|---------|--------|--------------------|-----------------|-----------|----------------|--|------------------|---|-------------------|-------------|--------|-------|----------|
| ID              | Reference                         | System   | Location                                      | Climate            | Building Type |                  | Adaptive Typology | State   |        | Changing Behaviour |                 | Timeframe | Configurations | Evaluation Method(s)                       | Control Strategy | Control Sensors                                 | Design Objectives |             |        |       |          |
|                 |                                   |  |   |                    | Conventional  | Non-Conventional |                   | Dynamic | Static | Geometrical Based  | Materials Based |           |                |  |                  |   | Thermal Comfort   | Daylighting | Energy | Glare | View Out |
| 1               | (Tzempelikos and Athienitis 2007) | Roller shade   | Canada/ Montreal                              | Humid continental  | O             | ✓                | BM                | ✓       |        | ✓                  |                 | D         | 6              | TRNSYS                                     | FF               | Solar radiation                                 |                   | ✓           | ✓      |       |          |
| 2               | (Nielsen et al. 2011b)            | Automated blinds   | Denmark                                       | Temperate          | O             | ✓                | BM                | ✓       |        | ✓                  |                 | H         | 3              | iDbuild                                    | F                | Indoor temperature                              |                   | ✓           | ✓      | ✓     |          |
| 3               | (Tabadkani et al. 2018)           | Rosette pattern  | Tahran/Iran                                   | Hot-arid           | O             |                  | CM                | ✓       |        | ✓                  |                 | S         | 6480           | DIVA /Grasshopper                          | N                | Task illuminance                                |                   | ✓           |        | ✓     |          |
| 4               | (`wdqTabadkani et al. 2020)       | Venetian blinds  | Melbourne, Australia                          | Temperate          | O             | ✓                | BM                | ✓       |        | ✓                  |                 | H         | 4              | Honeybee (EnergyPlus, (EMS)/Daysim)        | F                | Daylight Glare Index (DGI) and task illuminance |                   | ✓           | ✓      | ✓     |          |
| 5               | (Giovannini et al. 2019)          | Thermochromic glazing  | Abu Dhabi (UAE)/ Turin (ITA)/ Östersund (SWE) | Different climates | O             |                  | SM                | ✓       |        |                    | ✓               | H         | 5              | Honeybee (EnergyPlus, Daysim) Python (EMS) | N                | Surface temperature                             |                   | ✓           | ✓      |       |          |
| 6               | (Giovannini et al. 2015)          | Shape Variable Mashrabiya (SVM)                                      | UAE/ Abu Dhabi                                | Hot-arid           | O             |                  | CM                | ✓       |        | ✓                  |                 | H         | 3              | DIVA- Grasshopper /EnergyPlus              | FF               | Sun position                                    |                   | ✓           | ✓      |       |          |
| 7               | (Kim et al. 2015)                 | Origami  | UAE/ Abu Dhabi                                | Hot-arid           | O             |                  | CM                | ✓       |        | ✓                  |                 | H         | 10             | Dynamo/Revit/ GBS/ eQUEST                  | FF               | Sun position                                    |                   |             | ✓      |       |          |
| 8               | (Bui et al. 2020)                 | Electrochromic glazing   | Melbourne, Australia                          | Temperate          | O             |                  | SM                | ✓       |        |                    | ✓               | H         | 5              | Revit, GBS, Eppy (Python, EnergyPlus)      | FF               | Surface temperature                             |                   | ✓           | ✓      | ✓     |          |
| 9               | (Borkowski et al. 2018)           | Adaptive blinds  | London, UK                                    | Temperate          | O             | ✓                | BM                | ✓       |        | ✓                  |                 | H         | 6              | EnergyPlus EMS Dymola                      | FF               | Solar radiation                                 |                   |             | ✓      | ✓     |          |
| 10              | (Shi et al. 2020)                 | Transformable modules  | Singapore                                     | Tropical           | O             |                  | CM                | ✓       |        | ✓                  |                 | H         | 75             | Grasshopper (Honeybee & Ladybug)           | N                | Sun position                                    |                   | ✓           | ✓      |       |          |
| 11              | (ElGhazi and Mahmoud 2016)        | Origami  | Egypt/Cairo                                   | Hot-arid           | O             |                  | CM                | ✓       |        | ✓                  |                 | H         | 3              | DIVA-Grasshopper                           | N                | -   |                   | ✓           |        |       |          |
| 12              | (Hammad and Abu-Hijleh 2010)      | Dynamic Louvres  | UAE/ Abu Dhabi                                | Hot-arid           | O             | ✓                | BM                | ✓       |        | ✓                  |                 | H         | 18             | IES-VR                                     | N                | -   |                   |             | ✓      |       |          |
| 13              | (Kuru et al. 2021)                | Photovoltachromic (PVC) glazing)/ origami-like folding component/SMA | Sydney, Australia                             | Humid subtropical  |               |                  | B SM CM           | ✓       |        | ✓                  | ✓               | H         | 600            | EnergyPlus /EMS                            | FF               | Solar irradiance/ surface temperature           | ✓                 |             |        |       |          |
| 14              | (Sheikh and Asghar 2019)          | Folding external shading   | Lahore, Pakistan                              | Hot-humid          | O             |                  | B                 | ✓       |        | ✓                  |                 | H         | 3              | Revit/Insight 360 Ecotect                  | N                | Solar radiation                                 |                   | ✓           | ✓      |       |          |

**CHAPTER 2: LITERATURE REVIEW**

| Adaptive Façade |                             |  |   |                    | Adaptability  |              |                  |                   |         |        |                    |                 | Performance |                |  |                  |  |                   |             |        |       |          |
|-----------------|-----------------------------|--|---|--------------------|---------------|--------------|------------------|-------------------|---------|--------|--------------------|-----------------|-------------|----------------|--|------------------|--|-------------------|-------------|--------|-------|----------|
| ID              | Reference                   | System   | Location                                | Climate            | Building Type | Conventional | Non-Conventional | Adaptive Typology | State   |        | Changing Behaviour |                 | Timeframe   | Configurations | Evaluation Method(s)   | Control Strategy | Control Sensors  | Design Objectives |             |        |       |          |
|                 |                             |  |   |                    |               |              |                  |                   | Dynamic | Static | Geometrical Based  | Materials Based |             |                |  |                  |  | Thermal Comfort   | Daylighting | Energy | Glare | View Out |
| 15              | (Hosseini et al. 2019a)     | Two, and three-dimensional shape- change façades | Yazd, Iran                              | Hot-arid           | O             |              | ✓                | CM                | ✓       |        | ✓                  |                 | H           | 36             | Honeybee (EnergyPlus) DIVA (Radiance)                        | N                | Sun position   | ✓                 | ✓           |        | ✓     |          |
| 16              | (Masera et al. 2018)        | Origami shading with SMAs                        | Milan, Italy                            | Humid subtropical  | O             |              | ✓                | CM                | ✓       |        | ✓                  |                 | H           | -              | Honeybee (EnergyPlus) DIVA (Radiance)                        | N                | -  |                   | ✓           | ✓      | ✓     |          |
| 17              | (Tabadkani et al. 2019a)    | Hexagonal adaptive solar façade                  | Tehran, Iran                            | Hot-arid           | O             |              | ✓                | CM                | ✓       |        | ✓                  |                 | H           | 1800           | Grasshopper (Honeybee & Ladybug)                             | N                | Daylight Glare Index (DGI)   |                   | ✓           |        | ✓     |          |
| 18              | (Lee 2019)                  | Vertical panels, wedge-shaped flat planes        | Abu Dhabi, Hanoi, and Seoul             | Different climates | O             |              | ✓                | CM                | ✓       |        | ✓                  |                 | H           | 10             | IES, VE/ SketchUp  | N                | Solar radiation  |                   |             | ✓      |       |          |
| 19              | (Favoino et al. 2015)       | Adaptive photochromic glazing                    | Helsinki, London, and Rome              | Different climates | O             |              | ✓                | SM                | ✓       |        | ✓                  |                 | H           |                | EnergyPlus EMS   | FF               | Surface temperature  | ✓                 |             | ✓      |       |          |
| 20              | (Pesenti et al. 2015)       | Ron Resch Origami shading with SMAs              | Milan, Italy                            | Humid subtropical  | O             |              | ✓                | CM                | ✓       |        | ✓                  |                 | H           | 3              | Grasshopper (Honeybee & Ladybug) EnergyPlus                  | N                |  |                   | ✓           | ✓      | ✓     |          |
| 21              | (Grobman et al. 2017)       | Dynamic louvres                                  | Mediterranean region                    | Mediterranean      | O             | ✓            |                  | BM                | ✓       |        | ✓                  |                 | H           | -              | Grasshopper, DIVA, Radiance/DAYSIM                           | N                | Sun position   |                   | ✓           |        |       |          |
| 22              | (Konstantoglou et al. 2013) | Dynamic louvres                                  | Greece                                  | Mediterranean      | O             | ✓            |                  | BM                | ✓       |        | ✓                  |                 | H           | 7              | EnergyPlus   | F                | Illuminance levels, Daylight Glare Index (DGI)                                     |                   | ✓           | ✓      | ✓     |          |
| 23              | (Ricci et al. 2020)         | Self-adaptable panels                            | Copenhagen, Munich, Bologna, and Athens | Different climates | O             |              | ✓                | BM                | ✓       |        | ✓                  |                 | H           | -              | Grasshopper (Honeybee & Ladybug)/ EnergyPlus                 | N                | Illuminance, air, temperature, relative humidity, solar radiation, air temperature | ✓                 | ✓           | ✓      |       |          |
| 24              | (Eltaweel and Su 2017b)     | Automated Venetian blinds                        | Egypt/Cairo                             | Hot-arid           | O             | ✓            |                  | BM                | ✓       |        | ✓                  |                 | S           |                | Grasshopper (Honeybee & Ladybug)/ Radiance/DAYSIM EnergyPlus | FF               | Sun position, sun direction  |                   | ✓           |        | ✓     |          |
| 25              | (Kasinalis et al. 2014)     | Venetian blinds                                  | Netherlands                             | Temperate          | O             | ✓            |                  | BM                | ✓       |        | ✓                  |                 | S           | 7              | TRNSYS/ DAYSIM   | FF               | Indoor temperature, solar radiation  | ✓                 |             | ✓      |       |          |
| 26              | (Yun et al. 2014)           | Venetian blinds                                  | South Korea/ Seoul                      | Humid subtropical  | O             | ✓            |                  | BM                | ✓       |        | ✓                  |                 | H           | 4              | EnergyPlus, Grasshopper, DIVA                                | F                | Illuminance level  |                   | ✓           | ✓      | ✓     |          |
| 27              | (Skarning et al. 2017)      | Roller shade                                     | Italy /Rome-Copenhagen                  | Multi climate      | R             | ✓            |                  | BM                | ✓       |        | ✓                  |                 | H           | 4              | EnergyPlus   | FF               | Solar radiation, outdoor temperature   |                   | ✓           | ✓      |       |          |
| 28              | (Touma and                  | Venetian blinds                                  | Qatar                                   | Hot-arid           | O             | ✓            |                  | BM                | ✓       |        | ✓                  |                 | H           | 3              | EnergyPlus   | FF               | Solar radiation,   |                   | ✓           | ✓      | ✓     |          |

**CHAPTER 2: LITERATURE REVIEW**

| Adaptive Façade |                          |                                   |                        |                  |               |   |                  | Adaptability      |         |        |                    |                 |           | Performance    |                      |                  |                     |                   |             |        |       |          |
|-----------------|--------------------------|-----------------------------------|------------------------|------------------|---------------|---|------------------|-------------------|---------|--------|--------------------|-----------------|-----------|----------------|----------------------|------------------|---------------------|-------------------|-------------|--------|-------|----------|
| ID              | Reference                | System                            | Location               | Climate          | Building Type |   | Non-Conventional | Adaptive Typology | State   |        | Changing Behaviour |                 | Timeframe | Configurations | Evaluation Method(s) | Control Strategy | Control Sensors     | Design Objectives |             |        |       |          |
|                 |                          |                                   |                        |                  | Conventional  |   |                  |                   | Dynamic | Static | Geometrical Based  | Materials Based |           |                |                      |                  |                     | Thermal Comfort   | Daylighting | Energy | Glare | View Out |
|                 | Ouahrani 2017)           |                                   |                        |                  |               |   |                  |                   |         |        |                    |                 |           |                |                      |                  | indoor temperature  |                   |             |        |       |          |
| 29              | (Cannavale et al. 2018)  | Electrochromic smart window       | Rome, Italy            | Mediterranean    | O             | ✓ |                  | SM                | ✓       |        |                    | ✓               | D         | 8              | EnergyPlus           | -                | Surface temperature |                   | ✓           | ✓      | ✓     |          |
| 30              | (Sadek and Mahrous 2018) | Thermochromic glazing material    | Cairo, Egypt           | Hot-Arid         | R             | ✓ |                  | SM                | ✓       |        |                    | ✓               | H         | -              | EnergyPlus/ EMS      | FF               | Surface temperature |                   |             | ✓      |       |          |
| 31              | (Elzeyadi 2017)          | Six typologies of kinetic shading | ASHRAE Climate zone 4C | Moderate climate | O             |   | ✓                | BM, CM, SM        | ✓       |        | ✓                  |                 | -         | -              | IES-VR               |                  | Glare               |                   | ✓           | ✓      | ✓     |          |

**Type of the Building:** O: office building, E: educational building, R: residential building

**Adaptive Typology:** BM: basic movement, CM: complex movement, B: biomimetic, SM: smart material

**Timeframe:** H: hourly, D: daily, M: monthly, S: Seasonal, A: annual

**Control Strategy:** FF: feedforward, F: feedback, N: no control assigned



## **2.6. Challenges for Performance Prediction of Adaptive Façades**

Innovative materials and technologies have been developed in the AF field, and these can be enhanced with the use of building performance predictions. Additionally, in the design of AFs, it is crucial to predict the building performance accurately to achieve high performance buildings. Therefore, assessing the applicability of AFs during the early stages of the design is extremely significant, but it is mostly restricted to the existing simulation tools for faster quantification (Tabadkani et al. 2021a). Geyer and Singaravel (2018) indicated the importance of the early integration of performance in design processes, while Loonen et al. stated that predicting the performance of buildings with AFs is a challenging task that is mostly determined by the local boundary conditions, interactions with the building's users, and other building systems. When modelling and simulating an AF system, the façade system must be represented as a sequence of time-varying states or properties rather than as a static representation. The authors also examined the methods of simulation in both conventional static building envelopes and adaptive envelopes. In traditional static envelopes, the simulation process is less complex and requires some factors, such as the U-value and g-value for predictions to be made. On the other hand, an AF is more complex and has a variety of factors, which makes accurately predicting the building performance of an AF more challenging. Some of these factors are (1) the time variation behaviour, (2) modelling the dynamic operation of the façade adaptation, and (3) the multi physical domains. Therefore, some of the existing simulation tools were not developed for predicting performance with an AF specifically. Moreover, some of these tools are limited and provide misleading information for adaptive systems (Loonen et al. 2017). Two main factors that determine the applicability of AFs are as follows:

- **Modelling time-varying façade properties:** Façade specifications (i.e., material properties or position of components) need to be changeable during simulation runtime to properly account for transient heat transfer and energy storage effects in building constructions" (Loonen et al. 2017). Many state-of-the-art BPS tools have restricted functionalities for accomplishing this feature.
- **Modelling the dynamic operation of façade adaptation:** During the operation of adaptive systems, the performance of the system is entirely dependent on the scheduling strategy (i.e., control logic) that is utilised to change the façade.

## **CHAPTER 2: LITERATURE REVIEW**

Favoino et al. (2018) highlighted the issues regarding the existing building performance simulations of AFs and concluded that the information in this subject is fragmented. Loonen et al. also stated that designers and researchers who aim to assess an AF system with the current BPS tools are faced with different challenges, and to overcome these obstacles, they need to find a workaround to develop their simulation strategy. In addition, according to the literature, most designers evaluate AF with their own simulation strategy because there is no straightforward approach to assess the performance of AFs for energy performance (Attia 2019). Therefore, inaccurate results might be obtained when assessing their performance and applicability in the long term (Tabadkani et al. 2020).

### **2.7. BPS Tools and their Ability to Simulate Time Changes**

There are several tools available for estimating a building's energy performance. Each software program is unique in terms of model resolution, solution algorithms, intended target audience, modelling possibilities, and simplicity of use vs. flexibility, among other characteristics (Loonen et al. 2017). Software with the most advanced modelling capabilities and the most extensive validation studies are all legacy software simulation packages (e.g., EnergyPlus, ICE, ESP-r, TRNSYS, and IES VE) (Loonen et al. 2017). Even though these tools have active development communities and receive regular updates and enhancements to their modelling capabilities, their fundamental concepts and software architecture remain constant. The majority of tools were developed at a time when the adaptability of building components was not a concern for architects and engineers (Oh and Haberl 2016). As a result, these tools often do not permit modifying the shape of the building or its material properties during the simulation run, which limits the possibilities for simulating adaptive building envelope systems (Loonen 2018; Favoino 2016). However, existing parametric tools allow the integration with EnergyPlus which makes it feasible to simulate and model the time-variation of AF systems.

EnergyPlus has seen the largest increase in AF computational capabilities. EnergyPlus Runtime Language (ERL) is primarily responsible for these enhancements (Crawley 2007). By connecting sensors, control, and actuators, the ERL allows users to incorporate several EMS into their systems. Some examples of EMS actuators include the thermophysical characteristics of the building envelope materials. During simulation running, these actuators can be modified using user-defined IF-ELSE statements.

Parametric tools have been used to simulate different AF systems with shifting morphologies. For example, Grasshopper and Dynamo are two parametric tools that work in conjunction with architectural 3D modelling software which allow for the parametric control

## **CHAPTER 2: LITERATURE REVIEW**

and modelling of adaptive system design. In addition, these plugins assist in decision-making via the addition of add-ons such as Ladybug/Honeybee, which integrate simulation engines such as EnergyPlus. Furthermore, by utilising parametric modelling tools, it is possible to incorporate add-ons that offer flexibility to the modelling process. As an example, Grasshopper can integrate Python into a workflow similar to that of an EMS, allowing for control customisation. To this end, parametric modelling tools indicate significant potential for modelling and simulating AFs that change their shape in response to time variations and incorporate control logic that takes into consideration surrounding environmental conditions.

Adaptive building materials are the focus of most research on systems with physiology-changing properties (Al-Masrani and Al-Obaidi 2019; Kuru et al. 2021). Several of the simulated smart materials incorporate various glazing methods. As previously stated, most of software programs are limited in their ability to simulate a variety of complex geometrical architectural components controlled by 'sensors.' While this is true for AFs with changing morphologies, modelling and evaluating their performance in Grasshopper using EnergyPlus EMS and Python is still achievable. Nonetheless, modelling and simulating AFs that change geometrically continue to be a challenge with current PBS tools, and they were investigated in a very limited number of studies (Sheikh and Asghar 2019).

### **2.7.1. Parametric Tools**

The improvements in parametric design tools have had an impact on the architectural design process by allowing designers to express their creativity while still maintaining design dependencies and links between iterations. As a result, architects employ these tools to keep control over design parameters, enabling them to examine and optimise design solutions for a variety of architectural problems throughout the early stages of the design (Eltaweel and SU 2017). The term "parametric" refers to the method of digitally modelling a series of design iterations whose relationships to one another are determined by one or more mathematical relationships (parameters), which results in the creation of a parametric form capable of compressing a large number of related but distinct shapes (Eltaweel and SU 2017).

Parametric tools have been utilised to evaluate the performance of adaptive systems in recent years. A significant advantage of using parametric tools is that users can make changes to any parameter without having to repeat the procedure and generate new designs. Furthermore, it allows for the exploration of new forms in relation to a variety of parameters, assisting architects and designers in proposing ideal designs and behaviours

## **CHAPTER 2: LITERATURE REVIEW**

that adaptable to a range of different climates and environmental situations. Bacha and Bourbia (2016) stated that parametric tools can be utilised as a design tool since they permit users to develop complex models and use them during the early phases of design with numerous design values for certain context and scenarios. Hofer et al. (2016) demonstrated how parametric tools can be used to investigate the appearance of the building envelope and solar radiation from PV dynamic modules through the examination of module shading and SI, which can then be integrated with an electrical model to analyse electrical performance. The authors calculated the current voltage curves of PV modules to assess the electrical energy consumption associated with various parameters and module interconnections (Hofer et al. 2016).

### **2.7.2. Grasshopper**

Grasshopper is a parametric design tool developed in 2007 as a Rhinoceros software plugin by David Rutten, Robert McNeel, and associates (ElGhazi et al. 2014). It is a graphical algorithm editor that enables users to write customised scripts in VB.NET "(a version of Microsoft's Visual Basic that makes Web services applications easier to develop) or C# (a general object-oriented programming language for networking and Web development)" via various components, and model simple and complicated geometries (Hofer et al. 2016). This enables architects to easily generate parametric settings or forms without the need for scripting knowledge or any formal programming language. The integration of the Grasshopper interface with the Rhino modelling tool enables direct observation of Grasshopper algorithm modifications in Rhino. Moreover, the Grasshopper tool has commonly been utilised as a modelling tool among designers due to its ability to generate a variety of forms, its intuitive interface, and the quantity of plugins that significantly enhance its capability.

Hofer et al. (2016) designed a parametric shading system in the shape of a rectangular pattern using Rhinoceros 3D software and Grasshopper. Sharaidin et al. (2012) used Grasshopper in combination with Ecotect software to determine the ideal closing and opening percentages of a kinetic component based on daylight simulation. As a result, authors are able to achieve the most complex geometric configurations possible.

### **2.7.3. Parametric Integrated Simulation Tools**

Numerous Grasshopper plug-ins have been developed to facilitate the integration of parametric geometry with simulation software, such as the following:

### **2.7.3.1 Honeybee**

Honeybee integrates parametric models with validated tools, such as EnergyPlus, Radiance, Daysim, and OpenStudio, for the purpose of simulating energy and daylighting in buildings (Roudsari et al. 2013).

### **2.7.3.1. Ladybug**

Ladybug is an open-source environmental plugin for Grasshopper3D that assists in the development of an architecturally conscious approach to environmental design. The plug-in imports EnergyPlus Weather standard files (.EPW) into Grasshopper and generates a variety of interactive three-dimensional representations to assist in early design decision-making (Roudsari et al. 2013).

## **Part (C) Machine Learning (ML)**

### **2.8. Machine Learning (ML) – Overview**

Machine learning (ML) is a branch of artificial intelligence (AI) that allows the software to learn without being explicitly programmed (Chakraborty and Elzarka 2019). Mitchell (1997a) defined it as a system that learns from past experience (i.e., data) to predict future performance (Mitchell 1997b). In other words, ML could use existing data to predict or to respond to future data. After training and learning, it is expected that the system should obtain a better predictive performance on the same trained task or related tasks. As well as the idea of self-improving automatically, ML also offers other advantages, such as collecting and clustering useful information from a complex large set of data (Chakraborty and Elzarka 2019).

Over the last years, ML algorithms have become widely popular in several fields, such as marketing, social media services, medicine, architecture, design etc. For example, existing medical records can be integrated with ML to form a knowledge source to diagnose new patients (Oh et al. 2011). Similarly, in the architecture field, ML has been proposed in several studies to estimate heating and cooling loads, building performance, annual energy consumption predications, and architectural image recognition (Seyedzadeh et al. 2018). Nevertheless, the architecture field is considered one of the slowest industries to integrate ML, and it has resisted adopting it compared to other fields (Khean et al. 2018). Carpo (2017) argued that architecture seems to be disregarding the potential of ML and its ability to predict performance, categorise large sets of data, and form optimisation and advanced form findings.

## CHAPTER 2: LITERATURE REVIEW

ML algorithms can be categorised into distinct learning types: supervised learning, unsupervised learning, and reinforcement learning. Figure (2.19) shows the main approaches of ML algorithms in a graphical way including some examples of the algorithms used in each approach and examples of applications (Rafique and Velasco 2018). This research focuses on the supervised ML in the regression approach.

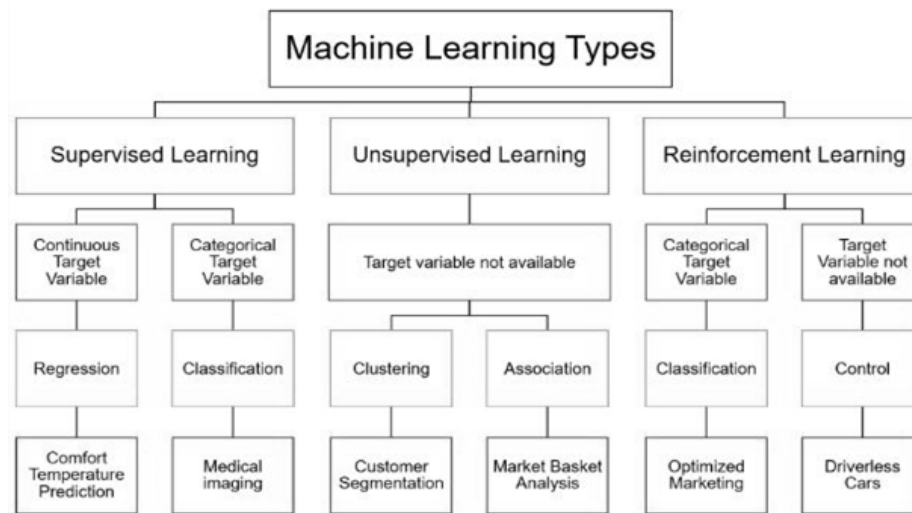


Figure 2.19: Types of machine learning (adapted from Ramasubramanian and Singh, 2019).

### **2.8.1. Supervised Learning (SL)**

In supervised learning (SL), the learning system is trained with a set of inputs and the corresponding desired outputs, where the outputs are known and are labelled data. In this process, the learning system should learn the relationship between input-output data before training the system Figure (2.20). Once the system is trained, it can predict the desired output with the new presented data (Koola et al. 2016). Similarly, humans are likely to be able to predict new outcomes once they have learned from previous examples (Koola et al. 2016). The training process in this approach is usually done by humans and has a significant impact on the quality of the outcomes data. Therefore, the pre-processing of trained data, inconsistencies, contradictions, and other errors are all important factors that need to be considered in SL. Additionally, the training data should be sufficient, and have a range of all the potential inputs and desired output (Hopmann et al. 2017). SL algorithms can be classified also into different learning algorithms; however, the most popular SL algorithms are backpropagation neural networks, deep learning neural networks, support vector machines, linear regression, decision trees, and Bayesian networks (Koola et al. 2016). The neural network is chosen in this study because it has shown in several studies its sufficiency in the prediction of building performance (Zhao and Magoulès 2012a).

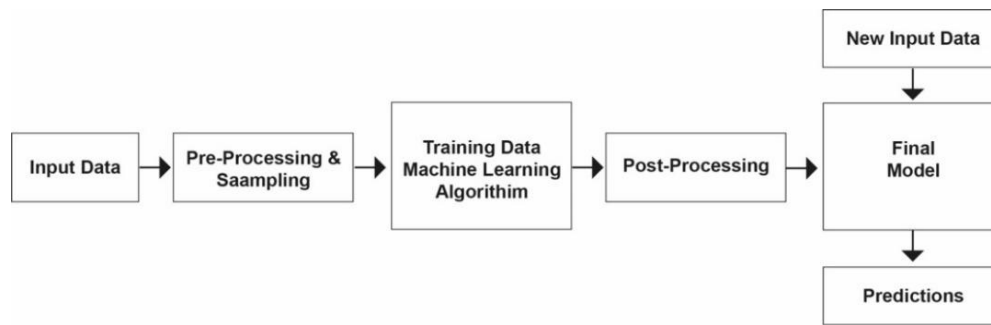


Figure 2.20: Supervised machine learning process (adapted from Alaaeddine and Wu 2020).

### 2.8.2. Unsupervised Learning (USL)

In unsupervised learning, the expected result is not known before initiating the analysis of the data (Mat Daut et al. 2017). Numerous studies on unsupervised learning have been conducted in the fields of data visualisation and classification as applications of unsupervised learning. The most used unsupervised learning technique is clustering (Raza and Khosravi 2015). For instance, Papadopoulos et al. (2018) used unsupervised learning with k-means clustering to effectively cluster the energy consumption of a mixed group of commercial and residential buildings (Papadopoulos et al. 2018).

### 2.9. Surrogate Model for Building Performance

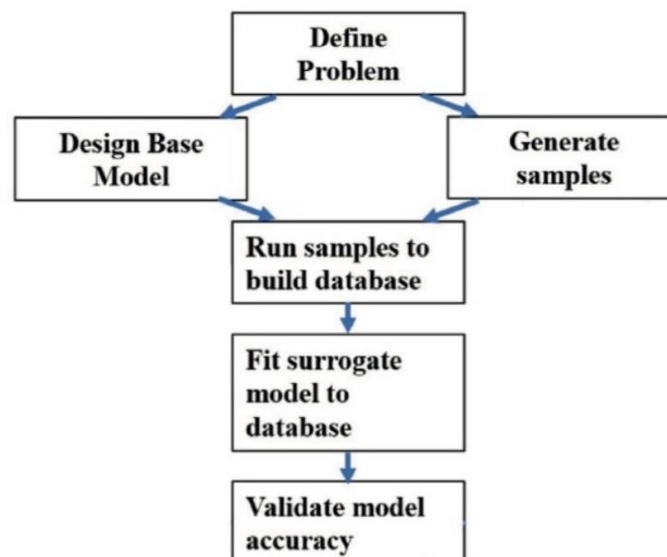
Surrogate models (SM), also known as meta-models, have the promise of providing a building's performance assessment that is significantly faster than simulation-based methods. Moreover, surrogate modelling is a statistical approach to emulate a high-fidelity, high-cost model, in this case, a building simulation model. The surrogate model is trained using a set of simulated input and output data. Once proven to accurately approximate the detailed simulation model, it can be used to almost instantaneously anticipate the outcomes of the high-fidelity simulation given an adequate collection of building design data. According to the literature, surrogate modelling is found to considerably assist four stages of the building design process: conceptual design stage, sensitivity analysis, uncertainty analysis, and optimisation (Westermann and Evins 2019b). Regarding the early design stages, building simulation is currently unable to keep up with the speed in this stage (Østergård et al. 2016). Because setting up a simulation to test a single concept requires the manual definition of a large number of parameters. Thus, the creativity process of the architect will be disrupted by the simulation's lengthy run time, which is better described as the program's feedback time (Miller 1968).

Surrogate modelling enables two distinct modes of engagement between the architect and the process of building simulation. First, because surrogates are evaluated instantaneously

## **CHAPTER 2: LITERATURE REVIEW**

(<0.01 seconds ), they can provide instant point estimates or probability distribution estimates of the building's performance (Van Gelder et al. 2014; Westermann and Evins 2019b). This enables designers to conduct a more rapid analysis and exploration of design concepts. Another advantage of surrogate models over simulation-based parametric analysis is that they establish a constant connection between design variables and building performance measures. The complexity of recent surrogate models enables them to capture variable interactions and extract non-linear, multi-modal behaviour (Østergård et al. 2017). Additionally, surrogate models have a simple computational layout and can be easily integrated into existing modelling tools (Ritter et al. 2015).

To create a surrogate model, it is necessary to identify the design issue and the associated design parameters. The building designer then creates an initial model of the building and selects design samples for simulation using a sampling approach. For each sample, the underlying model is changed, and building simulations are run using the parameters defined for each sample. After that, the simulation results are stored in a database. Following that, the input-output data are fitted with a surrogate model. Finally, the model is validated by determining its accuracy and quantifying the difference in prediction accuracy between surrogate predictions and simulation outcomes for a given set of inputs (Westermann and Evins 2019b). The stages involved in developing a surrogate model are represented in Figure (2.21).



*Figure 2.21: Stages to develop ML surrogate models (Westermann and Evins 2019b).*

Performing a surrogate derivation in a sequential manner is the most common method. After samples have been generated, the surrogate model is fitted. Because the samples are defined in advance of the simulation and are not altered in response to the model results,



## **CHAPTER 2: LITERATURE REVIEW**

this strategy is referred to as static sampling. This offers a global surrogate model that is accurate for the entire design space. On the other hand, in adaptive sampling, the database is expanded iteratively based on surrogate predictions and simulation outcomes. Most of the researchers adopted adaptive sampling for optimisation purposes (Westermann and Evins 2019). Westermann and Evins (2019) stated that 81% of researchers used static sampling, while 19% used the adaptive sampling method depending on the objective of the model. The authors compared the two sampling methods and found that neither of the two sampling methods clearly outperforms the other. The results also showed that adaptive sampling may be considered if the sample size is very small (Westermann and Evins 2019a).

### **2.9.1. Data Pre-Processing**

Pre-processing of data is critical for any data-driven method, as any wrong or inconsistent data might lead to inaccurate results. Numerous studies have demonstrated that pre-processing data can help improve prediction accuracy when using ML algorithms (Kuster et al. 2017; Amasyali and El-Gohary 2018; Zhang et al. 2021). Frequently, collected data contain errors, such as missing values, duplicate data, inconsistent data, noise, and outliers. The term "data pre-processing" refers to the process of cleaning, integrating, transforming, and/or sampling data (Hellerstein and Berkeley 2008). Data cleaning is the process of identifying and fixing, modifying, removing, and replacing incorrect or noisy data. For instance, data collected from sensors is frequently imprecise and incomplete. Data integration relates to the process of gathering multiple pieces of data from several sources into a single collection of data. For instance, data on external weather conditions and hourly electricity use are obtained from separate sources but integrated into a single dataset for training and testing purposes (Amasyali and El-Gohary 2018). Data transformation is the process of converting data into a format that the ML algorithm can understand. As a result, the network is able to identify patterns more easily and produce more accurate outputs. Each input data is scaled between 0 and 1 during the standard normalisation technique. Normalisation can be performed on individual input variables or on a collection of input variables. The normalisation technique may enhance the network's capacity for learning, resulting in more accurate predictions (Raza and Khosravi 2015). Data transformation includes normalisation, smoothing, aggregation/disaggregation, and/or generalisation of the data (Amasyali and El-Gohary 2018).

Surrogate modelling requires input and output data formats that are compatible with the chosen method. For instance, most approaches require numerical rather than category inputs. After that, categorical variables can be transformed into dummy variables. Once the

## **CHAPTER 2: LITERATURE REVIEW**

data is properly structured, it is divided into training and testing samples. A random separation sample of 20% of the data is suitable for training and testing (Westermann and Evins 2019b).

### **2.9.2. Model Training and hyperparameter tuning**

Following data preparation, a specific training technique is utilised to determine the data's parameters and weights. To train ANNs, for example, the well-known backpropagation technique is used. Along with the model weights for training, hyper-parameters must be specified. Hyper-parameters make it possible to fine-tune the variance of the surrogate's predictions by adjusting their values. They should be tuned to achieve a good balance between variance and bias to avoid overfitting the model to the training data. A model that is overfitted performs poorly when applied to new data. In order to determine the hyperparameters, multiple different settings are evaluated in a grid search or K-fold cross validation technique (Claesen and De Moor 2015). In addition, the tuning of hyperparameters may be performed manually using rules-of-thumb. However, these approaches fall short of reproducibility requirements and are impracticable when the number of hyperparameters is large. As a result of these shortcomings, the idea of automating the hyperparameter search is gaining attention in ML. Automated techniques have already been demonstrated to outperform a manual search on several problems. According to Ayoub (2020), the

“key hyperparameters to tune ANN before training include: the number of hidden layers; the number of hidden neurons; the learning rate that defines the update frequency to adjust the errors; the number of epochs that identifies the number of iterations such ANN undergoes for the whole training dataset; the batch size to control the number of propagated training samples through the network before updating the model; and the activation function that introduces non-linear properties to ANN and converts inputs of neurons to outputs”.

### **2.9.3. Performance evaluation**

Model testing is the process of evaluating a prediction model using established evaluation criteria. Validation of the model is carried out utilising dedicated test data. There is a variety of performance indicators to quantify the model's accuracy and determine the model's precision. Based on the literature, most used metrics include the mean absolute error (MAE), root mean squared error (RMSE), and coefficient of determination ( $R^2$ ), which

## **CHAPTER 2: LITERATURE REVIEW**

measures how much of the variance in the data is explained by the model (Raza and Khosravi 2015).

### **2.9.4. Data Types**

Three types of data are used to develop a surrogate model: (1) real data (e.g., smart meters, internet of things (IoT) sensors, and building management systems), (2) simulated data (results of building simulation tools), and (3) public stock data (e.g., annual energy demand and floor area for a large set of buildings) (Amasyali and El-Gohary 2018; Westermann and Evins 2019b).

Real data can be obtained from a variety of sources, including utility bills, energy assessments, smart meters, sensors, building management systems (BMS), and weather stations (Westermann and Evins 2019b). For instance, sensor-based techniques have a number of benefits and drawbacks that must be evaluated. A sensor-based technique offers real-time data on the indoor environment and energy usage levels. However, there is an added expense and effort that comes with installing sensors, not only in terms of installation but also in terms of testing and ensuring the quality of the data obtained (Edwards et al. 2012). Furthermore, sensor data may contain noise, missing values, and/or outliers, reducing the performance of prediction models.

Simulated data that can be collected using existing simulation tools, such as EnergyPlus, allow the designer to simulate a real or hypothetical building and collect the necessary data (Wong et al. 2010; Keshtkarbanaeemoghadam et al. 2018). According to Li et al. (2015), existing software tools for measuring the efficiency of energy-saving techniques in buildings are sometimes insufficient. While real data are preferred, simulations are a viable alternative when it is impossible or impractical to instrument a building for technical and/or financial reasons.

Other studies have used publicly available benchmark datasets, such as the ASHRAE and the CIBSE dataset, which can be easily accessible. With this type of data collection, it is possible to compare the performance of different models (Edwards et al. 2012; Hong et al. 2014; Paterson et al. 2017; Chakraborty and Elzarka 2019).

### **2.10. Artificial Neural Networks (ANN) - Overview**

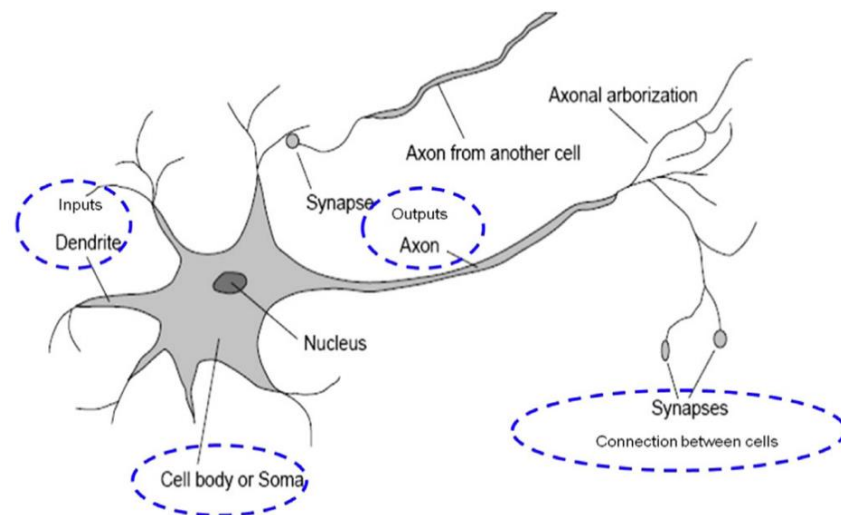
The ANN model has been widely utilised as a predictive tool in many fields (Chew et al. 2004). For example, ANNs have been implemented in a variety of fields and applications, such as mathematics, medicine, engineering, architecture, the environment, robotics, pattern recognition, forecasting, manufacturing, optimisation, etc. (Benedetti et al. 2016).

## **CHAPTER 2: LITERATURE REVIEW**

Moreover, regression analysis has long been the most widely used modelling method in the field of energy research. However, the application of ANNs in energy studies has increased recently. ANNs are becoming increasingly used today due to their flexibility and adaptability in modelling complex nonlinear systems (Sözen et al. 2004). A variety of energy-related studies have utilised ANNs for prediction, classification, and problem solving.

Regarding the building energy consumption situations, researchers have used ANNs to investigate heating/cooling load, power consumption, and optimisation, etc. (Zhao and Magoulès 2012a) because ANN predictions do not require the development of a physical model compared to conventional computational methodologies (Id et al. 2020). The ANN method was introduced by MacCulloch-Hopfield in the early 1960s, but its development started in 1985 (Haykin 1992). At that time, McCulloch and Pitts carried out an experiment to represent bio-systems with nets of simple logical operations for a simple nonlinear model of a real neuron. This experiment expanded the boundaries of computational calculation. The ANN model has the capability to deal with complex systems and nonlinear problems, which resemble the structure and functionality of biological neural configurations that take place in the human brain (Haykin 1992).

Neural networks are responsible for the information processing done by the brain. The brain can learn concepts over time by analysing and processing the primary information, which may be noise, complex, irrelevant, or absent. The brain's extraordinary capabilities come from its large, complex, and parallel neural networks. It is capable of processing, classifying, and even simulating the information, which it receives via senses to form an internal model (Samarasinghe 2007). The biological neuron processes occurring in the human brain are visualised in Figure (2.22). Each neuron's axon uses an electrochemical medium known as a neurotransmitter to transfer information to nearby neurons via synapses in the brain. The synapses of a neuron receive information from approximately 10,000 other neurons. The biological neuron is the inspiration for ANNs. The human brain contains approximately 100 billion interconnected neurons. Thus, repeated activation of neurons in a network produces a brain response (Safa 2011).

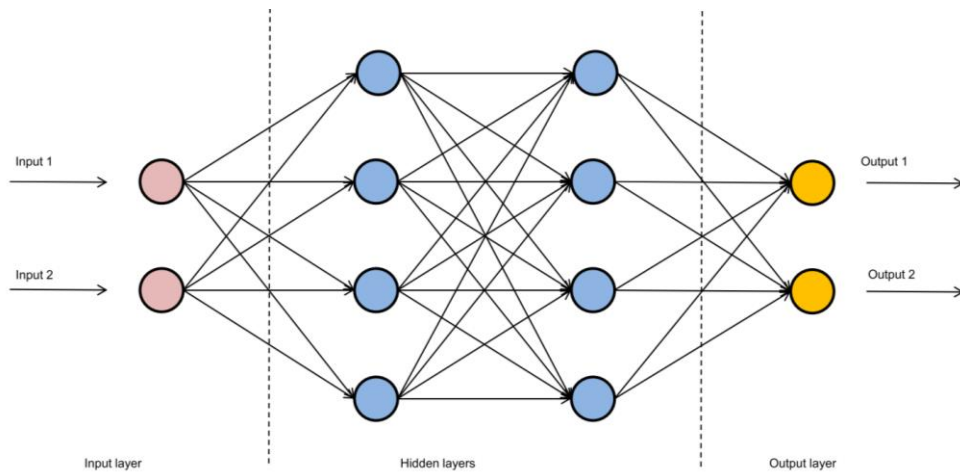


*Figure 2.22: Structural diagram of neuron (Raza and Khosravi 2015).*

According to Kuster et al. (2017), an ANN is a technique of intelligent ML that mimics the structure of the human brain. Similar to the human brain, an ANN is composed of neurons and connections arranged in multiple layers. Nonetheless, while existing ANNs do not even come close to mimicking the complexity of the human brain, they are effective pattern-detection tools (Kuster et al. 2017).

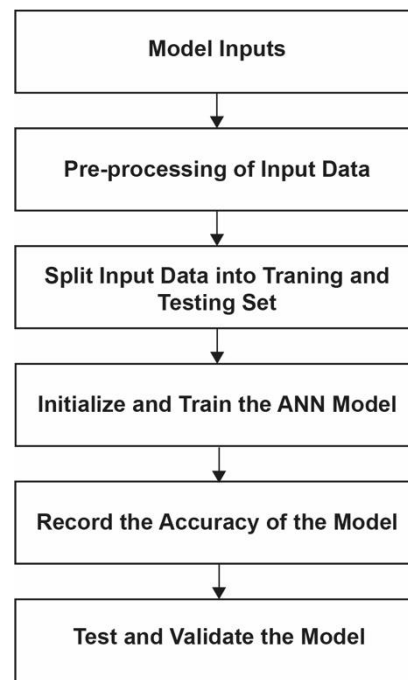
### **2.10.1. Fundamentals of Artificial Neural Networks**

The ANN model consists of interconnected units called neuros and is composed of three layers: the input layer, the output layer, and one or more hidden layers in between. Each layer is made up of some interconnected neurons which have an activation function. Figure (2.23) shows a schematic diagram of a two-layered architecture of a feedforward neural network. The number of hidden layers can vary depending on the nature and complexity of the problem. ANNs work as black-box models and learn the relationship between inputs and outputs without requiring any system-specific knowledge (Ahmad et al. 2017a). ANNs are typically defined by three types of parameters: the interconnection patterns between neurons in different layers, the learning process of updating the weights of the interconnection, and the activation function that transforms the weighted input of a neuron into its output activation (Wang and Srinivasan 2017).



*Figure 2.23: Schematic diagram of two-layered architecture network (Ahmad et al. 2017b).*

A neuron can receive or transmit a normalised signal from or to other neurons within the network. Each wire entering a neuron from another neuron is referred to as a "weight"  $w_{kp}$ . Additional inputs of +1 are added to each neuron, which is known as the bias value ( $b$ ), and its associated weight is represented by the mathematical symbol ( $w_{k0}$ ). To generate the output, the total of the weighted inputs is processed and applied to the activation function. Adjustments are made to the network's weights and biases in order to reduce the gap between the generated output and the required output of the network (Raza and Khosravi 2015). In another words, weights are modified over training in each iteration so that the error is minimised. Learning can also occur in batch mode, where weights are updated after the processing of a group of training vectors by the network. The transfer function can be nonlinear or linear transfer functions. Some common activation functions are available, and these will be discussed in section (2.10.3). The output is determined by the transfer function used. The primary steps to develop the ANN model are shown in Figure (2.24).



*Figure 2.24: The primary steps to develop the ANN model.*

In the case of complex issues, it is necessary to use more than one layer; these neural networks are known as multilayer neural networks or multilayer perceptions (MLPs) Figure (2.25). The multilayer network is constructed using a backpropagation (BP) rule that minimises the output error by backpropagating the error from the output to the hidden layer, consequently altering the weights. One or two hidden neurons may be adequate for straightforward nonlinear issues. However, many neurons may be required to replicate accurately the proper input-output relationships when dealing with extremely nonlinear problems involving several input variables. Using current tools, it is possible to determine the number of neurons and layers through an iterative process using different approaches to tune these parameters during the training process to select the optimal network architecture. When there are fewer hidden neurons than necessary, network errors increase, and the correlation between inputs and outputs decreases. In contrast, when the number of hidden neurons exceeds what is necessary, overlearning increases prediction variance (Kermanshahi and Iwamiya 2002).

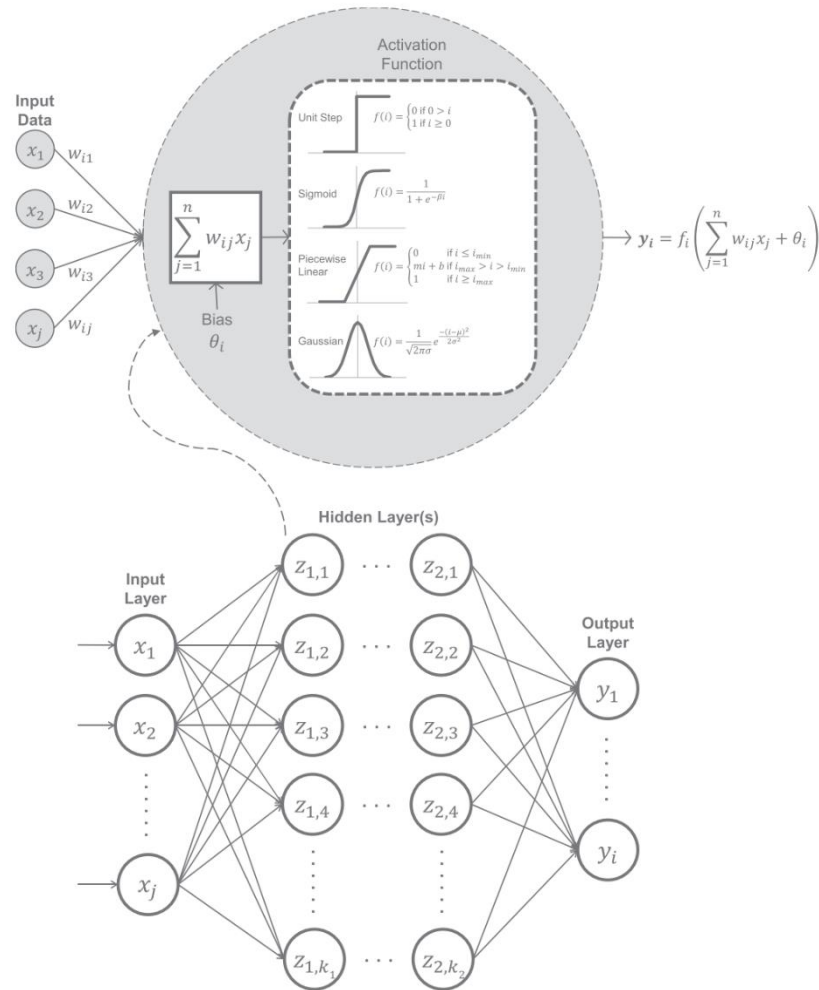
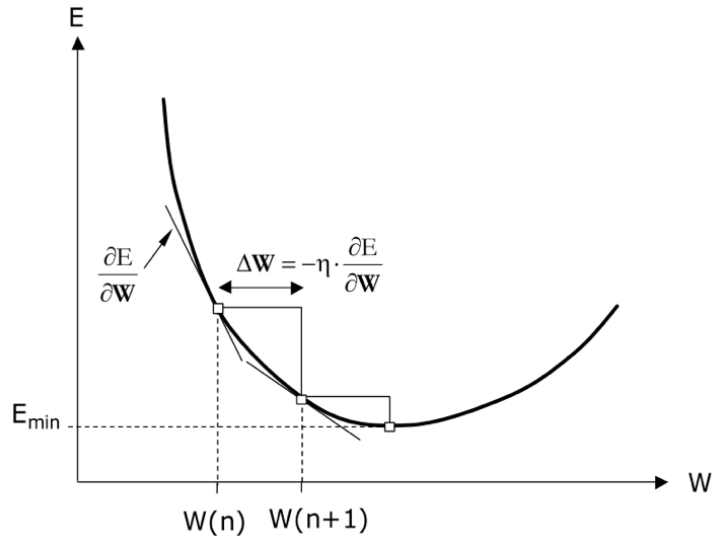


Figure 2.25: ANN architecture with multiple hidden layers (Ayoub 2020).

**2.10.2. Neural Network Architecture**

To meet the network's objective function, the error data is back propagated from the output of the network to the input. As the inputs change, the network seeks to reach a new equilibrium state from the prior state, as the change in inputs is applied (Raza and Khosravi 2015). Neural networks can handle dynamic and complex processes as well as time-varying or time-lagged patterns (Hahn et al. 2009). Back propagation (BP) relies on gradient descent as its foundation. To achieve the lowest feasible level of error as quickly as possible, the weights should be adjusted according to the gradient of the error surface with respect to the weights. In addition, the weights are modified by an increment determined by the learning algorithm after each cycle (Safa 2011).





*Figure 2.26: Gradient based to update the weights of the network (Raza and Khosravi 2015).*

The neural network's ability to learn is dependent on the errors it generates during training. The network error is defined as the squared difference between the desired and the actual values. For instance, the mean square error (MSE) of the network can be used during the training process to measure the differences. Other evaluation metrics or error functions are also possible, such as RMSE,  $R^2$ , etc. The calculated outputs (error) are utilised to alter the network's weights so as to lower the error level. An epoch occurs each time the network processes the entire collection of data (both forward and backward runs). In this approach, the network is trained by decreasing the error with each epoch until an acceptable error level is reached (Haykin 1992; Du and Swamy 2006; Kaiadi 2006). Then, a separate validation dataset is utilised to test the model's predictions.

The rate of learning controls the distance of descent. This rate is often positive and between zero and one. When training the network with a lower rate, the process will take longer, but the results will be more stable. While selecting larger learning rates may result in quicker training, the weights may oscillate near the minimum and never reach it, and the results will be less accurate (Kalogirou 2000; Samarasinghe 2007). Multiple learning rates should be applied during the process of adjusting the hyperparameters to get the best accuracy learning rate. The amount of time it takes to train a network could also be affected by other factors, such as the complexity of the network (number of hidden neurons and layer), and the amount of input.

In addition, when using a gradient descent approach, the slope of the error is always from the highest to the lowest to find the global minimum. To avoid getting trapped in a shallow valley known as a local minimum, the network weight values are modified based on small intervals. Even if the weights are constantly updated, it is challenging to escape the valley at

## CHAPTER 2: LITERATURE REVIEW

the local minimum point. Thus, the problem of local minima is also a significant consideration when deciding on a neural network training algorithm (Gori and Tesi 2000). The objective of the training algorithm is to achieve the global minimum value on the error surface as shown in Figure (2.27). According to the literature, the issue of local minima can be avoided by using a more efficient network training method (Raza and Khosravi 2015).

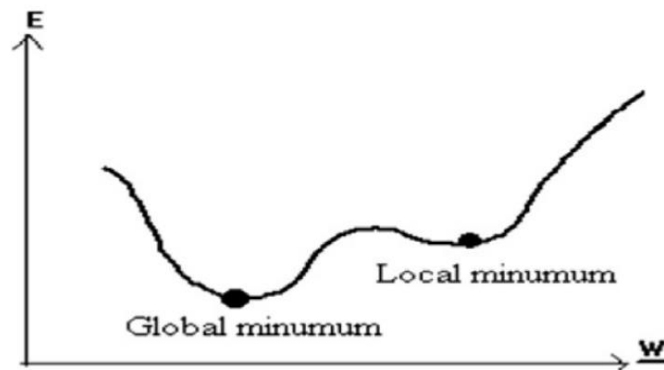


Figure 2.27: The global minimum value on the error surface (Raza and Khosravi 2015).

A model's ability to predict the output with minimal error is supported by an adequate number of variables. The size of the data sample is crucial, as neural networks cannot determine the proper correlations without sufficient samples. The sample size can range from a few to thousands of cases. The quantity of the dataset is determined based on the problem's complexity and the data's quality. Using more neurons than required results in overfitting, which is the most common problem in neural network training. Overfitting can be avoided by employing a technique known as "early stopping", in which a calibration dataset, extracted from the training dataset, is used at regular intervals during training to assess the model's performance and stop training at the point where overfitting occurs and when the prediction error on the calibration dataset begins to increase. K-fold cross validation is among the ways offered to automate the selection of the optimal number of hidden neurons (Samarasinghe 2007). Generalisation refers to the ability of a neural network to adapt to a variety of inputs. When a network's output is close enough to target values that were not included in its input, it is considered well-generalised. The number of parameters affecting generalisation include the quantity and quality of training data, the network's architecture, and its complexity.

### **2.10.3. Activation Function**

The activation function works as a compression function to convert weighted inputs into network outputs. There are a variety of activation functions available, including linear function, sigmoid function, logistic function, Rectified Linear Unit (ReLU) function, and step

## CHAPTER 2: LITERATURE REVIEW

function, etc. Nevertheless, activation might vary based on the neural network's architecture, the number of inputs, and the kind of the problem. However, there is no clear rule of thumb for finding the optimal activation function to maximise network output. The literature review demonstrates that alterations to the activation function can affect the network's output (Zhang et al. 1998). The activation function is a two-step linear combination of input weights and transfer function. In addition, the transfer function translates the weighted total of all inputs into the target unit (Raza and Khosravi 2015). The most two commonly employed activation function are sigmoid function, and, ReLU function as shown in Figure (2.28) (Lee et al. 2019b).

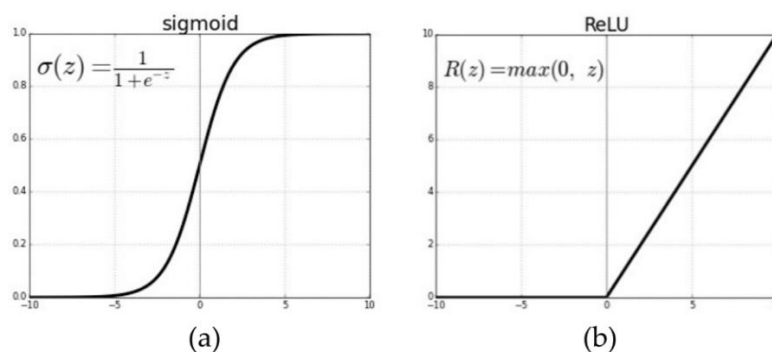
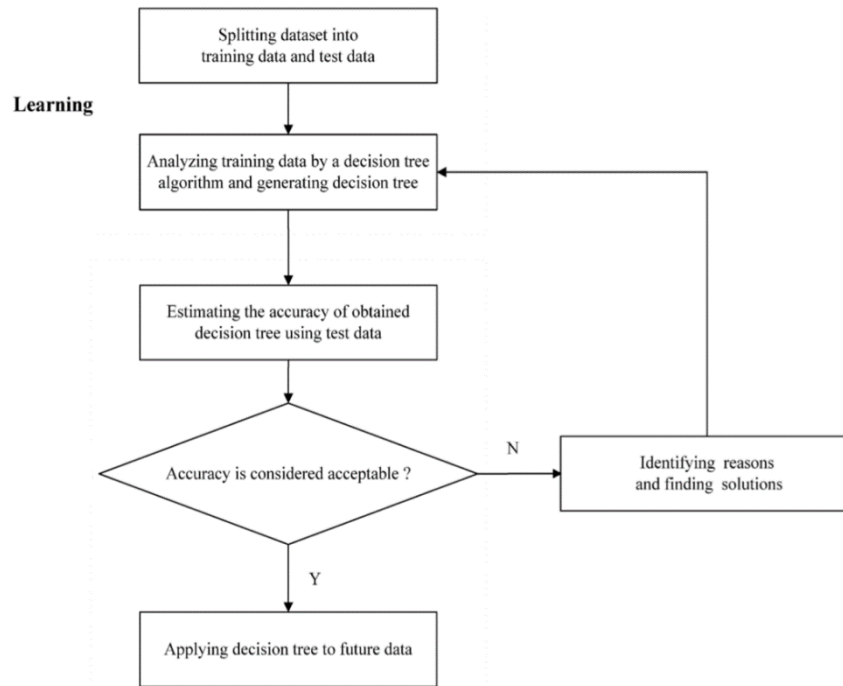


Figure 2.28: Two commonly employed activation functions (Lee et al. 2019b).

### **2.11. Decision Tree (DT)**

Decision tree (DT) is a method that has been commonly used for classification and prediction in many fields (Tung et al. 2005). DT "uses a flowchart-like tree structure to segregate a set of data into various predefined classes, thereby providing the description, categorization, and generalization of given datasets" Figure (2.29) (Yu et al. 2010a). The DT model has advantages over other models because of its ease of use and the ability to predict accurately without requiring excessive computation time. While this method has the ability to process both numerical and categorical data, DT usually performs better with categorical than with numerical data (Yu et al. 2010a). DTs are very desirable as ML algorithms because of their speed of computation. In addition, the method's training is straightforward, making it easy to generalise over a huge dataset. Due to their simplicity, usability, and interpretability, DTs have become a widely used ML technique in recent years (Thompson et al. 1974). Diverse studies have addressed the deficiencies of conventional DTs, such as their unsatisfactory performance and lack of robustness (Ahmad et al. 2017b). As a result of these efforts, an ensemble of trees was formed, and this was followed by a vote for the most popular class, which was labelled a forest (Breiman 2001).



*Figure 2.29: Procedure for Decision tree development (Yu et al. 2010a).*

One of the most common ensembles learning techniques is random forest (RF). RF is a method for classifying and predicting future outcomes. Using data training, the algorithm generates several DTs (Svetnik et al. 2003). This implies that the outcome for a particular set of inputs is determined by the training. This algorithm is applied to both category and numerical output data. RFs for numerical data produce the mean of the values generated by several DTs (regression). Using categorical data, the median of several DTs' generated values is the output (classification). For instance, if 7 out of the 10 DTs predict a Yes answer, and the other three predict a No answer, then the RF answer will be Yes (Madhusudanan 2019). According to (Ahmad et al. 2017b). "The primary characteristics of RF are as follows: (1) bootstrap resampling, (2) random feature selection, and (3) full depth decision tree growing". Figure (2.30) illustrates a DT derived from an RF for predicting the hotel's HVAC energy use. It is important to note that this DT serves merely as an example. Actual RF outcomes include DTs with more depth and complexity (Ahmad et al. 2017b).

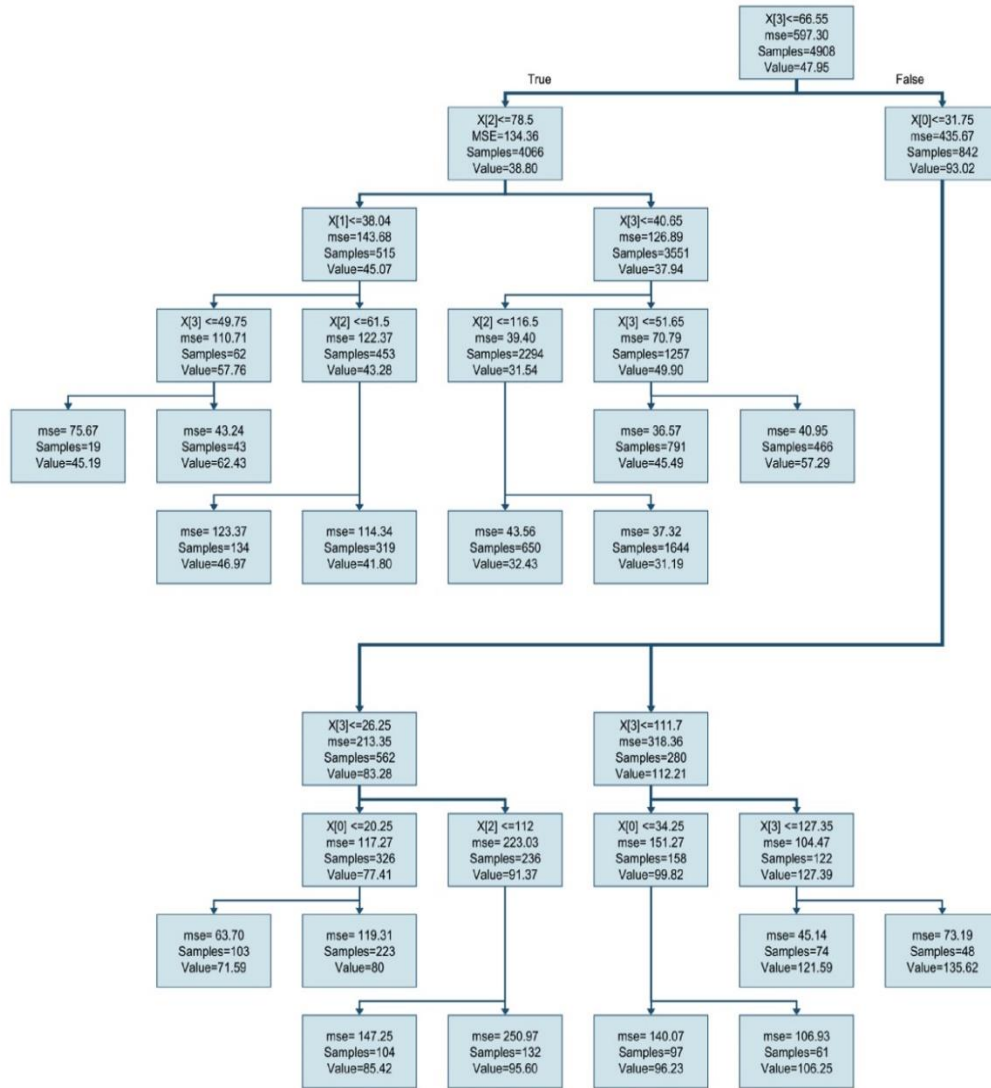


Figure 2.30: A decision tree showing how the decisions are made (Ahmad et al. 2017b).

## 2.12. Existing Studies

This section examines existing studies that used ANN or DT methods for building performance prediction focusing mainly on energy studies and solar radiation studies; nevertheless, it is not a thorough review. Zhang et al. (2021) reviewed various works on ML for predicting building loads. The authors identified a problem with the reported information, namely, that ML model development is frequently sporadic, and critical information is absent. Many articles, for instance, merely indicate the data used for modelling without providing additional information such as data resolution, training/testing data split, etc. Therefore, a standardised information table was recommended for future publishing in order to provide a complete picture of the described ML and modelling methodologies and to make it easy for readers to acquire information from the research (Zhang et al. 2021). Thus, this study utilised the recommended information table by Zhang et

## **CHAPTER 2: LITERATURE REVIEW**

al. (2021, p. 18), which is divided into four primary sections: (1) general information, (2) data description, (3) algorithm, and (4) performance evaluation. The general information section includes the following parameters: building type, prediction type, forecasting, etc. The data description section consists of the following: source of data, sampling interval of data, training/validation/ testing data description, etc. The algorithm and performance section includes main algorithm structure used, tuning methodology, other support techniques, and error metrics used Table (2.3).

### **2.12.1. Neural Networks Studies**

ML techniques can predict a building's energy consumption based on data such as climatic conditions, architectural characteristics, and occupancy status. ML techniques have been widely used in the field of building energy usage prediction because of their strong prediction capabilities. Predicting building energy usage has already been compared with various methods using ML. For instance, Neto and Fiorelli (2008) conducted a comparison study between ANN and EnergyPlus to predict energy building usage. Turhan et al. (2014) performed a similar study, in which the authors compared ANN with KEP-IYTE- ESS, an energy simulation software, for forecasting the heating load of residential buildings. The researchers found that, in comparison to traditional methods like engineering and hybrid models, ML-based approaches have a greater advantage in terms of model simplification, computation speed, and the ability to learn. Although energy simulation engines such as EnergyPlus are capable of simulating complex systems, their sequential software structure makes them significantly slower than ML techniques; for instance, the space temperature is updated hourly based on feedback from the HVAC module (Wang and Srinivasan 2017).

In recent years, several studies have been conducted integrating the ML approach for the prediction of building performance, which includes building energy performance, estimating heating and cooling loads, daylighting, building energy consumption, and solar radiation. Zhao and Magoulès (2012) agreed that the ML approach has proven to be efficient in the prediction of building performance. Unlike conventional modelling methods, supervised ML has major benefits in terms of requiring less computation time and less effort and of being computationally unexpansive (Huang et al. 2015). Additionally, the accuracy and simplification of predictions has inspired researchers to investigate this possible alternative method for predicting building performance and occupant behaviour (Wang and Srinivasan 2017), and to replace building performance simulations by using data analytics (Geyer and Singaravel 2018).

## **CHAPTER 2: LITERATURE REVIEW**

Regarding the prediction of energy demand, Paterson et al. (2017) developed a design tool where ANN is integrated to predict energy consumption in real-time in the early design stages. The study focuses on school building design in England as a case study, and ANN was trained for the assumption of the annual energy consumption of schools using the CIBSE existing heating and electrical energy database to train the model. A more recent study by Asl et al. (2017) proposed a model called the Energy Model Machine (EMM) using ML algorithms, (ANN and RF), to predict instant energy performance in the early stages of the design process. The authors tested the EMM model in a medium-sized office building as a case study to demonstrate the usefulness of this method. The model generated 7,000 building design options with their energy performance, which can help designers make informed decisions during the conceptual design process. The researchers found that the use of ML to estimate energy performance during the process of design exploration and optimisation is a feasible approach for achieving high-performance buildings. The RF surrogate model of their study resulted an accuracy with an  $R^2$  score of 0.999715.

Geyer and Singaravel (2018) presented a component-based method developed by ML for both parameterised whole building design and components of the design. The study examined construction-level components (wall, windows, floors, roof, etc.), and zone-level components. The results of the study show that “high prediction quality may be achieved with errors as low as 3.7% for cooling and 3.9% for heating” (Geyer and Singaravel 2018). Chakraborty and Elzarka (2019) compared multiple ML methods for the generation of a more accurate energy model. The study indicated that XGBoost and ANN produce accurate energy models compared to others. A few studies have implemented neural networks to predict daylighting and illuminance. A study by Lee et al. (2019) proposed a new method based on their exploration of the relationship between existing daylighting metrics and building design attributes. In addition, Kazanasmaz et al. (2009) effectively predicted the horizontal illuminance in office buildings using neural network-based modelling. The study resulted in a low average error of 3% once it was compared to measured illuminances. A more recent study by Clara Lorenz and Jabi (2017) analysed the efficiency of integrating supervised ML through using ANN to predict daylight autonomy levels for a typical office room. The study found that more accurate results can be achieved when a large set of data is sufficiently trained, which shows the potential of using this method to estimate the daylight autonomy of interior spaces.

Regarding a simulation-based model approach, Keshtkarbanaeemoghadam et al. (2018) developed an ANN model, trained by a BP algorithm, to estimate the total heating energy

## **CHAPTER 2: LITERATURE REVIEW**

demand of a shelter located in Iran. The study obtained the data by conducting 328 computer simulations using a Grasshopper plugin linked to the EnergyPlus engine. Nine inputs were selected to train and test the NN: "wall thickness, wall U-value, wall R-value, window U-value, window R-value, number of occupants, equipment load, and infiltration rate". In addition, different ANN models were examined with one or two hidden layers to select the most suitable architecture network. According to the results, the best ANN model had an MSE of 0.73, which indicates that the ANN model is a promising approach and can substitute other methods to predict the heating energy demand in buildings.

In another similar approach, Wong et al. (2010) conducted a simulation using EnergyPlus to generate a database of daily energy consumption for office buildings with daylighting. Then, these generated data were used to train and test the developed ANN model to predict daily building energy usage in fully air-conditioned office buildings in the early design stages. Nine dynamic inputs were selected that related to external weather conditions, building envelope design, and time variables using the feedforward MLP model. Regarding the output of the model, four nodes at the output layers were defined to estimate daily energy consumption for cooling, heating, electric lighting, and total building energy. The accuracy prediction of the model was measured using the Nash–Sutcliffe efficiency coefficient (NSE), and the results for "cooling, heating, electric lighting and total building electricity were 0.994, 0.940, 0.993, and 0.996, respectively", which represents a highly predictive model.

Ascione et al. (2017) proposed an ANN model to assess energy consumption and thermal comfort to predict the energy performance for office buildings in Italy. The study developed two network models; the first model was for existing building stock, and the second one was for renovated buildings in the presence of energy retrofit measures. The outcome data of the performed simulation by EnergyPlus were used to train and test the ANN network. Then, a "Simulation-based Large-scale sensitivity/uncertainty Analysis of Building Energy performance" (SLABE) was implemented to improve and optimise the network. Three different outputs were addressed for the first network (existing building): "primary energy consumption of space heating and cooling; the ratio of yearly discomfort hours"; and geometry, envelope, operation, and HVAC were selected as inputs of the network.

Khayatian et al. (2016) utilised the Italian CENED database to train the ANN model for the evaluation of energy performance certificates in the residential sector. The aim of the study was to replace the manual evaluation of assessing every building, which is time consuming, with the ANN approach for faster predictions. Several models with various combinations of direct and derived inputs were tested to develop the most reliable model. In addition, the



## **CHAPTER 2: LITERATURE REVIEW**

selected inputs were optimised to achieve a high prediction accuracy model. The researchers observed that the selection of 12 inputs from all the examined inputs was sufficient to predict the heat demand indicator, which indicates that inputs have a significant impact on the model's accuracy performance.

Zhang et al. (2015) compared different models to estimate the HVAC in an office building. Based on the results of the study, the ANN model did not perform well compared to other models because the model needs adequate data to "accurately capture the relationship between the input and output variables".

Another study by Kialashaki and Reisel (2013) conducted a comparison between two ML techniques, namely, ANN and MLR, to forecast the future energy demand for the US domestic sector. The ANN model was trained using the BP technique with seven inputs: population, gross domestic product, median household income, house size, cost of residential electricity, natural gas, and oil. The architecture of the ANN consists of three layers, specifically, the input layer, hidden layer, and output layer. In the hidden layer, each neuron includes a nonlinear activation function by using the sigmoidal logistic function, which influences the performance accuracy of the model. Historical data from several sources were used from the period 1984-2010 to estimate the future energy demand for the period 2010-2030.

Deb et al. (2016) used a data-driven technique of three institutional buildings in a university campus in Singapore to forecast future daily cooling demand. Their results show that the ANN model is able to predict cooling demand for the next 20 days using the 5 previous days as inputs with a good accuracy between the measured and predicted data (Deb et al. 2016).

Platon et al. (2015) compared two ML models, namely, ANN and Case Based Reasoning CBR, to predict hourly building electricity use in an institutional facility. Data were collected over 15 months to be used for training and testing the developed models. According to their comparison results, ANN model prediction is more accurate than CBR for predicting the energy consumption of the building on an hourly basis. However, it was found that CBR is more appropriate when dealing with a small amount of data, while a large amount of data is necessary for ANN modelling and training in order to achieve a high level of accuracy (Platon et al. 2015).

Regarding the prediction of the hourly cooling demands of the building. Li et al. (2009) et al. presented four modelling methodologies: MLFFNN, RBFNN, GRNN, and SVM. The relative prediction errors of the training samples for the four models were found to be less than 0.02%, which indicates that the models can accurately estimate building cooling demands.

## **CHAPTER 2: LITERATURE REVIEW**

Shakouri and Banihashemi (2019) conducted a different study in which they constructed a predictive model based on ANN to evaluate the performance of windows with regard to the heating and cooling loads. There was a total of ten influential factors that were fed into the network as input layers. These inputs include the following: the U-factor, emissivity, Solar Heat Gain Coefficient (SHGC), Dry Bulb Temperature (DBT), Wind Speed (WS), Solar Radiation (SR), diffuse SR, Humidity (H) Orientation (O), and month. Meanwhile, heating and cooling loads were the output of the network.

To date, no studies have explored the integration of ANN into predicting the energy performance of AFs. In addition to the mentioned studies related to the existing performance-simulation tools, these tools are not developed specifically for AFs but provide limited and misleading information for adaptive systems (Loonen et al. 2017). Therefore, this lack emphasises the need to examine different approaches for the performance of AFs in the initial design stage for advances in and the improvement of overall building performance.

Regarding solar radiation predictions, Mohandes et al. (1998) modelled global solar radiation using an ANN model as a function of latitude, longitude, altitude, and sunshine duration for ten different cities in Saudi Arabia. The MLFFNN with a BP algorithm were used to train the network. The optimal network consists of 4, 10, and 1 neuron in the input, hidden, and output layers respectively (Mohandes et al. 1998). Ouammi et al. (2012) built an ANN model to estimate the monthly solar radiation in different Moroccan cities. Inputs for the networks are normalised values of longitude, latitude, and elevation from 1998 to 2010, and predict that solar irradiation varies from 5030 to 6230 W/m<sup>2</sup>/day. In another study, Abdulazeez (2011) trained the ANN model with the following parameters: wind speed, relative humidity, air temperature, and soil temperature. The model has an accuracy of 94% in predicting the hourly global solar radiation. The author utilised a feedforward with a BP ANN model to forecast the monthly average global solar irradiation on a horizontal surface in Gusau, Nigeria. The desired output is SI, while the input parameters are sun duration, maximum temperature, and relative humidity. The results reveal that the estimated and measured values of global sun irradiation are in good agreement.

Benghanem et al. (2009) constructed an ANN model to predict solar radiation in Al-Madinah (Saudi Arabia). A neural network was trained using the data from the previous 4 years, and then it was tested and validated using data from the most recent year. The model was trained with three inputs, namely, air temperature, relative humidity, sunshine duration, and the day of the year. Yadav and Chandel (2014) demonstrated that ANN approaches are more effective than traditional, linear, nonlinear, and fuzzy logic models for predicting solar

## **CHAPTER 2: LITERATURE REVIEW**

radiation. Marzouq et al. (2017) conducted a comprehensive evaluation of ANN-based radiation prediction studies on a monthly, daily, and hourly basis. It was found that only a few studies had utilised hourly forecasts for their results. In addition, the author noted the lack of literature on ANN-based direct and diffuse solar radiation prediction.

Qazi et al. (2015) stated that ANN models can reliably estimate solar radiation in various climatic circumstances because ANNs accept more inputs than empirical models, hence enhancing their reliability. The study suggested employing ANN approaches for hourly solar prediction in future research for improved results. In addition to discussing potential inputs, the study emphasised that selecting the appropriate parameters is vital for doing the prediction with greater precision. Reddy and Ranjan (2004) created an ANN algorithm in India, where solar radiation data from thirteen stations were collected. Month, time, air temperature, relative humidity, latitude, longitude, altitude, wind speed, and precipitation were used as inputs. Comparing the findings of the ANN model to those of other empirical models revealed that the performance of the ANN model was superior.

Hasni et al. (2012) used month, day, hour, temperature, and relative humidity values as inputs to estimate global solar radiation in the southwest region of Algeria. A BP ANN approach was used to train the network. The first set of data (from February 2, 2011, to May 31, 2011) was used to train the network, while the second part was used to test the network. The results had an MAPE of 2.9971% and an  $R^2$  of 99.999%, indicating that the predicted solar global radiation values for the period between February 2 and May 31, 2011, were extremely close to the measured data. In another study, an ANN-based solar radiation estimation model developed by Koca et al. (2011) was used to predict solar radiation for seven cities in the Mediterranean region of Turkey's Anatolia. Six distinct combinations of inputs were utilised to determine the optimal ANN configuration for prediction: latitude, longitude, altitude, months, average temperature, average cloudiness, average wind velocity, and sunshine duration. The data of years 2005, 2007 and 2008 were utilised for training, while data from 2006 were utilised to test the network model. The results show that ANN-based solar radiation prediction models were highly accurate in the chosen region based on the prediction error values presented in this study (Koca et al. 2011).

Notton et al. (2012) developed three ANN models with five inputs, namely, declination angle, hour, zenith angle, hourly horizontal irradiation, and hourly global irradiation, to predict hourly global radiation on inclined planes.  $R^2$  values for the first, second, and third ANN models were 99.79%, 99.82%, and 99.70%, respectively. Ozgoren et al. (2012) estimated daily total global solar radiation using three distinct ML algorithms: multi-linear

## **CHAPTER 2: LITERATURE REVIEW**

regression (MLR), multi-nonlinear regression (MNL), and feedforward ANN approaches. The models made use of the recorded solar duration, air temperature, wind speed, and year (monthly and daily). The approaches that were created had been implemented and tested in the city of Adana in Turkey, with an MAPE of 9.23% and an  $R^2$  of 97.5%.

Mellit and Pavan (2010) built an ANN-based solar irradiance forecast model for predicting the next 24 hours. The network consisted of three layers with three inputs: the mean daily SI, the mean daily air temperature, and the date, while the output layer offered 24 hours of SI for the following day. SI and air temperature were collected between July 1, 2008, and May 23, 2009, and November 23, 2009, and January 1, 2010, which served as the network's training and testing data. For the purpose of validating the model, K-fold cross-validation was utilised. On sunny days, the correlation coefficient between predicted and measured SI was greater than 98%, whereas on cloudy weather, it was less than 95%.

### **2.12.2. Decision Tree Studies**

Limited applications have implemented DT techniques in relation to building studies compared to ANN or other ML models (Ahmad et al. 2017a; Ahmad et al. 2017b). Tso and Yau (2006) presented a comparison study between three modelling techniques to estimate average weekly electricity energy consumption in Hong Kong (Tso and Yau 2007). They found that both DT and ANN are applicable models compared to a regression model because of their understanding of energy consumption patterns and the prediction of energy usage. In another study by Yu et al. (2010a), the researchers developed a predictive model to improve building energy performance based on the use of DT (Yu et al. 2010a). They applied the use of DT on a residential building to predict the energy use intensity (EUI) level. The authors concluded that the use of the DT method makes it possible to classify and predict the energy usage of the building accurately, which would lead to a high energy performance building.

Regarding RF algorithms, Breiman (2001), stated that RF was initially designed to optimise the conventional DT approach. The author suggested employing an RF as a predictive regression technique for energy studies. Ahmad et al. (2017) predicted the hourly electricity consumption of HVAC systems at a Madrid hotel using an RF algorithm. Ma and Cheng (2016) used RFs to identify the relevant amounts of 171 parameters connected with the regional energy consumption intensity of residential buildings.

DTs were used by Yu et al. to predict energy usage. The authors modelled building energy usage intensity levels to calculate residential building energy performance indices. According to the findings, DT-based algorithms can produce fairly accurate predictions and can be used

## **CHAPTER 2: LITERATURE REVIEW**

by users without any experience of computer programming (Yu et al. 2010b). In another study by Hong et al. the authors developed the DT method to reduce electricity consumption in school buildings. Moreover, DTs can be used to classify educational facilities according to their electric energy use. The results showed that using a DT method increased prediction accuracy by 1.83–3.88% (Hong et al. 2012a). Similarly, Hong et al. [23] clustered multifamily dwelling complexes based on their gas consumption. Different ML algorithms were used, such as an ANN, a genetic algorithm, and a multiple regression analysis. According to the results, the predictive accuracy of the DT model increased by 0.06–0.145%. These results clearly highlight the significance and use of DTs for forecasting (Hong et al. 2012b).

Tsanas and Xifara (2012) compared a traditional linear method to an RF to determine which method was optimal for making predictions. The effect of eight input factors on residential building cooling and heating loads was evaluated. The eight input variables included relative compactness, surface area, wall area, roof area, overall height, orientation, glazing area, and distribution of glazing area. For the simulations, a total of 768 distinct houses were used. Ecotect was used to evaluate which of the two models was better. The value for the heating load was 0.51 and the value for the cooling load was 1.42. The results demonstrated the potential of RF algorithms as an alternative to traditional regression techniques (Tsanas and Xifara 2012).

### **2.12.3. Discussion of the Review**

Figure (2.31) shows the distribution of the studies based on different factors including building type, data collection, target of the developed model, data-splitting procedure, prediction term, and performance metrics used to validate the model. Based on the examined studies, most studies have focused on office buildings and residential buildings with 44% and 28% respectively. These studies focused on energy building studies instead of other factors due to the high energy consumption of these buildings. This analysis focused only on ANNs or DTs or on studies that compared these two algorithms with other ML models. The analysis showed that 47% of the studies utilised an ANN to train their models, while 28% of the studies utilised DTs method. On the other hand, 25% of the studies used multiple models as a comparison study. In terms of prediction capability, current studies focused more on yearly time prediction with 45% compared to other prediction terms, such as hour, day, week, and month; these represent 23%, 15%, 2%, and 12%, respectively. This indicates the need to examine other predictions terms for future research.

## **CHAPTER 2: LITERATURE REVIEW**

The analysis revealed that 59% of the current analysed studies used real data to train the model, while 41% utilised simulated data. Using real data is advantageous when they are easily accessible; however, simulation data are useful in some cases where real data are limited, for instance, when it is difficult to instrument a building due to technical or financial constraints. Regarding the performance evaluation metrics, the most commonly used evaluation metrics are the RMSE,  $R^2$ , and MAE. Overall, 29%, 27%, and 10% of the reviewed studies evaluated their models using RMSE,  $R^2$  and MAE, respectively. According to the current study, most studies did not include information regarding the process of splitting the data. The reason is that data split is one of the hyperparameters that can be tuned during the training process, which may vary depending on the size of data used, and other parameters. Westermann and Evins (2019) reviewed the use of surrogate modelling for sustainable building design; in this study, the authors stated that a random separation of 80% for training and 20% for testing is suitable once the data are properly structured. According to Amasyali and El-Gohary (2018), "A machine learning model predicts energy consumption based on a set of features. These features can be related to outdoor weather conditions, indoor environmental conditions, building characteristics, time, occupancy and occupant energy use behavior, and/or historical energy consumption". Existing studies used different features or inputs based on the target of their model.

**CHAPTER 2: LITERATURE REVIEW**

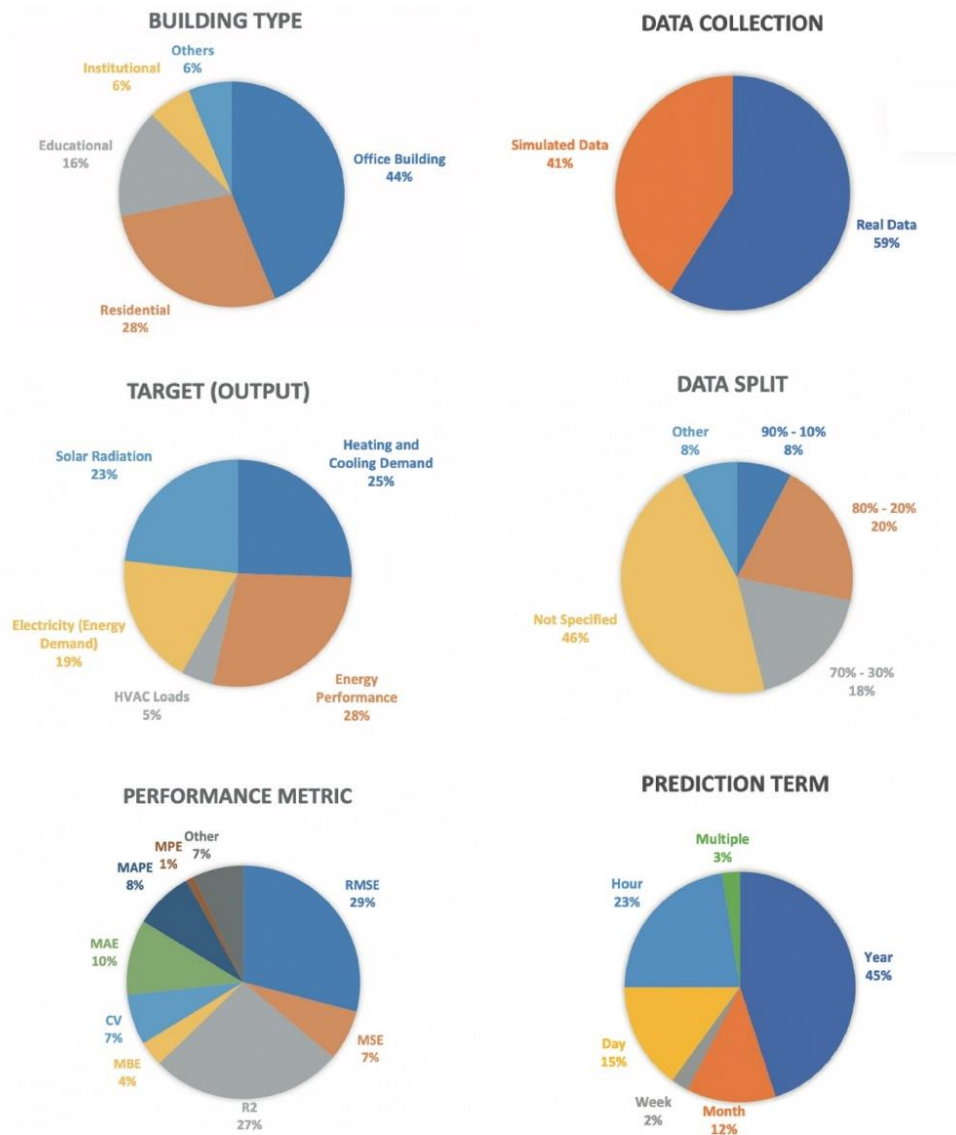


Figure 2.31: Analysis of the existing studies that used ANN or DT methods for building performance prediction.

**CHAPTER 2: LITERATURE REVIEW**

Table 2.3. ANN and DT application techniques to building-energy-related areas.

| ID | Study (Reference)                    | Building Type   | Target             | Inputs   | Outputs  | Data   |                               |   | Data Collection | ML Method        |  |                  | Tools                            | Performance Metric  |
|----|--------------------------------------|-----------------|--------------------|--|--|--|-------------------------------|---|-----------------|------------------|--|------------------|----------------------------------|---------------------|
|    |                                      |                 |                    |  |  | Volume   | Availability                  | Data Split  |                 | Model/ Structure | Function   | Predictio n Term |                                  |                     |
| 1  | (Keshtkarban aemoghadam et al. 2018) | Residential     | Heating demand     | “Nine input variables: (Wall thickness, wall u-value, wall R-value, window u-value, window R-value, number of occupants, area, equipment load, infiltration rate)”   | Heating energy demand  | 328 computer simulations                       | -                             | 70% training, 30% testing, and 30% validating.      | Simulation      | ANN              | Logistic sigmoid and purlin (linear)                 | Year             | Energy-plus, Grasshopper, MATLAB | MSE, R <sup>2</sup> |
| 2  | (Wong et al. 2010)                   | Office building | Energy performance | “Four inputs for external weather conditions, four inputs for the building envelope, and day type (i.e., weekdays, Saturdays and Sundays)”   | Daily electricity for cooling, heating, electric lighting and daily total electricity use. | 8760 hourly records of generic office building | -                             | 70%, 30% for training, testing.                     | Simulation      | ANN              | Logistic sigmoid                                     | Day              | Energy-Plus, MATLAB              | RMSE, MBE           |
| 3  | (Kalogirou et al. 1997)              | Office building | Heating load       | “Window area, external wall area, partition area, floor area, roof, window type, wall type, and room temperature”.   | Heating loads  | 250 cases                                      | -                             | 90%, 10% for training and testing.                  | Real Data       | ANN              | Three hidden slabs of different activation functions | Year             | -                                | R <sup>2</sup>      |
| 4  | (Paterson et al. 2017)               | Educational     | Energy performance | “Building characteristics: Floor area, surface exposure ratio, building depth ratio, orientation, construction year, glazing ratio, phase of education, ventilation strategy, adjacency, number of pupils, and occupancy hours”. | Annual energy use (EUI), thermal energy use, electrical energy use                         | 502 school buildings                           | (DEC), and (CIBSE)            | 80%, 10%,10% for training, testing, and validating. | Real Data       | ANN              | tangent sigmoid                                      | Year             | MATLAB                           | RMSE                |
| 5  | (Hong et al. 2014)                   | Educational     | Energy performance | “Construction year, phase of education, number of pupils,  | Fossil-thermal energy use  | 465 primary and secondary                      | UK Display Energy Certificate | 80%, 10%,10% for training, testing, and             | Real Data       | ANN              | -  | Month            | MATLAB                           | RMSE, CV, MAPE      |



**CHAPTER 2: LITERATURE REVIEW**

| ID | Study (Reference)            | Building Type   | Target             | Inputs   | Outputs   | Data  |   |                                 | Data Collection | ML Method        |                    |                  | Tools                           | Performance Metric        |
|----|------------------------------|-----------------|--------------------|--|---|---|---|---------------------------------|-----------------|------------------|--------------------|------------------|---------------------------------|---------------------------|
|    |                              |                 |                    |  |   | Volume  | Availability  | Data Split                      |                 | Model/ Structure | Function           | Predictio n Term |                                 |                           |
|    |                              |                 |                    | internal environmental conditioning, site exposure, orientation, adjacency, floor area, building depth ratio, compactness ratio, surface exposure ratio, glazing ratio, glazing type, roof shape, Heating degree-days, and Cooling degree-days". | (heating, and electricity use.                                      | school buildings  | (DEC) records   | validating.                     |                 |                  |                    |                  |                                 |                           |
| 6  | (Ascione et al. 2017)        | Office building | Energy performance | "Geometry, Envelope, Operation, and HVAC"  | Energy consumption for heating and cooling,                         | 8800 building stock   | Italian office building stock                                     | 90%, 10% for Training, Testing. | Simulation      | ANN              | sigmoidal function | Year             | Energy-Plus, MATLAB             | RMSE                      |
| 7  | (Khayatian et al. 2016)      | Residential     | Energy performance | "Several combinations of inputs were tested such as thermal conductivity i.e. walls, windows, roof and basement, volume, floor area, etc".   | Energy performance certificates / predicting heat demand indicators | 187587 Energy labels  | The online CENED database   | -                               | Real Data       | ANN              | -                  | Year             | MATLAB                          | R value, MAPE             |
| 8  | (Zhang et al. 2015)          | Office building | HVAC loads         | "Weather data (ambient dry bulb temperature) as an input variable".  | HVAC hot water energy consumptions                                  | Three months data collected   | -   | -                               | Real Data       | GPR, GMM, ANN    | Tangent sigmoid    | Day              | Monitored building energy usage | R <sup>2</sup> , RMSE, CV |
| 9  | (Kialashaki and Reisel 2013) | Residential     | Energy demands     | "Population, gross domestic product, median household income, house size, cost of residential electricity, natural gas and oil".   | Energy demand in the US residential sector                          | Data from the period of 1984–2010                                   | The data obtained from the Energy Information Administration (US) | -                               | Real Data       | ANNMLR           | logistic sigmoid   | Year             | -                               | R <sup>2</sup> , MSE, Cp  |
| 10 | (Deb et al. 2016)            | Institutional   | Cooling loads      | "Energy data for five consecutive days"  | Cooling demand  | The data of one to two years were gathered from three institutional | -   | -                               | Real Data       | ANN              | -                  | Day              | MATLAB                          | R <sup>2</sup>            |

**CHAPTER 2: LITERATURE REVIEW**

| ID | Study (Reference)           | Building Type   | Target                    | Inputs   | Outputs   | Data   |              |   | Data Collection | ML Method                   |                  |                  | Tools                           | Performance Metric   |
|----|-----------------------------|-----------------|---------------------------|--|---|--|--------------|---|-----------------|-----------------------------|------------------|------------------|---------------------------------|----------------------|
|    |                             |                 |                           |  |   | Volume   | Availability | Data Split  |                 | Model/ Structure            | Function         | Predictio n Term |                                 |                      |
|    |                             |                 |                           |  |   | buildings in the campus  |              |   |                 |                             |                  |                  |                                 |                      |
| 11 | (Naji et al. 2016)          | Residential     | Energy performance        | “Insulation K value, and insulation thickness”.  | Total heating and cooling energy                    | 180 data of different material thicknesses and insulation properties | -            | 70%, 30% for Training, Testing.   | Simulation      | ANNELM GP                   | sigmoid function | Year             | EnergyPlus, MATLAB              | RMSE, R <sup>2</sup> |
| 12 | (Platon et al. 2015)        | Institutional   | Electricity demand        | “Hourly measurements related to building operation, weather data, air temperature and relative humidity”.  | Hourly electricity consumption                      | An institutional facility (data collected over 15 month)             | -            | “Data from 2013 was used for model training, and the 2014 measurements were used as validation data”. | Real Data       | ANNCBR                      | -                | Hour             | -                               | CV, RMSE             |
| 13 | (Li et al. 2009)            | Office building | Cooling load              | “Outdoor weather parameters and indoor change of occupancy, starting and stopping of the equipment, OAT, H, and SR”  | Total cooling loads                                 | -  | -            | -   | Simulation      | ANNSVM BPNN, RBFNN and GRNN | Log              | Hour             | DeST, MATLAB                    | RMSE, MRE            |
| 14 | (Geyer and Singaravel 2018) | Office building | Cooling and heating loads | “Outdoor air-dry bulb temperature, Outdoor air relative humidity, wind speed, wind direction, sky temperature, diffuse and direct solar radiation, azimuth and latitude solar angle, solar hour angle, WWR, Orientation, Wall, window, Roof, Floor, Ground Floor, Zone”. | Total yearly heating and cooling energy consumption | 800 design combinations  | -            | 70% for training, 15% for validation, and 15% for testing   | Simulation      | ANN                         | Sigmoid function | Month , Year     | Energy Plus, MATLAB, TensorFlow | R <sup>2</sup>       |

**CHAPTER 2: LITERATURE REVIEW**

| ID | Study (Reference)              | Building Type   | Target                    | Inputs   | Outputs                                   | Data   |                                 |   | Data Collection | ML Method                 |   |                  | Tools  | Performance Metric              |
|----|--------------------------------|-----------------|---------------------------|--|---|--|---------------------------------|---|-----------------|---------------------------|---|------------------|--|---------------------------------|
|    |                                |                 |                           |  |   | Volume   | Availability                    | Data Split  |                 | Model/ Structure          | Function  | Predictio n Term |  |                                 |
| 15 | (Asl et al. 2017)              | Office building | Energy performance        | “Geometry parameters, construction parameters, and load parameters”  | Annual energy use                         | 180,000 data points  | -                               | 67% training set and 33% test sets  | Simulation      | ANN, DT                   | Rectified Linear Unit (RELU), softmax, sigmoid and linear | Year             | Autodesk Insight energy, Keras library with Scikit Learn package in Python | RMSE, R <sup>2</sup>            |
| 16 | (Chakraborty and Elzarka 2019) | Office building | Cooling and heating loads | “Year, month, day of the week, hour, holiday, daylight saving, temperature, relative humidity etc”   | Cooling electricity, Heating gas          | Four years of energy data- of a large-size office building (2012–2015) | US Department of Energy         | Year 2012 used for training the energy, and years from 2013 to 2015 used for testing. | Simulation      | ANNXG Boost OLS           | Logistic sigmoid  | Year             | EnergyPlus, Python   | RN_RMSE, R <sup>2</sup>         |
| 17 | (Lee et al. 2019b)             | Residential     | Energy performance        | “Age, income, gender, education level, job, and indoor time”.  | User based Energy Consumption             | Surveys of 5240 users  | “2014 Korean Time Using Survey” | 70%, 15%, 15% for Training, Testing, and Validating.                                  | Real Data       | ANN                       | ReLU function,  | Year             | EnergyPlus, Survey, MATLAB   | MSE                             |
| 18 | (Chou and Bui 2014)            | Office building | Cooling and heating loads | “Relative compactness, surface area, wall area, roof area, overall height, orientation, glazing area, glazing area distribution”   | (Cooling load (CL) and heating load (HL)) | 768 cases of CL and HL   | -                               | -   | Simulation      | ANN SVR, CART, CHAID, GLR | Sigmoid   | Year             | Ecotect,   | RMSE, MAE, MAPE, R <sup>2</sup> |
| 19 | (Ahmad et al. 2017a)           | Educational     | Energy performance        | “Occupancy schedule, outdoor dry-bulb temperature, indoor air temperature, blind schedule, altitude angle, month of the year, diffuse solar radiation, hour of the day, azimuth angle, total transmitted so- lar radiation and direct solar radiation” | Energy consumption , Daylight Illuminance | -  | -                               | -   | Simulation      | ANN, DT                   |   |                  | EnergyPlus, neurolab, scikit-learn   | RMSE, CV, R <sup>2</sup>        |
| 20 | (Hassanabadi and Namini)       | Residential     | Saved cooling and heating | “U-factor, SHGC, emissivity, monthly average DBT, monthly average H, monthly   | Monthly total Saved Cooling and Heating   | 400 simulations  | -                               | 80% for training, and 20% for validation  | Simulation      | ANN (MLFFN N)             | Tanh, and Log   | Monthly          | EnergyPlus   | MAPE, RMSE, R <sup>2</sup>      |

**CHAPTER 2: LITERATURE REVIEW**

| ID | Study (Reference)        | Building Type   | Target                        | Inputs   | Outputs                  | Data  |              |   | Data Collection | ML Method       |                                     |                 | Tools                            | Performance Metric        |
|----|--------------------------|-----------------|-------------------------------|--|--------------------------|---|--------------|---|-----------------|-----------------|-------------------------------------|-----------------|----------------------------------|---------------------------|
|    |                          |                 |                               |  |                          | Volume  | Availability | Data Split  |                 | Model/Structure | Function                            | Prediction Term |                                  |                           |
|    |                          |                 |                               | average WS, monthly average direct SR, monthly average diffuse SR, O, month of the year”                                 |                          |   |              |   |                 |                 |                                     |                 |                                  |                           |
| 21 | (Ilbeigi et al. 2020)    | Office building | Energy demands                | “Wall U-value, equipment load rate, lighting density, infiltration rate, number of people, and roof U-value. Apparently” | Energy use intensity EUI | 1602 simulated cases  | -            | 70%, 15%, 15% for Training, Testing, and Validating   | Simulation      | ANN             | Logistic sigmoid                    | Year            | Energy-Plus, Grasshopper, MATLAB | MSE, R                    |
| 22 | (Kazanasmaz et al. 2009) | Office building | Electrical energy consumption | “Date, hour, OAT, SR, H, UV index, UV dose, distance to window, O, floor ID, room ratio, point ID and illuminance”       | Illuminance              | The period between the months of November 2007 and January 2008 | -            | -   | Real data       | ANN (MLFFNN)    | Tanh                                | Hourly          | Digital lightmeter               | PE                        |
| 23 | (Hasni et al. 2012)      | -               | Solar radiation               | “Month, Day, Hour, TEMP, RH”   | Global solar radiation   | 02 Feb-31 May 2011  | -            | 80% for training, and 20% for testing   | Real data       | ANN             | Hyperbolic tangent sigmoid, purelin | Hourly          | MATLAB                           | RMSE, MAE, R <sup>2</sup> |
| 24 | (Koca et al. 2011)       | -               | Solar radiation               | “Lat, lon, alt, month, average cloudiness sunshine duration average wind velocity average humidity average TEMP”         | Global solar radiation   | Jan 2006 Dec 2006   | -            | Data from 2005, 2007 and 2008 were used for training, while data from 2006 was utilised to test the network model | Real data       | ANN             | Tangent sigmoid activation          | Monthly         | MATLAB                           | RMSE, R <sup>2</sup>      |
| 25 | (Ozgoren et al. 2012)    | -               | Solar radiation               | “Lat, lon, alt, month, mean land surface temperature”  | Global solar radiation   | 206 data records  | -            | 90% - 10%   | Real data       | ANN             | Sigmoid function                    | Monthly         | MATLAB                           | RMSE, R <sup>2</sup>      |
| 26 | (Notton et al. 2012)     | -               | Solar radiation               | “Hour, declination, zenith angle, horizontal global solar irradiation, extra-terrestrial horizontal solar irradiation”   | Global solar radiation   | Jan 2006 - Dec 2010 1st   | -            | 60% - 40%   | Real data       | ANN             | Sigmoid transfer function           | Monthly         | -                                | RMSE, MAE                 |

**CHAPTER 2: LITERATURE REVIEW**

| ID | Study (Reference)       | Building Type | Target             | Inputs  | Outputs                               | Data                                    |  |            | Data Collection | ML Method       |          |                 | Tools        | Performance Metric                  |
|----|-------------------------|---------------|--------------------|---|---------------------------------------|---|--|------------|-----------------|-----------------|----------|-----------------|--------------|-------------------------------------|
|    |                         |               |                    |   |                                       | Volume                                  | Availability                             | Data Split |                 | Model/Structure | Function | Prediction Term |              |                                     |
| 27 | (Mellit and Pavan 2010) | -             | Solar radiation    | “Daily solar irradiance, mean daily air TEMP, DOM”  | Global solar radiation                | -                                       | -  | -          | Real data       | ANN             | -        | Day             | MATLAB       | RMSE, MBE                           |
| 28 | (Benghanem et al. 2009) | -             | Solar radiation    | “Air temperature, relative humidity, sunshine duration, and the day of year”  | The global horizontal solar radiation | Data from 1998 to 2002                  | The National Renewable Energy Laboratory | -          | Real data       | ANN             | -        | Day             | MATLAB       | RMSE, MBE, MPE                      |
| 29 | (Tso and Yau 2007)      | Residential   | Electricity demand | “Flat size, number of members in the household, and ownership of air-conditioner”   | Electricity energy consumption        | 1201 records of household’s energy data | -  | -          | Real data       | DT              | -        | Week            | -            | RASE                                |
| 30 | (Yu et al. 2010b)       | Residential   | Energy demand      | “Annual average air temperature, house type, construction type, floor area (m2), heat loss coefficient (W/m2K), equivalent leakage area (cm2/m2), number of occupants, space heating, hot water supply kitchen”       | Energy use intensity EUI              | 80 residential buildings in Japan       | -  | -          | Real data       | DT              | -        | Year            | -            | -                                   |
| 31 | (Ahmad et al. 2017b)    | Hotel         | HVAC loads         | “DBT: outdoor air temperature, DPT: dew-point temperature, RH: relative humidity, HR: hour of the day, Mon: month of the year, Day: day of the week, WS: wind speed”  | Hourly HVAC energy consumption        | Data from Jan/2015 until April/2016     | -  | -          | Real data       | DT              | -        | Hour            | scikit-learn | RMSE, CV, MAPE, MAD, R <sup>2</sup> |
| 32 | (Hong et al. 2012a)     | Educational   | Electricity demand | “Location (e.g., region), building (e.g., founder type, structure type, elapsed years, building area, No. of stories, and total floor area), and inhabitants (e.g., No. of students, No. of teachers, No. of classes, | Energy consumption                    | 6282 elementary schools’ buildings      | -  | -          | Real data       | DT              | -        | Year            | -            | -                                   |

**CHAPTER 2: LITERATURE REVIEW**

| ID | Study (Reference)        | Building Type   | Target             | Inputs  | Outputs                                     | Data                                 |  |  | Data Collection | ML Method        |          |                  | Tools                | Performance Metric        |
|----|--------------------------|-----------------|--------------------|---|---|--------------------------------------|--|--|-----------------|------------------|----------|------------------|----------------------|---------------------------|
|    |                          |                 |                    |   |   | Volume                               | Availability                           | Data Split   |                 | Model/ Structure | Function | Predictio n Term |                      |                           |
|    |                          |                 |                    | and No. of students per class)”   |   |                                      |  |  |                 |                  |          |                  |                      |                           |
| 33 | (Tsanas and Xifara 2012) | Residential     | Energy performance | “Relative compactness<br>surface area<br>wall area<br>roof area, overall height<br>orientation<br>glazing area<br>glazing area distribution<br>”  | Total heating and cooling energy            | 768 distinct houses                  | -                                      | -  | Simulation      | DT               | -        | Year             | Ecotect              | MAE, MSE                  |
| 34 | (Ahmad et al. 2017c)     | Educational     | Energy performance | “Solar altitude angle, solar azimuth angle, direct normal radiation, diffuse horizontal radiation, day of the week, hour of the day, month of the year, outdoor dry-bulb air temperature, wind speed, outdoor air relative humidity, window blind position, occupancy “ | Daylight illuminance and energy consumption | Classroom model in a school building | -                                      | -  | Simulation      | DT               | -        | Year             | EnergyPlus           | RMSE, CV, R <sup>2</sup>  |
| 35 | (Ma and Cheng 2016)      | Residential     | Energy demand      | “Building, economy, education, environment, households, surrounding, and transportation”  | Energy use intensity (EUI)                  | 3640 multi-family Houses             | The Department of City Planning of NYC | -  | Real data       | DT               | -        | Year             | -                    | MSE, RMSE                 |
| 36 | (Alammar et al. 2021)    | Office building | Solar radiation    | “Hour, month, building contexts (b00, b01, b02, b03), façade floor level, orientation, and façade level height, features are x/y/z coordinates of the test points”  | Incident solar radiation                    | 50,545 total number of iterations    | -                                      | 80% for training, 6.67% for validation, and 13.37% for testing | Simulation      | (RF)/ANN         | ReLU     | Hour             | Grasshopper, PyTorch | RMSE, MAE, R <sup>2</sup> |
| 37 | (Barus 2021)             | Office building | Solar radiation    | “Location of the PV Module, size of the panel, orientation of the   | Annual solar radiation (ASR)                | 2200 random layouts were generated   | -                                      | -  | Simulation      | (RF)             | -        | Year             | Revit                | MAPE, R <sup>2</sup>      |

**CHAPTER 2: LITERATURE REVIEW**

| ID | Study (Reference)   | Building Type | Target          | Inputs  | Outputs                        | Data  |                                     |            | Data Collection | ML Method        |          |                  | Tools | Performance Metric        |
|----|---------------------|---------------|-----------------|---|--------------------------------|---|-------------------------------------|------------|-----------------|------------------|----------|------------------|-------|---------------------------|
|    |                     |               |                 |   |                                | Volume  | Availability                        | Data Split |                 | Model/ Structure | Function | Predictio n Term |       |                           |
|    |                     |               |                 | PV module, and size and orientation of panels above the PV module”                |                                |   |                                     |            |                 |                  |          |                  |       |                           |
| 38 | (Moosa et al. 2019) | -             | Solar radiation | “Temperature, relative, humidity, pressure, rainfall, wind speed, wind direction” | Global horizontal irradiation  | Year (2017) for training. from January 2018 to April 2018 for testing | Solar radiation data (SoDa) website | -          | Real data       | (RF)             | -        | Hour             | -     | RMSE, MAE                 |
| 39 | (Wei 2017)          | -             | Solar radiation | “Ground weather, satellite remote-sensing, and sun position”                      | Hourly surface solar radiation | hourly data for 7 years (2010–2016)                                   | -                                   | -          | Real data       | (RF)             | -        | Hour             | -     | MAE, RMSE, R <sup>2</sup> |

### **2.13. Identified Gaps and Conclusions**

Section (2.5.2) reviewed the previous research on AFs in the area of BPS. Each of the studies is classified according to their AF system technology, which includes (whether the system is conventional or non-conventional, the AF system type, the building type, and the climate), their ability to simulate dynamic or static states, and whether the adaptation is based on geometric or material changes. In addition, the evaluation methods used in these studies according to its capabilities and challenges, their control strategy, control sensors, and the design objective of the system.

Current studies showed that simulation software tools have difficulties when modelling complicated AF systems that modify their geometry components based on different time steps either per minute, hour, or season. Additionally, there is no straightforward method, and there is a lack of well-accepted methods to evaluate the adaptive behaviour of a façade. In recent studies, the automatic control system to automate non-conventional AF systems was not properly considered during the simulation due to the complexity and the interface limitations of current PBS systems. However, the automatic control system was employed in the case of dynamic façades with basic movement (conventional façade), such as Venetian blinds, roller shades, dynamic blinds, and louvres. In these shading systems, the adaptive behaviour is not complex, and modelling and simulating the model is integrated into most BPS software packages. Lastly, studies confirmed that setting up the model for simulating the AF system is time consuming and challenging with the current PBS tools.

Since the development of AFs has increased significantly in recent years (Elzeyadi 2017; Hosseini et al. 2019b; Böke et al. 2020; Bui et al. 2020; Panya et al. 2020; Shi et al. 2020), it is essential to find an alternative approach that requires less computational knowledge and that is less time consuming for predicting their performance efficiently during the early design stages. To the best of the author's knowledge, no studies have used ML algorithms to predict the energy performance of AFs. The lack of well-accepted strategies and the mentioned limitation to simulate the adaptive behaviour of a façade, therefore, points to the need to find an alternative method, such as ANN or DT as emulators surrogate models to predict the energy performance of AFs. Thus, ANN and RF will be developed and validated to predict the performance of AF systems in significantly less time compared to BPS tools. The specific research methods concerned with filling the identified gaps in literature are detailed in the next chapter.



## **CHAPTER THREE**

### **RESEARCH DESIGN AND METHODOLOGY**

**CHAPTER 3: RESEARCH DESIGN AND METHODOLOGY**

**3.1. Introduction**

This research will frame a suitable research design, including the development of appropriate techniques and methods, to conduct this study rigorously. The chapter begins by describing the research design and methodology for this investigation, as well as reviewing the philosophical paradigms, approaches, strategies, and methodologies utilised in this study, and providing the rationale behind their selection. In addition, it presents the data collection and analysis methods utilised to ensure that the research questions, objectives, and aims have been addressed.

Numerous disciplines have a common research process; however, what varies per domain is the nature of the research challenges and objectives. Research challenges and questions in architectural design relate to buildings, their occupants, the environment, and their design, as well as construction processes, building systems and materials, the design process, etc. It is possible to address a wide range of issues, including both basic and applied research, but they all centre on buildings, their occupants, their environments, and the nature of certain design stages (Aksamija 2021). Figure (3.1) shows typical architectural design phases, starting with pre-design, conceptual design, schematic design, design development, construction documentation, construction administration, building operation, and post-construction activities.

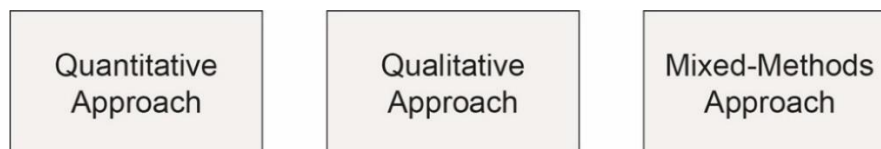
**DESIGN PHASES**



*Figure 3.1: Typical architectural design phases.*

## **3.2. Research Methodology and Methods**

A research methodology is a comprehensive framework that supports the fundamental concepts associated with a research paradigm (O’Leary 2017). Aksamija (2021) defined research methods as the mechanisms used to examine the established research questions. Researchers use research methods to test their theories and hypotheses. According to Kothari (2004), a research methodology is a systematic inquiry designed to answer research questions. The following section will discuss the three common research methodologies, namely, quantitative, qualitative, and mixed methods, in addition to their related techniques and methods. A unique set of strategies and procedures are used in each of these methods. Figure (3.3) shows the basic characteristics of the three research methodologies.



*Figure 3.2: The basic characteristics of the three research approaches.*

### **3.2.1. Quantitative Approach**

The objective of a quantitative approach is to collect factual data to explore the correlations between facts. It includes variables and data that have been measured and analysed statistically (Genot 2018). Research questions and hypotheses can be tested using numerical data obtained through this method. Quantitative methods generally use experimental and survey design strategies including questionnaires, structured interviews, and structured observations for collecting data (Aksamija 2021). The most common quantitative methods in architectural research include simulation and modelling, quantitative surveys, and correlational research. These research methods are objective by their nature. They can be used to predict the future performance of buildings, analyse human behaviour and opinion, test hypotheses, and investigate building performance and the built environment (Aksamija 2021).

Simulations use models to imitate real-world scenarios and to study their behaviour, interactions, performance, etc. It is possible to use simulations in architectural research to investigate the efficiency of building systems and materials, energy-consumption of buildings, structural studies, daylighting, and the flow of people through a space. Typically, simulations rely on computer-generated models of the system or process being studied to predict their behaviour. As a result, a model represents an object or process, and there are three different types: visual, mathematical, and computational.

### **3.2.2. Qualitative Approach**

The qualitative research method seeks to comprehend the participants' perspective. For example, it can be used to study participants' reactions to a phenomenon as well as their ideas, behaviours, and feelings prior to experiencing it (Groat and Wang 2013; Saunders et al. 2016). It collects qualitative data to study specific research issues, often concentrating on human, social, behavioural, cultural, historical, or theoretical aspects of architectural research (Creswell 2014). This method is primarily employed in the fields of the humanities, sociology, and anthropology (Braun and Clarke 2015). This method is usually associated with the inductive approach, where researchers collect evidence to develop concepts and form theories instead of testing hypotheses as in the deductive approach. Qualitative approaches collect data from a variety of sources, including interviews, observations, focus groups, archival research, and existing documents. Therefore, data analysis and interpretation by researchers are crucial elements of the qualitative research process.

### **3.2.3. Mixed-Methods Approach**

Many researchers prefer quantitative research methods to qualitative methods, or vice versa. Each of these methods has its advantages and disadvantages. However, a mixed-methods approach combines qualitative and quantitative methodologies by employing various strategies (Creswell and Clark 2011). For studies with numerous goals, a mixed-methods approach is ideal since it promotes generalisations and shared findings (Kumar 2014). Different phases of research, including data collection, data processing, interpretation, and dissemination, might employ a mixed methods approach. The findings from the various approaches can be used to compare, corroborate, or disprove the research's claims (Kumar 2014). According to Bryman (2016), conducting a mixed-methods research project requires additional time and money. Consequently, the researcher must arrange for sufficient resources, in terms of both cost and time.

## **3.3. Choosing a Quantitative Approach**

The method selected for this research was determined by the research questions, aim, and objectives derived from the research problems and the study's rationale. The research methodology employs a quantitative approach to data collection with the objective of developing a surrogate model as alternative to the existing Building Performance Simulation tools (BPS) for predicting the performance of AFs in office buildings in the early stages of the design, using data that are expressed numerically, such as solar radiation, shade factor, operative temperature, cooling loads, hours, months, etc., Moreover, the methodology used

in this research is underpinned by simulation and modelling and by case studies of office buildings in a numerical manner. Thus, these methods of data collection are quantitative as opposed to qualitative methods. According to Punch (2005) and Saunders et al. (2016), quantitative research typically employs numerical data and has a predetermined or fixed structure, predetermined research questions, and predetermined objectives. In addition, Creswell (2014) described certain features of quantitative studies, such as the use of closed-ended questions, a predetermined technique, and the numerical observation of data.

The rationale behind adopting a quantitative research method as opposed to a qualitative one is that it makes possible the testing of hypotheses and the determination of whether a theory is supported. In addition, it allows for the generalisation or replication of research results due to its alignment with a deductive approach (Allwood 2012; Creswell 2014). Based on the defined hypothesis, data are obtained to either confirm or deny the hypothesis and provide additional insight into the topic. This study is not concerned with the social aspects of a phenomenon; rather, it focuses on the environmental impact of AFs on workplace cooling energy usage. As a result, the method for social studies was not implemented.

### **3.4. Research Design**

A research design is defined as “the ways which the data will be collected, analysed in order to answer the research questions posed and to provide a framework for undertaking the research” (Knight and Ruddock 2009). Furthermore, it is up to “the plan, structure, and strategy of investigation to find answers to research questions as validly, objectively, accurately, and economically as possible” (Groat and Wang 2013). The quality of research is determined by the way the research activities are organised, by the appropriate methods used to gather and analyse data, and by the fulfilment of the study's objective. The following section outlines the framework for conducting this research. It will detail how the data were obtained, stored, trained, and validated to develop a predictive surrogate model using computational algorithmic workflow and machine learning techniques.

### **3.5. Research Framework**

Undertaking a research study requires an early indication of the various stages of the research (Kumar 2014). Thus, the researcher must plan the data collection, analysis, and assessment phases of an investigation after the topic and research approach have been selected. The research plan for the overall procedure is represented in Figure (3.4). This research was carried out in five phases to achieve its objectives. These phases are identified in the section below:

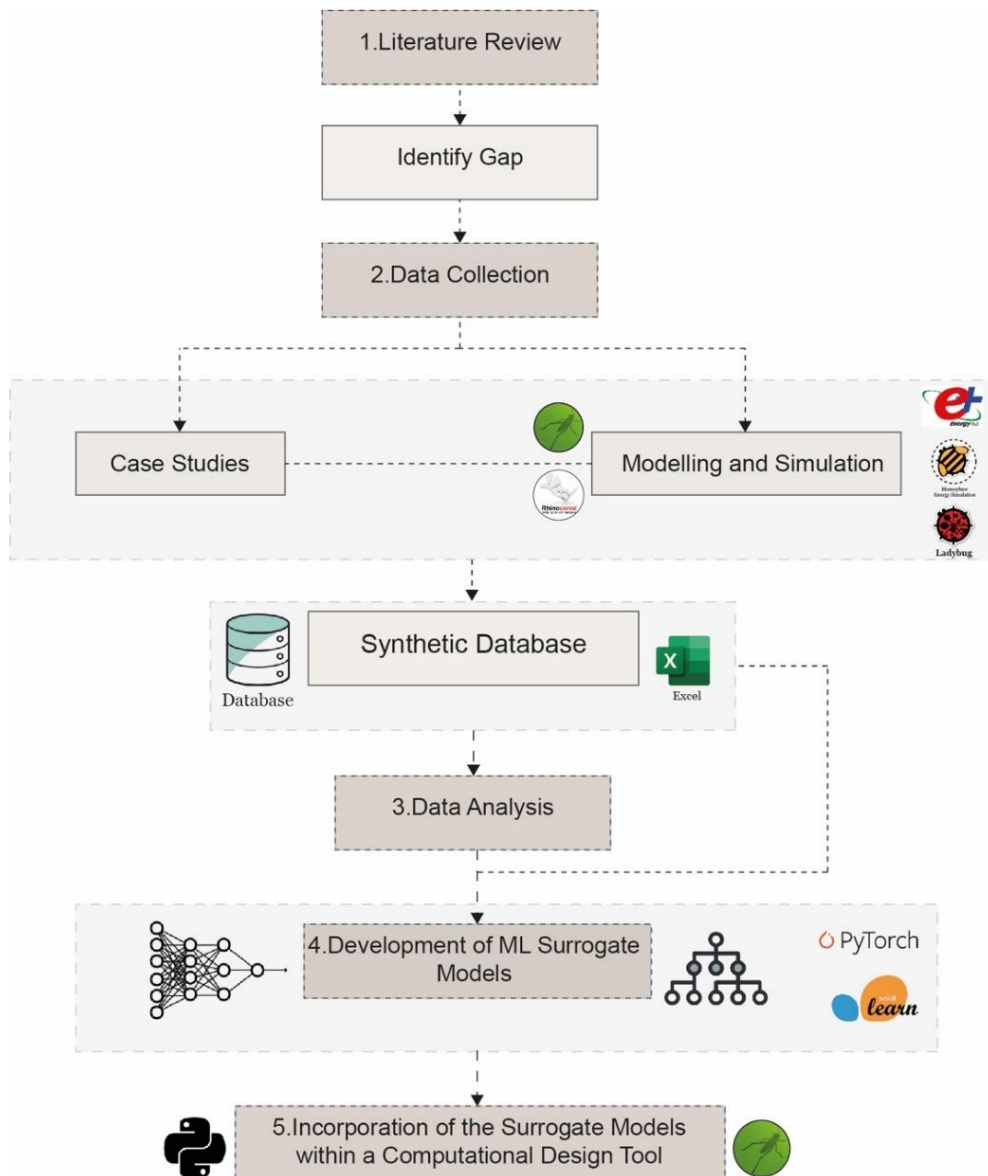


Figure 3.3: The overall research framework.

### 3.5.1. Literature Review

During this phase, the researcher studied the relevant literature to identify the knowledge gaps and gain a comprehensive grasp of the issue. Conducting an ongoing literature review allows the researcher to keep abreast of new developments in the field and gain from knowledge shared by others in the area (Wisker 2007). Murray and Hughes (2008) stated that it is helpful to review previous studies and their findings, as the in-depth knowledge of other researchers helps to uncover knowledge gaps (Murray and Hughes 2008). In addition to helping in the development of a research technique, the literature review aids in understanding the existing systems, methodologies, and technical approaches for a study.

## **CHAPTER 3: RESEARCH DESIGN AND METHODOLOGY**

The data for this study were extracted from a variety of sources, such as highly ranked peer-review journals and databases, Google Scholar, credible websites, books, e-books, and government websites. The literature review for this study is organised into three sections; part (1) presents an introduction to AFs, their history, similar terms used by scholars and their distinctions, and the influences of AFs on buildings' energy consumption. In addition, this section analyses the usage of automatic control systems to automate the AF, as well as their responsive time scales, and adaptation scales.

Part (2) explored the challenges and difficulties designers face in predicting the performance of an AF shading system using the existing BPS tools. In addition, some of the current simulation tools are examined and their limitations regarding AF performance prediction are highlighted. This part also discusses the existing AF studies by looking at three main factors: (1) AF system type, including whether the system is conventional or non-conventional, building type, and climate; (2) adaptability; and (3) performance. The adaptability and performance group includes the following parameters: adaptive typology, the state and type of change it generates, the behaviour changes generated by the system (whether geometrical or material-based), the timeframe of adaptability and its various configurations, the evaluation methods used, the control strategy, the control sensors, the physical domain of the performance evaluation, and the design objective of the system.

Part (3) reviewed machine learning techniques and their potential use for building performance predictions. In addition, two machine learning models, namely, Artificial Neural Network (ANN) and Decision Tree (DT), were reviewed as well as the process of development of a surrogate model. This part also covers current research that employed ANN, DT or RF approaches for predicting building performance, with an emphasis on energy and solar radiation studies. The review is organised primarily according to the following factors: (1) general information, (2) data description, (3) algorithm, and (4) performance evaluation.

### **3.5.2. Data Collection**

Data collection was the second phase of the research, which consisted of two main activities: case studies, and modelling and simulation. The section below provides a comprehensive explanation of the collected data.

#### **3.5.2.1. Case studies**

The chosen case studies were the base of the modelling and simulation phase. These case studies were used and analysed numerically to help in forming the prototype physics (design

### **CHAPTER 3: RESEARCH DESIGN AND METHODOLOGY**

factors) of the base case model of the study, such as the building plan, floor height, floor plate efficiency, leasing depth, number of floors, gross floor area (GFA), net leasable area (NLA), core dimensions, and glazing orientation, etc. This process was useful to accomplish the first stage for creating and setting up the digital model and its input parameters, the aim being to define the existing typical office building, and the design characteristics of high-rise office buildings in the studied region, Riyadh city. In addition, the base office model was developed with the consideration for building regulations, design guidelines, benchmarks, and the integration of knowledge from the literature. Therefore, the prototype could be representative of actual case study buildings.

A total of twenty-four high rise office cases were selected, and these cases were located at the central area of downtown Riyadh and the downtown area of King Abdullah financial district. These case study data were collected from design documents, architecture firms' webpages, books, magazines, and internet websites. The selection process was based on the following criteria:

- The study focuses on office towers in high rise buildings located in hot-arid climates as the chosen case is Riyadh city; thus, the selection of cases covered only high-rise office buildings in Riyadh.
- Availability of drawings and illustrations.
- Cases with a minimum of thirteen storeys were selected, as this defines the minimum height of high-rise office buildings.

#### **3.5.2.2. Data Collection Using Modelling and Simulation**

Machine learning (ML) models demand employing a sufficient database to construct the surrogate model to achieve highly accurate prediction results. Hence, a synthetic database was generated in this phase using a simulation technique due to the absence of real data for developing a ML surrogate model, which will be discussed on phase (4). Therefore, this phase examined in detail the modelling and simulation of an office tower with AF, situated in a hypothetical urban context. Results of the analysis in phase (1) were used to inform the digital model before conducting the simulation aiming to create a prototype that would represent the real case of office buildings.

This phase had two main objectives: (1) developing an algorithmic workflow to predict the energy consumption of AFs using a computational parametric tool to propose a workflow to overcome the existing challenges as discussed in section (2.5), and (2) building a database of hourly cooling loads, hourly solar radiation, and hourly shade factor to be used for training



### **CHAPTER 3: RESEARCH DESIGN AND METHODOLOGY**

the machine learning model. Thus, the framework for developing this phase to generate the required database could be structured in four primary stages:

- (1) Development of the hypothetical base model and its surrounding context.
- (2) Validation of the model.
- (3) Implementation of AF system.
- (4) Automation of the system based on different external and internal dynamic conditions.

Three evaluation approaches have been identified in the literature: field measurements and surveys, numerical calculations, and simulation tools. Experiments are the most precise but also the most costly and time-consuming way, whereas numerical calculations, such as mathematical formulas and simulations, require validation. Simulation was used in this study to collect data because it is the most cost-effective way when time and money are the main constraints, and it has advantage of being cheaper and, of being used in early predictions, and of being a widely used method especially given the unavailability of a physical building in which to conduct experiments. Furthermore, with simulations, it is possible to analyse a wide range of design scenarios and complex modelling that cannot be accomplished easily on a real-world scale. In addition, there was no available access to real data. This research develops a simulation-based framework to predict the performance of AF for reducing the annual cooling energy consumption in office towers as well as for building a database to support the research framework. To achieve this, a computational parametric tool 'Rhinoceros 3D' and its plug-in 'Grasshopper' were used to facilitate the parametric generation and simulation of the AF system. Moreover, Ladybug and Honeybee plug-ins were used, that is linked to Energy Plus and Radiance, to calculate energy loads and solar radiation. The proposed algorithmic workflow created a link between plug-ins including Ladybug, Honeybee tools, and Energy plus for running the simulation with an energy management system (EMS) to program a code that would be able to automate the AF system before each time step of the simulation, and lastly, with a Colibri plug-in tool to step through all the design variations automatically to create the dataset. Then, TT toolbox stored the resulted data in an Excel spreadsheet. The use of the algorithmic approach offered a flexible multidisciplinary platform for simulating AFs that respond to dynamic boundary conditions, as well as they help in performing a large number of simulation iterations.

The initial step was to develop a prototype with its multiple configurations. As the study aim is to investigate the effect of AF on energy consumption; thus, understanding the model inputs is critical to the study's investigation, as some will be static, and others will be

dynamic. if these parameters are correct and valid, and simulation tools are used accurately, then the evaluation process can begin, and the output data should be reliable. In this study, the prototype of a building without an AF (base model) must be developed and validated prior to the completion of simulations on prototypes with AF systems. The validation process ensures that the base case model accurately represents real office buildings by comparing its simulation outputs.

McHaney (1991, p. 95) defined the validation technique as “The process of determining that the real-world system being studied is accurately represented by the simulation model. This process ensures that the conceptual model is correct. It establishes an acceptable level of confidence that the conclusions drawn from running the simulation will give insight to the true operating characteristics of the system being modelled. The validation process should begin during the initial stage of a simulation project and continue until the end... Model validation can be best determined through the analysis of the simulation output data. If the model output closely represents the expected values for the system’s real-world data, it is considered to be valid”.

Chapter 4 will describe in detail the prototype's development phase, the simulation, and the validation of the base case prior to evaluation. The steps of the conducted simulations are outlined below:

- 1- Modelling (Rhino, Grasshopper, and Colibri)**
- 2- Validation of the Base Model**
- 3- Solar Radiation Analysis (SR) (Ladybug tool)**
- 4- Shade Factor Analysis (SF) (Ladybug tool)**
- 5- Energy Simulations (Honeybee tool, which was linked to Energy Plus)**
- 6- Adaptive Façade Automatic Control System (Energy Management System EMS)**
- 7- Database Recording (Colibri and TT toolbox (Excel))**

Because machine learning requires sufficient data for training the surrogate model, parametric design tools were used, as they help in performing a large number of simulation iterations. However, conducting simulations is time consuming and requires high computational power. Therefore, this research used a set of cloud-based machines to overcome the issue of time consumption, which will be discussed below.

Regarding simulation time, running a simulation of this scale demands a high level of computational power that standard computers cannot provide. Consequently, in addition to a powerful PC, a series of cloud-based machines were customised via the Paperspace web-based platform (<https://www.paperspace.com>). Each machine was composed of the

## **CHAPTER 3: RESEARCH DESIGN AND METHODOLOGY**

following hardware properties: Quadro P5000, 8 CPU, 30GBRAM, 50GB SSD (Internal Storage), 100GB SSD (External Storage), and dedicated GPU.

### **3.5.3. Data Analysis**

The data analysis was the third phase of the research where the outcomes of the simulations were analysed and compared. This phase evaluated the following:

- Engineering parameters, such as exterior wall and glazing types.
- External shading system types including fixed vertical shading, fixed horizontal shading, AF with scaling movement, and AF with folding movement.
- Different control scenarios including (C1: incident solar radiation on window (W/m<sup>2</sup>), C2: transmitted solar radiation (W/m<sup>2</sup>), C3: direct solar radiation (W/m<sup>2</sup>), and C4: both incident solar radiation and operative temperature).
- Office orientation.
- Building contexts.
- Shading state variations.

### **3.5.4. Development of Machine Learning Surrogate Models**

Based on the discussed studies, machine learning models can be used to predict the energy performance of buildings. This can be achieved by developing a model which requires sufficient data to train, test, and validate the model. Therefore, in this phase, the synthetic database that was generated using simulation in phase 2 was translated and pre-processed into two machine learning models: ANN, and RF. The collected cooling loads database and solar radiation database were used to construct, train, and validate these models. The constructed predictive tool aims to assist architects to predict the energy performance of AFs during the early phases of the design in significantly less time compared to PBS tools. Different steps were undertaken to develop the surrogate model as follows (Figure 3.5):

- Data pre-processing.
- Model training, testing, and hyper-parameter tuning.
- Model validation.

The research developed different surrogate machine learning models include (1) Artificial Neural Network (ANN) to predict hourly solar radiation, (2) Random Forest (RF) to predict hourly solar radiation, (3) Artificial Neural Network (ANN) to predict hourly cooling loads, (4) Random Forest (RF) to predict hourly cooling loads, and (5) Random Forest (RF) considering the time series data.

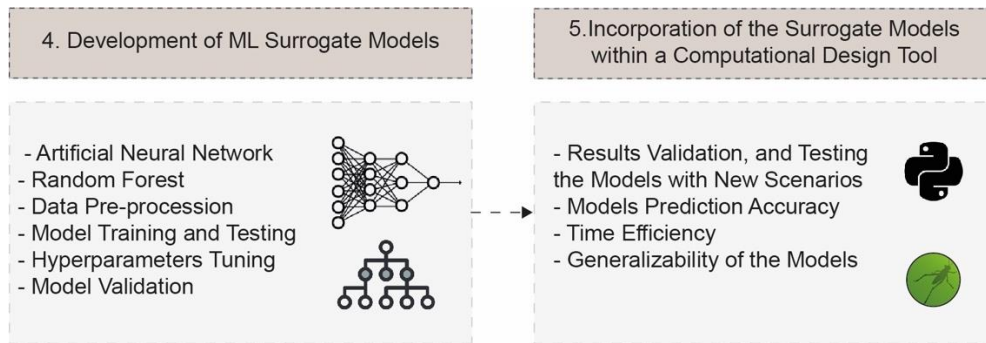


Figure 3.4: A diagram showing (Phase 4: Development of ML surrogate models), and (Phase 5: Incorporation of the surrogate model within a computational design tool).

A comparison was conducted between ANN and RF in both cases of the design objectives: hourly solar radiation and hourly cooling loads regarding model predictions. In addition, a comparison was conducted to examine the time series inputs using RF modelling. To analyse the effect of time in the data, two sets of experiments were carried out including the time window approach and the time differencing approach. These models were developed using Python programming language (Pytorch framework) and (scikit-learn). The experiment used two PCs with the following specifications: Intel Xeon E5-2630 CPU, 80 GB RAM, and Nvidia GeForce GTX 1080-Ti GPU, and Intel Core i9-10920X - 12 Cores 3.5 GHz, NVIDIA GeForce RTX 3080 10 GB GDDR6X, 16 GB DDR4.

**The Artificial Neural Network (ANN) was structured as follow:**

**(1) Modelling and training settings:**

- The ANN type used was the Multilayer's feedforward with the back propagation technique.
- Input data were pre-processed prior to training (some were treated as categorical or discrete, while others were treated as continuous).
- The performance of the network was evaluated with the root mean square error (RMSE), mean absolute error (MAE) and  $R^2$ -score.

**(2) Optimization**

- The optimization is a critical process in the development of machine learning models; it ensures an appropriate network is chosen to avoid the under fitting or over fitting of the data and to achieve a better generalization of the network. The experiment of hyper-parameters tuning was carried out using two different procedures: (A) *Optimization using grid-structure*, and (B) *K-fold cross validation*.

**(3) Validation and Testing**

### **CHAPTER 3: RESEARCH DESIGN AND METHODOLOGY**

- After selecting the optimal architecture network, a new model was constructed using the entire training data set. Then, the developed model was tested with the unseen testing data set.
- Random cases were tested to compare the prediction accuracy between simulated data prediction with ANN model prediction.

***The Random Forest (RF) was structured as follows:***

**(1) Modelling and training settings:**

- Input data were processed prior to training (some were treated as categorical or discrete, while others were treated as continuous).
- The performance of the network was evaluated with the root mean square error (RMSE), mean absolute error (MAE), and R<sup>2</sup>-score.

**(2) Optimization**

- The experiment of hyper-parameters tuning was carried out using two different procedures: (A) *Optimization using grid-structure*, and (B) *K-fold cross validation*.

**(3) Validation and Testing**

- The developed model was tested with the unseen testing data set.
- Random cases were tested to compare the prediction accuracy between simulated data prediction with ANN model prediction.

#### **3.5.5. Incorporation of the Surrogate Models within a Computational Design Tool, and Validation of the Results.**

The trained surrogate models were imported into a computational design tool (Grasshopper) to establish a workflow to predict the energy performance (cooling loads) of the design scenarios of an AF system in the early stages of the design for design decision-making. The surrogate models (ANN and RF) were saved as a pickle file (PyTorch file), which is a specialized format that helps to run ML models in an external environment. The surrogate models were evaluated in terms of prediction accuracy, time efficiency, and their generalisation prediction capability. To validate the result, the results obtained from the developed surrogate models (ANN and RF) were compared to the simulation results for both hourly cooling loads and hourly solar radiation. Moreover, the time required to make a prediction was compared between the simulated results and the predicted results using the surrogate models.

Following that, a new design scenario was created to test new cases with the developed ML models in phase (4) and to predict the outcomes within the Grasshopper interface. The new design considers several office towers in different urban contexts compared to the original

### **CHAPTER 3: RESEARCH DESIGN AND METHODOLOGY**

model done during the simulation phase. The aim is to test large scale modelling and compare the time required to make predictions using ANN and RF models with the time required to make predictions using simulation tools. Furthermore, different cities that shared hot climate characteristics similar to those of the current study were tested regarding the prediction accuracy of the developed surrogate models.

### **3.6. Chapter Summary**

This chapter presented the research design and approach adopted, as well as the data collection, data analysis, model development, and validation and testing processes. To meet the research objectives, a quantitative approach was employed. Table (3.1) presents the research objectives and methodologies employed. Figure (3.6) shows the research framework of all stages.

*Table 3.1: Research objectives and methods*

|   | <b>Research Objectives</b>   | <b>Research Methods</b>  |
|---|--|--|
| 1 | - Investigate the impact of adaptive façade on energy performance.   | Literature search  |
| 2 | - Develop an algorithmic workflow to evaluate the energy performance of AF shading system.   | Computational approach<br>Ladybug, Honeybee tools,<br>EnergyPlus & EMS |
| 3 | - Generate a synthetic database of AF cooling energy loads of offices to train and test the surrogate models.                                    | Computational approach<br>(Modelling and simulation)                   |
| 4 | - Develop machine learning models to predict energy performance of AF in the early stage of the design.  | Machine learning (ANN and RF)  |
| 5 | - Establish a workflow that incorporates the surrogate model within a computational design tool to assist in early-stage design-decision making. | Computational approach<br>(Grasshopper- GH C Python)                   |

**CHAPTER 3: RESEARCH DESIGN AND METHODOLOGY**

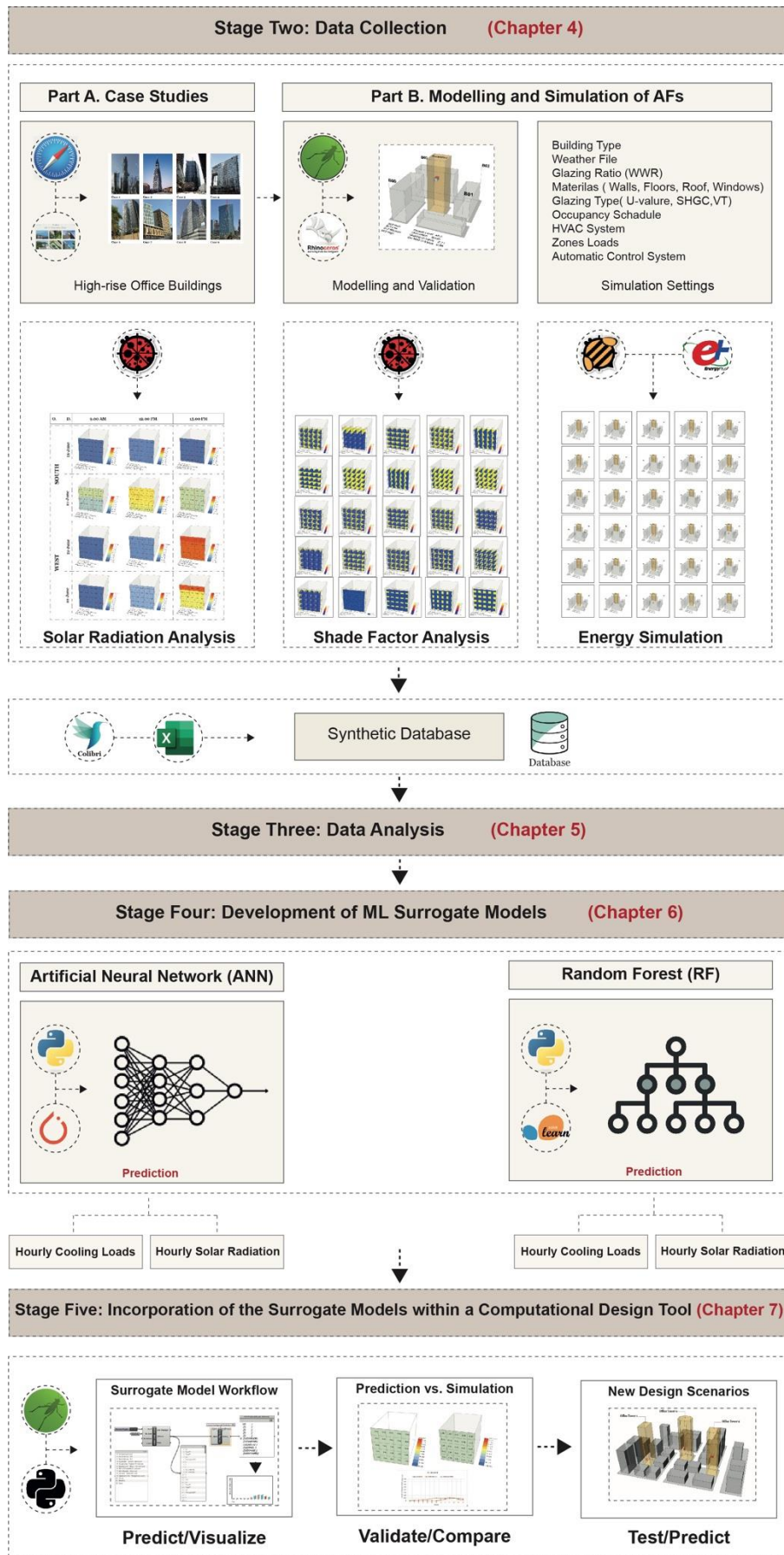


Figure 3.5: The research framework.

## **CHAPTER FOUR**

# **SYNTHETIC DATABASE GENERATION USING SIMULATION APPROACH**



## **CHAPTER 4: SYNTHETIC DATABASE GENERATION USING SIMULATION APPROACH**

### **4.1. Introduction**

This chapter aims to consider the data generated using the simulation approach for developing the machine learning (ML) models. In the building domain, researchers can collect data to establish a surrogate model from three different resources: (1) data collected from sensors, such as smart meters, building management systems, and the internet of things (IoT), (2) data collected from building stock, such as annual energy demand, and (3) data collected from building simulations, such as the results from building simulation tools (Westermann and Evins 2019b). The study adapted the synthetic databases (simulation-based approach) to develop the surrogate model because the data can be generated using simulation software within a reasonable time compared to actual data, the collection of which could take years. In addition, in most cases, real data is not as easily accessible as such data obtained from simulation. Furthermore, with simulations, it is possible to analyse a wide range of design scenarios and complex modelling that cannot be accomplished easily on a real-world scale.

The first phase of this chapter examines different case studies of high-rise office buildings in the studied region to inform the modelling in phase (2) by looking at the architectural characteristics of high-rise office buildings and the building regulations and guidelines for constructing office buildings. By analysing these cases, the study aims to identify the main architectural characteristics for developing the base case model prior to conducting the energy simulation. In the second phase of this chapter (Part 2: Synthetic Database Generation, Modelling-Simulation Based), the modelling and simulation were carried out detailing how data were collected to then form the synthetic databases. A generative parametric office tower and its urban context were designed and simulated, and this model then served as the base case model for all the conducted simulations of the study. Moreover, this section presents in detail the workflow conducted to simulate the AF energy performance; this involves setting up the model; establishing the hypothetical building for the study; validating the model; exploring how the model was parametrically generated; setting up the parameters of the office tower; and determining the input variables. The workflow also involves the implementation of fixed and adaptive shading systems, the simulation settings, and the approach followed to overcome the challenges of the AF simulation as discussed in the literature. Furthermore, it presents the automatic control

system applied to actuate the AF on an hourly basis with consideration of different environmental parameters. Lastly, this section presents the generated databases: solar radiation (SR) (KWh/m<sup>2</sup>) database, shade factor (SF) database, and energy (cooling loads) (KW/m<sup>2</sup>) database for different shading systems.

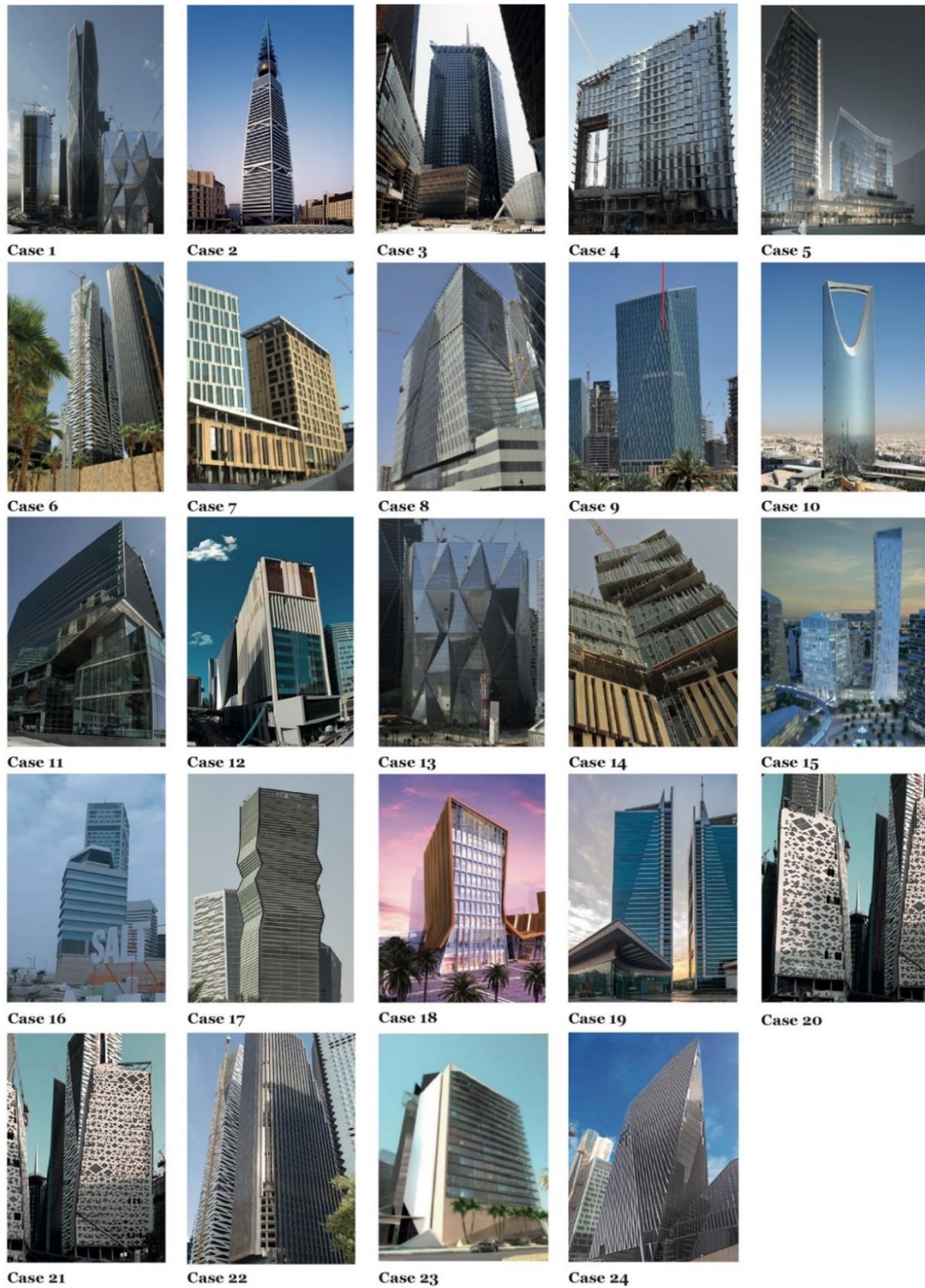
### **4.2. High-Rise Office Building Characteristics**

In this phase, the study investigated different existing case studies of office buildings that were located in the same area as this study. This process is useful to accomplish the first stage for setting up the model and its input parameters, and it aims to define the existing prototypes and design characteristics of high-rise office buildings in the studied region. This is in addition to considering the design guidelines suggested by the Saudi Building Code (SBC) and reliable benchmarks, as presented in Section (4.4.4) of the simulation settings.

A total of twenty-four high-rise office cases were selected, and these cases were located at the central area of downtown Riyadh and the downtown King Abdullah financial district (Figure 4.1). The selection process was based on the pre-defined criteria to inform the modelling stage of the simulation. The analysis of cases is based on parameters concerning the design consideration of high-rise office buildings. These cases consider the following parameters: heights of high-rise office buildings, floor plate efficiency, leasing depth, number of floors, floor-to-ceiling height, gross floor area (GFA), net leasable area (NLA), core dimensions, and core configuration as shown in (Appendix B). Data from the buildings were obtained from design documents, architecture firms' webpages, books, magazines, and websites. The case study analysis focused on two stages: the first stage looked at general information about the building, while the second stage provided more details about the considerations for office design. Figure (4.2) shows the twenty-four selected office buildings in the pictures numbered from 1 to 24.



*Figure 4.1: Geographical map showing the locations of the selected high rise building cases.*

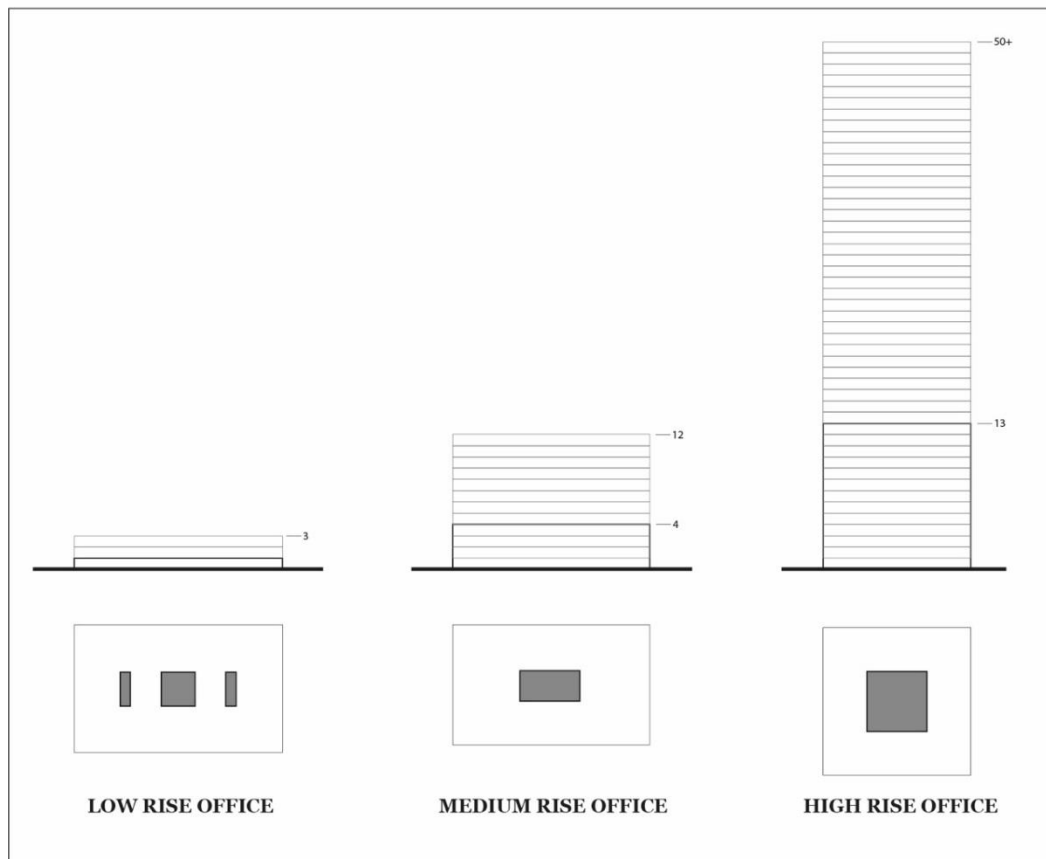


*Figure 4.2: High-rise office buildings: selected cases*

High-rise office buildings are defined as structures with thirteen or more storeys which are found in the high-density urban context of a city (Marfella 2015). Generally, sites in these urban locations are very small with an extremely expensive property value. Therefore, developers tend to derive maximum value from the site by constructing vertically to attain the maximum profit from the rentable office spaces. On the other hand, mid-rise office

buildings are defined as four to twelve storey buildings located in high density areas and suburban locations. Figure (4.3).

**OFFICE BUILDING TYPES**



*Figure 4.3: Office building types.*

**4.2.1. Floor Efficiency**

The feasibility of high-rise office buildings can be accomplished when the gross area and NLA are maximized for the selected site (Kim and Elnimeiri 2004). In this case, developers and owners can obtain the maximum returns from the high-cost values of the land. The floor efficiency is the ratio of NLA over the GFA Figure (4.4). Commonly, space efficiency is required to be no less than 80% in current real state standards (Marfella 2015). According to the analysed case studies, space efficiency ranges from 70% to 85% with an average of 80% Figure (4.5). In addition, the average of GFA is 1,225 sqm, so the typical floor office should produce between 980 sqm and 1,040 sqm NLA.



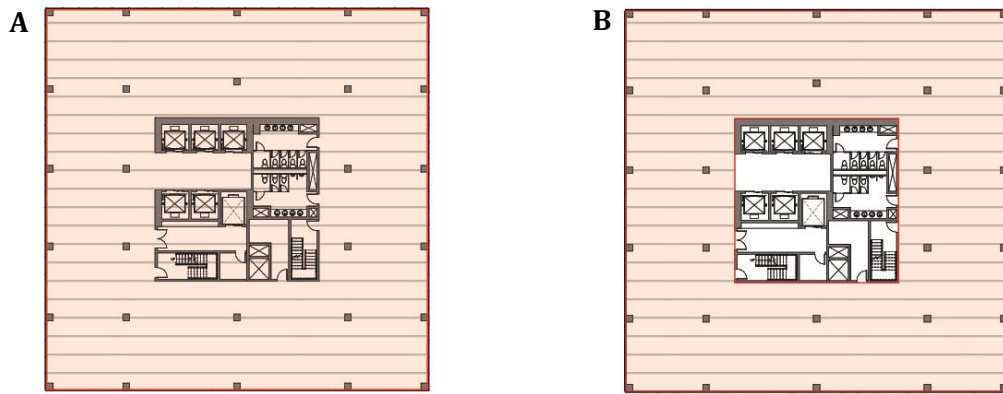


Figure 4.4: (A) Gross Floor Area (GFA), and (B) Net Lettable Area (NLA).

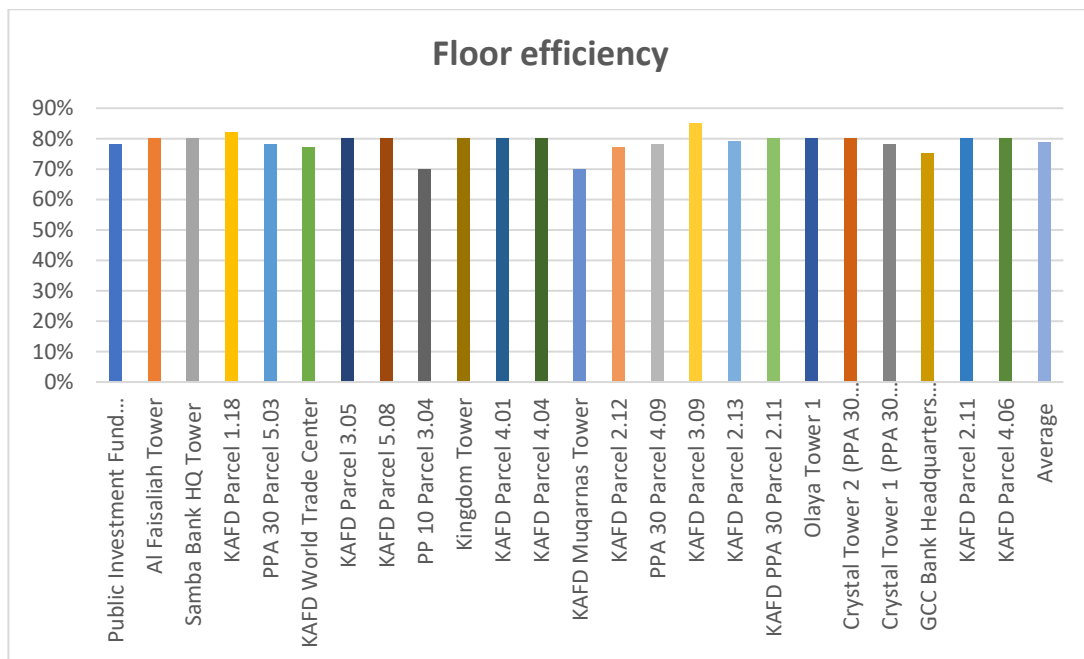


Figure 4.5: Graph showing the floor efficiency parameter of the analysed cases.

#### 4.2.2. Leasing Depth

Another parameter that is closely related to space efficiency is the amount of usable space between the exterior wall (building envelope) and the core area (services). This area is known as the leasing depth or lease span; it is an important factor that influences other parameters, such as natural daylight, layout of interior offices, and subdivisions of rentable spaces. Smaller office spaces from the core to the exterior envelope allow workers to connect with the outside and benefit from natural daylight Figure (4.6). From the collected data as shown in (Appendix B), the leasing depths for the 24 different cases studied range from 9 m to 15 m with an average lease depth of 10 m Figure (4.7).

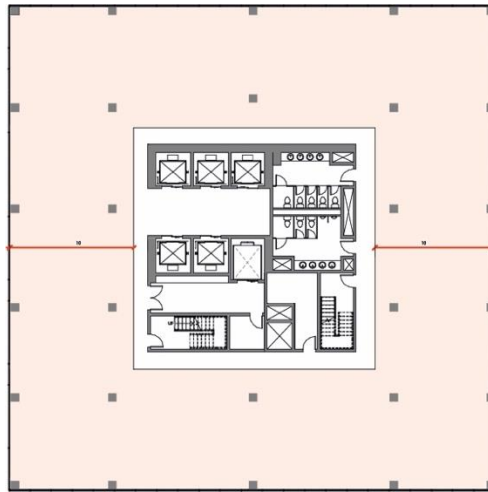


Figure 4.6: Lease span in the office tower zone

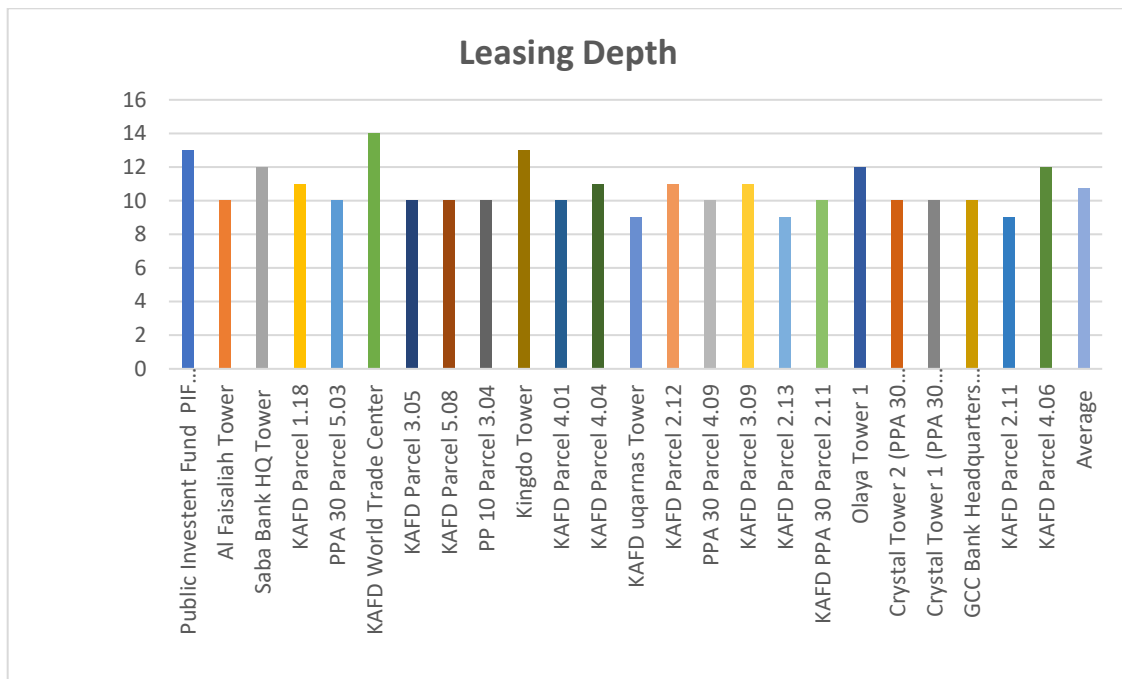


Figure 4.7: Graph showing the average leasing depth.

### 4.2.3. Number of Floors - Floor Height

The floor-to-floor height of high-rise office buildings is mostly consistent for all occupied storeys except for spaces such as the lobby, restaurants, and spaces for special functions. Based on the collected cases, the floor-to-floor height ranges from 3.80 m and 4.20 m with an average height of 4.0 m. The number of floors ranges from 11 floors to 77 floors with an average of 30 floors Figure (4.8). Most of the cases located the core at the centre of the floor plan.

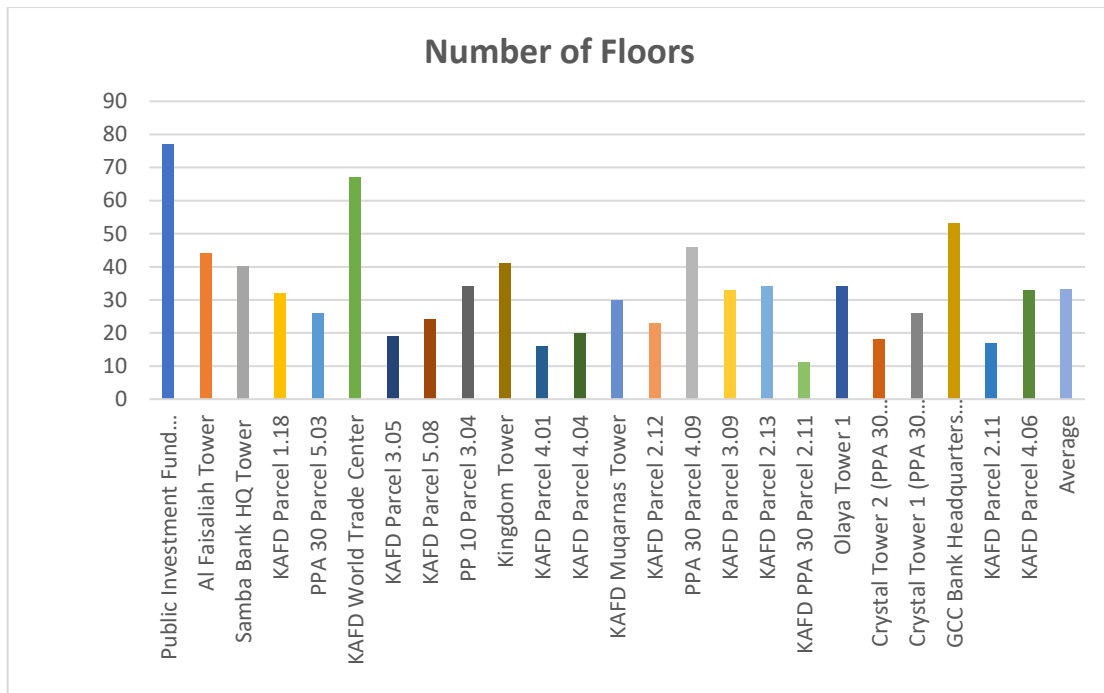


Figure 4.8: Number of floors of the analysed office cases.

#### 4.2.4. Buildings Heights

To determine the average height of the buildings in the context being studied, the study looked at a sufficient number of high-rise office buildings that were located in the downtown area. The building features such as building name, building height, number of floors, tall building type, year of construction, glazing orientation, external shading existence, and building geometry are presented in (Appendix B). Regarding the building height parameter, the data looked at both building height and number of floors. As can be seen from Figure (4.9), building heights range from a minimum of 36 m to a maximum of 385 m with an average height of 120 m.



**CHAPTER 4: SYNTHETIC DATABASE GENERATION USING SIMULATION APPROACH**

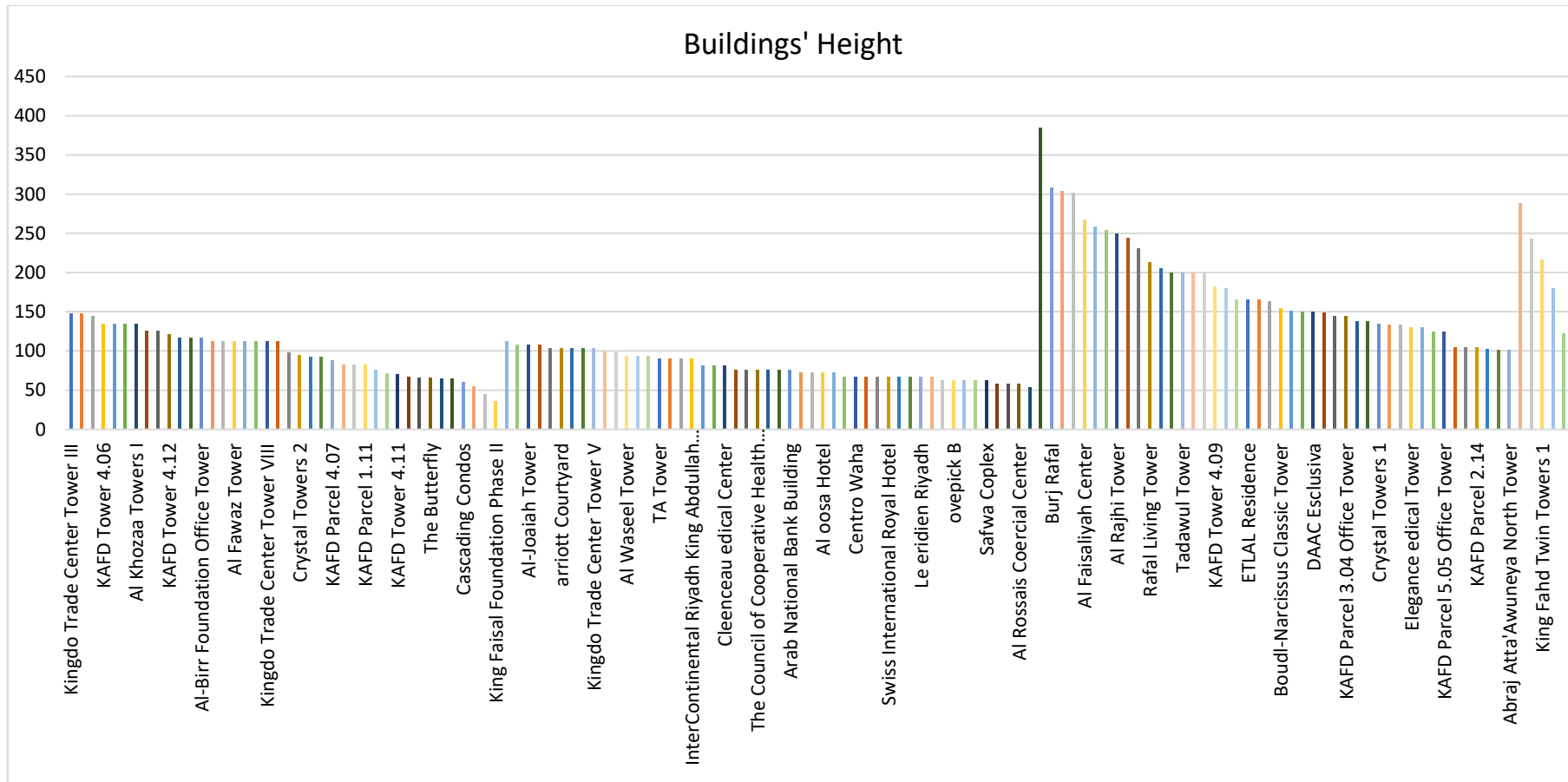
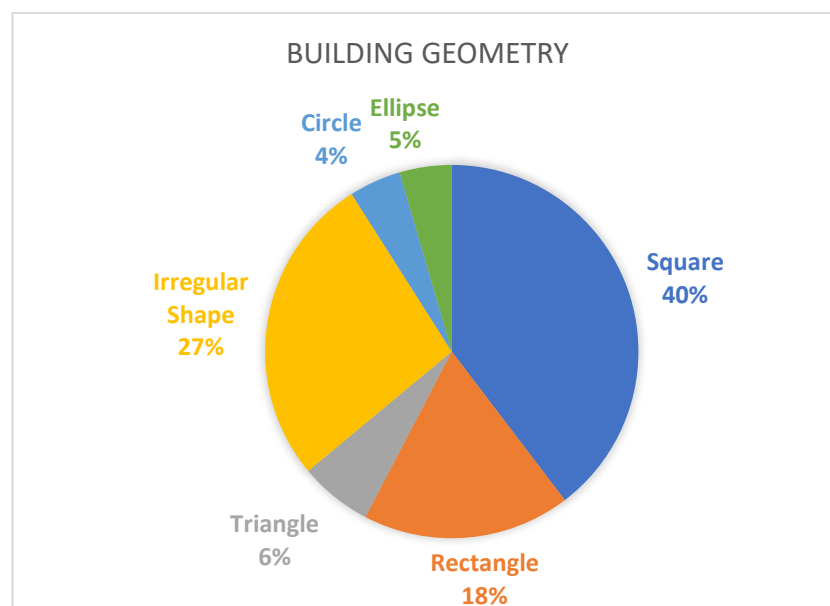


Figure 4.9: Graph showing the heights of high-rise office buildings in the studied context.

### **4.2.5. Building Geometry and Shading System**

The architectural shapes of tall buildings are believed to have evolved from the traditional extrusion of basic forms to the dynamic evolution of variants of computer-produced complex forms (Wells 2005). The main shapes of high-rise buildings, for example, can be viewed in basic forms, such as squares, triangles, and circles (Ching 2007). Other basic forms and irregular forms can be produced, such as an elliptical floor plan generated from a circle, and a rectangle which is generated from a square (Onyenobi et al. 2006). This method of conceptualising and altering the width, length, and height of a fundamental shape is widely employed in high-rise buildings, particularly in contemporary design approaches. According to Onyenobi et al. (2006), a form can be altered by removing a portion of its volume or as indicated by Wells (2005), by conducting many transformations on selected fundamental forms.

Most high-rise buildings around the world are constructed with square and rectangular floor plans (Alaghmandan et al. 2014). In the case of Riyadh city, different forms can be seen in high-rise buildings. This study examined the form parameter of different high-rise buildings and found that various shapes were used to design these buildings, such as square, rectangle, circle, triangle, ellipse, and irregular shapes as presented in (Appendix B). Based on the analysis of 137 case studies of tall buildings in Riyadh, the results revealed that square and irregular plan shapes are the most commonly applied forms in high-rise buildings in Riyadh city with 40% and 27% respectively as shown in Figure (4.10). Thus, this thesis examines the square plan form, as it is the most widely used layout for high-rise buildings in the area under study and is also popular worldwide.

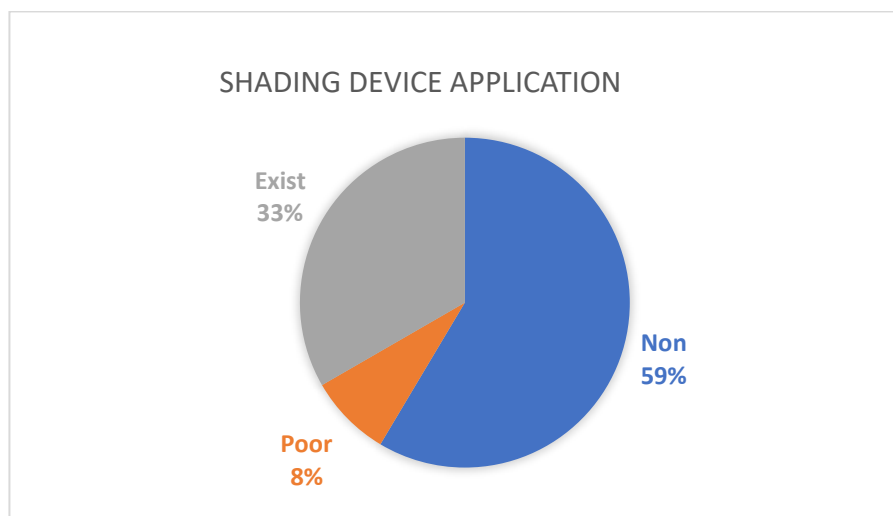


*Figure 4.10: Most applied forms in high-rise buildings.*

#### **CHAPTER 4: SYNTHETIC DATABASE GENERATION USING SIMULATION APPROACH**

Furthermore, the analysis examined whether or not a shading system existed for the investigated high-rise buildings to emphasise the significance of incorporating shading during the design phase. The results of the investigation revealed the lack of consideration given to installing a shading system in high-rise buildings in the studied region. As demonstrated in Figure (4.11), only 33% of tall constructions used shading devices, while nearly 60% of tall buildings were constructed without considering the use of shading devices to the building envelope. As discussed in the literature, different researchers agreed that the use of shading systems assists in reducing the energy demands of buildings. Another finding of the analysis showed that in recent years, there has been an increase in the application of shading systems in high-rise buildings, as demonstrated in Figure (4.12), due to the demand for sustainable green buildings. These buildings were constructed recently and were mostly found to be located in KAFD, which is an urban project that aims to promote energy efficient buildings.

Regarding the glazing orientation parameter, the study indicates that 82% of these buildings used a fully glazed façade in all orientations. A few tall buildings selected full glazing on the east and north façades and avoided the west and south façades, as they receive the longest period of solar radiation in hot arid climates. These buildings were the earliest examples of tall buildings in Riyadh city as discussed in (chapter one). This practice followed the traditional building design that uses small windows to control the harsh climatic conditions. From this analysis, support can be offered for the findings of Elkhatieb (2016) study, which revealed that these high-rise buildings followed the international design style using a fully glazed façade and thus neglecting the variations of the local climatic conditions, the use of shading systems, and the cultural requirements of each city, while a few buildings were found that had considered the use of shading systems.



*Figure 4.11: Existence of shading devices in current high-rise buildings in the studied region.*

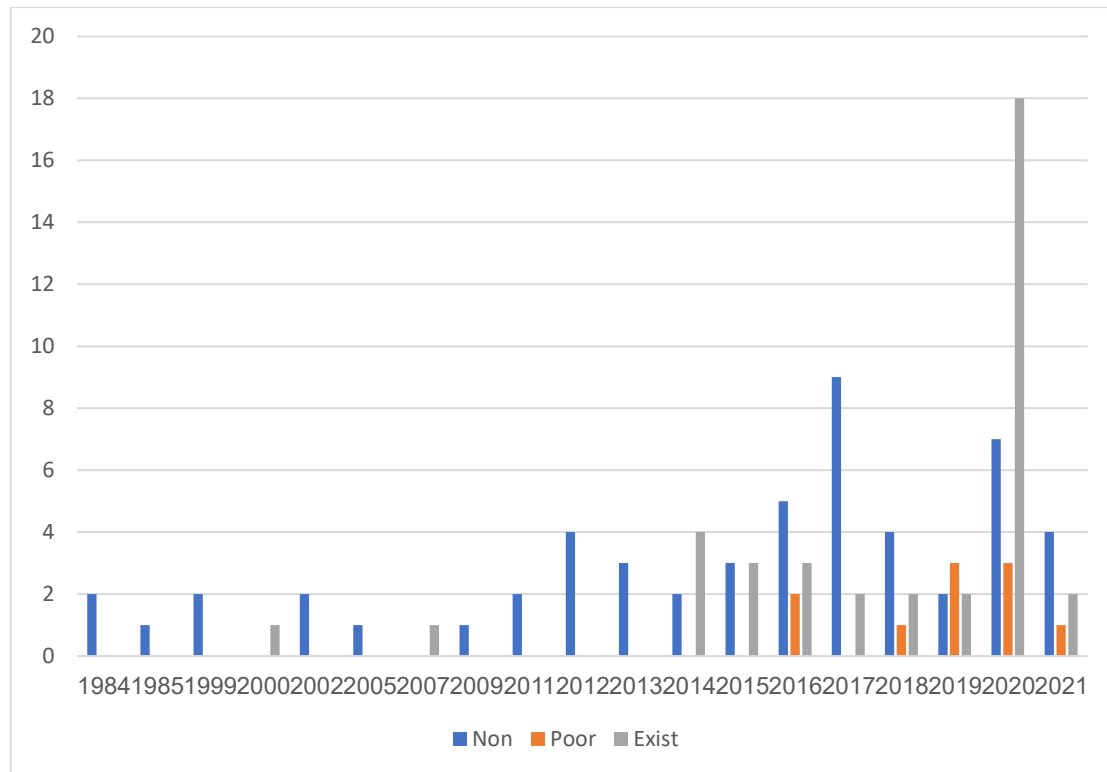


Figure 4.12: Correlation between time and the application of shading systems in high-rise buildings.

#### 4.2.6. Case Studies Summary

This phase of data analysis examined different cases of high-rise buildings to inform the modelling phase, which will be discussed in detail in the second phase. The case studies examined the following parameters: general building information, building height, number of floors, floor height, year of building construction, floor plan efficiency, GFA, typical floor area, NLA, leasing depth, building geometry, existence of shading system, and glazing orientations. These architectural characteristics were considered and implemented for the parametric study's base case. The development of the base case will be explained in detail in Section (4.4). Table (4.1) shows the average of each parameter of the investigated cases.

Table 4.1. Summary of the examined parameters.

| Examined Parameters                 | Average of Case Studies |
|-------------------------------------|-------------------------|
| Floor Efficiency                    | 80%                     |
| Gross Floor Area (GFA)              | 1,225 sqm               |
| Typical Floor NFA (m <sup>2</sup> ) | 980 sqm                 |
| Floor Efficiency                    | 80%                     |
| Leasing Depth                       | 10.00 m                 |
| Floor Height                        | 4.00 m                  |
| Number of Floors                    | 30                      |
| Building Height                     | 120 m                   |

### **4.3. Generation of Synthetic Database Based on Modelling and Simulation**

The main aim of the second phase is to build a synthetic database for testing and training the ML models using a simulation-based framework and to predict the performance of AF for reducing annual cooling energy consumption in office towers. Thus, a computational parametric tool 'Rhinoceros 3D', with its plugin 'Grasshopper' were used to facilitate the parametric generation and simulation of an adaptive system. Moreover, Ladybug and Honeybee plugins were used, which were linked to EnergyPlus and Radiance to calculate energy loads and solar radiation. The proposed algorithmic workflow creates a link between plugins including Ladybug, Honeybee tools, and EnergyPlus for running the simulation with an energy management system (EMS) to program a code that can automate the AF system before each time step of the simulation and lastly with the Colibri plugin tool to work through all the design variations automatically to create the dataset.

As reviewed in Chapter (2), section (2.5.1), the current simulation tools have not been developed for such complex cases, such as the AF system. The study integrated both solar radiation analysis and energy simulation for future prediction through the ML approach to minimize the time consumed by the simulation process in the early stages of the design. Unlike conventional simulation methods, supervised ML has major benefits in terms of requiring less computation time and less effort and of being computationally unexpensive (Huang et al. 2015). The workflow of the simulation process was developed to fulfil the aim of the study. The systematic framework of this phase is presented in Figure (4.13).

**CHAPTER 4: SYNTHETIC DATABASE GENERATION USING SIMULATION APPROACH**

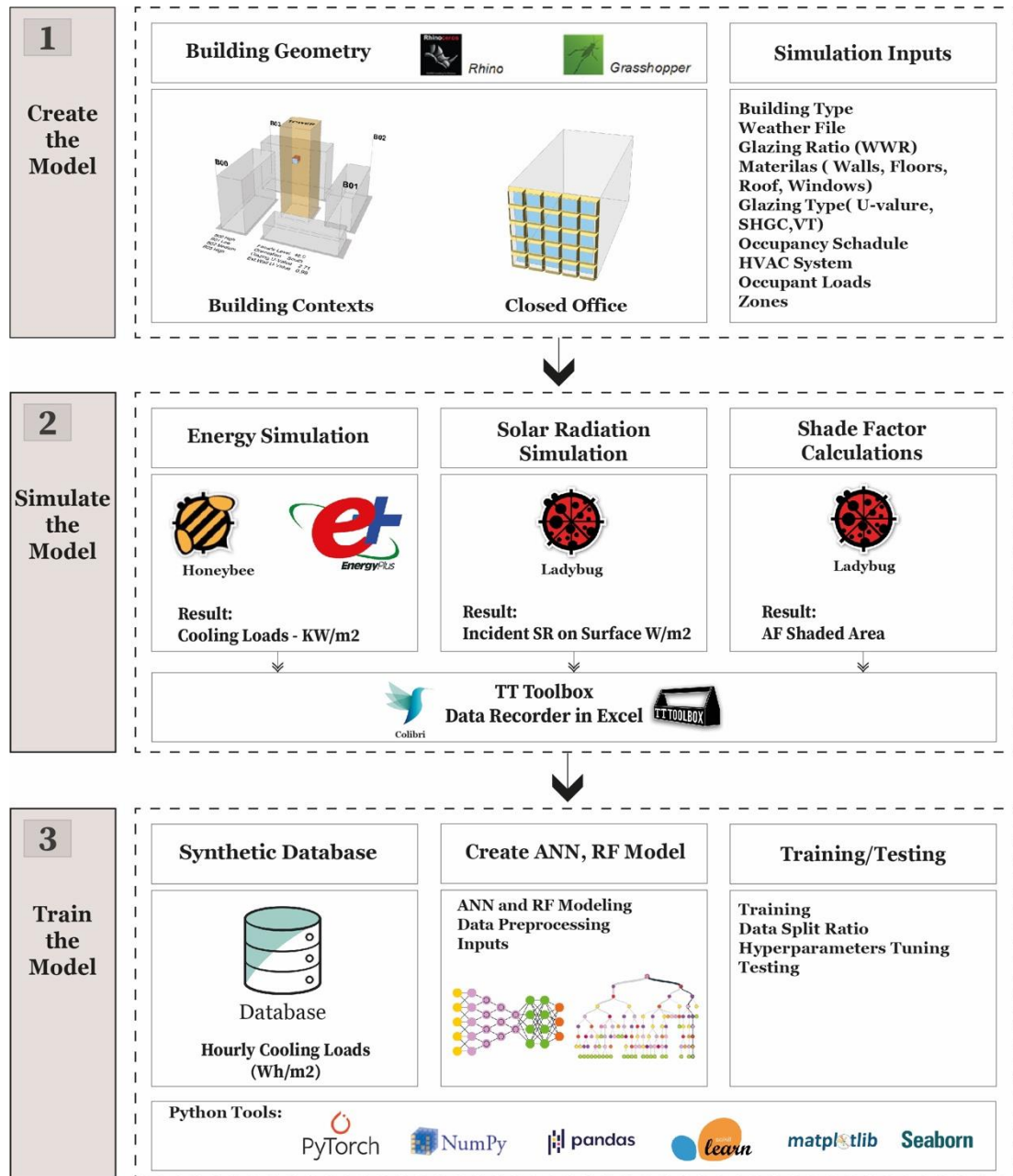


Figure 4.13: Schematic framework of the modeling and simulation phase, and the surrogate model development phase.

## **4.4. Base Case and Adaptive Façade Modelling**

### **4.4.1. Modelling Stage**

After the typical characteristics of office buildings found in the existing case studies had been analysed, the modelling stage took place to conduct the simulation. This section explains in detail the process of modelling the base case model, the urban context, how the model was generated pragmatically, the rules of the parametric generation, and the implemented prototypes of shading systems. Then, a validation of the base model was carried out to ensure the validity of the proposed model. Firstly, the study developed a high-rise office building as a base case in a hypothetical urban context located in the centre of Riyadh, Saudi Arabia. The developed base case model was utilised as a unit of measurement to quantify the variations in cooling demands in relation to the applied shading type. To establish the base model, consideration was given to the main high-rise building design parameters, such as number of floors, building height, floor-to-floor height, core location, building plan geometry, NLA, leasing depth, floor efficiency, and floor area. The architectural design, building services, and interior spaces are represented with a degree of abstraction during the modelling process to limit the number of model blocks, which might otherwise interfere with the output and cause unneeded software instability (Hamza 2004).

The developed office building has 30 floors with a height of 120 m, which is the average height situation found in the centre of the KAFD. This office building was located in a theoretical site and was assumed to be surrounded by several mid-rise office buildings, which created direct, diffuse, and reflected solar gains on the building surface Figure (4.14, left) (Trigaux and De Troyer 2015). These solar gains would affect the annual energy demand of each office room of the building. The model was tested to examine a hot, arid climate such as Riyadh city, where overheating is a crucial factor.

The dimensions of the layout and core area are fixed in all floors of the building as follows: (35 m \* 35 m), with a total area of 1,225 m<sup>2</sup> Figure (4.14, right). In this study, only shared side-lit office zones with an adaptive shading system were examined on each floor of the proposed office building, which faces the main orientations (north, south, east, west) to quantify solar radiation and the impact of an AF on building energy performance. The layout of each floor consists of the core and the offices zone. The core is situated at the centre of the floor plan and includes all the operational components of the office building. The typical office rooms are distributed according to the density of occupation. The area of the core services is 225 m<sup>2</sup> (15 m \* 15 m), and the NLA of the offices zone is 980 m<sup>2</sup>. The model

incorporated most of the design conditions of a high-rise office building according to the analysed studied cases in phase one as well as the design regulations by the SBC.

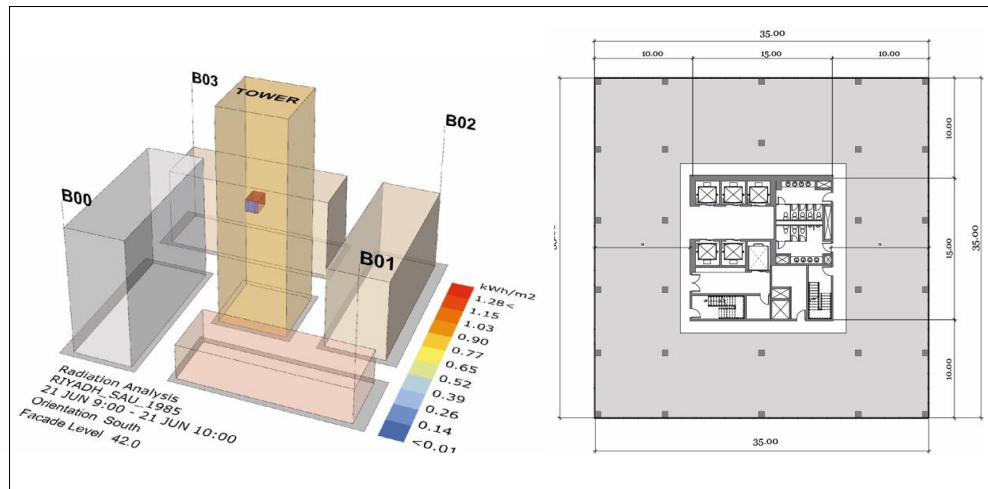


Figure 4.14: (Left) 3D parametric urban context, which varies in each simulation, and (Right) a detailed typical floor plan.

#### 4.4.2. Typical Closed Office

The study examined only a typical side-lit office room facing the main orientations (north, south, east, and west) with different floor levels that varied based on the surrounding contexts Figure (4.15). The spatial dimensions of the office room are 4 m wide by 6 m deep, making a rectangular zone with a floor-to-ceiling height of 4 m. These dimensions represent a space that can hold two workstations. This closed office room was designed with a fully glazed working environment, giving a window-wall ratio (WWR) of 80%. Figure (4.16) shows the office zone created using Honeybee tool.

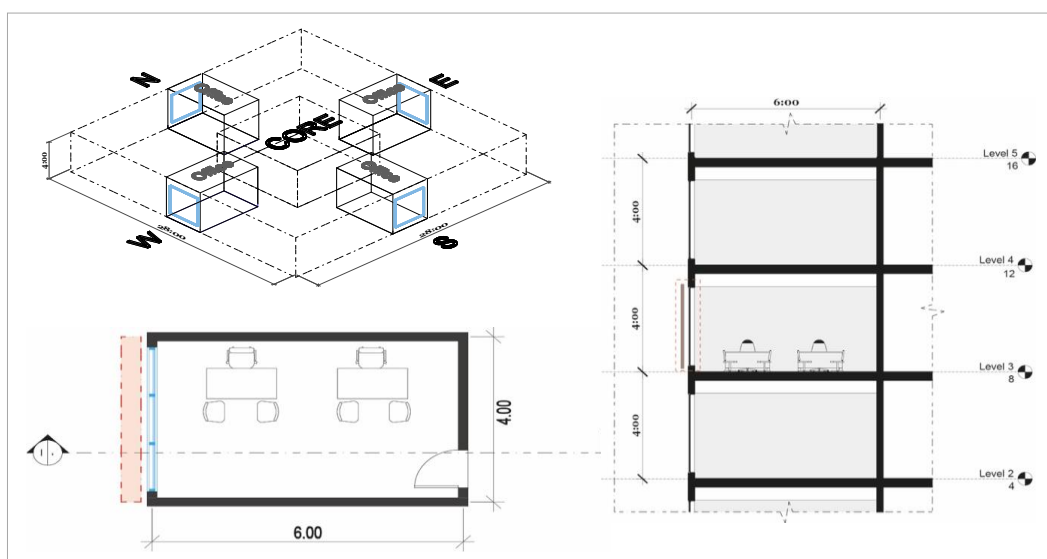


Figure 4.15: Single closed office space within the office tower facing main orientations.



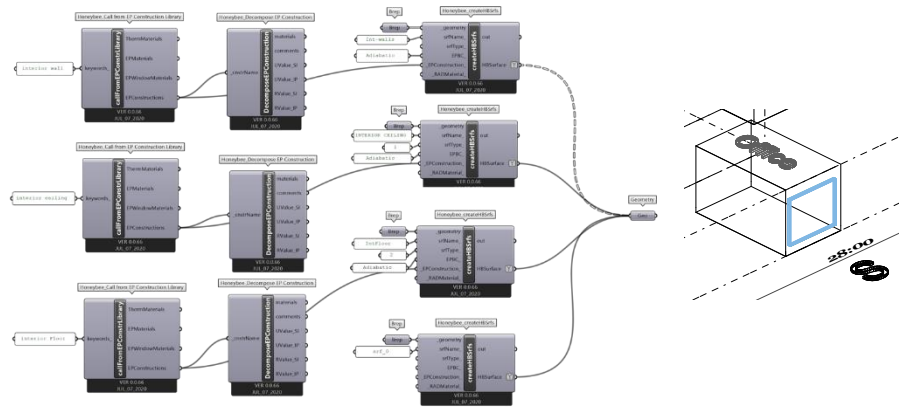


Figure 4.16: Scripting to create the office zone using Honeybee tools.

**4.4.3. Setting Up the Model Parametrically - Generative Parametric Tower**

Computational tools can be applied effectively to gather quantitative information about both the building’s performance and its design in the schematic design stage. In this research, Honeybee and Ladybug Grasshopper plugins were used to generate and simulate the model in terms of energy consumption. Grasshopper is a parametric modelling plugin for the Rhinoceros 3D modelling software, which allows designers to create simple, complex, or free forms without scripting experiences (Banihashemi et al. 2017). Sadeghipour Roudsari et al. (2013) developed Ladybug and Honeybee, which are plugin simulation tools on the Grasshopper platform. These tools perform hourly calculations of different analyses, such as the total energy demand. In addition, Ladybug provides a solar radiation analysis for calculating the energy collected on the building surface (Kim et al. 2012). These plugins are linked to EnergyPlus, a robust building energy simulation engine. In recent years, several researchers, engineers, and architects have considered EnergyPlus software as the most suitable engine for modelling the energy performance of buildings (Evins et al. 2011). Therefore, the simulation was carried out using both Ladybug and Honeybee for energy analysis, solar radiation, and SF calculations Figure (4.17).

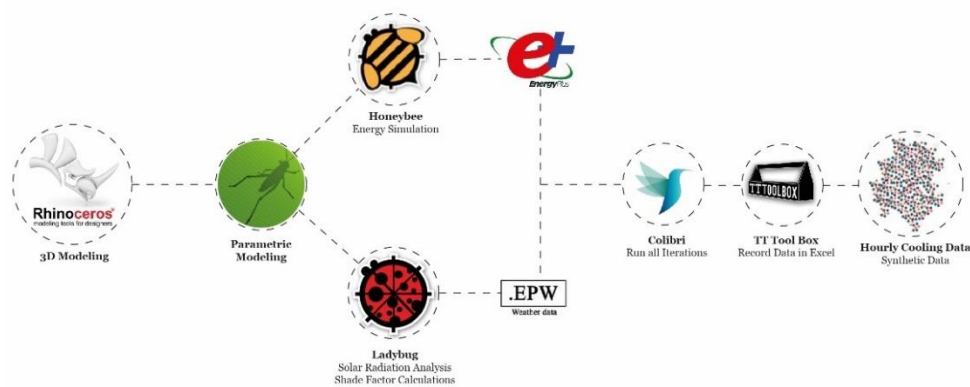


Figure 4.17: Parametric modelling and simulation tools used in the study.

## CHAPTER 4: SYNTHETIC DATABASE GENERATION USING SIMULATION APPROACH

The building context varied in each simulation (low, medium, and high) to test solar radiation and energy loads on all the levels and in all the main orientations (north, south, east, and west). The variation of heights of the surrounding contexts acted as one of the main features of geometrical variation in the study. In addition, the average height of the surrounding buildings was used parametrically to control the vertical location of the office room in each orientation in accordance with a lower-than-average, average, and higher-than-average height setting. This was intended to simulate the varying amounts of sunlight and daylight that the offices in a building receive. The generative parametric office tower rules and their urban context are illustrated in Figures (4.18) and (4.19). The vertical location of the office was calculated using the following formula.

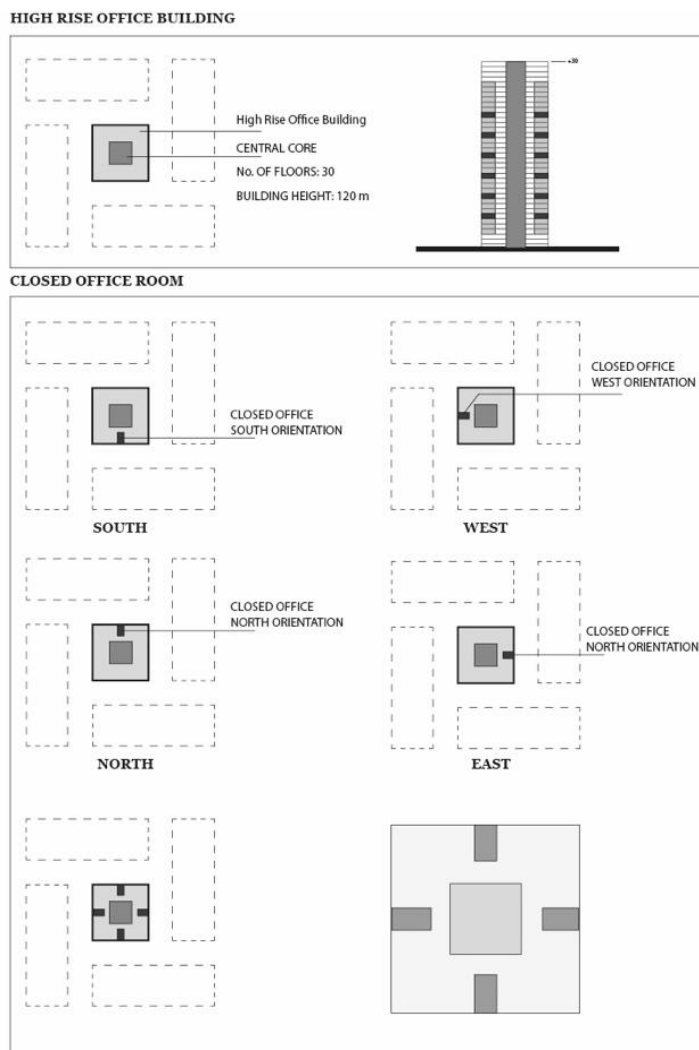
$$a = \sum B00 + B01 + B02 + B03 / n$$

$$l = (a) * 0.50$$

$$h = (a) * 1.50$$

Where  $a$  = Average,  $l$  = Lower than average,  $h$  = Higher than average

$B$  = Building context,  $n$  = Number of variables



## CHAPTER 4: SYNTHETIC DATABASE GENERATION USING SIMULATION APPROACH

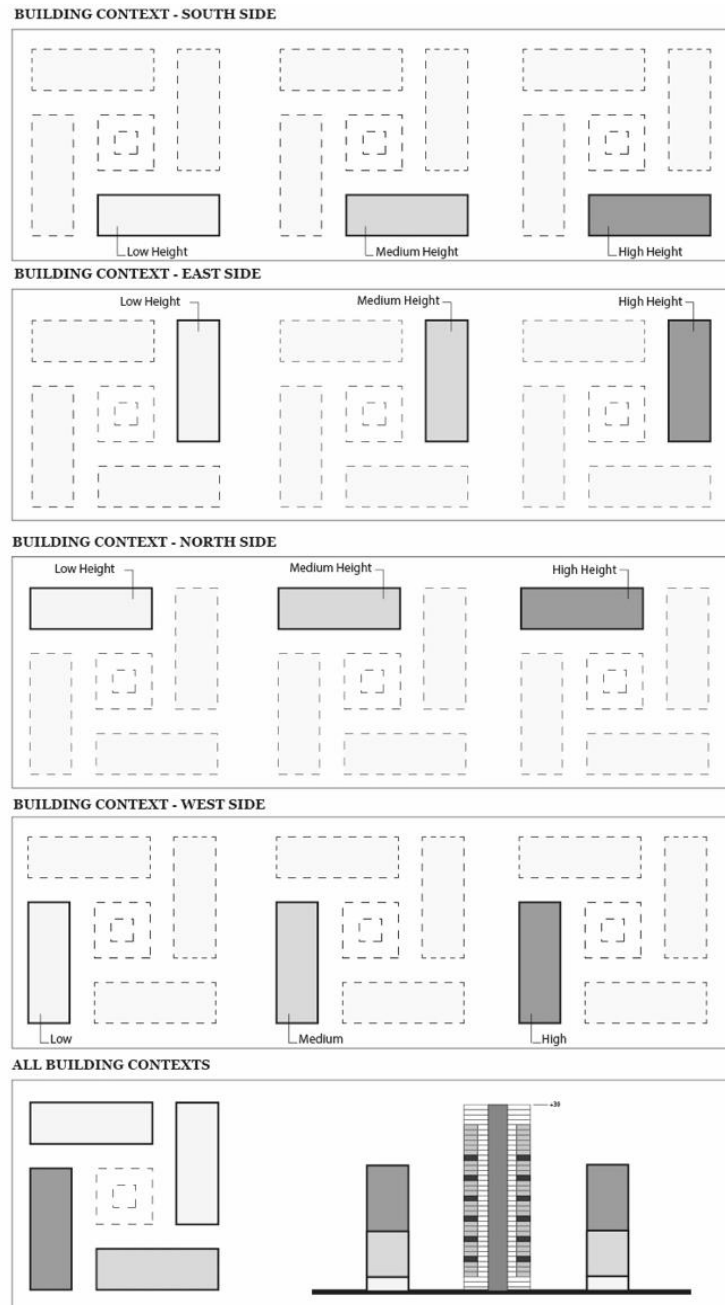


Figure 4.18: Parametric modelling generation rules.

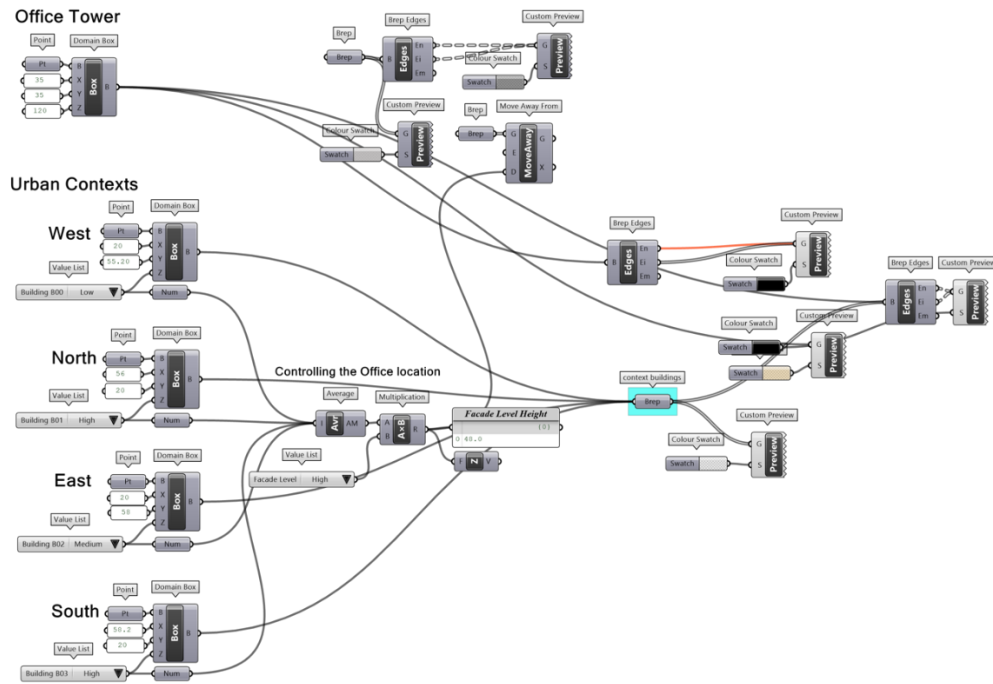


Figure 4.19: Scripting for setting up the geometry in a parametric way.

#### 4.4.4. Climatic Analysis

The development of any type of shade system to increase the energy efficiency of a building is dependent on the geographic location, latitude, and climate. Therefore, the city of Riyadh in Saudi Arabia was selected for this study. Riyadh is located in central Saudi Arabia, which has a hot, dry climate with cold winters and extremely hot summers Figure (20). In the summer, the average temperature may exceed 45 degrees Celsius, but the ambient temperature may approach 50 degrees Celsius Figure (4.21). In addition, the global horizontal radiation varies from 300Wh/m<sup>2</sup> to 1060W/m<sup>2</sup> highlighting the intensity of radiation buildings could receive as shown in Figure (4.22). As described in Chapter (1), Saudi Arabia has three distinct climate zones, with Riyadh's climate being Zone 1 - hot and dry. Before initiating the simulation, the Riyadh weather data were downloaded from the EnergyPlus weather map and then imported into the Grasshopper interface using the Ladybug tool.

## CHAPTER 4: SYNTHETIC DATABASE GENERATION USING SIMULATION APPROACH

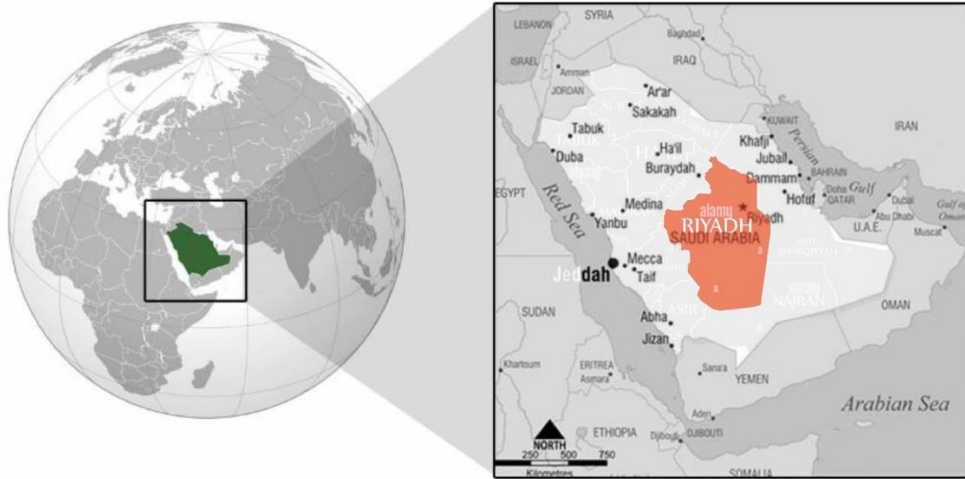


Figure 4.20: The location and borders of Saudi Arabia and the location of Riyadh (USNews, 2019).

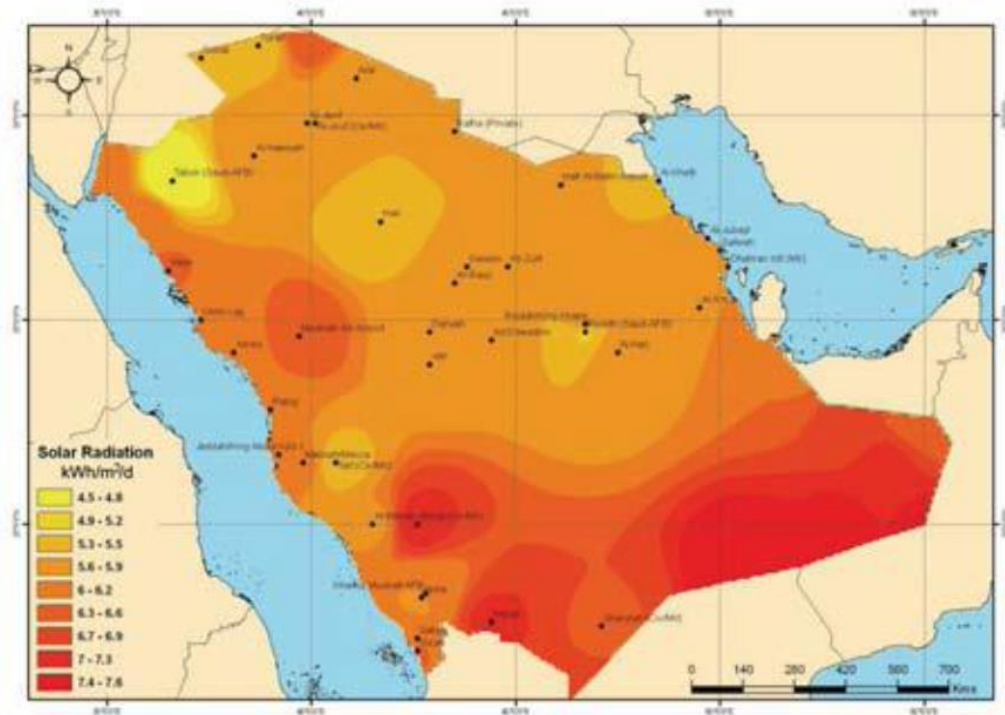


Figure 4.21: The average annual daily solar radiation in KSA.

## CHAPTER 4: SYNTHETIC DATABASE GENERATION USING SIMULATION APPROACH

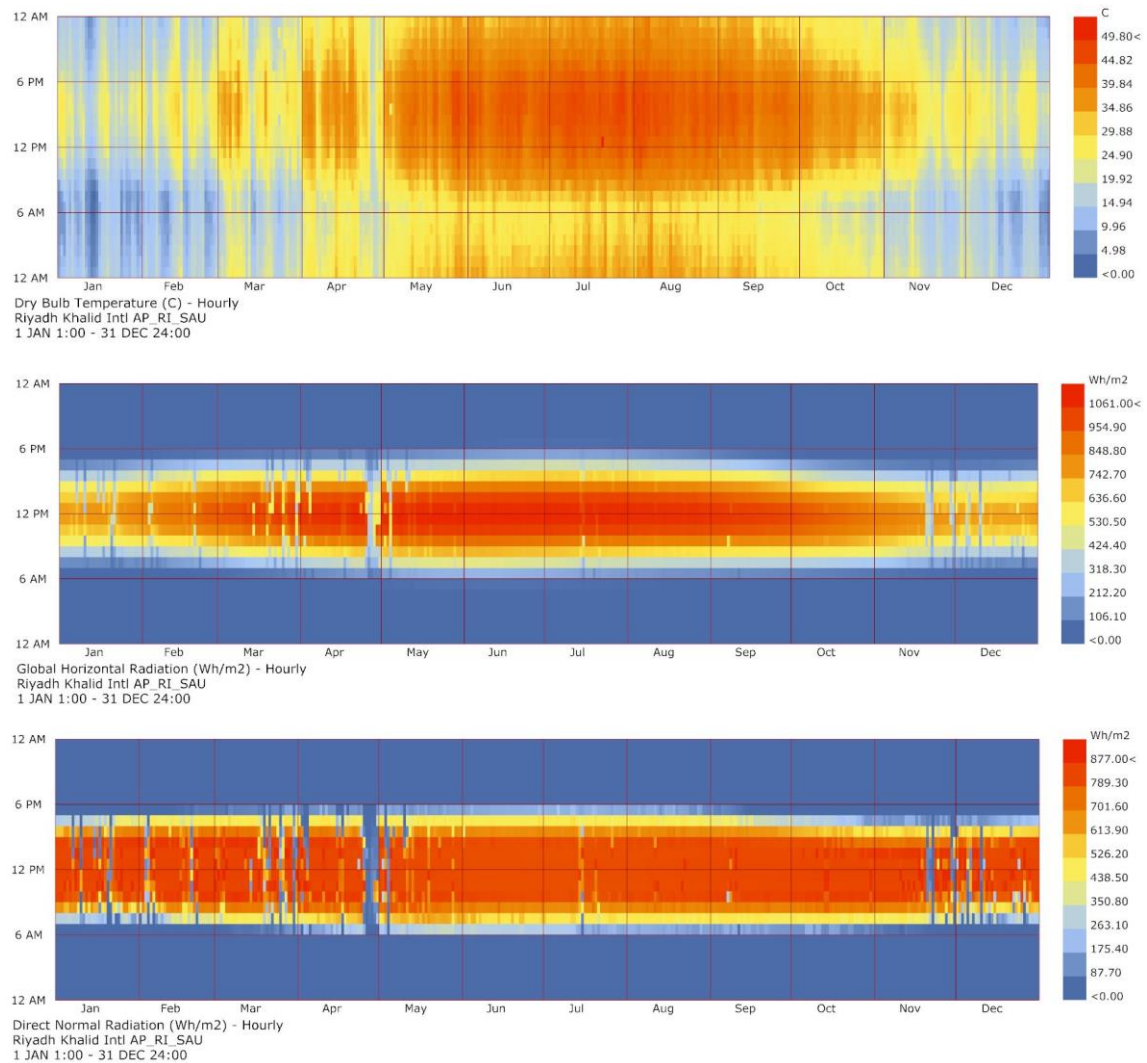


Figure 4.22: Dry bulb temperature (top), global horizontal radiation (middle), and direct solar radiation (bottom).

### 4.4.5. Simulation Settings

The accuracy of the predicated results performed in the simulation process depends heavily on the accuracy of the model inputs (Alnusairat 2018). Therefore, the simulation input values were defined based on the review of key building standards, benchmarks, and other related studies to ensure the accuracy of the model's inputs: occupancy density, construction of materials, U-values of materials, shading materials, occupancy schedule, lighting schedule, equipment load per area, building services and thermal setting, cooling system, program, and zones. In the simulation settings, fixed inputs were kept identical throughout all the design iterations except the inputs of variables that were considered to be the influential parameters in the study.

The study reviewed the following different benchmarks and office building guidelines during the simulation process to comply with the studied region and to ensure that the simulation

was as close to the real situation as possible: ASHREA 90.1-2010 (ANSI/ASHRAE/IESNA 2010), ASHRAE (2013), ANSI/ASHRAE Standard 209-2018 Energy Simulation Aided Design for Buildings, CIBSE Guides A for Environmental Design (2015), CIBSE Guide F for Energy Efficiency in Buildings (2012), Saudi Building Code (SBC,2010), and Saudi Building Code (Energy Conservation). The SBC was developed based on ASHRAE /IESNA standard 90.1 and the International Energy Conservation Code (IECC).

#### **4.5. Validation of the Base Model**

Validation is an essential step in the simulation process to ensure that the hypothetical model is correct and represents the real environment. Several researchers have examined the validation process of simulation models and their guidelines to validate the model in their studies (Sargent 2010; Qudrat-Ullah 2012; Rehman and Pedersen 2012; Hora and Campos 2015; Murray-Smith 2016; Zeigler and Nutaro 2016). These guidelines were provided to ensure that the model set up was correctly formulated and close to reality. Furthermore, Law (2009) stated that simulation models need to be validated before they can be used to make judgements. In general, the most definitive validation method is to compare model results with existing cases. In this section of the thesis, examples of case studies are used to support the validity of the base model.

Base case model validation is necessary to ensure that the simulation results are representative of typical Riyadh office buildings and that all simulations have been validated, as stated in Chapter 3. In fact, the prototypes with the AF system were developed from the base case model, which does not feature an AF system. The base case model must represent typical high rise office buildings. If the simulation generates energy loads of the base case that match the energy loads of office buildings in Riyadh, the base case accurately represents Riyadh office buildings. In this situation, the outcomes of all prototypes developed from the base case can likewise be valid.

The base model was established based on existing case studies and design guidelines for office buildings which exemplify the typical characteristics of office buildings in Riyadh. In addition, the simulation settings and parameters were determined using a reliable benchmark. The validation process in the current study was carried out in two parts. In the first part, the results of the base model's annual energy consumption and annual cooling energy were compared to case studies published in the same region as the current study (Fasiuddin and Budaiwi 2011). The second part of the validation process entailed comparing the base case model with a good practice case study. Both processes are discussed below.



#### **CHAPTER 4: SYNTHETIC DATABASE GENERATION USING SIMULATION APPROACH**

Firstly, the annual energy consumption for the base model of the study, which does not integrate an AF system, shows coherence with the five case studies examined. Fasiuddin and Budaiwi (2011) conducted a study on five commercial buildings in Saudi Arabia and provided detailed statistics for various factors, among which was annual energy consumption data. The annual energy consumption data for these case studies were obtained from the utility bills provided by the management or by the Saudi Electric Company (SEC). The annual and monthly energy consumption of the examined buildings revealed minor variations in energy use, with the lowest value being 250kWh/m<sup>2</sup>/year and the maximum value being 275kWh/m<sup>2</sup>/year Table (4.2) (Fasiuddin and Budaiwi 2011).

*Table 4.2. The annual energy consumption of the examined buildings.*

|   | Cases from Fasiuddin and Budaiwi (2011) |          |          |          |          | By Author |
|---|---|----------|----------|----------|----------|-----------|
|   | Case (A)                                | Case (B) | Case (C) | Case (D) | Case (E) | Base Case |
| <b>Annual Consumption (kWh/m<sup>2</sup>)</b> | 273.5                                   | 267.8    | 275.5    | 249.9    | 263.5    | 232.7     |

Based on the above cases, the average annual consumption per unit area (m<sup>2</sup>) for all five buildings is approximately 266 kWh/m<sup>2</sup>/year. The developed base model was validated by comparing the simulation energy results with the annual energy consumption of the above reviewed case studies. The EUI of 266 kWh/m<sup>2</sup>/year serves as a typical annual consumption for commercial buildings in the studied region and provides the basis for comparison. Thus, an average annual consumption per square metre less than or equal to the above value is considered to be performing within the normal range of energy consumption. However, this value could be optimised when implementing the AF system. Demirbas et al. (2017) stated that “70% of Saudi electricity is consumed for air conditioning and cooling and the summer demand is about twice the winter demand.” Moreover, the King Abdullah Petroleum Studies and Research Centre (KAPSARC) reported that “cooling accounts for around 70% of buildings’ electricity consumption” (Alshehri et al. 2020). Thus, if the average annual energy consumption of the five buildings is 266kWh/m<sup>2</sup>/year, which is then multiplied by 70%, then 186.2kWh/m<sup>2</sup>/year is the average annual cooling energy in office buildings.

For the studied base case, the annual energy consumption result generated from the simulation averages 232.7kWh/m<sup>2</sup>/year (base case-south orientation = 263.2kWh/m<sup>2</sup>/year, base case-west orientation = 270.9kWh/m<sup>2</sup>/year, base case-north orientation = 184.6kWh/m<sup>2</sup>/year, and base case-east orientation = 212kWh/m<sup>2</sup>/year) Figure (4.23). In addition, the average energy cooling load is 176.5kWh/m<sup>2</sup>/year (base case-south orientation



#### CHAPTER 4: SYNTHETIC DATABASE GENERATION USING SIMULATION APPROACH

= 211.1kWh/m<sup>2</sup>/year, base case-west orientation = 217.3kWh/m<sup>2</sup>/year, base case-north orientation = 122.6kWh/m<sup>2</sup>/year, and base case-east orientation = 155.2kWh/m<sup>2</sup>/year) Figure (4.24).

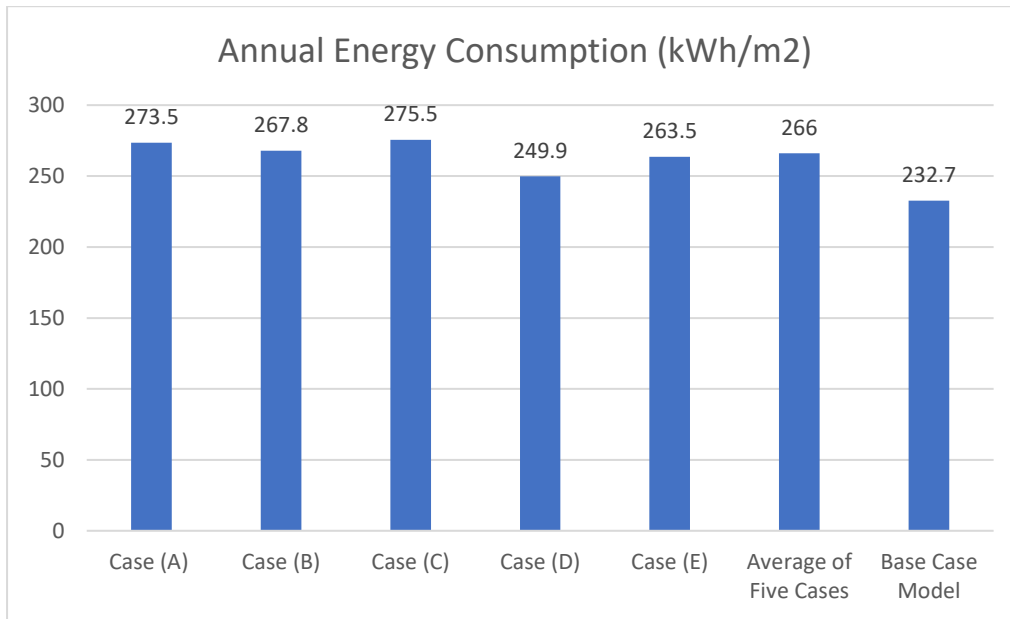


Figure 4.23: Annual energy consumption results of the examined building compared to base model.

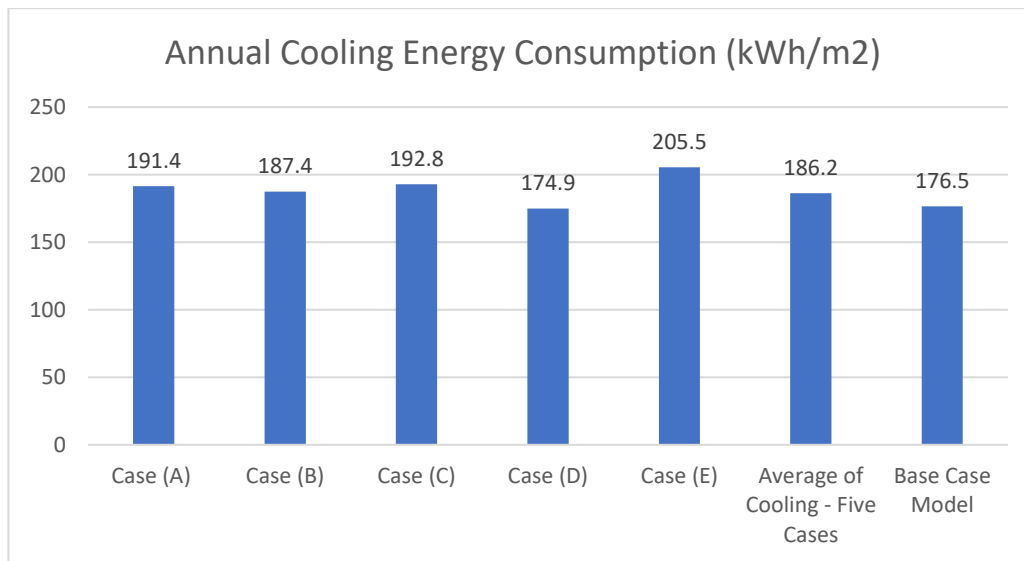


Figure 4.24: Annual cooling energy consumption of the examined cases compared to base model.

The values of 186.2KWh/m<sup>2</sup> for the average cooling of five cases and 176.5KWh/m<sup>2</sup> for cooling loads of base case model are not significantly different, and the difference between the energy consumption values in the case studies and the base model is due to the use of some different settings. For example, the lighting density was higher in the case studies compared to the base case model. The model of the study considers 5.00 W/m<sup>2</sup> based on the considered benchmarks, whereas the case studies consider a value of 10.8 W/m<sup>2</sup>. In

#### CHAPTER 4: SYNTHETIC DATABASE GENERATION USING SIMULATION APPROACH

addition, the case studies use a range of 8 to 11 W/m<sup>2</sup> for equipment power density, whereas the base model considers 4W/m<sup>2</sup> to be the average benchmark value (ASHRE, 2010). This comparison verifies the capability of the study's base model and the validity of the simulation outcomes.

Secondly, an office building located in the same region of the study was examined by looking at its electricity bills to compare the base case model with a good practice case study. The utility bills were collected from the management team for a one-year period (2019). Moreover, other factors were obtained, such as building information, the building's main measurements, floor area, glazing type, glazing ratio, etc. The main differences between the case study (F) and the examined five cases is the glazing type composition used and the specifications for construction materials. When examining the electricity bills of case F, the annual energy consumption recorded is 175.1kWh/m<sup>2</sup>/year and the cooling energy consumption is 122.5kWh/m<sup>2</sup>/year. For the studied base case, the average annual energy consumption result generated from the simulation is 177.1kWh/m<sup>2</sup>/year (base case-south orientation = 184.6kWh/m<sup>2</sup>/year, base case-west orientation = 194.8kWh/m<sup>2</sup>/year, base case-north orientation = 159.4kWh/m<sup>2</sup>/year, and base case-east orientation = 169.9kWh/m<sup>2</sup>/year). The differences in energy consumption between the base case model and the good practice case are considered to be marginal. In addition, Figure (4.25) shows that the maximum cooling demand occurred during the summer months, which is acceptable given that the case study was conducted in a hot, arid climate. Therefore, the energy consumption results for the base model are reasonable, and the model could be employed for the research investigation.

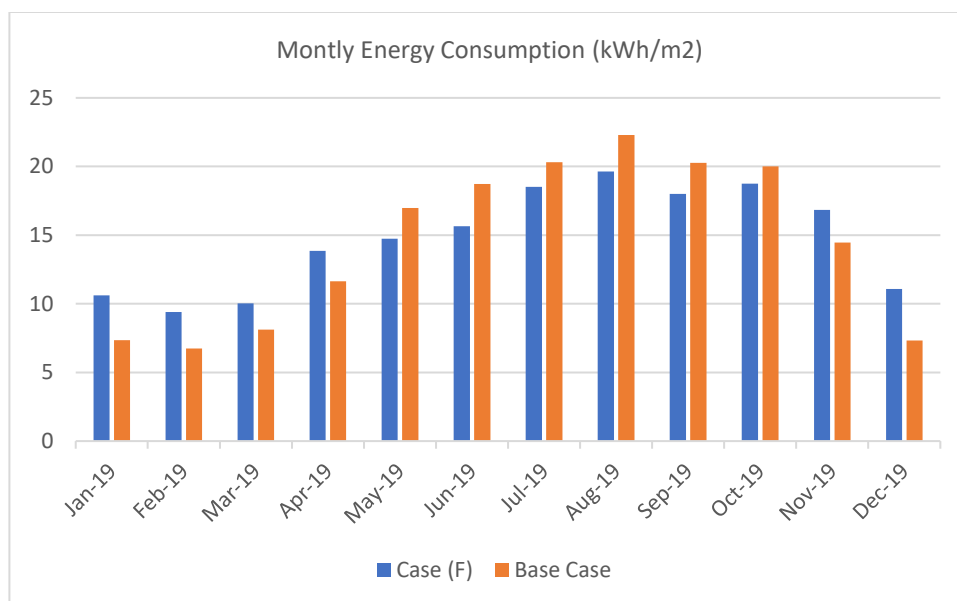


Figure 4.25: Monthly energy consumption comparison between case study (F), which obtained from electricity bills and the simulated base case model.

## **4.6. Implementation of Adaptive Façade Shading System**

The main benefit of AF external shading systems is their ability to manage and reduce solar gains, which can significantly decrease cooling loads and eliminate glare. When designing an AF shading system, it is essential to consider aspects such as location, time, daylighting, environmental conditions, and control system, as they can block useful daylight from entering the space, thereby creating a need for artificial lighting. Dekay (2001) stated that successful exterior shading depends on the designer's awareness of when to allow and block the sun, considering the outdoor climatic conditions in each month. Internal shading is beneficial, as it provides privacy as well as visual and thermal comfort; however, it has the potential to trap heat that is radiated from inside surfaces and raise cooling demands during periods of excessive heat (Kirimtat et al. 2016). This research investigated only the implementation of external shading devices, as internal shading is mostly determined by human behaviour and is therefore outside the scope of this study. After the base case model had been validated, different prototypes of fixed and adaptive shading systems were installed to evaluate their impacts on energy performance compared to the base case model:

Prototype (1) represents the base case model with no shading system, Prototype (2) represents fixed vertical shading, Prototype (3) represents fixed horizontal shading, Prototype (4) represents a scaling and translating movement, and lastly, Prototype (5) represents a folding movement Figure (4.26). The aim of these two movement patterns is to provide hierarchical configurations and self-shading geometry for the envelope (Hosseini et al. 2019b). Figure (4.27) shows the panel is scaling and folding within a rectangular grid of (0.80 cm \* 0.80 cm), which was fixed throughout the analysis process. Six different shading states were designed, ranging from 100% fully open to 0% fully closed with intermediate states Figure (4.27). Furthermore, vertical and horizontal fixed shading systems were modelled based on the recommendations of previous studies (Sabry et al. 2014; Ghabra 2019). These external fixed shadings consist of simple sun breakers, evenly spaced with (0.3cm) wide spacing and depth. The aim of implementing fixed shading systems is to compare this type of system with the adaptive shading system in terms of energy consumption in a shared office space within a tower building. However, these fixed shading devices are not the focus of this research, as they are used only to provide a comparison analysis with AF shading systems, which will be presented in the results chapter (5).

**CHAPTER 4: SYNTHETIC DATABASE GENERATION USING SIMULATION APPROACH**

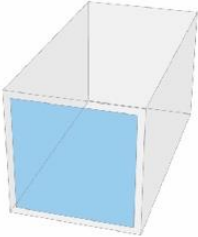

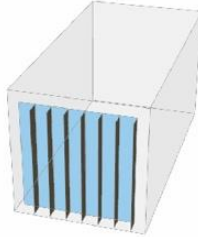

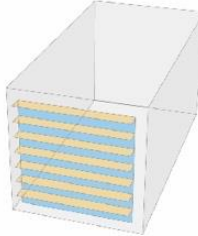

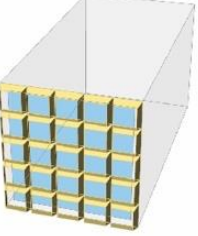
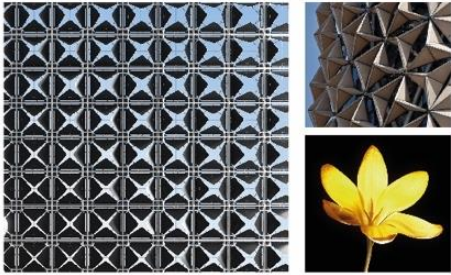
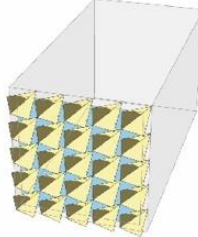

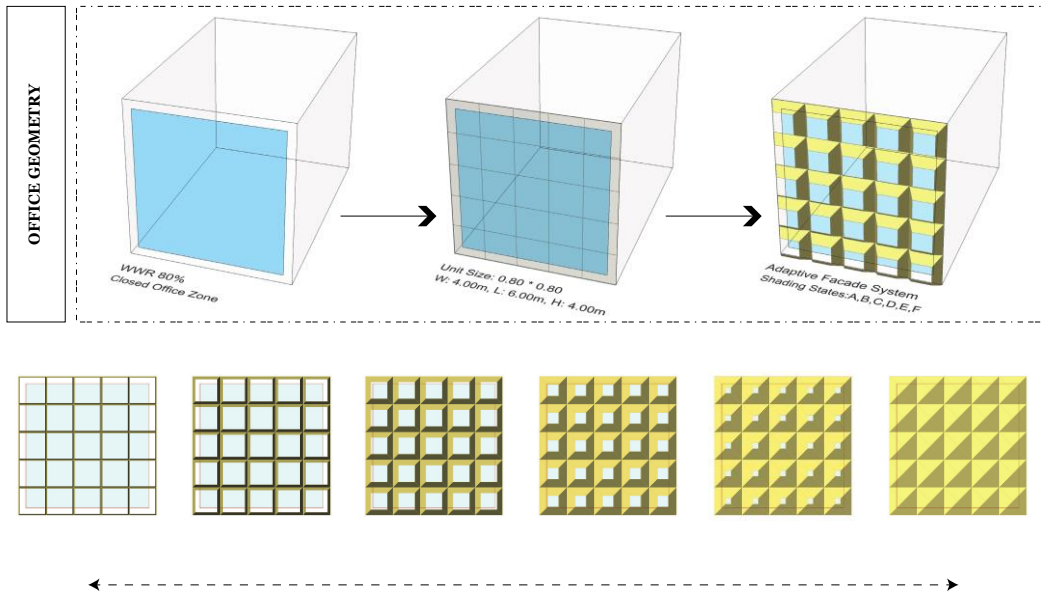
|             | Motion   | Reference Cases  |
|-------------|--|--|
| Prototype 1 | <p>Base Case Model</p>            |    |
| Prototype 2 | <p>Fixed Vertical Shading</p>     |    |
| Prototype 3 | <p>Fixed Horizontal Shading</p>  |   |
| Prototype 4 | <p>AF - Scaling Movement</p>    |  |
| Prototype 5 | <p>AF - Folding Movement</p>    |  |

Figure 4.26: Different prototypes of an adaptive façade with different movement motions.

(A) Scaling and translating movement



(B) Folding movement

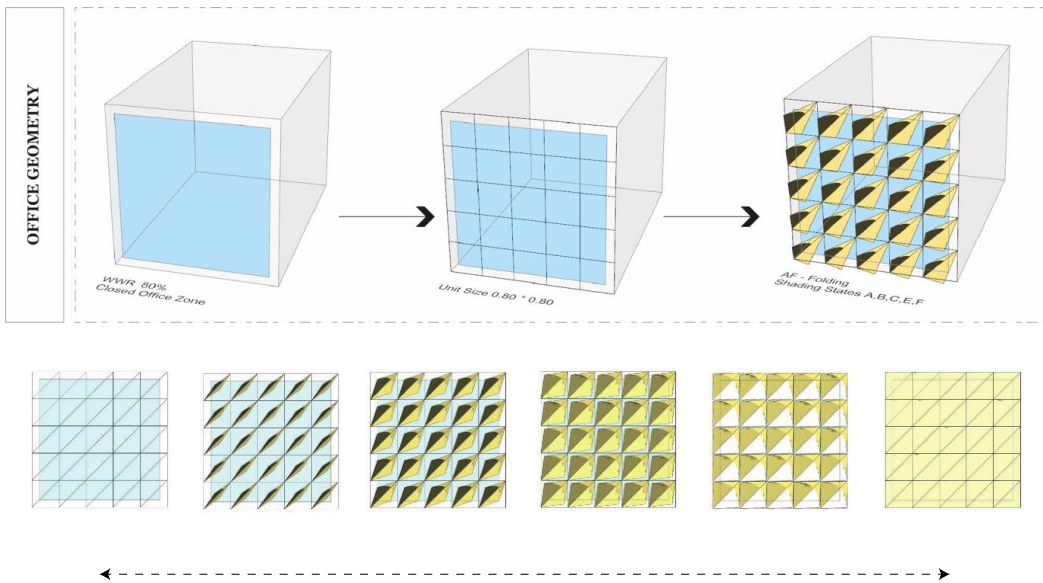


Figure 4.27: Modelling process of the AF geometry. (A) Scaling movement, and (B) Folding movement, which shows the variation of adaptive façade shading states.

### **4.7. Adaptive Façade Energy Simulation**

The studies examined in the literature review in Chapter (2) section (2.5.2) revealed the significant impact of an AF shading system on reducing energy consumption in office buildings. Furthermore, it shows the lack of a well-accepted framework to simulate the AF system in the early stages of the design that architects can follow. Thus, this study proposed an algorithmic workflow to evaluate the energy performance of an AF system using computational parametric tools. The energy simulation process comprised several steps as follows: (1) calculating the hourly incident solar radiation on the façade; (2) calculating the hourly shade factor of the proposed shading states in both scaling and folding movements; (3) defining the simulation settings such as input parameters, construction materials, thermal settings, HVAC system, zone loads, occupancy schedule, etc.; (4) assigning an automatic control system; and (5) running the simulation to calculate the hourly cooling loads. Figure (4.28) shows the modelling and simulation and the database framework of phase two. The modelling stage was reviewed in the previous section. This section mainly explores how the simulations were conducted with detailed information about each step.

## CHAPTER 4: SYNTHETIC DATABASE GENERATION USING SIMULATION APPROACH

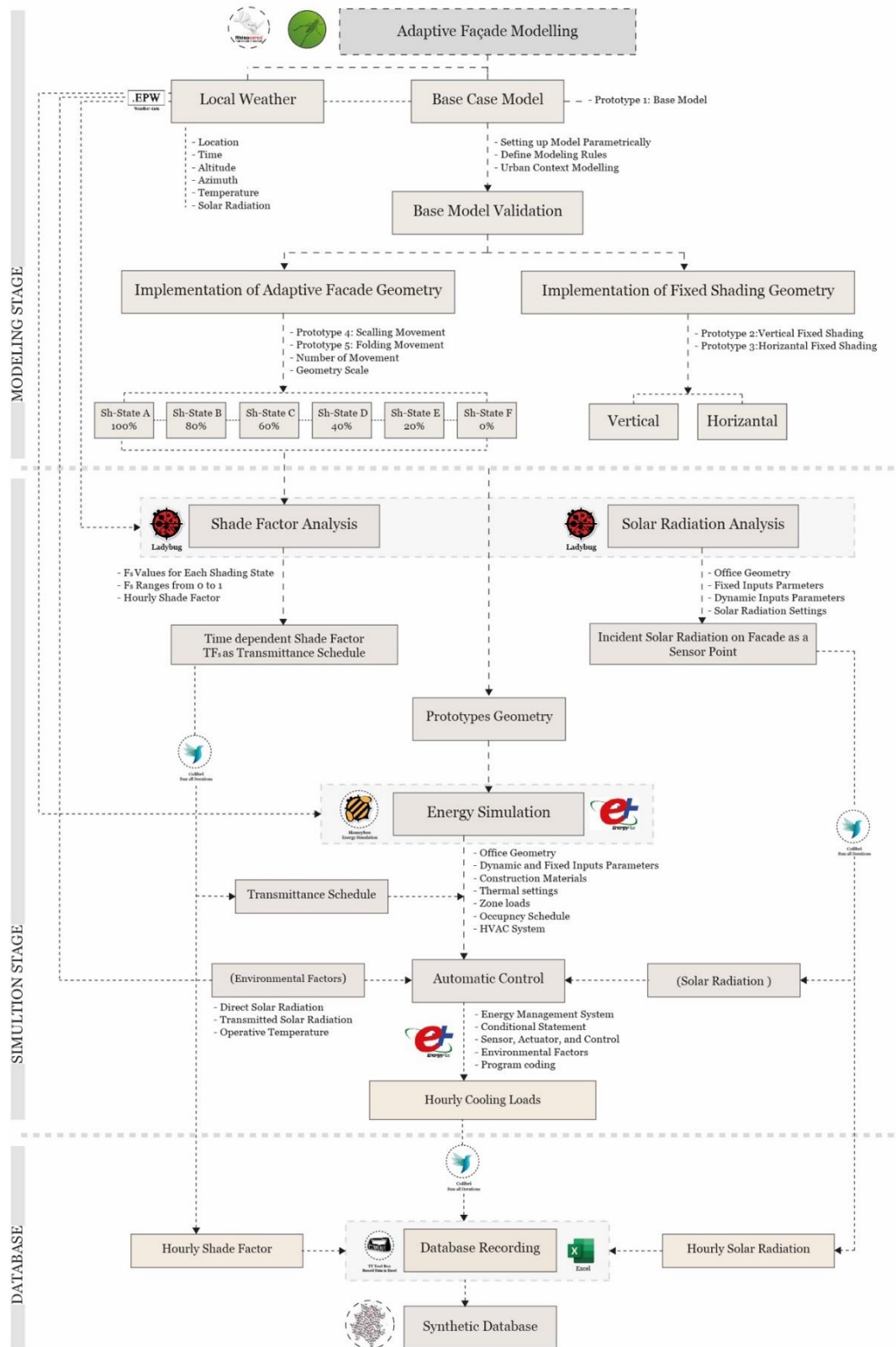
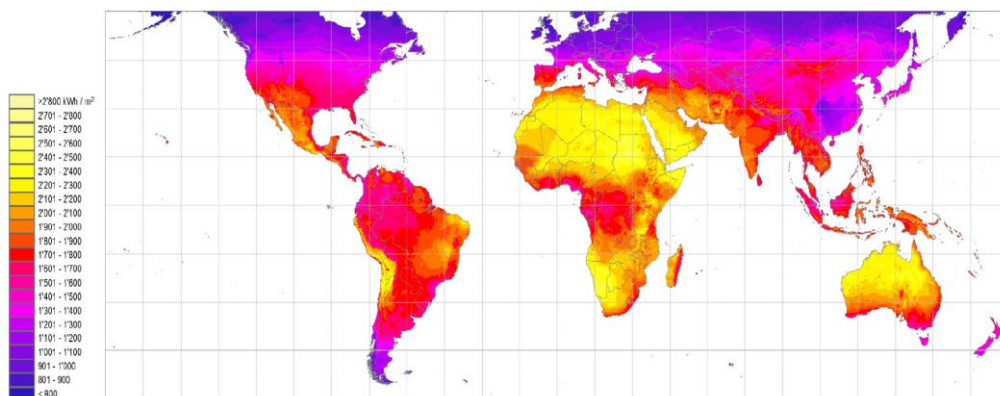


Figure 4.28: Framework of the three conducted stages: modelling, simulation, and database recording.



## **4.8. Solar Radiation Analysis**

In terms of energy efficiency, the primary function of an external adaptive shading system is to regulate solar radiation passing through windows, which influences solar heat gain and the indoor daylight level. The main goal of conducting the solar radiation analysis is to collect the hourly incident radiation on the façade surface to be used as a sensor point for actuating the AF system. As mentioned in the literature, AFs can vary based on different environmental factors either internally or externally. These environmental factors, such as temperature, humidity, solar radiation, airflow, etc., have a major impact on the energy requirements of a building. This research focuses on solar radiation and temperature factors because of the excessive heat gain from solar radiation and the problem of high temperatures in hot, arid climates as shown in Figure (4.29). Throughout most of the year, severe weather conditions are common in hot regions such as Riyadh city. High levels of solar radiation influence a variety of surfaces, particularly during the long summer months (Zell et al. 2015). Hence, glazed façades create a variety of issues that must be thoroughly examined, mitigated, and solved to justify their use in such a scenario.



*Figure 4.29: Annual solar radiation map of the world (Asif 2016).*

Solar radiation was selected since it is one of the most often cited control inputs in the research literature (Yun et al. 2017). The average hourly solar radiation for a surface in Riyadh is  $262.19 \text{ Wh/m}^2$ . The solar radiation varies from  $300 \text{ Wh/m}^2$  to  $1060 \text{ Wh/m}^2$  during the daytime over a year. The incident solar radiation was evaluated on the west façade of a vertical wall in Riyadh city. It can be noticed from Figure (4.30) during specific hours in April and September, the solar radiation exceeds  $825 \text{ W/m}^2$ .



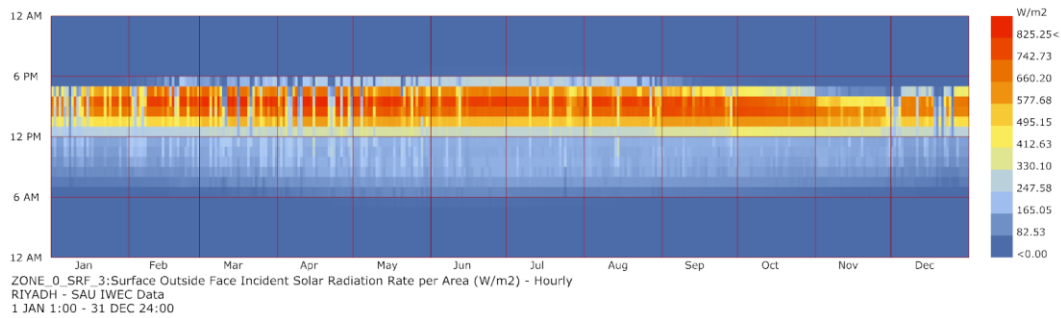


Figure 4.30: Incident solar radiation on a west-facing wall, Riyadh.

#### 4.8.1. Validation of Tool Accuracy

In the field of environmental studies, several studies have validated Grasshopper, Honeybee, and Ladybug plugins that are linked to EnergyPlus and Radiance. Therefore, these plugins were used in this study to conduct solar radiation and energy simulation (Aksamija 2011; Donato et al. 2017; Elwy et al. 2018). Researchers have widely proven that Ladybug and Honeybee tools can provide accurate results when comparing simulation results with measured results, as well as their ability to adapt to different environmental conditions. According to Ibrahim et al. (2020) study, the Ladybug tool proved to be reliable when comparing the simulated data with measured data as well as when comparing the outcome of the simulation with other simulation software such as Envi-met. In another study, Poon et al. (2020) examined the differences between the simulated and measured data of the solar radiation that was received by the building envelope in Singapore's weather conditions. It was found that the data from the Ladybug simulation had an error of less than 12%.

In order to demonstrate the accuracy of the Ladybug tool and validate the solar radiation output, the study validated and compared its solar radiation results against experimental studies conducted by Touma and Ouahrani (2018) and Ghabra (2019). Both of these studies were conducted in a climate similar to that of the study, that is, in hot climate zones. Touma and Ouahrani (2018) performed their experiments on 20 June and 20 December of the year using different measurement sensors, such as the CMP 11 Pyranometer K-type for solar radiation, K-type thermocouples for surface temperature, and the Hygro-thermo Transmitter for room air temperature. Each day, the experiment was performed continuously for 24 hours. The temperature and solar radiation measurements for the experimental days in Doha, Qatar are presented in Figure (4.31). The study simulated the two examined days to validate the results. The results of Touma and Ouahrani's (2018) experiment showed that on 20 June, the temperature ranged from 33.8°C at 4:00 am to 43.3°C at 6:00 pm, while solar radiation striking the glazed façade reached a maximum of

327 W/m<sup>2</sup> at 11:00 am as shown in Figure (4.31, top). On the other hand, the winter temperature on 20 December ranged from 16.1 to 27.2°C, while solar radiation reached 666 W/m<sup>2</sup> at 11 am, as shown in Figure (4.31, bottom). As a result of the country's latitude in the northern hemisphere, south-facing vertical surfaces receive greater solar radiation during the winter, such as in November than during the summer, such as in June. In contrast, west-facing surfaces receive a greater amount of solar radiation during the summer months. The simulated results reveal a similar hourly pattern of solar radiation striking the surface to the experimental study, which peaked at 250 W/m<sup>2</sup> at 11:00 am, while the temperature varied between 29.9°C and 41.0°C on 20 June during the hot summer Figure (4.32, top). In addition, the winter day (20 December) shows an hourly pattern comparable to that of the experimental investigation, with solar radiation reaching 843.4 W/m<sup>2</sup> at 11:00 am Figure (4.32, bottom).

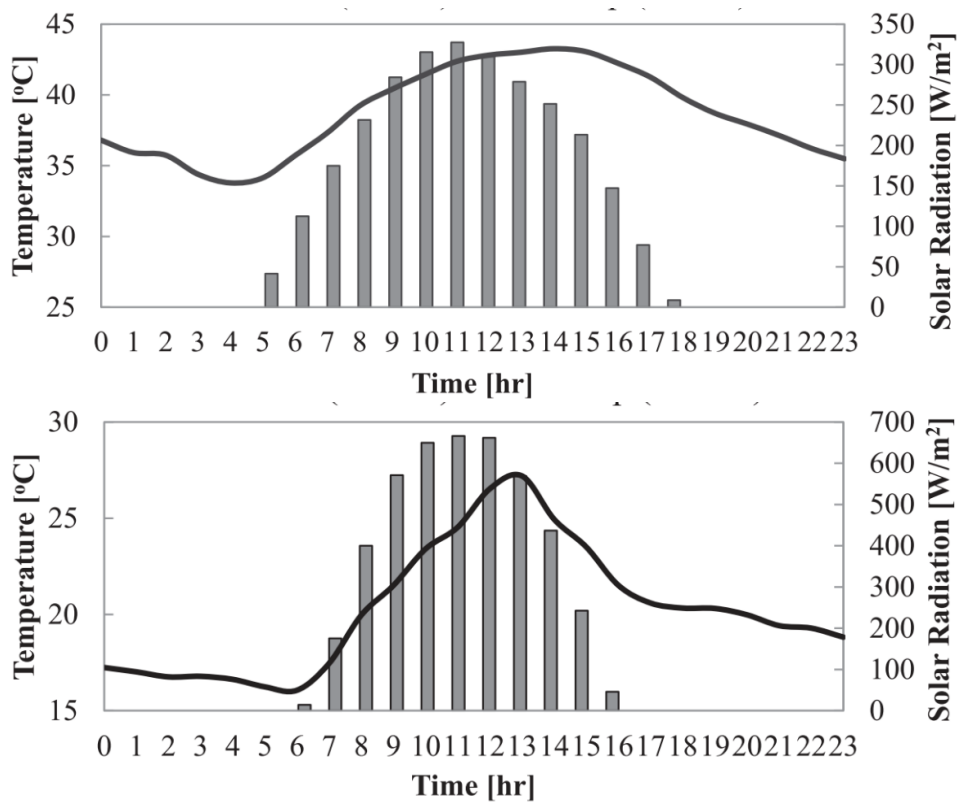
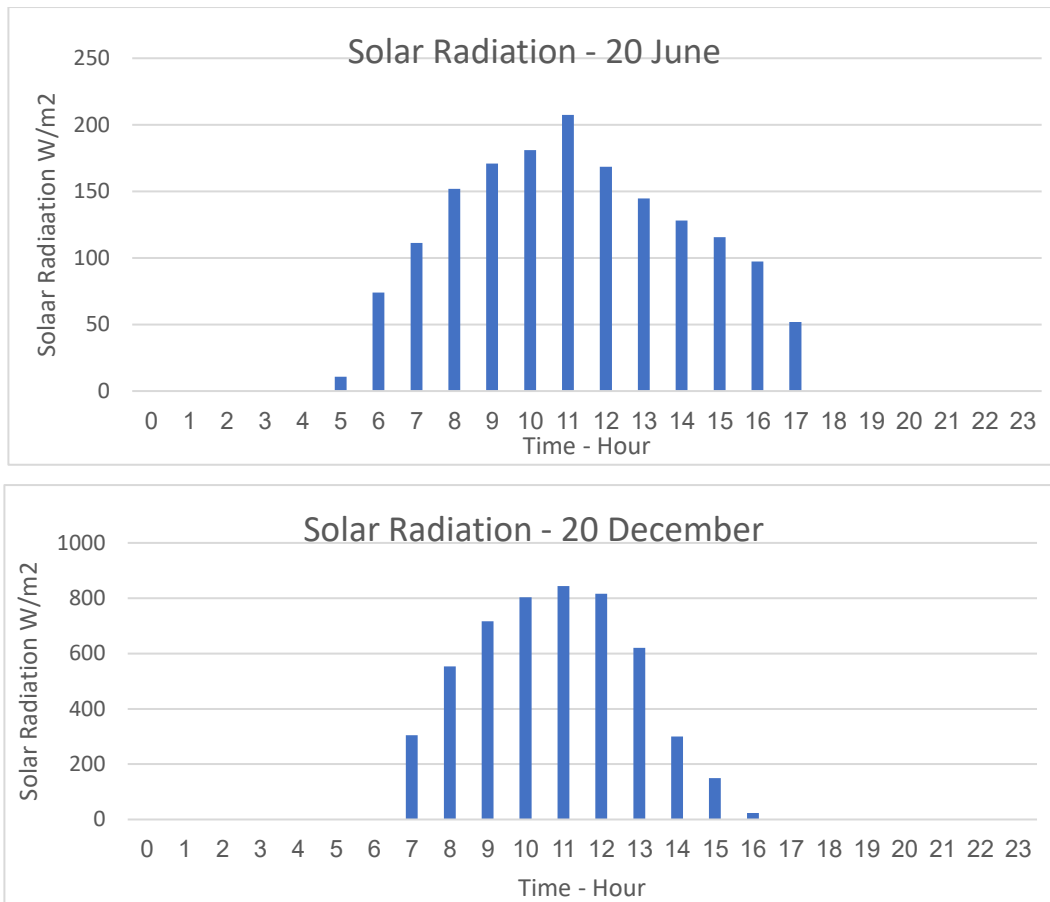


Figure 4.31: Temperature and solar radiation striking south-facing surface during (top) 20 June and (bottom) 20 December (Source: Touma and Ouahrani 2018).



*Figure 4.32: Solar radiation striking south-facing surface during (top) 20 June and (bottom) 20 December for the conducted study.*

In the second study by Ghabra (2019), the average monthly incident solar radiation (kWh/m<sup>2</sup>) was evaluated for four main orientations in Jeddah city, Saudi Arabia. According to their findings, the east and west façades received the maximum solar radiation between April and September, highlighting the necessity to shade these surfaces during the summer. On the other hand, the south façade received the highest incidence solar radiation values during the winter months Figure (4.33). A similar pattern was observed for all orientations indicating the accuracy of the simulation outcomes Figure (4.34).

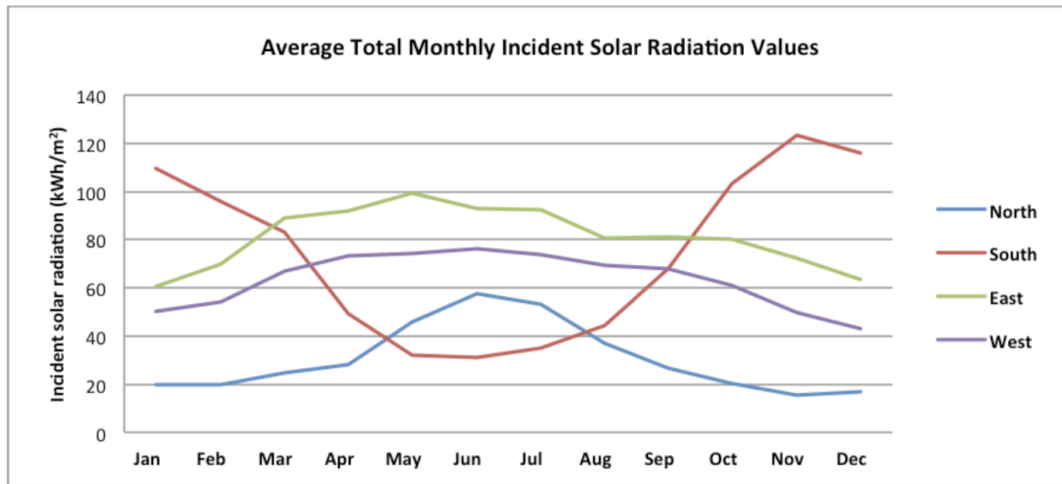


Figure 4.33: Average monthly total incident solar radiation on four main orientations in Jeddah. Source: Ghabra (2019)

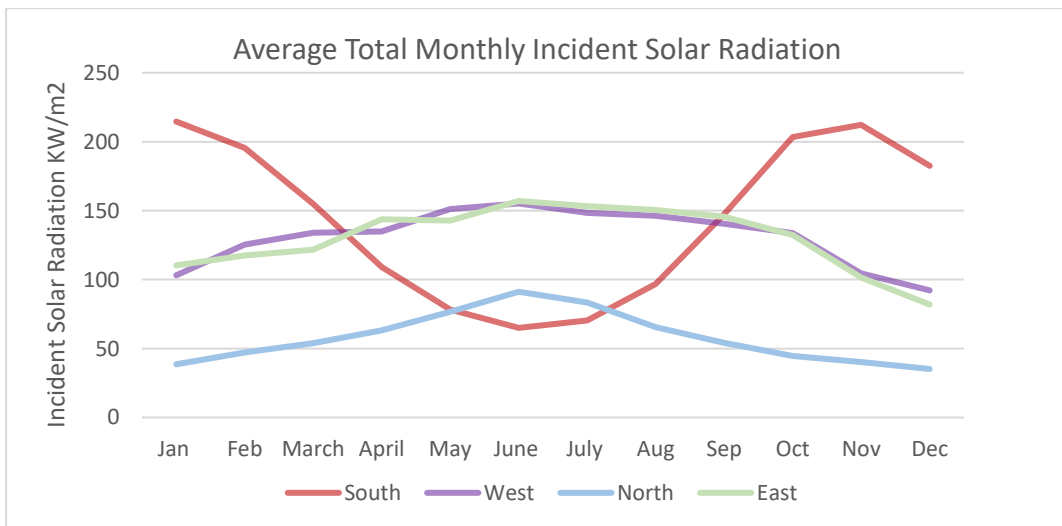


Figure 4.34: Average monthly total incident solar radiation on four main orientations for the conducted study.

#### 4.8.2. Solar Radiation Settings

Solar radiation simulation was conducted using the data from the weather file of Riyadh city, which was imported via the Ladybug plugin tool (Roudsari et al. 2013). This EPW weather file contains essential meteorological information, including hourly global horizontal radiation, direct normal radiation, dry bulb temperature, etc. Ladybug utilised the Gen-cumulative Sky module to generate an annual cumulative sky illuminance model, which utilises Radiance to simulate global and diffuse irradiance (Hensen and Lamberts 2011). The Ladybug Radiation Analysis Tool utilises the position of the sun at each hour of the year to calculate the amount of radiation received by external surfaces. Due to the implementation of the Perez diffuse

#### **CHAPTER 4: SYNTHETIC DATABASE GENERATION USING SIMULATION APPROACH**

radiation model and ray-tracing technique, Radiance has been thoroughly proven to be more accurate and efficient for solar irradiance simulation studies (Freitas et al. 2015).

The generated model in section (4.4) and its urban contexts is used in this phase to conduct the solar radiation analysis. The incident solar radiation that strikes the window surface on each office room was calculated considering the urban context variation. Since solar radiation differs based on different parameters, such as surrounding context, orientation, hour of the day, month, etc., a generative design process was conducted parametrically with varied parameters to simulate most of the design settings. To that end, solar radiation analysis was performed considering the following main parameters: (1) office operational time, which was considered to be from 8:00 am to 6:00 pm; (2) month, which was selected seasonally (March, June, September, and December) throughout all the simulations (Tabadkani et al. 2018); (3) surrounding context, which varies in each iteration from low, to medium, to high; and (4) main orientations, which are south, west, north, and east.

The workflow of the solar radiation analysis consisted of the following: (1) assigning building geometry and the surrounding urban contexts, (2) importing an EPW weather file of Riyadh city from the EnergyPlus weather map, (3) selecting the Sky matrix and defining the analysis period (month, day, and hour), (4) specifying the grid cell size for solar radiation on the tested façade surface, (5) specifying the offset distance of the test point grid from the input tested façade surface, and (6) running the radiation analysis to calculate the results on the selected façade surface Figure (4.35). The process used to conduct the solar radiation analysis in Grasshopper using the Ladybug tool are shown in Figure (4.36).

**CHAPTER 4: SYNTHETIC DATABASE GENERATION USING SIMULATION APPROACH**

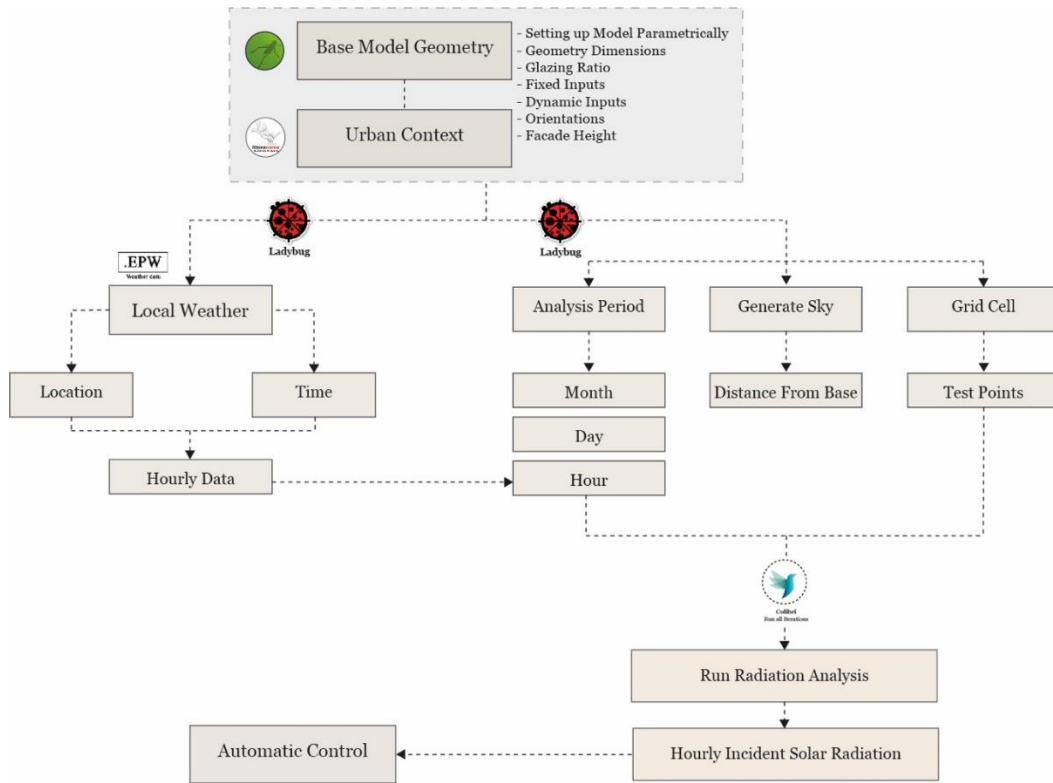


Figure 4.35: Workflow used to conduct the solar radiation analysis.

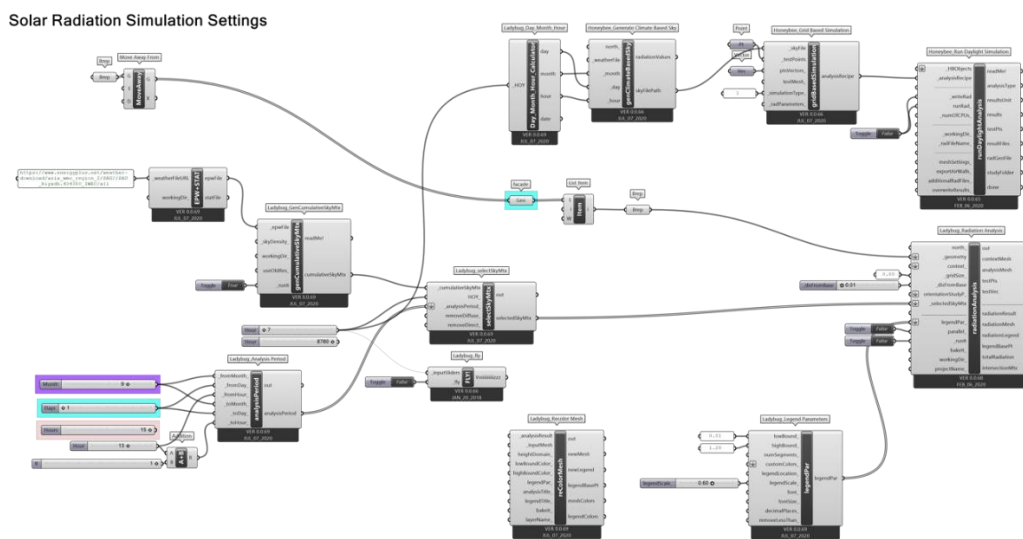


Figure 4.36: Scripting process used to conduct the solar radiation analysis in Grasshopper using the Ladybug tool.

**4.8.3. Solar Analysis Input Parameters**

For the solar radiation experiments, different dynamic inputs were determined. The first parameter is the building context, which varies in each simulation iteration. The building contexts produced a total of 324 different urban configurations that varied in height (low=12 m, medium=28 m, high=44 m). The main office tower is located in the middle of the urban context, and four buildings surround the tower from four sides: (B00 building from the west side, B01 building from the south side, B02 building from the east side, and B03 building from the north side). Then, these were also multiplied with four orientations (south, west, north, and east), 13-day time office hours from 6:00 am until 18:00 pm, and four months (March, June, September, and December). Regarding fixed input parameters, the following inputs were fixed throughout all iterations: (1) the geometry dimensions of both the office room within the tower and the urban context, (2) the curtain wall was fixed with an 80% glazing ratio, (3) the grid cell of the test points was fixed with an 0.80 \* 0.80 grid size, (4) the number of test points was 25 points, and (5) the distance from the tested surface was set to 0.01.

Figure (4.37) lists in detail these dynamic input parameters together with the fixed inputs used in this study to conduct the solar radiation analysis that strike the building façade surface. The Colibri plugin tool in Grasshopper was applied within the simulation workflow to step through all the design solutions automatically to create the dataset Figure (4.38). Then, Colibri stored the result of the solar radiation data and its coordinates in an Excel spreadsheet (Natanian et al. 2019).

| Fixed Input Parameters  |                           | Dynamic Input Parameters  |                           |                   |
|-------------------------|---------------------------|---|---------------------------|-------------------|
| Input                   | Assigned Values           | Input   | Assigned Values           | No. of Iterations |
| Site Location           | Riyadh, Saudi Arabia      | Month   | 0,1,2,3                   | 4                 |
| Space type              | Shared Office Room        | Hour  | 6:00 to 18:00             | 13                |
| Room width              | 4.00 m                    | B00   | L(12 m), M(28 m), H(44 m) | 3                 |
| Room floor height       | 4.00 m                    | B01   | L(12 m), M(28 m), H(44 m) | 3                 |
| Room length             | 6.00 m                    | B02   | L(12 m), M(28 m), H(44 m) | 3                 |
| Glazing ratio           | 80 %                      | B03   | L(12 m), M(28 m), H(44 m) | 3                 |
| Grid size               | 0.80 * 0.80               | Orientation   | South, West, North, East  | 4                 |
| Distance from base      | 0.01                      | Façade Height   | l(0.50), a(1.00),h(1.50)  | 3                 |
| Day                     | 1-31                      | <b>Total No of iterations</b>   |                           | <b>50,544</b>     |
| Test Points coordinates | 25 coordinates of X, Y, Z | 0= March, 1=June, 2=September, 3= December<br>B= Building Context Height , A total of 4 surrounding buildings<br>L=Low(12m), M=Medium(28m), H=Height(44m)<br>l=lower than average, a=Average, h=Higher than average |                           |                   |

Figure 4.37: Fixed and dynamic model parameters.

## CHAPTER 4: SYNTHETIC DATABASE GENERATION USING SIMULATION APPROACH

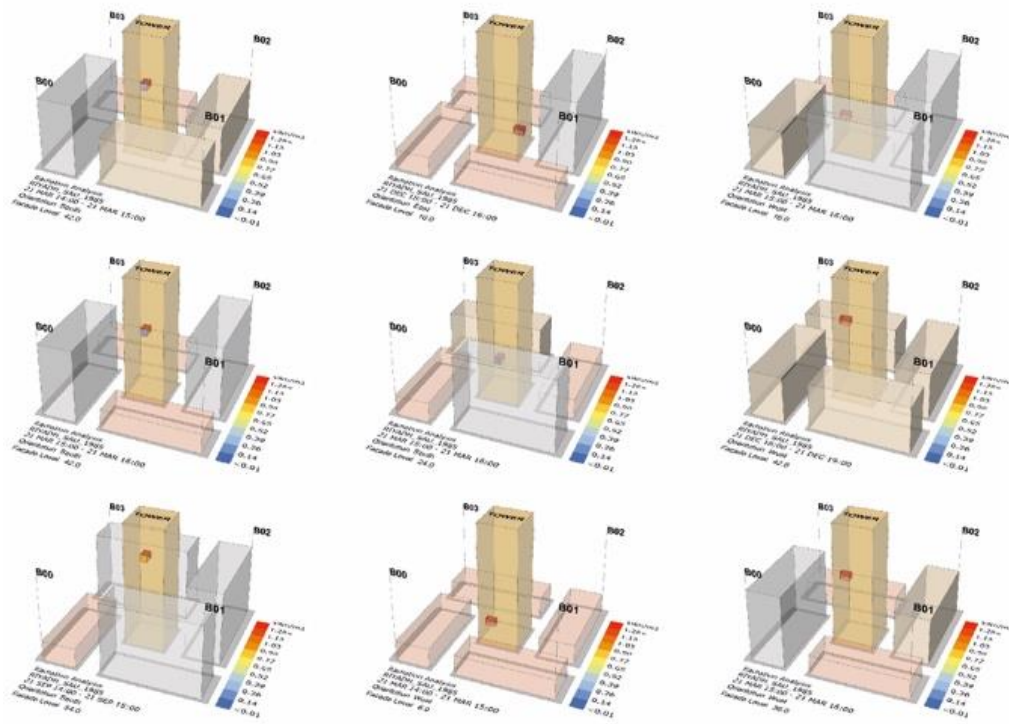


Figure 4.38: Sample of the solar radiation data generated automatically in the simulation process, which produced different SR results in each design situation.

The output of each iteration consists of several test points that fall on the tested surface with X, Y, and Z coordinates to perform the radiation analysis, and these values are measured in  $\text{KWh/m}^2$  Figure (4.39). The total number of test points is 1,263,600 (25 test points of each surface \* 50,545 total number of iterations). The total radiation results in  $\text{KWh/m}^2$  are calculated through the mass addition of results at each of the test points multiplied by the area of the face that the test point is representing Figure (4.40).



**CHAPTER 4: SYNTHETIC DATABASE GENERATION USING SIMULATION APPROACH**

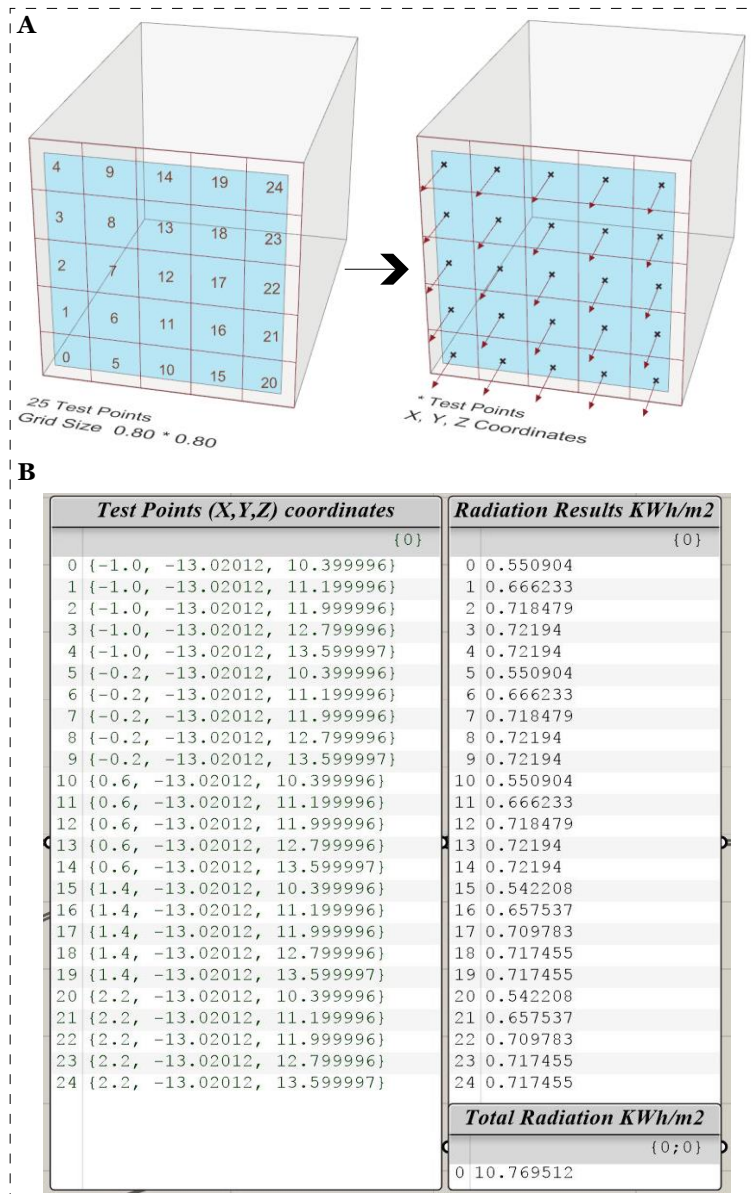


Figure 4.39: (A) Test point coordinates, (B) Radiation results based on each test point.

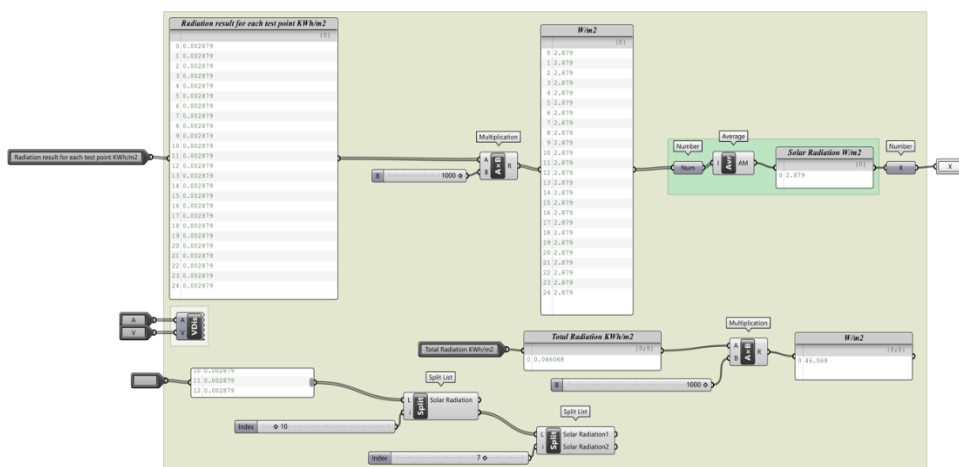


Figure 4.40: Pre-processing of solar radiation results.

**4.8.4. Solar Radiation Database**

A total of 50,545 solar radiation iterations were generated in the simulation process examining different orientations. Figure (4.41) shows an example of some samples of the conducted simulation for solar radiation results in two different orientations and at different hours of the day. The whole database is stored on one Excel sheet that contains all the design iterations in the following order: hour; day; month; building context B00; building context B01; building context B03; building context B04; façade floor height; X, Y, and Z coordinates of (test point 0, test point 1, test point 2, test point 3, test point 4, test point 5, test point 6, test point 7, test point 8, test point 9, test point 10, ....., test point 24); (output of test point 0, output of test point 1, output of test point 2, output of test point 3, output of test point 4, output of test point 5, output of test point 6, output of test point 7, output of test point 8,....., output of test point 24); and image of each iteration. The Excel sheet consists of 56 columns representing the input parameters and 50,545 rows representing the number of design iterations, which in total is 2,830,520 data points. A sample of the solar radiation recorded database is shown in (Appendix D).

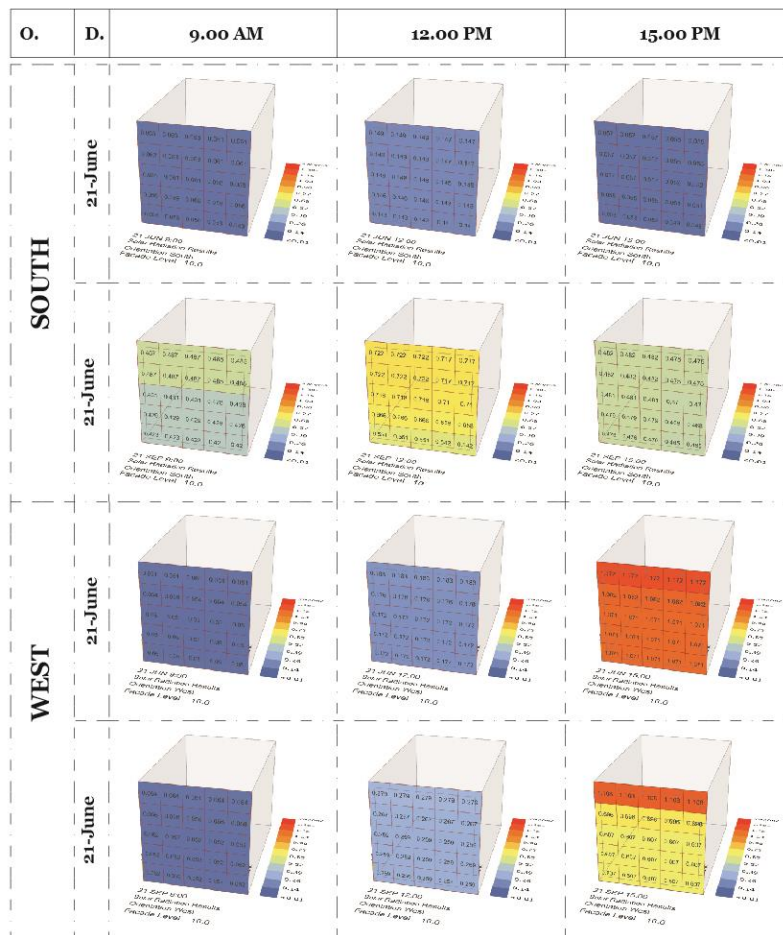


Figure 4.41: An example of two different cases of solar radiation results within different orientations and based on the variation of building contexts and time.

## **4.9. Shade Factor Analysis**

As discussed in chapter (2), the current simulation tools are limited when it comes to mimicking the time-dependent nature of an AF that alters the dynamic heat transition when physical and material parameters are considered. This is primarily the result of the shading effect of the AF on the thermal energy stored in the building materials, which causes a thermal lag between each time interval. This concept can be done in the case of Venetian blinds because the BPS tool supports only this shading system. Therefore, to fill this gap, this section discusses an alternative method to model and simulate the energy performance of AF shading systems, which will be discussed in more detail in the coming sections.

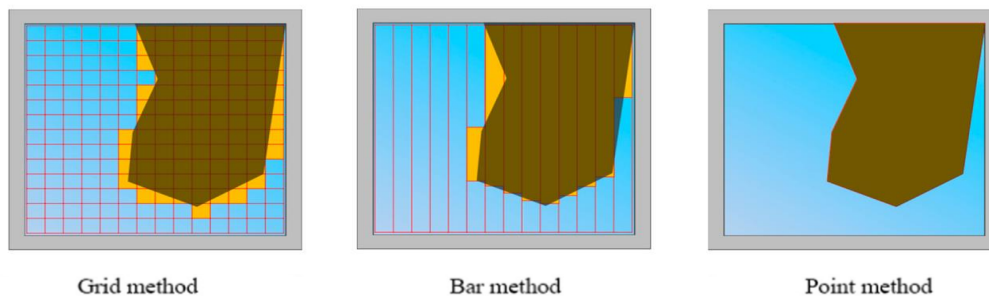
The thermal model in EnergyPlus considers the thermal interactions between the shade layer and the glass when a shading system is applied, and calculations are made based on the following factors (EnergyPlus 2020).

- “Exterior shading device: Long-wave radiation (IR) from the surround absorbed by shading device or transmitted by the shading device and absorbed by the adjacent glass. For interior shading the surround consists of the other zone surfaces. For exterior shading the surround is the sky and ground plus exterior shadowing surfaces and exterior building surfaces “seen” by the window”.
- “Inter-reflection of IR between the shading device and adjacent glass”.
- “Direct and diffuse solar radiation absorbed by the shading device”.
- “Inter-reflection of solar radiation between shading layer and glass layers”.
- “Convection from shading layer and glass to the air in the gap (or, for between-glass shading, gaps) between the shading layer and adjacent glass”.
- “Natural convection airflow in the gap (or, for between-glass shading, gaps) between shading layer and adjacent glass”.

The SF can be calculated by simplifying the irregular AF geometry into flat shaded areas on the glazed part of the façade. Depending on the amount of direct solar radiation received from the sun, any shading system installed on the window surface may provide either complete or partial shading protection. Hence, the glazed area is separated into two distinct regions: (1) shaded area and (2) un-shaded area. The SF is defined as a number between 0 and 1 and refers to the percentage of the glazed surface that is not exposed to incident solar radiation as a result of the shading system (Choi et al. 2017a).

### **4.9.1. Shade Factor Methods**

The SF is calculated in response to the hourly changes of the opening ratio of each shading state. In the literature, the shaded area created by the external dynamic movements of a shading system can be calculated using any of the following three methods: (1) the grid method, (2) the bar method, and (3) the polygon method (Choi et al. 2017a; Choi et al. 2017b) Figure (4.42). Both the grid and the cell methods involve dividing the window area into a grid of cells, and the SF is calculated by excluding the area of cells that receive direct SR from the total window area. However, the only difference between these two approaches is the shape of the division segments. These two methods have been widely used within different software, such as EnergyPlus, Ecotect, and Radiance (Tabadkani et al. 2020). On the other hand, the polygon method projects the shading system coordinates into the target window area, and the SF is calculated by the projected geometrical figure defined by the shadow's coordinates. The polygon method is more accurate and time consuming compared to the first two methods, which are less accurate but have the advantage of allowing fast calculation (Choi et al. 2017b). Since the grid method is similar to the ray-tracing method found within the Ladybug plugin, which is linked to the Radiance software, this method was adopted in this research to calculate the shaded area of all of the six proposed shading states for a total of 8,760 hours of the year.



*Figure 4.42: Shade factor (SF) calculations adapted from Choi et al. (2017b).*

### **4.9.2. Shade Factor Settings**

Shading control can be defined in the EnergyPlus under the Window Property: Shading Control section. Adjusting the slat angle in this section is possible depending on one of three controls: (a) the static slat angle, (b) the cut-off or blocked angle, and (c) the scheduled slat angle. Hence, the last approach was chosen for this investigation since it allows hourly slat angles to be overriding by an hourly transmittance fixed schedule. The SF ranges from 0 to 1 based on the percentage openness of the shading system, sun angle, and sun position, where the SF is mostly equal to 1 (fully shaded). In addition, a grid cell size of 1 cm<sup>2</sup> was

assigned on the window surface as inputs for the SF simulation. Figure (4.43) illustrates the framework for the SF calculation method where the AF system is simplified using the grid (ray-tracing approach) in the Ladybug tool.

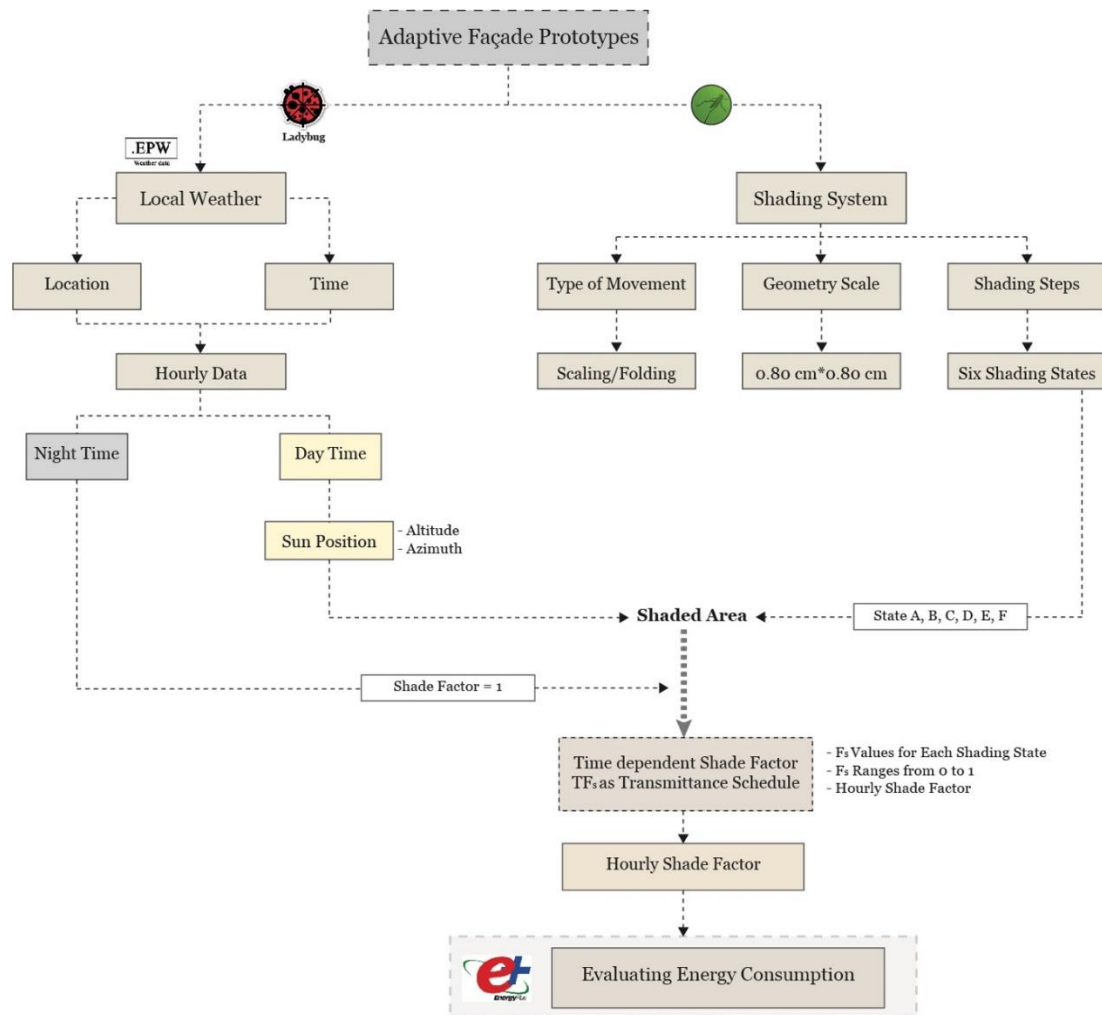


Figure 4.43: Workflow used to conduct the shade factor analysis.

To conduct an SF analysis in response to the developed AF shading states, different steps were followed:

- (1) Firstly, an EPW local weather file was assigned to create hourly sun position and define the day-time hours and night-time hours during the year through the analysis period component.
- (2) In the second step, the sun azimuth and altitude were defined for a certain time of day. Then, the urban context and AF shading system that were modelled in section (4.6) which determined the type of shading movement (scaling or folding), geometry scale, and number of shading states (shading state A-100%, shading state B-80%, shading state C-60%, shading state D-40%, and shading state E-20%) was linked to a ray-tracing component within the shade factor workflow analysis Figure (4.44).

## CHAPTER 4: SYNTHETIC DATABASE GENERATION USING SIMULATION APPROACH

- (3) In the next step, the SF was calculated for each simulation iteration by dividing the total number of grid cells on the window area that received solar radiation by the total number of grid cells on the window area. This process was repeated every hour for each shading state.
- (4) Finally, an iterative process was done using the Colibri tool to step through all the hours of the year for each shading state.

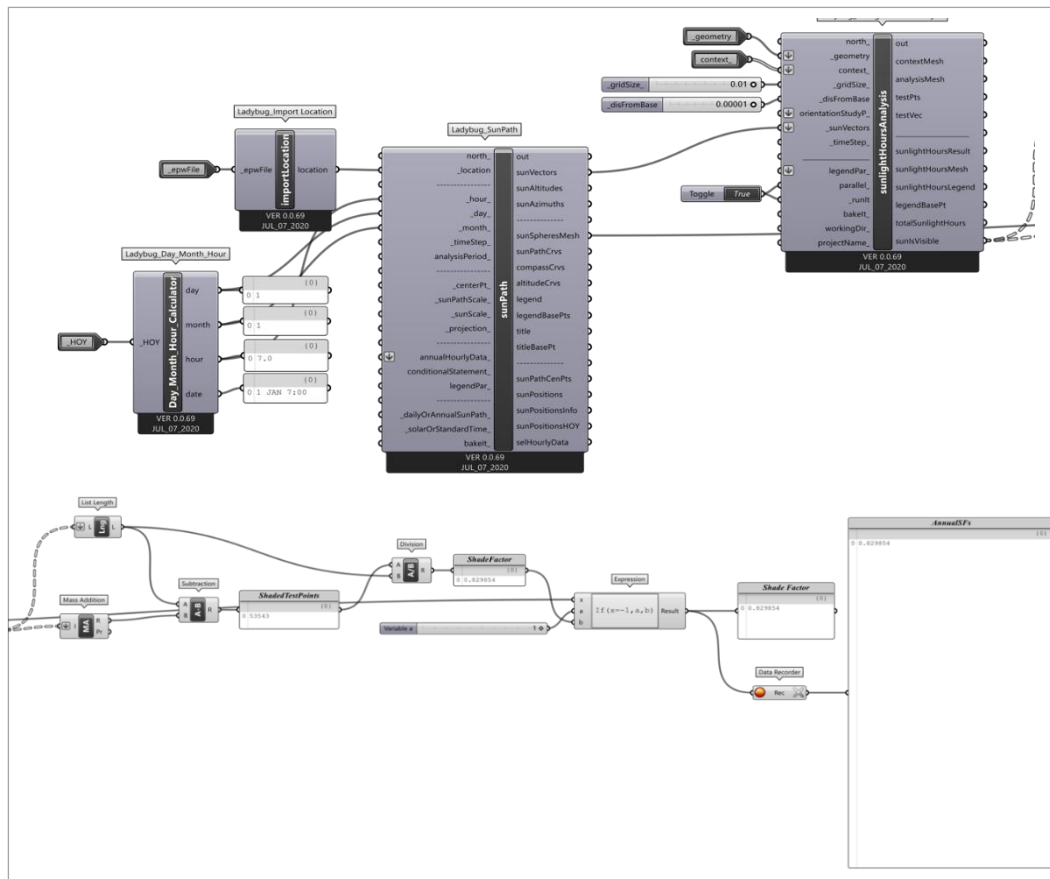


Figure 4.44: Scripting process to conduct the shade factor analysis in Grasshopper using the Ladybug tool.

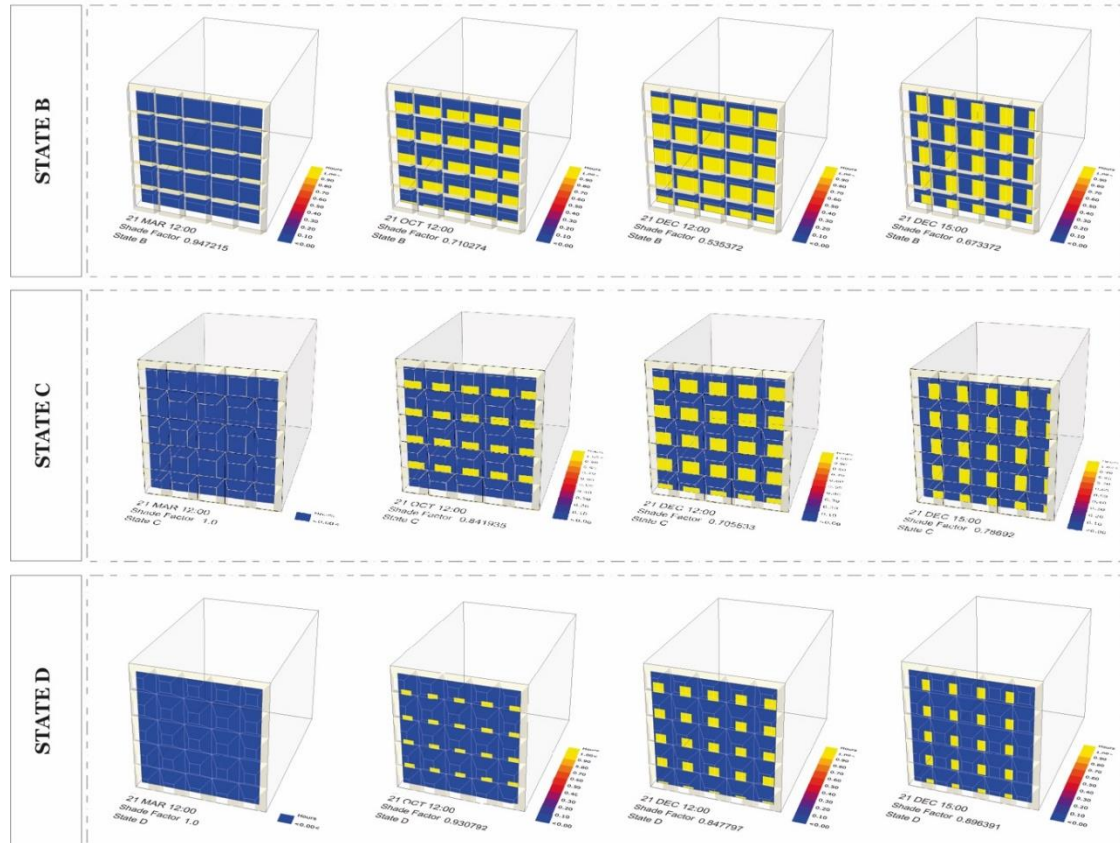
### 4.9.3. Shade Factor Database

The output of the hourly SF of each shading state was recorded on an Excel sheet of hourly SFs. The database was stored in the following order: hour, day, month, SF state A, SF state B, SF state C, SF state D, SF state E, and SF state F. The Excel sheet contains of 8 columns identifying SF states and 8,760 rows identifying the number of hours in a year. As an example of the output, Figure (4.45) shows different shading states when the shading system is 80% and 40% open with the grid method for SF calculations. To this end, the calculated shaded area of the distinct shading states was then translated into the transmittance schedule so it could be used within the EMS interface to select the state



## CHAPTER 4: SYNTHETIC DATABASE GENERATION USING SIMULATION APPROACH

based on the defined threshold, as will be explored in the following sections. The aim of this analysis along with the solar radiation analysis performed in previous section is to evaluate the energy performance of the AF shading system, specifically, the hourly cooling loads. A sample of the shade factor database is shown in (Appendix D).



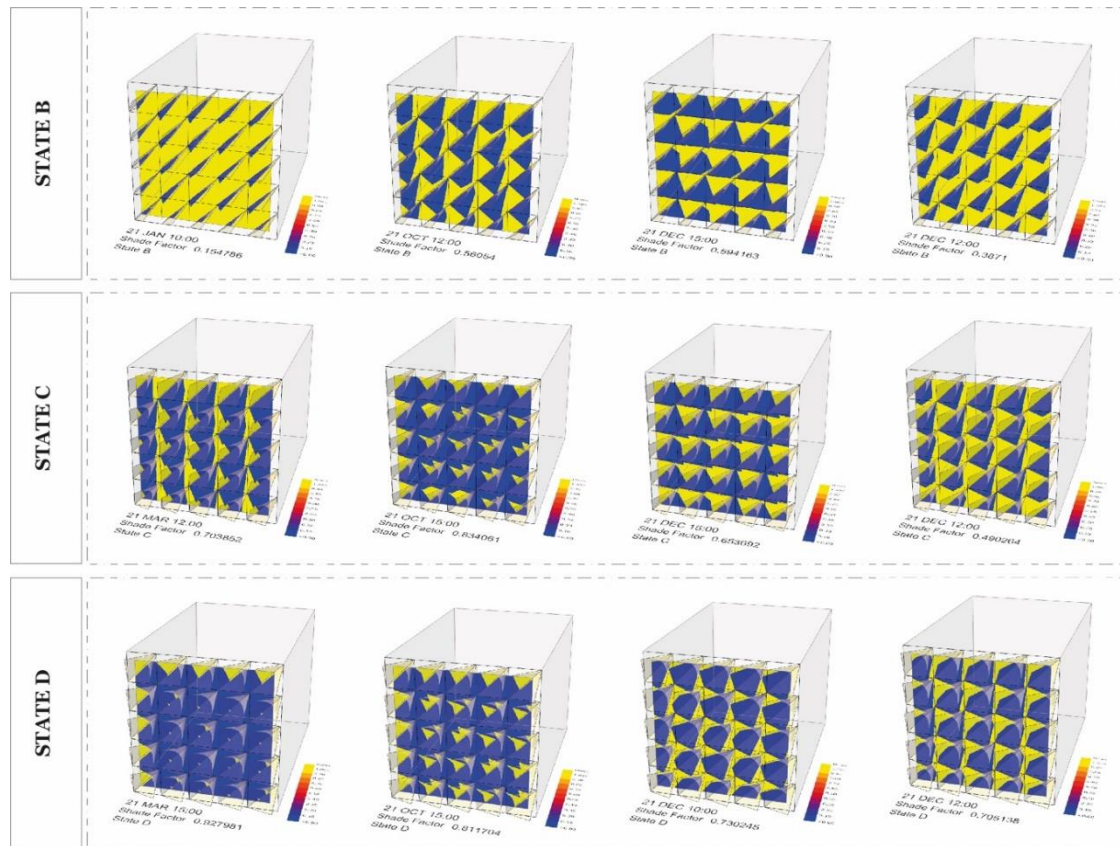


Figure 4.45: Shade factor calculation for some selected cases for two AF movements (scaling and folding).

### 4.10. Energy Simulation

The generated models in section (4.4) were simulated with an AF system in terms of energy consumption using EnergyPlus, which served to generate the training data Figure (4.46). Simulation settings, input parameters, material properties, occupant loads, zone program, occupancy schedule, and thermal setting were determined and valued according to the benchmark standard and office building guidelines to conduct a detailed energy analysis (Hensen and Lamberts 2011). Then, an automatic shading control was employed to control the AF system on an hourly basis using various environmental sensors. The aim of these two stages was to assess the impact of AFs on the energy performance of a shared office room and to create a large synthetic database of an hourly cooling energy demand (Wh/m<sup>2</sup>) for training the surrogate model, which will be presented in Chapter (6). Figure (4.47) shows the algorithmic workflow of the parametric modelling and simulation in the Grasshopper environment. The next sections discuss in detail the energy simulation settings, the parameters used, and the assigned control system. The study evaluates the energy performance for the parametrically modelled office space considering the following scenarios:



## CHAPTER 4: SYNTHETIC DATABASE GENERATION USING SIMULATION APPROACH

- base case model (no shading assigned)
- vertical fixed shading (no automatic control assigned)
- horizontal fixed shading (no automatic control assigned)
- AF scaling movement (automatic control is assigned)
- AF folding movement (automatic control is assigned)

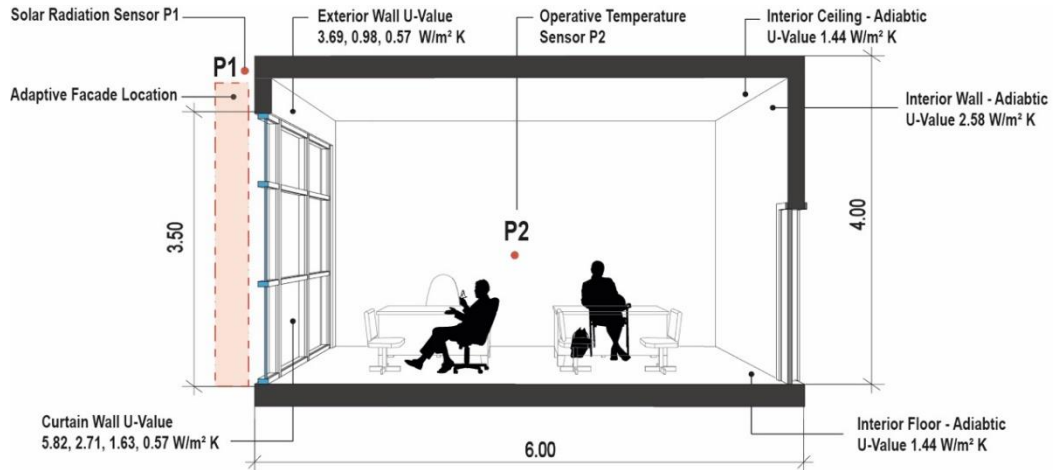


Figure 4.46: Closed office room with detailed constructions and location of sensor.

**CHAPTER 4: SYNTHETIC DATABASE GENERATION USING SIMULATION APPROACH**

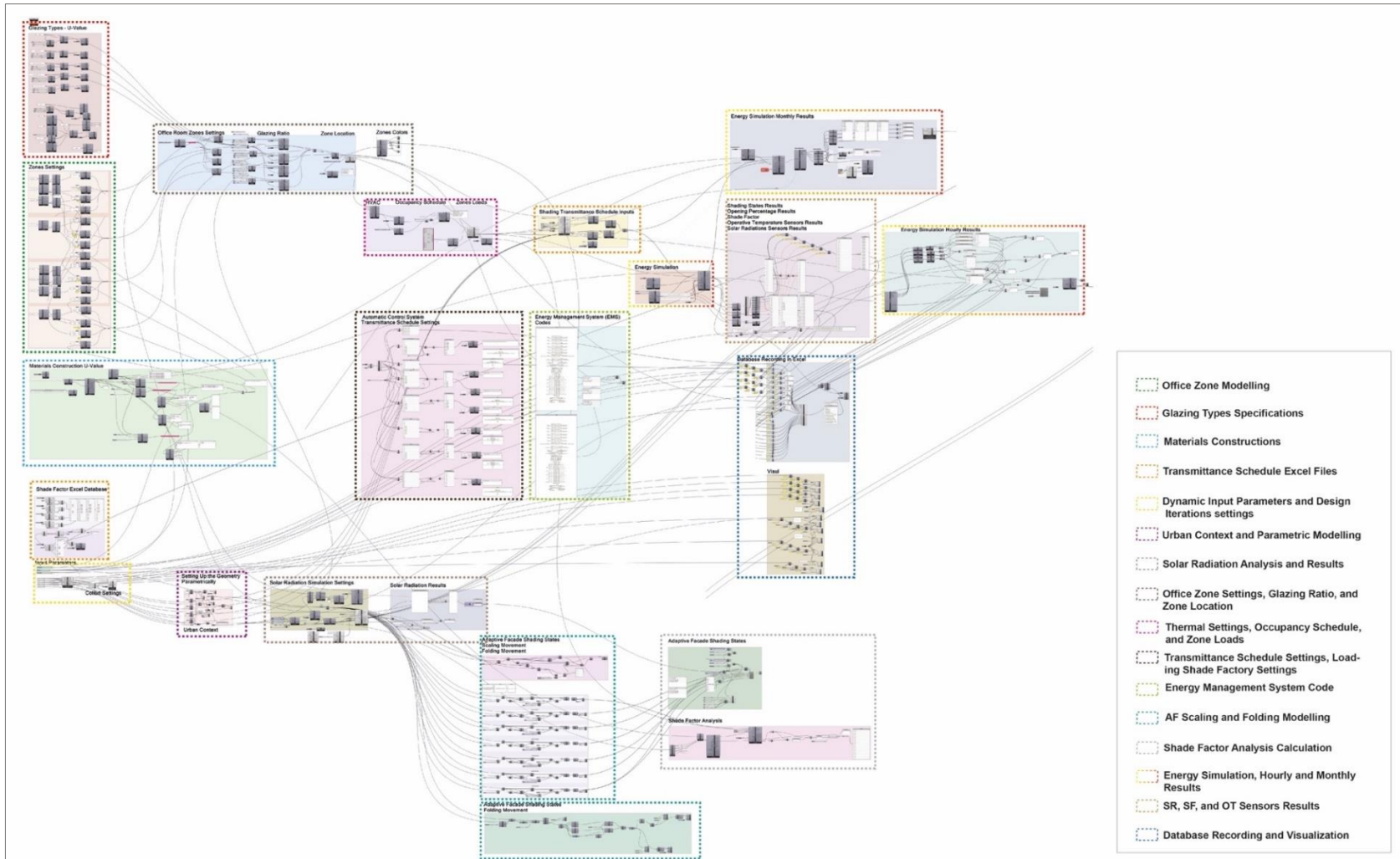


Figure 4.47: Algorithmic workflow of the parametric modelling and simulation in Grasshopper environment.

### **4.10.1. Input Parameters**

The dynamic input parameters of this research were selected considering the building envelope properties and the dynamic behaviour changes of the AF shading system including hour, day, month, orientation, building context, external wall U-value, glazing type U-value, solar radiation setpoint, operative temperature setpoint, SF, and opening ratio, which will be discussed in detail below. According to the literature, different parameters should be tested to find the most effective parameters in terms of energy-use reduction. A study by Pacheco et al. (2012) revealed that building orientation, shape, envelope system, passive heating, cooling mechanisms, shading, and glazing were the most influential features in regard to energy consumption. In addition, as found in the literature review, AF systems have significantly reduced the total energy consumption of buildings, as a building envelope that includes a dynamic shading system may significantly affect the amount of energy consumption. Thus, in this study, the focus was only on specific parameters to evaluate the potential effect of an AF system, together with the envelope's physical properties, on enhancing the energy performance of buildings. The selected dynamic inputs were as follows:

- Responsive time scale:

#### *Hour*

The AF shading system modifies its configurations based on a variety of time scales ranging from seconds to seasons and is influenced by a wide range of environmental conditions. Thus, the time scale selected in this study was based on an hourly basis, as that was the time scale most frequently found in literature that is suitable for SR as discussed in Chapter 2 section (2.5.2), as well as considering the computational time that could increase the scale of simulations when conducting the investigation based on minutes or seconds.

#### *Month*

The simulation of each skin configuration was performed for all months of the year to provide a complete evaluation analysis; however, the study focused on the four extreme and mediate times of the year to minimize the computational time required to train the ML models in the next phase (Tabadkani et al. 2019b). The four different seasons of the year considered for energy simulation were March, June, September, and December, as these months represent maximum, equinox, and minimum availability of sunlight around the year (Eltaweel and Su 2017a).

### *Day*

The simulation was run for all days of the months (Day 1 to Day 31), and the office operational time was considered to be from 8:00 am to 18:00 pm.

#### - Orientation:

Examining different orientation is an essential input parameter for energy simulation when designing AF shading systems, as each orientation varies in terms of solar radiation intensity values received on façades depending on climate and location. For instance, in the studied climate zone, the west and east orientation received the highest solar radiation during summer months (from April to September) compared to south orientation façades, which received the highest solar radiation during the cold months. Thus, this highlights the importance of considering orientation parameters as a dynamic input for investigating when to block or allow solar radiation to penetrate into the internal the space for AF shading systems. Therefore, this input variable was tested on the main orientations (south, west, north, and east).

#### - Surrounding building context

When estimating the energy consumption of a building, it is important to account for the effect of surrounding buildings for solar radiation reflections and convective heat transfer. The solar radiation reflected by surrounding buildings can have a significant impact on the amount of solar heat received on the façade of the buildings, and thereby, can affect the energy required for cooling and heating a space (Allegrini et al. 2016). Therefore, the amount of direct and reflected solar irradiation received by the building's façade determines when the AF shading system opens and closes.

#### - Glazing type

This variable was investigated using various glazing systems ranging from single to triple glazing with varying thermal transmittance (U-Value) of the opaque and transparent elements, the glazing composition, and the thermal and visual features of glazing, such as the visual transmittance (VLT), and solar heat gain coefficient (SHGC). This parameter along with the glazing ratio has been evaluated in several studies, which have demonstrated their significant impact on reducing the cooling requirements of office buildings (Hammad and Abu-Hijleh 2010; Gadelhak and Lang 2016). However, the glazing ratio was not

#### **CHAPTER 4: SYNTHETIC DATABASE GENERATION USING SIMULATION APPROACH**

investigated as one of the input variables because the most commonly used glazing ratio is 80%, according to the cases analysed in section (4.2).

- External wall

This variable was also tested using different construction materials and finishing layers and will be discussed in detail in the following section.

- Environmental parameters

As mentioned in the literature, buildings are exposed to different environmental factors that are highly dynamic and change continuously throughout the day and the season. Thus, the study investigated different environmental parameters, such as incident and transmitted solar radiation, and operative temperature, to automatically control the AF shading openness once it reaches a certain threshold. Solar radiation varies based on the amount of incident solar gain the façade receives hourly, which has been evaluated in section (4.8). The selected control parameters will be discussed in detail in section (4.10.4).

- Shade factor

The complex form was simplified to a flat shaded area on the window that ranged from a value of 0 to 1, which has been evaluated in section (4.9).

- Shades Transmittance

This variable represents the un-shaded area that is exposed to incident solar radiation allowed by the shading system.

Tables (4.3) and (4.4) list the fixed and dynamic input parameters used in this research to conduct the energy analysis using the EnergyPlus engine. Figure (4.48) shows the iteration process using Colibri tool to iterate through all design solutions.

*Table 4.3. Fixed simulation parameters*

| <b>Parameter</b>                          | <b>Assigned Value(s)</b>                   |
|---|--|
| <i>Location</i>                           | <i>Riyadh, Saudi Arabia</i>                |
| <i>Space type</i>                         | <i>Shared Office Room</i>                  |
| <i>Zone program</i>                       | <i>Closed Office Zone</i>                  |
| <i>Glazing ratio</i>                      | <i>80 %</i>                                |
| <i>Room width</i>                         | <i>4.00 m</i>                              |
| <i>Room floor height</i>                  | <i>4.00 m</i>                              |
| <i>Room length</i>                        | <i>6.00 m</i>                              |
| <i>Shading reflectance</i>                | <i>70 %</i>                                |
| <i>Interior wall, ceiling, floor</i>      | <i>Adiabatic</i>                           |
| <i>Cooling set points</i>                 | <i>24 C</i>                                |
| <i>Heating set points</i>                 | <i>22 C</i>                                |
| <i>HVAC system</i>                        | <i>ideal air load system</i>               |
| <i>Number of people</i>                   | <i>2 people</i>                            |
| <b>Zone loads</b> <i>Lighting density</i> | <i>5.00 W/m<sup>2</sup></i>                |
| <i>Number of occupants</i>                | <i>2 Occupants (0.2 ppl/m<sup>2</sup>)</i> |

## CHAPTER 4: SYNTHETIC DATABASE GENERATION USING SIMULATION APPROACH

| Parameter                           | Assigned Value(s)   |
|-------------------------------------|---|
| Equipment load (W/m <sup>2</sup> )  | 4 W/m <sup>2</sup>  |
| Infiltration ratio                  | 0.04 cfm/sf (~0.000203 m <sup>3</sup> /s m <sup>2</sup> façade) |
| Schedule                            | Sun.-Thur. 08:00 – 18:00  |
| Prototype unit                      | 0.80 * 0.80 c   |
| Shadow calculation method           | Time step frequency   |
| Solar radiation sensor point 1 (P1) | 3.00 m height   |
| Operative temperature point 2 (P2)  | 1.5 m height  |

Table 4.4. Dynamic simulation parameters

| Dynamic Input Parameter          | Assigned Value(s)                                    | No. of Iterations |
|----------------------------------|--|-------------------|
| Orientation                      | south, west, north, east                             | 4                 |
| Building context 00              | low, medium, high                                    | 3                 |
| Building context 01              | low, medium, high                                    | 3                 |
| Façade level height              | lower than average, average, and higher than average | 3                 |
| Exterior wall – U-value          | 0, 1, 3 W/m <sup>2</sup> K                           | 3                 |
| Glazing type – U-value           | 0, 1, 2, 3 W/m <sup>2</sup> K                        | 4                 |
| Total no. of iterations          |  | 1,296             |
| Month                            | March, June, September, December                     | -                 |
| Day                              | 01 – 31  | -                 |
| Hour                             | 1:00 - 24:00   | -                 |
| Shading states                   | A, B, C, D, E, F                                     | -                 |
| Total no. of hourly cooling data |  | 3,794,688         |

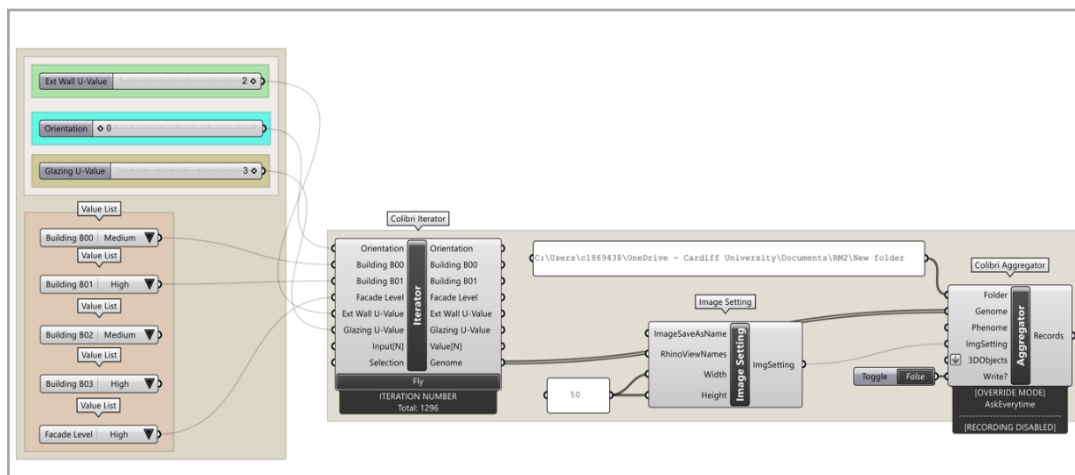


Figure 4.48: Scripting process using Colibri tool to iterate through design solutions.

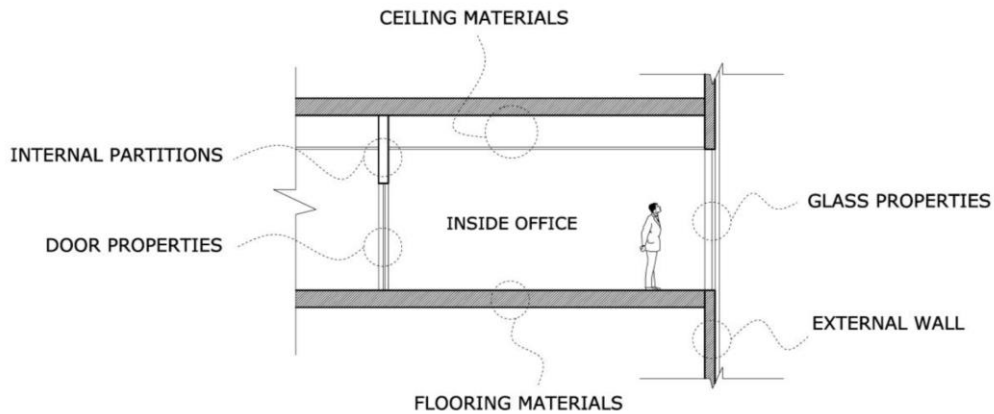
### 4.10.2. Construction Materials and Thermal Settings

The material parameters of the office were defined based on ASHRAE 90.1-2010 climate region number 1, a database provided by EnergyPlus (ASHRAE materials databases) as the recommended materials for the climate zone of the study, which were assigned for a hot-dry climate region. ASHRAE database construction materials were employed for the following building elements as illustrated in Figure (4.49):

- external walls construction materials and finishing layers
- interior partition materials and finishing layers
- ceiling materials

## **CHAPTER 4: SYNTHETIC DATABASE GENERATION USING SIMULATION APPROACH**

- interior floor construction materials and finishing layers
- glazing system properties



*Figure 4.49: Construction parameters considered for this study.*

Different types of external walls for the office room were considered with distinct U-values. Partitions/interior walls were assumed to be adiabatic and to be gypsum board with a U-value of 2.58 (ASHRAE 90.1-2010), which means there was no heat transfer across the interior walls. In addition, glazing is one of the main variables in the energy simulation of the model. This is because the SHGC affects the total solar heat transmittance of the glass and its components (Baenas and Machado 2017). The glazing shading coefficient measures the glazing's capacity to block solar radiation. A low shading coefficient value reduces the amount of solar heat gain that penetrates through the glass. Changing the SHGC value has an impact on the cooling loads and daylighting performance of a building with an AF (Hammad and Abu-Hijleh 2010). Therefore, different types of glazing system (single, double, and triple glazing) were investigated for the studied model, which has different solar heat coefficient values and thermal transmittance U-values (Gadelhak and Lang 2016). Table (4.5) lists the specifications for the construction material parameters that were implemented in this study.

A closed office program zone according to the EnergyPlus US Department of Energy's (DOE) office building zones (DOE 2016) was selected in all offices. These closed offices were conditioned with the default set of an ideal air load system in EnergyPlus for HVAC, which was the most appropriate system in the early stages of the design when taking calculation time into consideration (Zhang et al., 2017). In addition, the model was set for an hourly time step to calculate the energy demand of the office room. The operating time for cooling and heating was assumed to be five days per week, Monday to Friday from 8:00 am to 18:00 pm. The temperature setpoints of the HVAC system were considered to be 24°C for cooling

## CHAPTER 4: SYNTHETIC DATABASE GENERATION USING SIMULATION APPROACH

and 22°C for heating. The HVAC system was set to work automatically to maintain the desired internal temperature.

Table 4.5. Characteristics of materials used in the simulation.

| Name of material  | Thickness (m) | Layers   | U-value (W/m <sup>2</sup> K) | R-value (K m <sup>2</sup> /W) |
|---|---------------|--|------------------------------|-------------------------------|
| ASHRAE 90.1-2010<br>EXTWALLMASS<br>CLIMATEZONE 1              | 0.2412        | 1IN Stucco<br>8IN CONCRETE HW RefBldg<br>1/2IN Gypsum  | 3.690821                     | 0.270942                      |
| ASHRAE 90.1-2010<br>EXTWALL MASS<br>CLIMATEZONE ALT-<br>RES 1 | 0.277737      | 1IN Stucco<br>8IN CONCRETE HW RefBldg<br>Mass Wall Insulation R-4.23 IP<br>1/2IN Gypsum        | 0.983672                     | 1.016599                      |
| ASHRAE 90.1-2010<br>EXTWALL METAL<br>CLIMATEZONE 1-2          | 0.154367      | Metal Siding<br>Metal Building Wall Insulation<br>R-9.45 IP<br>1/2IN Gypsum                    | 0.573406                     | 1.743964                      |
| ASHRAE 90.1-2010<br>INTERIOR WALL                             | 0.188         | G01a 19 mm gypsum board<br>F04 Wall air space resistance<br>G01a 19 mm gypsum board            | 2.580645                     | 0.3875                        |
| ASHRAE 90.1-2010<br>INTERIOR FLOOR                            | 0.7291        | F16 Acoustic tile<br>F05 Ceiling air space<br>resistance<br>M11 100 mm lightweight<br>concrete | 1.449209                     | 0.690031                      |
| ASHRAE 90.1-2010<br>INTERIOR CEILING                          | 0.3007        | M11 100mm lightweight<br>concrete<br>F05 Ceiling air space<br>resistance<br>F16 Acoustic tile  | 1.449209                     | 0.690031                      |

| Glazing Type (Glaz)                     | U-value (W/m <sup>2</sup> K) | Solar Heat Gain Coefficient (SHGC) | Visual Transmittance (τ <sub>vis</sub> ) |
|---|------------------------------|------------------------------------|--|
| Single glazing (SG)                     | 5.82                         | 0.82                               | 0.88                                     |
| Double glazing - clear (DG)             | 2.71                         | 0.72                               | 0.80                                     |
| Double glazing - low-e<br>coating (DG)  | 1.63                         | 0.28                               | 0.65                                     |
| Triple glazing - Krypton<br>filled (TG) | 0.57                         | 0.23                               | 0.47                                     |

### 4.10.3. Zone Loads

Internal gains for the office room, such as the equipment load, infiltration ratio, and number of occupants, were selected based on ASHRAE (2016) standard recommendations. Equipment loads per area typically range from 2 W/m<sup>2</sup> for just one laptop in the zone to 15 W/m<sup>2</sup> when the office is filled with computers and appliances. In addition, ASHRAE recommends different values of infiltration ratio based on the area of the façade exposed to outdoors, which ranges from 0.0001 (m<sup>3</sup>/s m<sup>2</sup>) to 0.0003 (m<sup>3</sup>/s m<sup>2</sup>) for an average building. The selected infiltration ratio is 0.04 cfm/sf (~0.000203 m<sup>3</sup>/s m<sup>2</sup> façade). Furthermore, the number of occupants per area typically ranges from 0.02 ppl/m<sup>2</sup> for a lightly occupied space



to 0.5 ppl/m<sup>2</sup> for a tightly packed space. The lighting peak internal load was determined at 5.00 W/m<sup>2</sup> in accordance with ASHRAE-90.1 (2016), specifying that LED bulbs were used for each square metre of lighting devices. When daylight exceeds 500 lux, lighting control is activated, and the lights are automatically turned off. The 500 lux is suggested as the optimal threshold for enhancing worker productivity (Tabadkani et al. 2020a). The electric lighting fixtures are controlled through a continuous dimming control, from 0 to 500 lux. When natural daylight decreases, a linear algorithm interpolates steadily to increase the lighting power (EnergyPlus 2013) Figure (4.50).

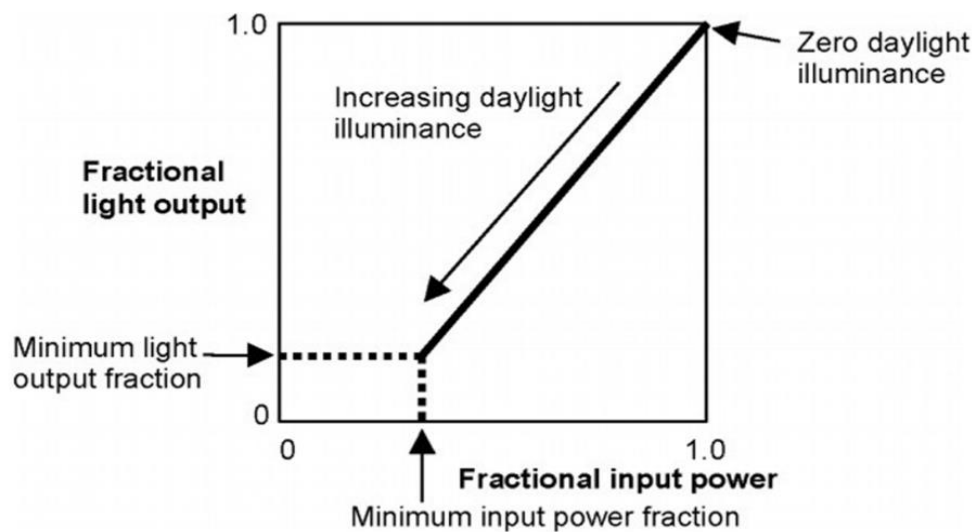


Figure 4.50: Artificial lighting – continuous dimming control (EnergyPlus 2013).

#### 4.10.4. Automatic Control System

AF systems rely heavily on control strategies as their base. They consist of a range of variables that interact with indoor and outdoor conditions, creating a high degree of complexity. As a result, their programming is highly dependent on simulation tools and demands high-level modelling techniques (Attia et al. 2022). Moreover, simulating the adaptive behaviour of a façade is not fully supported by the existing tools, and there is a lack of any well-accepted approach that designers can follow to set a control logic to evaluate the AF shading system in the early stages of the design. However, the automatic control of the shading can be applied only in the case of a conventional shading system, such as Venetian blinds, as it is supported by most BPS tools. Therefore, to overcome these limitations, the study implemented the following steps to control the changing behaviour of the AF: (1) controlling the opening size of the external AF shading system based on outdoor and indoor sensors, (2) translating the SF to transmittance schedule, (3) calculating the incident SR on the exterior surface on an hourly basis, and (4) establishing a control scheme

#### **CHAPTER 4: SYNTHETIC DATABASE GENERATION USING SIMULATION APPROACH**

through an EMS, which is an embedded function in EnergyPlus to define sensors, control, and actuators on hourly time steps (Hong and Lin 2013) Figure (4.51).

According to the literature, an AF shading system is triggered automatically by environmental stimuli, such as SR, relative humidity, surface temperature, etc. Thus, in this study, an automatic control based on different environmental parameters including (C1) incident solar radiation on window ( $W/m^2$ ), (C2) transmitted solar radiation from window ( $W/m^2$ ), (C3) direct solar radiation ( $W/m^2$ ), and (C4) both incident solar radiation ( $W/m^2$ ) and operative temperature (C) have been employed as sensors to adjust the opening ratio of the AF shading system in an automatic way with the integration of either closed (feedback) loop or open loop control mechanisms (Table 4.6). These control parameters were chosen to compare their effects on energy loads to select the most effective control strategy. Several studies (Sadeghi et al. 2016; Bustamante et al. 2017; Yun et al. 2017; Attia et al. 2022) have often used these control parameters; however, as stated by several researchers (Moeseke et al. 2007; Evola et al. 2017; Tabadkani et al. 2020a), the combination of two parameters that is based on outdoors and indoors, provided the best system in terms of energy performance and human comfort.

Control scenario C1) employs solar radiation in the form of outdoor incident vertical solar radiation on the window, while (C2) activates the shading based on the internal window surface, and (C3) uses horizontal direct solar radiation using an open-loop control mechanism. On the other hand, (C4) activates the shading in response to both exterior incident solar radiation on the window and indoor operative temperature through a closed-loop control mechanism. For scenario (C4), the first sensor point (P1) was placed at the corner of the exterior wall to collect the incident solar radiation on the surface, while the second sensor point (P2) was located at the middle of the room at a height of 1.5 m to record the room air temperature.



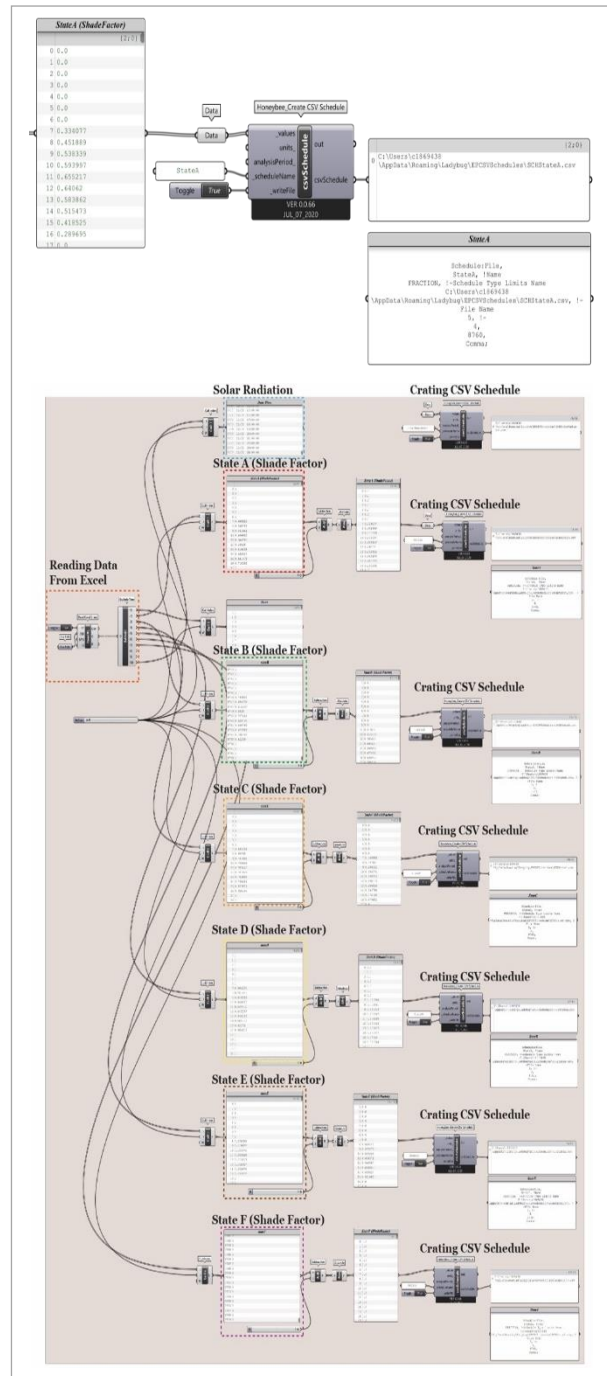
*Figure 4.51: Energy management system (EMS) principles.*

**CHAPTER 4: SYNTHETIC DATABASE GENERATION USING SIMULATION APPROACH**

Table 4.6. Control scenario parameters.

| S  | Parameter  | Location           | Parameter in (EnergyPlus)  | Domain                  |
|----|--|--------------------|--|-------------------------|
| C1 | Incident solar radiation (W/ m2)                               | Outdoor            | Surface Outside Face Incident Solar Radiation per Area                         | 50 – 450 W              |
| C2 | Transmitted solar radiation (W/ m2)                            | Indoor             | Surface Window Transmitted Solar Radiation Rate per Area                       | 50 – 450 W              |
| C3 | Direct solar radiation (W/ m2)                                 | Outdoor            | Site Direct Solar Radiation Rate per Area                                      | 50 – 450 W              |
| C4 | Incident solar radiation (W/ m2) and operative temperature (C) | Indoor and Outdoor | Surface Outside Face Incident Solar Radiation per Area – Operative Temperature | 50 – 450 W<br>21 – 25 C |

Both the hourly shade factor database and hourly solar radiation database that were generated in previous sections were loaded back within the energy simulation workflow using the Read Excel Sheet component in Grasshopper. This component makes it possible to read different columns and rows of the developed data. Then, a schedule of hourly shade factors was created for each of the developed shading states as well as a schedule of hourly solar radiation using the Honeybee Create\_CSV Schedule, which allows users to write a custom .csv schedule in EnergyPlus. These created hourly schedules will be called out based on the defined thresholds in the EMS. Furthermore, the schedules will be formatted based on the EnergyPlus schedule format and connected as additional strings in the Honeybee\_Run Energy Simulation, thus permitting users to write advanced codes, such as the EMS coding control. EnergyPlus processes the SF data under the Group Schedules as an external sub-hourly schedule file (Object – Schedule:File) to assess the energy performance of the building (DOE 2020). Figure (4.52) illustrates the scripting used in Grasshopper to develop the hourly schedule prior to running the energy simulation.



*Figure 4.52: Scripting process to create hourly shading states schedules in grasshopper using Honeybee tool.*

After that, the six developed shading states in both movements that varied in terms of their opening ratio (State-A 100%, State-B 80%, State-C 60%, State-D 40%, State-E 20%, State-F 0%) were selected based on the defined thresholds. The pre-calculated SF from the previous SF analysis were used to generate this algorithmic approach considering daytime hours. During night-time, the shade factor is equal to 1 (representing a 100% shaded area), whereas during working hours, the shading system will comply with the specified thresholds. To prevent overheating during the summer and maximise solar gain during the winter, a

#### **CHAPTER 4: SYNTHETIC DATABASE GENERATION USING SIMULATION APPROACH**

control logic was programmed for the shading system to be closed or open when the defined thresholds exceeded a chosen set point. During winter, shading state A, which is a fully open shading state, was applied to maximise solar gain, while in other seasons, the control logic was applied to be open or closed by checking the environmental thresholds. The SR range varies between 0 W and 450 W with a 50 W step, while the OT ranges from 21 C to 24 C. These thresholds were determined based on some of the previous studies discussed in Chapter 2 section (2.4), which recommended an appropriate activation threshold for each climate zone (Al Touma and Ouahrani 2017; Yun et al. 2017; Tabadkani et al. 2020b).

To apply the control logic, four different scripts with conditional statements were coded within the EMS interface and added to the simulation model to adjust the AF shading based on the defined program logic. Figure (4.53) shows one example of the EMS script that is added within the Ladybug and Honeybee tools. For instance, in the case of (C4), the shading (state A) is fully open when the SR is equal to or below 50 W and the OT is equal to or below 21 C. On the other hand, shading (state F) is fully closed when the SR is equal to or above 450 W, and the OT is higher than 24 C. Other intermediate shading states were considered in between these thresholds. Lastly, the derived transmittance schedule from this stage was used as the input to calculate energy demands.

## CHAPTER 4: SYNTHETIC DATABASE GENERATION USING SIMULATION APPROACH

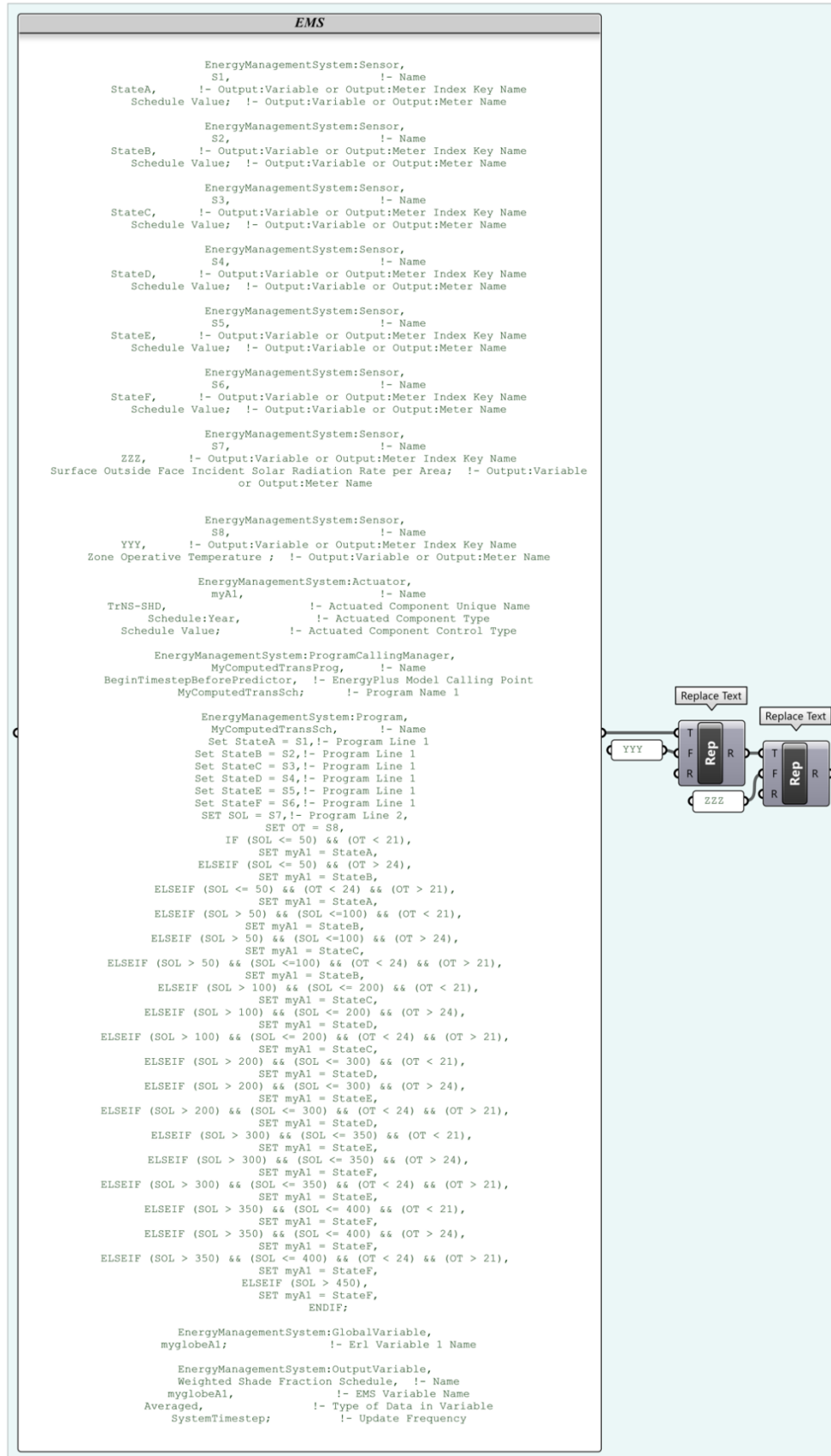


Figure 4.53: EMS conditional (IF, ELSE-IF) statement to control the AF opening ratio based on a predefined threshold.

### **4.10.5. Simulation Challenges**

Different challenges were faced during the simulation process, such as the computational time consumed to perform all design iterations, preparation of the simulation and storage of the output data, and data visualization.

- In terms of time consumption, the study evaluates two different movements of AF based on hourly measurements with the consideration of different variables. In addition, it evaluates the static shading system for comparison with AF performance, calculates the hourly shade factor for all shading states for two developed movements, and calculates hourly incident solar radiation. All of these tasks require the performance of large-scale simulations. It might take minutes to hours to complete only one of these design iterations using a typical PC computer or laptop. Thus, the completion of all simulations could take months, particularly if debugging is required during the modelling process.
- Preparing a large number of simulations and storing their output data is a difficult task. Hence, early decisions about file arrangement and unique names had to be made to manage large numbers of files, which required a local hard drive. However, dealing with a large number of files and their size could present additional difficulties.
- It is highly challenging to visualise the entire dataset in a feasible manner due to the massive volume of data, especially when modelling the shading system on an hourly basis.

Two main solutions were considered to address the above constraints and make the simulation possible:

- In terms of simulation time, simulations of this scale require a high degree of computational power that is beyond the capabilities of regular computers. Therefore, the Paperspace web-based platform (<https://www.paperspace.com>) was used to customise a number of cloud-based machines in addition to a powerful machine. The following hardware specifications applied to each machine: Quadro P5000, 8 CPU, 30GBRAM, 50GB SSD (Internal Storage), 100GB SSD (External Storage), and dedicated GPU.
- Parametric design tools were utilised; these allow for a high number of simulation iterations to be performed, as well as the management of design variations. As an algorithmic platform, the combination of the Rhino and Grasshopper programmes enables designers to connect parametric modelling with design variables and

## CHAPTER 4: SYNTHETIC DATABASE GENERATION USING SIMULATION APPROACH

connect various plugins, such as the Honeybee and Ladybug environmental analysis tools that were linked to EnergyPlus and Radiance. This is in addition to the possibility of integrating the data organisation and storage in the desired manner.

### 4.10.6. Simulation Matrices

Based on the dynamic input parameters discussed in section (4.10.1), the simulation matrix for all studied prototypes, their inputs, and the number of iterations was defined as shown in Tables (4.7), (4.8), and (4,9). Each combination was named with unique abbreviations that represent each input.

For example, combination case (P-AF-SCM-C4\_Or\_B00Low\_B01Low\_FLLow\_ExtW2\_Glaz3) refers to a particular case for an AF with control scenario C4. The first letter refers to the prototype (P), the second letter (C) represents the control scenario used, (Or) refers to the office room orientation, (B00) and (B01), refer to building context height, (FL) refers to the façade level height, (ExtW) refers to the exterior wall type U-value used, and lastly, (Glaz) refers to the glazing type U-value used. These unique abbreviations/names were made to manage large numbers of files and for results analysis.

Table 4.7. Dynamic simulation matrix for base case model.

| Prototype (P)                     | Orientation (Or.) | Building Context |        | Façade Level (FL) | Exterior wall U-Value (ExtW) | Glazing Type U-Value (Glaz) | No. of Iterations |
|-----------------------------------|-------------------|------------------|--------|-------------------|------------------------------|-----------------------------|-------------------|
|                                   |                   | B00              | B01    |                   |                              |                             |                   |
| Base Case (Base-M)                | South (0)         | Low              | Low    | Low               | Type 0 (3.69)                | SG 0 (5.82)                 | 324               |
|                                   |                   | Medium           | Medium | Medium            | Type 1 (0.98)                | DG 1 (2.71)                 |                   |
|                                   |                   | High             | High   | High              | Type 2 (0.57)                | DG 2 (1.63)                 |                   |
|                                   |                   |                  |        |                   |                              |                             |                   |
|                                   | West (1)          | Low              | Low    | Low               | Type 0 (3.69)                | SG 0 (5.82)                 | 324               |
|                                   |                   | Medium           | Medium | Medium            | Type 1 (0.98)                | DG 1 (2.71)                 |                   |
|                                   |                   | High             | High   | High              | Type 2 (0.57)                | DG 2 (1.63)                 |                   |
|                                   |                   |                  |        |                   |                              |                             |                   |
|                                   | North (2)         | Low              | Low    | Low               | Type 0 (3.69)                | SG 0 (5.82)                 | 324               |
|                                   |                   | Medium           | Medium | Medium            | Type 1 (0.98)                | DG 1 (2.71)                 |                   |
|                                   |                   | High             | High   | High              | Type 2 (0.57)                | DG 2 (1.63)                 |                   |
|                                   |                   |                  |        |                   |                              |                             |                   |
|                                   | East (3)          | Low              | Low    | Low               | Type 0 (3.69)                | SG 0 (5.82)                 | 324               |
|                                   |                   | Medium           | Medium | Medium            | Type 1 (0.98)                | DG 1 (2.71)                 |                   |
|                                   |                   | High             | High   | High              | Type 2 (0.57)                | DG 2 (1.63)                 |                   |
|                                   |                   |                  |        |                   |                              |                             |                   |
| <b>Total Number of Iterations</b> |                   |                  |        |                   |                              |                             | <b>1296</b>       |



**CHAPTER 4: SYNTHETIC DATABASE GENERATION USING SIMULATION APPROACH**

Table 4.8. Dynamic simulation matrix for fixed shading system.

| Prototype (P)                     | Orientation (Or.) | Building Context |        | Façade Level (FL) | Exterior wall U-Value (ExtW) | Glazing Type U-Value (Glaz) | No. of Iterations |
|-----------------------------------|-------------------|------------------|--------|-------------------|------------------------------|-----------------------------|-------------------|
|                                   |                   | B00              | B01    |                   |                              |                             |                   |
| Fixed Shading Vertical (FS-V)     | South (0)         | Low              | Low    | Low               | Type 0 (3.69)                | SG 0 (5.82)                 | 324               |
|                                   |                   | Medium           | Medium | Medium            | Type 1 (0.98)                | DG 1 (2.71)                 |                   |
|                                   |                   | High             | High   | High              | Type 2 (0.57)                | DG 2 (1.63)                 |                   |
|                                   |                   |                  |        |                   |                              |                             |                   |
|                                   | West (1)          | Low              | Low    | Low               | Type 0 (3.69)                | SG 0 (5.82)                 | 324               |
|                                   |                   | Medium           | Medium | Medium            | Type 1 (0.98)                | DG 1 (2.71)                 |                   |
|                                   |                   | High             | High   | High              | Type 2 (0.57)                | DG 2 (1.63)                 |                   |
|                                   |                   |                  |        |                   |                              |                             |                   |
|                                   | North (2)         | Low              | Low    | Low               | Type 0 (3.69)                | SG 0 (5.82)                 | 324               |
|                                   |                   | Medium           | Medium | Medium            | Type 1 (0.98)                | DG 1 (2.71)                 |                   |
|                                   |                   | High             | High   | High              | Type 2 (0.57)                | DG 2 (1.63)                 |                   |
|                                   |                   |                  |        |                   |                              |                             |                   |
| East (3)                          | Low               | Low              | Low    | Type 0 (3.69)     | SG 0 (5.82)                  | 324                         |                   |
|                                   | Medium            | Medium           | Medium | Type 1 (0.98)     | DG 1 (2.71)                  |                             |                   |
|                                   | High              | High             | High   | Type 2 (0.57)     | DG 2 (1.63)                  |                             |                   |
|                                   |                   |                  |        |                   |                              |                             | TG 3 (0.57)       |
| Fixed Shading Horizontal (FS-H)   | South (0)         | Low              | Low    | Low               | Type 0 (3.69)                | SG 0 (5.82)                 | 324               |
|                                   |                   | Medium           | Medium | Medium            | Type 1 (0.98)                | DG 1 (2.71)                 |                   |
|                                   |                   | High             | High   | High              | Type 2 (0.57)                | DG 2 (1.63)                 |                   |
|                                   |                   |                  |        |                   |                              |                             |                   |
|                                   | West (1)          | Low              | Low    | Low               | Type 0 (3.69)                | SG 0 (5.82)                 | 324               |
|                                   |                   | Medium           | Medium | Medium            | Type 1 (0.98)                | DG 1 (2.71)                 |                   |
|                                   |                   | High             | High   | High              | Type 2 (0.57)                | DG 2 (1.63)                 |                   |
|                                   |                   |                  |        |                   |                              |                             |                   |
|                                   | North (2)         | Low              | Low    | Low               | Type 0 (3.69)                | SG 0 (5.82)                 | 324               |
|                                   |                   | Medium           | Medium | Medium            | Type 1 (0.98)                | DG 1 (2.71)                 |                   |
|                                   |                   | High             | High   | High              | Type 2 (0.57)                | DG 2 (1.63)                 |                   |
|                                   |                   |                  |        |                   |                              |                             |                   |
| East (3)                          | Low               | Low              | Low    | Type 0 (3.69)     | SG 0 (5.82)                  | 324                         |                   |
|                                   | Medium            | Medium           | Medium | Type 1 (0.98)     | DG 1 (2.71)                  |                             |                   |
|                                   | High              | High             | High   | Type 2 (0.57)     | DG 2 (1.63)                  |                             |                   |
|                                   |                   |                  |        |                   |                              |                             | TG 3 (0.57)       |
| <b>Total Number of Iterations</b> |                   |                  |        |                   |                              |                             | <b>2592</b>       |

Table 4.9. Dynamic simulation matrix for adaptive façade shading system.

| Prototype (P)                | Or.       | Building Context |        | Façade Level (FL) | Exterior wall U-Value (ExtW) | Glazing Type U-Value (Glaz) | Automatic Control (C) | No. of Iterations |
|------------------------------|-----------|------------------|--------|-------------------|------------------------------|-----------------------------|-----------------------|-------------------|
|                              |           | B00              | B01    |                   |                              |                             |                       |                   |
| AF Scaling Movement (AF-SCM) | South (0) | Low              | Low    | Low               | Type 0 (3.69)                | SG 0 (5.82)                 | Control (C1)          | 1,296             |
|                              |           | Medium           | Medium | Medium            | Type 1 (0.98)                | DG 1 (2.71)                 | Control (C2)          |                   |
|                              |           | High             | High   | High              | Type 2 (0.57)                | DG 2 (1.63)                 | Control (C3)          |                   |
|                              |           |                  |        |                   |                              |                             | TG 3 (0.57)           |                   |
|                              | West (1)  | Low              | Low    | Low               | Type 0 (3.69)                | SG 0 (5.82)                 | Control (C1)          | 1,296             |
|                              |           | Medium           | Medium | Medium            | Type 1 (0.98)                | DG 1 (2.71)                 | Control (C2)          |                   |
|                              |           | High             | High   | High              | Type 2 (0.57)                | DG 2 (1.63)                 | Control (C3)          |                   |
|                              |           |                  |        |                   |                              |                             | TG 3 (0.57)           |                   |

**CHAPTER 4: SYNTHETIC DATABASE GENERATION USING SIMULATION APPROACH**

| Prototype (P)                | Or.                               | Building Context |        | Façade Level (FL) | Exterior wall U-Value (ExtW) | Glazing Type U-Value (Glaz) | Automatic Control (C) | No. of Iterations |              |
|------------------------------|-----------------------------------|------------------|--------|-------------------|------------------------------|-----------------------------|-----------------------|-------------------|--------------|
|                              |                                   | B00              | B01    |                   |                              |                             |                       |                   |              |
|                              | North (2)                         | Low              | Low    | Low               | Type 0 (3.69)                | SG 0 (5.82)                 | Control (C1)          | 1,296             |              |
|                              |                                   | Medium           | Medium | Medium            | Type 1 (0.98)                | DG 1 (2.71)                 | Control (C2)          |                   |              |
|                              |                                   | High             | High   | High              | Type 2 (0.57)                | DG 2 (1.63)                 | Control (C3)          |                   |              |
|                              |                                   |                  |        |                   |                              | TG 3 (0.57)                 | Control (C4)          |                   |              |
|                              | East (3)                          | Low              | Low    | Low               | Type 0 (3.69)                | SG 0 (5.82)                 | Control (C1)          | 1,296             |              |
|                              |                                   | Medium           | Medium | Medium            | Type 1 (0.98)                | DG 1 (2.71)                 | Control (C2)          |                   |              |
|                              |                                   | High             | High   | High              | Type 2 (0.57)                | DG 2 (1.63)                 | Control (C3)          |                   |              |
|                              |                                   |                  |        |                   |                              | TG 3 (0.57)                 | Control (C4)          |                   |              |
| AF Folding Movement (AF-FOM) | South (0)                         | Low              | Low    | Low               | Type 0 (3.69)                | SG 0 (5.82)                 | Control (C4)          | 324               |              |
|                              |                                   | Medium           | Medium | Medium            | Type 1 (0.98)                | DG 1 (2.71)                 |                       |                   |              |
|                              |                                   | High             | High   | High              | Type 2 (0.57)                | DG 2 (1.63)                 |                       |                   |              |
|                              |                                   |                  |        |                   |                              | TG 3 (0.57)                 |                       |                   |              |
|                              | West (1)                          | Low              | Low    | Low               | Type 0 (3.69)                | SG 0 (5.82)                 | Control (C4)          | 324               |              |
|                              |                                   | Medium           | Medium | Medium            | Type 1 (0.98)                | DG 1 (2.71)                 |                       |                   |              |
|                              |                                   | High             | High   | High              | Type 2 (0.57)                | DG 2 (1.63)                 |                       |                   |              |
|                              |                                   |                  |        |                   |                              | TG 3 (0.57)                 |                       |                   |              |
|                              | North (2)                         | Low              | Low    | Low               | Type 0 (3.69)                | SG 0 (5.82)                 | Control (C4)          | 324               |              |
|                              |                                   | Medium           | Medium | Medium            | Type 1 (0.98)                | DG 1 (2.71)                 |                       |                   |              |
|                              |                                   | High             | High   | High              | Type 2 (0.57)                | DG 2 (1.63)                 |                       |                   |              |
|                              |                                   |                  |        |                   |                              | TG 3 (0.57)                 |                       |                   |              |
|                              | East (3)                          | Low              | Low    | Low               | Type 0 (3.69)                | SG 0 (5.82)                 | Control (C4)          | 324               |              |
|                              |                                   | Medium           | Medium | Medium            | Type 1 (0.98)                | DG 1 (2.71)                 |                       |                   |              |
|                              |                                   | High             | High   | High              | Type 2 (0.57)                | DG 2 (1.63)                 |                       |                   |              |
|                              |                                   |                  |        |                   |                              | TG 3 (0.57)                 |                       |                   |              |
|                              | <b>Total Number of Iterations</b> |                  |        |                   |                              |                             |                       |                   | <b>6,480</b> |

**4.10.7. Energy Simulation Database**

Figure (4.54) shows a sample of the generated energy data, which vary based on each design solution. In addition, Figure (4.55) and (4.56) shows a sample of some cases for specific days of the year (21 March, 21 June, 21 September, and 21 December), with the selection of three different hours of the day (9.00 am, 12.00 pm, and 15.00 pm), according to the

#### **CHAPTER 4: SYNTHETIC DATABASE GENERATION USING SIMULATION APPROACH**

defined automatic control system. Once all simulation settings were defined, and the fixed and dynamic inputs and the automatic control settings were selected, energy simulation could be run using the Honeybee\_Run Energy Simulation component, which was linked to EnergyPlus to calculate the hourly cooling loads. This process was conducted iteratively using the Colibri iterator component in Grasshopper to generate all design iterations from the dynamic input's sliders. For example, the database of the two movements of AF shading systems was stored in Excel as follows: date (hour, day, and month), orientation, building context 00, building context 01, building context 03, building context 04, façade level height, glazing type - U-value, exterior wall - U-value, AF shading states, AF transmittance values, AF shade factor, environmental parameters (C1, C2, C3 and C4), out: hourly cooling loads - KW/m<sup>2</sup>, out: hourly heating loads - KW/m<sup>2</sup>, out: hourly lighting loads - KW/m<sup>2</sup>, out: hourly equipment loads - KW/m<sup>2</sup>, out: total cooling loads - KW/m<sup>2</sup>, out: total heating loads - KW/m<sup>2</sup>, out: total lighting loads - KW/m<sup>2</sup>, out: total equipment loads - KW/m<sup>2</sup>, out: annual energy use intensity - KW/m<sup>2</sup>, and out: solar heat gain - KW/m<sup>2</sup>. On the other hand, the database of the base case and the fixed shading systems was stored in a similar order excluding the variable inputs associated with the AF shading system. A sample of the energy simulation database is shown in (Appendix D).

**CHAPTER 4: SYNTHETIC DATABASE GENERATION USING SIMULATION APPROACH**

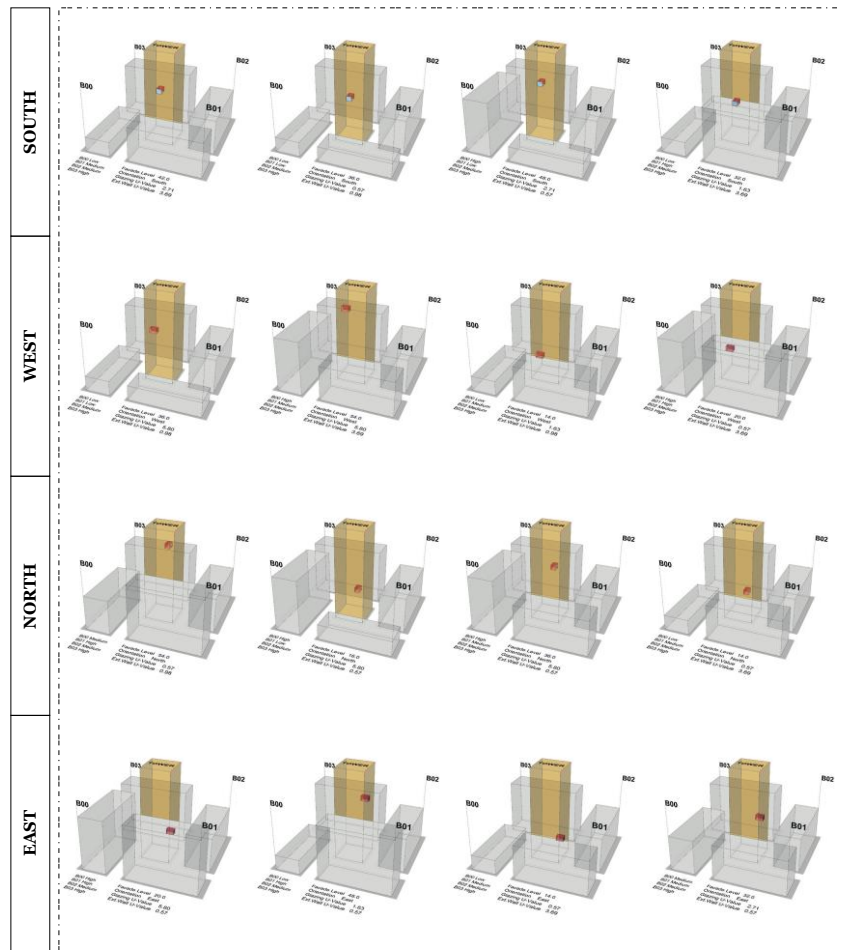


Figure 4.54: Sample of the generated energy data, which vary based on each design solution.

**CHAPTER 4: SYNTHETIC DATABASE GENERATION USING SIMULATION APPROACH**

| Case Location | O.           | Date                  | 9.00 AM                                   | 12.00 PM                                  | 15.00 PM                                  |                       |        |
|---------------|--------------|-----------------------|---|---|---|-----------------------|--------|
|               | <b>SOUTH</b> | <b>21-March</b>       | <br>Shading State B<br>Opening Ratio 80%  | <br>Shading State C<br>Opening Ratio 80%  | <br>Shading State B<br>Opening Ratio 80%  |                       |        |
|               |              | Shading State         | B   | Shading State                             | C   | Shading State         | B      |
|               |              | Solar Radiation       | 61.79                                     | Solar Radiation                           | 116.08                                    | Solar Radiation       | 82.07  |
|               |              | Operative Temperature | 21.03                                     | Operative Temperature                     | 23.58                                     | Operative Temperature | 24.4   |
|               |              | <b>21-June</b>        | <br>Shading State A<br>Opening Ratio 100% | <br>Shading State A<br>Opening Ratio 100% | <br>Shading State A<br>Opening Ratio 100% |                       |        |
|               |              | Shading State         | A   | Shading State                             | A   | Shading State         | A      |
|               |              | Solar Radiation       | 31.67                                     | Solar Radiation                           | 30.04                                     | Solar Radiation       | 25.57  |
|               |              | Operative Temperature | 25.3                                      | Operative Temperature                     | 26.14                                     | Operative Temperature | 26.89  |
|               |              | <b>21-September</b>   | <br>Shading State C<br>Opening Ratio 80%  | <br>Shading State D<br>Opening Ratio 80%  | <br>Shading State A<br>Opening Ratio 100% |                       |        |
|               |              | Shading State         | C   | Shading State                             | D   | Shading State         | A      |
|               |              | Solar Radiation       | 124.24                                    | Solar Radiation                           | 263.05                                    | Solar Radiation       | 142.98 |
|               |              | Operative Temperature | 25.31                                     | Operative Temperature                     | 27.17                                     | Operative Temperature | 27.73  |
|               |              | <b>21-December</b>    | <br>Shading State A<br>Opening Ratio 100% | <br>Shading State C<br>Opening Ratio 80%  | <br>Shading State A<br>Opening Ratio 100% |                       |        |
|               |              | Shading State         | A   | Shading State                             | C   | Shading State         | A      |
|               |              | Solar Radiation       | 23.03                                     | Solar Radiation                           | 135.66                                    | Solar Radiation       | 32.75  |
|               |              | Operative Temperature | 19.24                                     | Operative Temperature                     | 20.29                                     | Operative Temperature | 19.61  |

Figure 4.55: Sample of cases for hourly shading states in three selected hours (9:00 am, 12:00 pm, 15:00 pm).

**CHAPTER 4: SYNTHETIC DATABASE GENERATION USING SIMULATION APPROACH**

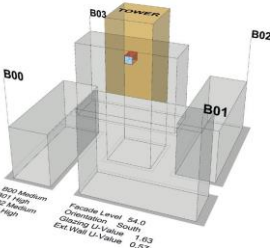
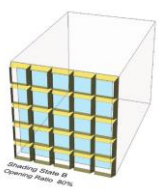
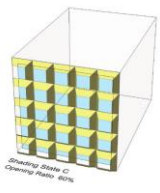
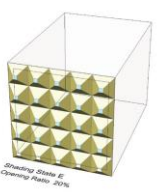
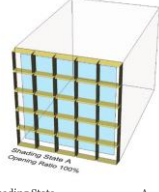
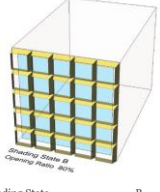
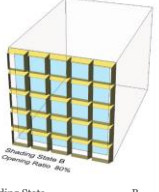
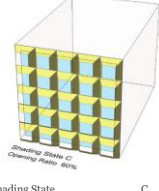
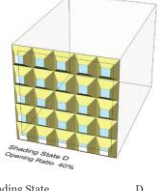
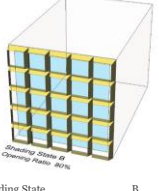
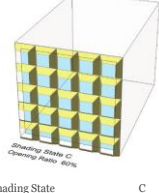
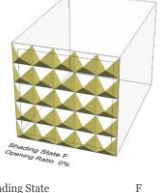
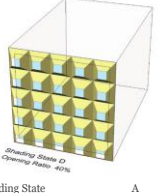
| Case Location   | O.           | Date                  | 9.00 AM   | 12.00 PM  | 15.00 PM  |                       |        |
|---|--------------|-----------------------|---|---|---|-----------------------|--------|
|  <p>                     B00 Medium<br/>                     827 High<br/>                     822 Medium<br/>                     853 High<br/>                     Facade Level: 54.0<br/>                     Orientation: South<br/>                     Glazing (U-Value): 1.63<br/>                     Ext. Wall U-Value: 0.57                 </p> | <b>SOUTH</b> | <b>21-March</b>       |  <p>Shading State D<br/>Opening Ratio: 80%</p>   |  <p>Shading State C<br/>Opening Ratio: 80%</p>  |  <p>Shading State E<br/>Opening Ratio: 80%</p>   |                       |        |
|   |              | Shading State         | B   | Shading State   | C   | Shading State         | E      |
|   |              | Solar Radiation       | 87.34   | Solar Radiation   | 109.49  | Solar Radiation       | 274.78 |
|   |              | Operative Temperature | 20.56   | Operative Temperature   | 21.92   | Operative Temperature | 25.78  |
|   |              | <b>21-June</b>        |  <p>Shading State A<br/>Opening Ratio: 100%</p>  |  <p>Shading State B<br/>Opening Ratio: 80%</p>  |  <p>Shading State B<br/>Opening Ratio: 80%</p>   |                       |        |
|   |              | Shading State         | A   | Shading State   | B   | Shading State         | B      |
|   |              | Solar Radiation       | 41.64   | Solar Radiation   | 94.37   | Solar Radiation       | 86.44  |
|   |              | Operative Temperature | 25.63   | Operative Temperature   | 20.96   | Operative Temperature | 21.82  |
|   |              | <b>21-September</b>   |  <p>Shading State C<br/>Opening Ratio: 80%</p>   |  <p>Shading State D<br/>Opening Ratio: 40%</p>  |  <p>Shading State B<br/>Opening Ratio: 80%</p>   |                       |        |
|   |              | Shading State         | C   | Shading State   | D   | Shading State         | B      |
|   |              | Solar Radiation       | 124.24  | Solar Radiation   | 204.31  | Solar Radiation       | 135.58 |
|   |              | Operative Temperature | 25.31   | Operative Temperature   | 26.70   | Operative Temperature | 27.18  |
|   |              | <b>21-December</b>    |  <p>Shading State C<br/>Opening Ratio: 80%</p> |  <p>Shading State F<br/>Opening Ratio: 0%</p> |  <p>Shading State D<br/>Opening Ratio: 80%</p> |                       |        |
|   |              | Shading State         | C   | Shading State   | F   | Shading State         | A      |
|   |              | Solar Radiation       | 145.91  | Solar Radiation   | 386.76  | Solar Radiation       | 135.66 |
|   |              | Operative Temperature | 19.20   | Operative Temperature   | 23.16   | Operative Temperature | 23.80  |

Figure 4.56: Sample of cases for hourly shading states in three selected hours (9:00 am, 12:00 pm, 15:00 pm).

### **4.11. Chapter Summary**

This chapter presents the analysis of the studied high rise office cases to inform the modelling stage. Then, a generative parametric office tower and its urban context were designed and simulated in a generative way to create the synthetic database. It also presents the algorithmic framework that linked between different plugins within grasshopper tool to simulate the energy performance of AF shading system in the office tower. Moreover, it details the automatic control system used to evaluate AF based on an hourly time basis. This chapter concludes by presenting the created databases for different shading systems, including the solar radiation (KWh/m<sup>2</sup>) database, the shade factor (SF) database, and the energy (cooling loads) (KW) database.

## **CHAPTER FIVE**

### **SIMULATION RESULTS**



## **CHAPTER 5: SIMULATION RESULTS**

### **5.1. Introduction**

This chapter presents the results of the simulation described in the previous chapter. The analysis of the simulation results initially evaluated the engineering parameters in terms of cooling loads and solar heat gain prior to conducting external shading simulations. Then, a comparison was made between different fixed and adaptive shading systems and the differences in cooling load reductions and solar heat gain reductions were analysed. Moreover, different control scenarios of AFs were analysed in terms of cooling and lighting loads in relation to different parameters. Lastly, the most effective control scenario was further evaluated in greater detail in terms of cooling loads, shading states, and hourly variations, in relation to different parameters, such as building orientation and urban context. Due to the massive volume of generated data, a web-based data visualization tool (Design Explorer) was used for visualisation and analysis.

### **5.2. Evaluation based on Engineering Parameters**

The study examined different building envelope parameters, such as exterior wall and glazing types, with different values in a parametric evaluation, as these parameters have an impact on the cooling energy loads of the building. A total of 1,296 sets of simulations were conducted, which represents the building envelope combination of three wall types and four glazing types with other parameters, such as orientation, building context, and vertical location of the office. This analysis focuses on the building envelope prior to implementing the shading system to understand the most influential parameter affecting the cooling loads. The results were expressed using the annual cooling loads per square metre of floor area output metric (kWh/m<sup>2</sup>).

The results of the simulation were presented in accordance with the orientation of the four examined offices in terms of annual cooling demands and in relation to solar gain. The entire set of simulation data is visualised in a web-based comparison website, as visualisation of the entire dataset cannot be presented in a feasible manner. The 48 cases presented in this section are based on only one fixed urban context setting (B00: Low, B01: Low, B02: Medium, B03: High), and for an office room that is located on the second floor of the office tower.

Figure (5.1) compares the annual cooling loads per square meter for 48 combinations of building envelope parameters (exterior wall and glazing type) for the main orientations

## **CHAPTER 5: SIMULATION RESULTS**

(south, west, north, and east). Based on this analysis, the results revealed that the case of the combination (P-Base-M\_ExtW2\_Glaz3) performed the best in terms of cooling loads and solar heat gain in all tested orientations. The cooling loads results achieved based on orientation are as follows: south: 92.52 kWh/m<sup>2</sup>/year, west: 97.23 kWh/m<sup>2</sup>/year, north: 74.34 kWh/m<sup>2</sup>/year, and east: 80.70 kWh/m<sup>2</sup>/year. This is to be expected, given that the glazing type in this case has a lower solar heat gain coefficient value with low U-value and is combined with higher insulation exterior wall composition, thus contributing to a higher performance outcome. On the other hand, the poor exterior wall insulation, which has a higher U-value of 3.6 with a higher solar heat gain coefficient value of 0.82 in the single glazing type of 5.8 U-value and is highlighted in red (P-Base-M\_ExtW0\_Glaz0), performed the worst in all orientations and combinations of the examined 48 cases. This is because the U-value of the exterior wall is quite high, and a high value of shading coefficient was chosen for the glazing system. Moreover, the findings show that west orientations performed worst across all scenarios since they were subjected to the most solar radiation.

Furthermore, the results were analysed with regard to solar heat gains, as the purpose of this section was to determine which engineering parameter had the most impact on the cooling loads of the tower building envelope. Comparing the results of the various orientations for each combination revealed similar patterns in each zone. The south and west rooms scored the worst in the evaluation. Figure (5.2) shows that in the case of (P-Base-M\_ExtW0\_Glaz0), solar gain is the highest due to the use of glazing with a shading coefficient value that permits a greater solar gain into the zone. This resulted in higher cooling loads together with the lack of any thermal insulation in the opaque wall. In contrast, solar gain is reduced in the cases (P-Base-M\_ExtW0\_Glaz3, P-Base-M\_ExtW1\_Glaz3, and P-Base-M\_ExtW2\_Glaz3), which have a lower shading coefficient value of 0.23. Therefore, altering the shading coefficient value of the glazing components can have a significant impact on solar gains. In the cases discussed above, the low SHGC value reduced solar heat gain by up to 72% compared to the worst-case scenario (P-Base-M\_ExtW0\_Glaz0) as presented in Figure (5.2).

In general, as can be seen in Table (5.1), there is a 56% difference between the optimal combination (P-Base-M\_ExtW2\_Glaz3) and the worst combination (P-Base-M\_ExtW0\_Glaz0). This highlights the significant influence that the parameters of the building envelope can have in terms of energy performance.

**CHAPTER 5: SIMULATION RESULTS**

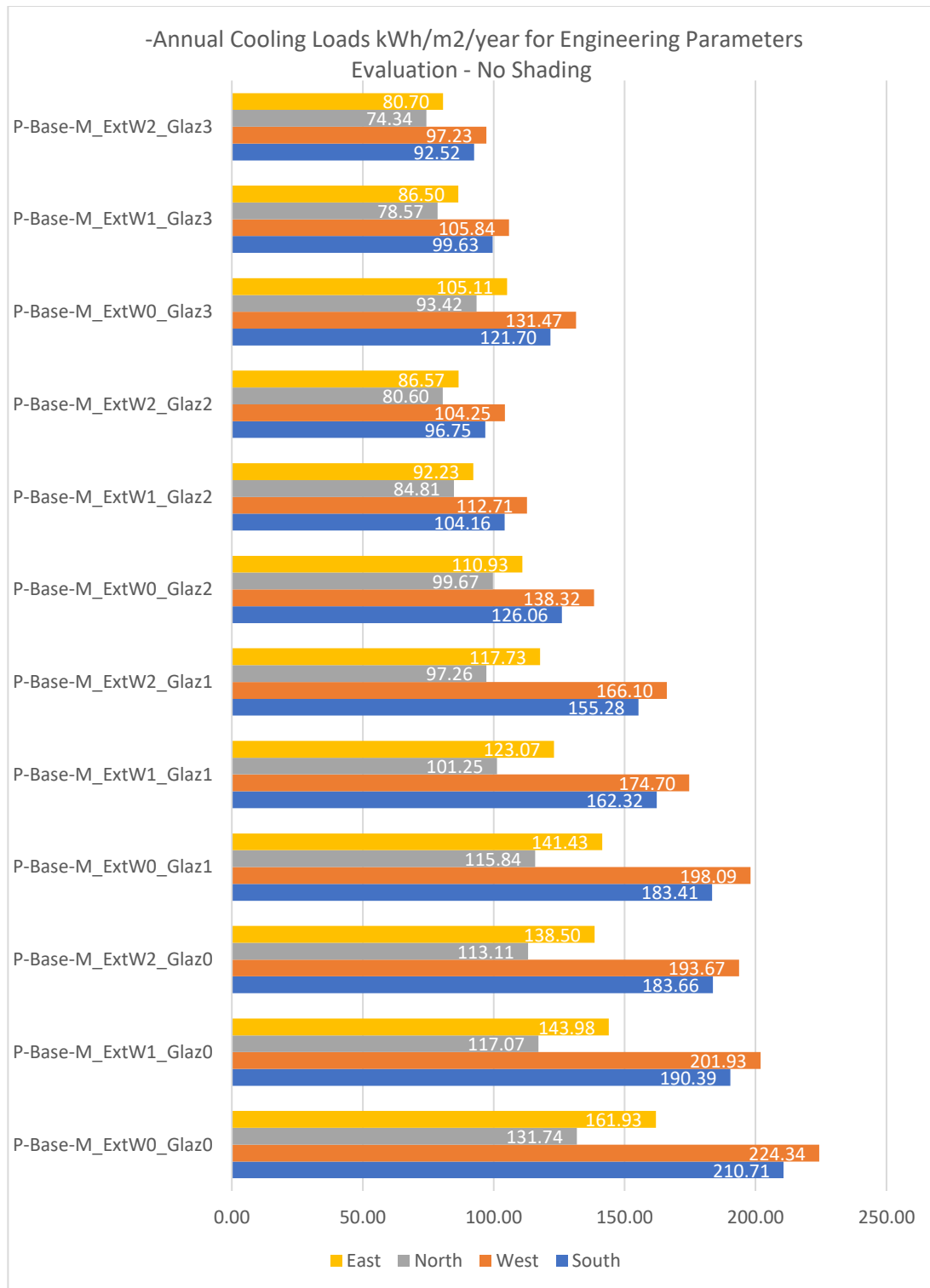


Figure 5.1: Simulation results of engineering parameters in terms of cooling loads within different orientations.

**CHAPTER 5: SIMULATION RESULTS**

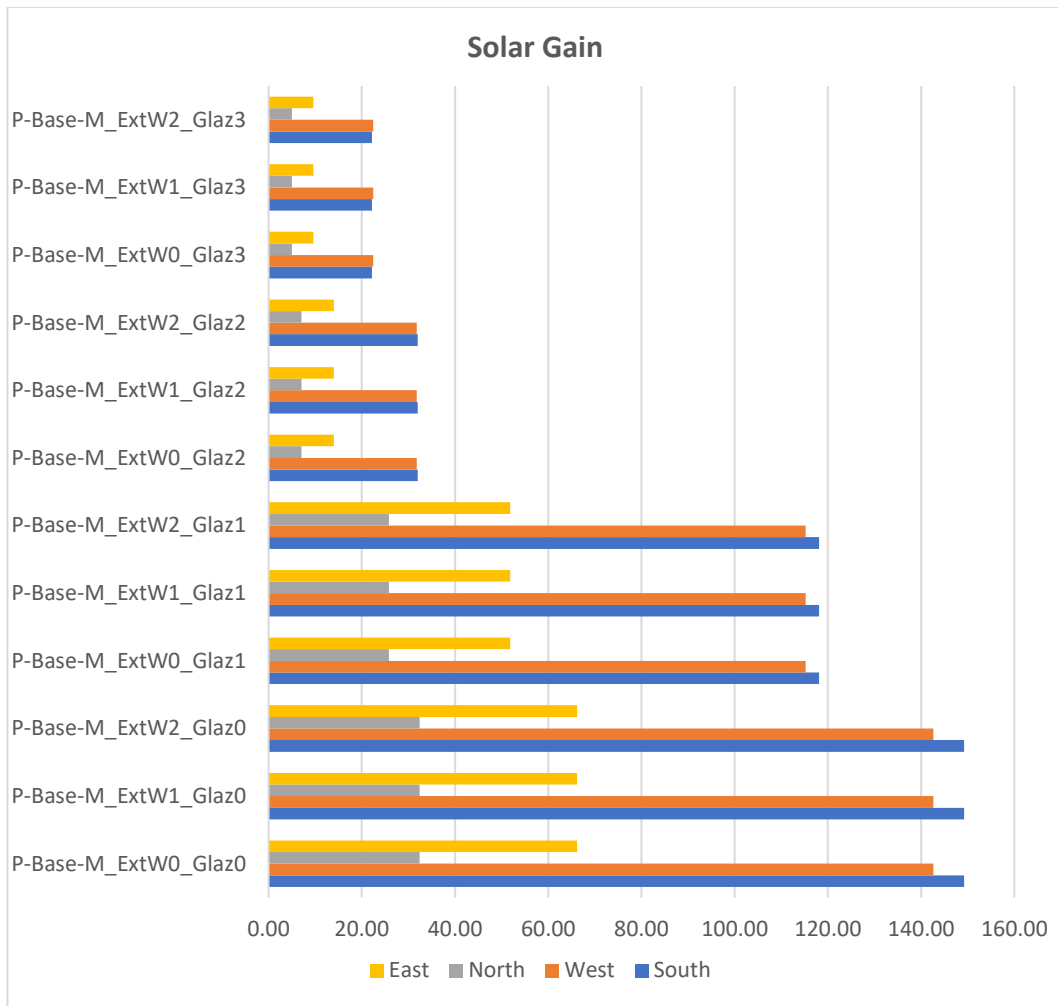


Figure 5.2: Solar heat gain results for 48 cases.

Table 5.1. The simulation results for cooling loads, the orange row representing the optimal-case scenario and the yellow row representing the worst-case scenario.

|                      | South  | West   | North  | East   |
|----------------------|--------|--------|--------|--------|
| P-Base-M_ExtW0_Glaz0 | 210.71 | 224.34 | 131.74 | 161.93 |
| P-Base-M_ExtW1_Glaz0 | 190.39 | 201.93 | 117.07 | 143.98 |
| P-Base-M_ExtW2_Glaz0 | 183.66 | 193.67 | 113.11 | 138.50 |
| P-Base-M_ExtW0_Glaz1 | 183.41 | 198.09 | 115.84 | 141.43 |
| P-Base-M_ExtW1_Glaz1 | 162.32 | 174.70 | 101.25 | 123.07 |
| P-Base-M_ExtW2_Glaz1 | 155.28 | 166.10 | 97.26  | 117.73 |
| P-Base-M_ExtW0_Glaz2 | 126.06 | 138.32 | 99.67  | 110.93 |
| P-Base-M_ExtW1_Glaz2 | 104.16 | 112.71 | 84.81  | 92.23  |
| P-Base-M_ExtW2_Glaz2 | 96.75  | 104.25 | 80.60  | 86.57  |
| P-Base-M_ExtW0_Glaz3 | 121.70 | 131.47 | 93.42  | 105.11 |
| P-Base-M_ExtW1_Glaz3 | 99.63  | 105.84 | 78.57  | 86.50  |
| P-Base-M_ExtW2_Glaz3 | 92.52  | 97.23  | 74.34  | 80.70  |

### **5.3. Evaluation based on Shading System Type**

In hot climate zones, where the air temperature is high and there is a great deal of solar radiation, the shading coefficient of the glazing system plays a crucial role in reducing cooling energy requirements in relation to solar gain, as shown on previous simulations that incorporated engineering parameters. This suggests that solar heat gain can be reduced by decreasing the shade coefficient. These findings indicate that developing shading elements may have a significant impact on cooling energy loads, and that relying on a prescriptive approach by modifying the engineering parameter values for the building envelope may not achieve the required reductions in solar gains, given that solar gains are the most important factor in cooling loads.

In this analysis, a comparison of fixed and adaptive shading systems was carried out, and their performance was evaluated in terms of cooling loads in relation to solar heat gain. The purpose of this analysis and evaluation was to determine the extent to which external shading can contribute to energy efficiency in high-rise office buildings in regions with hot climates. The simulation of all previous cases presented in section (5.2), which is (1,296) design iterations with no shading system, was simulated again after implementing each shading system. Different fixed and adaptive external shading systems were simulated, such as fixed vertical shading, fixed horizontal shading, AF with scaling movement, and AF with folding movement, and the results were analysed according to the annual energy cooling requirements. The same 48 cases presented in section (5.2) were used for shading system analysis, and the entire dataset is presented in a web page analysis.

In general, the integration of different shading devices, whether fixed or adaptive, further improved the performance of all glazing types by decreasing the incident solar radiation values on the window. However, the greater reduction of cooling was achieved by both scaling and folding AF systems compared to fixed shading as shown in Figure (5.3). The case presented in Figure (5.3) is the combination case (ExtW2\_Glaz3), which is the best performing case in terms of values of engineering parameters. The results in Figure (5.3) revealed that both the scaling and the folding movements consume almost the same amount of cooling energy. Thus, the folding shading system will not be studied in any more depth in the next analysis.

Figure (5.4) shows that AFs with scaling and folding movements for the combination case (ExtW2\_Glaz3), produced the best performance in terms of cooling load reduction in all studied orientations (south, west, north, and east) with a reduction of 30.5%, 32.2%, 21.5%, and 22.3% respectively, compared with the base cases. Moreover, solar heat gain was also

**CHAPTER 5: SIMULATION RESULTS**

reduced for all orientations compared to base model. On the other hand, in the case of the fixed vertical shading system, the cooling loads were reduced by varying amounts (south: 12.6%, west: 9.7%, north: 9.5%, and east: 9.1%) compared to the base case.

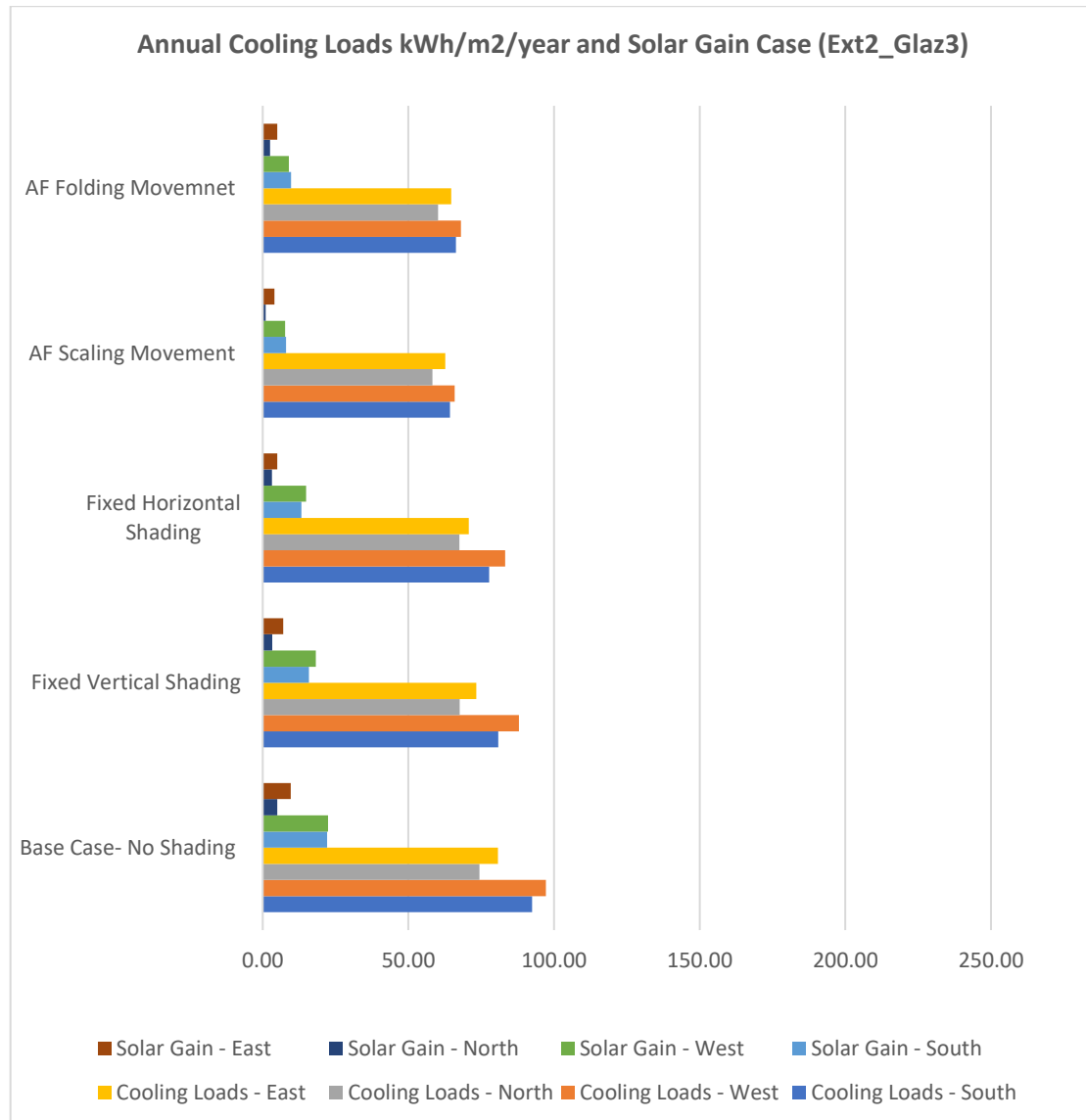
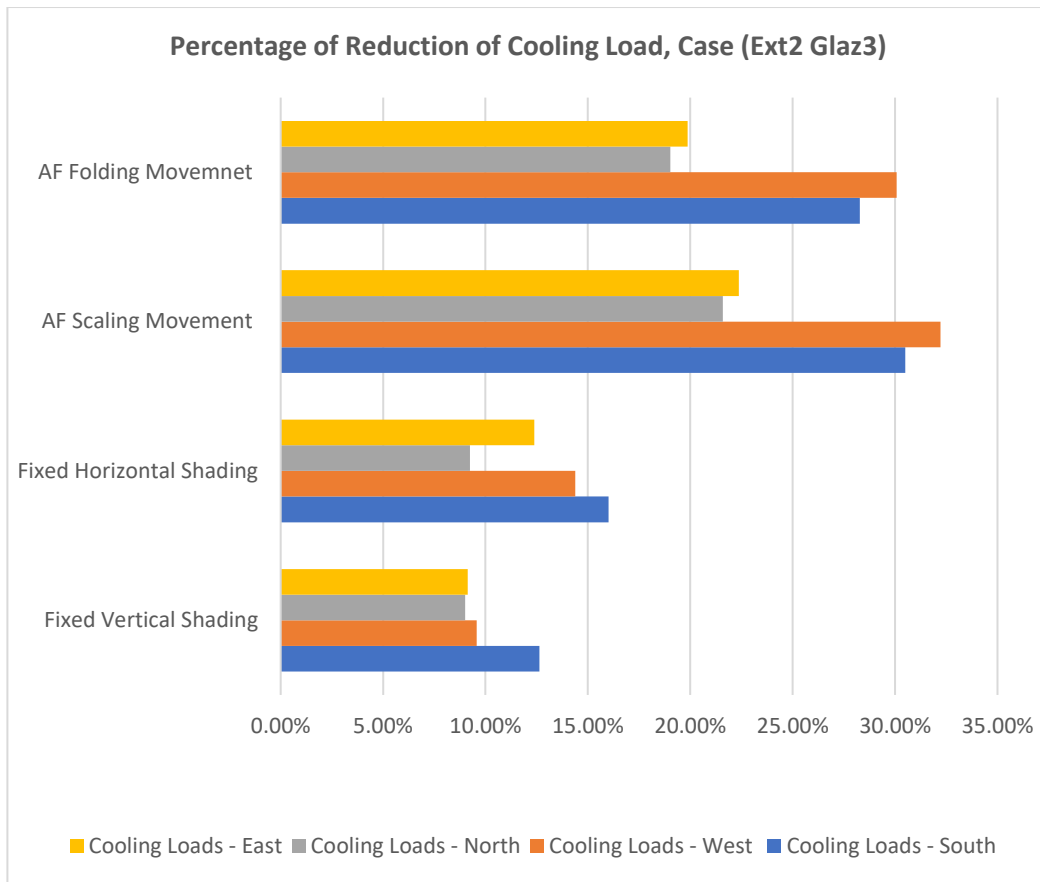


Figure 5.3: Comparison of external shading systems for (Ext2 Glaz3) in terms of cooling loads and solar heat gain.



*Figure 5.4: Comparison of external shading systems for case (Ext2\_Glaz3), in terms of cooling load reduction and solar heat gain reduction.*

A further reduction of cooling loads was observed in the cases with glazing types that have higher SHGC values, such as the case (Ext0 Glaz0), since these glazing types block solar radiation, which helps to compensate for the poor shading quality of the glazing Figure (5.5). In the case of the AF with a scaling movement, the cooling loads were reduced (south: 36.7%, west: 34.6%, north: 33.6%, and east: 33.8%) compared to the base case as shown in Figure (5.6). On the other hand, when the AF with a scaling movement was compared to the fixed vertical shading system, the cooling loads were reduced by (south: 27.3%, west: 27.2%, north: 26.3%, and east: 26.9%). Thus, these results indicate that the application of an AF system is more effective in terms of cooling load reductions compared to fixed shading systems.

**CHAPTER 5: SIMULATION RESULTS**

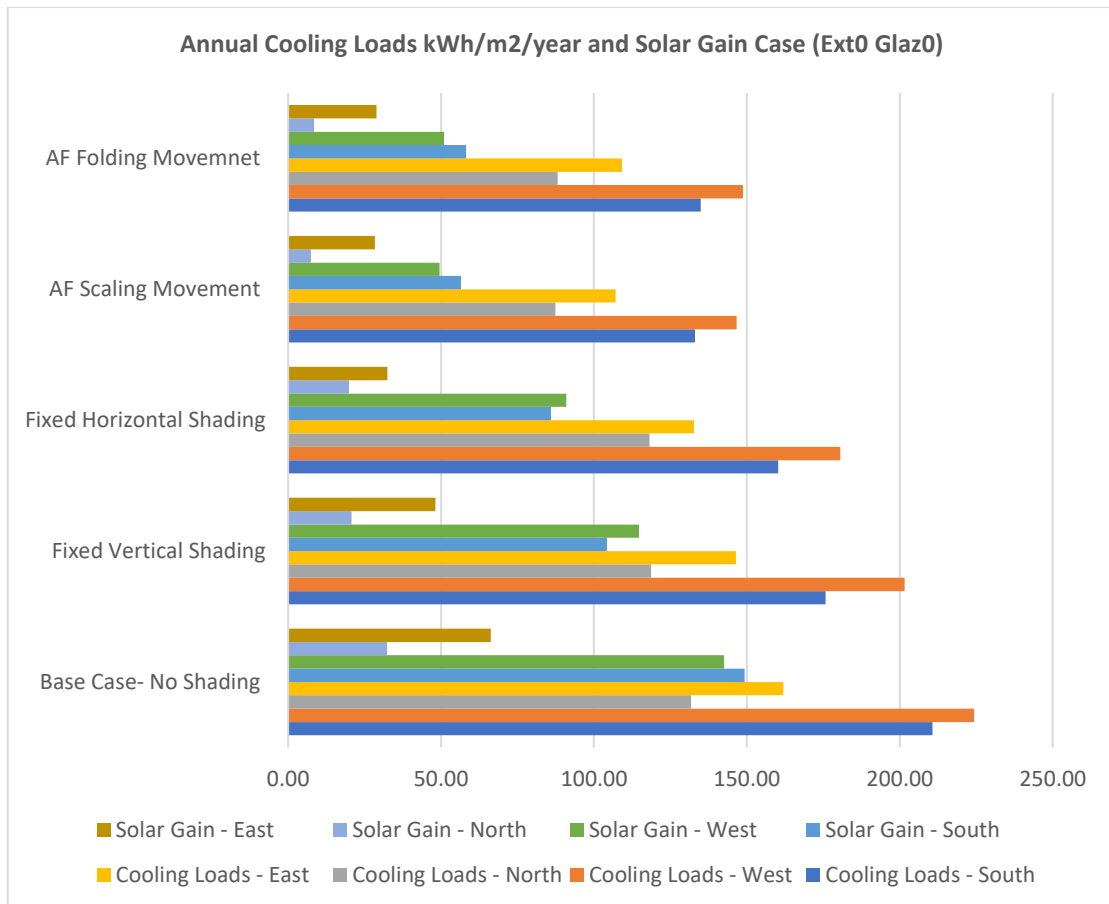


Figure 5.5: Comparison of external shading systems for case (Ext0- Glaz0), in terms of cooling loads and solar heat gain.

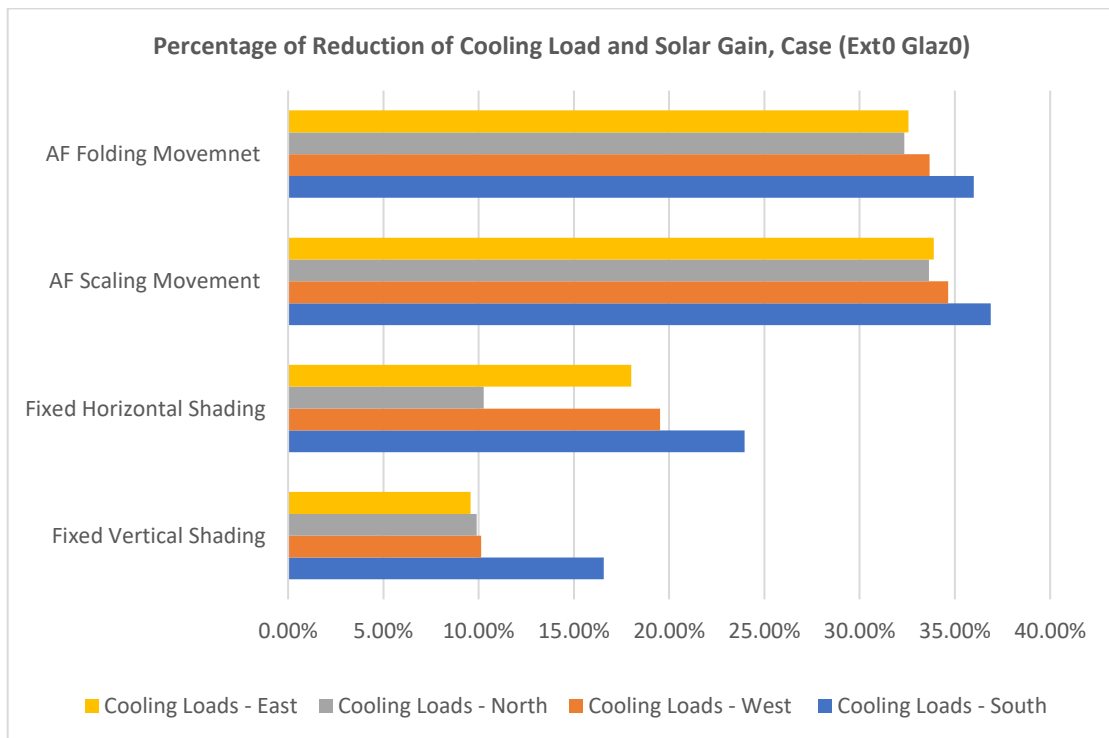


Figure 5.6: Comparison of external shading systems for case (Ext0- Glaz0), in terms of cooling load reduction and solar heat gain reduction.



## **CHAPTER 5: SIMULATION RESULTS**

The next analysis examined the reduction in cooling loads for the four study zones for the 48 combinations to determine which orientation benefited the most from using the adaptive shading system or the fixed shading system. Overall, the AF system performed better in all orientations compared to fixed shading; however, the amount of reduction of cooling varied depending on each orientation. The results demonstrate the effectiveness of the AF shading system on the south and west orientations with a reduction in annual cooling loads of up to 36% and 34% respectively, while north and east orientations benefited most with cases that used glazing types with higher SHGC values. Figures (5.7-5.10) demonstrate the annual cooling loads for all the 48 combinations for different fixed and adaptive shading systems in relation to orientation and engineering parameters. The finding indicates that both solar gain and cooling loads were reduced when an external shading system was applied for all 48 combinations. However, the best performing results achieved in all 48 combinations are for the AF prototype. Furthermore, in all external shading systems, the reduction of solar heat gain is more evident in the cases that combined glazing type (Glaz2, and Glaz3) and a well-insulated exterior wall, which results in a better cooling energy performance.

In conclusion, the findings proved that AF shading devices are the best at reducing cooling requirements in relation to solar gains. However, it is crucial to assess how they affect visibility and views. External shading devices can significantly improve the thermal performance of the building envelope and the energy efficiency of office buildings; however, their efficiency may be compromised if the thermal performance of the wall and glazing types is not well studied. As the adaptive system achieved a predominantly higher cooling energy performance compared to the other shading types. In the following section, the study further evaluates AFs using different automatic control scenarios for the studied cases in terms of cooling loads. The analysis examines only AFs with scaling movement excluding folding movement as both systems behave almost similarly in terms of energy loads.

**CHAPTER 5: SIMULATION RESULTS**

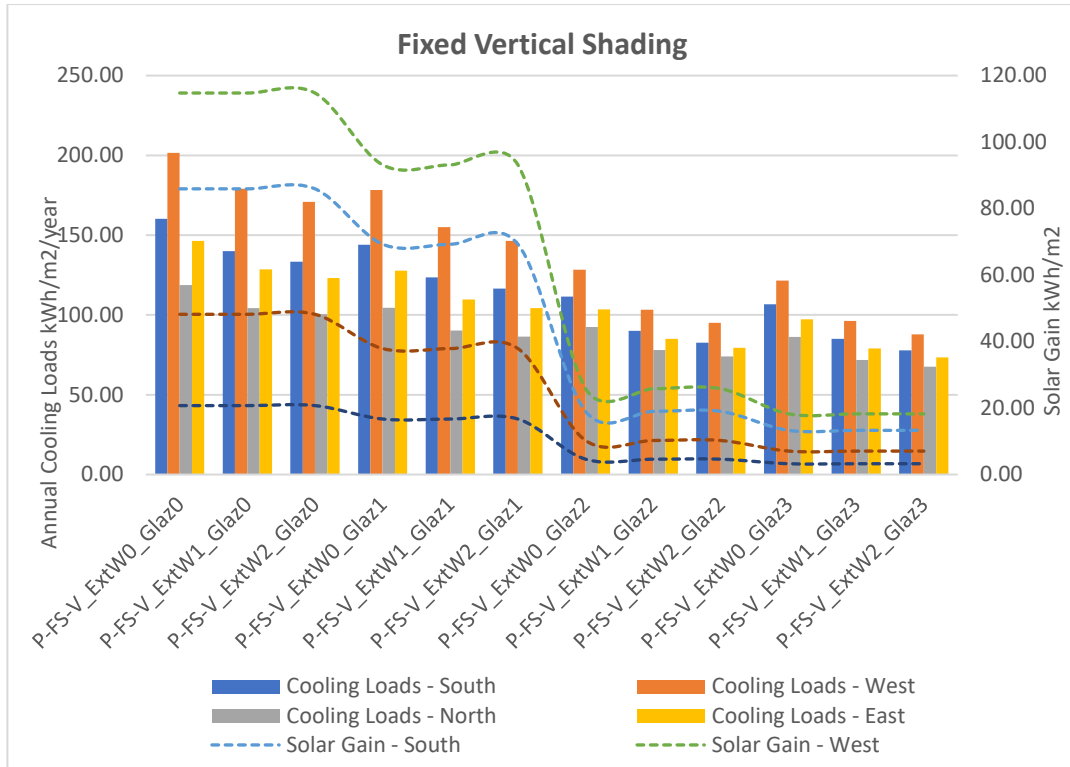


Figure 5.7: Simulation results of fixed vertical shading in terms of cooling loads and solar heat gain within different orientations.

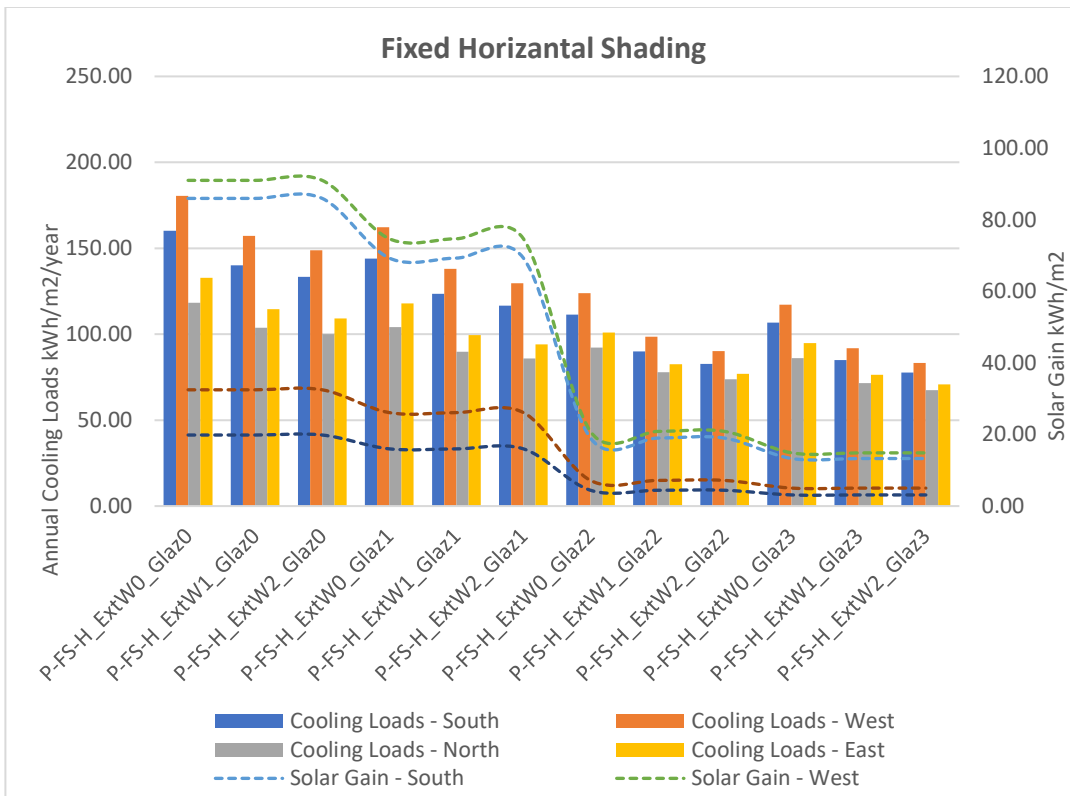


Figure 5.8: Simulation results of fixed horizontal shading in terms of cooling loads and solar heat gain within different orientations.

**CHAPTER 5: SIMULATION RESULTS**

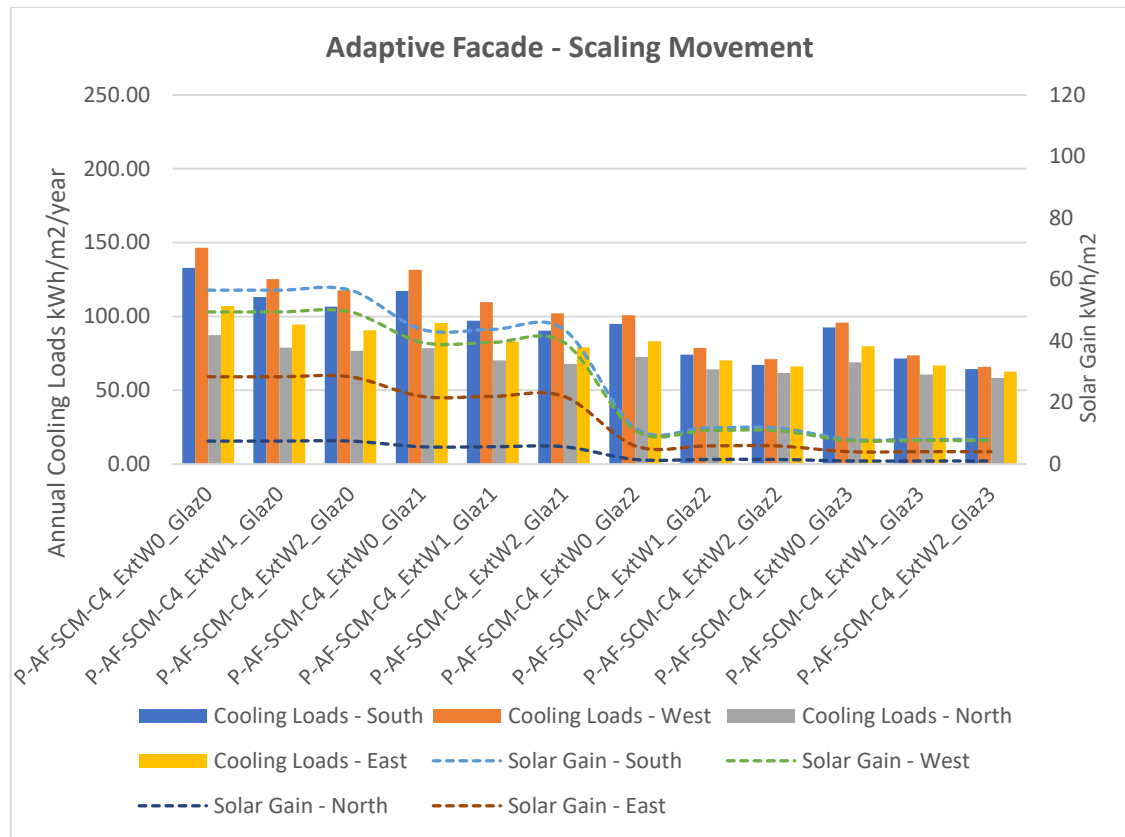


Figure 5.9: Simulation results of adaptive faced (scaling movement) in terms of cooling loads and solar heat gain within different orientations.

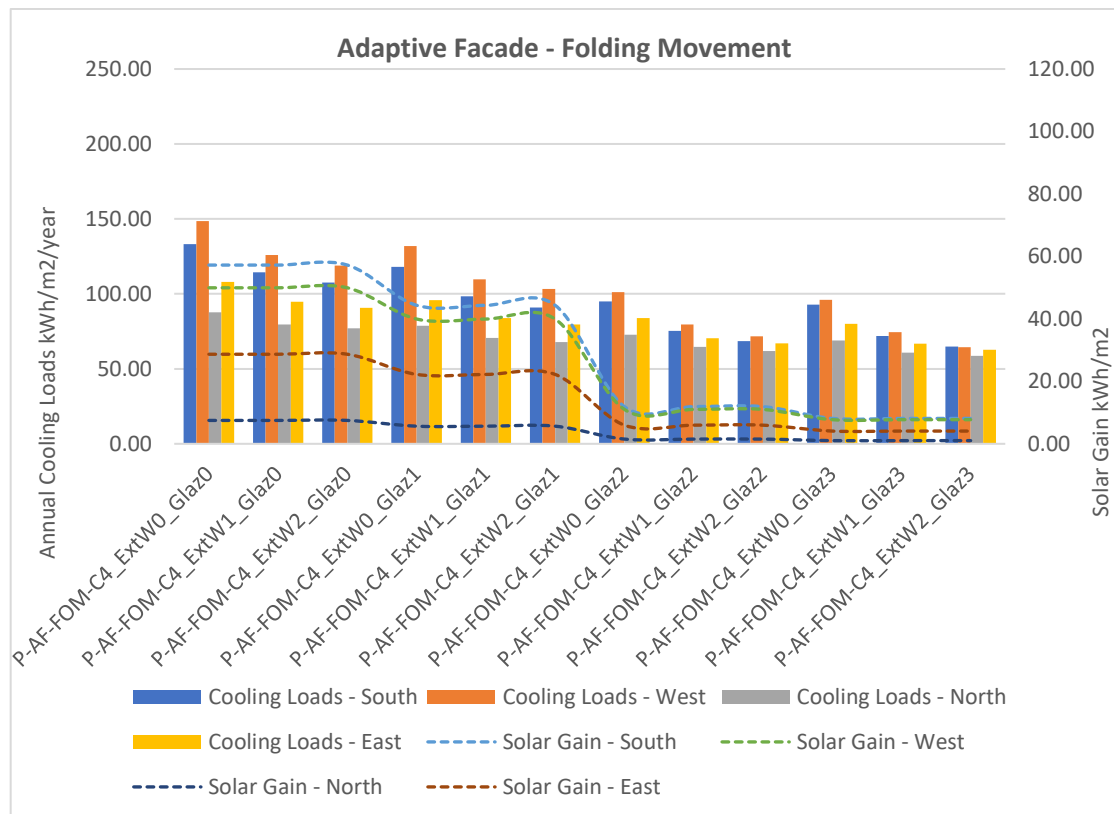


Figure 5.10: Simulation results of adaptive façade (folding movement) in terms of cooling loads and solar heat gain within different orientations.

## **5.4. Evaluation based on Control Scenarios**

This analysis evaluates the use of different automatic control strategies, as these are the basis of any AF system. The goal of this comparison is also to explore the impact of environmental parameters, either interior or exterior, on the performance of adaptive systems, which will result in the selection of the appropriate shading control scenario. The result of the simulation is presented in accordance with the orientation of the four examined offices in terms of annual cooling demands and lighting loads. The study tested four different control scenarios including (C1: incident solar radiation on window (W/m<sup>2</sup>), C2: transmitted solar radiation (W/m<sup>2</sup>), C3: direct solar radiation (W/m<sup>2</sup>), and C4: combinations of incident solar radiation and operative temperature), two exterior parameters, one interior parameter, and one that combined both interior and exterior parameters.

The simulation was carried out for all 48 combinations for the adaptive façade with scaling movement prototype; however, the analysis looked closely at the best performing case (ExtW2\_Glaz3) that was presented in section (5.2). Other cases were stored in a web-based comparison website. In general, all four control scenarios tested resulted in improving the cooling energy loads when compared to the fixed shading and base case; however, some scenarios performed the worst in terms of savings to lighting loads and providing adequate natural daylight. The results demonstrated that weather conditions considerably affect the shading control scenario. Figure (5.11) shows the results of the automatic shading control, which are grouped based on each orientation. The results also indicate that the performance of automatic shading control can be influenced by building orientation, which exploits the sun's position and its positive or negative effects on the interior environment. Thus, the energy cooling loads, solar gain, and lighting loads varied in each orientation. The findings show that south and west orientations consumed more cooling loads in hot climate regions; however, these orientations benefited the most in terms of cooling load reductions when compared to the case model with an average reduction of up to 30%, while lighting load variations were quite similar among each orientation except in the case of the control scenario (C3). Moreover, all control scenarios in the north orientations behaved similarly in terms of annual cooling loads due to the low values of solar radiation intensity that strike this façade. Thus, the AF is mostly open except for the time that received more radiation during the summer period from May to August in the morning and afternoon time to block the northwest and northeast solar radiation.

Regarding control scenarios, the AF with control C3 and C4 achieved the best performance in terms of cooling load reduction with 33.8%, and 30.5% respectively compared to the base

## **CHAPTER 5: SIMULATION RESULTS**

model. However, in the case of C3, which used direct solar radiation as a trigger, it improved the cooling loads, while it increased lighting loads due to the high number of times that the shade system was completely closed as shown in Figure (5.12). Figure (5.12, top) shows the hourly direct solar radiation which reached up to 1031.42 W/m<sup>2</sup>, and Figure (5.12, bottom) shows the adaptive shading with control C3 where the shading states corresponded to the direct solar radiation sensor hourly, resulting in the system being closed, as it exceeded the threshold. On the other hand, control scenario C2, which applied a transmitted solar radiation sensor, achieved the lowest performance compared to other controls, as it maximised the cooling loads as shown in Figures (5.13 and 5.14). These observations show that outdoor-based control scenarios perform better than using solely indoor controls. Moreover, the results demonstrate the capability of such control scenarios to close the shades prior to allowing the penetration of undesired solar gains to indoor spaces. The results also reveal that when taking into consideration the need to reduce both cooling loads and lighting loads, the most efficient energy performance was achieved with control scenario C4, as it considered both outdoor and indoor parameters. The C4 control strategy minimised cooling loads and lighting loads while maintaining natural lighting at an acceptable level. Overall, the performance across the control scenarios can be ranked from C2 as the worst performance to C3 as the best performance. However, as discussed previously, C3 scored the highest because the control system closed the shading position for most of the time; thus, the reliance on artificial lighting increased. Consequently, if outdoor views are a priority, this control strategy poses potential concerns in addition to lighting-saving issues. In the next analysis, the study closely analysed control scenario C4, as it was the most efficient strategy.

Regarding other combinations, all 48 combinations behaved the same as the presented case above (ExtW2\_Glaz3); the variations of cooling loads occurred based on the engineering parameters used (exterior wall values and glazing type values). For instance, Figure (5.15) shows a different combination (ExtW1\_Glaz2) of exterior wall and glazing types that varied in terms of its outputs, but the control scenarios behaved in a very similar way.

**CHAPTER 5: SIMULATION RESULTS**

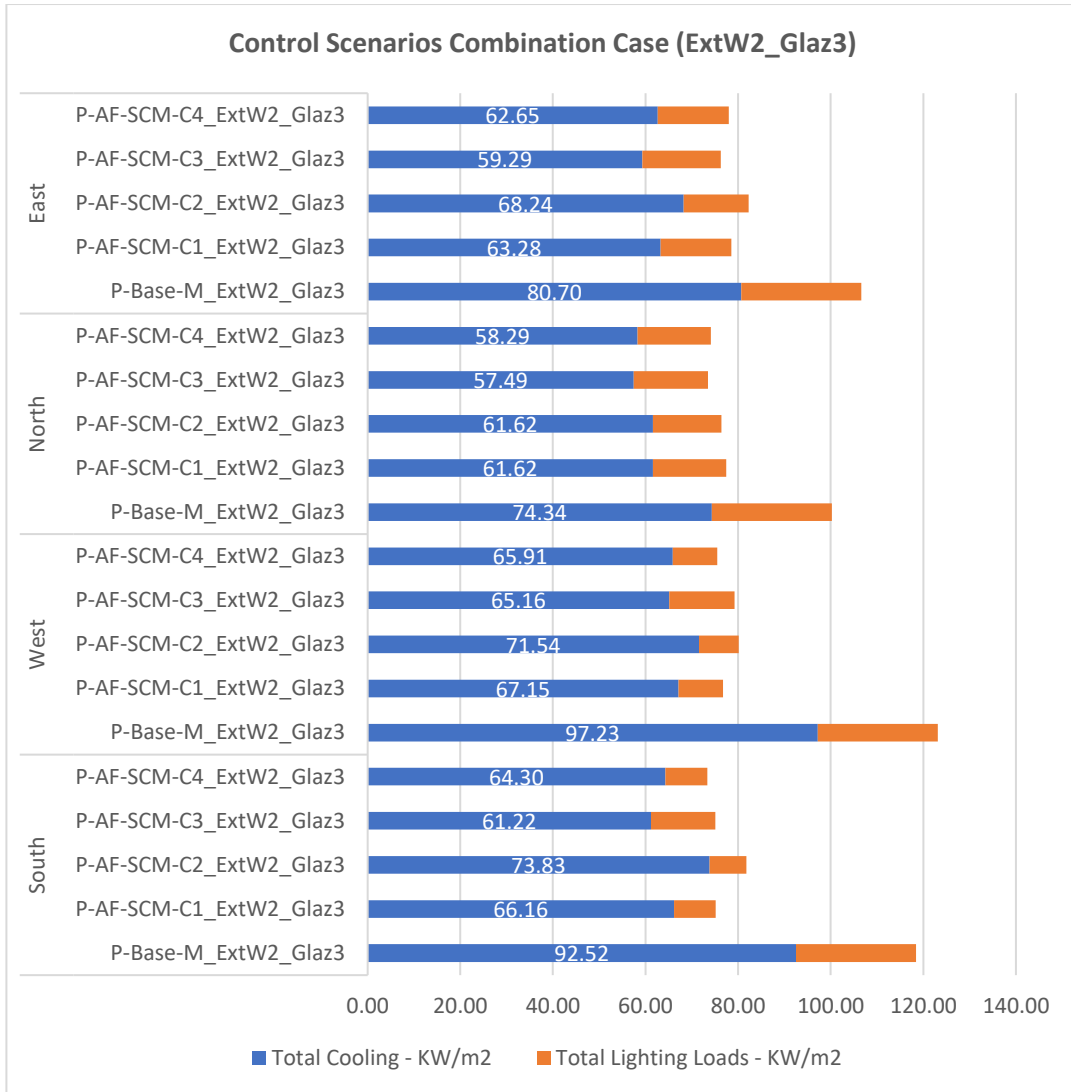


Figure 5.11: Comparison of control scenarios in terms of cooling and lighting loads within different orientations, case (ExtW2\_Glaz3).

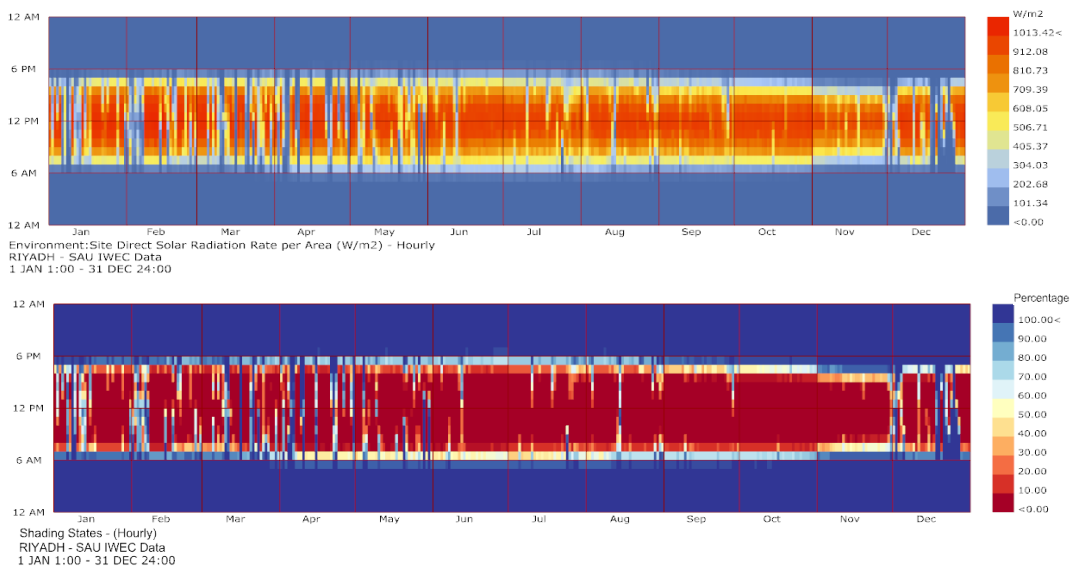


Figure 5.12: Simulation outputs for (C3) (south orientation), hourly direct solar radiation (top), and the hourly corresponding shading states (bottom).

## CHAPTER 5: SIMULATION RESULTS

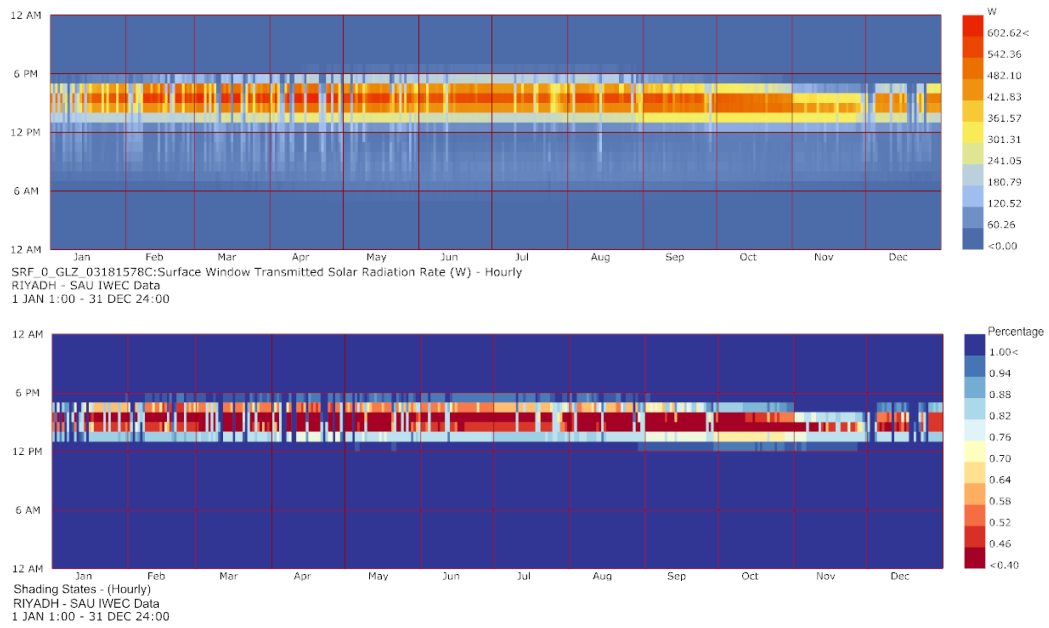


Figure 5.13: Simulation outputs for (C2) (west orientation), hourly transmitted solar radiation (top), and the hourly corresponding shading states (bottom).

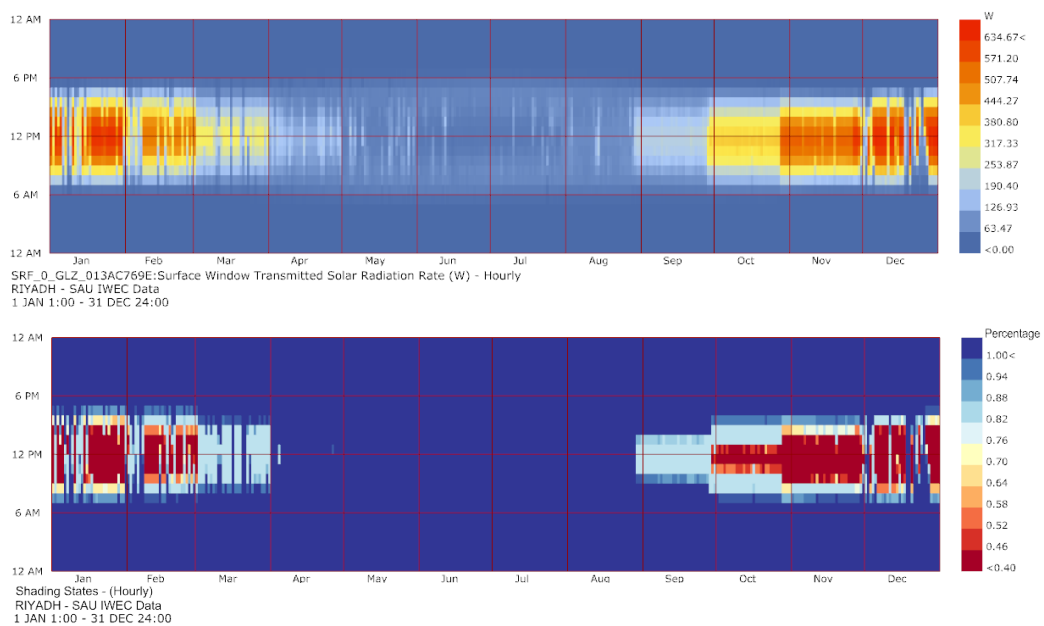


Figure 5.14: Simulation outputs for (C2) (south orientation), hourly transmitted solar radiation (top), and the hourly corresponding shading states (bottom).

**CHAPTER 5: SIMULATION RESULTS**

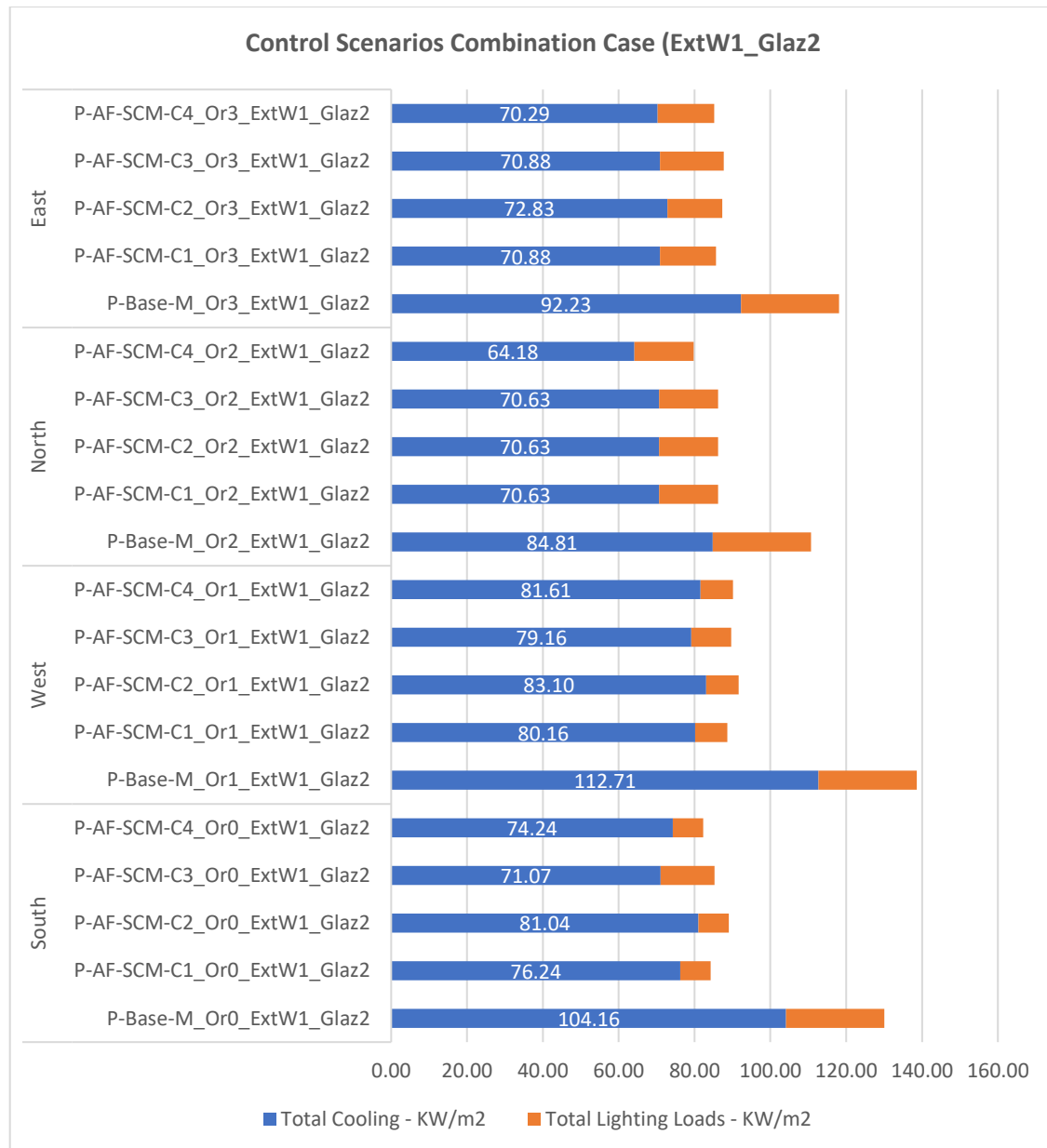


Figure 5.15: Comparison of control scenarios in terms of cooling and lighting loads within different orientations, case (ExtW1\_Glaz2).

The entire data of this experiment were loaded into design explorer to visualize all control scenarios. All design solutions for each control scenarios are presented in (Appendix C), and the overall findings of this experiment is outlined below. In addition, a scatter plot of all design cases in relation to cooling loads and annual energy consumption are shown in (Appendix C).

- The annual cooling loads for (C1) range from 58.15 kWh/m<sup>2</sup>/year to 181.71 kWh/m<sup>2</sup>/year.
- The annual lighting loads for (C1) range from 7.60 kWh/m<sup>2</sup>/year to 15.07 kWh/m<sup>2</sup>/year.



## **CHAPTER 5: SIMULATION RESULTS**

- The optimum case in terms of cooling loads is case (P-AF-SCM-C1\_Or2\_B00High\_B01High\_FLHigh\_ExtW2\_Glaz3), while the worst case is (P-AF-SCM-C1\_Or3\_B00Low\_B01Medium\_FLMedium\_ExtW0\_Glaz0).
- The annual cooling loads for (C2) range from 61.12 kWh/m<sup>2</sup>/year to 174.22 kWh/m<sup>2</sup>/year.
- The annual lighting loads for (C2) range from 9.57 kWh/m<sup>2</sup>/year to 16.17 kWh/m<sup>2</sup>/year.
- The optimum case in terms of cooling loads is case (P-AF-SCM-C2\_Or2\_B00Low\_B01Low\_FLLow\_ExtW2\_Glaz3), while the worst case is (P-AF-SCM-C2\_Or1\_B00Low\_B01Low\_FLMedium\_ExtW0\_Glaz0).
- The annual cooling loads for (C3) range from 57.84 kWh/m<sup>2</sup>/year to 136.93 kWh/m<sup>2</sup>/year.
- The annual lighting loads for (C3) range from 11.98 kWh/m<sup>2</sup>/year to 21.68 kWh/m<sup>2</sup>/year.
- The optimum case in terms of cooling loads is case (P-AF-SCM-C3\_Or2\_B00High\_B01High\_FLHigh\_ExtW2\_Glaz3), while the worst case is (P-AF-SCM-C3\_Or1\_B00Medium\_B01Low\_FLHigh\_ExtW0\_Glaz0).
- The annual cooling loads for (C4) range from 59.40 kWh/m<sup>2</sup>/year to 148.70 kWh/m<sup>2</sup>/year.
- The annual lighting loads for (C4) range from 7.53 kWh/m<sup>2</sup>/year to 15.92 kWh/m<sup>2</sup>/year.
- The optimum case in terms of cooling loads is case (P-AF-SCM-C4\_Or2\_B00Low\_B01Medium\_FLLow\_ExtW2\_Glaz3), while the worst case is (P-AF-SCM-C4\_Or1\_B00Medium\_B01Low\_FLHigh\_ExtW0\_Glaz0).

### **5.5. Evaluation based on Control Scenario (C4)**

As a result of the large number of simulation iterations, a web-based data visualization tool (Design Explorer) was utilised to present design solutions depending on specific objectives. For the purpose of this study, control scenario (C4) was selected to investigate its different variants in more depth since it was the most effective control system based on the results presented in the previous section. Designers can use Design Explorer to generate parallel coordinate charts for evaluating several design scenarios and for determining the optimal solution. Thus, all the simulation results of control scenario (C4) were presented in the Design Explorer web page ([https://tt-acm.github.io/DesignExplorer/?ID=BL\\_3eJReGq](https://tt-acm.github.io/DesignExplorer/?ID=BL_3eJReGq)) as shown in Figure (5.16). As illustrated in Figure (5.16), the inputs are labelled in the black column, while the outputs are labelled in the blue column. In addition, the inputs, results, and graphs of each case are presented.

**CHAPTER 5: SIMULATION RESULTS**

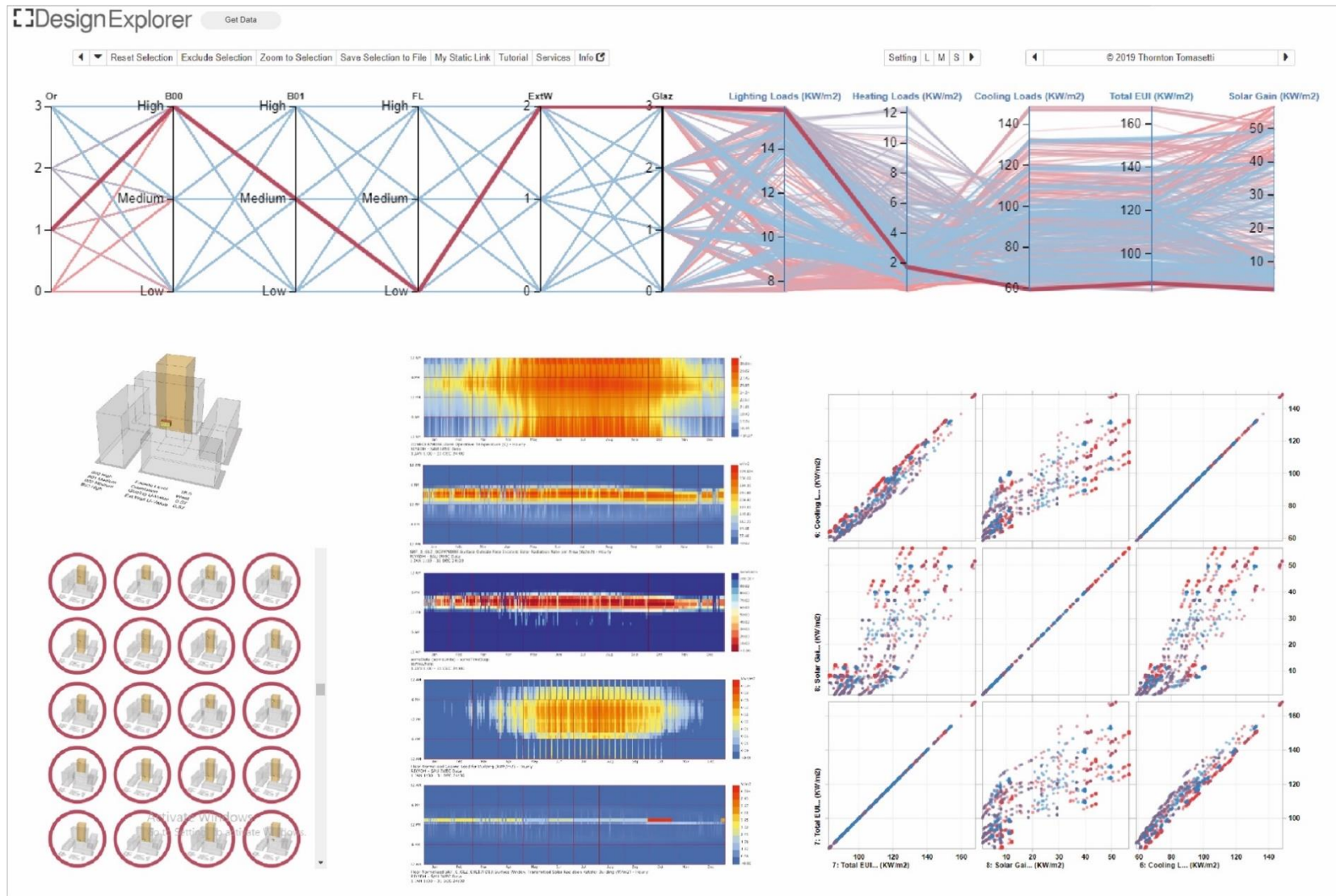


Figure 5.16: The interface webpage of Design Explorer allowing parallel coordinate chart.

## **CHAPTER 5: SIMULATION RESULTS**

Figure (5.17) shows some examples, and the following outcomes are outlined:

- Annual cooling loads range from 59.40 kWh/m<sup>2</sup>/year to 148.70 kWh/m<sup>2</sup>/year.
- Annual lighting loads range from 7.53 kWh/m<sup>2</sup>/year to 15.92 kWh/m<sup>2</sup>/year.
- Solar gain ranges from 1.05 kWh/m<sup>2</sup> to 56.5 kWh/m<sup>2</sup>.
- Optimum cooling loads (south orientation): Figure (5.17) shows that case (P-AF-SCM-C4\_Or0\_B00High\_B01High\_FLLow\_ExtW2\_Glaz3) performed the best for the south orientation with a cooling load of 60.62 kWh/m<sup>2</sup>/year, while the worst case is (P-AF-SCM-C4\_Or0\_B00Low\_B01Low\_FLLow\_ExtW0\_Glaz0) with a cooling load of 132.98 kWh/m<sup>2</sup>/year.
- Optimum cooling loads (west orientation): records show that case (P-AF-SCM-C4\_Or1\_B00High\_B01Medium\_FLLow\_ExtW2\_Glaz3) is the optimum case which achieved a cooling load of 59.40 kWh/m<sup>2</sup>/year. On the other hand, the worst performing case is (P-AF-SCM-C4\_Or1\_B00Medium\_B01Low\_FLHigh\_ExtW0\_Glaz0) with a cooling load of 148.70 kWh/m<sup>2</sup>/year.
- Optimum cooling loads (north orientation): Figure (5.17) shows that case (P-AF-SCM-C4\_Or2\_B00Low\_B01Medium\_FLLow\_ExtW2\_Glaz3) with cooling loads of 58.51 kWh/m<sup>2</sup>/year, while the worst performing case is (P-AF-SCM-C4\_Or2\_B00Medium\_B01Low\_FLHigh\_ExtW0\_Glaz0) with a cooling load of 135.47 kWh/m<sup>2</sup>/year.
- Optimum cooling loads (east orientation): The best performance case is (P-AF-SCM-C4\_Or3\_B00Low\_B01High\_FLLow\_ExtW2\_Glaz3) with a cooling load of 62.75 kWh/m<sup>2</sup>/year. On the other hand, the worst performing case is (P-AF-SCM-C4\_Or3\_B00Low\_B01Medium\_FLMedium\_ExtW0\_Glaz0) with a cooling load of 132.41 kWh/m<sup>2</sup>/year.

## CHAPTER 5: SIMULATION RESULTS

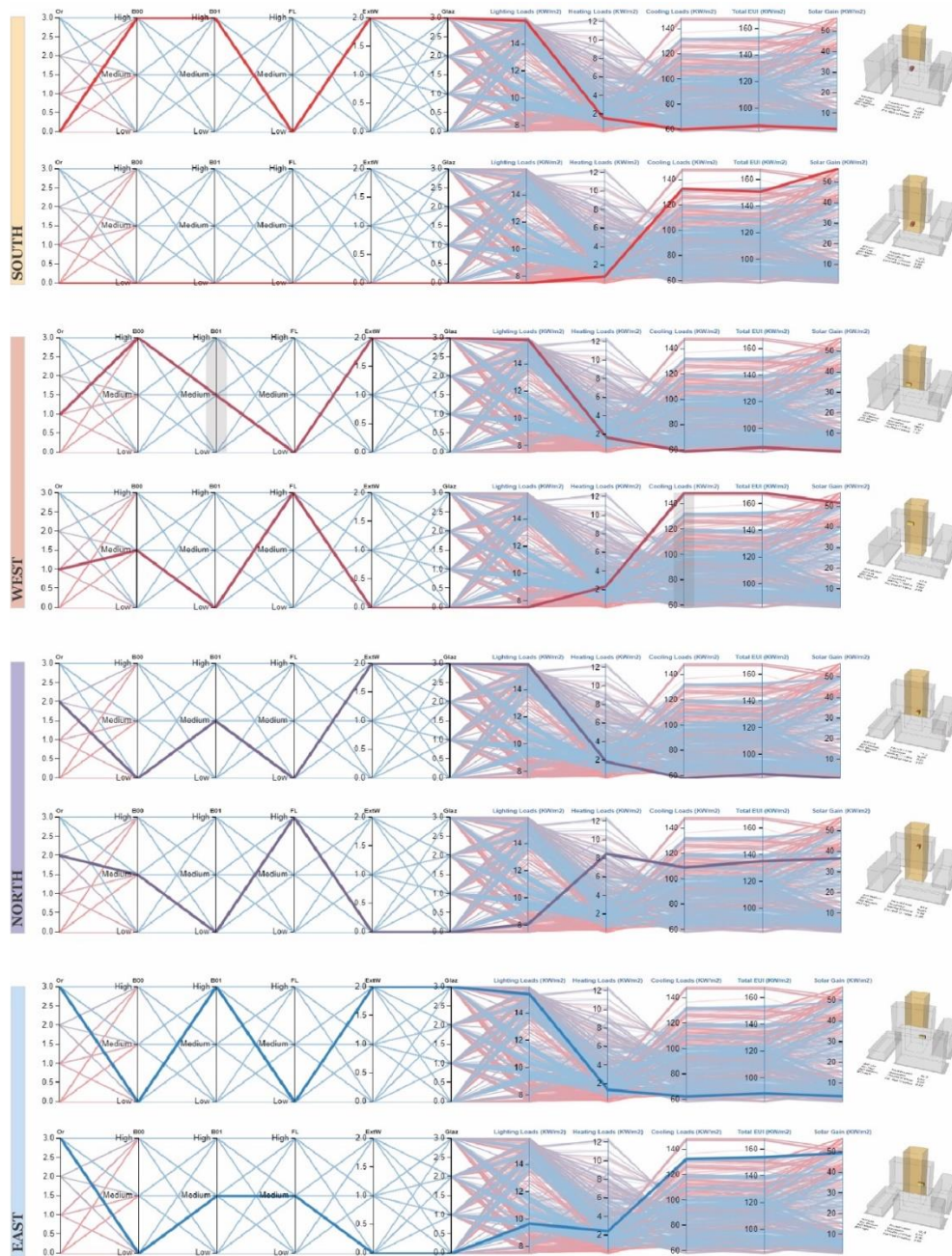


Figure 5.17: Web-based comparison of energy performance for control scenario (C4) showing optimum and worst cases for all orientations.

In this study, shading states were designed from fully open 100% (A) up to fully closed 0% (F), with four different shading states in between (80%: B, 60%: C, 40%: D, and 20%: E) as explained in chapter (4). Hence, in each orientation, the shading states performed differently, as orientations varied in terms of the solar radiation received on the building envelope and the level of operative temperature inside the room. According to the conditional statement that was coded within EMS on an hourly basis as explained in chapter (4), section (4.10.4), Figure (5.18) shows that AF in the west orientation was mostly closed (State, F) during the summertime from May to September in the afternoon between 2:00



## CHAPTER 5: SIMULATION RESULTS

pm to 4:00 pm, which refers to the hours that exceeded the SR and OT thresholds. Meanwhile, it was fully open (State, A) in the morning from 6:00 am until 12:00 pm, where SR and OT values were in the acceptable range. Then, the adaptive shading altered to different states after 12:00 pm, which were adjusted mostly between 20% (state E) up to 80% (state B) for the hours from 12:00 pm to 2:00 pm and from 6:00 pm.

Furthermore, a similar behaviour was also observed for the east façade during summer months; however, during the morning time, the west and the east façades received the highest solar radiation during summer as shown in Figure (5.19). On the other hand, the adaptive shading automated the shading states differently on the south façade. Although the south façade received the highest values of solar radiation, this was mostly during the winter months. Thus, the shading states were not fully closed during summer season, and the alteration of states occurred only in April, May, August, September, and October, while in June, and July the shading states remained mostly open. Figure (5.20) demonstrates the adaptive shading behaviour on the south façade, where the shading states most of the time were adjusted between 40% up to 80% during the summer season since SR did not exceed 250 W/m<sup>2</sup> and OTs were equal to or below 25. Regarding the north façade, the results in Figure (5.21) show that adaptive shading was mostly open throughout the year except for the summer period from May to August, and particularly in June for the morning and afternoon times.

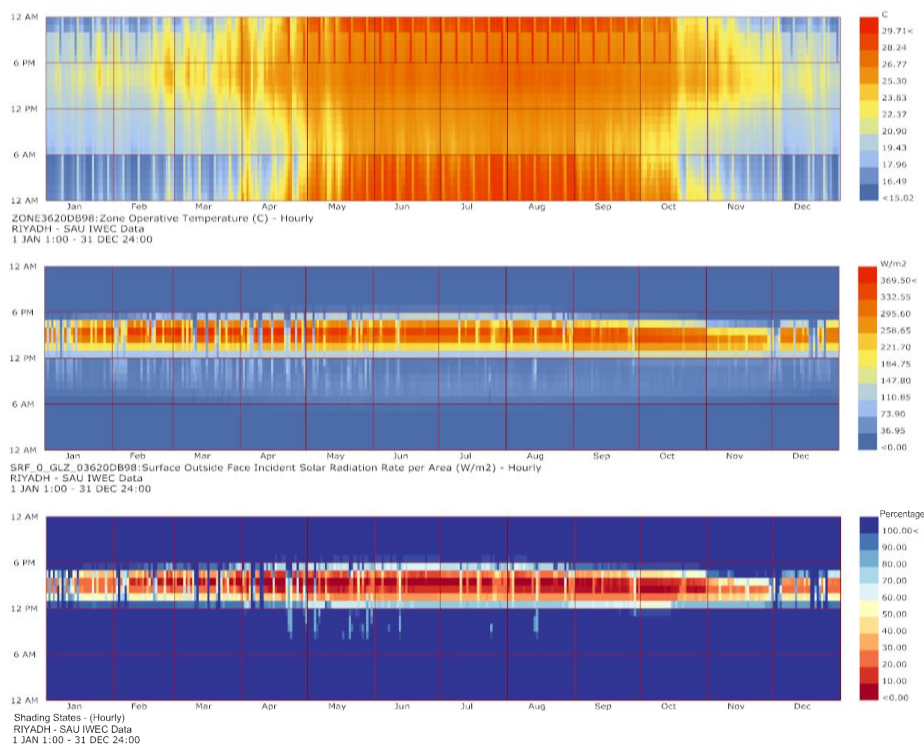


Figure 5.18: Simulation outputs for (C4), (west orientation): operative temperature (top), solar radiation (middle), and hourly variations of shading states based on SR and OT (bottom).

## CHAPTER 5: SIMULATION RESULTS

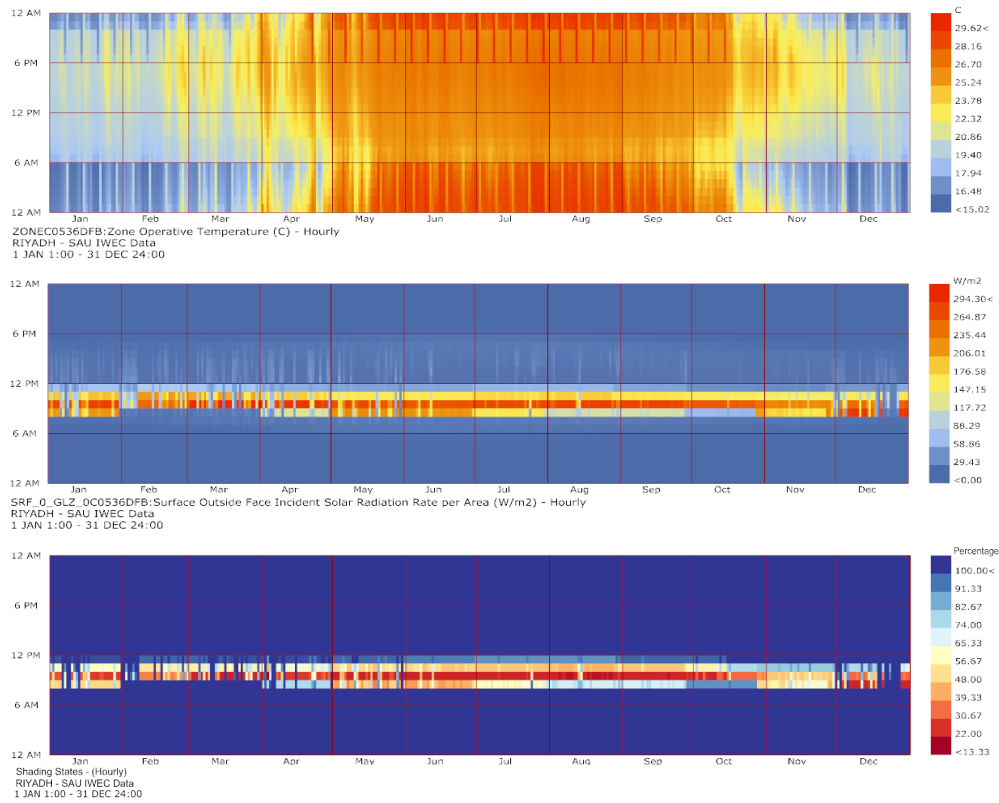


Figure 5.19: Simulation outputs for (C4), east orientation): operative temperature (top), solar radiation (middle), and hourly variations of shading states based on SR and OT (bottom).

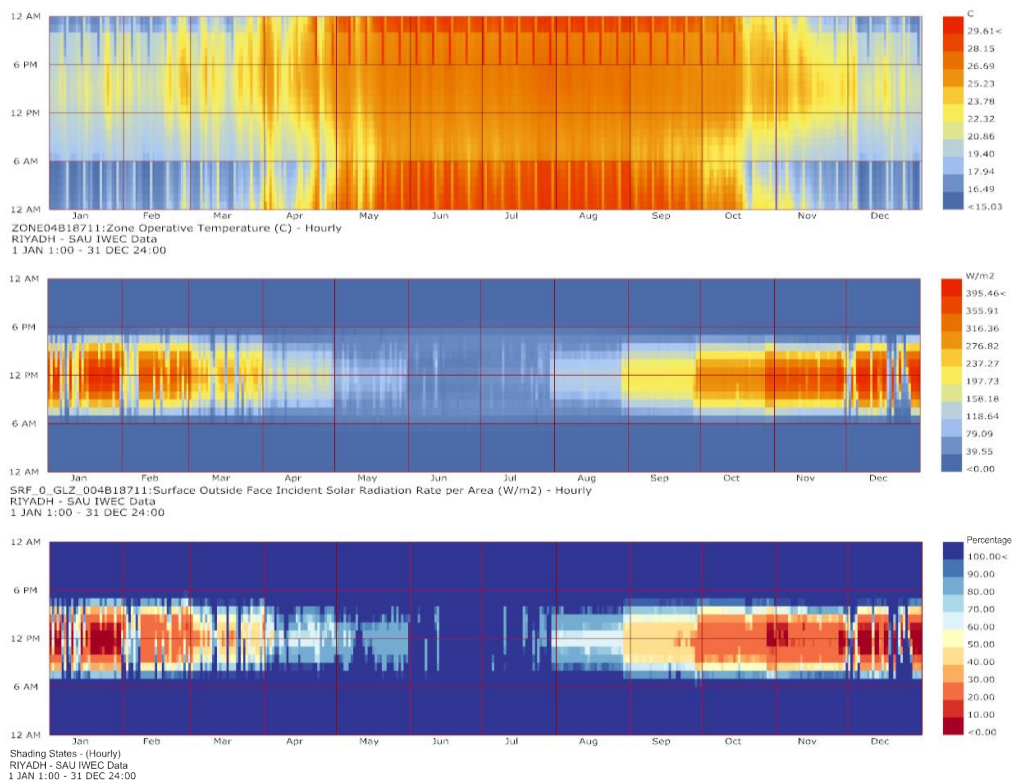


Figure 5.20: Simulation outputs for (C4), (south orientation): operative temperature (top), solar radiation (middle), and hourly variations of shading states based on SR and OT (bottom).

## CHAPTER 5: SIMULATION RESULTS

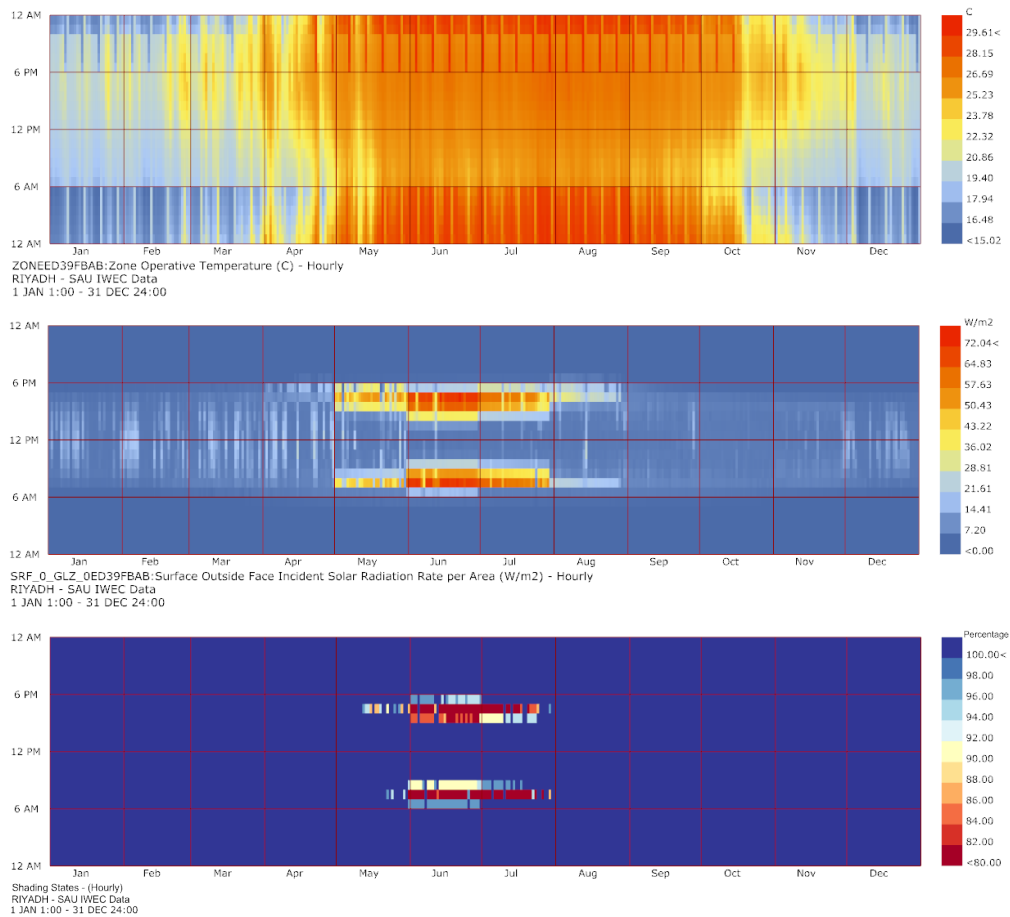
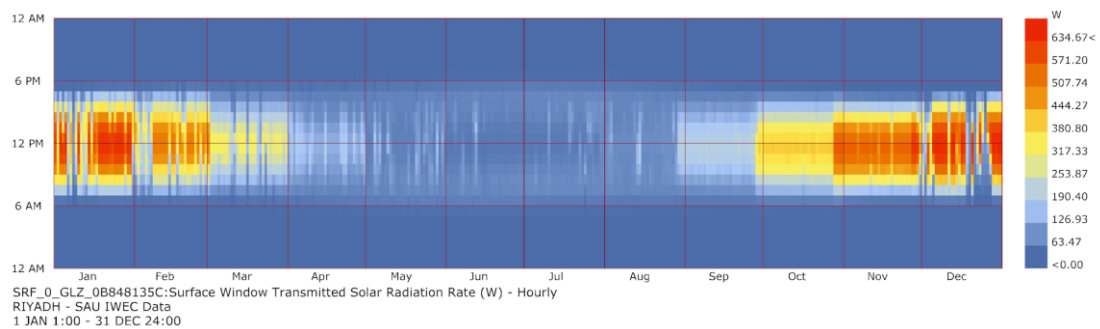


Figure 5.21: Simulation outputs for (C4), (north orientation): operative temperature (top), solar radiation (middle), and hourly variations of shading states based on SR and OT (bottom).

Regarding solar radiation transmittance through the window, the results indicate a significant reduction in the solar radiation that was transmitted through the window after the implementation of an adaptive shading system for all orientations as illustrated in Figures (5.22-5.25). These figures highlight the differences in solar radiation transmittance through the window, which in the (top, A) shows the situation of transmitted solar radiation prior to applying the AF, and (bottom, B) shows the results after the implementation of the AF.





## CHAPTER 5: SIMULATION RESULTS

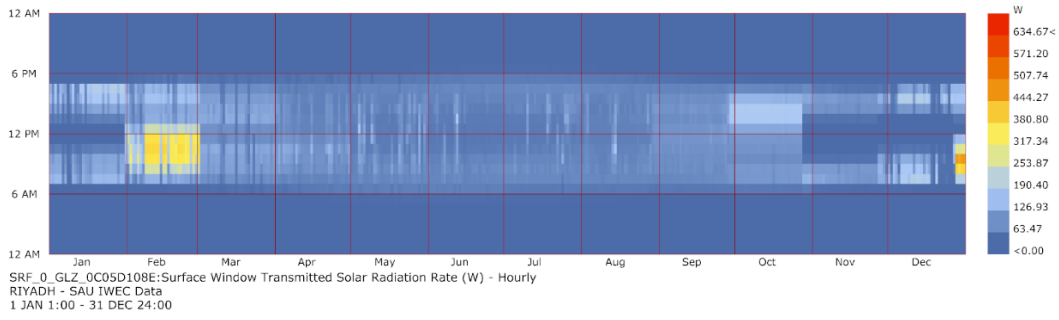


Figure 5.22: Hourly transmitted solar radiation through window (south orientation), prior to implementing the AF shading (top), and after implementing the AF shading (bottom).

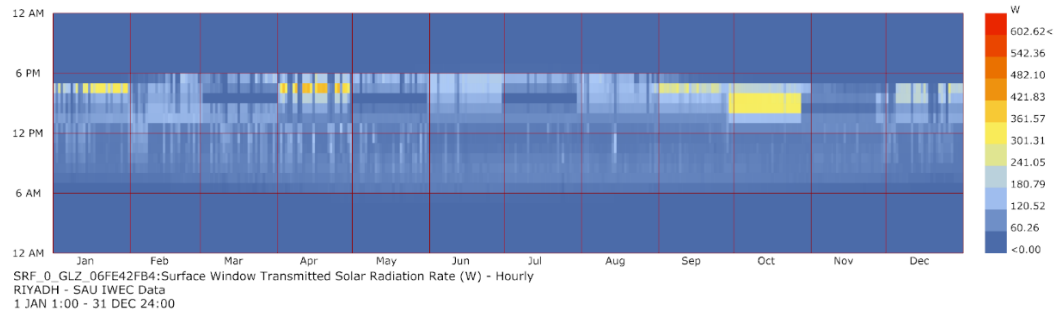
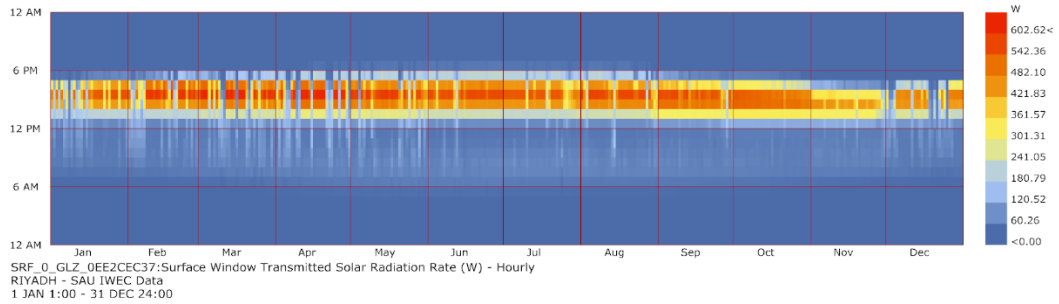


Figure 5.23: Hourly transmitted solar radiation through window (west orientation), prior to implementing the AF shading (top), and after implementing the AF shading (bottom).

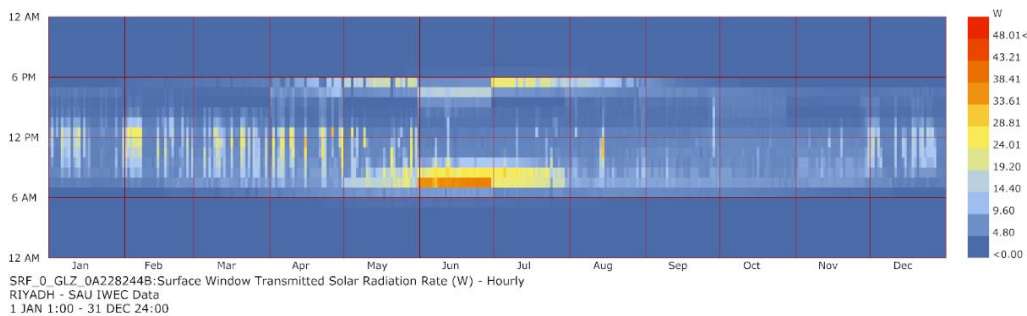
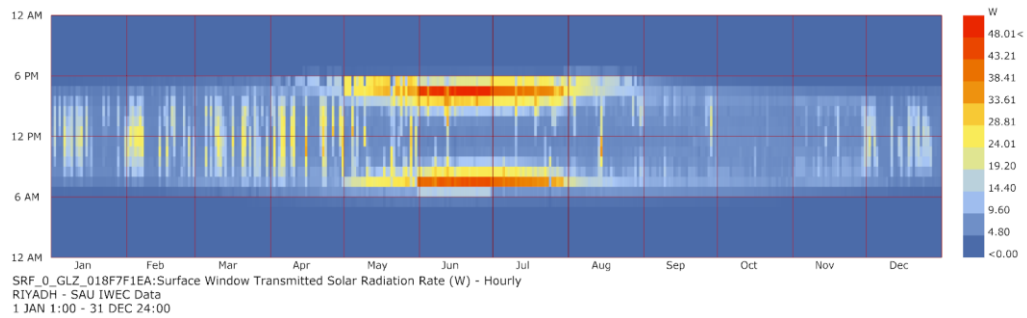


Figure 5.24: Hourly transmitted solar radiation through window (north orientation), prior to implementing the AF shading (top), and after implementing the AF shading (bottom).

## CHAPTER 5: SIMULATION RESULTS

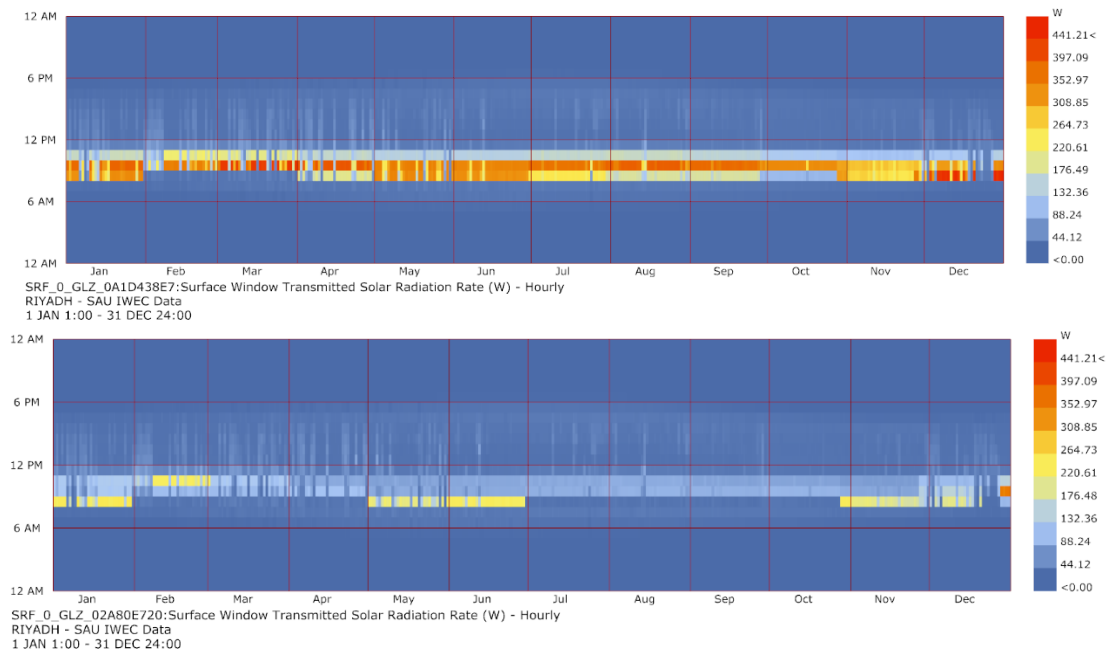


Figure 5.25: Hourly transmitted solar radiation through window (east orientation), prior to implementing the AF shading (top), and after implementing the AF shading (bottom).

Regarding building context variations, beside the environmental parameters, the AF shading states transformed according to the urban context and the location of the office room. In some cases, the urban context had a greater effect on alterations to the shading states while in other cases, slight differences in the shading states were observed due to the similar settings of the urban context. This variation was expected, as the urban context created shadows and reflected solar radiation on the building envelope. In this analysis, configurations for a total of 324 different urban contexts are analysed in terms of their effect on the transformation of shading states and, thereby, on the cooling load results. Figures (5.26) and (5.27) show the analysis of three different combinations of urban contexts that surrounded the office tower on four sides as follows:

1. P-AF-SCM-C4\_Or\_B00Low\_B01Low\_FLLow\_ExtW2\_Glaz3
2. P-AF-SCM-C4\_Or\_B00High\_B01Medium\_FLLow\_ExtW2\_Glaz3
3. P-AF-SCM-C4\_Or\_B00High\_B01High\_FLLow\_ExtW2\_Glaz3

Measuring their effect on shading states for the south and west façades revealed that their shading states were fully open (State A) most of time in the urban case (high, high, medium, high) with a cooling load of 60.62 kWh/m<sup>2</sup>/year. The openness for the same hours in the other two cases (low, low, medium, high), and (high, medium, medium, high) was varied and had a cooling load of 65.77 kWh/m<sup>2</sup>/year and 64.04 kWh/m<sup>2</sup>/year respectively.

Furthermore, the total number of hours spent in each shading state for the C4 scenario throughout the year excluding night times are presented in Table (5.2). This evaluation

## CHAPTER 5: SIMULATION RESULTS

highlights the influence of both orientations and the urban context on the behaviour of the shading states and the results for the cooling loads. In addition, a detailed results of two specific days of the year (21 March and 21 September) for the south and west façades are shown in (Appendix C). To prevent overheating during the summer and to maximise solar gain during the winter, the conditional statement in EMS was modified to maintain a fully open shading system during the winter season. However, a slight difference was noticed in terms of cooling loads while a greater reduction was observed for heating loads.

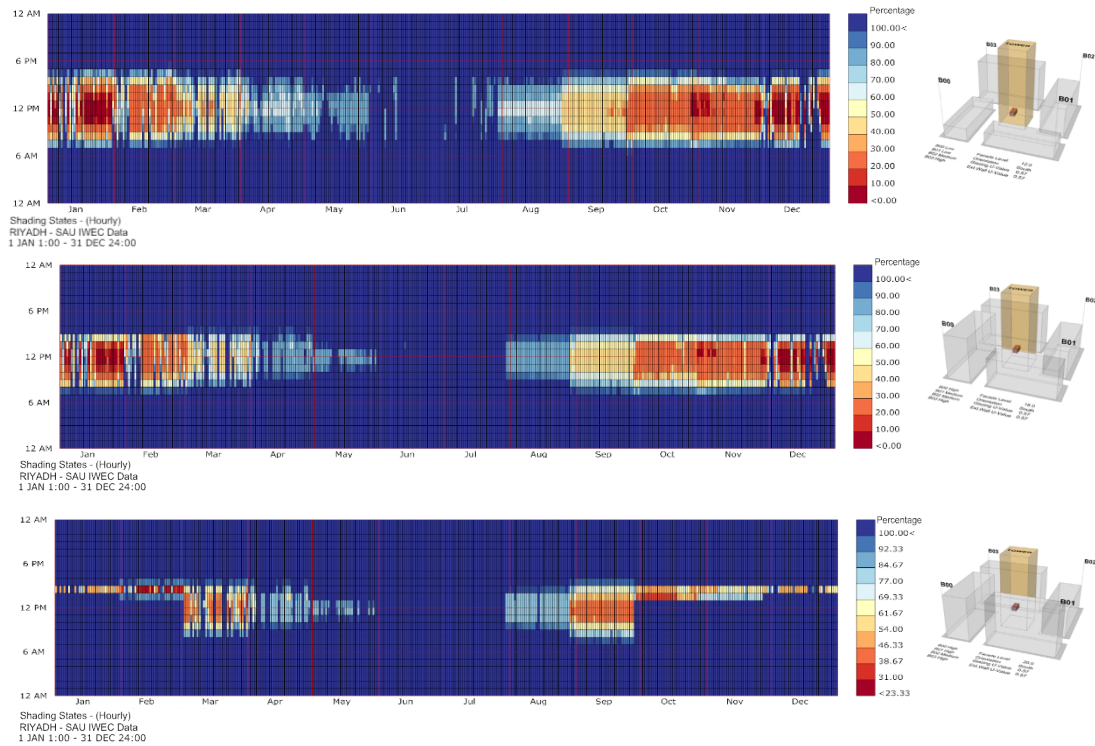


Figure 5.26: Relation between shading states variations, and urban contexts and its impact on cooling loads for South orientation.

## CHAPTER 5: SIMULATION RESULTS

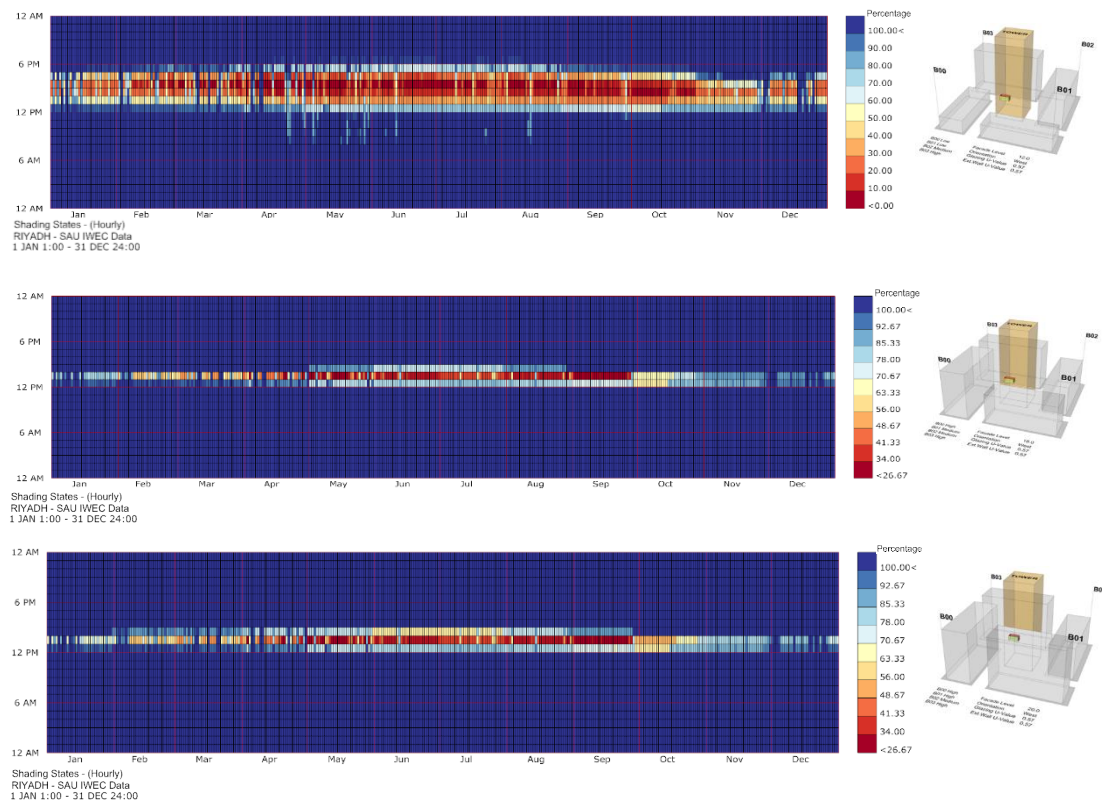
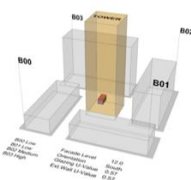
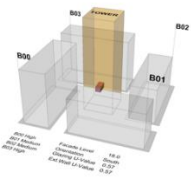
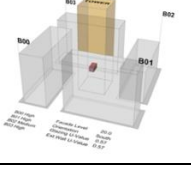


Figure 5.27: Relation between variations in shading states, and urban contexts and their impact on cooling loads for west orientation.

Table 5.2. Total number of hours spent in each shading state for some specific cases in different orientations and urban contexts.

|   |        |      |     |     |     |     |     |
|---|--------|------|-----|-----|-----|-----|-----|
| <b>P-AF-SCM</b><br><b>C4_Or_B00Low_B01Low_FLLow_ExtW2_Glaz3</b><br>      | States | A    | B   | C   | D   | E   | F   |
|   | South  | 2070 | 829 | 481 | 455 | 592 | 318 |
|   | West   | 2670 | 420 | 420 | 215 | 554 | 466 |
|   | North  | 4487 | 159 | 99  | 0   | 0   | 0   |
|   | East   | 3534 | 344 | 202 | 370 | 276 | 19  |
| <b>P-AF-SCM-</b><br><b>C4_Or_B00High_B01Medium_FLLow_ExtW2_Glaz3</b><br> | States | A    | B   | C   | D   | E   | F   |
|   | South  | 2774 | 664 | 301 | 387 | 475 | 144 |
|   | West   | 3982 | 330 | 244 | 59  | 130 | 0   |
|   | North  | 4442 | 215 | 88  | 0   | 0   | 0   |
|   | East   | 3229 | 374 | 186 | 367 | 418 | 171 |
| <b>P-AF-SCM-</b><br><b>C4_Or_B00High_B01High_FLLow_ExtW2_Glaz3</b><br>   | States | A    | B   | C   | D   | E   | F   |
|   | South  | 3711 | 513 | 210 | 273 | 38  | 0   |
|   | West   | 3868 | 331 | 336 | 78  | 132 | 0   |
|   | North  | 4402 | 343 | 0   | 0   | 0   | 0   |
|   | East   | 2974 | 504 | 276 | 328 | 456 | 0   |

## **5.6. Chapter Summary**

This chapter presents the results and findings of the conducted simulations. The analysis discussed the engineering parameters used to perform the simulation prior to implementing the shading system to understand the most influential parameter affecting the cooling loads. Then, different external shading systems (fixed, and adaptive) were compared to find the most effective shading system that can reduce the energy cooling loads of the office tower. In addition, different control scenarios were evaluated to actuate the AF shading system based on indoor and outdoor environmental conditions.

The results demonstrated that external shading devices can greatly enhance the thermal performance of the building envelope and the energy efficiency of office buildings; however, their effectiveness may be compromised if the thermal performance of the wall and glazing types is not thoroughly investigated. Moreover, the findings proved that AF shading devices have better performance than static façades at reducing cooling requirements in relation to solar gains. It was also found that, it is crucial to examine different control scenarios to select the appropriate shading control system. The next chapter will utilise the collected database based on the simulation to develop the ML surrogate models for predicting AF cooling loads. Different ML models will be developed and compared to achieve a highly accurate model. In addition, it will present in detail the workflow conducted to train, test, and validate the developed models.

The database is loaded into the web-based data visualization tool (Design Explorer):

Adaptive Façades Control Scenario (C1).

[https://tt-acm.github.io/DesignExplorer/?ID=BL\\_3SEYQbY](https://tt-acm.github.io/DesignExplorer/?ID=BL_3SEYQbY)

Adaptive Façades Control Scenario (C2).

[https://tt-acm.github.io/DesignExplorer/?ID=BL\\_3BSZP1I](https://tt-acm.github.io/DesignExplorer/?ID=BL_3BSZP1I)

Adaptive Façades Control Scenario (C3).

[https://tt-acm.github.io/DesignExplorer/?ID=BL\\_3ULMJeZ](https://tt-acm.github.io/DesignExplorer/?ID=BL_3ULMJeZ)

Adaptive Façades Control Scenario (C4).

[https://tt-acm.github.io/DesignExplorer/?ID=BL\\_3eJReGq](https://tt-acm.github.io/DesignExplorer/?ID=BL_3eJReGq)

Adaptive Façades All Control Scenarios.

[https://tt-acm.github.io/DesignExplorer/?ID=BL\\_3E7vqPE](https://tt-acm.github.io/DesignExplorer/?ID=BL_3E7vqPE)

## **CHAPTER SIX**

# **DEVELOPMENT OF A SURROGATE MODEL FOR ADAPTIVE FAÇADE PERFORMANCE IN THE EARLY DESIGN STAGES**

## **CHAPTER 6: DEVELOPMENT OF A SURROGATE MODEL FOR ADAPTIVE FAÇADE PERFORMANCE IN THE EARLY DESIGN STAGES**

### **6.1. Introduction**

The aim of this chapter is to develop a surrogate model that can predict the performance of adaptive façades (AFs) in the early stages of the design. As mentioned in the literature, surrogate models offer a promising approach to assess the performance of buildings based on physical knowledge significantly faster than simulation-based methods. Additionally, existing simulation tools have a high computational cost, and setting up the model for simulation is time intensive (Attia et al. 2012). Building simulation tools are currently unable to keep up with the pace of early design phases (Østergård et al. 2017) because creating a simulation to test a single idea requires carefully defining a large number of parameters. As a result, the architect's creative process will be disrupted by the extended run time of the simulation as well as the complexity of the AF system (Miller 1968). Therefore, this research proposes a surrogate model to assess the performance of AFs. In this chapter, the process of constructing the surrogate model is examined in detail following three main steps: (1) data pre-processing, (2) model training and hyperparameter tuning, and (3) model validation.

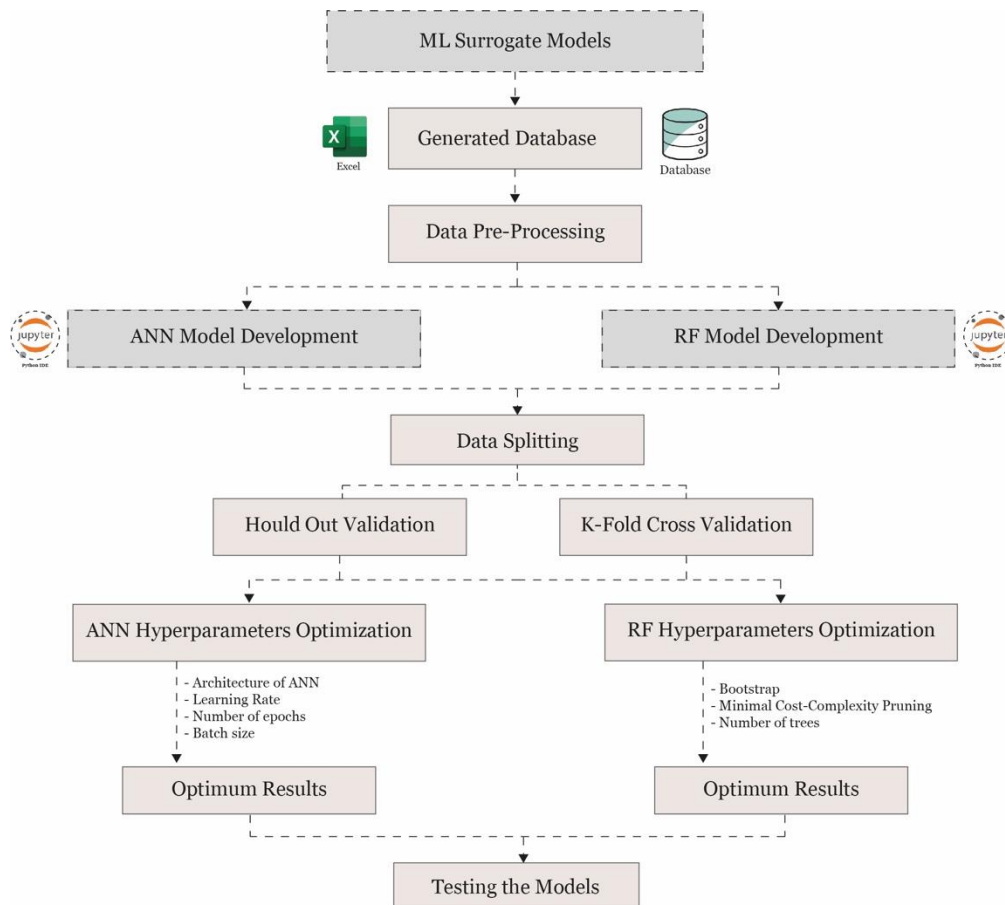
Part of the methodology followed in chapter 4 demands the analysis of solar radiation prior to analysing the energy performance of an AF, which increases the simulation time of the prediction. Thus, in this chapter, the study experimented initially with solar radiation data that were generated using simulation to avoid the need to conduct solar radiation simulation again when predicting the energy cooling demands of AF using ML. In addition, the study investigated the performance of ML models as potential emulators of simulation tools. For this investigation, two different ML algorithms were used to test and compare the prediction accuracy, starting with ANN algorithms, as this ML method is the most frequently applied in the literature to predict building performance and are best capable of dealing with complex nonlinear problems, as discussed in chapter 2 section (2.10). Following that, the RF algorithm was used as another method due to its ability to process both numerical and categorical data as well as its training simplicity and ability to generalize over a huge dataset.

After the solar radiation surrogate model was developed, confirming the suitability of ML techniques to emulate building performance, the second phase involved constructing another surrogate model to predict the energy cooling loads of AF shading systems using the data generated through simulation. In this phase, approaches similar to those in phase one

## **CHAPTER 6: DEVELOPMENT OF A SURROGATE MODEL FOR ADAPTIVE FAÇADE PERFORMANCE IN THE EARLY DESIGN STAGES**

were followed by developing two different ML learning algorithms, namely, ANN and RF, for testing and comparison of the cooling results accuracy. In both investigations, data were pre-processed prior to training the models. Then, the data were split into different sets, namely, a training set, a testing set, and a validation set, using two different methods of splitting the data: (1) hold out validation, and (2) K-fold cross validation, which will be detailed in this chapter. Following that, a hyperparameter tuning procedure was carried out to optimize the models and select the suitable parameters. The workflow used to develop the surrogate models is presented in Figure (6.1).

Lastly, the time series nature of the data was considered using RF modelling to examine the effect of time series inputs on the performance of the surrogate models. To model the time series nature of the data, two different approaches were applied, namely, the time differencing approach and the time window approach.



*Figure 6.1: Workflow used to develop the surrogate models*



## **6.2. Solar Radiation Prediction Using Machine Learning**

As mentioned earlier, the data extracted from the simulation were imported into two ML algorithms, ANN, and RF, to undergo training. From the simulation model, only data describing the design changes, referring to input features, were imported alongside the corresponding hourly solar radiation results. In this study, a total of eleven variables were used as input parameters to train the two models. This section describes in detail how the data were pre-processed prior to training, model development, data-splitting procedure, optimization, and validation.

## **6.3. Data Pre-processing**

Pre-processing the data can help to improve prediction accuracy when using ML algorithms as stated in various studies (Chou and Bui 2014; Kuster et al. 2017; Zhang et al. 2021). Firstly, the data were checked to identify incorrect or noisy data and to make sure the input features were valid. Then, data transformation was done to convert the input data into a format that ML algorithms could understand. For this experiment, input features were defined as either categorical or continuous inputs. For example, hour, month, building contexts (B00, B01, B02, B03), orientation, and façade level height were considered categorical features, and they were one-hot encoded, which is a common way of converting categorical inputs into a suitable format for ML models (Seger 2018). The remaining input features were x/y/z coordinates of the test points. They were treated as continuous inputs, and pre-processing was not applied to these features. The output of the model is the solar radiation of the corresponding location. Each of these input features had different ranges that defined the number of design iterations of the model as illustrated in Table (6.1). The ranges of each feature were as follows:

- Hour ranges from 6:00 am to 18:00 pm in step of 1
- Month (0: March 1: June 2: September, and 3: December)
- Orientation (0: South, 1: West, 2: North, 3: East)
- Building context B00 height - west side of the building (0: Low, 1: Medium, 2: High)
- Building context B01 height - north side of the building (0: Low, 1: Medium, 2: High)
- Building context B03 height - east side of the building (0: Low, 1: Medium, 2: High)

## **CHAPTER 6: DEVELOPMENT OF A SURROGATE MODEL FOR ADAPTIVE FAÇADE PERFORMANCE IN THE EARLY DESIGN STAGES**

- Building context B04 height - south side of the building (0: Low, 1: Medium, 2: High)
- Façade height ranges from 6 to 66
- X-coordinate (-11.08, 12.28)
- Y-coordinate (-13.06, 10.26)
- Z-coordinate (6.40, 69.60)

*Table 6.1. The input data used for the machine learning modelling.*

| <b>Input</b>  | <b>Input Neuron Type</b> | <b>Data Range</b>     |
|---------------|--------------------------|-----------------------|
| Hour          | Discrete                 | 6 to 18 in steps of 1 |
| Month         | Discrete                 | 0,1,2,3               |
| B00           | Discrete                 | 0,1,2                 |
| B01           | Discrete                 | 0,1,2                 |
| B02           | Discrete                 | 0,1,2                 |
| B03           | Discrete                 | 0,1,2                 |
| Orientation   | Discrete                 | 0,1,2,3               |
| Façade height | Discrete                 | 6 to 66               |
| X-coordinate  | Continuous               | [-11.08, 12.28]       |
| Y-coordinate  | Continuous               | [-13.06, 10.26]       |
| Z-coordinate  | Continuous               | [6.40, 69.60]         |

### **6.4. ANN Model Development**

In this section, ANNs were used for the modelling in the form of regression learning and were trained by a backpropagation (BP) algorithm to predict solar radiation Figure (6.2). The BP technique minimises the output error by backpropagating the error from the output to the hidden layer, consequently altering the weights. This approach has been followed by many researchers as discussed in chapter (2), section (2.10).

ANNs use a network of neurons with variable weighted connections to process and transfer data. An input layer receives training data, one or more hidden layers build a pattern of connections to replicate functions, and an output layer generates predictions. During training, the input features were sent to the input layer neurons, while the solar radiation results were transferred to the output layer neurons. In order to reduce the MSE (mean squared error) between the simulated and predicted outputs, the networks adjusted the weights of the connections between neurons during epoch-based training. The performance of the network was evaluated with the root mean square error (RMSE), mean absolute error (MAE) and coefficient of determination ( $R^2$ ) score, which were calculated using the following formulae.

$$RMSE = \sqrt{\frac{1}{n} \sum_{i=1}^n (y_i - f(x_i))^2}$$

$$MAE = \frac{1}{|n|} \sum_{i=1}^{|n|} |y(i) - f(x_i)|$$

$$R^2 = 1 - \frac{\sum_{i=1}^{|n|} (y(i) - f(x_i))^2}{\sum_{i=1}^{|n|} (y(i) - \bar{y})^2}$$

In the above equations, it is assumed that there are  $n$  number of testing data points,  $y_i$  is the output of the  $i^{\text{th}}$  data point corresponding to the input  $x_i$ ,  $f(x_i)$  is the predicted value of the  $i^{\text{th}}$  data point where  $f(x)$  is the function approximated by the neural network, and  $\bar{y} = \frac{1}{|n|} \sum_{i=1}^{|n|} f(x_i)$ . In an ideal modelling case, the RMSE and MAE values are expected to be zero and the  $R^2$  score to be 1.

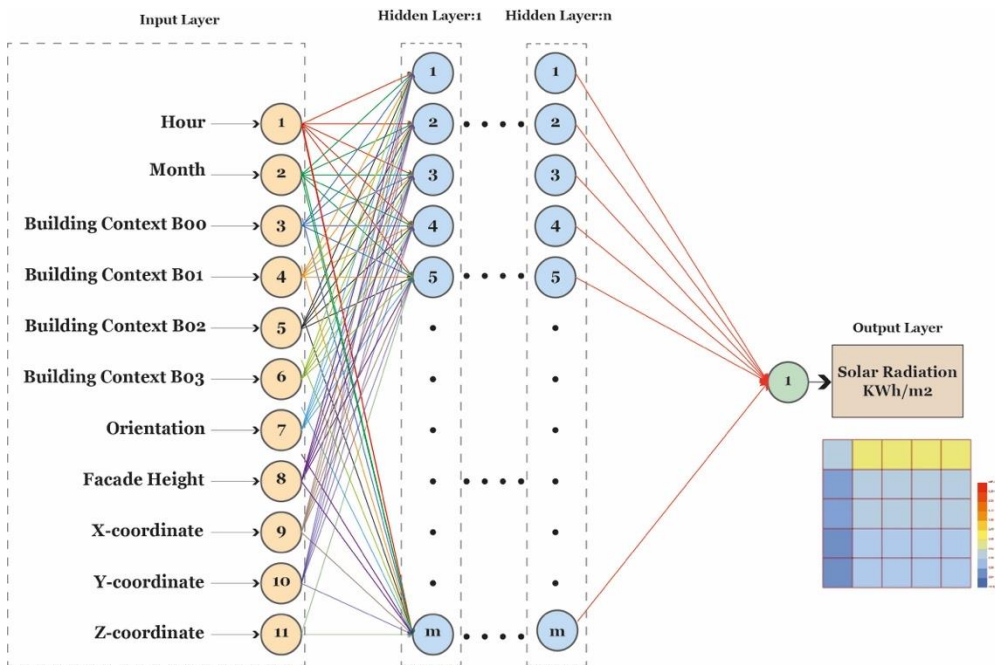


Figure 6.2: Architecture of the ANN model.

#### 6.4.1. Training Process

During the training process, a feedforward passing was performed with each feature of the data; then the prediction output was calculated. During training, the weights of the layers were updated by propagating the errors backwards from the output layer to the input layer. The input data were applied in stochastic mode, and the optimization algorithm used was the gradient descent. The weights of the layers were initialized using the Kaiming initialization method (Kaiming et al. 2015). The one-hot encoded categorical features were fed into an embedding layer. The purpose of this layer was to give a vector embedding to

**CHAPTER 6: DEVELOPMENT OF A SURROGATE MODEL FOR ADAPTIVE FAÇADE PERFORMANCE IN THE EARLY DESIGN STAGES**

the one-hot encoded input rather than using them as such. This approach has been found to give more representational power for the categorical inputs. Similarly, the continuous features were fed into the batch normalizing layer (Ioffe and Szegedy 2016). Its purpose was to make the continuous data follow the same probability distribution so that the learning of the network was optimized.

For the non-linear activation of the inputs in the neurons, the Rectified Linear Unit (ReLU) function, defined as  $f(x) = \max(0, x)$ , was used (Nair and Hinton, 2017). The output of the ReLU was batch normalized, and then the dropout regularization was applied. Dropout is a mechanism to ensure the generalization capability of the network by avoiding overfitting (Srivastava et al. 2016). For each layer of the network, the data were processed as – linear layer à ReLU activation à batch normalization à dropout. The output neuron of the network is a trivial neuron where no activations are applied, and the output is taken from the previous layer Figure (6.3). In this study, implementation of the network was conducted using the PyTorch environment with Python tools as illustrated in Figure (6.4) (Paszke et al. 2019). The experiment was performed with one-layer, two-layer, three-layer, and four-layer networks, and the dropout rate used for the experiment was 0.2.

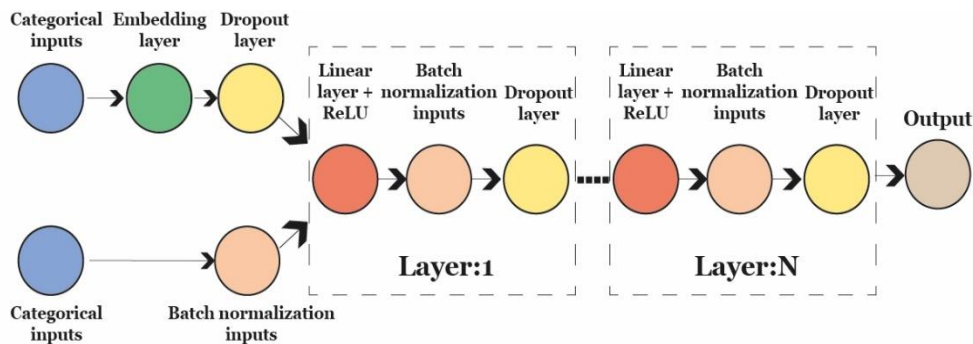


Figure 6.3: ANN components.

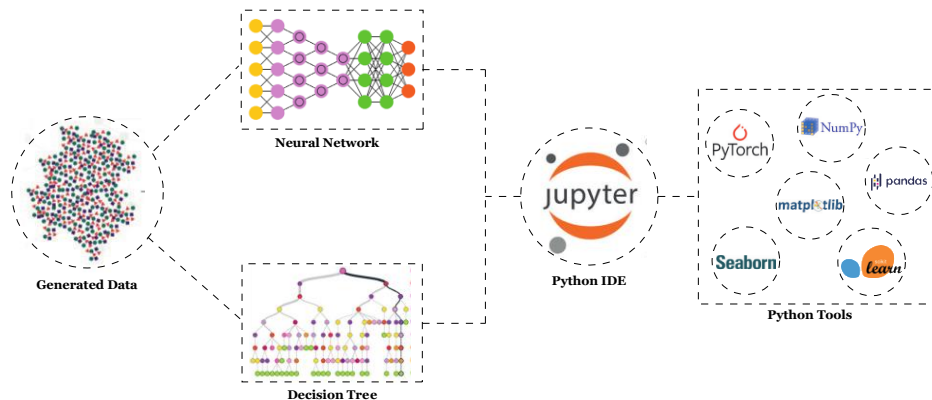
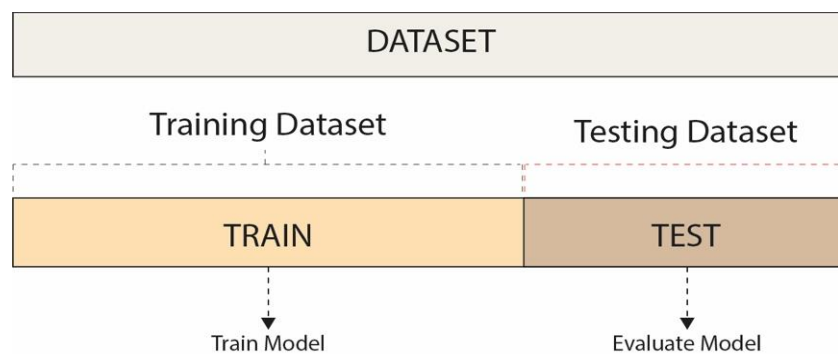


Figure 6.4: Tools used in the study to train and test both models.

### **6.4.2. Data Splitting Procedure (Hold Out Validation)**

This section discusses investigation of the data split. It started with the hold out validation approach, which is a simpler data split procedure, and it was then investigated with the K-fold cross validation, which will be discussed in a later section. Prior to computing the model, the data were separated into the training set and the testing set. The training dataset was used for developing the model, while the testing dataset was used to evaluate the model performance Figure (6.5). The training and testing set split was done in the ratio of 0.8, that is, 80% of the data were assigned to the training set and 20% to the testing set (Westermann and Evins 2019c). The 20% of the test data were not used for training purposes; these data were maintained at the end of the training process to evaluate the performance after tuning the hyperparameters.



*Figure 6.5: Hold out validation splitting procedure*

### **6.4.3. Optimization of Hyperparameters (Grid-Structure)**

Tuning the hyperparameters is an important step in the training process of the ANN model to achieve the best outcome, as discussed in chapter (2), section (2.9.2). Optimization of the hyperparameters was performed in a grid structure approach with respect to the following parameters: architecture of the network, learning rate, number of epochs, and batch size, as detailed below. The goal of this experiment was to act as a sanity check on these parameters for the next experiment.

- 1) Architecture of the neural network: Choosing an appropriate network is important to avoid the under fitting and overfitting of the data and for better generalization of the network to be used with the unseen future data. The aim is to fix the number of layers and number of neurons in each layer.
- 2) Learning rate: This is the parameter used to update the weights of the networks as part of the mathematical optimization of the network. This value controls how much a weight is updated during optimization. When considering a high learning rate, it may result in skipping the minima and oscillating around the minima region. In

## **CHAPTER 6: DEVELOPMENT OF A SURROGATE MODEL FOR ADAPTIVE FAÇADE PERFORMANCE IN THE EARLY DESIGN STAGES**

contrast, when its value is too low, the search towards the local minima will be too slow; this results in a high number of epochs, which consumes more time (Kalogirou 2000; Samarasinghe 2007).

- 3) Number of epochs: An epoch represents the number of times the entire set of training data is fed into the neural network. The number of epochs must be considered to determine the optimum value. This is because when a low value is considered, the network model may not learn as intended. On the other hand, selecting a high value may result in extra unnecessary running time, and the learning gets saturated.
- 4) Batch size: This is the number of training data points that are fed into the neural network at a time. This value is regulated by the hardware memory constraints and time of execution of the program. Some studies have found that varying the batch size can have an effect on the performance of the neural network modelling (Ayoub 2020).

### **6.4.3.1. Architecture of the Neural Network**

Since the performance of ANN models is highly dependent on the design of the network, this study evaluated several ANN architectures starting with one hidden layer and employing a variety of hidden neurons. The objective was to select the optimal network architecture for the ANN model. This experiment modelled ANNs with one hidden layer, two hidden layers, three hidden layers, and four hidden layers. The experiments were repeated for the cases with a different number of neurons in each layer (64, 80, 128, 256, 512 and 1,024). Table (6.2) details the models used in the experiment and their associated RMSE results. Figure (6.6) shows a comparison of all the examined combinations of the ANN models.

*Table 6.2. The different number of layers experimented in the study.*

| <b>Serial No.</b> | <b>No. of layers</b> | <b>No. of neurons in each layer</b> | <b>RMSE</b> |
|-------------------|----------------------|-------------------------------------|-------------|
| 1                 | 1                    | 64                                  | 0.022570    |
| 2                 | 1                    | 80                                  | 0.021322    |
| 3                 | 1                    | 128                                 | 0.020274    |
| 4                 | 1                    | 256                                 | 0.018792    |
| 5                 | 1                    | 512                                 | 0.017913    |
| 6                 | 1                    | 1024                                | 0.018077    |
| 7                 | 2                    | 64                                  | 0.018284    |
| 8                 | 2                    | 80                                  | 0.015763    |
| 9                 | 2                    | 128                                 | 0.015238    |
| 10                | 2                    | 256                                 | 0.014368    |
| 11                | 2                    | 512                                 | 0.015892    |
| 12                | 2                    | 1024                                | 0.014912    |
| 13                | 3                    | 64                                  | 0.016262    |

**CHAPTER 6: DEVELOPMENT OF A SURROGATE MODEL FOR ADAPTIVE FAÇADE PERFORMANCE IN THE EARLY DESIGN STAGES**

| Serial No. | No. of layers | No. of neurons in each layer | RMSE     |
|------------|---------------|------------------------------|----------|
| 14         | 3             | 80                           | 0.015605 |
| 15         | 3             | 128                          | 0.015195 |
| 16         | 3             | 256                          | 0.014479 |
| 17         | 3             | 512                          | 0.014109 |
| 18         | 3             | 1024                         | 0.014478 |
| 19         | 4             | 64                           | 0.016198 |
| 20         | 4             | 80                           | 0.016176 |
| 21         | 4             | 128                          | 0.015801 |
| 22         | 4             | 256                          | 0.015468 |
| 23         | 4             | 512                          | 0.015031 |
| 24         | 4             | 1024                         | 0.014350 |

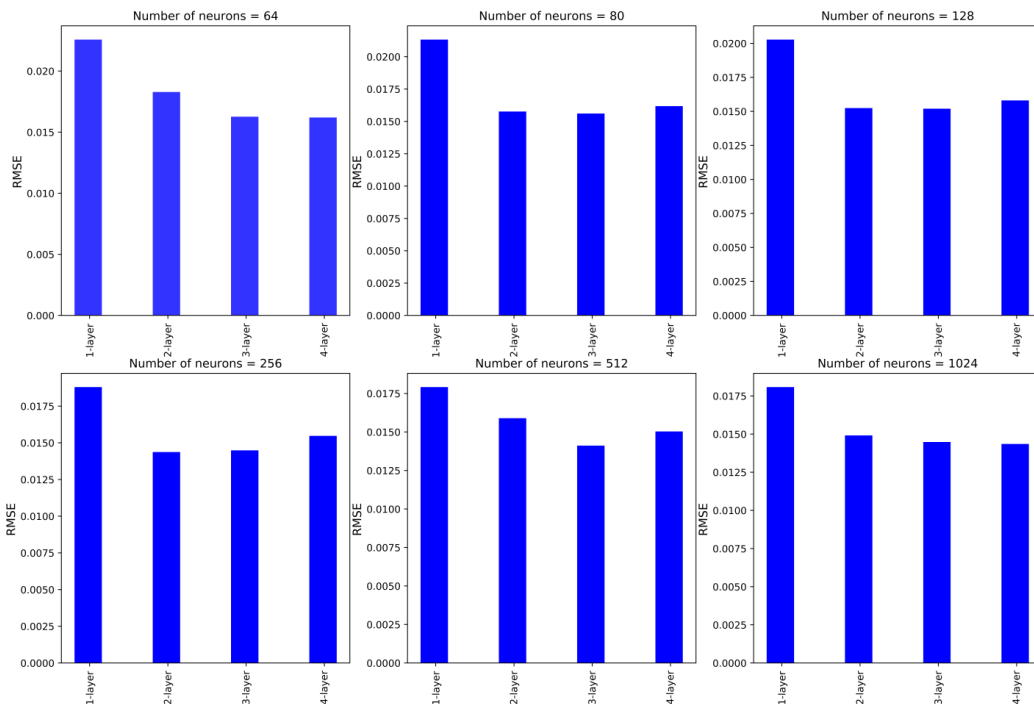


Figure 6.6: A comparison of all examined ANN models.

Based on the evaluated architecture models, the following observations were made:

- The results show that RMSE decreased as the number of layers increased. However, there was no significant decrease between the performance of three-layer and four-layer networks.
- Out of the networks that used 64 neurons in each layer, the RMSE decreased as the network depth increased, as shown in the above figure, and the best RMSE was 0.016198.
- For networks that had 1,024 neurons in each layer, the RMSE also decreased. However, the best RMSE was lower than that of the 64-neuron networks, which was 0.014350.

## **CHAPTER 6: DEVELOPMENT OF A SURROGATE MODEL FOR ADAPTIVE FAÇADE PERFORMANCE IN THE EARLY DESIGN STAGES**

- This decrease was expected since the representation capabilities of the neural networks also increased as the number of layers increased.
- For the 80-neuron networks, the best RMSE was 0.015605 for three-layer networks. For 128-neuron networks, it was 0.015195 for three layers. For 256-neuron networks, it was 0.014368 for two layers. For 512-neuron networks, it was 0.014109 for three layers.
- Based on the previous observation, it can be seen that for most of the investigated cases, the RMSE value of a four-layer network was slightly higher than for its three-layer counterparts.
- The results concluded that the three-layer network was the most suitable architecture, since selecting higher layers may result in overfitting.

To that end, the architecture that was considered was the three hidden layer neural network with 512 neurons in each layer. For all experimented models, the learning rate was 0.01, the number of epochs was 60, and the batch size was 8,000.

### **6.4.3.2. Learning Rate**

As the learning rate influences the outcome of the ANN model, thus, multiple values should be considered to get the best accuracy learning rate as shown in Table (6.3). The results of this analysis indicate that when specifying a lower learning rate, the RMSE resulted in a very high value, which was 0.091769. Hence, this implies that this value of the learning rate is unsuitable for neural network modelling. As a result, the updated weights did not occur in the desired amount, and learning was stagnant. As the learning rate value increased slightly at 0.0001, the RMSE significantly improved to 0.020789. The above two values show the significance of carefully choosing the value of the learning rate. It was again further reduced as the rate was decreased. The learning rate was fixed as 0.01, and the network used was a three-layer network with 512 neurons, the number of epochs was 60, and the batch size was 8,000.

*Table 6.3. Different values of learning rate.*

| <b>Learning rate</b> | <b>RMSE</b> |
|----------------------|-------------|
| 0.00001              | 0.091769    |
| 0.0001               | 0.020789    |
| 0.001                | 0.011144    |
| 0.01                 | 0.011000    |

### **6.4.3.3. Number of Epochs**

Once it had been decided that the learning rate was to be fixed as 0.01, this analysis was done by varying the number of epochs as shown in Table (6.4). The network used for this



## **CHAPTER 6: DEVELOPMENT OF A SURROGATE MODEL FOR ADAPTIVE FAÇADE PERFORMANCE IN THE EARLY DESIGN STAGES**

analysis was a three-layer network with 512 neurons, the learning rate was 0.01, and the batch size was 8,000. The results obtained when varying the number of epochs reveal that after epoch 60, there was no significant improvement in the RMSE value. When selecting a value of 100 and 200 for the number of epochs, there was no change in the RMSE. In the case of 300 epochs, the RMSE difference was extremely negligible. Therefore, based on this experiment, the number of epochs was fixed as 100.

*Table 6.4. Variations of the number of epochs.*

| Number of epochs | RMSE     |
|------------------|----------|
| 60               | 0.011189 |
| 100              | 0.011185 |
| 200              | 0.011185 |
| 300              | 0.011186 |

### **6.4.3.4. Batch Size**

The analysis considered various batch sizes for training the data, as listed in Table (6.5). The network used for this analysis was a three-layer network with 512 neurons, the learning rate was 0.01, and the number of epochs was 100. The learning rate was high for the lowest batch size, and the time taken to run the program was also very high. As the batch size increased, there was no significant improvement in the RMSE, but there was a reduction in the runtime. The runtime after a limit of batch size was mostly the same, which can be attributed to the computing powers of the GPU and other related hardware used. Mostly, the values were in the range 0.010 to 0.012. Thus, considering this in addition to the running time, the batch size was fixed as 16,000.

*Table 6.5. Different batch sizes used in the analysis.*

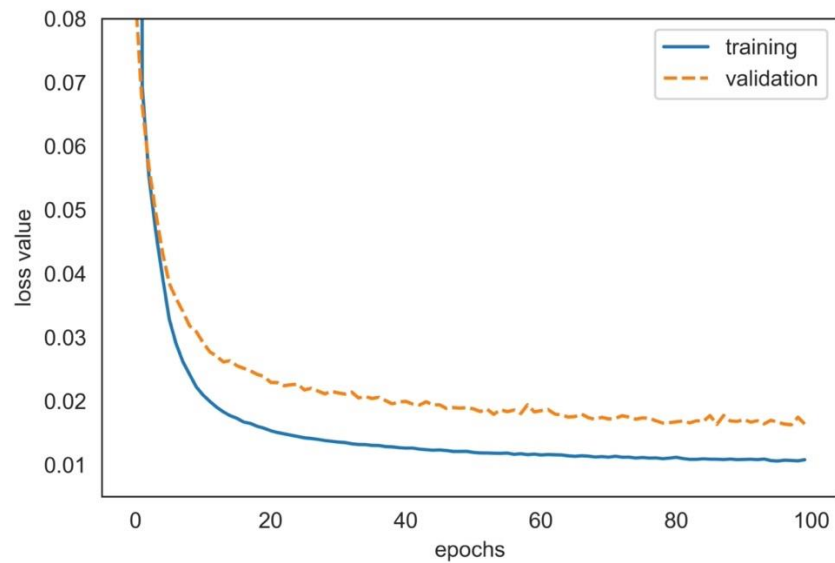
| Batch size | RMSE     | Time taken |
|------------|----------|------------|
| 100        | 0.013214 | 6h 40m     |
| 500        | 0.011034 | 1h 37m     |
| 1000       | 0.010987 | 1h 23m     |
| 2000       | 0.011362 | 1h 08m     |
| 4000       | 0.011864 | 1h 05m     |
| 8000       | 0.011426 | 1h 04m     |
| 16000      | 0.010929 | 1h 02m     |
| 32000      | 0.011134 | 0h 59m     |

### **6.4.3.5. Results of Hyperparameters**

In this experiment with neural networks modelling, the best result was obtained with a three-layer network with 512 neurons in each layer with an RMSE value of 0.010929. The learning rate was 0.01, the number of epochs 100, and the batch size 16,000. The training loss and validation loss of the developed network is plotted in Figure (6.7). The Figure illustrates that the training loss starting from 0.63 decreased steeply to less than 0.01 in the first few iterations. This indicates that the neural network had learned in the desired way.

## **CHAPTER 6: DEVELOPMENT OF A SURROGATE MODEL FOR ADAPTIVE FAÇADE PERFORMANCE IN THE EARLY DESIGN STAGES**

From iteration 15 onwards, the rate of decrease in the loss was very low. Similarly, the validation loss started slowly decreased as the epochs proceeded.



*Figure 6.7: Training and validation loss against epochs.*

### **6.4.4. K-fold Cross Validation**

The purpose of the initial experiment was to determine the appropriate range of parameter values, such as learning rate, batch size, and number of epochs. This section investigates K-fold cross validation as a novel method for improving the accuracy prediction of an ANN model. As mentioned in the literature, K-fold cross validation has the ability to train on multiple train-test splits and provide more accurate approximations of generalization. However, it requires more computational power and time for training.

As the K-fold cross validation consumes time and requires computational power, the study considered only the architecture of the ANN for fine-tuning. As stated by Keshtkarbanaeemoghadam et al. (2018), ANN models are significantly dependent on the architectures of the network. Other parameters were obtained from first experiment in section (6.4.3), which include learning rate, batch-size, dropout rate, and number of epochs, as these parameters were already fixed in a previous experiment. For this experiment, the data were split into training, validation, and test sets. The models were tested using the training and validation data splits, and the selected model was tested with the test data. The test data were treated as unseen data and were not used for selecting the right architecture of ANN.

Initially, the whole dataset was split into training, validation, and testing sets: 80% of the data were assigned to the training set, 6.67% to the validation set, and the remaining 13.37% to the testing set. The k-fold cross validation was then conducted on the training

## **CHAPTER 6: DEVELOPMENT OF A SURROGATE MODEL FOR ADAPTIVE FAÇADE PERFORMANCE IN THE EARLY DESIGN STAGES**

fold, and the chosen value of  $k$  was 5. The data split procedure is graphically represented in Figure (6.8). During  $k$ -fold cross validation, one among the fold becomes the testing set, and the remaining ones become the training set. In this case, one-third of the testing case was reserved as a validation set for that particular instance of the validation procedure. For the cross-validation experiments, the learning rate was fixed at 0.01, the dropout rate at 0.2, and the batch size at 16,000. The experiments were run for 100 epochs with an early stopping criterion of 10 epochs.

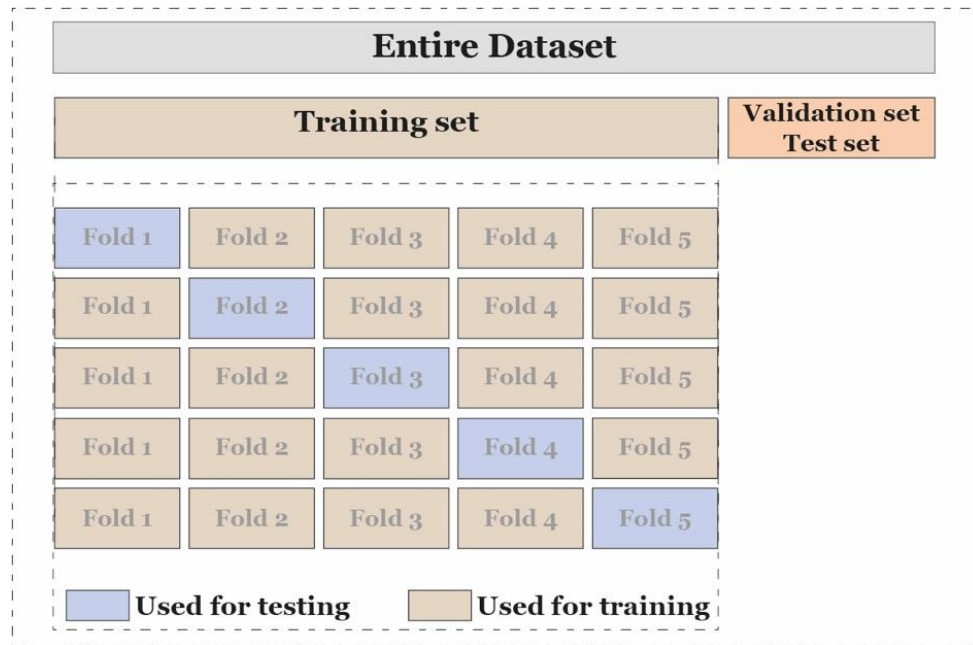


Figure 6.8: The data split procedure.

### **6.4.5. Optimization of Hyperparameters**

$K$ -fold cross validation was utilized to select the optimal architecture for the ANN in terms of the required number of layers and the number of neurons per layer. The experiment employed one-, two-, three-, and four-hidden layer network architectures. Each network was tested with 64, 128, 256, 512, and 1,024 neurons in each layer. The details of the experiment are presented in Table (6.6), and the following conclusions were drawn.

The results revealed that as the number of layers increased, the RMSE decreased. This was expected since the representation capabilities of the ANN also increased as the number of layers increased. However, there was a slight increase in the RMSE when it came to the three-layer network with 1,024 neurons and four-layer networks. A similar trend was also observed with the MAE and  $R^2$  scores. Hence, for the data modelling problem, the three-layer network was suitable, as considering a higher number of layers could result in overfitting Figure (6.9). The architecture selected after the five-fold cross validation experiment was a three-layer network with 256 neurons in each layer Figure (6.10).

**CHAPTER 6: DEVELOPMENT OF A SURROGATE MODEL FOR ADAPTIVE FAÇADE PERFORMANCE IN THE EARLY DESIGN STAGES**

Table 6.6. Architecture optimization of ANN by k-fold cross validation.

| Serial No. | No. of layers | No. of neurons in each layer | RMSE    | MAE      | R <sup>2</sup> |
|------------|---------------|------------------------------|---------|----------|----------------|
| 1          | 1             | 64                           | 0.02164 | 0.08616  | 0.6872         |
| 2          | 1             | 128                          | 0.01964 | 0.08144  | 0.716          |
| 3          | 1             | 256                          | 0.01898 | 0.0804   | 0.7254         |
| 4          | 1             | 512                          | 0.01842 | 0.07976  | 0.7334         |
| 5          | 1             | 1024                         | 0.01922 | 0.0835   | 0.7226         |
| 6          | 2             | 64                           | 0.01658 | 0.07134  | 0.7606         |
| 7          | 2             | 128                          | 0.01528 | 0.06708  | 0.7798         |
| 8          | 2             | 256                          | 0.01524 | 0.06716  | 0.7794         |
| 9          | 2             | 512                          | 0.01626 | 0.07186  | 0.7646         |
| 10         | 2             | 1024                         | 0.01784 | 0.0808   | 0.7426         |
| 11         | 3             | 64                           | 0.01705 | 0.07238  | 0.7549         |
| 12         | 3             | 128                          | 0.01520 | 0.067586 | 0.7816         |
| 13         | 3             | 256                          | 0.01509 | 0.06596  | 0.7832         |
| 14         | 3             | 512                          | 0.0161  | 0.07155  | 0.7686         |
| 15         | 3             | 1024                         | 0.02275 | 0.09761  | 0.6729         |
| 16         | 4             | 64                           | 0.01708 | 0.072567 | 0.7546         |
| 17         | 4             | 128                          | 0.01539 | 0.06675  | 0.7789         |
| 18         | 4             | 256                          | 0.01559 | 0.06779  | 0.7759         |
| 19         | 4             | 512                          | 0.01754 | 0.07589  | 0.7841         |
| 20         | 4             | 1024                         | 0.01807 | 0.07878  | 0.7403         |

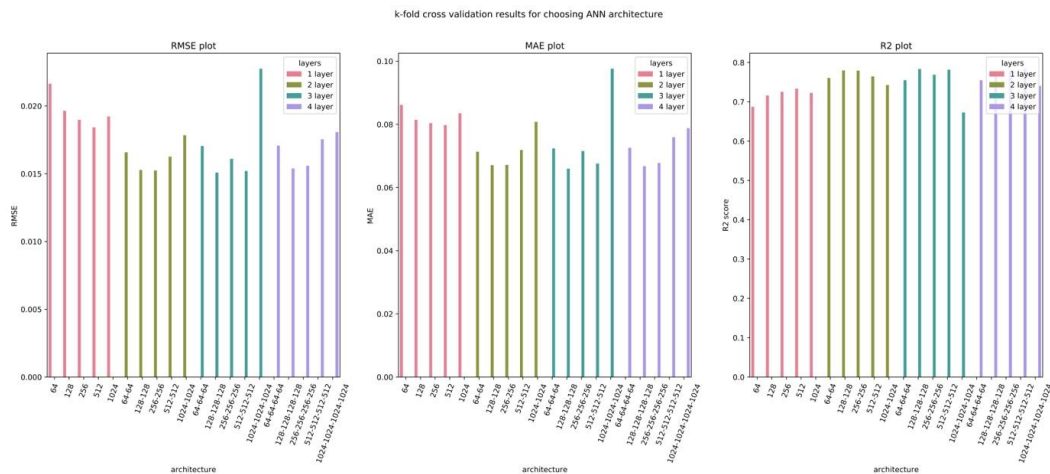


Figure 6.9: k-fold cross validation results for choosing the architecture

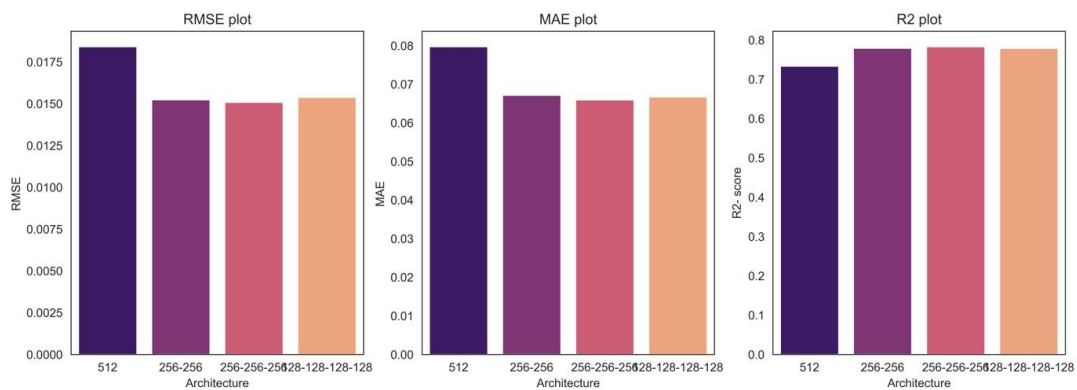


Figure 6.10: The performance metric comparison of best performing model among one-, two-, three-, and four-layer networks

### 6.4.6. Testing the Architecture

The three-layer network with 256 neurons in each layer, which was selected through k-fold cross validation, was applied with the validation set and test set. For this purpose, a new model was built using the entire training set. This model was tested with the test set. The results obtained are as follows: RMSE=0.011415, MAE=0.052188, and  $R^2$  score=0.831315. For the experiment, the learning rate used was 0.01, the dropout rate was 0.2, the number of epochs was 100, and the batch size was 16,000. Figure (6.11) shows a sample of the hourly solar radiation prediction using ANN for a set of 25 coordinates to test the model.

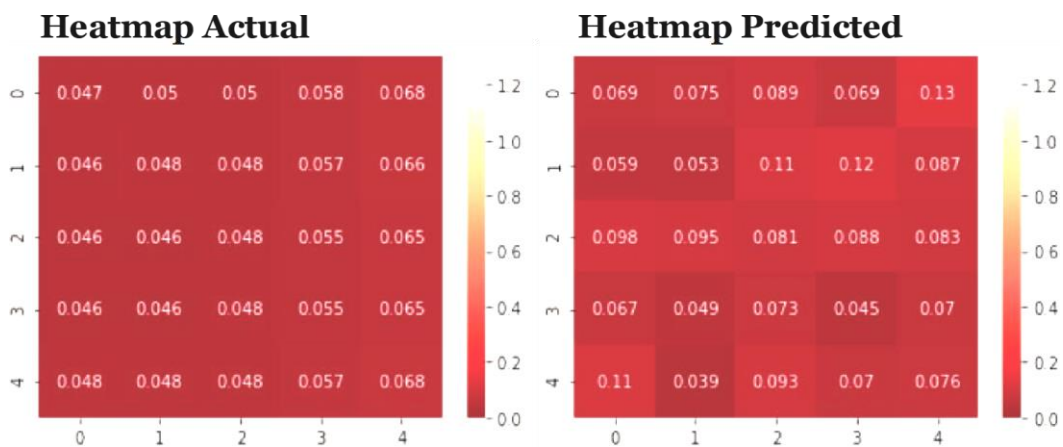
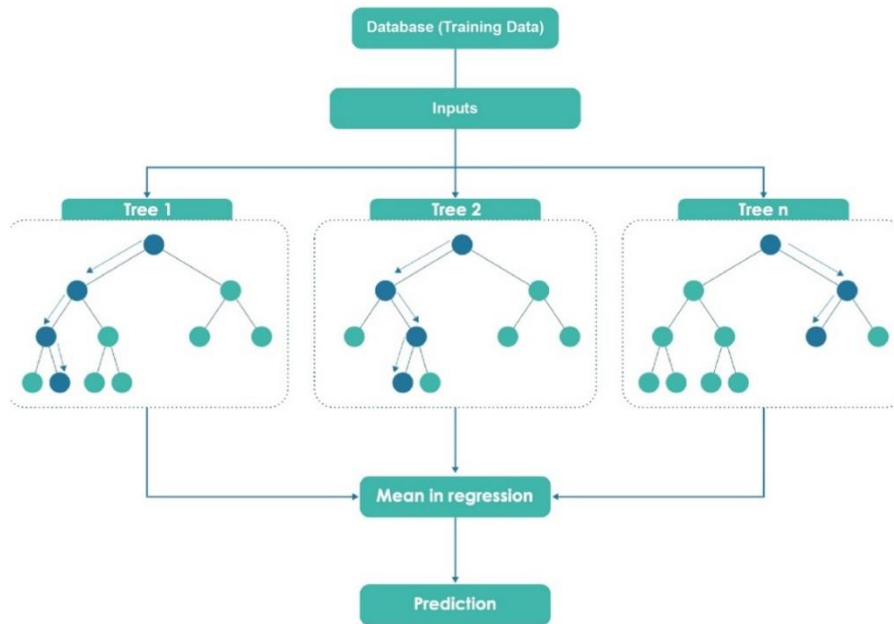


Figure 6.11: The actual and predicted solar radiation values by ANN for a set of 25 coordinates.

## 6.5. Random Forest Model Development

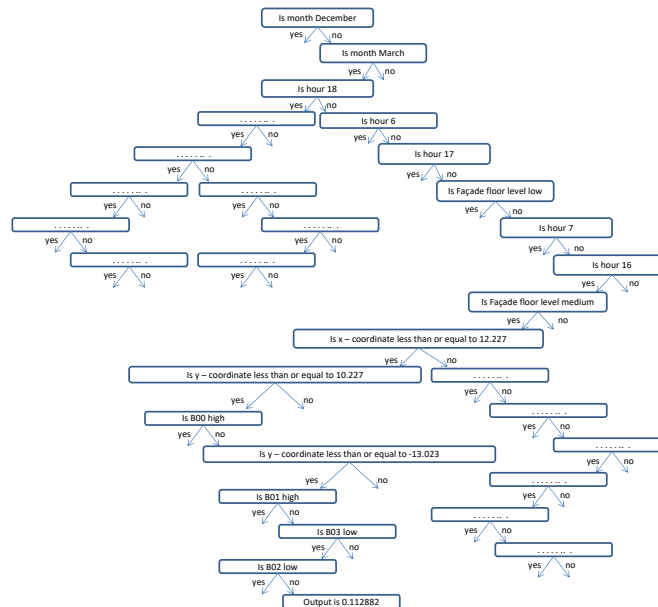
Random forest (RF) is an advancement of DT and the model used in the form of regression learning. RF algorithms were employed as another ML algorithm to compare the prediction accuracy with that of the ANN model output. Figure (6.12, top) illustrates the modelling of RF and how the decision is made in RF algorithms Figure (6.12, down). In terms of input features, the same data as were discussed in section (6.3) which underwent pre-processing as a preparation for ANN modelling were employed in this section. The output was the solar radiation of the corresponding location. Similarly with ANN modelling and to allow comparison, the performance of the network was evaluated with the RMSE, MAE, and  $R^2$  scores.

**CHAPTER 6: DEVELOPMENT OF A SURROGATE MODEL FOR ADAPTIVE FAÇADE PERFORMANCE IN THE EARLY DESIGN STAGES**



A testing case :

|                     |          |
|---------------------|----------|
| Hours               | 16       |
| B00                 | Medium   |
| B01                 | Low      |
| B02                 | High     |
| B03                 | Low      |
| Month               | March    |
| Façade Floor Level  | Medium   |
| Orientation         | 0        |
| Façade Level Height | 24       |
| x - coordinate      | -1       |
| y - coordinate      | -13.0319 |
| z - coordinate      | 24.39999 |
| solar radiation     | 0.108169 |



Predicted output: 0.112882

Figure 6.12: The modelling of RF (top), and how the decision is made in the decision tree algorithm (down).

**6.5.1. Optimization of Hyperparameters**

Optimization of the hyperparameters for RF was performed in a grid structure approach with respect to the following parameters: bootstrap, minimal cost-complexity pruning, and number of trees. These are discussed in more detail below.

**6.5.1.1. Bootstrap**

Bootstrap is a process of random sampling from the training data. In bootstrap, the training data are selected with a uniform probability of replacement. In each time, a data point is

## **CHAPTER 6: DEVELOPMENT OF A SURROGATE MODEL FOR ADAPTIVE FAÇADE PERFORMANCE IN THE EARLY DESIGN STAGES**

selected; it is equally likely to be selected again and re-added to the training set. This procedure helps reduce the high variance of the RF models and prevents them from overfitting (Breiman 2001). If the bootstrap option is not enabled, the RF is learned using the whole dataset. The experiment was done with and without the bootstrap option enabled, and the results are recorded in Table (6.7). The number of trees used for the experiments was 30, and the minimal cost-complexity pruning parameter was 0.0. From the experiments, it can be observed that the bootstrap sampling option helped to reduce the RMSE to a significant level.

*Table 6.7. Experiments using bootstrap.*

| <b>Bootstrap</b> | <b>RMSE</b> |
|------------------|-------------|
| Enabled          | 0.000342    |
| Disabled         | 0.000447    |

### **6.5.1.2. Minimal Cost-Complexity Pruning**

Tree pruning is a procedure to avoid overfitting in RF models. In the pruning technique, the trees are not allowed to grow beyond a predetermined depth. The minimal cost complexity pruning is a pruning technique proposed in a study by Dietterich (2000a). This experiment was done by varying the pruning hyperparameter  $\alpha$  in the set [0, 0.001, 0.002, 0.003, 0.004, 0.005] Table (6.8). The experiments were done with a split 80/20, the number of trees was 30, and the bootstrap option was enabled. The experimental observation indicates that there is no significant difference in applying pruning to the default setting of no pruning ( $\alpha = 0$ ). Therefore, it can be concluded that the data were not overfitting the RF model.

*Table 6.8. Experiments using various hyperparameters of  $\alpha$ .*

| <b>Value of <math>\alpha</math></b> | <b>RMSE</b> |
|-------------------------------------|-------------|
| 0.000                               | 0.000342    |
| 0.001                               | 0.000351    |
| 0.002                               | 0.000344    |
| 0.003                               | 0.000366    |
| 0.004                               | 0.000360    |
| 0.005                               | 0.000349    |

### **6.5.1.3. Number of Trees**

The number of trees indicates the number of individual decision tree estimators used in the random forest algorithm. The experiment was carried out considering different numbers of trees starting from a value of 10 trees, then adding more in sequence as follows (10, 20, 30, 40, 50, 60, 70, 80, 90, 100) as shown in Table (6.9). The results show that the RMSE decreased until it reached the value of 30 for the number of trees. The lowest value achieved was for 30 trees, for which the RMSE result was 0.000306. Then, the results show that as the value for the number of trees increased, the corresponding RMSE values showed

## **CHAPTER 6: DEVELOPMENT OF A SURROGATE MODEL FOR ADAPTIVE FAÇADE PERFORMANCE IN THE EARLY DESIGN STAGES**

a slightly increasing trend. Thus, based on these experiments, the number of trees was fixed as 30.

*Table 6.9. Experiments using different number of trees.*

| Split | RMSE     |
|-------|----------|
| 10    | 0.000451 |
| 20    | 0.000431 |
| 30    | 0.000306 |
| 40    | 0.000439 |
| 50    | 0.000433 |
| 60    | 0.000449 |
| 70    | 0.000321 |
| 80    | 0.000338 |
| 90    | 0.000371 |
| 100   | 0.000327 |

### **6.5.2. K-fold Cross Validation**

To find the proper values for the hyperparameters, an experiment was conducted similar to the one described in Section (6.2.6). A five-fold cross validation was applied on the training set alone to fix the hyperparameters. To test the model in the testing set, a model was built using the entire training set whose hyperparameters were those fixed by the k-fold cross validation.

### **6.5.3. Optimization of Hyper parameters**

For the K-fold cross validation, the selected hyperparameters include (1) number of trees, (2) bootstrap, and (3) minimal cost-complexity pruning parameters. The results of the k-fold cross validation are shown in Table (6.10). The results showed that there was no significant variation in the RMSE value as the number of trees increased as shown in Figure (6.13). The best performance was observed with a ccp-alpha value of 0.0 regardless of the number of trees and the bootstrap option. When a non-zero value was specified, there was a greater drop in the performance. The performance when the bootstrap option was enabled was better than with the models where it was disabled. The best result was observed when the number of trees was 80, the ccp-alpha value was 0, and the bootstrap option was enabled. In this setting, the RMSE value was 0.000354, the MAE was 0.00457, and the  $R^2$  score was 0.993 Figure (6.14). To that end, the final model was built with the above specified hyperparameters. The final test results were as follows: the RMSE was 0.000514, the MAE was 0.00661, and the  $R^2$  score was 0.99228. Figure (6.15) illustrates a sample of the solar radiation prediction using RF for a set of 25 coordinates to test the model.



**CHAPTER 6: DEVELOPMENT OF A SURROGATE MODEL FOR ADAPTIVE FAÇADE PERFORMANCE IN THE EARLY DESIGN STAGES**

Table 6.10. The k-fold cross validation results for RF.

| SI No. | Trees | RMSE     | MAE      | R <sup>2</sup> -score |
|--------|-------|----------|----------|-----------------------|
| 1      | 10    | 3.52E-04 | 4.42E-03 | 9.92E-01              |
| 2      | 20    | 3.48E-04 | 4.41E-03 | 9.93E-01              |
| 3      | 30    | 3.48E-04 | 4.40E-03 | 9.95E-01              |
| 4      | 40    | 3.48E-04 | 4.39E-03 | 9.95E-01              |
| 5      | 50    | 3.45E-04 | 4.40E-03 | 9.95E-01              |
| 5      | 60    | 3.52E-04 | 4.48E-03 | 9.94E-01              |
| 7      | 70    | 3.45E-04 | 4.39E-03 | 9.92E-01              |
| 8      | 80    | 3.54E-04 | 4.57E-03 | 9.93E-01              |
| 9      | 90    | 3.41E-04 | 4.38E-03 | 9.95E-01              |
| 10     | 100   | 3.50E-04 | 4.40E-03 | 9.95E-01              |

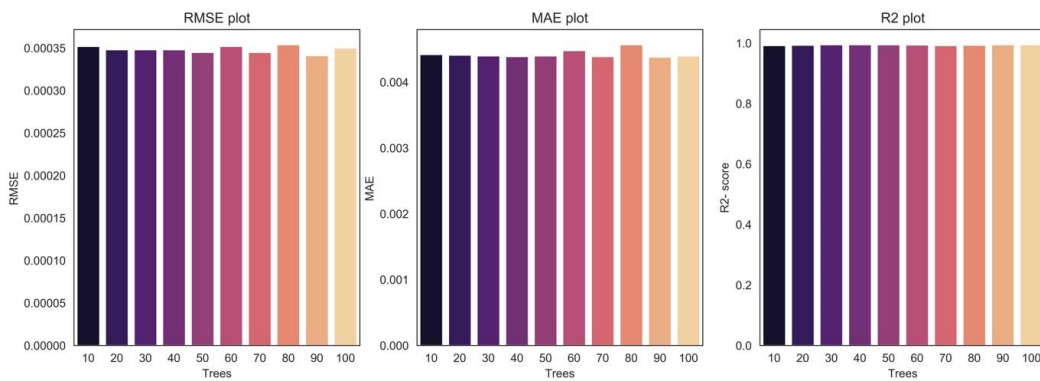


Figure 6.13: The performance metric visualization for the best model when the number of trees is considered.

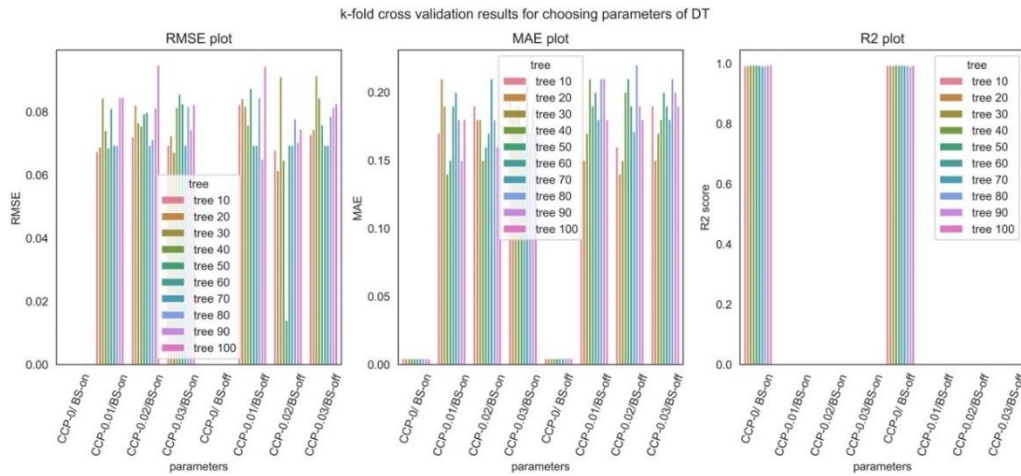


Figure 6.14: The result visualization of hyperparameter tuning in RF, CCP stands for the CCP alpha value chosen, and BS stands for bootstrap option.

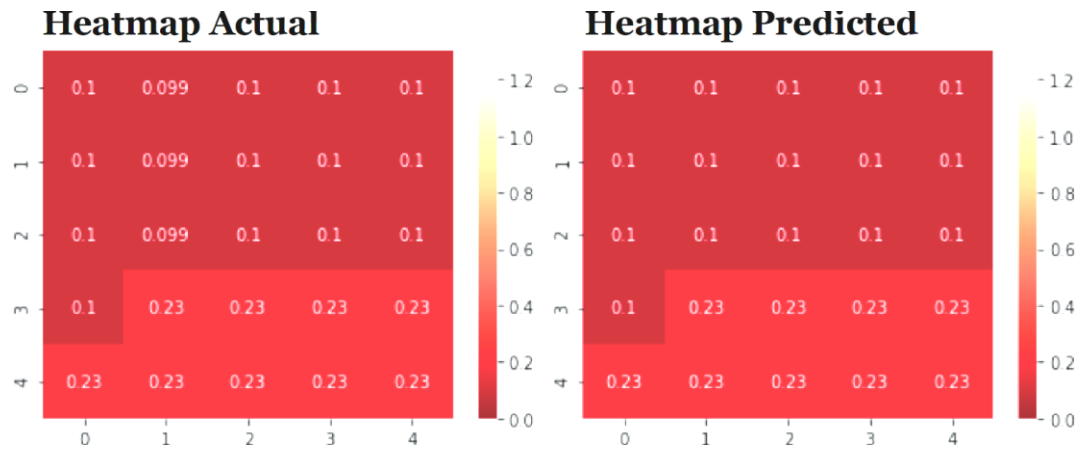


Figure 6.15: The actual and predicted solar radiation values by RF for a set of 25 coordinates plotted as a heatmap.

### 6.6. Comparison of ANN and RF

After the experiment with these different parameters, the best result achieved for the neural network in terms of RMSE was 0.011415 and for the RF was 0.000514. While both methods provided an acceptable level of accuracy, the performance by RF was significantly higher than that of ANN as given in Table (6.11). This is due to the following reasons:

- Most of the inputs were categorical; thus, this was a highly compatible learning scenario for the RF. Since the decision trees are highly suitable for categorical inputs in the learning setting, RF modelling has a significant advantage over neural network modelling.
- An RF is an ensemble algorithm. Ensemble algorithms are a class of ML algorithms where a set of learning programs are combined together to give accurate predictions (Dietterich 2000b). Instead of relying on a single algorithm, the predictions from such multiple algorithms are considered, and the error is reduced significantly. Since this feature is implicitly embedded with RF modelling, its performance was significantly better than that of neural networks in this case.
- The generalizability of either RF or ANN to a new modelling problem is dependent on the nature of the inputs and the modelling tasks. However, the study observed that if the input data were mostly categorical, the RF algorithm could perform better than an ANN.

Table 6.11. Performance comparison of ANN and RF for solar radiation data.

| Performance metric    | Neural network | Random Forest |
|-----------------------|----------------|---------------|
| RMSE                  | 0.011415       | 0.000514      |
| MAE                   | 0.052188       | 0.00661       |
| R <sup>2</sup> -score | 0.831315       | 0.99228       |

## 6.7. Cooling Loads Prediction Using Machine Learning

After confirming the suitability of ML techniques to predict hourly solar radiation in stage one, this section develops another surrogate model to predict the energy cooling loads of AF shading systems using the data generated through simulation. This chapter discusses an approach similar to that followed in phase one by developing two different ML learning algorithms, ANN and RF, for testing and comparing the cooling result accuracy. As mentioned in chapter 2 section (2.9), employing sufficient data is essential to achieve a highly accurate predictive ANN model that can predict the hourly cooling energy demand. For this purpose, 1,296 simulation iterations of an office room with AF with control scenario (C4) were performed by the Honeybee plugin in chapter (4), with various inputs to train the model. A total of 3,794,688 (1296 \* 4 months (122 days) \* 24 hours) items of hourly cooling energy data were recorded corresponding mainly to the variation of the AF system per hour together with other input parameters Figure (6.16). Cooling loads  $\text{KW/m}^2$  were generated as an output of the ANN model, and a total of thirteen variables were used as inputs as follows: hour, month, day, orientation, building 00, building 01, façade level height, glazing type U-value  $\text{W/m}^2\text{K}$ , exterior wall U-value  $\text{W/m}^2\text{K}$ , AF opening ratio, AF-SF, SR  $\text{W/m}^2$ , and OT. The input data feature and ranges of each input are illustrated in Table (6.12).

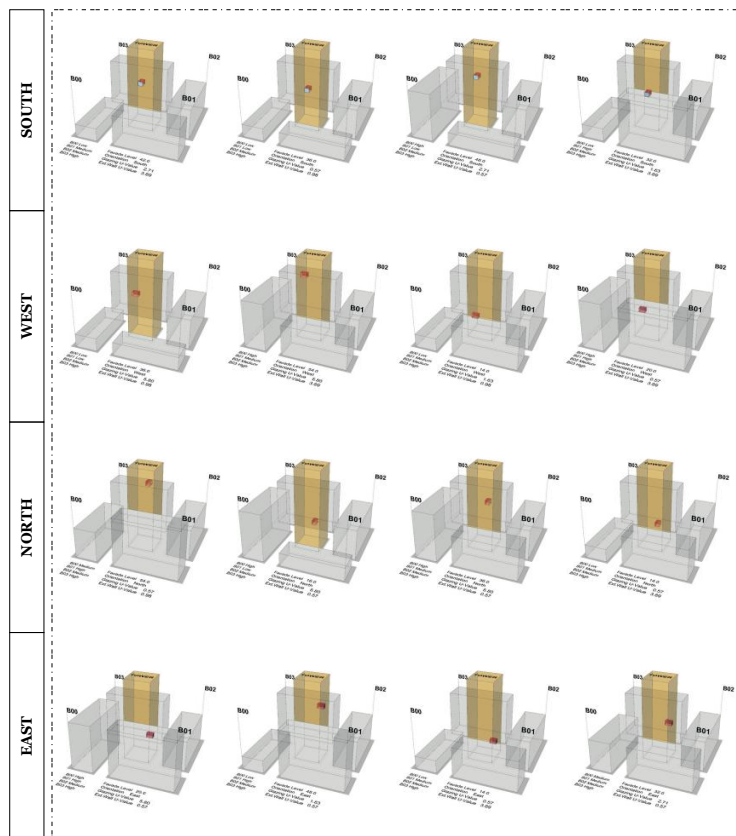


Figure 6.16: Sample of the data generated based on simulation.

**CHAPTER 6: DEVELOPMENT OF A SURROGATE MODEL FOR ADAPTIVE FAÇADE PERFORMANCE IN THE EARLY DESIGN STAGES**

Table 6.12. The input data used for the ANN modelling

| Input parameter               | Input neuron type | Data range   |
|-------------------------------|-------------------|--|
| Hour                          | Discrete          | (1, 2, ..., 24)  |
| Month                         | Discrete          | (0, 1, 2,3) (March, June, September, December)   |
| Day                           | Discrete          | (1, 2, ...,31)   |
| Orientation                   | Discrete          | (0, 1, 2, 3) – (South, West, North, East)  |
| Building 00                   | Discrete          | (0, 1, 2) – (Low, Medium, High)  |
| Building 01                   | Discrete          | (0, 1, 2) – (Low, Medium, High)  |
| Facade Level Height           | Continuous        | 8 - 60   |
| Glazing Type - U-value W/m2K  | Discrete          | (0,1,2,3) – (SingleG0, DBL-Glz001-Clear, DBL-Glz002-low-e coating, TripleGlz-Krypton Filled) |
| Exterior Wall - U-value W/m2K | Discrete          | (0,1,2)  |
| AF-Opening Ratio              | Continuous        | 0 - 1  |
| AF-Shade Factor               | Continuous        | 0 - 1  |
| Solar Radiation - W/m2        | Continuous        | 0 – 550  |
| Operative Temperature - C     | Continuous        | 14.00 – 30.00  |

The ANN was used for the ML modelling because of the universal approximation theorem. The theorem states that an ANN with one hidden layer can approximate any continuous function for inputs within a specific range. In other words, an ANN can find an approximation of a function to be learned from a set of inputs via a dataset. It is a network of different layers consisting of a set of basic computing units called neurons. Each neuron takes the input from the previous layer where the inputs are multiplied with weights Figure (6.17). The output of a neuron is a non-linear function of the linear combination of weighted inputs as shown in the figure (6.17) and described by the following equation. The data flow overview of the modelling process is described in Figure (6.18).

$$y = \sigma (x_1w_1 + x_2w_2 + x_3w_3)$$

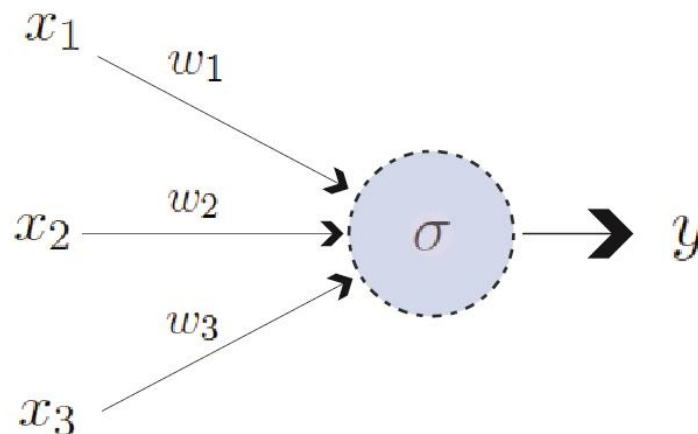


Figure 6.17: An artificial Neuron.

The non-linear function  $\sigma$  is called the activation function. In the experiments, the activation used was the ReLU, which is defined as follows:

$$\sigma(x) = \max(0, x).$$

**CHAPTER 6: DEVELOPMENT OF A SURROGATE MODEL FOR ADAPTIVE FAÇADE PERFORMANCE IN THE EARLY DESIGN STAGES**

The network architectures used were one-, two-, three-, and four-layer networks with 64, 128, 256, and 512 neurons. In the case of multilayer neural networks, the underlying equation can be written as follows:

$$y = \sigma \dots \sigma(\sigma(X_1 W_1)) W_2 \dots W_N$$

Here,  $X_1$  is the input matrix of dimensions  $n \times d$ ;  $n$  is the number of data points, and  $d$  is the dimension of the data.  $W_1$  is the weight matrix in the first layer of dimensions  $d \times d_1$ . Similarly,  $\sigma(X_1 W_1)$  forms the input for the second layer, and  $W_2$  is the weight matrix for the second layer and has the dimensions  $d_1 \times d_2$ .

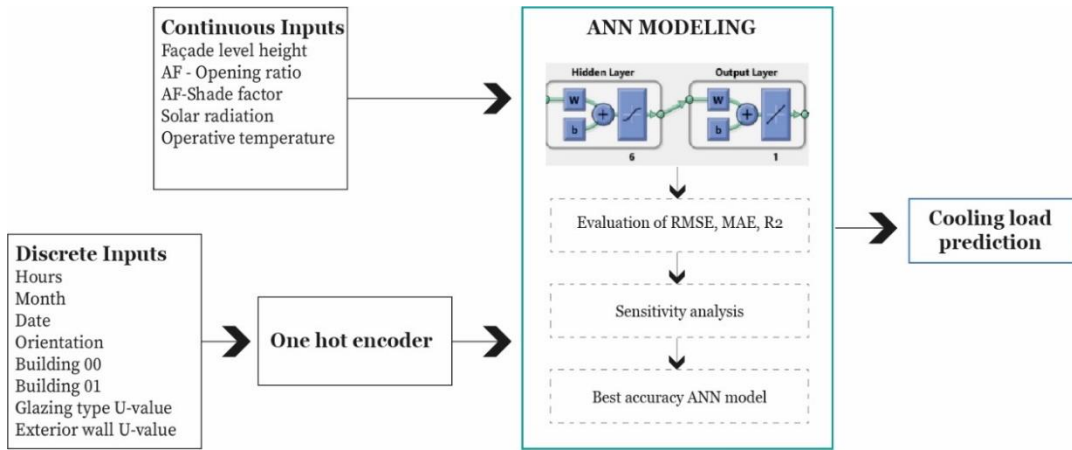


Figure 6.18: Data flow overview

The performance of the network was evaluated with the RMSE value, MAE, and  $R^2$  score. The performance metrics were calculated using the following formulae.

$$RMSE = \sqrt{\frac{1}{|y|} \sum_{i=1}^n (y_i - \hat{y}(i))^2}$$

$$MAE(y, \hat{y}) = \frac{1}{|y|} \sum_{i=1}^{|y|} |y(i) - \hat{y}(i)|$$

$$R^2(y, \hat{y}) = 1 - \frac{\sum_{i=1}^{|y|} (y(i) - \hat{y}(i))^2}{\sum_{i=1}^{|y|} (y(i) - \bar{y})^2}$$

In the above equation,  $y_i$  is the output of the  $i^{\text{th}}$  data point,  $\hat{y}(i)$  is the predicted value of the  $i^{\text{th}}$  data point, and  $\bar{y}$  is the mean of  $y$ . Here,  $\hat{y}(\cdot)$  is the function approximated by the NN, and it is assumed that there are  $|y|$  number of prediction cases.

The RMSE value describes the square of the difference between the actual cooling load values and the predicted ones. On the other hand, the MAE describes the absolute value of the difference between the two. The difference is also known as the residual. Both the values can take any value greater than zero, and a model is said to be performing well when both the values are as low as possible.

## **CHAPTER 6: DEVELOPMENT OF A SURROGATE MODEL FOR ADAPTIVE FAÇADE PERFORMANCE IN THE EARLY DESIGN STAGES**

The  $R^2$ -value evaluates the scatter of the predicted values around the regression line. In statistics, it is also called the coefficient of determination. It is defined as the ratio of variance explained by the model to the total variance.

### **6.8. Data Pre-processing**

The discrete inputs used for the modelling were hour, month, date, orientation, building 00, building 01, glazing type U-value, and exterior wall U-value. These inputs were first one-hot encoded. One-hot encoding is a mechanism to represent categorical variables as a mathematical vector that contains zeros and ones (Seger 2018). The vector will have a dimension equal to the number of possible values it can take. One is given for the coordinate corresponding to the value taken by the variable, and the remaining coordinates will be zero.

For example, if a variable takes values of either high, medium, or low, high is represented as [1, 0, 0], medium is represented as [0, 1, 0], and low is represented as [0, 0, 1]. The one-hot encoded categorical features are fed into an embedding layer. In this layer, the one-hot encoded vector already created will again be changed to another meaning vector rather than using it in its original form of just ones and zeros. This approach has been found to give greater representational power for the categorical inputs.

The continuous inputs used for the modelling were façade level height, AF (opening percentage), AF-SF, SR, and OT. These inputs were fed into the batch normalizing layer (Ioffe and Szegedy 2016). Then, the data were fed into the ANN in batches. Since the network was not fed with the entire dataset, the data distribution tended to vary, as each batch was processed. This caused some instability with the learning process. To rectify this effect, batch normalization was introduced. It standardized the input in the form of batches that had been fed to the ANN layers. It helped to stabilize the learning process and reduced the number of epochs required to train the networks.

### **6.9. ANN Model Development**

This section describes the ANN model development process for predicting the cooling loads. Several ANN models were examined and trained based on the data obtained from simulation Figure (6.19). In addition to determining the optimum ANN model, a hyperparameter optimization method was performed considering the following parameters: the architecture of the model, the data split ratio, the learning rate, the batch size, and the number of epochs. Implementation of the network was done using the PyTorch framework (Paszke et al. 2019). The dropout rate used for the experiment was 0.5 (Srivastava et al.

**CHAPTER 6: DEVELOPMENT OF A SURROGATE MODEL FOR ADAPTIVE FAÇADE PERFORMANCE IN THE EARLY DESIGN STAGES**

2016). The hardware used was Intel Xeon E5-2630 CPU, 80 GB RAM, and Nvidia GeForce GTX 1080-Ti GPU. In the algorithm, first, a feedforward passing was performed with each item of the data, the prediction was calculated, and then the weights of the layers were updated by propagating the errors backwards from the output layer to the input layer. The data may be applied in stochastic or batch mode, and the optimization algorithm used was the gradient descent. The weights of the layers were initialized using the Kaiming initialization method (Kaiming et al. 2015). The ANN components and operations used in the experiments are shown in Figure (6.20).

The experiment of hyperparameter tuning was carried out using two different procedures to find the optimum hyperparameters of the ANN model. The first one was a systematic parameter tuning procedure to find the optimal architecture, learning rate, batch size, and number of epochs. The second one was a k-fold cross validation technique to tune the architecture.

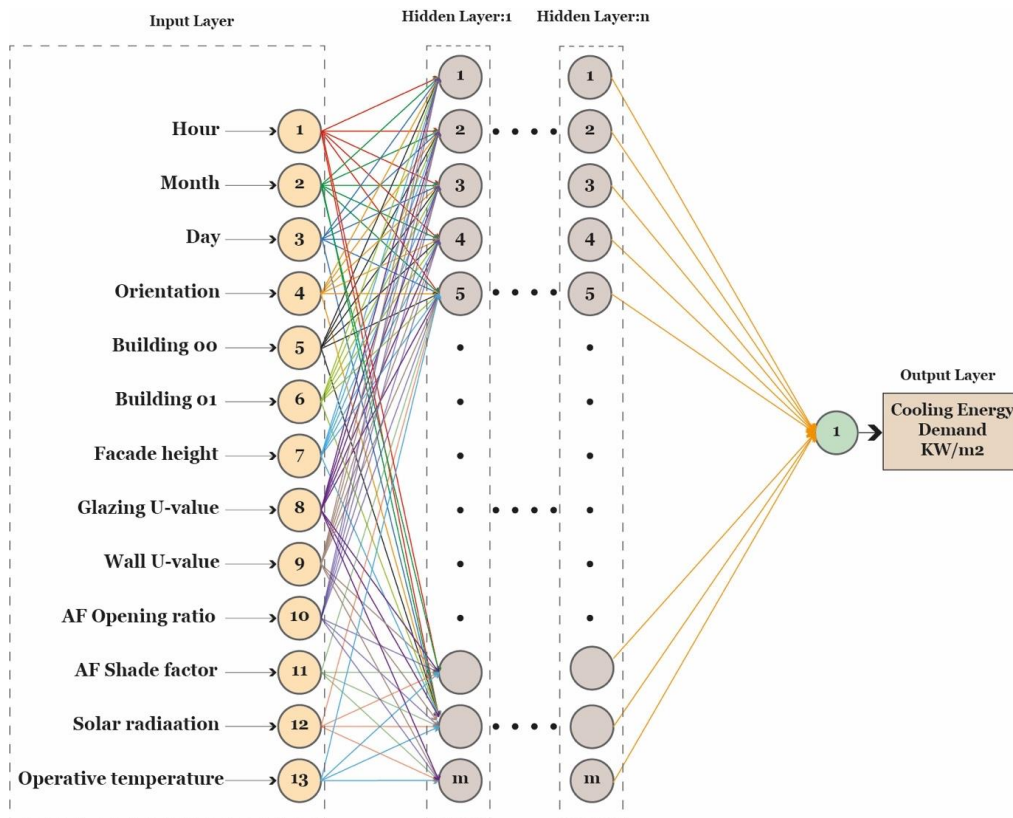


Figure 6.19: Architecture of the ANN model.

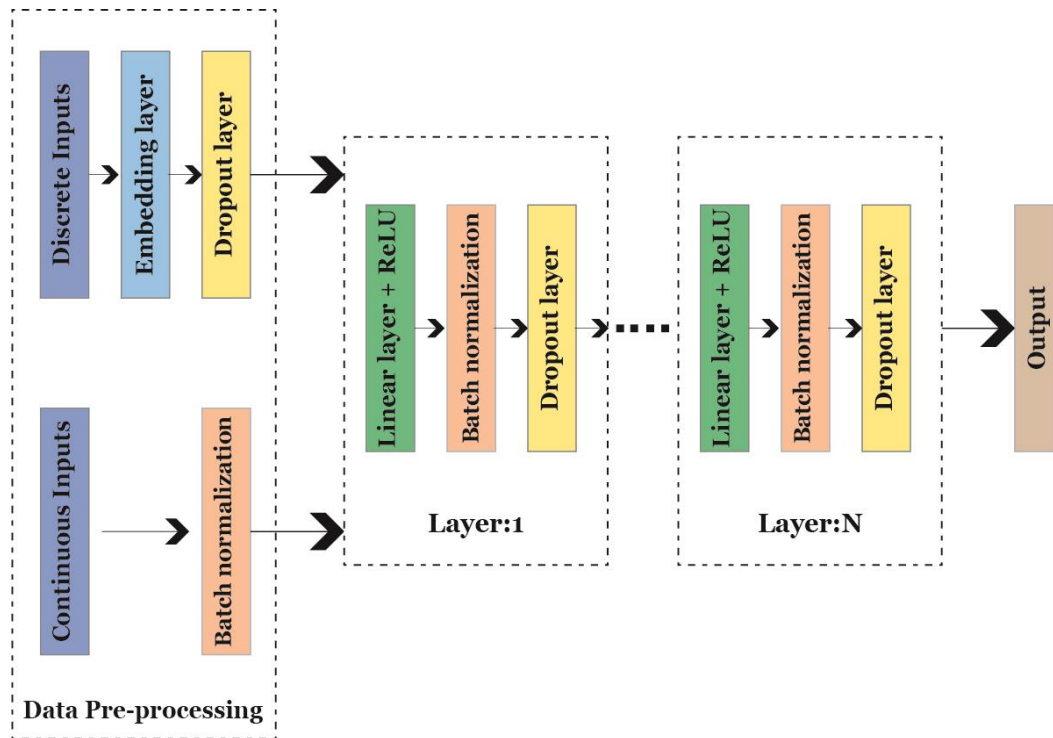


Figure 6.20: ANN components.

The operations inside the layers are as follow:

a) **Linear layer + ReLU:**

The input to the network was given to a dense or linear layer. For the non-linear activation of the inputs in the neurons in the linear layer, the ReLU function defined as  $f(x) = \max(0, x)$  was used.

b) **Batch normalization:**

The output of ReLU was batch normalized. Batch normalization concepts were discussed in the previous section.

c) **Dropout regularization:**

Dropout is a mechanism to ensure the generalizability of the network by avoiding overfitting. It is the process of disabling certain neurons randomly so that the learning process becomes robust, and dependency on specific neurons will be decreased. The percentage of neurons to be disabled is treated as a hyperparameter; it was taken as 0.5 out of 1 in the experiments.

d) **Output of the network:**

The output of the network was a neuron without any activation function, that is, the input of the neuron was multiplied by the weight, and no further processing was done.



## **CHAPTER 6: DEVELOPMENT OF A SURROGATE MODEL FOR ADAPTIVE FAÇADE PERFORMANCE IN THE EARLY DESIGN STAGES**

### **6.9.1. Optimization of Hyperparameters (Grid-Structure)**

The training dataset was used for developing the model, while the testing dataset was used to evaluate the model performance. The training and testing set split was done in the ratio of 0.8, that is, 80% of the data were assigned to the training set and 20% to the testing set. The optimization of the hyperparameters was carried out considering the architecture of the network, learning rate, batch size, and epochs.

#### **6.9.1.1. Architecture of the Neural Network**

ANN can have a different number of layers where each layer can have a different number of neurons. Choosing an appropriate network is important to avoid the under-fitting and overfitting of the data and for better generalization of the network to be used in the unseen future data. To achieve this, the experiment started with a one-layer network, and numbers of neurons were added to it in steps. Firstly, 32 neurons were given, then 64, and then 128. Next, the experiment was repeated for two-layer and three-layer networks. The models used in the experiment and the corresponding RMSE are given in Table (6.13).

*Table 6.13. Experiments using different ANN architecture.*

| <b>Serial No.</b> | <b>No. of layers</b> | <b>No. of neurons in each layer</b> | <b>RMSE</b> | <b>MAE</b>  | <b>R<sup>2</sup> score</b> |
|-------------------|----------------------|-------------------------------------|-------------|-------------|----------------------------|
| 1                 | 1                    | 64                                  | 0.000269399 | 0.011253547 | 0.758151442                |
| 2                 | 1                    | 128                                 | 0.000253705 | 0.011068318 | 0.772240334                |
| 3                 | 1                    | 256                                 | 0.000240284 | 0.010677113 | 0.784288583                |
| 4                 | 1                    | 512                                 | 0.000283188 | 0.012195355 | 0.745772501                |
| 5                 | 2                    | 64                                  | 0.000194905 | 0.009196877 | 0.825026787                |
| 6                 | 2                    | 128                                 | 0.000166843 | 0.008723773 | 0.850219593                |
| 7                 | 2                    | 256                                 | 0.000175501 | 0.008926978 | 0.842446943                |
| 8                 | 2                    | 512                                 | 0.000958364 | 0.024877253 | 0.139643104                |
| 9                 | 3                    | 64                                  | 0.000194224 | 0.009385868 | 0.825638646                |
| 10                | 3                    | 128                                 | 0.000143462 | 0.007910841 | 0.871209485                |
| 11                | 3                    | 256                                 | 0.000417632 | 0.01416273  | 0.625077461                |
| 12                | 3                    | 512                                 | 0.001052363 | 0.026886282 | 0.055257404                |
| 13                | 4                    | 64                                  | 0.000182201 | 0.008812156 | 0.836432209                |
| 14                | 4                    | 128                                 | 0.000152965 | 0.00791995  | 0.862677845                |
| 15                | 4                    | 256                                 | 0.000750953 | 0.021309711 | 0.325843067                |
| 16                | 4                    | 512                                 | 0.000470598 | 0.015197082 | 0.57752796                 |

The results are graphically represented as shown in Figure (6.21). From the figure, the following observation were drawn.

- The performance score varied drastically for deeper networks with a large number of neurons (256 and 512), and the performance was low compared to other shallow networks. For example, for networks with three to four layers

**CHAPTER 6: DEVELOPMENT OF A SURROGATE MODEL FOR ADAPTIVE FAÇADE PERFORMANCE IN THE EARLY DESIGN STAGES**

with 256 neurons, the RMSE was 0.000417632 and 0.000750953 respectively while on the other hand, for one- to two-layer-networks, it was 0.000240284 and 0.000175501 respectively. A similar trend could be observed with models containing 512 neurons.

- On the other hand, the performance of deeper networks with a lower number of neurons (64 and 128) was comparatively better than the previous case. For example, for 64 neurons, the RMSEs were 0.000269399, 0.000194905, 0.000194224, and 0.000182201 for networks one, two, three, and four layers respectively.

The results show that the performance was increasing up to three-layer networks. Then, when four-layer networks were selected, the performance dropped. The best result achieved was for the three-layer network with 128 neurons on each layer as shown in Figure (6.22). Thus, based on the experiments, the architecture chosen was a three-layer neural network with 128 neurons. For all these experiments, the train/test ratio of the data used was 80/20%, the learning rate was 0.01, the number of epochs was 60, and the batch size was 25,000.

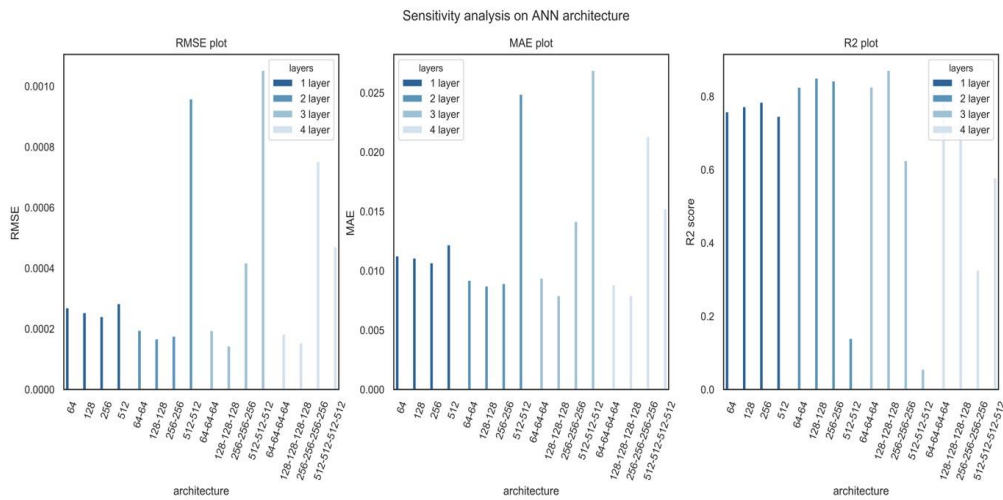


Figure 6.21: Results of sensitivity analysis on ANN architecture.

**CHAPTER 6: DEVELOPMENT OF A SURROGATE MODEL FOR ADAPTIVE FAÇADE PERFORMANCE IN THE EARLY DESIGN STAGES**

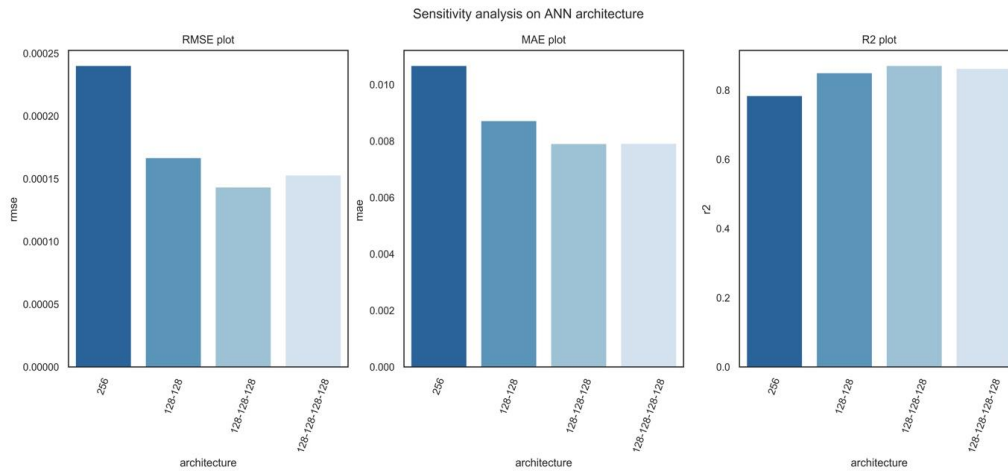


Figure 6.22: RMSE, MAE and R<sup>2</sup> score of the best performing models among the one-, two-, three- and four-layer networks.

**6.9.1.2. Learning Rate**

This parameter was used to adjust the network weights as part of the network's mathematical optimization. The details of the experiments are presented in Table (6.14) and visually represented in Figure (6.23). The experiments were done considering a value of 60 as the number of epochs. It can be seen from Table (6.14) that when the learning rate was lowest, the RMSE had a very high value, which was 0.001057556. This revealed that this value of the learning rate was too low for the neural network modelling, and a large number of epochs would be required to obtain the desired results. On the other hand, when the value increased to 0.001, the RMSE result significantly improved to 0.000496417. In addition, further reduction could be observed as the rate decreased. Therefore, these results indicate that consideration should be given while determining the value of the learning rate. To that end, the learning rate was fixed as 0.01, as it was the lowest RMSE of 0.000143462. For the experiments, the network used was a three-layer network with 128 neurons, the train/test split was 80/20, the number of epochs was 60, and the batch size was 25,000.

Table 6.14. Experiment using different values of learning rate.

| SI No. | Learning rate | RMSE        | MAE         | R <sup>2</sup> score |
|--------|---------------|-------------|-------------|----------------------|
| 1      | 0.1           | 0.000205214 | 0.009361184 | 0.81577201           |
| 2      | 0.01          | 0.000143462 | 0.007910841 | 0.871209485          |
| 3      | 0.001         | 0.000496417 | 0.015957664 | 0.554348964          |
| 4      | 0.0001        | 0.001057556 | 0.026922022 | 0.050594843          |

**CHAPTER 6: DEVELOPMENT OF A SURROGATE MODEL FOR ADAPTIVE FAÇADE PERFORMANCE IN THE EARLY DESIGN STAGES**

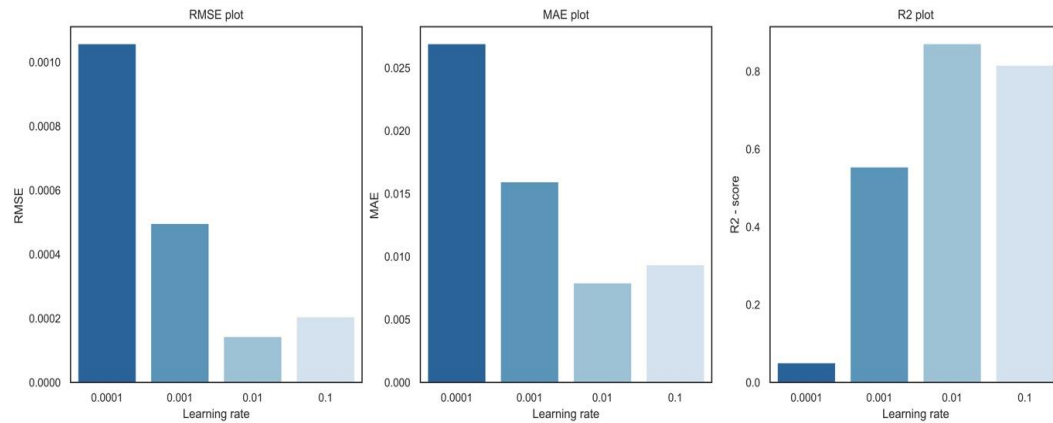


Figure 6.23: RMSE, MAE and R<sup>2</sup> score for the learning rate.

**6.9.1.3. Batch Size**

The experiment confirmed that batch size influences the performance of the ANN model. The finding shows that when batch size increases, performance increases up to a certain limit and then decreases. For example, the RMSE for a batch size of 2,500 was 0.00012724, for 10,000 it was 0.00011567, and for 250,000 it was 0.00010494. However, the RMSE increased significantly for higher batch sizes of 100,000 and 250,000 to 0.0006451 and 0.00068948 respectively. The results of the experiment with varied batch sizes are presented in Table (6.15) and Figure (6.24). Based on the experiment, the batch size was fixed as 25,000, and the network used employed was a three-layer network with 128 neurons, the train/test split was 80/20, the number of epochs was 60, and the learning rate was 0.01.

Table 6.15. Experiment using different batch size.

| SI No | Batch size | RMSE       | MAE       | R <sup>2</sup> - score |
|-------|------------|------------|-----------|------------------------|
| 1     | 2500       | 0.00012724 | 0.0072207 | 0.885772563            |
| 2     | 10000      | 0.00011567 | 0.0076822 | 0.892154514            |
| 3     | 25000      | 0.00010494 | 0.0062125 | 0.905787265            |
| 4     | 100000     | 0.0006451  | 0.0197306 | 0.420871584            |
| 5     | 250000     | 0.00068948 | 0.0198572 | 0.381028919            |

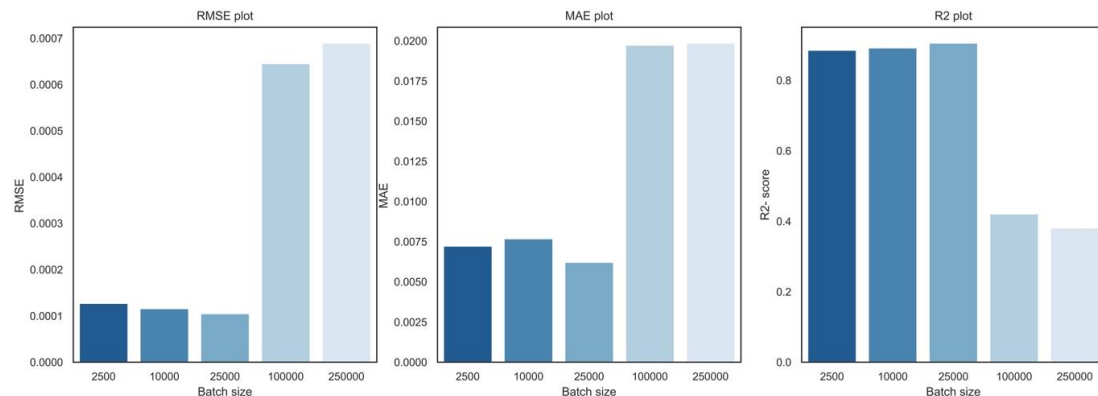


Figure 6.24: RMSE, MAE and R<sup>2</sup> score for the batch size.

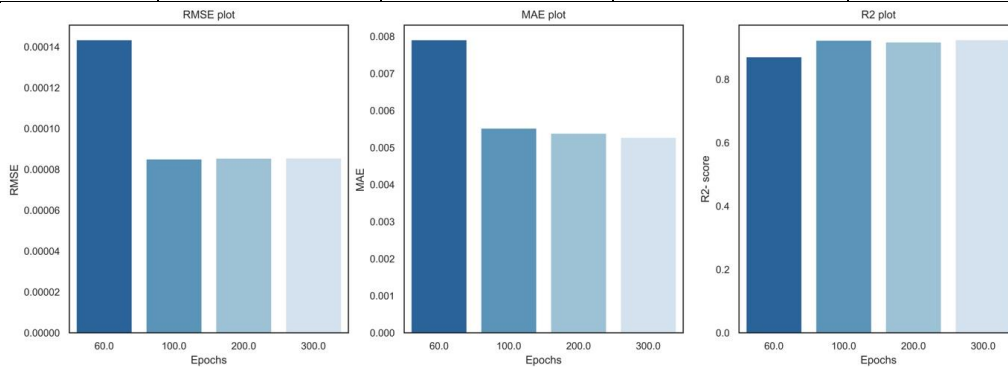
**CHAPTER 6: DEVELOPMENT OF A SURROGATE MODEL FOR ADAPTIVE FAÇADE PERFORMANCE IN THE EARLY DESIGN STAGES**

**6.9.1.4. Number of Epochs**

The epoch refers to the method by which data are entered into the network. The data should be fed multiple times to allow the network to learn effectively. The 'number of epochs' represents the number of times data have been fed into the network, which should be considered during the tuning of the hyperparameters to select the optimal number of epochs. This experiment was conducted by altering the number of epochs, with the learning rate maintained constant at 0.01. The details of the investigations are summarized in Table (6.16) and Figure (6.25). In the experiments, a three-layer network with 128 neurons was utilised, the train/test split was 80/20, the learning rate was 0.01, and the batch size was 25,000. After 100 epochs, a significant improvement was noted in the RMSE value. However, for values of 200 and 300 epochs, the RMSE stayed consistent. Thus, considering these findings, the number of epochs was determined at 100.

*Table 6.16 Experiment using different number of epochs.*

| SI No | Epochs | RMSE       | MAE         | R <sup>2</sup> - score |
|-------|--------|------------|-------------|------------------------|
| 3     | 60     | 0.00014346 | 0.0079108   | 0.871209485            |
| 4     | 100    | 0.00008509 | 0.005525503 | 0.92360919             |
| 3     | 200    | 0.00008554 | 0.0053893   | 0.917816795            |
| 4     | 300    | 0.00008562 | 0.005276    | 0.924930709            |



*Figure 6.25: RMSE, MAE, and R<sup>2</sup> score for the number of epochs*

**6.9.1.5. Results for Hyperparameters**

The best result achieved for an ANN model was for a three-layer network with 128 neurons. The RMSE value was 0.00008509, the MAE was 0.005525503, and the R<sup>2</sup> score was 0.92360919. For this experiment, the learning rate was 0.01, the number of epochs was 100, and the batch size was 25,500. A validation dataset was preserved to test the performance of the model. The training loss and validation loss of this network is plotted in Figure (6.26). As can be seen from the plot training, the loss started with 0.019 and decreased steeply to less than 0.001 in the first few iterations. This indicates that the ANN model had learned in

**CHAPTER 6: DEVELOPMENT OF A SURROGATE MODEL FOR ADAPTIVE FAÇADE PERFORMANCE IN THE EARLY DESIGN STAGES**

the desired way. Similarly, the validation loss slowly decreased as the epochs proceeded. Table shows the training and validation accuracy against the epochs in ten steps.

The results in Table (6.17) reveal that the training process of the ANN modelling proceeded in the desired way. In addition, Figure (6.27) shows a scatter plot of actual and predicted values for 100 randomly chosen testing cases. In addition, for more details, some tested cases in different orientation predicted using ANN compared to simulation are shown in (Appendix E). These results prove that the ANN model could predict the cooling load with good accuracy.

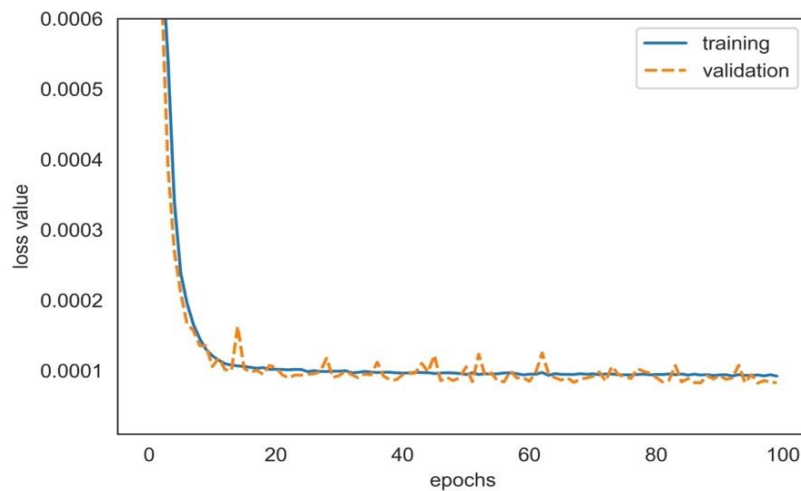


Figure 6.26: Training and validation loss against epochs.

Table 6.17. Training and validation loss against epochs.

| Epoch | Training loss | Validation loss |
|-------|---------------|-----------------|
| 1     | 0.019771      | 0.000877        |
| 10    | 0.00013       | 0.000135        |
| 20    | 0.000102      | 0.000108        |
| 30    | 0.0000993     | 0.0000905       |
| 40    | 0.0000970     | 0.0000872       |
| 50    | 0.000096      | 0.0000899       |
| 60    | 0.000094      | 0.0000905       |
| 70    | 0.0000949     | 0.0000896       |
| 80    | 0.0000941     | 0.0000966       |
| 90    | 0.0000932     | 0.0000884       |
| 100   | 0.0000923     | 0.0000831       |

## CHAPTER 6: DEVELOPMENT OF A SURROGATE MODEL FOR ADAPTIVE FAÇADE PERFORMANCE IN THE EARLY DESIGN STAGES

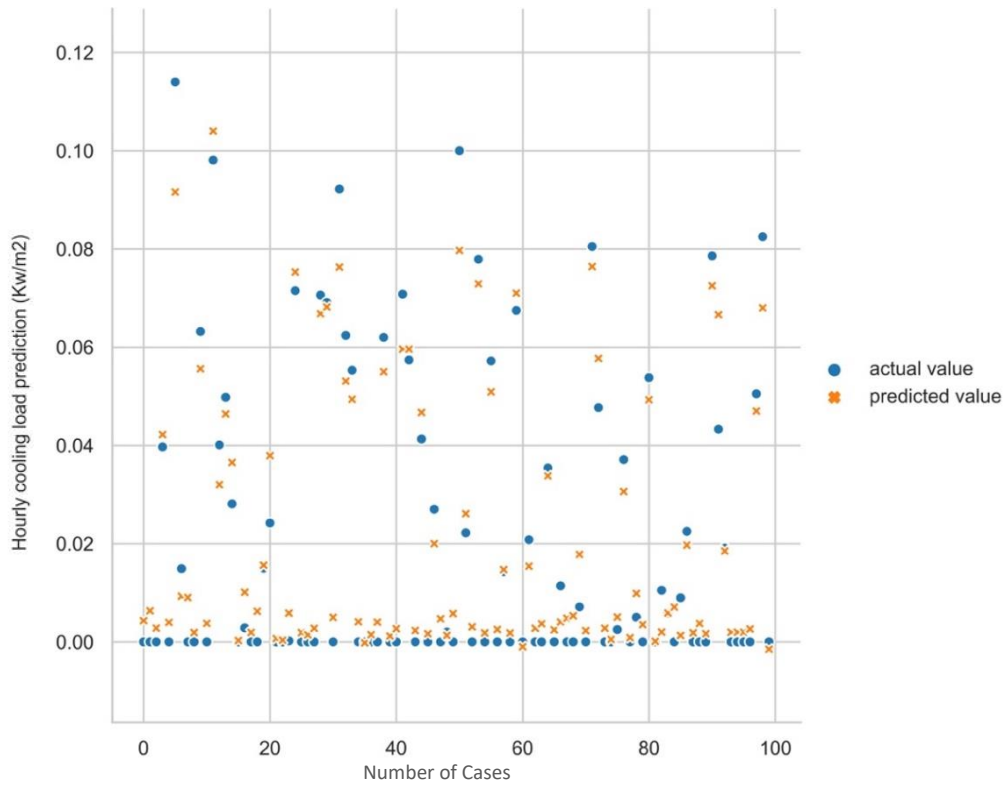


Figure 6.27: Plot of actual and predicted values for 100 testing cases.

### K-Fold Cross Validation

The optimal hyperparameter values were determined using an experiment similar to that which was explained in Section (6.4.4). The dataset was split into training, validation, and testing sets: 80% of the data were assigned to the training set, 6.67% to the validation set, and the remaining 13.37% to the testing set. The training set alone was then subjected to five-fold cross validation to tune the hyperparameters. After fine-tuning the network's parameters, a model was constructed using the entire training set and then tested using the testing unseen data. The details of the cross-validation are shown in Figure (6.28).

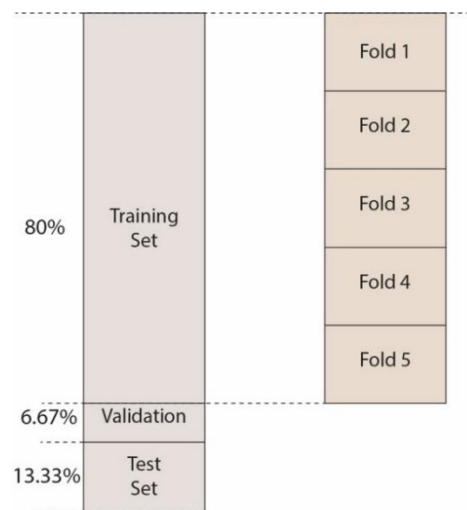


Figure 6.28: The data split procedure.

## **CHAPTER 6: DEVELOPMENT OF A SURROGATE MODEL FOR ADAPTIVE FAÇADE PERFORMANCE IN THE EARLY DESIGN STAGES**

### **6.9.2. Optimization of Hyperparameters**

This experiment started with a one-layer network, and numbers of neurons were added to it in steps. Firstly, 32 neurons were given, then 64, and then 128. Following that, the experiment was repeated for two-layer, three-layer, and four-layer networks, and the data were split into training, validation, and test sets (Table 6.18). The models were trialed using the training and validation data splits, and the model finally chosen was tested with the test data.

*Table 6.18. Results of hyperparameter tuning for ANN architecture*

| Serial No. | No. of layers | No. of neurons in each layer | RMSE     | MAE     | R <sup>2</sup> score |
|------------|---------------|------------------------------|----------|---------|----------------------|
| 1          | 1             | 64                           | 0.000485 | 0.03821 | 0.836432             |
| 2          | 1             | 128                          | 0.000478 | 0.0383  | 0.862678             |
| 3          | 1             | 256                          | 0.000482 | 0.03793 | 0.642886             |
| 4          | 1             | 512                          | 0.000857 | 0.04861 | 0.57725              |
| 5          | 2             | 64                           | 0.000551 | 0.04171 | 0.750268             |
| 6          | 2             | 128                          | 0.000547 | 0.04106 | 0.75022              |
| 7          | 2             | 256                          | 0.00057  | 0.04226 | 0.644694             |
| 8          | 2             | 512                          | 0.000799 | 0.0469  | 0.496431             |
| 9          | 3             | 64                           | 0.000651 | 0.04564 | 0.638646             |
| 10         | 3             | 128                          | 0.000703 | 0.04616 | 0.620949             |
| 11         | 3             | 256                          | 0.000583 | 0.04301 | 0.597746             |
| 12         | 3             | 512                          | 0.001891 | 0.06814 | 0.552574             |
| 13         | 4             | 64                           | 0.000635 | 0.0471  | 0.646                |
| 14         | 4             | 128                          | 0.00074  | 0.0492  | 0.690268             |
| 15         | 4             | 256                          | 0.000688 | 0.04673 | 0.584307             |
| 16         | 4             | 512                          | 0.002813 | 0.08081 | 0.577528             |

The results are graphically represented as shown in Figure (6.29). From the figure, the following findings were outlined.

- As the number of layers increased, the RMSE increased. The best results were achieved for networks with only one layer.
- The performance score dropped for deeper networks compared to shallow networks.
- This indicates that having deeper networks with a large number of neurons resulted in overfitting or poor generalization to the data.
- On the other hand, the performance of deeper networks with a lower number of neurons (64 and 128) was comparatively better than those with a larger number of neurons.

Based on the experiments, the architecture chosen was a one-layer neural network with 128 neurons as shown in Figure (6.30). For all these experiments, the train/test ratio of the data



**CHAPTER 6: DEVELOPMENT OF A SURROGATE MODEL FOR ADAPTIVE FAÇADE PERFORMANCE IN THE EARLY DESIGN STAGES**

used was 80%/20%, the learning rate was 0.01, the number of epochs was 100, and the batch size was 25,000.

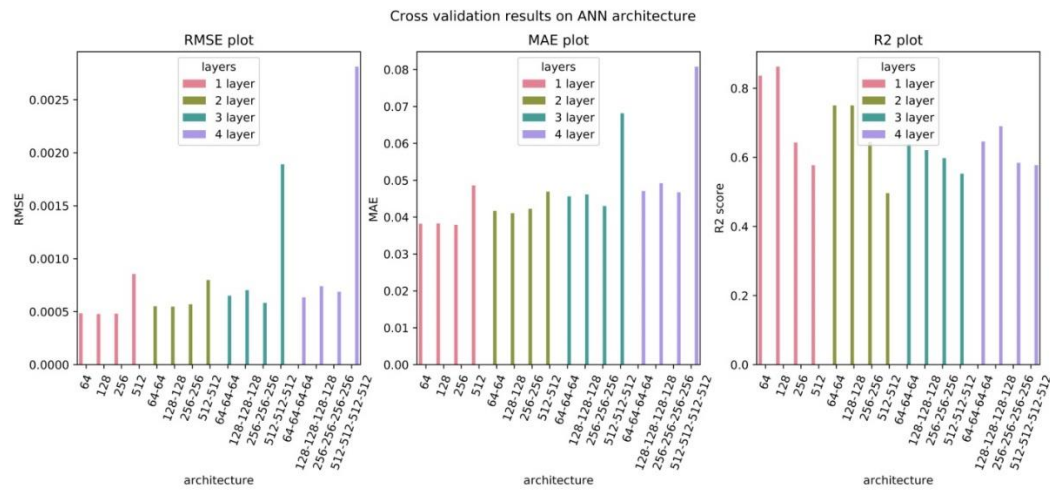


Figure 6.29: K-fold cross validation results on choosing ANN architecture

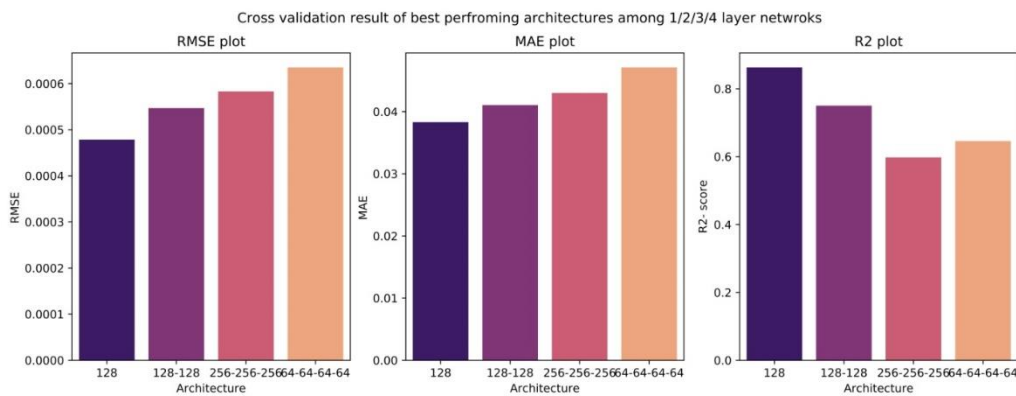


Figure 6.30: RMSE, MAE, and  $R^2$  score of the best performing models among the one-, two-, three-, and four-layer networks

**6.9.3. Testing the Architecture**

The one-layer network with 128 neurons was the one selected through the k-fold cross validation applied with the validation set and test set as explained in Figure 52. For this purpose, a new model was built using the entire training set. This model was tested with the test set. The results obtained are as follows: RMSE value was 0.00008809, MAE was 0.00718157, and the  $R^2$  score was 0.8531965. For the experiment, the learning rate used was 0.01, the number of epochs was 100, and the batch size was 25,000. The training loss and validation loss of this network is plotted as shown in Figure (6.31). This figure shows that the training loss starting from 0.20 decreased steeply until it reached less than 0.00012 in the first few iterations. Thus, this indicated that the neural network had learned in the desired way. For more details, a plot of actual and predicted values for some randomly

## **CHAPTER 6: DEVELOPMENT OF A SURROGATE MODEL FOR ADAPTIVE FAÇADE PERFORMANCE IN THE EARLY DESIGN STAGES**

selected testing cases on different days and building orientations are shown in (Appendix E). The results reveal that the ANN model could predict the cooling load with a good accuracy.

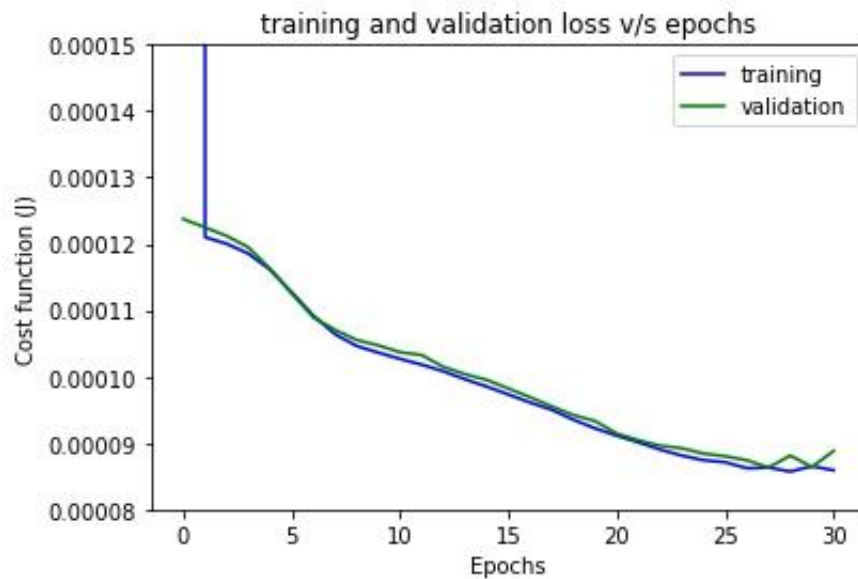


Figure 6.31: Training and validation loss against epochs

### **6.10. Random Forest Model Development**

After the experiment on ANN modelling and training in the previous section to predict cooling loads, this section investigates using a different algorithmic method, which followed a similar modelling process to that presented in section (6.5).

#### **6.10.1. K-Fold Cross Validation**

As mentioned earlier, the purpose of k-fold cross validation is to choose a suitable combination of hyperparameters such as the number of trees and bootstrap. To tune these hyperparameters, a systematic search with a k-fold cross-validation experiment was undertaken. In k-fold cross validation, the data were split into k folds. Among these k number of folds, (k-1) folds belonged to the training data and the remainder to the testing data. The experiments were performed k times, and each time, the testing fold varied without repetition. The benefit is that each fold in one or other experiment becomes part of the training as well as the testing. Hence, the bias that can result from the binary splits was avoided. Regarding the dataset splitting procedure, the experiment utilised a similar process to that presented in section (6.4.4) by using K-fold cross validation to split the data.

### 6.10.2. Optimization of Hyperparameters

Numerous hyperparameters are required for RF modelling to achieve a model with greater accuracy. This experiment considered the following parameters: (1) number of trees, (2) bootstrap, and (3) minimal cost-complexity pruning parameter.

### 6.10.3. Results of Cooling Prediction using RF

This section discusses the prediction of the cooling load from the input data. The result of k-fold cross validation is given in Figure (6.32). The figure contains the average RMSE, MAE and R<sup>2</sup> score for each of the parameter combinations. On the x-axis, bootstrap combinations are given separately along with their performance with different options for the number of trees (visualised as bars). From the experiments, the following observations can be made.

- The performance of the whole parameter combinations was excellent because the RMSE varied between the range of  $2 \times 10^{-8}$  to  $4 \times 10^{-8}$ , MAE varied in the range  $3.5 \times 10^{-5}$  to  $4 \times 10^{-5}$ , and the R<sup>2</sup> score was close to one.
- There was no significant difference whether the bootstrap option was enabled or not.
- Increasing the number of trees caused the performance to exhibit an oscillatory behaviour, although the difference in performance was negligible.
- From the experiments, the optimal model had the following hyperparameter combination: Bootstrap option enabled and a total of 30 trees.

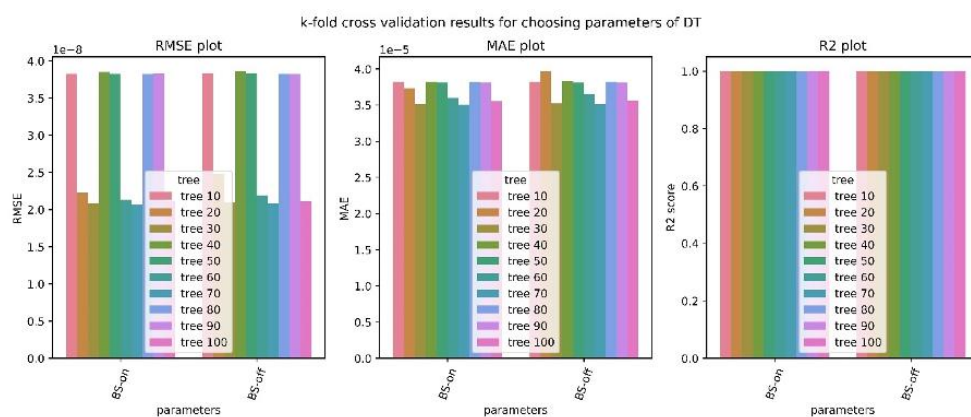


Figure 6.32: The result of cooling load prediction. The figure corresponds to the visualization of the results of hyperparameter tuning in RF (BS stands for bootstrap option).

Figure (6.33) illustrates the performance metrics corresponding to the best performing models with respect to the number of trees. The results are for the bootstrap option enabled. In the k-fold cross validation, the optimal result was observed when the number of trees was 30, the ccp-alpha value was 0, and the bootstrap option was enabled. The final test results were as follows: the RMSE was  $1.986 \times 10^{-8}$ , MAE was  $3.168 \times 10^{-5}$ , and the R<sup>2</sup>

**CHAPTER 6: DEVELOPMENT OF A SURROGATE MODEL FOR ADAPTIVE FAÇADE PERFORMANCE IN THE EARLY DESIGN STAGES**

score was 0.99985. These results correspond to the model performance selected after cross-validation with the entire training data and tested with the 20% test data. A result visualisation of RF prediction for a randomly chosen 100 points is given in Figure (6.34). It can be seen that for most of the data points, the actual and predicted value was almost the same, or the prediction was very accurate. This is why, visually, one might not be able to read the actual values since they might be directly underneath the predicted values. With regard to prediction accuracy, the results show that the RF model predicted the cooling loads with high accuracy compared to the ANN model, with RMSE that was very close to zero as shown in Table (6.19).

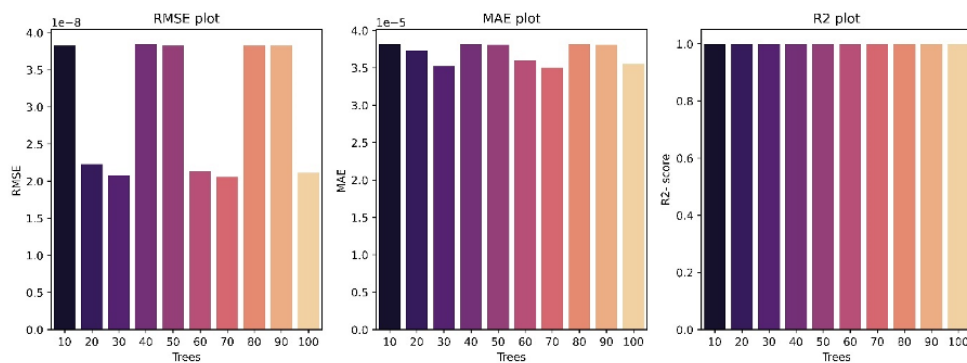


Figure 6.33: Performance metrics corresponding to the best performing models.

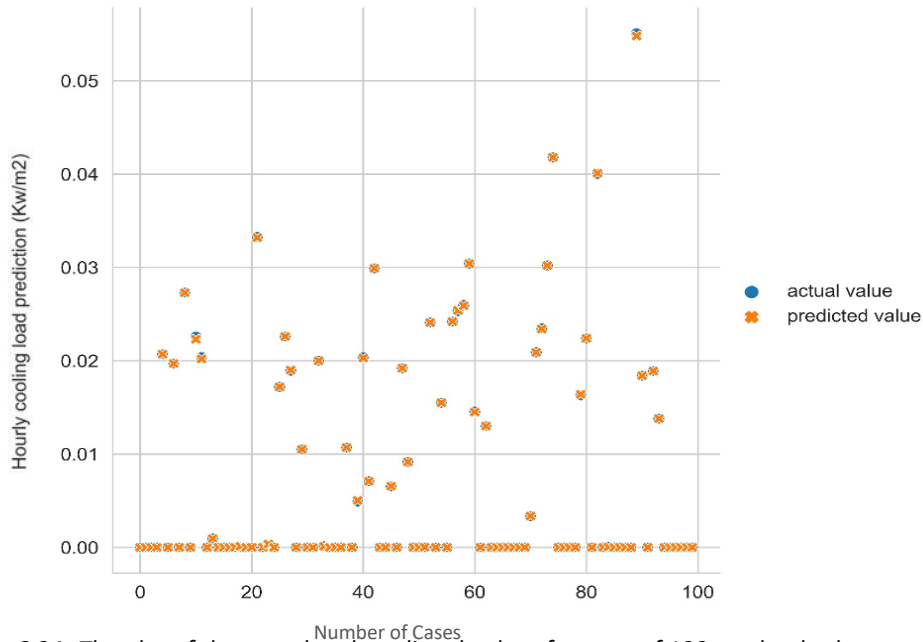


Figure 6.34: The plot of the actual and predicted values for a set of 100 randomly chosen test points in the case of cooling load prediction.

Table 6.19. Performance comparison of ANN and RF for cooling loads data.

| Performance metric   | Neural Network | Random Forest |
|----------------------|----------------|---------------|
| RMSE                 | 0.00008809     | 0.0000001986  |
| MAE                  | 0.00718157     | 0.00003168    |
| R <sup>2</sup> score | 0.8531965      | 0.99985       |

## **6.11. 6.11 Experiment to Analyse Time Series Nature of the Data**

This section examined the time series nature of the data since the cooling loads data was generated dependent on time. In the simulation, it was generated in an hourly basis for the whole year for different configurations. As discussed in section (6.7), inputs were pre-processed, and most of the data were categorical (non-time series data) except solar radiation, and operative temperature. To analyse the effect of time in the data two sets of experiments were carried out.

### **6.11.1. Modelling Particularly the Time Series Inputs**

The time-varying features in the input data were solar radiation and operative temperature. An experiment was conducted to predict hourly cooling loads using these specific inputs. The purpose of this experiment was to analyse whether the time varying inputs would be sufficient to perform the prediction task compared to including all the other categorical and continuous inputs. In addition, the aim was to examine the effect of time series inputs on the performance of the surrogate models. To model the time series nature of the data, two different approaches were experimented as explained below (Brillinger 2001).

#### **6.11.1.1. Approach 1 (Time Differencing)**

Time differencing is a conventional method in statistics to represent time series data. In the real world, time series data mostly are non-stationary (Salles et al. 2019). Thus, the differencing approach was used, which helped to make the data stationary (Fan and Yao 2004). In the experiment, the one-step time difference was calculated for the inputs as per the equation given below.

$$y_t \rightarrow y_t - y_{t-1}$$

That is, the solar radiation and operative temperature values at time step  $t$  are represented as the difference of the values at time steps  $t$  and  $t-1$ . Hence, the data at time step  $t$  denoted as  $(X_t)$  is represented as follows:

$$X_t = [s_t, o_t, s_t - s_{t-1}, o_t - o_{t-1}, c_t$$

where  $s$ ,  $o$ , and  $c$  denote solar radiation, operative temperature, and cooling load respectively.

#### **6.11.1.2. Approach 2 (Time Window)**

Time window is a method that is commonly used in machine learning (ML) to represent time series data for predictive analytics. In this approach, the values of the time series for a past time window are also taken to the modelling (Felix et al. 2002). In the experiment, the

## **CHAPTER 6: DEVELOPMENT OF A SURROGATE MODEL FOR ADAPTIVE FAÇADE PERFORMANCE IN THE EARLY DESIGN STAGES**

window was chosen as 10 hours; that is, values of solar radiation and operative temperature for the previous 10 hours were used to predict the current time step. Hence, the data at time step  $t$  for the modelling took the following form:

$$X_t = [S_{t-10}, S_{t-9}, \dots, S_{t-1}, S_t, O_{t-10}, O_{t-9}, \dots, O_{t-1}, O_t, c_t ]$$

Then, the data prepared in approach 1 and 2 were given to an RF regressor for the modelling.

### **6.11.2. Modelling the Time Series and Non-Time Series Inputs.**

Along with the time varying inputs, categorical inputs including orientation, glazing type, and exterior wall were considered. In this modelling, the time series nature of the time varying inputs was modelled with the two approaches as explained above.

In approach 1, the data at time step  $t$  denoted as  $(X_t)$  are represented as follows:

$$X_t = [S_t, O_t, S_t - S_{t-1}, O_t - O_{t-1}, r, g, e, c_t ]$$

where  $s$ ,  $o$ , and  $c$  denote solar radiation, operative temperature, and cooling load respectively, which are time varying data, and  $r$ ,  $g$ , and  $e$  denote orientation, glazing type, and exterior wall, which are non-time varying inputs.

In approach 2, the data are represented as follows:

$$X_t = [S_{t-10}, S_{t-9}, \dots, S_{t-1}, S_t, O_{t-10}, O_{t-9}, \dots, O_{t-1}, O_t, r, g, e, c_t ].$$

The data prepared in approaches 1 and 2 were given to an RF regressor for the modelling.

### **6.11.3. Random Forest Model Development**

This section investigates using different algorithmic methods; the modelling process followed was similar to that presented in sections (6.5, 6.10).

### **6.11.4. K-Fold Cross Validation**

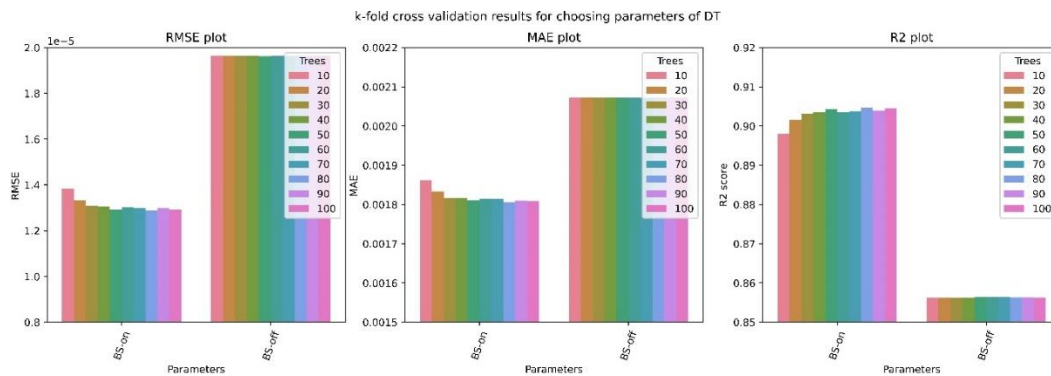
The data for training and testing were split by preserving the chronology. In other words, data from January to September were chosen for the training and the remaining data for testing. The training data were then used for k-fold cross validation as explained earlier in section (6.10.1). The purpose of k-fold cross validation is to choose a suitable combination of hyperparameters, such as the number of trees and bootstrap. To tune these hyperparameters, a k-fold cross-validation experiment was undertaken.

**6.11.5. Optimization of Hyperparameters**

**6.11.5.1. Experiment (1): Time Differencing Approach with only Time Series inputs.**

The results of k-fold cross validation are shown in Figure (6.35). This figure shows the average RMSE, MAE, and R<sup>2</sup> score for each of the parameter combinations. On the x-axis, bootstrap combinations are given separately along with their performance with different options for the number of trees (visualised as bars). The results of this experiments revealed the following:

- The performance of the whole parameter combinations is as follows - RMSE varied between the range of  $1.2 \times 10^{-5}$  to  $2 \times 10^{-5}$ , the MAE varied in the range 0.0018 to 0.0022, and the R<sup>2</sup> score in the range 0.85 to 0.91.
- The difference in performance depending on whether the bootstrap option was enabled or not is not a significant one, but without the bootstrap option, performance is low.
- Increasing the number of trees caused a general trend of improvement in the performance.
- From the experiments, the optimal model had the following hyperparameter combination: bootstrap option enabled, and a total of 80 trees.



*Figure 6.35: The result of cooling load prediction in the time differencing approach with only time varying inputs. The figure corresponds to the visualisation of the results of hyperparameter tuning in RF (BS stands for bootstrap option).*

Figure (6.36) illustrates the performance metrics corresponding to the best performing models with respect to the number of trees. The results are for the bootstrap option enabled. The final test results were as follows: the RMSE was  $4.582 \times 10^{-6}$ , the MAE was 0.000881, and the R<sup>2</sup> score was 0.845101. A result visualisation of the RF prediction for a randomly chosen week is presented in Figures (6.37), and (6.38). It can be seen that for most of the data points, the actual and predicted values were almost the same, or following a similar pattern of the actual points.

**CHAPTER 6: DEVELOPMENT OF A SURROGATE MODEL FOR ADAPTIVE FAÇADE PERFORMANCE IN THE EARLY DESIGN STAGES**

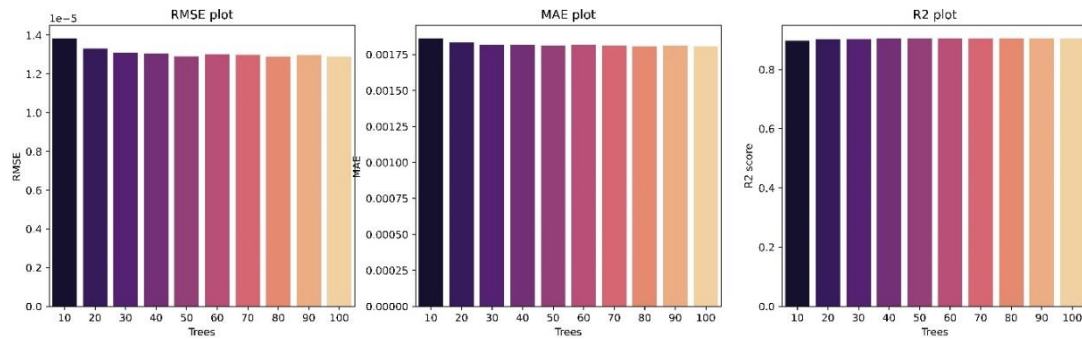


Figure 6.36: Performance metrics corresponding to the best performing models.

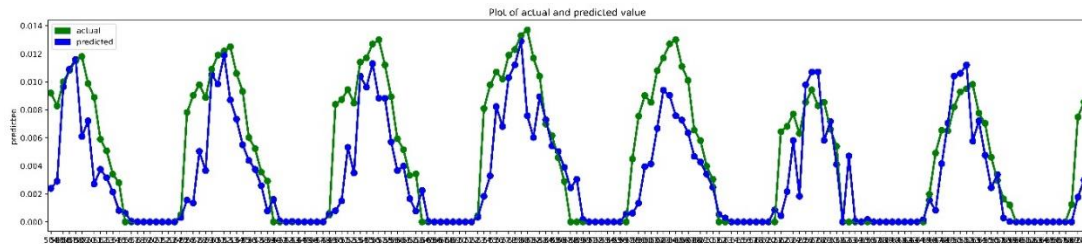


Figure 6.37: The plot of the actual and predicted values for third week of October in the case of hourly cooling load prediction (Experiment 1).

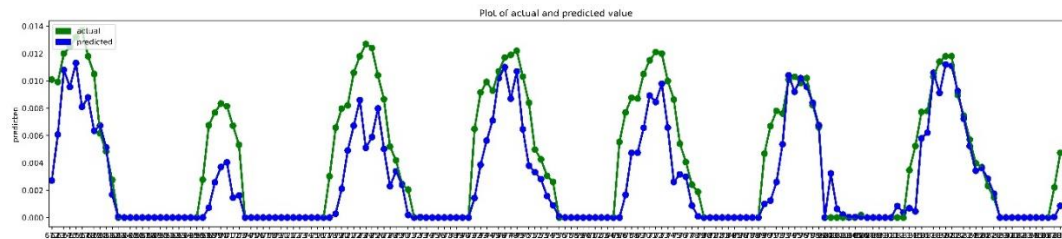


Figure 6.38: The plot of the actual and predicted values for fourth week of October in the case of hourly cooling load prediction (Experiment 1).

**6.11.5.2. Experiment (2): Time Window Approach with Only Time Series Inputs**

The results of k-fold cross validation are shown in Figure (6.39). From the experiments, the following observations were made.

- The performance of the whole parameter combinations is as follows - RMSE varied between the range of  $3.5 \times 10^{-6}$  to  $6.0 \times 10^{-6}$ , the MAE varied in the range 0.00105 to 0.00140, and the  $R^2$  score in the range 0.95 to 0.97.
- The difference in performance depending on whether the bootstrap option was enabled or not is not a significant one, but without the bootstrap option, performance is low.
- Increasing the number of trees caused a general trend of improvement in the performance, but for a larger number of trees, the performance starts dropping.
- From the experiments, the optimal model had the following hyperparameter combination: bootstrap option enabled and a total of 80 trees.



**CHAPTER 6: DEVELOPMENT OF A SURROGATE MODEL FOR ADAPTIVE FAÇADE PERFORMANCE IN THE EARLY DESIGN STAGES**

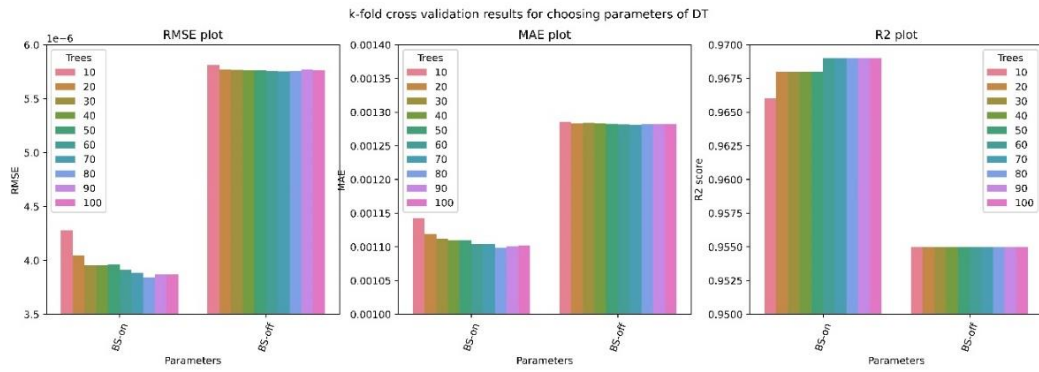


Figure 6.39: The result of cooling load prediction in the time window approach with only time varying inputs. The figure corresponds to the visualisation of the results of hyperparameter tuning in RF (BS stands for bootstrap option).

Figure (6.40) demonstrates the performance metrics corresponding to the best performing models with respect to the number of trees. The results are for the bootstrap option enabled. The final test results were as follows: the RMSE was  $2.194 \times 10^{-6}$ , the MAE was 0.000697, and the  $R^2$  score was 0.925818. A resulting visualisation of RF prediction for a randomly chosen week is shown in Figures (6.41), and (6.42).

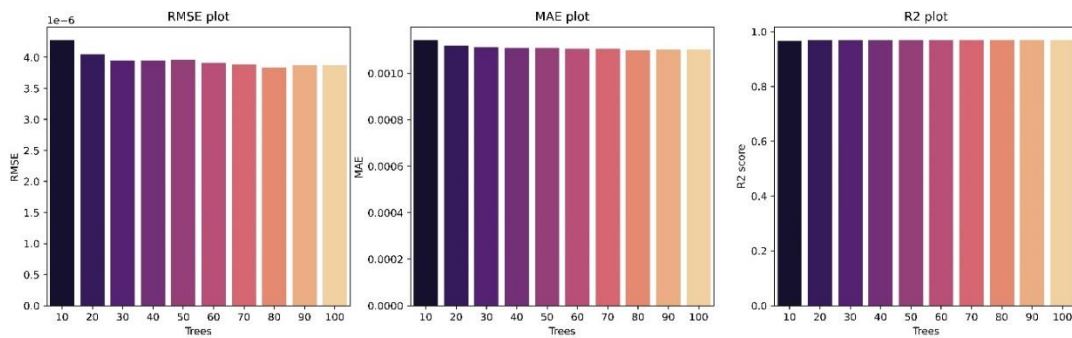


Figure 6.40: Performance metrics corresponding to the best performing models.

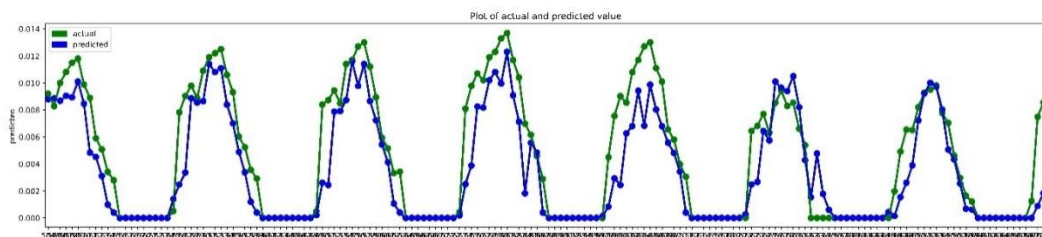


Figure 6.41: The plot of the actual and predicted values for third week of October in the case of hourly cooling load prediction (Experiment 2).

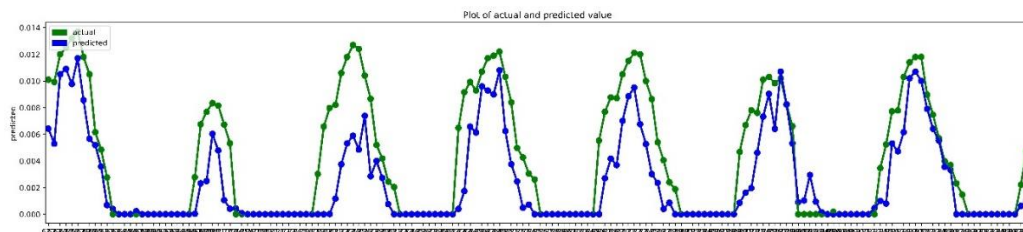


Figure 6.42: The plot of the actual and predicted values for fourth week of October in the case of hourly cooling load prediction (Experiment 2).

## CHAPTER 6: DEVELOPMENT OF A SURROGATE MODEL FOR ADAPTIVE FAÇADE PERFORMANCE IN THE EARLY DESIGN STAGES

### 6.11.5.3. Experiment (3): Time Differencing Approach with Time Series and Time Non-Series Inputs.

The result of k-fold cross validation is given in Figure (6.43). The results of this experiments revealed the following:

- The performance of the whole parameter combinations is as follows - RMSE varied between the range of  $2.5 \times 10^{-6}$  to  $5.5 \times 10^{-6}$ , the MAE varied in the range 0.00085 to 0.00110, and the  $R^2$  score in the range 0.95 to 0.98.
- The difference in performance depending on whether the bootstrap option was enabled or not is not a significant one, but without the bootstrap option, performance is low.
- Increasing the number of trees caused an oscillatory behaviour in the performance; that is, the performance improved when the number of trees was increased to 60, but it increased for 70 and 80. However, the best result was found when the number of trees was increased to 90.
- From the experiments, the optimal model had the following hyperparameter combination: bootstrap option enabled and a total of 90 trees.

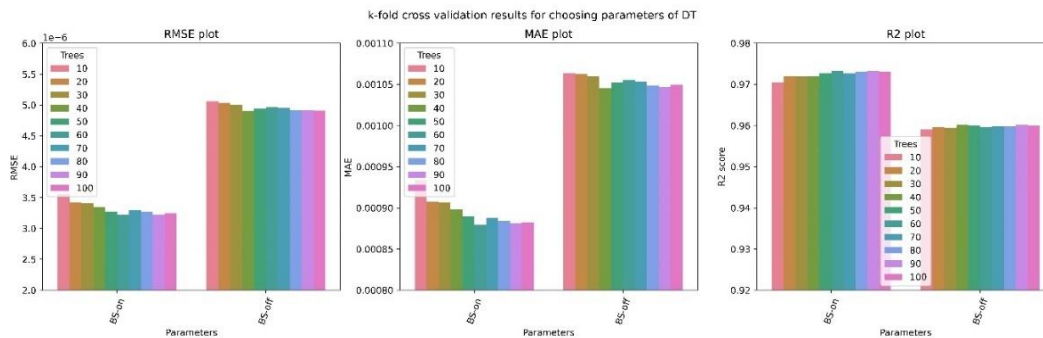


Figure 6.43: The result of cooling load prediction in the time window approach with only time varying inputs. The figure corresponds to the visualisation of the results of hyperparameter tuning in RF (BS stands for the bootstrap option).

Figure (6.44) illustrates the performance metrics corresponding to the best performing models with respect to the number of trees. The final test results were as follows: the RMSE was  $2.997 \times 10^{-6}$ , the MAE was 0.000709, and the  $R^2$  score was 0.898690. A result visualisation of the RF prediction for a randomly chosen week is given in Figures (5.45), and (6.46).

**CHAPTER 6: DEVELOPMENT OF A SURROGATE MODEL FOR ADAPTIVE FAÇADE PERFORMANCE IN THE EARLY DESIGN STAGES**

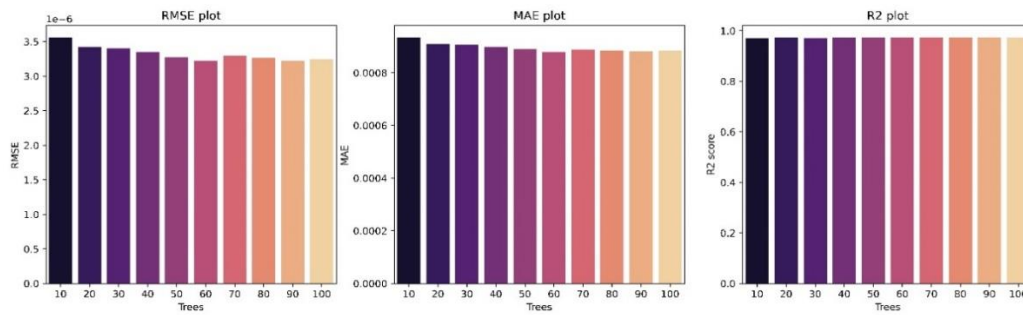


Figure 6.44: Performance metrics corresponding to the best performing models.

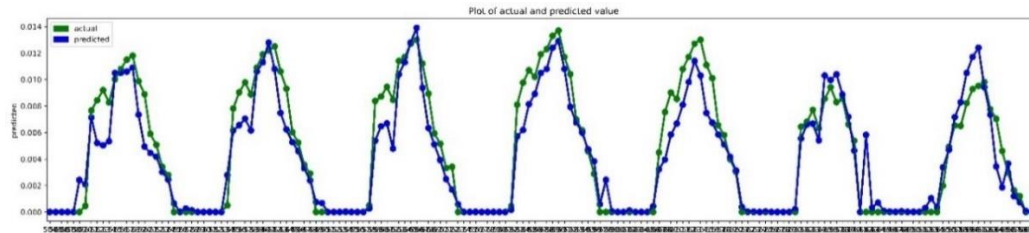


Figure 6.45: The plot of the actual and predicted values for third week of October in the case of cooling load prediction (Experiment 3).

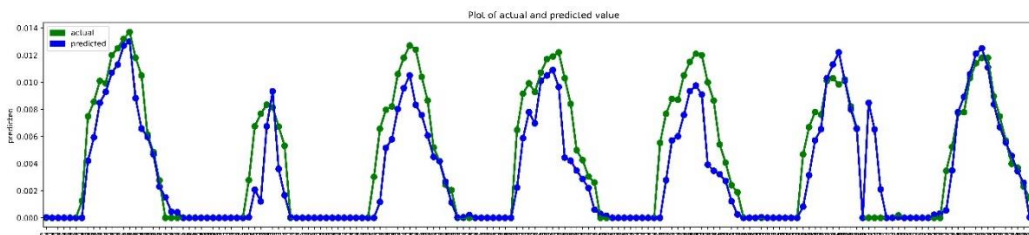


Figure 6.46: The plot of the actual and predicted values for fourth week of October in the case of cooling load prediction (Experiment 3).

**6.11.5.4. Experiment (4): Time Window Approach with Time Series and Time Non-Series Inputs**

The result of k-fold cross validation is given in Figure (6.47). From the experiments, the following observations were made.

- The performance of the whole parameter combinations is as follows - RMSE varied between the range of  $2.5 \times 10^{-6}$  to  $5.5 \times 10^{-6}$ , the MAE varied in the range 0.00085 to 0.00110, and the  $R^2$  score in the range 0.95 to 0.98.
- The difference in performance depending on whether the bootstrap option was enabled or not is not a significant one, but without the bootstrap option, performance is low.
- Increasing the number of trees caused an oscillatory behaviour in the performance; that is, the performance improved and degraded as the number of trees increased.

**CHAPTER 6: DEVELOPMENT OF A SURROGATE MODEL FOR ADAPTIVE FAÇADE PERFORMANCE IN THE EARLY DESIGN STAGES**

- From the experiments, the optimal model had the following hyperparameter combination: bootstrap option enabled and a total of 100 trees.

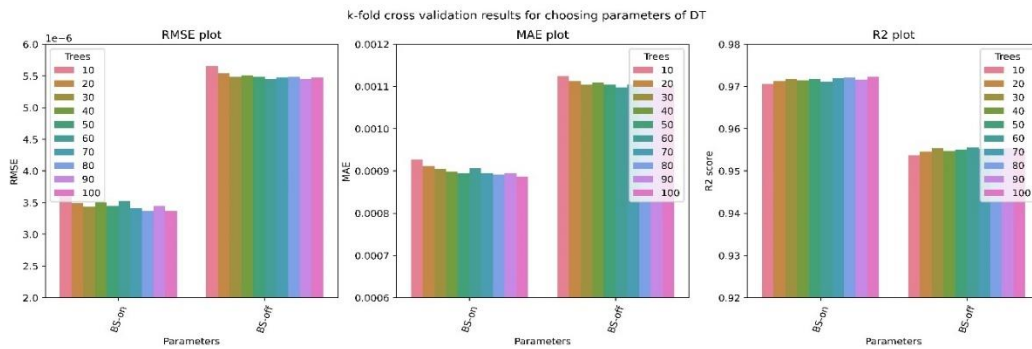


Figure 6.47: The result of the cooling load prediction in the time window approach with only time varying inputs. The figure corresponds to the visualisation of the results of hyperparameter tuning in RF (BS stands for bootstrap option).

Figure (6.48) shows the performance metrics corresponding to the best performing models with respect to the number of trees. The final test results were as follows: the RMSE was  $4.307 \times 10^{-6}$ , the MAE was 0.000898, and the  $R^2$  score was 0.854395. A result visualisation of the RF prediction for a randomly chosen week is presented in Figures (6.49), and (6.50).

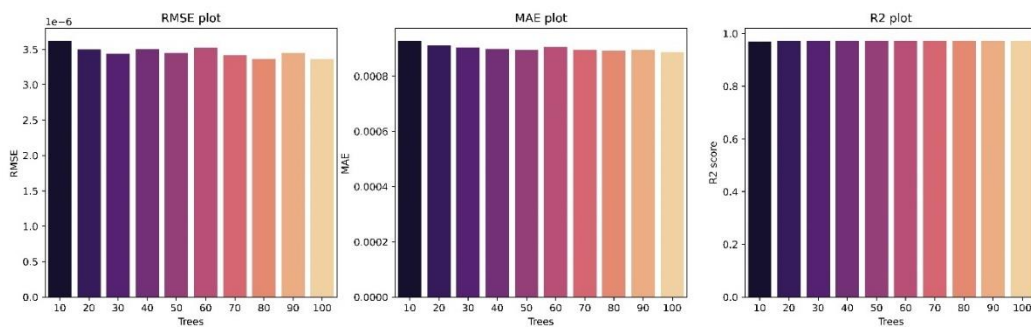


Figure 6.48: Performance metrics corresponding to the best performing models.

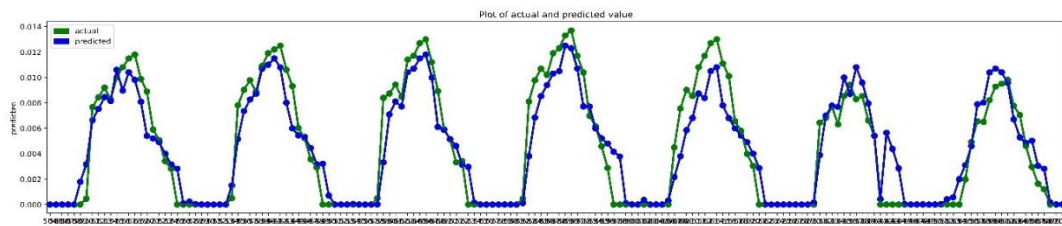


Figure 6.49: The plot of the actual and predicted values for third week of October in the case of cooling load prediction (Experiment 4).

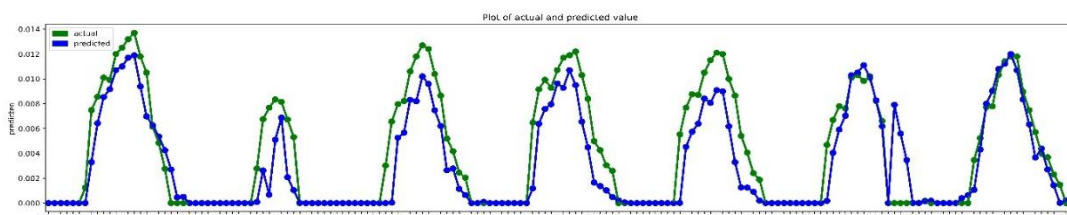


Figure 6.50: The plot of the actual and predicted values for fourth week of October in the case of cooling load prediction (Experiment 4).

## **CHAPTER 6: DEVELOPMENT OF A SURROGATE MODEL FOR ADAPTIVE FAÇADE PERFORMANCE IN THE EARLY DESIGN STAGES**

### **6.11.6. Comparative Analysis**

The best results achieved were for the initial experiment (RF without a time dynamic), as its performance was better than the time series modelling. This initial experiment consists of time varying inputs - solar radiation and operative temperature and other categorical and continuous inputs. The result of the initial modelling is presented along with the four conducted experiments in this section as shown in Table (6.20).

*Table 6.20. Performance comparison of the four conducted experiments.*

| <b>Model</b>                                 | <b>RMSE</b>              | <b>MAE</b> | <b>R<sup>2</sup>-score</b> |
|--|--------------------------|------------|----------------------------|
| Initial Experiment (RF without Time dynamic) | 1.986 x 10 <sup>-8</sup> | 0.000031   | 0.999850                   |
| Experiment 1                                 | 4.582 x 10 <sup>-6</sup> | 0.000881   | 0.845101                   |
| Experiment 2                                 | 2.194 x 10 <sup>-6</sup> | 0.000697   | 0.925818                   |
| Experiment 3                                 | 2.997 x 10 <sup>-6</sup> | 0.000709   | 0.898690                   |
| Experiment 4                                 | 4.307 x 10 <sup>-6</sup> | 0.000898   | 0.854395                   |

Based on these experiments, the following observations can be made:

- When comparing experiments (1) and (2), which employed only time series inputs, the results showed that the time window approach achieved better performance compared to the time differencing approach.
- When comparing experiments (3) and (4), which employed both time series and non-time series data, the results revealed that the time differencing approach achieved better performance.
- In experiments (3) and (4), categorical inputs, including orientation, glazing type, and exterior wall, were added to the time varying inputs. However, the performance of the models is poorer than with the time window approach of experiment (2).
- The best results achieved among the four conducted experiments were for the time window approach that considered only time series data.
- It can be concluded that adding non-time series inputs to a time series modelling can possibly diminish the performance of the model that processes only time series input. Therefore, time series modelling should be conducted when all inputs are dependent on time.
- It can also be concluded that depending on the modelling situation and the goal of the developed model, sometimes non-time series inputs are important and cannot be neglected. Thus, in this case, the conventional method of modelling can be more effective due to the influence of non-time series inputs in the prediction.

## **6.12. Chapter Summary**

This chapter developed an alternative approach to evaluating the performance of AF shading systems in the early stages of the design using ML algorithms. This approach aimed to resolve the obstacles faced when making prediction of AF shading system with current BPS tools. As mentioned earlier, this technique is beneficial, as it saves time that would otherwise be mostly consumed during the simulation process to inform the shading design decision instantly. In this chapter, the experiment was conducted in two different stages.

In stage one, an experiment was undertaken for solar radiation analysis because predicting the energy performance of AF depends on first evaluating the solar radiation in the initial process of the design and confirming the suitability of using a surrogate model to evaluate the hourly cooling loads of AFs. Two different machine algorithms, ANN, and RF were investigated for incident solar radiation prediction on the building envelope to discover if using another ML model type could influence the accuracy prediction outcome.

The second stage of the chapter presented the development of the surrogate model for predicting the hourly cooling load of AFs. The data were collected from the simulation that was performed in (chapter 4) and were then fed into two ML algorithms in an approach similar to that followed in stage one. Several fixed and dynamic inputs were chosen that would reflect the dynamic fluctuation of the AF system, design conditions, and building envelope parameters with cooling loads as the targeted outcome. Subsequently, the data obtained were used to train, validate, and test the proposed models. To optimize the models, a hyperparameter tuning process was carried out in both stage one and stage two with the consideration of various parameters. Lastly, different approaches of time series modelling were followed to examine the time series nature of the data using RF modelling.

The results indicated that ML techniques can predict the hourly cooling loads of AFs with a high level of accuracy in the range of 85% to 99%. In particular, the RF model showed a 17% improvement in  $R^2$  accuracy over the ANN model in predicting the hourly cooling loads of AFs. Regarding time series data modelling, it was found that time window approach achieved better performance compared to time differencing approach.

## **CHAPTER SEVEN**

### **DEPLOYMENT OF THE DEVELOPED SURROGATE MODELS**

## **CHAPTER 7: DEPLOYMENT OF THE DEVELOPED SURROGATE MODELS**

### **7.1. Introduction**

The central goal of using ML surrogate models was to efficiently predict the energy performance (hourly cooling loads) of AF shading and (hourly solar radiation) in the early stages of the design. This chapter presents the results obtained from the developed surrogate model and compares them with the simulation results, with the aim of further validating the results. The results presented in this chapter are based on hourly cooling loads (KWh/m<sup>2</sup>) and hourly solar radiation (KWh/m<sup>2</sup>). The model was also evaluated in terms of prediction accuracy, time efficiency, and its generalisation prediction capability. In addition, the surrogate model was tested in terms of its applicability in predicting other similar hot-climate cities. To achieve this, after training and validating the model in chapter (6), the trained surrogate models were imported into a workflow within a computational design tool (Grasshopper environment) using the GH-C Python tool. The workflow was then used to predict the energy performance (cooling loads) of the design scenarios of the AF system.

### **7.2. Model Deployment**

After the training and validation had been conducted with ANN and RF, the best performing model (RF) was imported into the Grasshopper interface using GH-C Python to predict solar radiation and cooling loads for different design scenarios. GH-C Python was developed for the integration of the Grasshopper and GH-C Python languages (Abdelrahman 2017). This plug-in tool allows users to incorporate Python libraries such as NumPy, SciPy, Matplotlib, pandas, Scikit-learn, PyTorch, etc. into Grasshopper and link the pre-trained model to make predictions. The developed codes and models were saved as a pickle file (PyTorch file), which is a specialized format that helps to run ML models in an external environment. Then, in Grasshopper, the codes were loaded inside the GH-C Python component, and a Python script was coded as illustrated in Figure (7.1). After that, the input parameters of the model were added into the slider components in Grasshopper; each slider component represents an input with its variants. For example, in the case of solar radiation prediction within the orientation slider, four options can be selected: (0) represents South, (1) represents West, (2) represents North, and (3) represents East, and within the building context sliders, three options can be selected (low, medium, and high) as shown in Figure (7.2). All the defined inputs that were used to train the model need to be defined to make a prediction with the RF model. These inputs include hours, months, orientations, the four surrounding building



## CHAPTER 7: DEPLOYMENT OF THE DEVELOPED SURROGATE MODELS

contexts, façade level and height, and the X, Y, and Z coordinates of façade. After prediction, the results were processed to visualise the solar radiation data as a heatmap on the building envelope of the studied office room. A similar approach was followed in the case of cooling load inputs as shown in Figure (7.3). The cooling load inputs include month, hour, day, orientation, building 00, building 01, façade level height, glazing type U-value W/m<sup>2</sup>K, exterior wall U-value W/m<sup>2</sup>K, AF opening ratio, AF-SF, SR W/m<sup>2</sup>, OT.

```

File Data Python
43 import pandas as pd
44 import numpy as np
45 import time
46 import matplotlib.pyplot as plt
47 import seaborn as sb # used to plot the heatmap
48 import pickle
49 from sklearn.preprocessing import OneHotEncoder
50 from sklearn.tree import DecisionTreeRegressor
51 from sklearn.ensemble import RandomForestRegressor
52 from sklearn.metrics import mean_squared_error, mean_absolute_error, r2_score
53
54 start = time.time()
55
56 ## Data loading and preprocessing
57
58 # In[2]:
59
60
61 # The data is read as a pandas data frame
62 data = pd.read_csv("C:/Users/ammaralumar/Documents/Grasshopper integration - DT/finalized_data.csv").dropna()
63
64
65 # In[3]:
66
67 def data_create( inp):
68
69
70
71
72
73
74
75
76
77
78
79
80
81
82
83
84
85
86
87
88
89
90
91
92
93
94
95
96
97
98
99
100
101
102
103
104
105
106
107
108
109
110
111
112
113
114
115
116
117
118
119
120
121
122
123
124
125
126
127
128
129
130
131
132
133
134
135
136
137
138
139
140
141
142
143
144
145
146
147
148
149
150
151
152
153
154
155
156
157
158
159
160
161
162
163
164
165
166
167
168
169
170
171
172
173
174
175
176
177
178
179
180
181
182
183
184
185
186
187
188
189
190
191
192
193
194
195
196
197
198
199
200
201
202
203
204
205
206
207
208
209
210
211
212
213
214
215
216
217
218
219
220
221
222
223
224
225
226
227
228
229
230
231
232
233
234
235
236
237
238
239
240
241
242
243
244
245
246
247
248
249
250
251
252
253
254
255
256
257
258
259
260
261
262
263
264
265
266
267
268
269
270
271
272
273
274
275
276
277
278
279
280
281
282
283
284
285
286
287
288
289
290
291
292
293
294
295
296
297
298
299
300
301
302
303
304
305
306
307
308
309
310
311
312
313
314
315
316
317
318
319
320
321
322
323
324
325
326
327
328
329
330
331
332
333
334
335
336
337
338
339
340
341
342
343
344
345
346
347
348
349
350
351
352
353
354
355
356
357
358
359
360
361
362
363
364
365
366
367
368
369
370
371
372
373
374
375
376
377
378
379
380
381
382
383
384
385
386
387
388
389
390
391
392
393
394
395
396
397
398
399
400
401
402
403
404
405
406
407
408
409
410
411
412
413
414
415
416
417
418
419
420
421
422
423
424
425
426
427
428
429
430
431
432
433
434
435
436
437
438
439
440
441
442
443
444
445
446
447
448
449
450
451
452
453
454
455
456
457
458
459
460
461
462
463
464
465
466
467
468
469
470
471
472
473
474
475
476
477
478
479
480
481
482
483
484
485
486
487
488
489
490
491
492
493
494
495
496
497
498
499
500
501
502
503
504
505
506
507
508
509
510
511
512
513
514
515
516
517
518
519
520
521
522
523
524
525
526
527
528
529
530
531
532
533
534
535
536
537
538
539
540
541
542
543
544
545
546
547
548
549
550
551
552
553
554
555
556
557
558
559
560
561
562
563
564
565
566
567
568
569
570
571
572
573
574
575
576
577
578
579
580
581
582
583
584
585
586
587
588
589
590
591
592
593
594
595
596
597
598
599
600
601
602
603
604
605
606
607
608
609
610
611
612
613
614
615
616
617
618
619
620
621
622
623
624
625
626
627
628
629
630
631
632
633
634
635
636
637
638
639
640
641
642
643
644
645
646
647
648
649
650
651
652
653
654
655
656
657
658
659
660
661
662
663
664
665
666
667
668
669
670
671
672
673
674
675
676
677
678
679
680
681
682
683
684
685
686
687
688
689
690
691
692
693
694
695
696
697
698
699
700
701
702
703
704
705
706
707
708
709
710
711
712
713
714
715
716
717
718
719
720
721
722
723
724
725
726
727
728
729
730
731
732
733
734
735
736
737
738
739
740
741
742
743
744
745
746
747
748
749
750
751
752
753
754
755
756
757
758
759
760
761
762
763
764
765
766
767
768
769
770
771
772
773
774
775
776
777
778
779
780
781
782
783
784
785
786
787
788
789
790
791
792
793
794
795
796
797
798
799
800
801
802
803
804
805
806
807
808
809
810
811
812
813
814
815
816
817
818
819
820
821
822
823
824
825
826
827
828
829
830
831
832
833
834
835
836
837
838
839
840
841
842
843
844
845
846
847
848
849
850
851
852
853
854
855
856
857
858
859
860
861
862
863
864
865
866
867
868
869
870
871
872
873
874
875
876
877
878
879
880
881
882
883
884
885
886
887
888
889
890
891
892
893
894
895
896
897
898
899
900
901
902
903
904
905
906
907
908
909
910
911
912
913
914
915
916
917
918
919
920
921
922
923
924
925
926
927
928
929
930
931
932
933
934
935
936
937
938
939
940
941
942
943
944
945
946
947
948
949
950
951
952
953
954
955
956
957
958
959
960
961
962
963
964
965
966
967
968
969
970
971
972
973
974
975
976
977
978
979
980
981
982
983
984
985
986
987
988
989
990
991
992
993
994
995
996
997
998
999
1000

```

Figure 7.1: The loaded codes inside GH\_CPython to make predictions within Grasshopper.

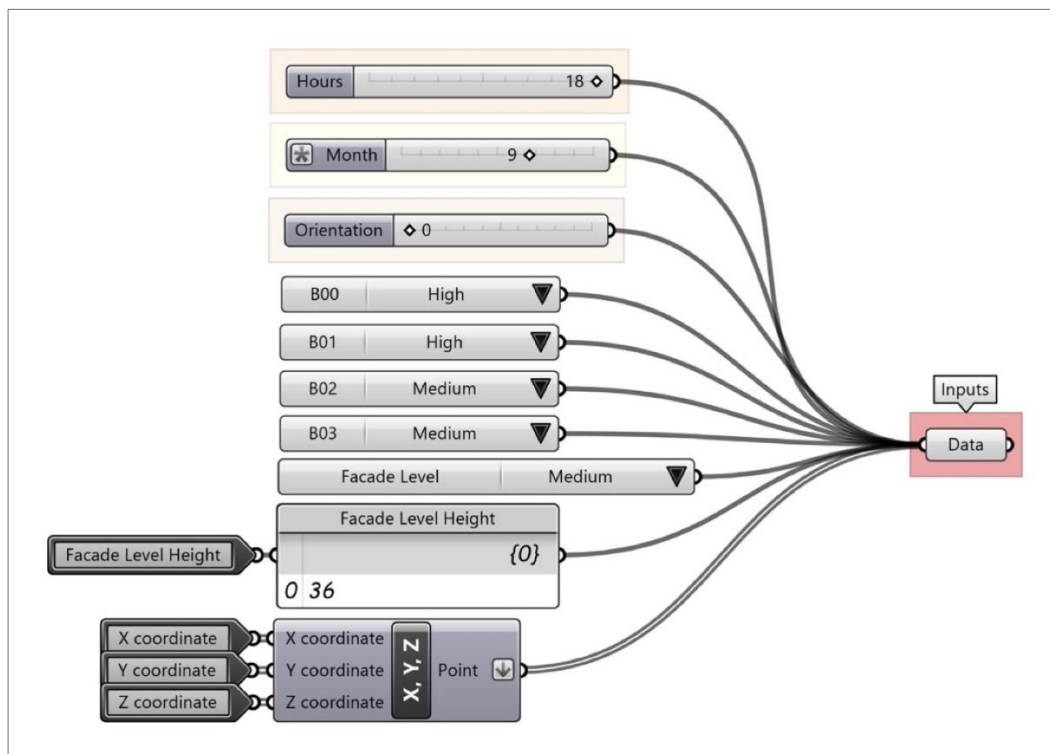
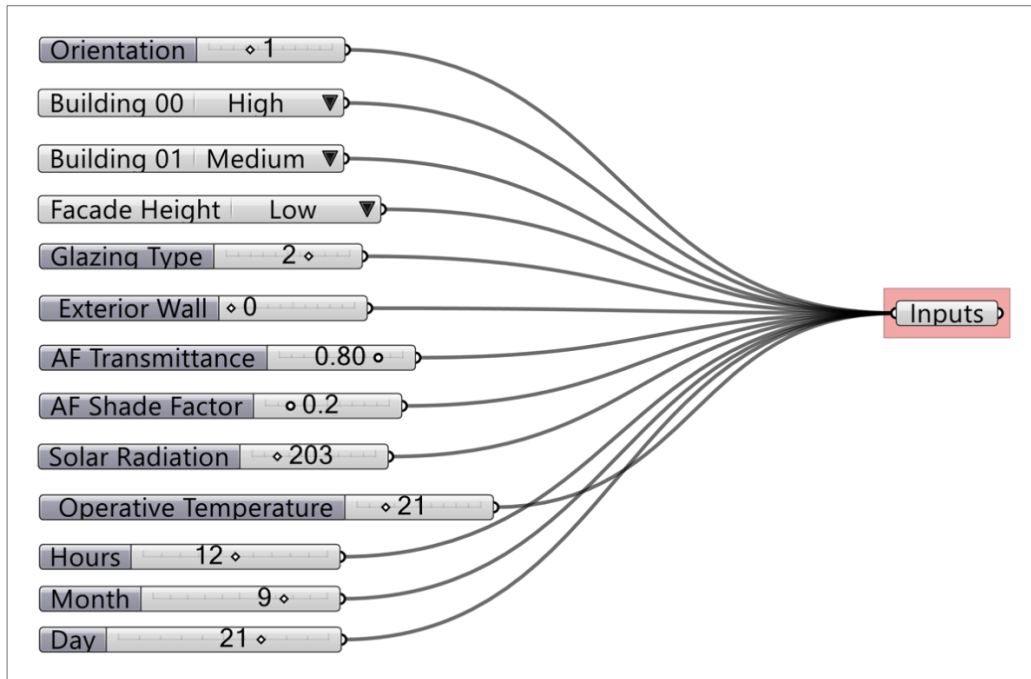


Figure 7.2: Inputs required to make predictions for solar radiation using the RF model.



*Figure 7.3: Inputs required to make predictions for cooling loads using the RF model.*

With respect to workflow comparison, the workflow of the RF model within Grasshopper is much simpler than the workflow conducted for the simulation as shown in Figure (7.4). With the RF model prediction, the inputs are the only parameters required to make a prediction. On the other hand, simulation requires different settings to be defined, such as setting up the model, setting up the solar radiation settings, processing the results etc. to make predictions, which consumes more time. This was also found in the case of the energy performance simulation (cooling loads) workflow of AF as presented in chapter (4), where the complexity of simulating the AF shading system is even more time consuming and requires significant effort and resources. The workflow to conduct the energy performance of AF shading requires setting up the model, analysing the climate, defining the simulation settings, determining the input parameters, selecting the construction material properties, defining the zone loads, determining the thermal setting, and assigning the automatic control system. Figures (7.5) and (7.6) show the workflow used to perform the simulation compared to the RF workflow. This highlights the time efficiency spent using ML techniques to make predictions compared to simulation tools. In addition, time is spent during the running time of the simulation, which will be discussed in the following sections.

**CHAPTER 7: DEPLOYMENT OF THE DEVELOPED SURROGATE MODELS**

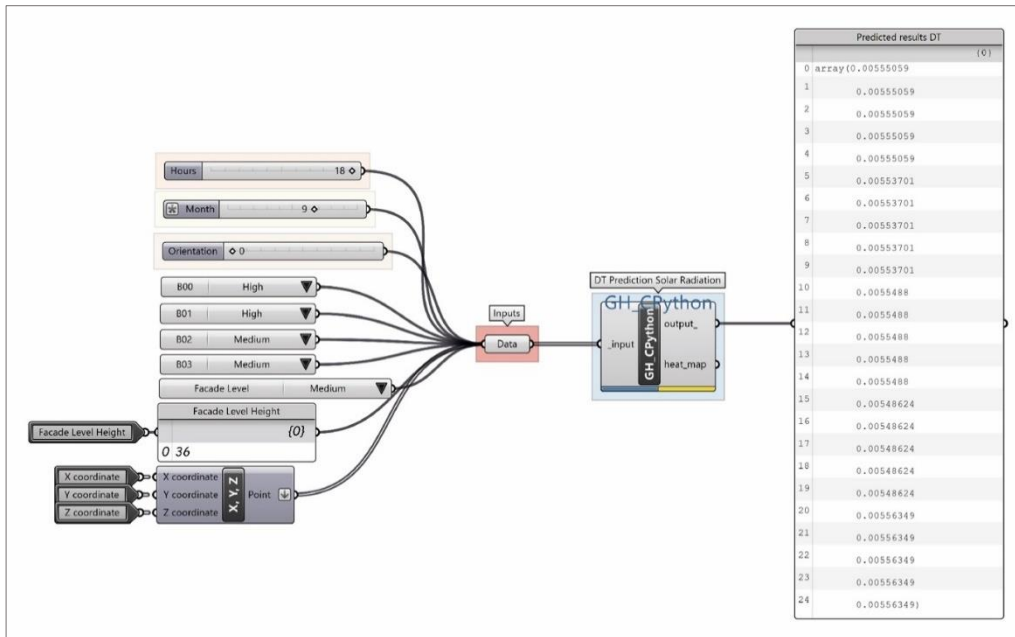


Figure 7.4: RF surrogate model workflow for predicting hourly solar radiation within Grasshopper.

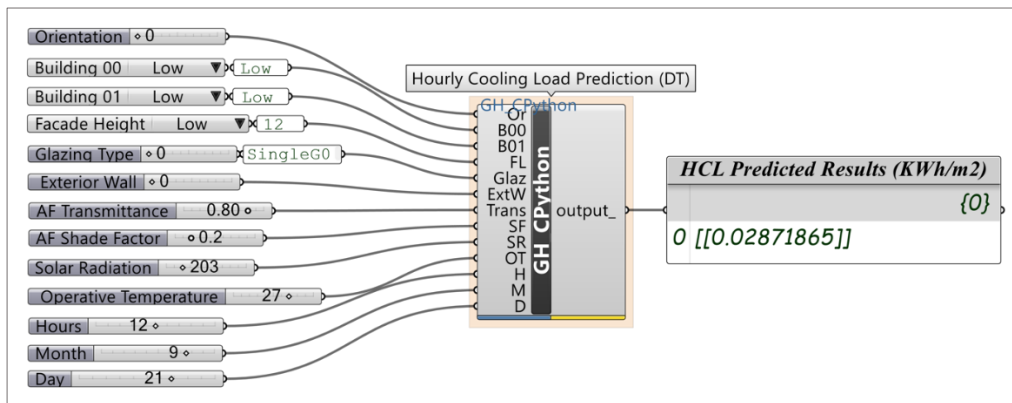
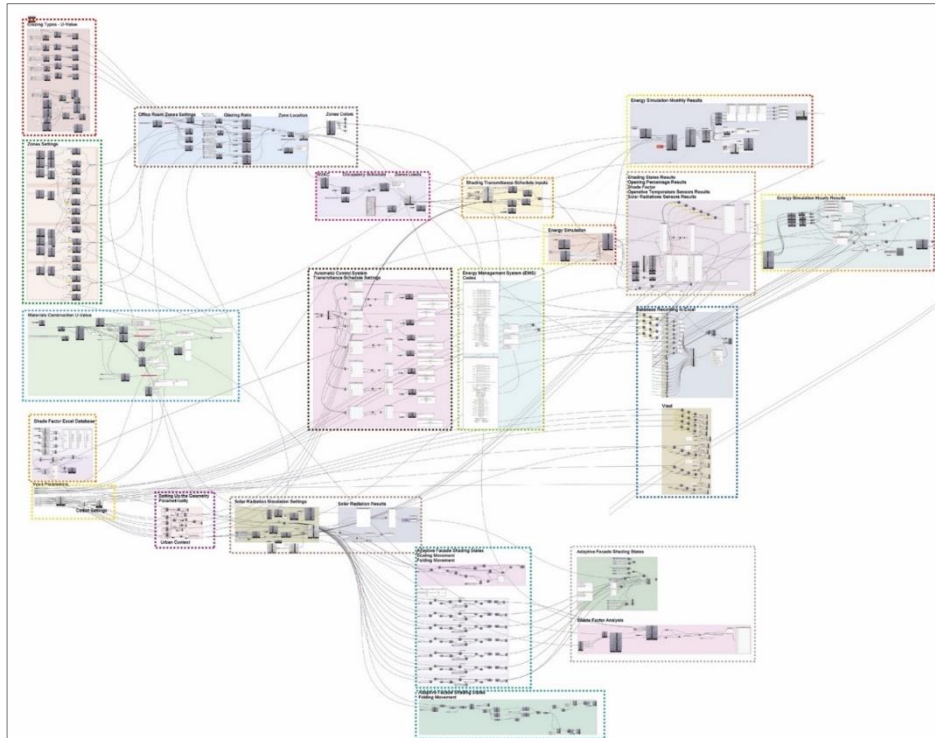


Figure 7.5: RF surrogate model workflow for predicting hourly cooling loads within Grasshopper.



*Figure 7.6: Workflow to conduct energy performance of AF shading system*

The following sections explain how the study initially presented and compared the solar radiation results using RF with the simulation results for different design scenarios. Then, a new design scenario was generated to evaluate the generalisability of the model, and the consumption time spent in making the prediction was calculated. Following that, a similar approach was followed for the cooling loads results of the AF shading systems considering different design solutions.

### **7.3. Solar Radiation (Predicated Design Scenarios vs. Simulated)**

As presented in chapter (6), the RF model performed better than the ANN model in terms of the prediction accuracy of the hourly solar radiation when tested with the 20% unseen data with an RMSE of 0.000514 compared to the ANN with an RMSE of 0.011415. Therefore, the study explored the integration of RF within the Grasshopper interface.

The study examined the combination cases:

- (Hours7\_Day21\_B00Medium\_B01Medium\_B02Medium\_B03Medium\_FacadeLevelMedium\_Orientation0).
- (Hours7\_Day21\_B00Medium\_B01Medium\_B02Medium\_B03Medium\_FacadeLevelMedium\_Orientation1).

These cases vary in terms of orientations, months, and hours. Detailed comparison analysis between the RF model prediction and the simulation prediction for an hourly solar radiation are shown in (Appendix E). The results revealed highly accurate prediction results where predicted case results with RF matched the simulation results. The results showed that the South and West orientations received most of the solar radiation in the afternoon time between 12:00 pm and 15:00 pm for the 21 September. In the South orientation, the solar radiation ranged from 450 KWh/m<sup>2</sup> to 900 KWh/m<sup>2</sup>, while in the West orientation, it ranged from 230 KWh/m<sup>2</sup> to 1280 KWh/m<sup>2</sup> on both 21 June and 21 September.

### **7.4. Solar Radiation Prediction for New Design Scenario**

After confirming the prediction accuracy of the examined cases within the Grasshopper environment, a new design scenario was generated that was not part of the data used to build ML models aiming to test the model in predicting unseen cases. The new design considered several office towers with new urban contexts as shown in Figure (7.7). To make predictions, the input parameters need to be defined either from the slider's components, from a text panel, or from a loaded CSV file Figure (7.8). The study experimented with 150 design cases generated within the office towers with different urban contexts. Since the number of cases was high, the inputs were loaded into Grasshopper using a CSV file to make predictions. Based on this experiment, the prediction accuracies for the solar radiation results of the new cases are shown in Figures (7.9) and (7.10), which are very close to the simulation prediction results.

With regard to time efficiency, using the RF model to predict hourly solar radiation for the 150 cases reduced the time spent on simulation. The time required to make a prediction was seconds compared to simulation, which took hours. Thus, for solar radiation prediction, it will be a cost-effective solution for the cases that require the large-scale generation of simulation data.





## CHAPTER 7: DEPLOYMENT OF THE DEVELOPED SURROGATE MODELS

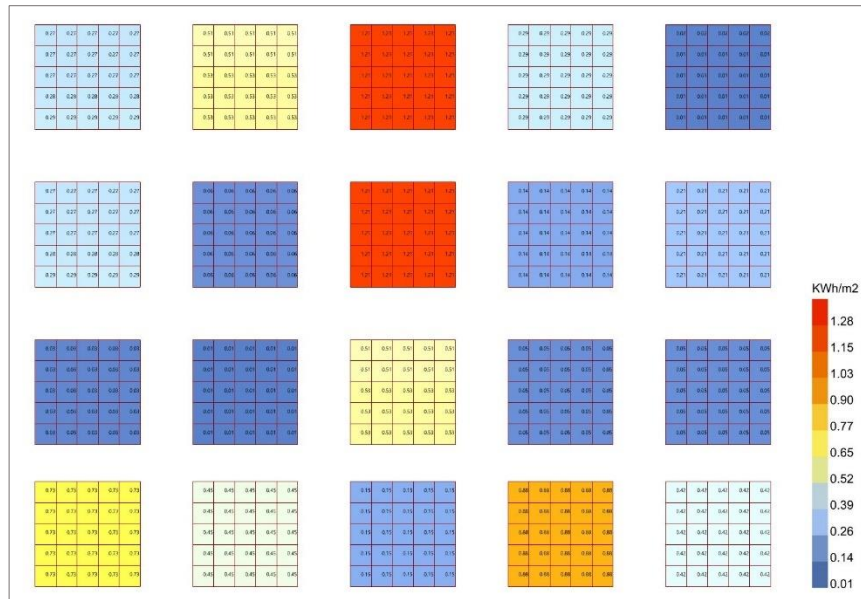


Figure 7.9: Sample of the hourly solar radiation output of the 150 cases as predicted by the RF surrogate model.

| <b>Simulated Results</b> |          | <b>Predicted results DT</b> |          | <b>Simulated Results</b> |          | <b>Predicted results DT</b> |            |
|--------------------------|----------|-----------------------------|----------|--------------------------|----------|-----------------------------|------------|
|                          | {0}      |                             | {0}      |                          | {0}      |                             | {0}        |
| 0                        | 0.890847 | 0                           | 0.890847 | 0                        | 0.658735 | 0                           | 0.665515   |
| 1                        | 0.890847 | 1                           | 0.890847 | 1                        | 0.658735 | 1                           | 0.665515   |
| 2                        | 0.890847 | 2                           | 0.890847 | 2                        | 0.658735 | 2                           | 0.665515   |
| 3                        | 0.890847 | 3                           | 0.890847 | 3                        | 0.658735 | 3                           | 0.665515   |
| 4                        | 0.890847 | 4                           | 0.890847 | 4                        | 0.658735 | 4                           | 0.665515   |
| 5                        | 0.890847 | 5                           | 0.890847 | 5                        | 0.658735 | 5                           | 0.665515   |
| 6                        | 0.890847 | 6                           | 0.890847 | 6                        | 0.658735 | 6                           | 0.665515   |
| 7                        | 0.890847 | 7                           | 0.890847 | 7                        | 0.658735 | 7                           | 0.665515   |
| 8                        | 0.890847 | 8                           | 0.890847 | 8                        | 0.658044 | 8                           | 0.665515   |
| 9                        | 0.890847 | 9                           | 0.890847 | 9                        | 0.658044 | 9                           | 0.665515   |
| 10                       | 0.890847 | 10                          | 0.890847 | 10                       | 0.658735 | 10                          | 0.665515   |
| 11                       | 0.890847 | 11                          | 0.890847 | 11                       | 0.658044 | 11                          | 0.665515   |
| 12                       | 0.890847 | 12                          | 0.890847 | 12                       | 0.658044 | 12                          | 0.665515   |
| 13                       | 0.890847 | 13                          | 0.890847 | 13                       | 0.658044 | 13                          | 0.665515   |
| 14                       | 0.890847 | 14                          | 0.890847 | 14                       | 0.658044 | 14                          | 0.66567856 |
| 15                       | 0.890847 | 15                          | 0.890847 | 15                       | 0.658044 | 15                          | 0.66567856 |
| 16                       | 0.890847 | 16                          | 0.890847 | 16                       | 0.658044 | 16                          | 0.66567856 |
| 17                       | 0.890847 | 17                          | 0.890847 | 17                       | 0.658044 | 17                          | 0.66567856 |
| 18                       | 0.890847 | 18                          | 0.890847 | 18                       | 0.658044 | 18                          | 0.66567856 |
| 19                       | 0.890847 | 19                          | 0.890847 | 19                       | 0.658044 | 19                          | 0.66584311 |
| 20                       | 0.890847 | 20                          | 0.890847 | 20                       | 0.655535 | 20                          | 0.66584311 |
| 21                       | 0.890847 | 21                          | 0.890847 | 21                       | 0.655535 | 21                          | 0.66584311 |
| 22                       | 0.890847 | 22                          | 0.890847 | 22                       | 0.655535 | 22                          | 0.66584311 |
| 23                       | 0.890847 | 23                          | 0.890847 | 23                       | 0.653807 | 23                          | 0.66584311 |
| 24                       | 0.890847 | 24                          | 0.890847 | 24                       | 0.653807 | 24                          | 0.66584311 |

Figure 7.10: Comparison between simulated solar radiation results using Ladybug and the predicted results using the RF surrogate model for two random cases

**7.5. Cooling Loads (Predicted Design Scenarios vs. Simulated)**

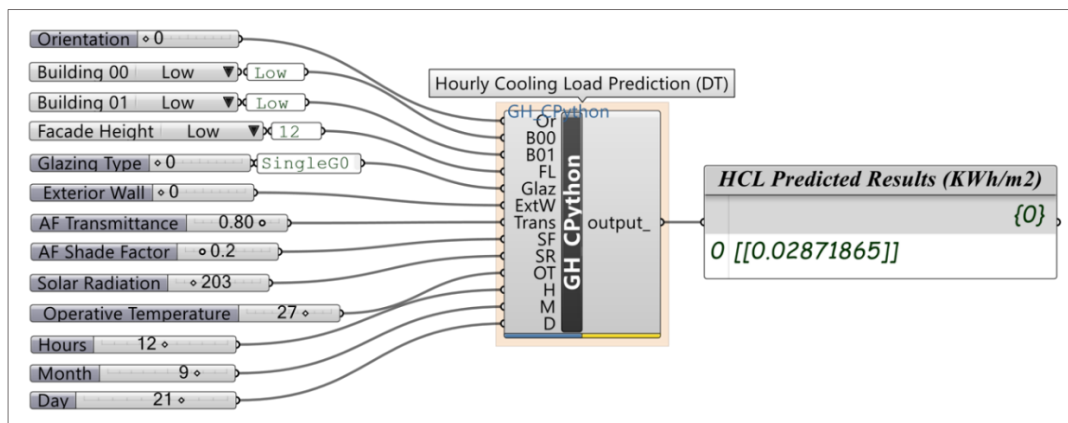
For the cooling loads experiment conducted in chapter (6), even though both the RF and ANN achieved highly accurate prediction results, the results of the RF outperformed the ANN model in terms of prediction accuracy with an RMSE that was close to 0 (0.00000001986) compared to the ANN with an RMSE of (0.00008809) Table (7.1). In this section, the study integrated the developed models within the computational design tool (Grasshopper) to validate the results and develop the workflow of the proposed surrogate model.

*Table 7.1. Performance comparison of ANN and RF for cooling load data.*

| Performance metric    | Artificial Neural Network (ANN) | Random Forest (RF) |
|-----------------------|---------------------------------|--------------------|
| RMSE                  | 0.00008809                      | 0.00000001986      |
| MAE                   | 0.00718157                      | 0.00003168         |
| R <sup>2</sup> -score | 0.8531965                       | 0.99985            |

The workflow of the surrogate model was developed with three different scripts to define the inputs of the model depending on the number of cases required to make a prediction of hourly cooling loads. Once the office room was generated in Grasshopper, inputs could be entered into G-H CPython from the following selections:

- Defining the inputs from slider components, which allows the prediction only of hourly cooling loads for individual cases as shown in Figure (7.11).
- Defining the inputs through a panel text, which allows the prediction only of hourly cooling loads for multiple design scenarios as shown in Figure (7.12).
- Defining the inputs from a CSV. File, which allows the prediction only of hourly cooling loads for an unlimited number of design scenarios as shown in Figure (7.13).



*Figure 7.11: Selection of inputs from the slider component*



## CHAPTER 7: DEPLOYMENT OF THE DEVELOPED SURROGATE MODELS

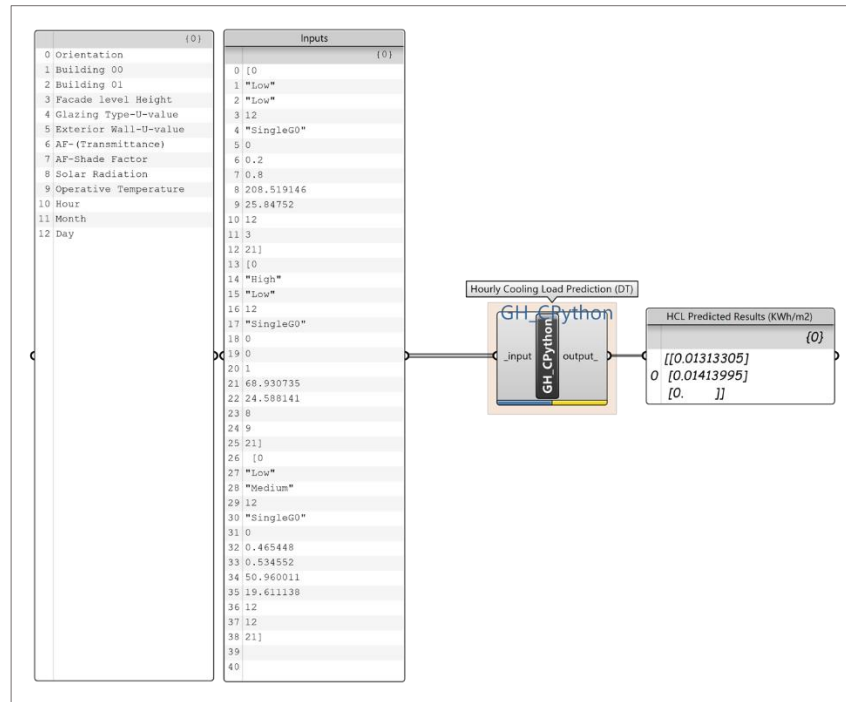


Figure 7.12: Selection of inputs from a panel component for three different design scenarios

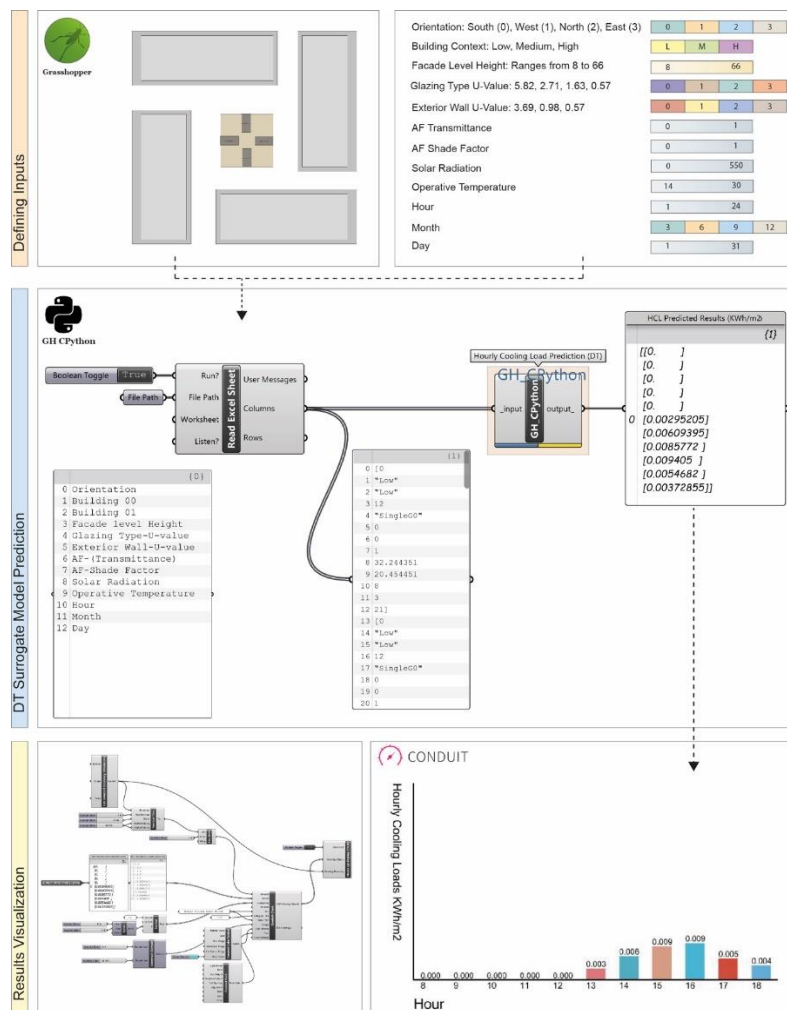


Figure 7.13: The developed workflow to predict hourly cooling loads within the Grasshopper interface

## **CHAPTER 7: DEPLOYMENT OF THE DEVELOPED SURROGATE MODELS**

Two different random cases were selected which varied in terms of input parameters to compare the hourly cooling load results of the RF and ANN model prediction to simulation.

- (P-AF-SCM C4\_Or0\_B00Low\_B01Low\_FLLow\_ExtW0\_Glaz0).
- (P-AF-SCM C4\_Or1\_B00High\_B01Low\_FLMedium\_ExtW1\_Glaz3).

The first case is located in the South orientation of the office tower, with an office height of 12m, and surrounded by low building contexts. Meanwhile, the second case is in located in the West orientation, with an office height of 24m, and surrounded by a mix of high and low building contexts Table (7.2). The experiment examined four months of the year (March, June, September, and December) in the daytime working hours of the day (6:00 am to 18:00 pm) to test the model prediction accuracy. The office room dimensions were fixed for all predicted cases with an area of 24m<sup>2</sup>, the window wall ratio was fixed at 80%, and the floor height was fixed at 4m. Detailed comparison analysis between the RF model predictions, the ANN model predictions, and the simulation predictions for an hourly cooling load for the two examined cases are presented in (Appendix E). The results show highly accurate prediction results where the predicted case results matched or were close to the simulation results. However, the RF model prediction performed best compared to the ANN model in terms of the accuracy of the hourly cooling loads prediction, which matched or almost matched the simulation results with a significantly minimal squared error as shown in Figures (7.14). These graphs show that the RF model was able to accurately predict the hourly cooling loads of case (1) for different months of the year (March, June, September, and December) for the examined daytime hours. Similarly, the RF model was able to accurately predict the hourly cooling loads of case the second case as shown in Figures (7.15).

*Table 7.2. The specifications of the examined cases.*

| <b>Case (1) – (P-AF-SCM C4_Or0_B00Low_B01Low_FLLow_ExtW0_Glaz0)</b> |                               |
|---|-------------------------------|
| Orientation   | South                         |
| Building Contexts B00   | Low                           |
| Building Contexts B01   | Low                           |
| Building Contexts B02   | Medium                        |
| Building Contexts B03   | High                          |
| Façade Height   | 12 m                          |
| Glazing Type – U-value  | Single glazing (SG) - 5.82    |
| Exterior Wall – U-value   | 3.69                          |
| Transmittance, Shade Factor, SR, and OT                             | Varied Hourly                 |
| Month   | March-June-September-December |
| Hours   | 6:00 AM – 18:00 PM            |

## **CHAPTER 7: DEPLOYMENT OF THE DEVELOPED SURROGATE MODELS**

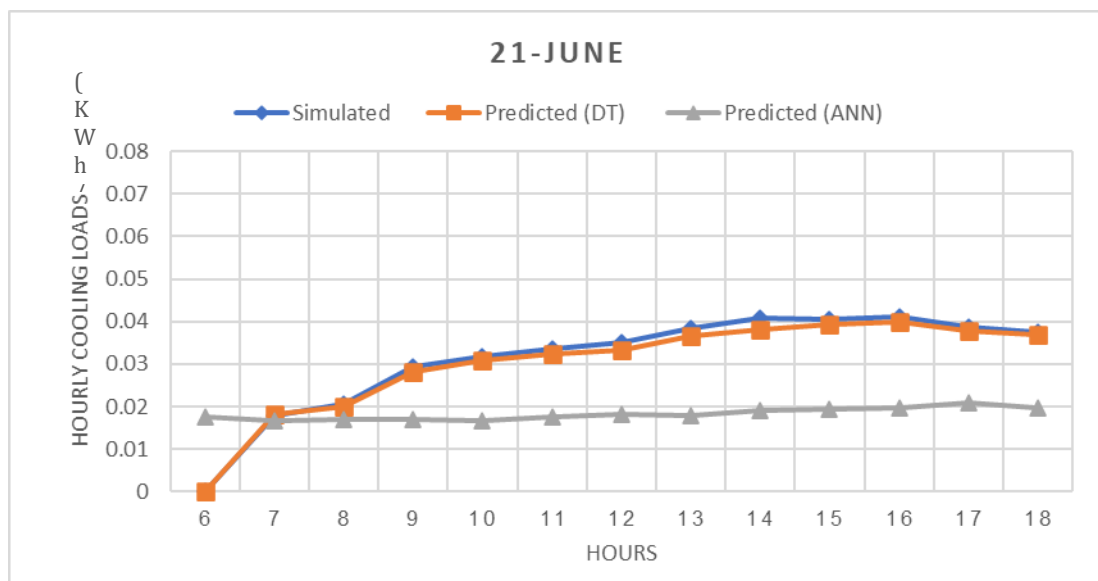
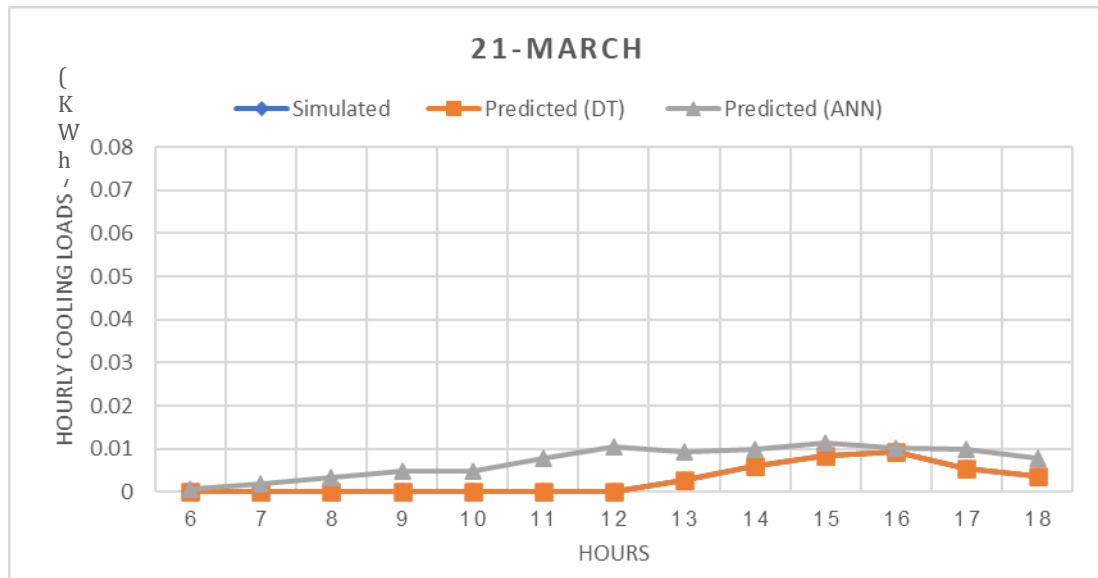
|  |                               |
|--|-------------------------------|
| Day  | 21                            |
| <b>Case (2)- (P-AF-SCM C4_Or1_B00High_B01Low_FLMedium_ExtW1_Glaz3)</b> |                               |
| Orientation  | West                          |
| Building Contexts B00  | High                          |
| Building Contexts B01  | Low                           |
| Building Contexts B02  | Medium                        |
| Building Contexts B03  | High                          |
| Façade Height  | 24 m                          |
| Glazing Type – U-value   | Triple glazing (TG) – 0.57    |
| Exterior Wall – U-value  | 0.98                          |
| Transmittance, Shade Factor, SR, and OT                                | Varied Hourly                 |
| Month  | March-June-September-December |
| Hours  | 6:00 AM – 18:00 PM            |
| Day  | 21                            |

Regarding time efficiency, the energy simulation was performed for the AF shading system model with a total time of 86 hours to generate 1,296 AF design solutions excluding the debugging during the simulation and modelling process. In addition, the completion of the modelling, the simulation settings, and the development of the algorithmic workflow of the AF systems that involve incident solar radiation analysis, shade factor analysis, and energy simulation took months. Solar radiation simulation for 50,545 design iterations in an hourly simulation consumed a total of 140 hours, and hourly shade factor analysis for each shading state (A, B, C, D, E, and F), with 8,760 hours for each state, consumed 17 hours with a total of 102 hours. On the other hand, training and testing the RF model consumed a total of 14 hours, and training and testing the ANN model consumed a total of 60 hours excluding the time spent generating the data for both models. Both ML models predicted the hourly cooling loads to within 2 to 3 seconds. This comparison highlights the significant time reduction when using ML models to predict cooling loads compared to existing BPS tools. This approach will be even more effective when simulating large scale projects.

The study focused on hot climate regions; thus, predicting cases for different climates would require the generation of new data and the retraining of the surrogate model for the new climate. However, there is no need to train a new shading geometry because the trained model is derived from the numeric shaded area parameter. Therefore, regardless of the geometry, only the shaded area is required as input to make the prediction. To make a generalized model, future work can be carried out to generate a variety of building contexts to train the model. In addition, further work needs to be carried out to test if removing all building contexts from the surrogate model and training it only on solar radiation and

## CHAPTER 7: DEPLOYMENT OF THE DEVELOPED SURROGATE MODELS

operative temperature is sufficient to achieve accurate results. With this approach, the indoor and outdoor sensor point is needed; this can be obtained by generating a range of solar radiation that covers a variety of cases. This can produce a generalized model regardless of the building contexts and geometry, as the building contexts were added to test the diffuse and reflected solar rays on the building.



**CHAPTER 7: DEPLOYMENT OF THE DEVELOPED SURROGATE MODELS**

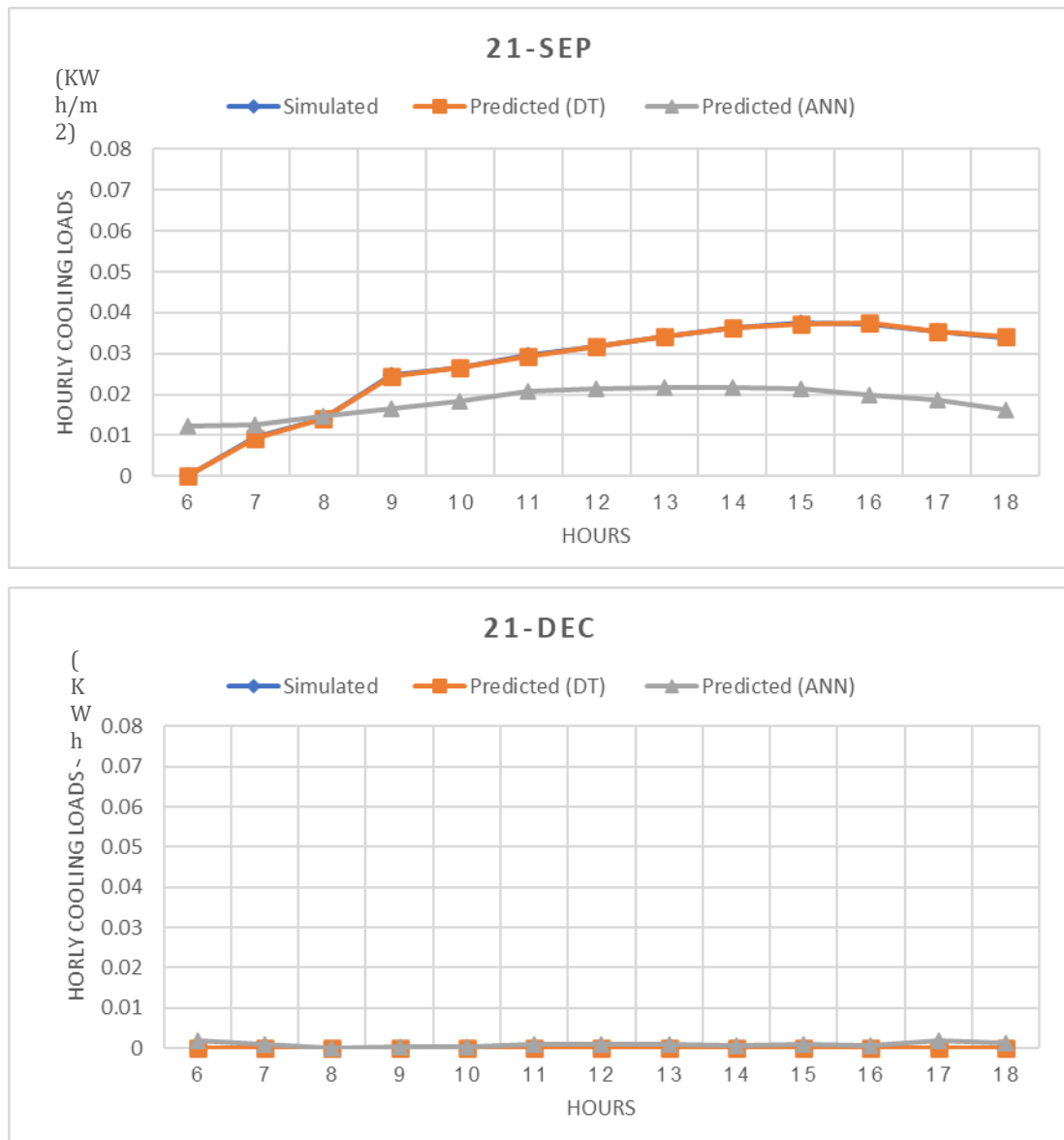
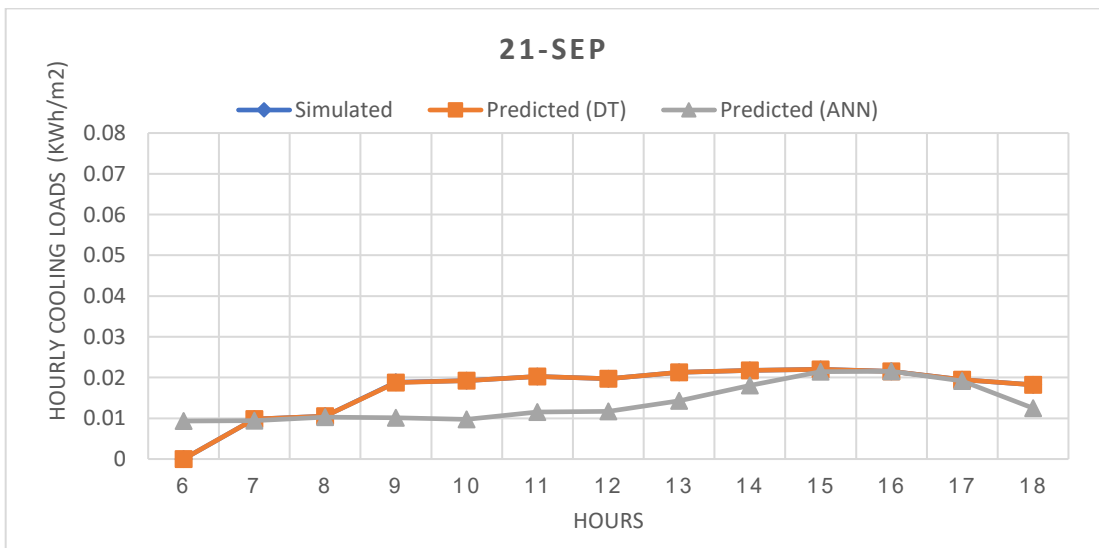
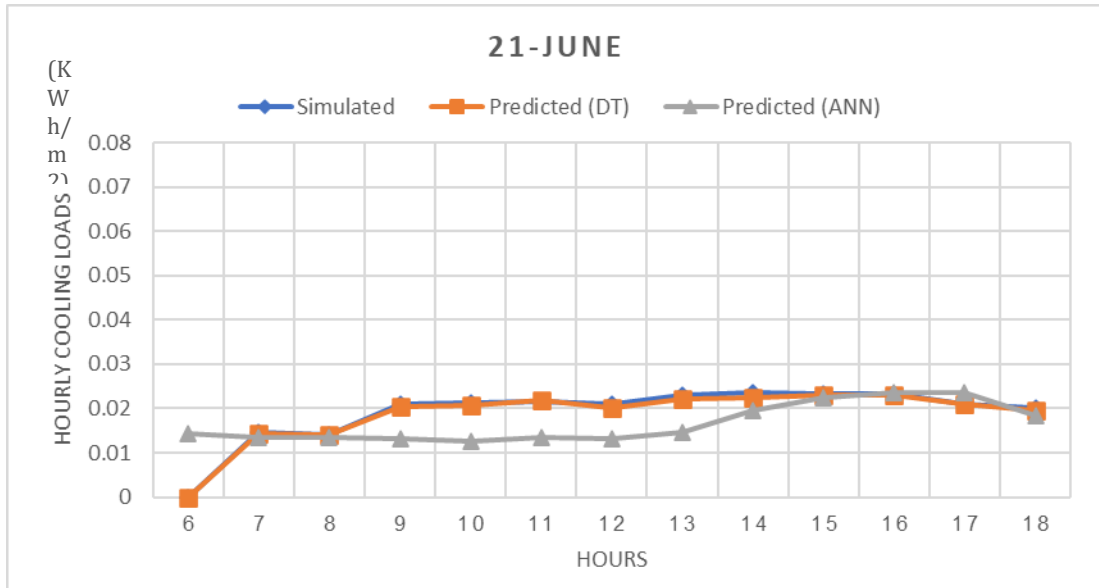
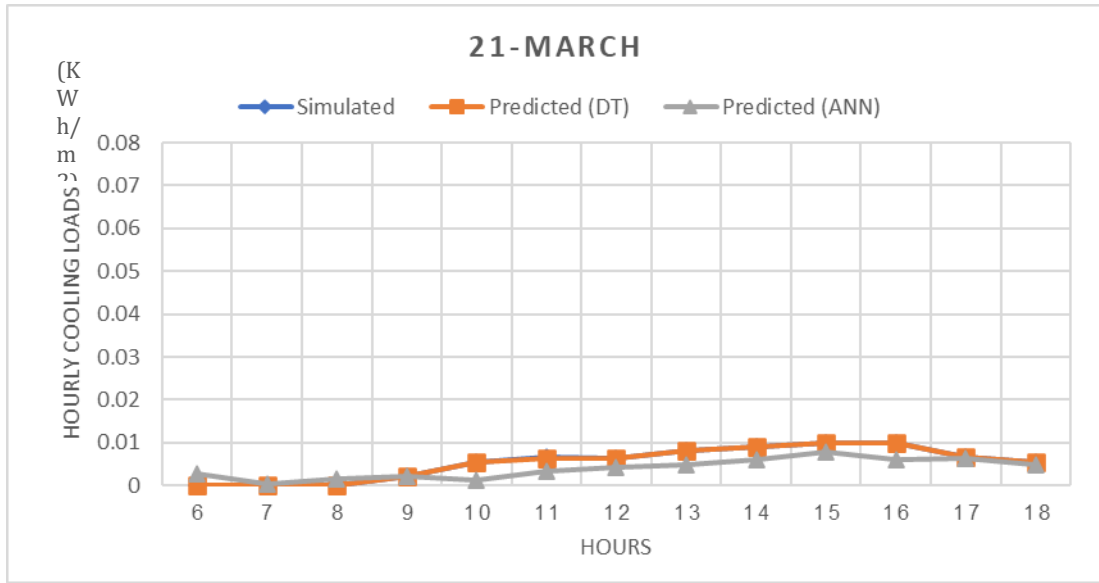


Figure 7.14: Comparison between RF model predictions, ANN model predictions, and simulation predictions of hourly cooling loads for four months of the year (March, June, September, and December).

**CHAPTER 7: DEPLOYMENT OF THE DEVELOPED SURROGATE MODELS**



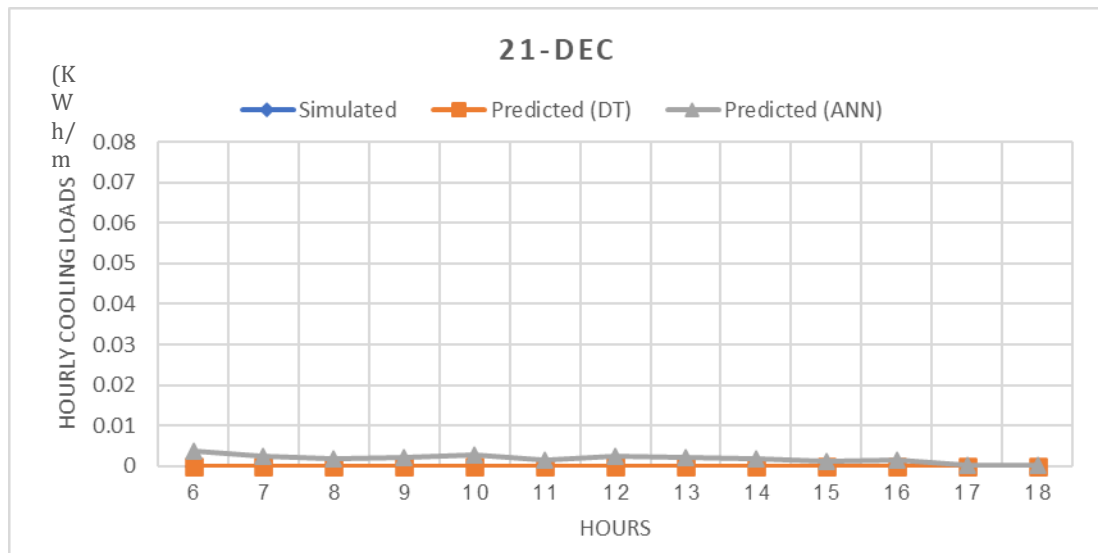
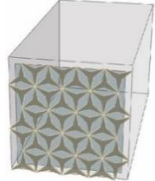


Figure 7.15: Comparison between RF model predictions, ANN model predictions, and simulation predictions of hourly cooling loads for four months of the year (March, June, September, and December).

### 7.6. Cooling Loads Prediction for Different Cities

The study examined different random cities that shared similar hot climate characteristics as the city in the current study. The aim of this experiment is to test the developed ML surrogate model’s applicability to predict the cooling loads of a new design of AF for other similar climates. The selected four cities are Jeddah SA, Kuwait KWT, Phoenix AZ, and Tucson AZ; they were chosen from climate zone 1B, which is characterised as a hot climate zone. Table (7.3) shows the input parameters used to test the accuracy of the developed surrogate models for the examined four cities. The study performed a simulation for the examined case in each city to compare the surrogate model’s accuracy prediction to the simulation prediction.

Table 7.3. Input parameters of the examined four cities.

|   |                            |
|---|----------------------------|
| P-AF-SCM C4_Or0_B00Medium_B01Low_FLLow_ExtW1_Glaz2                                  |                            |
|  |                            |
| Orientation   | South                      |
| Building Contexts B00   | Medium                     |
| Building Contexts B01   | Low                        |
| Building Contexts B02   | Medium                     |
| Building Contexts B03   | High                       |
| Façade Height   | 12 m                       |
| Glazing Type – U-value  | Double Glazing (DG) – 1.63 |
| Exterior Wall – U-value   | 0.98                       |

**CHAPTER 7: DEPLOYMENT OF THE DEVELOPED SURROGATE MODELS**

|   |                                 |
|---|---------------------------------|
| Transmittance, Shade Factor, SR, and OT | Varied Hourly                   |
| Month                                   | September                       |
| Hours                                   | 6:00 AM – 18:00 PM              |
| Day                                     | 21                              |
| Location                                | Jeddah, Kuwait, Phoenix, Tucson |

Based on the analyses, the results revealed that the RF model is more accurate than the ANN model to predict the hourly cooling loads of AF with a significant minimal error when compared to the simulated results. Moreover, the results demonstrate the prediction accuracy for all the examined hours, which proved that the ML surrogate models were able to make predictions that were very close to the simulation results when the input parameters are within the range of the trained inputs. For example, predicting hourly cooling loads for Jeddah and Kuwait was highly accurate, as these cities have a similar climatic pattern as the city in the current study as shown in Figures (7.16). On the other hand, predicting hourly cooling loads for Phoenix and Tucson was less accurate because solar radiation and operative temperature ranges varied compared to the current study as shown in Figures (7.17). Detailed results of the analysis are presented in (Appendix E).

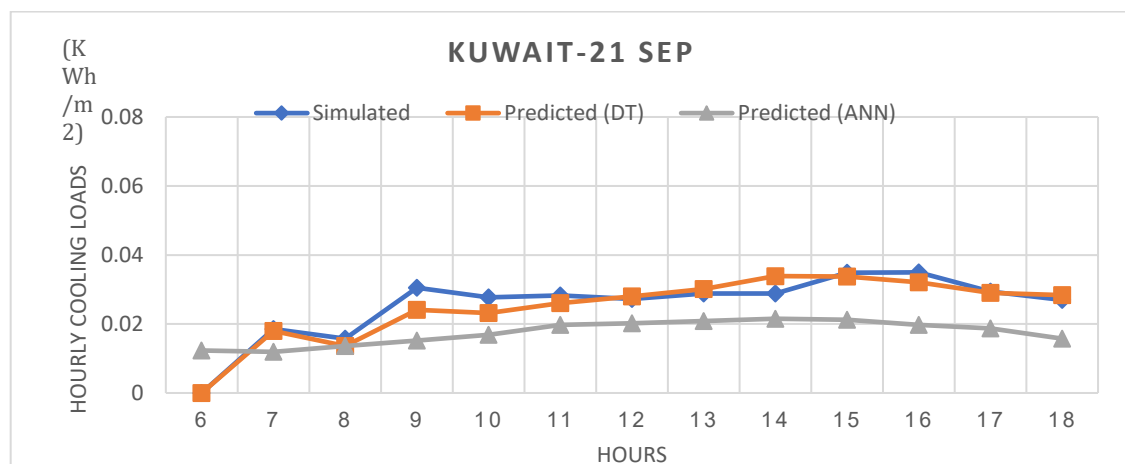
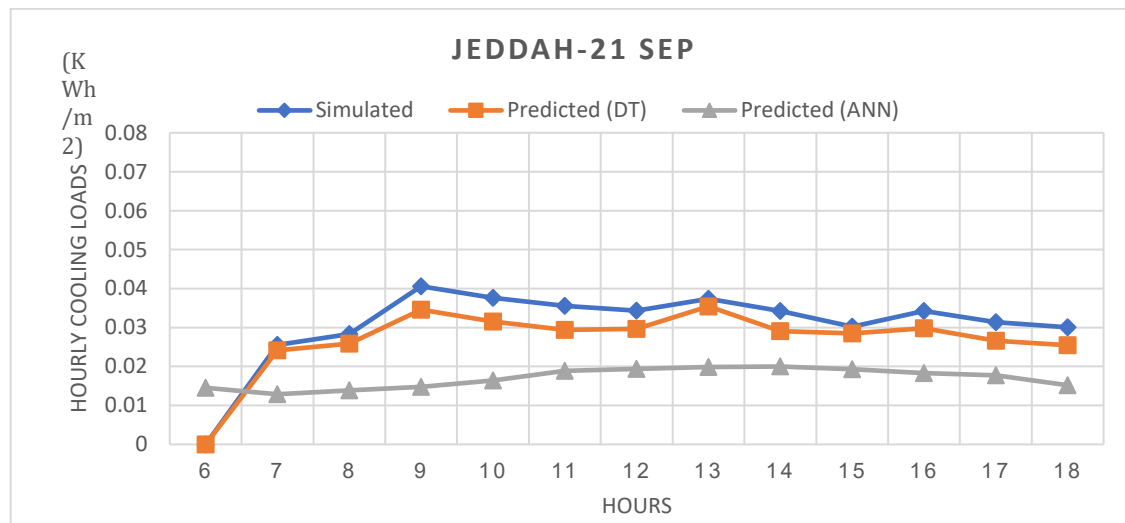


Figure 7.16: Comparison between surrogate models’ prediction and simulation prediction for Jeddah and Kuwait cities.



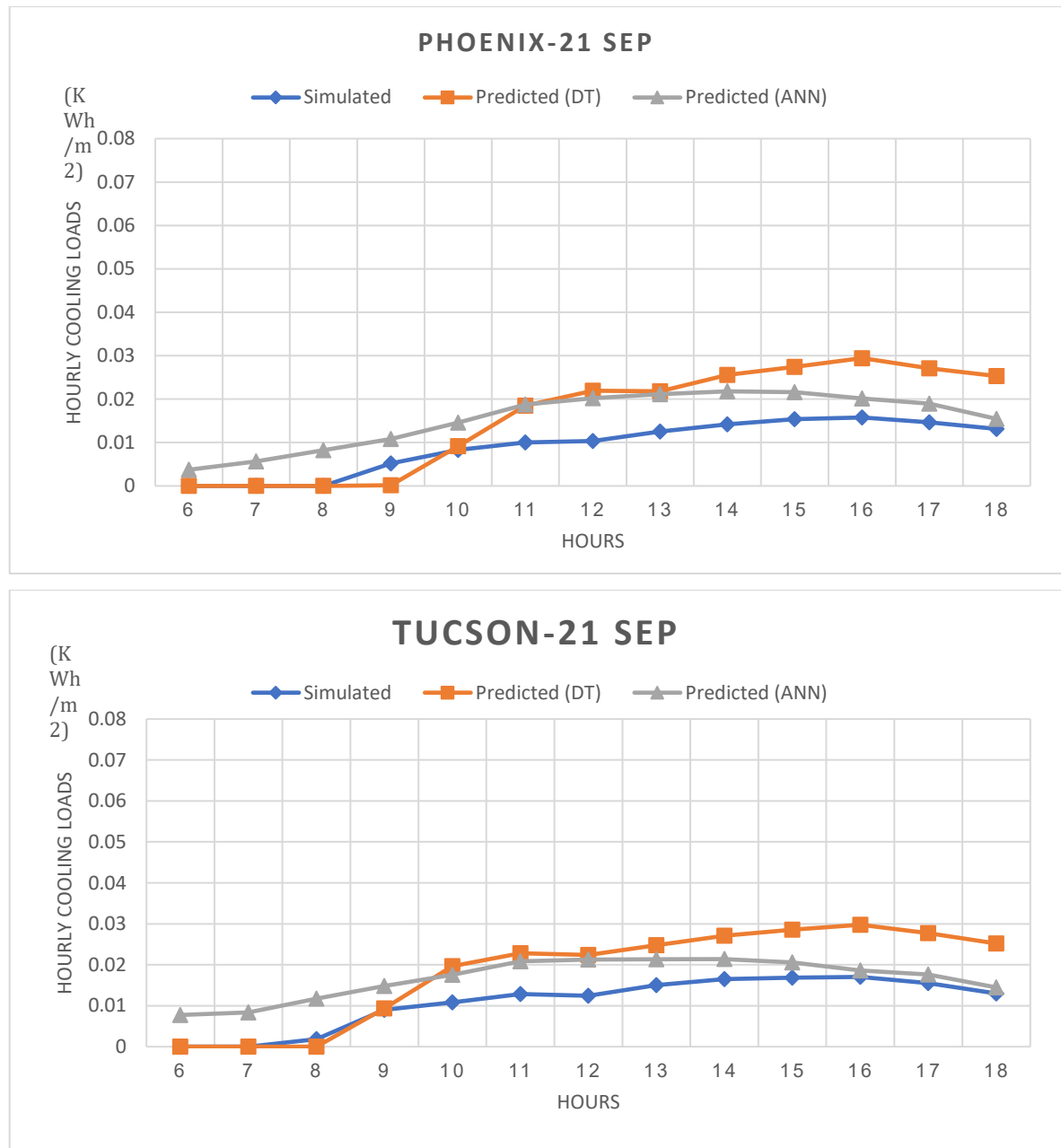


Figure 7.17: Comparison between surrogate models' prediction and simulation prediction for Phoenix and Tucson cities.

## **7.7. Chapter Summary**

This chapter presented the results of the surrogate models and compared them with the simulation results. The evaluation of the RF and ANN surrogate models was carried out based on the model prediction accuracy of new cases, time consumed to train and test the developed models, and time consumed to make a prediction against the time spent to make a prediction during simulation. In addition, the chapter presented the surrogate model workflow within a computational design tool to allow for instant feedback between the new design model and the energy performance evaluation. Different new design scenarios were examined to test the generalisability of the surrogate model to other scenarios. The findings of this chapter concluded that ML surrogate models can predict with greater accuracy both hourly cooling loads and hourly solar radiation. It was found that the RF model performed best in terms of prediction accuracy compared to the ANN model. The results also demonstrated that predicting new design scenarios would be more accurate if the new design ranges are within the input parameters on which the ML models were trained. However, once the input parameters vary more than the range of inputs of the surrogate model, the prediction is less accurate. Lastly, the surrogate model offered a significant time reduction in making predictions compared to simulation. The implementation codes of this experiment and the files are available at the following links:

[https://github.com/archammar/Predicting-Hourly-Cooling-Loads-of-Adaptive-Facades Using-Machine-Learning.git](https://github.com/archammar/Predicting-Hourly-Cooling-Loads-of-Adaptive-Facades-Using-Machine-Learning.git)

<https://github.com/archammar/Solar-radiation-prediction-for-office-tower-using-machine-learning.git>

## **CHAPTER EIGHT**

### **DISCUSSION AND CONCLUSION**

## **CHAPTER 8: DISCUSSION AND CONCLUSION**

### **8.1. Introduction**

This chapter presents a review and discussion of the results that emphasise the ability of AF shading systems to reduce the energy consumption in office buildings in regions with a hot climate. The chapter also discusses the findings of the machine learning (ML) surrogate models, which proved to be an effective method for predicting the performance of AFs during the early stages of design. It also revisits the research objectives of the study and explores how these objectives have been achieved. In addition, this chapter highlights the contributions to the current body of knowledge and states the limitations of the study. Finally, it concludes with recommendations for architects and façade engineers that are likely to promote the application of AFs in buildings, and it highlights suggestions for further work that have emerged as a result of the findings of this study.

### **8.2. Discussion of Research Findings**

The study aimed to answer the four research questions established initially to achieve the study's aim and objectives. The main results are discussed in relation to the research questions, which are covered in the subsections below.

#### **8.2.1. An Algorithmic Framework to Evaluate the Energy Performance of Adaptive Façades**

Assessing the performance of AFs during the design stages remains difficult due to their time-varying dynamic behaviour. In the majority of cases, the process concludes with experimental validations over mock-up scales, which increase expenses for stakeholders and limit their application in practice. Most existing studies focus primarily on the development of AF technologies that are capable of changing only their physiological properties in order to quantify their energy and environmental performance, such as switchable, thermochromic (TC), and photovoltaic-chromic (PVC) glazing systems. In addition, based on the analysed literature, it was found that limited studies examine the geometry-changing behaviour of AFs that adapt to outdoor climatic conditions due to the limitations and complexity of the simulation tools as discussed in chapter (2). Furthermore, the literature review revealed that most studies implement the control strategy system for conventional dynamic façades, such as venetian blinds, roller shades, dynamic blinds, louvres, etc., that are characterised by having a basic movement. This is because the adaptive behaviour is not

complex, and modelling and simulating the systems is embedded in most BPS software packages.

The analysed studies showed that 48% of developed AF systems did not implement an automatic control system, where an automatic system was applied mostly with conventional façades. Moreover, 39% of studies used a feed-forward control system, while 13% used a feedback control system to automate the shading system. It was also found that the limited studies that experimented with the time-varying behaviour used parametric tools in conjunction with EnergyPlus, Daysim and Radiance to model and simulate AF systems to analyse various environmental parameters. Therefore, in order to fill the gap in the body of knowledge, the study developed an algorithmic framework that considers the automatic control system of AF systems in relation to the environmental parameters. The study implemented the following steps to automate the changing behaviour of the AF: (1) controlling the opening size of the external AF shading system based on different outdoor and indoor sensors, (2) translating the calculated shade factor of each shading state into a transmittance schedule, (3) calculating the incident solar radiation on the exterior surface on an hourly basis, and (4) establishing a control scheme through an EMS, which is an embedded function in EnergyPlus to define sensors, control, and actuators in hourly time steps (Hong and Lin 2013). The developed algorithmic methodology permits the designer to evaluate various control scenarios during the design phase.

The proposed workflow confirmed what has been addressed in the literature regarding the complexity and difficulty in simulating the time-varying behaviour of AFs. The steps that were followed show that the process to simulate AFs requires computational effort, time, and programming knowledge.

### **8.2.2. The Impact of Adaptive Façades on Energy Performance in High Rise Office Buildings**

The results of this study confirm the saving potential of adaptive shading systems in hot climates for high rise office buildings. The following sections discuss the main findings of the simulation.

#### ***Building Envelope Parameters***

Prior to implementing the AF, the study examined different building envelope parameters, such as exterior wall and glazing types, with different values in a parametric evaluation, as these parameters affect the cooling energy loads of the building. The analysis focused on the building envelope to understand the most influential parameter affecting the cooling loads. The simulation results concluded that all combination cases that were simulated with a low

## **CHAPTER 8: DISCUSSION AND CONCLUSION**

SHGC value, with a low U-value of triple glazing and combined with higher thermal insulation, performed the best in terms of annual cooling loads. Meanwhile, the higher energy cooling consumption was observed with combination cases that had poor thermal insulation of exterior walls and used single-glazed windows. The results of the engineering parameters experiment revealed that in hot climate zones, where the air temperature is high and there is a great deal of solar radiation, the shading coefficient of the glazing system plays a crucial role in lowering the cooling energy demands in relation to solar gain. This indicates that the amount of solar heat gain can be lowered by decreasing the shading coefficient. Since solar gains are the most important factor in cooling loads, these findings suggest that developing shading elements may have a significant impact on cooling energy loads, and that relying on a prescriptive approach by modifying the values of the engineering parameters for the building envelope may not achieve the necessary reductions in solar gains.

### ***Fixed vs. Adaptive***

As presented in chapters 4 and 5, different scenarios of external shading systems include fixed vertical shading, fixed horizontal shading, AF with scaling movement, and AF with folding movement; these were simulated and compared to the base case model in terms of energy cooling consumption. Overall, all the examined external shading systems saved cooling energy loads since they reduced the solar heat gain. However, the simulation results revealed that the AFs with scaling and folding movements performed the best in terms of reducing the cooling loads compared to fixed shading and the base model. This is because AFs have the adaptability to react to short-term changes of the surrounding environment. The simulation results demonstrated that an AF with a light dimming strategy reduced the cooling loads by 36.7%, 34.6%, 33.6%, and 33.8% for the south, west, north, and east orientations, respectively compared to the base case model. On the other hand, when AFs were compared to the fixed shading system, the cooling loads were reduced by 27.3%, 27.2%, 26.3%, and 26.9% for the south, west, north, and east orientations, respectively. The obtained results align with several studies that compared AF shading with fixed shading and a base model (Hammad and Abu-Hijleh 2010; Giovannini et al. 2015; Lee 2019; Sheikh and Asghar 2019; Bui et al. 2021; Attia et al. 2022), which proved that an adaptive shading system is more effective in terms of cooling load reduction.

When the two proposed movements were compared, the results showed that both the scaling and the folding movements have almost a similar performance in terms of cooling energy loads. Based on the analysis, although external shading devices can greatly enhance

## **CHAPTER 8: DISCUSSION AND CONCLUSION**

the thermal performance of the building envelope and the energy efficiency of office buildings, their effectiveness may be compromised if the thermal performance of the wall and glazing types is not carefully examined.

### ***Automatic Control Scenarios***

Following that, the study examined different automatic control scenarios in terms of cooling loads, as these are the backbone of any AF shading system. Employing environmental sensors to automate the AF shading system in either an open loop or a closed loop mechanism can have a positive influence on energy loads. Therefore, the study evaluated four control scenarios, including (C1: incident solar radiation on window (W/m<sup>2</sup>), C2: transmitted solar radiation (W/m<sup>2</sup>), C3: direct solar radiation (W/m<sup>2</sup>), and C4: combinations of incident solar radiation and operative temperature), two exterior parameters, one interior parameter, and one that combined both exterior and interior parameters. Overall, the results showed that all four control scenarios resulted in a reduction in cooling energy loads; however, some scenarios were not effective in terms of lighting energy savings and providing adequate natural daylight.

The simulation results revealed that AF with control C3 and C4 achieved a better performance in terms of cooling load reduction. However, in the case of C3, which used direct solar radiation as a trigger, it improved the cooling loads while it increased lighting loads due to the high number of times that the shade system was completely closed. Consequently, if outdoor views are a priority, this control strategy poses potential concerns in addition to lighting-saving issues. On the other hand, control scenario C2, which applied a transmitted solar radiation sensor, achieved the lowest performance compared to other controls, as it maximised the cooling loads. Therefore, these observations indicate that outdoor-based control scenarios perform better than using solely indoor controls. Moreover, the results demonstrated the capability of such control scenarios to close the shades prior to allowing the penetration of undesired solar gains to indoor spaces.

The results also discovered that when taking into consideration the need to reduce both cooling loads and lighting loads, the most efficient energy performance was achieved with control scenario C4, as it applied a closed loop mechanism that considered both outdoor and indoor environmental parameters. Hence, a closed-loop control algorithm performed better than the proposed open-loop scenarios. Moreover, the results showed that control scenario C4 achieved an average energy saving of 30.5%. These findings are generally consistent with Tabadkani et al.'s (2021) study, which investigated the potential of different automatic control systems to reduce energy consumption in different climates.

## **CHAPTER 8: DISCUSSION AND CONCLUSION**

With respect to building orientation, the results observed that the performance of automatic shading control can be influenced by building orientation, which exploits the sun's position and its positive or negative effects on the interior environment. Consequently, the energy cooling loads, solar gain, and lighting loads varied based on the orientation. The findings demonstrated that the south and west orientations consumed higher cooling loads; however, these orientations benefited the most in terms of cooling load reductions, while lighting load variations were relatively similar among all orientations, except for control scenario (C3). On the other hand, all control scenarios with north orientation performed similarly in terms of annual cooling loads, due to the low levels of solar radiation intensity that strike this particular façade. Thus, the AF is mostly open, except during the summer months of May through to August, when it receives more sunlight in the morning and afternoon to block solar radiation from the northwest and northeast.

Furthermore, the results showed that the AF in the west orientation was mostly closed (state F) or 20% semi closed (State E) during the summertime from May to September in the afternoon between 2:00 pm and 4:00 pm, which refers to the hours that exceeded the SR and OT thresholds. Meanwhile, it was fully open (state A) in the morning from 6:00 am until 12:00 pm, where the SR and OT values were in the acceptable range. Then, the adaptive shading altered to different states after 12:00 pm, and were adjusted mostly between 20% (state E) up to 80% (state B) for the hours from 12:00 pm to 2:00 pm and from 4:00 pm to 6:00 pm. Hence, in each orientation, the shading states performed differently, as orientations varied in terms of the solar radiation received on the building envelope and the level of operative temperature inside the room.

### **8.2.3. Parametric Generative Database based on Simulation Approach**

Due to the absence of real data, the study generated a synthetic database parametrically using simulation. It was not possible to access real data, as there were no buildings in the studied region that implemented an AF shading system. Therefore, simulation was used in this study to collect data because it is the most cost-effective way when time and money are the main constraints and because it is a widely used method especially given the unavailability of a physical building in which to conduct experiments. Furthermore, with simulations, it was possible to analyse a wide range of design scenarios and complex modelling that could not be accomplished easily on a real-world scale. The study employed a parametric simulation technique within Grasshopper to perform a wide range of design iterations since ML demands a sufficiently large database. Different parameters were considered to create the database of AF shading systems including the building envelope, a



responsive time scale of AFs, orientation, building contexts, and environmental parameters. In terms of data processing, it was found that compared to real data, simulated data required less time for pre-processing prior to being used to train the ML models. This is because most real data contain errors, such as missing values, duplicate data, inconsistent data, and noise data.

### **8.2.4. Machine Learning (ML) Models to Predict Energy Performance of Adaptive Façades**

Due to the complexity and the enormous amount of time required to simulate AF shading systems, the study proposed the use of the ML method to provide alternative emulators of simulation tools. Thus, as presented in chapter (5), different supervised ML models were developed including Artificial Neural Network (ANN) and Random Forest (RF) models to predict both the hourly cooling loads (HCL) of AF and the hourly solar radiation (HSR) in the early design stages. These models were trained, tested, and validated using the generated synthetic database that were generated based on the simulation in chapter (4). The developed surrogate models were proposed to examine the potential of using ML techniques as alternative emulators of simulation tools for predicting the energy performance of AF shading systems. In general, the results demonstrated that surrogate modelling has immense potential to accurately predict the solar radiation and cooling loads of AFs in an office tower. In the case of ANN, the model achieved an accuracy of ( $R^2$ : 0.8531965) between the simulated and the predicted hourly cooling loads of AFs. On the other hand, in the case of RF, the model showed a high accuracy of ( $R^2$ : 0.99985) between the simulated and the predicted hourly cooling loads of AF.

These obtained results are generally consistent with other studies that employed ANN and RF models to predict energy performance in buildings (Wong et al. 2010; Kialashaki and Reisel 2013; Zhang et al. 2015; Deb et al. 2016; Khayatian et al. 2016; Ilbeigi et al. 2020; Yu et al. 2010; Ahmad et al. 2017b; Asl et al. 2017).

The results of the study revealed that both the ANN and RF models can predict HCL and HSR. However, the RF model performed better in terms of prediction accuracy compared to the ANN model in both the HCL and HSR predictions. This is because RF algorithms have a better performance when most of the input features are categorical. During training the model, it was found that random forest has a significant advantage over neural network modelling since DTs are highly suitable for categorical inputs in the learning setting. In addition, random forest is an ensemble algorithm; this is a class of ML where a set of learning programs are combined together to give accurate predictions Instead of relying on a single

## **CHAPTER 8: DISCUSSION AND CONCLUSION**

algorithm, the predictions from such multiple algorithms are considered, and the error is reduced significantly. Since this feature is implicitly embedded with random forest modelling, its performance was significantly better than that of neural networks in this case. These findings align with the findings of several studies (Tso and Yau 2007; Ahmad et al. 2017b; Ahmad et al. 2017a) that compared the use of ANN and RF and concluded that RF performed better in predicting the energy performance due to the nature of the inputs or features.

Furthermore, in both models (ANN and RF), there were no significant differences in the results achieved by K-fold cross validation experiments compared to hold-out validation experiments. It was also found that K-fold cross validation requires more computational power and time for training compared to hold-out validation. Regarding ANN efficacy, when training the ANN model to predict the energy performance, different parameters were found to significantly affect the efficacy of the ANN and its accuracies, such as the architecture of ANN, the learning rate, the batch size, and the number of epochs. With respect to the size of ANN architecture, the study found that selecting the optimum structure is an essential step to optimize the ANN model. Therefore, different numbers of hidden layers and numbers of neurons were tested to avoid the under-fitting and overfitting of the data and for better generalisation of the network to be used with unseen future data. In the case of cooling loads, it was found that as the number of layers and neurons increased, the performance score of the ANN model dropped compared to shallow networks. This indicates that having deeper networks with a large number of neurons resulted in the overfitting or poor generalisation of the data. On the other hand, the performance of deeper networks with a lower number of neurons (64 and 128) was comparatively better than those with a larger number of neurons (256 and 512). The experiments showed that as prediction accuracy converged, some measures should be specified in order to minimise ANN training time. For example, training should cease whenever the validation loss increases compared to training loss using an early stopping criterion.

In the case of solar radiation, it was found that as the number of hidden layers increased, the performance metrics decreased up to a three-layer network. Then, selecting a higher number of hidden layers and neurons did not make a significant difference in the accuracy of the model; therefore, the selected architecture was a three-layer network with 256 neurons in each layer. The results in both experiments revealed that ANN architecture can vary based

on the training sample size, the type of features, and the complexity of the relation between input and output variables.

Regarding RF efficacy, the number of trees was found to significantly affect the accuracy of the RF model. In the case of cooling loads, the results revealed that, as the number of trees increased, the performance of the RMSE score showed an oscillatory behaviour. On the other hand, in the case of solar radiation, the results showed that there was no significant variation in the RMSE value as the number of trees increased. In terms of training time, it was shown that it is faster to train and tune RF modelling than ANN modelling. The training time for the RF model was significantly less than for the ANN model (a few seconds compared to minutes). This is due to the simplicity and lower number of parameters used to tune the model compared to ANN training. It was evident that RF performed better with superior performance metrics values (lower RMSE, MAE, and higher  $R^2$  values). Both models showed a strong performance for non-linear mapping generalisation ability; hence, it can be concluded that both models can be effective in predicting the hourly solar radiation and hourly cooling loads of AF shading systems.

Regarding the time series data modelling, it was found that time window approach achieved better performance compared to time differencing approach. Moreover, the results revealed that processing both time series data and non-time series data together is not an effective approach. Depending on the modelling situation, sometimes non-time series inputs are important and cannot be neglected. Thus, the conventional method of modelling can be more effective due to the influence of non-time series inputs in the prediction.

### **8.2.5. Surrogate Model to Assist in Early Design Stages of AF for Decision Making**

Current building simulation tools are unable to keep up with the speed of early design phases since evaluating a single concept requires defining a large number of parameters. Therefore, the architect's creative process will be disrupted by the extended run time of the simulation and the AF system's complexities. After training and validating the model, the trained surrogate models were imported into a computational design tool (the Grasshopper environment) to develop a workflow for the proposed surrogate model to provide instant feedback between a new design model and energy performance evaluation. The study showed that the workflow of the surrogate model within Grasshopper was simplified in comparison to detailed simulation, and the prediction and computation time were drastically reduced, which is essential for early design phases. This highlights the time savings associated with using ML approaches for prediction as opposed to simulation tools.

## **CHAPTER 8: DISCUSSION AND CONCLUSION**

With regard to prediction accuracy, unseen cases and new design cases were tested to evaluate the developed surrogate model. In the case of hourly solar radiation prediction, random cases were selected, and the results revealed highly accurate prediction results where the predicted results using the RF model matched the simulation results. Moreover, the results demonstrated that the RF model predicted the solar radiation of the proposed 150 new cases with high accuracy, and the time required was reduced compared to simulation. In the case of hourly cooling loads, the results revealed highly accurate prediction results, with predicted case outcomes matching or reaching close to simulation outcomes. Nevertheless, RF model prediction outperformed ANN in terms of the prediction accuracy of hourly cooling loads, with a minimal squared error. In addition, a significant time reduction was observed for predicting cooling loads; thus, this approach will be even more effective when simulating large scale projects. The results also observed that predicting new design scenarios would be more accurate once the new design ranges within the input parameters of the ML models that were trained on. Once the input parameters vary more than the range of inputs of the surrogate model, the prediction will be less accurate.

Architects and façade engineers can utilise the developed surrogate model in practice in the early stage of the design for decision making regarding to any proposed adaptive skin that is within a hot climate zone and falls within the range of the trained data. To use the surrogate model, the input of the new geometry has to be defined and placed in the same order as the developed workflow. The workflow is easy to use for energy prediction because users are not required to have extensive knowledge regarding the use of ML algorithms or coding. However, parametric design skills are required to utilise the proposed workflow. The proposed surrogate model would be easier and more attractive for users if the model were applied as a design tool. Moreover, to investigate the easiness or the difficulties of using the proposed tool, a study can be conducted to evaluate the usability of the tool by using the system usability scale (SUS). This measurement will be useful in measuring how easy or difficult using the tool is in practice.

### **8.3. Achievement of the Research Objectives**

Five objectives were established as the central aim of the research. The following sections provide a detailed demonstration of how this research was effectively carried out through the use of a quantitative research method and how each of the objectives was achieved.

### ***Objective One: “Investigate the impact of adaptive façades on energy performance”***

This objective was addressed in Chapter 2 by conducting a comprehensive literature review regarding the impact of AFs on energy saving and the evaluation process of their performance. The literature review presented the existing AF studies looking at different factors including AF system type, the adaptability of the system, the performance, and the influences of AFs on buildings' energy consumption. In addition, the literature review explored the challenges and difficulties designers face in predicting the performance of an AF shading system using the current BPS tools. It also examined some of the current simulation tools, and their limitations regarding AF performance prediction were highlighted. The literature revealed that most simulation software tools have difficulty modelling complex AF systems whose geometry components vary based on minute, hour, or seasonal time steps. In addition, there was no straightforward approach for modelling the adaptive behaviour of a façade. It was also found that, due to the complexity and interface constraints of existing PBS systems, only a few researchers had adapted an automatic control system to automate non-conventional AF systems. However, automatic control was found mostly in the case of façades with basic movement, such as venetian blinds, roller shades, and dynamic blinds. It was discovered that studies in the literature addressed the capability of employing a co-simulation technique, such as Energy Management System (EMS), to evaluate and control the AF system.

### ***Objective Two: “Develop an algorithmic workflow to evaluate the energy performance of AF shading system”***

This objective was achieved in Chapter 4 through the use of a computational parametric tool ‘Rhino 3D’ and its plug-in ‘Grasshopper’ to assist in the parametric generation and simulation of the AF shading systems. Moreover, Ladybug and Honeybee plug-ins were utilised; they were linked to Energy Plus and Radiance to calculate energy loads and solar radiation. The algorithmic workflow created a link between plug-ins including Ladybug, the Honeybee tools, and Energy Plus for running the simulation with EMS to program a code to automate the AF system in each time step of the simulation. The workflow successfully addressed the time-varying dynamic behaviour of AFs in relation to indoor and outdoor environmental conditions. A coded conditional statement was used within EMS to define different environmental sensors including incident solar radiation, direct solar radiation, transmitted solar radiation, and operative temperature with a predefined threshold for each sensor. Moreover, this objective was addressed in (Chapter 5) to evaluate the energy

## **CHAPTER 8: DISCUSSION AND CONCLUSION**

performance of AFs. Different external shading systems (fixed and adaptive) were compared in terms of energy consumption. In addition, different automatic control scenarios were evaluated to select the one that performed best in terms of energy cooling reduction. The findings concluded that an AF shading system is more effective in terms of cooling load reduction compared to static façades. It was also found that control scenario C4, which triggers both incident solar radiation and operative temperature in a closed loop mechanism performed better than other control scenarios.

### ***Objective Three: “Generate a synthetic database of AF cooling energy loads of offices to train and test the surrogate models”***

To achieve this objective, both a simulation and parametric tools were used, which facilitated performing a large number of simulation iterations. A generative parametric office tower and its urban context were designed and simulated in a generative way. Different dynamic inputs were defined to create a range of different design scenarios. Within the simulation framework, the Colibri plug-in tool was integrated to step through all the design variations automatically to create the dataset. In addition, the TT toolbox plug-in tool was used to store the resultant data in an Excel spreadsheet of all the design iterations. To that end, different databases were generated including a solar radiation (KWh/m<sup>2</sup>) database, a shade factor (SF) database, and an energy (cooling loads) (KW/m<sup>2</sup>) database.

### ***Objective Four: “Develop machine learning models to predict energy performance of AF in the early stage of the design”***

This objective was achieved by employing two different supervised ML algorithms (ANN and RF) to predict the hourly cooling loads of AF in an office tower. The simulation created the synthetic database, which was afterwards imported and pre-processed into two ML models. The collected cooling loads database and solar radiation database were used to perform the training. The models were constructed utilising the Python programming language (PyTorch framework) and (scikit-learn). The development of the surrogate model consisted of three major steps: data pre-processing, model training, testing, and hyper-parameter optimisation, and model validation. Prior to the training of the surrogate model, the data were split into different sets, namely, a training set, a testing set, and a validation set. Following that, a hyperparameter tuning procedure was carried out to select the most suitable parameters. In addition, ANN and RF models were compared in both scenarios of the design objectives, namely, hourly solar radiation and hourly cooling loads, in terms of prediction accuracy. The results showed that the RF model performed better than the ANN model in terms of prediction accuracy. Therefore, ML surrogate models showed a promising

## **CHAPTER 8: DISCUSSION AND CONCLUSION**

approach to evaluate the AF hourly cooling loads in an office tower. It was also found that when developing an ML surrogate model, it is essential to employ a substantial dataset to ensure highly accurate prediction outcomes.

**Objective Five: “Establish a workflow that incorporates the surrogate model within a computational design tool to assist in decision making in the early design stages.”**

This objective was accomplished by deploying the developed surrogate models into a computational design tool (Grasshopper). The surrogate models (ANN and RF) were saved as a PyTorch file to run the models in an external environment. The models were then loaded into Grasshopper using GH-C Python to import in python libraries. The workflow in Grasshopper was created to predict the energy performance (cooling loads) of the design scenarios of an AF system early in the design process to assist in making design decisions. To define the inputs of the model, the workflow was developed with three alternative scripts: from a loaded CSV file, from the slider's components, or from a text panel. The hourly cooling loads and hourly solar radiation were visualised in GH-C Python and using the Conduit plugin tool. After that, the surrogate models were evaluated based on prediction accuracy, time efficiency, and potential for generalisability. The findings revealed that the workflow of the surrogate model in Grasshopper was easier than using simulation and that the amount of time needed for prediction and computation was dramatically reduced. The findings also showed that the input of new cases has to fall within the range of the input parameters of the trained ML models to achieve accurate results.

Architects and façade engineers can use the developed surrogate model in the early design phases to predict the energy cooling loads of an AF in an office tower instantly to assist in decision making, before other architecture, engineering, and construction systems are incorporated into the design. This workflow allows architects and façade engineers to evaluate the adaptive skin in terms of energy consumption and solar radiation analysis on the building envelope, and to evaluate the automatic control system. In addition, they can use the proposed model for large urban projects that required massive simulation runs, as the proposed model reduces the time spent on the simulation process, which often disturbs the thinking process in the early design phases.

### **8.4. Simulation Novelty and Surrogate Model Generalizability**

Existing building performance tools (BPS) were originally intended for evaluating static façades, where alterations to the façade's shape are neglected during the simulation

## **CHAPTER 8: DISCUSSION AND CONCLUSION**

process. The simulation technique for conventional fixed envelopes is straightforward and involves only a few variables, such as the U-value and g-value, to create accurate predictions. In contrast, an AF is more complex and comprises a greater number of components, making it more challenging to properly predict its building performance. These features include (1) the behaviour of time variation, (2) the modelling of the dynamic operation of the facade adaptation, and (3) the multiple physical domains. Recent studies have indicated that simulation software does not support modelling complex AF systems that fluctuate on a minute-by-minute, hourly, or monthly basis (Loonen et al. 2017).

Recent studies have not properly examined the automatic control system required to automate complex (non-conventional) AF systems dependent on various environmental parameters due to the complexity and interface limitations of current BPS systems. Nonetheless, the automatic control system was employed successfully for basic façades with basic movement (such as Venetian blinds, roller shades, dynamic blinds, and louvres). Driven by this knowledge gap, the simulation of non-standard AFs in this research includes a novel control technique that was developed to address the limitations of existing simulation interfaces. EnergyPlus includes a built-in function called EMS, which is where the controlling mechanism is implemented to modify the opening percentage on an hourly basis in response to varying internal and external environmental variables. The complex shading geometry is expressed as a shaded factor area on the window and translated into a transmittance schedule and called within the EMS prior to each simulation for the software to understand the geometry. It is important to note here that expressing the geometry as a shading factor makes the workflow generalizable to other shading geometries. As a result of this novel algorithmic workflow, architects and façade engineers can model and simulate a variety of adaptive façades and simulated their behaviour in a unified parametric computational environment.

The surrogate model was developed within a computational design tool to assess the energy performance of AFs in the early stages of the design in a significantly faster time compared to simulation. The proposed model is effective for large urban projects that required massive simulation runs, as the model reduces the time spent on the simulation process.

While the surrogate model achieved high accuracy on unseen data (99% accuracy), the time and resource limitations of this dissertation placed constraints on the scope and size of the dataset used for training. As a result, the surrogate model can only be applied to buildings within hot climatic regions. Its generalizability to other climatic regions will require further work and training on a larger and more diverse dataset. However, the contribution of this



research is in defining the framework and methodology required to accurately simulate AF and build surrogate model for any climatic region.

### **8.5. Contributions to the Body of Knowledge**

This research makes novel contributions to the knowledge as follows:

- A comprehensive literature review has revealed the impact of AF on energy performance as well as a knowledge gap in how to accurately simulate it.
- A comprehensive framework was developed that allows architects and façade engineers to evaluate the benefits of AFs in terms of energy saving in the early stages of the design, as there is no straightforward framework.
- A generative of a large synthetic database of AFs were performed with a different range of parameters considering the time-varying behaviour of AFs in a working environment. Then, this database was used to develop the ML surrogate models.
- This study is the first to explore the potential of ML models to predict the energy performance of AFs, thus overcoming the complexity of simulation tools and reducing the computation time of prediction.
- A surrogate model as developed within a computational design tool to assess the energy performance of AFs in the early stages of the design.

### **8.6. Research Limitations**

Although the findings of this study have been very encouraging, there are some limitations. The following present the limitations that the researcher encountered while carrying out this study:

- This research investigated the impact of AF shading systems on energy performance for the office buildings in Riyadh, Saudi Arabia. The scope of this research is limited to the assessment of AFs in regions with the characteristics of hot climates. Thus, the results obtained in this research cannot be generalised to other climate zones; however, it is feasible to apply the developed algorithmic framework of AFs to other different climates.
- Due to the non-existence of AF shading systems in the region of the study to obtain real data or to conduct on-site measurements, the researcher had to rely on a synthetic database using simulation approach.
- Due to computational power constraints, only six shading positions were considered, resulting in a restricted range of view ratio to the outdoors.

## **CHAPTER 8: DISCUSSION AND CONCLUSION**

- The developed framework is limited to AF types that have an extrinsic control system. Hence, AFs that have intrinsic controls or material-based actuators cannot apply the proposed control framework of this study.
- The operation and the maintenance of AFs require additional costs and resources that are not examined in this study.
- Due to the timeframe of the PhD and the computation time, this study examined a certain range of parameters to train the ML models, which would restrict the generalisability of the developed surrogate model to predict other parameters. Basically, the ML models are applicable only to the scenarios covered by the training data.
- The results confirmed that ML surrogate models are an effective method for emulating simulation tools to predict the energy performance of AFs and provide high prediction accuracies for a variety of design variables. Despite the strengths of this promising approach, a notable limitation concerns the unaddressed question of how surrogate models would perform in more complex design scenarios beyond the range of the examined inputs.

### **8.7. Recommendations and Future Work**

The findings of the study and limitations showed important recommendations and future research to be investigated.

- The study encourages architects and façade engineers to implement more AF shading systems in regions with hot climates, as they have been proven to be effective in saving energy in office buildings. In addition, to motivate architects to develop more AFs, it is feasible to implement the method to similar AFs in different climates.
- The study explored the impact of AF shading systems on the energy performance of buildings. However, there is still a lot of scope for investigation that researchers into AFs can explore including visual comfort, thermal comfort, and daylight quality.
- Future research should investigate the satisfaction of occupants based on post-occupancy evaluations. A post-occupancy assessment is an appropriate method for evaluating the performance of AFs with the help of surveys.
- The research recommends the use of a co-simulation approach within the parametric design tool to accurately simulate the performance of AFs and their time varying behaviour during the early stages of the design.
- ML methods are a promising approach in the field of architecture; nevertheless, big data is required to develop the models, and such data is not easily accessible or does not exist. Therefore, this study encourages public and private institutions in the KSA

to develop a national database similar to the Commercial Buildings Energy Consumption Survey (CBECS) system in the United States (US).

- In this research, the ANN architecture was optimised using different numbers of layers and neurones. Future research may employ alternative network architecture algorithms and training methods, such as the Recurrent Neural Network (RNN) and the Long-Short Term Memory (LSTM).
- This study developed ML surrogate models to predict only the hourly cooling loads of AFs; hence, additional research is needed to construct ML surrogate models to predict other performance metrics such as annual energy consumption, daylighting metrics, etc.
- The developed surrogate models particularly examined hot climate zones; thus, the models' applicability to other climates must be determined in future research.
- The study developed a workflow of the trained surrogate model within a computational design tool (Grasshopper) for instant design decision-making; however, future work is required to develop design tools that simplify such procedures and make them more attractive to designers.

### **8.8. Chapter Summary**

Throughout my research, I strived to conduct this work following the most accurate methods used by researchers in the literature. If I had to do my research again, I would conduct the experiment using real data instead of the simulation approach. Even though data obtained using simulation tools with the inevitable limitations are considered reliable, real data represent the actual settings more accurately. If I had the time, I would apply the surrogate model in a design tool for architects and façade engineers in a simple and attractive way, and I would test its usability. In addition, at the beginning of my research, there was a plan to include biomimicry as an inspiration for adaptive design; however, there was not enough time to conduct the experiment in an appropriate way.

Moreover, if I had the time, I would generate a variety of building contexts to make the model generalizable to different design settings. In addition, I would train a second model only on solar radiation and operative temperature to find out if the model could be generalized by following this approach. Lastly, I would test the developed model on real urban contexts in downtown Riyadh.

## **REFERENCES**

## REFERENCES

## REFERENCES

- Abdelrahman, M.M. 2017. Enhancing Computational Design with Python high performance scientific libraries : Integration of Grasshopper and CPython language. (November), pp. 2–3. doi: 10.13140/RG.2.2.27230.33600/1.
- Abdulazeez, M.. 2011. Artificial Neural Network Estimation of Global Solar Radiation Using Meteorological Parameters in Gusau , Nigeria. *Applied Science Research* 3(2), pp. 586–595.
- Addington, M. and Schodek, D. 2005. *Smart Materials and New Technologies For the architecture and design professions*. Oxford: Architectural Press.
- Aelenei, D., Aelenei, L. and Vieira, C.P. 2016. Adaptive Façade: Concept, Applications, Research Questions. *Energy Procedia* 91, pp. 269–275. Available at: <http://dx.doi.org/10.1016/j.egypro.2016.06.218>.
- Ahmad, M.W., Hippolyte, J.-L., Mourshed, M. and Rezgui, Y. 2017a. Random Forests and Artificial Neural Network for Predicting Daylight Illuminance and Energy Consumption. *5th Conference of International Building Performance Simulation Association* , pp. 1–7.
- Ahmad, M.W., Mourshed, M. and Rezgui, Y. 2017b. Trees vs Neurons: Comparison between random forest and ANN for high-resolution prediction of building energy consumption. *Energy and Buildings* 147, pp. 77–89. Available at: <http://dx.doi.org/10.1016/j.enbuild.2017.04.038>.
- Ahmad, M.W., Reynolds, J. and Rezgui, Y. 2017c. Random Forests and Artificial Neural Network for Predicting Daylight Illuminance and Energy Consumption. In: *Building Simulation.*, pp. 1–7.
- El Ahmar, S.A.S. 2011. Biomimicry as a tool for sustainable architectural design: towards morphogenetic architecture. (January)
- Ahmed, M.M.S., Abdel-Rahman, A.K., Bady, M. and Mahrous, E.K. 2016a. The thermal performance of residential building integrated with adaptive kinetic shading system. *International Energy Journal* 16(3), pp. 97–106.
- Ahmed, M.M.S., Abdel-Rahman, A.K., Bady, M., Mahrous, E.K. and Suzuki, M. 2016b. Optimum energy consumption by using kinetic shading system for residential buildings in hot arid areas. *International Journal of Smart Grid and Clean Energy* , pp. 121–128. doi: 10.12720/sgce.5.2.121-128.
- Aksamija, A. 2011. Methods for integrating parametric design with building performance analysis. In: *ARCC Conference Repository*. Available at: <https://www.arcc-journal.org/index.php/repository/article/view/459>.
- Aksamija, A. 2021. *Research Methods for the Architectural Profession*. 1st ed. New York: Routledge.
- Al-Masrani, S.M. and Al-Obaidi, K.M. 2019. Dynamic shading systems: A review of design parameters, platforms and evaluation strategies. *Automation in Construction* 102, pp. 195–216. doi: 10.1016/j.autcon.2019.01.014.
- Alaaeddine, R. and Wu, S. 2020. Application of supervised learning methods to better predict building energy performance. United Kingdom: University of Huddersfield
- Alaghmandan, M., Bahrami, P. and Elnimeiri, M. 2014. The Future Trend of Architectural Form and Structural System in High-Rise Buildings. *Architecture Research* 4(3), pp. 55–62. doi: 10.5923/j.arch.20140403.01.
- Alammar, A., Jabi, W. and Lannon, S. 2021. Predicting Incident Solar Radiation on Building ' s Envelope Using Machine Learning.

## **REFERENCES**

- Alardhi, A., S Alaboodi, A. and Almasri, R. 2020. Impact of the new Saudi energy conservation code on Saudi Arabia residential buildings. *Australian Journal of Mechanical Engineering* 00(00), pp. 1–15. Available at: <https://doi.org/10.1080/14484846.2020.1802919>.
- Albogami, S.M. and Boukhanouf, R. 2019. Residential building energy performance evaluation for different climate zones. *IOP Conference Series: Earth and Environmental Science* 329(1), pp. 1–8. doi: 10.1088/1755-1315/329/1/012026.
- Allegrini, J., Dorer, V. and Carmeliet, J. 2016. Impact of radiation exchange between buildings in urban street canyons on space cooling demands of buildings. *Energy and Buildings* 127, pp. 1074–1084. Available at: <http://dx.doi.org/10.1016/j.enbuild.2016.06.073>.
- Allwood, C.M. 2012. The distinction between qualitative and quantitative research methods is problematic. *Quality and Quantity* 46(5), pp. 1417–1429. doi: 10.1007/s11135-011-9455-8.
- Almushaikah, A.R.S. and Almasri, R.A. 2021. Evaluating the potential energy savings of residential buildings and utilizing solar energy in the middle region of Saudi Arabia – Case study. *Energy Exploration and Exploitation* 39(5), pp. 1457–1490. doi: 10.1177/0144598720975144.
- Alnusairat, S.F. 2018. *Approaches to Skycourt Design and Performance in High-Rise Office Buildings in a Temperate Climate*. Welsh School of Architecture, Cardiff University.
- Alrashed, F. and Asif, M. 2012. Prospects of renewable energy to promote zero-energy residential buildings in the KSA. *Energy Procedia* 18, pp. 1096–1105. Available at: <http://dx.doi.org/10.1016/j.egypro.2012.05.124>.
- Alrashed, F. and Asif, M. 2014. Trends in residential energy consumption in Saudi Arabia with particular reference to the Eastern province. *Journal of Sustainable Development of Energy, Water and Environment Systems* 2(4), pp. 376–387. doi: 10.13044/j.sdewes.2014.02.0030.
- Alshahrani, J. 2018. *Smart Solutions to Manage Peak Electricity Demand in Saudi Arabia*.
- Alshahrani, J. and Boait, P. 2019. Reducing High Energy Demand Associated with Air-Conditioning Needs in Saudi Arabia. *Energies*
- Alshehri, T., Howarth, N., Fuentes, R. and Odnoletkova, N. 2020. *The Future of Cooling in Saudi Arabia: Technology, Market and Policy Options*. Available at: files/167/Alshehri et al. - 2020 - The Future of Cooling in Saudi Arabia Technology, Market and Policy Options. Available at: [https://www.researchgate.net/publication/344285392\\_The\\_Future\\_of\\_Cooling\\_in\\_Saudi\\_Arabia\\_Technology\\_Market\\_and\\_Policy\\_Options](https://www.researchgate.net/publication/344285392_The_Future_of_Cooling_in_Saudi_Arabia_Technology_Market_and_Policy_Options).
- Alyami, M. and Omer, S. 2021. Building energy performance simulation: a case study of modelling an existing residential building in Saudi Arabia. *Environmental Research: Infrastructure and Sustainability* 1(3), p. 035001. doi: 10.1088/2634-4505/ac241e.
- Amasyali, K. and El-Gohary, N.M. 2018. A review of data-driven building energy consumption prediction studies. *Renewable and Sustainable Energy Reviews* 81(April 2017), pp. 1192–1205. Available at: <http://dx.doi.org/10.1016/j.rser.2017.04.095>.
- Armstrong, R. 2012. *Living Architecture: How Synthetic Biology Can Remake Our Cities and Reshape Our Lives*. Kindle Single, TED Books.
- Ascione, F., Bianco, N., De Stasio, C., Mauro, G.M. and Vanoli, G.P. 2017. Artificial neural networks to predict energy performance and retrofit scenarios for any member of a building category: A novel approach. *Energy* 118, pp. 999–1017. Available at: <http://dx.doi.org/10.1016/j.energy.2016.10.126>.
- ASHRAE 2018. ANSI/ASHRAE Standard 209-2018 Energy Simulation Aided Design for Buildings Except Low-Rise

## REFERENCES

Residential Buildings. 8400

- Asif, M. 2016. Growth and sustainability trends in the buildings sector in the GCC region with particular reference to the KSA and UAE. *Renewable and Sustainable Energy Reviews* 55, pp. 1267–1273. Available at: <http://dx.doi.org/10.1016/j.rser.2015.05.042>.
- Asl, M.R., Das, S., Tsai, B. and Molloy, I. 2017. Energy Model Machine ( EMM ). In: *eCAADe 35 - MATERIAL STUDIES - ENERGY.*, pp. 277–286.
- Attia, S. 2019. *Adaptive Facades Performance Assessment, interviews with facade experts*. Belgium: Cost Action TU1403.
- Attia, S., Bertrand, S., Cuchet, M., Yang, S. and Tabadkani, A. 2022. Comparison of Thermal Energy Saving Potential and Overheating Risk of Four Adaptive Façade Technologies in Office Buildings. *Sustainability (Switzerland)* 14(10). doi: 10.3390/su14106106.
- Attia, S., Bilir, S., Safy, T., Struck, C., Loonen, R. and Goia, F. 2018. Energy & Buildings Current trends and future challenges in the performance assessment of adaptive façade systems. *Energy & Buildings* 179, pp. 165–182. Available at: <https://doi.org/10.1016/j.enbuild.2018.09.017>.
- Attia, S., Favoino, F., Loonen, R., Petrovski, A. and Monge-barrio, A. 2015. Adaptive Façades System Assessment : An initial review. *10th Conference on Advanced Building Skins* , pp. 1265–1273. Available at: [https://orbi.ulg.ac.be/bitstream/2268/187576/1/Attia\\_Adaptive Façades System Assessment An initial review\\_v05.pdf](https://orbi.ulg.ac.be/bitstream/2268/187576/1/Attia_Adaptive_Façades_System_Assessment_An_initial_review_v05.pdf).
- Attia, S., Gratia, E., De Herde, A. and Hensen, J.L.M. 2012. Simulation-based decision support tool for early stages of zero-energy building design. *Energy and Buildings* 49, pp. 2–15. Available at: <http://dx.doi.org/10.1016/j.enbuild.2012.01.028>.
- Atzeri, A., Cappelletti, F. and Gasparella, A. 2014. Internal versus external shading devices performance in office buildings. In: *Energy Procedia*. doi: 10.1016/j.egypro.2014.01.050.
- Atzeri, A.M., Gasparella, A., Cappelletti, F. and Tzempelikos, A. 2018. Comfort and energy performance analysis of different glazing systems coupled with three shading control strategies. *Science and Technology for the Built Environment* 24(5), pp. 545–558. Available at: <https://doi.org/10.1080/23744731.2018.1449517>.
- Atzeri, A.M., Pernigotto, G., Cappelletti, F., Gasparella, A. and Tzempelikos, A. 2013. Energy performance of shading devices for thermal and lighting comfort in offices. *Building Simulation Applications* 2013-Janua, pp. 233–242.
- Ayoub, M. 2020. A review on machine learning algorithms to predict daylighting inside buildings. *Solar Energy* 202(March), pp. 249–275. Available at: <https://doi.org/10.1016/j.solener.2020.03.104>.
- Bacha, C. and Bourbia, F. 2016. Effect of kinetic facades on energy efficiency in office buildings -hot dry climates. In: *Advanced Building Skins*. Bern, Switzerland: 11th Conference on Advanced Building Skins
- Badarnah, L. 2017. Form Follows Environment: Biomimetic Approaches to Building Envelope Design for Environmental Adaptation. *Buildings* 7(4), p. 40. doi: 10.3390/buildings7020040.
- Badarnah, L. and Kadri, U. 2015. A methodology for the generation of biomimetic design concepts. *Architectural Science Review* 58(2), pp. 120–133. doi: 10.1080/00038628.2014.922458.
- Baenas, T. and Machado, M. 2017. On the analytical calculation of the solar heat gain coefficient of a BIPV module. *Energy and Buildings* 151(June), pp. 146–156. Available at: <http://dx.doi.org/10.1016/j.enbuild.2017.06.039>.

## REFERENCES

- Banihashemi, S., Tabadkani, A. and Hosseini, M.R. 2017. Modular coordination-based generative algorithm to optimize construction waste. (December). doi: 10.1016/j.proeng.2017.04.222.
- Barus, M.V. 2021. *Surrogate Modelling of Solar Radiation Potential for the Design of PV Module Layout on Entire Façade of Tall Buildings*.
- Bastiaansen, C.W.M., Schenning, A., Debije, M. and Broer, D.J. 2013. Nano-textured polymers for future architectural needs. *Journal of Facade Design and Engineering* 1(September 2016), pp. 97–104. doi: 10.3233/FDE-130002.
- Benedetti, M., Cesarotti, V., Introna, V. and Serranti, J. 2016. Energy consumption control automation using Artificial Neural Networks and adaptive algorithms: Proposal of a new methodology and case study. *Applied Energy* 165, pp. 60–71. Available at: <http://dx.doi.org/10.1016/j.apenergy.2015.12.066>.
- Benghanem, M., Mellit, A. and Alamri, S.N. 2009. ANN-based modelling and estimation of daily global solar radiation data: A case study. *Energy Conversion and Management* 50(7), pp. 1644–1655. Available at: <http://dx.doi.org/10.1016/j.enconman.2009.03.035>.
- Bishop, R.H. 1998. Modern Control Systems , 8th edition Modern Control Systems. *Books by Marquette University Faculty* . Available at: [http://epublications.marquette.edu/marq\\_fac-book/185](http://epublications.marquette.edu/marq_fac-book/185).
- de Boer, B., Ruijg, G., Loonen, R.C.G.M., Trčka, M., Hensen, J.L.M. and Kornaat, W. 2011. Climate adaptive building shells for the future – optimization with an inverse modelling approach. *Proceedings of ECEEE Summer Study 2011* (June), pp. 1413–1422.
- Böke, J., Knaack, U. and Hemmerling, M. 2020. Automated adaptive façade functions in practice - Case studies on office buildings. *Automation in Construction* 113(June 2019), p. 103113. Available at: <https://doi.org/10.1016/j.autcon.2020.103113>.
- Borkowski, E., Donato, M., Zemella, G., Rovas, D. and Raslan, R. 2018. Optimisation Of The Simulation Of Advanced Control Strategies For Adaptive Building Skins. (September), pp. 11–12.
- Braun, V. and Clarke, V. 2015. *Successful Qualitative Research a practical guide for beginners*. London: SAGE.
- Breiman, L. 2001. *Random forests*. Publishers, K. A. ed. The Netherlands. doi: 10.1201/9780367816377-11.
- Brillinger, D.R. 2001. *Time Series Data Analysis and Theory*. University of California, Berkeley.
- Bui, D.K., Nguyen, T.N., Ghazlan, A., Ngo, N.T. and Ngo, T.D. 2020. Enhancing building energy efficiency by adaptive façade: A computational optimization approach. *Applied Energy* 265(January). doi: 10.1016/j.apenergy.2020.114797.
- Bui, D.K., Nguyen, T.N., Ghazlan, A. and Ngo, T.D. 2021. Biomimetic adaptive electrochromic windows for enhancing building energy efficiency. *Applied Energy* 300(July), p. 117341. Available at: <https://doi.org/10.1016/j.apenergy.2021.117341>.
- Building, M. and Codes, E. 2013. Energy Codes. *ASHRAE Journal* 55(August)
- Bustamante, W., Uribe, D., Vera, S. and Molina, G. 2017. An integrated thermal and lighting simulation tool to support the design process of complex fenestration systems for office buildings. *Applied Energy* 198, pp. 36–48. Available at: <http://dx.doi.org/10.1016/j.apenergy.2017.04.046>.
- Cannavale, A., Ayr, U. and Martellotta, F. 2018. Innovative electrochromic devices: Energy savings and visual comfort effects. *Energy Procedia* 148(September), pp. 900–907. doi: 10.1016/j.egypro.2018.08.096.
- Carpo, M. 2017. *The second digital, turn design beyond intelligence*. The MIT Press.



## **REFERENCES**

- Chakraborty, D. and Elzarka, H. 2019. Advanced machine learning techniques for building performance simulation: a comparative analysis. *Journal of Building Performance Simulation* 12(2), pp. 193–207. doi: 10.1080/19401493.2018.1498538.
- Chew, M.Y.L., De Silva, N. and Tan, S.S. 2004. A neural network approach to assessing building façade maintainability in the tropics. *Construction Management and Economics* 22(6), pp. 581–594. doi: 10.1080/01446190310001631019.
- Ching, F.D.K. 2007. *Architecture: Form, Space, and Order*. Available at: <http://www.amazon.co.uk/Architecture-Francis-D-K-Ching/dp/0471752169>.
- Choi, S.J., Lee, D.S. and Jo, J.H. 2017a. Lighting and cooling energy assessment of multi-purpose control strategies for external movable shading devices by using shaded fraction. *Energy and Buildings* 150, pp. 328–338. Available at: <http://dx.doi.org/10.1016/j.enbuild.2017.06.030>.
- Choi, S.J., Lee, D.S. and Jo, J.H. 2017b. Method of deriving shaded fraction according to shading movements of kinetic façade. *Sustainability (Switzerland)* 9(8). doi: 10.3390/su9081449.
- Chou, J.S. and Bui, D.K. 2014. Modeling heating and cooling loads by artificial intelligence for energy-efficient building design. *Energy and Buildings* 82(2014), pp. 437–446. Available at: <http://dx.doi.org/10.1016/j.enbuild.2014.07.036>.
- Claesen, M. and De Moor, B. 2015. Hyperparameter Search in Machine Learning., pp. 10–14. Available at: <http://arxiv.org/abs/1502.02127>.
- Crawley, D. 2007. Simulation of energy management systems in energyplus. Beijing, China: Building Simulation, p. 2014.
- Creswell, J. and Clark, V. 2011. *Designing and conducting mixed methods research*. 2nd ed. SAGE Publications.
- Creswell, J.W. 2014. *Research design: Qualitative, quantitative, and mixed methods approaches*. SAGE Publications Asia-Pacific Pte. Ltd. doi: 10.1093/nq/s4-l.25.577-c.
- CTBUH 2017. The Global Tall Building Database of the CTBUH. Available at: <https://www.skyscrapercenter.com/city/riyadh>.
- Davies, M. 1981. *A Wall For All Seasons*. RIBA Journal.
- Deb, C., Eang, L.S., Yang, J. and Santamouris, M. 2016. Forecasting diurnal cooling energy load for institutional buildings using Artificial Neural Networks. *Energy and Buildings* 121, pp. 284–297. Available at: <http://dx.doi.org/10.1016/j.enbuild.2015.12.050>.
- Dekay, M. 2001. *Sun, Wind & Light: architectural design strategies*. 2nd editio. Canada: Wiley & Sons.
- Demirbas, A., Hashem, A.A. and Bakhsh, A.A. 2017. The cost analysis of electric power generation in Saudi Arabia. *Energy Sources, Part B: Economics, Planning and Policy* 12(6), pp. 591–596. Available at: <http://dx.doi.org/10.1080/15567249.2016.1248874>.
- Dietterich, T.G. 2000a. Ensemble Methods in Machine Learning. *Multiple Classifier Systems* 1857, pp. 1–15. Available at: [http://link.springer.com/chapter/10.1007/3-540-45014-9\\_1](http://link.springer.com/chapter/10.1007/3-540-45014-9_1).
- Dietterich, T.G. 2000b. Ensemble Methods in Machine Learning. In: *Multiple Classifier Systems*. Berlin, Heidelberg: Springer Berlin Heidelberg, pp. 1–15.
- DOE, U.S. 2020. *EnergyPlus™ Version 22.1.0 Documentation, Input Output Reference*.
- Donato, M., Zemella, G., Rapone, G., Hussain, J. and Black, C. 2017. An innovative APP for a parametric, holistic

## REFERENCES

- and multidisciplinary approach to early design stages. *Journal of Facade Design and Engineering* 5(2), pp. 113–127. doi: 10.7480/jfde.2017.2.1739.
- Du, K.L. and Swamy, M.N.S. 2006. Neural networks in a softcomputing framework. *Neural Networks in a Softcomputing Framework*, pp. 1–566. doi: 10.1007/1-84628-303-5.
- Edwards, R.E., New, J. and Parker, L.E. 2012. Predicting future hourly residential electrical consumption: A machine learning case study. *Energy and Buildings* 49, pp. 591–603. Available at: <http://dx.doi.org/10.1016/j.enbuild.2012.03.010>.
- Ekici, B.B. and Aksoy, U.T. 2009. Prediction of building energy consumption by using artificial neural networks. *Advances in Engineering Software* 40(5), pp. 356–362. Available at: <http://dx.doi.org/10.1016/j.advengsoft.2008.05.003>.
- ElDin, N.N., Abdou, A. and ElGawad, I.A. 2016. Biomimetic Potentials for Building Envelope Adaptation in Egypt. *Procedia Environmental Sciences* 34, pp. 375–386. Available at: <http://dx.doi.org/10.1016/j.proenv.2016.04.033>.
- ElGhazi, Y.S. and Mahmoud, A.H.A. 2016. Origami Explorations A Generative Parametric Technique For kinetic cellular façade to optimize Daylight Performance. *Conference: 34th Annual eCAADe Conference, At Oulu, Finland*. 2(August), pp. 399–408.
- ElGhazi, Y.S., Wagdy, A., Mohamed, S.A.A. and Hassan, A. 2014. Daylighting driven design: optimizing kaleidocycle facade for hot arid climate. In: *BauSIM2014 - IBPSA-Germany*. RWTH Aachen University, pp. 314–321. Available at: [https://www.researchgate.net/publication/266328925\\_Daylighting\\_Driven\\_Design\\_Optimizing\\_Kaleidocycle\\_faade\\_for\\_hot\\_arid\\_climate](https://www.researchgate.net/publication/266328925_Daylighting_Driven_Design_Optimizing_Kaleidocycle_faade_for_hot_arid_climate).
- Elkhatieb, M.A. 2016. *A Performance-Driven Design Model of Territorial Adaptive Building Skin (TABS) for Daylighting Performance Optimisation in Office Buildings in Egypt*. University of Liverpool. Available at: [https://www.bertelsmann-stiftung.de/fileadmin/files/BSt/Publikationen/GrauePublikationen/MT\\_Globalization\\_Report\\_2018.pdf](https://www.bertelsmann-stiftung.de/fileadmin/files/BSt/Publikationen/GrauePublikationen/MT_Globalization_Report_2018.pdf)  
[http://eprints.lse.ac.uk/43447/1/India\\_globalisation%2C\\_society\\_and\\_inequalities%28Isero%29.pdf](http://eprints.lse.ac.uk/43447/1/India_globalisation%2C_society_and_inequalities%28Isero%29.pdf)  
<https://www.quora.com/What-is-the>.
- Eltaweel, A. and Su, Y. 2017a. Controlling venetian blinds based on parametric design ; via implementing Grasshopper ' s plugins : A case study of an office building in Cairo. *Energy & Buildings* 139, pp. 31–43. Available at: <http://dx.doi.org/10.1016/j.enbuild.2016.12.075>.
- Eltaweel, A. and Su, Y. 2017b. Controlling venetian blinds based on parametric design; via implementing Grasshopper's plugins: A case study of an office building in Cairo. *Energy and Buildings* 139, pp. 31–43. Available at: <http://dx.doi.org/10.1016/j.enbuild.2016.12.075>.
- Eltaweel, A. and SU, Y. 2017. Parametric design and daylighting: A literature review. In: *Renewable and Sustainable Energy Reviews*., pp. 1086–1103. doi: 10.1016/j.rser.2017.02.011.
- Elwy, I., Ibrahim, Y., Fahmy, M. and Mahdy, M. 2018. Outdoor microclimatic validation for hybrid simulation workflow in hot arid climates against ENVI-met and field measurements. *Energy Procedia* 153, pp. 29–34. Available at: <https://doi.org/10.1016/j.egypro.2018.10.009>.
- Elzeyadi, I. 2017. The impacts of dynamic façade shading typologies on building energy performance and occupant's multi-comfort. *Architectural Science Review* 60(4), pp. 316–324. Available at: <https://doi.org/10.1080/00038628.2017.1337558>.
- EnergyPlus 2013. *EnergyPlus Engineering Reference*.
- EnergyPlus 2020. EnergyPlus Engineering Reference, The Reference to EnergyPlus Calculations. *The*

## **REFERENCES**

*Encyclopedic Reference to EnergyPlus Input and Output* (c), pp. 1996–2016.

- Evins, R., Pointer, P., Vaidyanathan, R., Happold, B. and Street, N. 2011. Multi-objective optimisation of the configuration and control of a double-skin facade. In: *Proceedings of Building Simulation 2011*. Sydney: 12th Conference of International Building Performance Simulation Association, pp. 14–16. Available at: [http://www.ibpsa.org/proceedings/BS2011/P\\_1463.pdf](http://www.ibpsa.org/proceedings/BS2011/P_1463.pdf).
- Evola, G., Gullo, F. and Marletta, L. 2017. The role of shading devices to improve thermal and visual comfort in existing glazed buildings. *Energy Procedia* 134, pp. 346–355. Available at: <https://doi.org/10.1016/j.egypro.2017.09.543>.
- Fan, J. and Yao, Q. 2004. *Nonlinear Time Series: Nonparametric and Parametric Methods*. doi: 10.1198/tech.2004.s746.
- Fasiuddin, M. and Budaiwi, I. 2011. HVAC system strategies for energy conservation in commercial buildings in Saudi Arabia. *Energy and Buildings* 43(12), pp. 3457–3466. Available at: <http://dx.doi.org/10.1016/j.enbuild.2011.09.004>.
- Favoino, F. et al. 2016. Simulating switchable glazing with EnergyPlus : an empirical validation and calibration of a thermotropic glazing model. In: *Cost Action 1403 Adaptive Facades Network*.
- Favoino, F., Goia, F., Perino, M. and Serra, V. 2014a. Experimental assessment of the energy performance of an advanced responsive multifunctional façade module. *Energy and Buildings* 68(PART B), pp. 647–659. Available at: <http://dx.doi.org/10.1016/j.enbuild.2013.08.066>.
- Favoino, F., Jin, Q. and Overend, M. 2014b. Towards an ideal adaptive glazed façade for office buildings. *Energy Procedia* 62(December), pp. 289–298. Available at: <http://dx.doi.org/10.1016/j.egypro.2014.12.390>.
- Favoino, F., Jin, Q. and Overend, M. 2017. Design and control optimisation of adaptive insulation systems for office buildings. Part 1: Adaptive technologies and simulation framework. *Energy* 127, pp. 301–309. Available at: <http://dx.doi.org/10.1016/j.energy.2017.03.083>.
- Favoino, F., Overend, M. and Jin, Q. 2015. The optimal thermo-optical properties and energy saving potential of adaptive glazing technologies. *Applied Energy* 156, pp. 1–15. Available at: <http://dx.doi.org/10.1016/j.apenergy.2015.05.065>.
- Felix, A.G., Eck, D. and Jürgen, S. 2002. Applying LSTM to Time Series Predictable Through Time-Window Approaches. In: *Perspectives in Neural Computing.*, pp. 88–100.
- Fiorito, F., Sauchelli, M., Arroyo, D., Pesenti, M., Imperadori, M., Masera, G. and Ranzi, G. 2016. Shape morphing solar shadings: A review. *Renewable and Sustainable Energy Reviews* 55, pp. 863–884. doi: 10.1016/j.rser.2015.10.086.
- Freitas, S., Catita, C., Redweik, P. and Brito, M.C. 2015. Modelling solar potential in the urban environment: State-of-the-art review. *Renewable and Sustainable Energy Reviews* 41, pp. 915–931. Available at: <http://dx.doi.org/10.1016/j.rser.2014.08.060>.
- Gadelhak, M. and Lang, W. 2016. Optimization of Office Building Façade To Enhance Daylighting , Thermal Comfort and Energy Use Intensity. *BSO 2016 Building Simulation & Optimization* (January 2017), pp. 1116–1124.
- Van Gelder, L., Das, P., Janssen, H. and Roels, S. 2014. Comparative study of metamodeling techniques in building energy simulation: Guidelines for practitioners. *Simulation Modelling Practice and Theory* 49, pp. 245–257. Available at: <http://dx.doi.org/10.1016/j.simpat.2014.10.004>.
- Genot, E.J. 2018. *The SAGE Handbook of Qualitative Research*. 5th Editio. SAGE Publications, Inc. doi: 10.1007/s11229-017-1319-x.

## REFERENCES

- Geyer, P. and Singaravel, S. 2018. Component-based machine learning for performance prediction in building design. *Applied Energy* 228(October 2017), pp. 1439–1453. Available at: <https://doi.org/10.1016/j.apenergy.2018.07.011>.
- Ghabra, N. 2019. *Energy Efficient Strategies for the Building Envelope of Residential Tall Buildings in Saudi Arabia*. University of Nottingham.
- Ghaffarianhoseini, A., Berardi, U., AlWaer, H., Chang, S., Halawa, E., Ghaffarianhoseini, A. and Clements-Croome, D. 2016. What is an intelligent building? Analysis of recent interpretations from an international perspective. *Architectural Science Review* 59(5), pp. 338–357. Available at: <http://dx.doi.org/10.1080/00038628.2015.1079164>.
- Giovannini, L., Favoino, F., Pellegrino, A., Lo Verso, V.R.M., Serra, V. and Zinzi, M. 2019. Thermochromic glazing performance: From component experimental characterisation to whole building performance evaluation. *Applied Energy* 251(May), p. 113335. Available at: <https://doi.org/10.1016/j.apenergy.2019.113335>.
- Giovannini, L., Lo Verso, V.R.M., Karamata, B. and Andersen, M. 2015. Lighting and energy performance of an adaptive shading and daylighting system for arid climates. *Energy Procedia* 78, pp. 370–375. Available at: <http://dx.doi.org/10.1016/j.egypro.2015.11.675>.
- Gori, M. and Tesi, A. 2000. On the Problem of Local Minima in Backpropagation.
- Groat, L. and Wang, D. 2013. *Architectural research Methods*. 2nd Editio. Hoboken, New Jersey: Wiley & Sons.
- Grobman, Y.J., Capeluto, I.G., Austern, G., Capeluto, I.G. and Austern, G. 2017. External shading in buildings : comparative analysis of daylighting performance in static and kinetic operation scenarios. 8628. Available at: <https://doi.org/10.1080/00038628.2016.1266991>.
- Grosso, A.E. Del and Basso, P. 2013. Design Concepts for Adaptive Multi-Functional. (June), pp. 24–26.
- Hadi, Y., Heath, T. and Oldfield, P. 2014. Vertical Public Realms : Creating Urban Spaces in the Sky. *CTBUH 2014 Shanghai Conference Proceedings* , pp. 112–119. Available at: [www.nottingham.ac.uk/abe](http://www.nottingham.ac.uk/abe).
- Haeusler, M. 2009. *Media Facades - History, Technology, Content*. 2nd Edition.
- Hahn, H., Meyer-Nieberg, S. and Pickl, S. 2009. Electric load forecasting methods: Tools for decision making. *European Journal of Operational Research* 199(3), pp. 902–907. Available at: <http://dx.doi.org/10.1016/j.ejor.2009.01.062>.
- Hammad, F. and Abu-Hijleh, B. 2010. The energy savings potential of using dynamic external louvers in an office building. *Energy and Buildings* 42(10), pp. 1888–1895. Available at: <http://dx.doi.org/10.1016/j.enbuild.2010.05.024>.
- Hamza, N.A. 2004. *The performance of double skin facades in office building refurbishment in hot arid areas*. University of Newcastle.
- Al Harbi, F. and Csala, D. 2019. Saudi Arabia’s Electricity: Energy Supply and Demand Future Challenges. In: *2019 IEEE.*, pp. 0–5.
- Hasni, A., Sehli, A., Draoui, B., Bassou, A. and Amieur, B. 2012. Estimating global solar radiation using artificial neural network and climate data in the south-western region of Algeria. *Energy Procedia* 18, pp. 531–537. Available at: <http://dx.doi.org/10.1016/j.egypro.2012.05.064>.
- Hasselaar, B.L.H. 2006. Climate adaptive skins: Towards the new energy-efficient façade. *WIT Transactions on Ecology and the Environment* 99(August), pp. 351–360. doi: 10.2495/RAV060351.

## REFERENCES

- Haykin, S. 1992. *Neural networks and learning machines*. 3rd Editio. Pearson.
- Heiselberg, P.K. 2007. *Integrated Building Design*.
- Hellerstein, J.M. and Berkeley, U.C. 2008. Quantitative Data Cleaning for Large Databases. *United Nations Economic Commission for Europe* , pp. 1–42. Available at: <http://db.cs.berkeley.edu/jmh/cleaning-unece.pdf%5Cnpapers2://publication/uuid/DC7173AB-6B26-4B8B-AEC3-4C7E65CEEED>.
- Hensen, J.L.M. and Lamberts, R. 2011. *Building Performance Simulation for Design and Operation*. New York: Spon Press. doi: 10.1201/9780429402296.
- Hofer, J., Groenewolt, A., Jayathissa, P., Nagy, Z. and Schlueter, A. 2016. Parametric analysis and systems design of dynamic photovoltaic shading modules. In: *Energy Science and Engineering.*, pp. 134–152. doi: 10.1002/ese3.115.
- Hoffmann, S., Lee, E.S., McNeil, A., Fernandes, L., Vidanovic, D. and Thanachareonkit, A. 2016. Balancing daylight, glare, and energy-efficiency goals: An evaluation of exterior coplanar shading systems using complex fenestration modeling tools. *Energy and Buildings* 112, pp. 279–298. Available at: <http://dx.doi.org/10.1016/j.enbuild.2015.12.009>.
- Hong, S.M., Paterson, G., Mumovic, D. and Steadman, P. 2014. Improved benchmarking comparability for energy consumption in schools. *Building Research and Information* 42(1), pp. 47–61. doi: 10.1080/09613218.2013.814746.
- Hong, T., Koo, C. and Jeong, K. 2012a. A decision support model for reducing electric energy consumption in elementary school facilities. *Applied Energy* 95, pp. 253–266. Available at: <http://dx.doi.org/10.1016/j.apenergy.2012.02.052>.
- Hong, T., Koo, C. and Park, S. 2012b. A decision support model for improving a multi-family housing complex based on CO 2 emission from gas energy consumption. *Building and Environment* 52, pp. 142–151. Available at: <http://dx.doi.org/10.1016/j.buildenv.2012.01.001>.
- Hong, T. and Lin, H.-W. 2013. Occupant Behavior: Impact on Energy Use of Private Offices. *ASim 2012-1st Asia conference of International Building Performance Simulation Association* (January)
- Hopmann, C., Augusto Santos Silva Eng Christian Luft, C., de Saldanha Gonçalves Matos Supervisor, J. and Augusto Santos Silva, C. 2017. *Machine Learning to improve indoor climate and building energy performance Energy Engineering and Management Examination Committee*. Available at: [https://fenix.tecnico.ulisboa.pt/downloadFile/1970719973966588/Master Thesis Christoph Hopmann.pdf](https://fenix.tecnico.ulisboa.pt/downloadFile/1970719973966588/Master%20Thesis%20Christoph%20Hopmann.pdf).
- Hora, J. and Campos, P. 2015. A review of performance criteria to validate simulation models. *Expert Systems* 32(5), pp. 578–595. doi: 10.1111/exsy.12111.
- Hosseini, S.M., Mohammadi, M. and Guerra-Santin, O. 2019a. Interactive kinetic façade: Improving visual comfort based on dynamic daylight and occupant’s positions by 2D and 3D shape changes. *Building and Environment* 165(June), p. 106396. Available at: <https://doi.org/10.1016/j.buildenv.2019.106396>.
- Hosseini, S.M., Mohammadi, M. and Guerra-Santin, O. 2019b. Interactive kinetic façade: Improving visual comfort based on dynamic daylight and occupant’s positions by 2D and 3D shape changes. *Building and Environment* . doi: 10.1016/j.buildenv.2019.106396.
- Huang, H., Chen, L. and Hu, E. 2015. A neural network-based multi-zone modelling approach for predictive control system design in commercial buildings. *Energy and Buildings* 97, pp. 86–97. Available at: <http://dx.doi.org/10.1016/j.enbuild.2015.03.045>.
- Ibrahim, Y., Kershaw, T. and Shepherd, P. 2020. A methodology For Modelling Microclimates : A Ladybug-tools

## **REFERENCES**

- and ENVI-met verification study. In: *PLEA 2020 A CORUÑA Planning Post Carbon Cities.*, pp. 1–7.
- Id, M.S., Su, Y. and Mohamed, G. 2020. Artificial Neural Network Intelligent Technique and Multiple Nonlinear Regression for Prediction and Optimization of the Transmittance of Lightpipes and Implementation in BIM.
- Ilbeigi, M., Ghomeishi, M. and Dehghanbanadaki, A. 2020. Prediction and optimization of energy consumption in an office building using artificial neural network and a genetic algorithm. *Sustainable Cities and Society* 61(June), p. 102325. Available at: <https://doi.org/10.1016/j.scs.2020.102325>.
- Ioffe, S. and Szegedy, C. 2016. Batch Normalization: Accelerating Deep Network Training by Reducing Internal Covariate Shift. *Journalism Practice* 10(6), pp. 730–743. doi: 10.1080/17512786.2015.1058180.
- Jain, S. and Garg, V. 2018. A review of open loop control strategies for shades, blinds and integrated lighting by use of real-time daylight prediction methods. *Building and Environment* 135(March), pp. 352–364. Available at: <https://doi.org/10.1016/j.buildenv.2018.03.018>.
- Johnsen, K. and Winther, F. V 2015. Dynamic facades , the smart way of meeting the energy requirements. *Energy Procedia* 78, pp. 1568–1573. Available at: <http://dx.doi.org/10.1016/j.egypro.2015.11.210>.
- Kaiadi, M. 2006. *Artificial Neural Networks Modelling for Monitoring and Performance Analysis of a Heat and Power Plant Mehrzad Kaiadi*.
- Kaiming, H., Zhang, X., Ren, S. and Sun, J. 2015. “Delving deep into rectifiers: Surpassing human-level performance on imagenet classification.” In: *Proceedings of the IEEE international conference on computer vision*.
- Kalogirou, S., Neocleous, C. and Schizas, C. 1997. Building Heating Load Estimation Using Artificial Neural Networks. *Proceedings of the 17th international conference on Parallel architectures and compilation techniques* (January 1997), pp. 1–8.
- Kalogirou, S.A. 2000. Artificial neural networks in renewable energy systems applications: A review. *Renewable and Sustainable Energy Reviews* 5(4), pp. 373–401. doi: 10.1016/S1364-0321(01)00006-5.
- Kasinalis, C., Loonen, R.C.G.M., Cóstola, D. and Hensen, J.L.M. 2014. Framework for assessing the performance potential of seasonally adaptable facades using multi-objective optimization. *Energy & Buildings* 79, pp. 106–113. Available at: <http://dx.doi.org/10.1016/j.enbuild.2014.04.045>.
- Kazanasmaz, T., Günaydin, M. and Binol, S. 2009. Artificial neural networks to predict daylight illuminance in office buildings. *Building and Environment* 44(8), pp. 1751–1757. doi: 10.1016/j.buildenv.2008.11.012.
- Kermanshahi, B. and Iwamiya, H. 2002. Up to year 2020 load forecasting using neural nets. *International Journal of Electrical Power and Energy Systems* 24(9), pp. 789–797. doi: 10.1016/S0142-0615(01)00086-2.
- Keshtkarbanaemoghadam, A., Dehghanbanadaki, A. and Kaboli, M.H. 2018. Estimation and optimization of heating energy demand of a mountain shelter by soft computing techniques. *Sustainable Cities and Society* 41(June), pp. 728–748. doi: 10.1016/j.scs.2018.06.008.
- Khayatian, F., Sarto, L. and Dall’O’, G. 2016. Application of neural networks for evaluating energy performance certificates of residential buildings. *Energy and Buildings* 125, pp. 45–54. Available at: <http://dx.doi.org/10.1016/j.enbuild.2016.04.067>.
- Khean, N., Fabbri, A., Haeusler, M.H., Learning, S. and Framework, E. 2018. Learning Machine Learning as an Architect , How to?, pp. 95–102.
- Kialashaki, A. and Reisel, J.R. 2013. Modeling of the energy demand of the residential sector in the United

## **REFERENCES**

- States using regression models and artificial neural networks. *Applied Energy* 108, pp. 271–280. Available at: <http://dx.doi.org/10.1016/j.apenergy.2013.03.034>.
- Kim, D., Jang, D. and Kim, S. 2012. A Symbiotic Interaction of Virtual and Physical Models in Designing Smart Building Envelope. 2, pp. 633–642.
- Kim, H.-I. and Elnimeiri, M. 2004. Space Efficiency in Multi-Use Tall Building. *CTBUH 2004 Seoul Conference* , pp. 748–755.
- Kim, H., Asl, M.R., Yan, W., Modeling, P. and Simulation, E. 2015. Parametric BIM-based Energy Simulation for Buildings with Complex Kinetic Façades. 1, pp. 657–664.
- Kimber, M., Clark, W.W. and Schaefer, L. 2014. Conceptual analysis and design of a partitioned multifunctional smart insulation. *Applied Energy* 114, pp. 310–319. Available at: <http://dx.doi.org/10.1016/j.apenergy.2013.09.067>.
- Kirimtat, A., Koyunbaba, B.K., Chatzikonstantinou, I. and Sariyildiz, S. 2016. Review of simulation modeling for shading devices in buildings. *Renewable and Sustainable Energy Reviews* 53(January), pp. 23–49. Available at: <http://dx.doi.org/10.1016/j.rser.2015.08.020>.
- Knight, A. and Ruddock, L. 2009. *Advanced Research Methods in the Built Environment*. Blackwell Publishing Ltd. doi: 10.1080/01446190902896637.
- Koca, A., Oztop, H.F., Varol, Y. and Koca, G.O. 2011. Estimation of solar radiation using artificial neural networks with different input parameters for Mediterranean region of Anatolia in Turkey. *Expert Systems with Applications* 38(7), pp. 8756–8762. Available at: <http://dx.doi.org/10.1016/j.eswa.2011.01.085>.
- Konstantoglou, M., Kontadakis, A. and Tsangrassoulis, A. 2013. Counterbalancing daylighting, glare and view out: the role of an external shading system control strategy. *Clima* , pp. 16–19.
- Konstantoglou, M. and Tsangrassoulis, A. 2016. Dynamic operation of daylighting and shading systems: A literature review. *Renewable and Sustainable Energy Reviews* 60, pp. 268–283. Available at: <http://dx.doi.org/10.1016/j.rser.2015.12.246>.
- Koola, P.M., Ramachandran, S. and Vadakkevedu, K. 2016. How do we train a stone to think? A review of machine intelligence and its implications. *Theoretical Issues in Ergonomics Science* 17(2), pp. 211–238. Available at: <https://www.tandfonline.com/action/journalInformation?journalCode=ttie20> [Accessed: 4 February 2019].
- Kothari, C.. 2004. *Research methodology: methods and techniques*. 2nd Editio. New Delhi: New Age International (P) Ltd., Publishers. Available at: <https://www.ptonline.com/articles/how-to-get-better-mfi-results>.
- Krarti, M., Dubey, K. and Howarth, N. 2017. Evaluation of building energy efficiency investment options for the Kingdom of Saudi Arabia. *Energy* 134, pp. 595–610. Available at: <http://dx.doi.org/10.1016/j.energy.2017.05.084>.
- Kumar, R. 2014. *Research Methodology: A Step-by-Step Guide for Beginners*. 4th Editio. London: SAGE Publications Ltd. Lang,.
- Kuru, A. 2020. Biomimetic adaptive building skins : An approach towards multifunctionality. (July)
- Kuru, A., Oldfield, P., Bonser, S. and Fiorito, F. 2021. Performance prediction of biomimetic adaptive building skins: Integrating multifunctionality through a novel simulation framework. *Solar Energy* 224(January), pp. 253–270. Available at: <https://doi.org/10.1016/j.solener.2021.06.012>.

## REFERENCES

- Kuster, C., Rezgui, Y. and Mourshed, M. 2017. Electrical load forecasting models: A critical systematic review. *Sustainable Cities and Society* 35(July), pp. 257–270. Available at: <http://dx.doi.org/10.1016/j.scs.2017.08.009>.
- Law, A.M. 2009. How to Build Valid and Credible Simulation Models. *Proceedings - Winter Simulation Conference 2019-Decem*, pp. 1402–1414. doi: 10.1109/WSC40007.2019.9004789.
- Leatherbarrow, D. and Mostafavi, M. 2005. *Surface Architecture*. Cambridge, Massachusetts.: The MIT Press.
- Lee, B. 2019. Heating, cooling, and lighting energy demand simulation analysis of kinetic shading devices with automatic dimming control for Asian Countries. *Sustainability (Switzerland)* 11(5). doi: 10.3390/su11051253.
- Lee, J., Boubekri, M. and Liang, F. 2019a. Impact of building design parameters on daylighting metrics using an analysis, prediction, and optimization approach based on statistical learning technique. *Sustainability (Switzerland)* 11(5). doi: 10.3390/su11051474.
- Lee, S., Jung, S. and Lee, J. 2019b. Prediction model based on an artificial neural network for user-based building energy consumption in South Korea. *Energies* 12(4). doi: 10.3390/en12040608.
- Li, Q., Meng, Q., Cai, J., Yoshino, H. and Mochida, A. 2009. Predicting hourly cooling load in the building: A comparison of support vector machine and different artificial neural networks. *Energy Conversion and Management* 50(1), pp. 90–96. Available at: <http://dx.doi.org/10.1016/j.enconman.2008.08.033>.
- Lienhard, J. 2015. *Bending-active structures*. doi: 10.1002/bate.201500007.
- Loonen, R.C.G.M., Hoes, P., Hensen, J.L.M., Loonen, R.C.G.M. and Hoes, P. 2014a. Performance prediction of buildings with responsive building elements challenges and solutions. (June), pp. 1–8. Available at: <https://pure.tue.nl/ws/portalfiles/portal/3992582/392669136570421.pdf>.
- Loonen, R.C.G.M., Hoes, P., Hensen, J.L.M., Loonen, R.C.G.M. and Hoes, P. 2014b. Performance prediction of buildings with responsive building elements challenges and solutions PERFORMANCE PREDICTION OF BUILDINGS WITH RESPONSIVE BUILDING ELEMENTS: CHALLENGES AND SOLUTIONS. (June), pp. 1–8. Available at: <https://pure.tue.nl/ws/portalfiles/portal/3992582/392669136570421.pdf>.
- Loonen, R.C.G.M. (2018) 2018. *Approaches for computational performance optimization of innovative adaptive façade concepts*.
- Loonen, R.C.G.M., Favoino, F., Hensen, J.L.M. and Overend, M. 2017. Review of current status, requirements and opportunities for building performance simulation of adaptive facades†. *Journal of Building Performance Simulation* 10(2), pp. 205–223. Available at: <https://doi.org/10.1080/19401493.2016.1152303>.
- Loonen, R.C.G.M., Rico-Martinez, J.M., Favoino, F., Brzezicki, M., Menezes, C., La Ferla, G. and Aelenei, L. 2015. Design for façade adaptability: Towards a unified and systematic characterization. *Proceedings of the 10th Conference on Advanced Building Skins* (November), pp. 1284–1294. Available at: [https://pure.tue.nl/ws/files/8287122/15\\_abs\\_loonen.pdf](https://pure.tue.nl/ws/files/8287122/15_abs_loonen.pdf).
- Loonen, R.C.G.M., Singaravel, S., Trčka, M., Cóstola, D. and Hensen, J.L.M. 2014c. Simulation-based support for product development of innovative building envelope components. *Automation in Construction* 45(2014), pp. 86–95. doi: 10.1016/j.autcon.2014.05.008.
- Loonen, R.C.G.M., Trcka, M., Cóstola, D. and Hensen, J.L.M. 2010. Performance simulation of climate adaptive building shells-Smart Energy Glass as a case study. In: *Proceedings of SSB. 8th International Conference on System Simulation in Buildings*, pp. 1–19. Available at: [http://www.bwk.tue.nl/bps/Hensen/publications/10\\_ssb\\_loonen.pdf](http://www.bwk.tue.nl/bps/Hensen/publications/10_ssb_loonen.pdf).



## **REFERENCES**

- Loonen, R.C.G.M., Trčka, M., Cóstola, D. and Hensen, J.L.M. 2013. Climate adaptive building shells: State-of-the-art and future challenges. *Renewable and Sustainable Energy Reviews* 25, pp. 483–493. doi: 10.1016/j.rser.2013.04.016.
- Loonen, R.C.G.M., Trčka, M. and Hensen, J.L.M. 2011. Exploring the potential of climate adaptive building shells. *Proceedings of Building Simulation 2011: 12th Conference of International Building Performance Simulation Association*, pp. 2148–2155.
- López, M., Rubio, R., Martín, S. and Ben Croxford 2017. How plants inspire façades. From plants to architecture: Biomimetic principles for the development of adaptive architectural envelopes. *Renewable and Sustainable Energy Reviews* 67, pp. 692–703. Available at: <http://dx.doi.org/10.1016/j.rser.2016.09.018>.
- Lorenz, C. and Jabi, W. 2017. International Conference for Sustainable Design of the Built Environment. In: *International Conference for Sustainable Design of the Built Environment SDBE*.
- Ma, J. and Cheng, J.C.P. 2016. Identifying the influential features on the regional energy use intensity of residential buildings based on Random Forests. *Applied Energy* 183, pp. 193–201. Available at: <http://dx.doi.org/10.1016/j.apenergy.2016.08.096>.
- Madhusudanan, C.R. 2019. A Machine Learning Framework for Energy Consumption Prediction.
- Marfella, G. 2015. Five Speculative Points for a Building Type. (July 2010). doi: 10.13140/RG.2.1.3310.8002.
- Marzouq, M., El Fadili, H., Lakhliai, Z. and Zenkouar, K. 2017. A review of solar radiation prediction using artificial neural networks. *2017 International Conference on Wireless Technologies, Embedded and Intelligent Systems, WITS 2017*. doi: 10.1109/WITS.2017.7934658.
- Masera, G., Pesenti, M. and Fiorito, F. 2018. Exploration of Adaptive Origami Shading Concepts through Integrated Dynamic Simulations. *Journal of Architectural Engineering* 24(4), p. 04018022. doi: 10.1061/(asce)ae.1943-5568.0000323.
- Mat Daut, M.A., Hassan, M.Y., Abdullah, H., Rahman, H.A., Abdullah, M.P. and Hussin, F. 2017. Building electrical energy consumption forecasting analysis using conventional and artificial intelligence methods: A review. *Renewable and Sustainable Energy Reviews* 70(December 2016), pp. 1108–1118. Available at: <http://dx.doi.org/10.1016/j.rser.2016.12.015>.
- Mellit, A. and Pavan, A.M. 2010. A 24-h forecast of solar irradiance using artificial neural network: Application for performance prediction of a grid-connected PV plant at Trieste, Italy. *Solar Energy* 84(5), pp. 807–821. Available at: <http://dx.doi.org/10.1016/j.solener.2010.02.006>.
- Miller, R. 1968. Response Time in Man-Computer Conversational Transactions. 33(pt 1), pp. 267–277. doi: 10.1145/1476589.1476628.
- Moeseke, G., Bruyère, I. and De Herde, A. 2007. Impact of control rules on the efficiency of shading devices and free cooling for office buildings. *Building and Environment* 42(2), pp. 784–793. doi: 10.1016/j.buildenv.2005.09.015.
- Mohamed, M. 2015. Traditional Ways of Dealing with Climate in Egypt. The Seventh International Conference of Sustainable Architecture and Urban Development (SAUD), pp. 247–266.
- Mohandes, M., Rehman, S. and Halawani, T.O. 1998. Estimation of global solar radiation using artificial neural networks. *Renewable Energy* 14(1–4), pp. 179–184. doi: 10.1016/S0960-1481(98)00065-2.
- Moosa, A., Shabir, H., Ali, H., Darwade, R. and Gite, B. 2019. Predicting Solar Radiation Using Machine Learning Techniques. *Proceedings of the 2nd International Conference on Intelligent Computing and Control Systems, ICICCS 2018 (Iciccs)*, pp. 1693–1699. doi: 10.1109/ICCONS.2018.8663110.

## **REFERENCES**

- Mukherjee, S., Birru, D., Cavalcanti, D., Shen, E., Patel, M., Wen, Y.-J. and Das, S. 2010. Closed Loop Integrated Lighting and Daylighting Control for Low Energy Buildings. *2010 ACEEE Summer Study on Energy Efficiency in Buildings*, pp. 9–252.
- Murray-Smith, D.J. 2016. *Testing and Validation of Computer Simulation Models: Principles, Methods and Applications*. Springer.
- Murray, N. and Hughes, G. 2008. *Writing up your university assignments and research projects : A practical handbook*. New York: McGraw-Hill. Available at: <http://mcgraw-hill.co.uk/html/033522718X.html>.
- Nady, R. 2017. Dynamic Facades: Environmental Control Systems for Sustainable Design. In: *Renewable Energy and Sustainable Development.*, pp. 118–127. doi: 10.21622/resd.2017.03.1.118.
- Nair, V. and Hinton, E., G. 2017. Rectified Linear Units Improve Restricted Boltzmann Machines. *Journal of Applied Biomechanics* 33(5), pp. 384–387. doi: 10.1123/jab.2016-0355.
- Naji, S., Keivani, A., Shamshirband, S., Alengaram, U.J., Jumaat, M.Z., Mansor, Z. and Lee, M. 2016. Estimating building energy consumption using extreme learning machine method. *Energy* 97, pp. 506–516. doi: 10.1016/j.energy.2015.11.037.
- Nashaat, B. and Waseef, A. 2018. (PDF) Kinetic Architecture: Concepts, History and Applications. (10.21275/ART20181560), pp. 750–758. Available at: [https://www.researchgate.net/publication/330349848\\_Kinetic\\_Architecture\\_Concepts\\_History\\_and\\_Applications](https://www.researchgate.net/publication/330349848_Kinetic_Architecture_Concepts_History_and_Applications).
- Natanian, J., Aleksandrowicz, O. and Auer, T. 2019. A parametric approach to optimizing urban form, energy balance and environmental quality: The case of Mediterranean districts. *Applied Energy*. doi: 10.1016/j.apenergy.2019.113637.
- Neto, A.H. and Fiorelli, F.A.S. 2008. Comparison between detailed model simulation and artificial neural network for forecasting building energy consumption. *Energy and Buildings* 40(12), pp. 2169–2176. doi: 10.1016/j.enbuild.2008.06.013.
- Nguyen, T.A. and Aiello, M. 2013. Energy intelligent buildings based on user activity: A survey. *Energy and Buildings* 56, pp. 244–257. Available at: <http://dx.doi.org/10.1016/j.enbuild.2012.09.005>.
- Nielsen, M.V., Svendsen, S. and Jensen, L.B. 2011a. Quantifying the potential of automated dynamic solar shading in office buildings through integrated simulations of energy and daylight. *Solar Energy*. doi: 10.1016/j.solener.2011.01.010.
- Nielsen, M.V., Svendsen, S. and Jensen, L.B. 2011b. Quantifying the potential of automated dynamic solar shading in office buildings through integrated simulations of energy and daylight. *Solar Energy* 85(5), pp. 757–768. Available at: <http://dx.doi.org/10.1016/j.solener.2011.01.010>.
- Notton, G., Paoli, C., Vasileva, S., Nivet, M.L., Canaletti, J.L. and Cristofari, C. 2012. Estimation of hourly global solar irradiation on tilted planes from horizontal one using artificial neural networks. *Energy* 39(1), pp. 166–179. Available at: <http://dx.doi.org/10.1016/j.energy.2012.01.038>.
- O’Leary, Z. 2017. *The Essential Guide to Doing Your Research Project*. 3rd Editio. New Zealand: The Australia and New Zealand School of Government.
- Oborn, P. 2013. *Al Bahr Towers: The Abu Dhabi Investment Council Headquarters*. John Wiley & Sons.
- Ochoa, C.E. and Capeluto, I.G. 2008. Strategic decision-making for intelligent buildings: Comparative impact of passive design strategies and active features in a hot climate. *Building and Environment* 43(11), pp. 1829–1839. doi: 10.1016/j.buildenv.2007.10.018.

## **REFERENCES**

- Oh, J., Hwang, J.-E., Smith, S.F. and Koile, K. 2011. Learning from Main street: A machine learning approach identifying neighborhood commercial districts. *Metropolis*, p. 20. Available at: <http://papers.cumincad.org/data/works/att/ddss2006-hb-325.content.pdf> [Accessed: 4 March 2019].
- Oh, S. and Haberl, J.S. 2016. Origins of analysis methods used to design high-performance commercial buildings: Whole-Building energy simulation. *Science and Technology for the Built Environment* 22(1), pp. 118–137. doi: 10.1080/23744731.2015.1063958.
- Olbina, S. and Hu, J. 2012. Daylighting and thermal performance of automated split-controlled blinds. *Building and Environment* 56, pp. 127–138. Available at: <http://dx.doi.org/10.1016/j.buildenv.2012.03.002>.
- Onyenobi, T., Hudson, J. and Ormerod, M. 2006. Impact of building geometry on fire spread rate. In: *Association of Researchers in Construction Management, ARCOM 2006 - Procs 22nd Annual ARCOM Conference.*, pp. 739–748.
- Østergård, T., Jensen, R.L. and Maagaard, S.E. 2016. Building simulations supporting decision making in early design - A review. *Renewable and Sustainable Energy Reviews* 61, pp. 187–201. Available at: <http://dx.doi.org/10.1016/j.rser.2016.03.045>.
- Østergård, T., Jensen, R.L. and Maagaard, S.E. 2017. Early Building Design: Informed decision-making by exploring multidimensional design space using sensitivity analysis. *Energy and Buildings* 142, pp. 8–22. Available at: <http://dx.doi.org/10.1016/j.enbuild.2017.02.059>.
- Ouammi, A., Zejli, D., Dagdougui, H. and Benchrifa, R. 2012. Artificial neural network analysis of Moroccan solar potential. *Renewable and Sustainable Energy Reviews* 16(7), pp. 4876–4889. Available at: <http://dx.doi.org/10.1016/j.rser.2012.03.071>.
- Ozgoren, M., Bilgili, M. and Sahin, B. 2012. Estimation of global solar radiation using ANN over Turkey. *Expert Systems with Applications* 39(5), pp. 5043–5051. Available at: <http://dx.doi.org/10.1016/j.eswa.2011.11.036>.
- Pacheco, R., Ordóñez, J. and Martínez, G. 2012. Energy efficient design of building: A review. *Renewable and Sustainable Energy Reviews* 16(6), pp. 3559–3573. doi: 10.1016/j.rser.2012.03.045.
- Pan, C.-A.P.C.-A. and Jeng, T.J.T. 2010. A robotic and kinetic design for interactive architecture. *SICE Annual Conference 2010, Proceedings of*, pp. 1792–1796.
- Panya, D.S., Kim, T. and Choo, S. 2020. A methodology of interactive motion facades design through parametric strategies. *Applied Sciences (Switzerland)* 10(4). doi: 10.3390/app10041218.
- Papadopoulos, S., Bonczak, B. and Kontokosta, C.E. 2018. Pattern recognition in building energy performance over time using energy benchmarking data. *Applied Energy* 221(February), pp. 576–586. Available at: <https://doi.org/10.1016/j.apenergy.2018.03.079>.
- Park, J.J. 2016. *Adaptive Biomimetic Façades: compound bio-inspired design strategy for multi-functional stadiums*. The University of Melbourne.
- Paszke, A. et al. 2019. PyTorch: An Imperative Style, High-Performance Deep Learning Library. (NeurIPS). Available at: <http://arxiv.org/abs/1912.01703>.
- Paterson, G., Mumovic, D., Das, P. and Kimpian, J. 2017. Energy use predictions with machine learning during architectural concept design. *Science and Technology for the Built Environment* 23(6), pp. 1036–1048. Available at: <https://doi.org/10.1080/23744731.2017.1319176>.
- Pesenti, M., Masera, G. and Fiorito, F. 2015. Shaping an origami shading device through visual and thermal simulations. *Energy Procedia* 78, pp. 346–351. Available at: <http://dx.doi.org/10.1016/j.egypro.2015.11.663>.

## REFERENCES

- Platon, R., Dehkordi, V.R. and Martel, J. 2015. Hourly prediction of a building's electricity consumption using case-based reasoning, artificial neural networks and principal component analysis. *Energy and Buildings* 92, pp. 10–18. Available at: <http://dx.doi.org/10.1016/j.enbuild.2015.01.047>.
- Poon, K.H., Kämpf, J.H., Tay, S.E.R., Wong, N.H. and Reindl, T.G. 2020. Parametric study of URBAN morphology on building solar energy potential in Singapore context. *Urban Climate* 33(April 2019), p. 100624. Available at: <https://doi.org/10.1016/j.uclim.2020.100624>.
- Punch, K. 2005. *Introduction to Social Research Quantitative and Qualitative Approaches*. 2nd Editio. SAGE Publications Ltd.
- Qazi, A., Fayaz, H., Wadi, A., Raj, R.G., Rahim, N.A. and Khan, W.A. 2015. The artificial neural network for solar radiation prediction and designing solar systems: A systematic literature review. *Journal of Cleaner Production* 104, pp. 1–12. Available at: <http://dx.doi.org/10.1016/j.jclepro.2015.04.041>.
- Qudrat-Ullah, H. 2012. On the validation of system dynamics type simulation models. *Telecommunication Systems* 51(2–3), pp. 159–166. doi: 10.1007/s11235-011-9425-4.
- Rafique, D. and Velasco, L. 2018. Machine Learning for Network Automation: Overview, Architecture, and Applications [Invited Tutorial]. *Journal of Optical Communications and Networking* 10(10), p. D126. Available at: <https://www.osapublishing.org/abstract.cfm?URI=jocn-10-10-D126>.
- Raza, M.Q. and Khosravi, A. 2015. A review on artificial intelligence based load demand forecasting techniques for smart grid and buildings. *Renewable and Sustainable Energy Reviews* 50, pp. 1352–1372. Available at: <http://dx.doi.org/10.1016/j.rser.2015.04.065>.
- Reddy, K.S. and Ranjan, M. 2004. Solar resource estimation using artificial neural networks and comparison with other correlation models. *Energy Conversion and Management* 44(15), pp. 2519–2530. doi: 10.1016/S0196-8904(03)00009-8.
- Rehman, M. and Pedersen, S.A. 2012. Validation of Simulation Models. *Journal of Experimental and Theoretical Artificial Intelligence* 24(3), pp. 351–363. doi: 10.1080/0952813X.2012.695459.
- Ricci, A., Ponzio, C., Fabbri, K., Gaspari, J. and Naboni, E. 2020. Development of a self-sufficient dynamic façade within the context of climate change. *Architectural Science Review* 8628. doi: 10.1080/00038628.2020.1713042.
- Ritter, A. 2007. *Smart materials in architecture, interior architecture and design*. Birkhäuser.
- Ritter, F., Geyer, P. and Bormann, A. 2015. Simulation-based Decision-making in Early Design Stages. *Proc. of the 32nd CIB W78 Conference 2015, 27th-29th October 2015, Eindhoven, The Netherlands*, pp. 657–666.
- Robson, C. and McCartan, K. 2011. *Real world research: a resource for users of social research methods in applied settings*. 4th Editio. London: Wiley, Chichester, West Sussex. Available at: <https://www.ptonline.com/articles/how-to-get-better-mfi-results>.
- Romano, R., Aelenei, L., Aelenei, D. and Mazzucchelli, E.S. 2018. What is an adaptive façade? Analysis of recent terms and definitions from an international perspective. *Journal of Facade Design and Engineering* 6(3), pp. 065–076. doi: 10.7480/jfde.2018.3.2478.
- Roudsari, M., Pak, M. and Smith, A. 2013. Ladybug: a Parametric Environmental Plugin for Grasshopper To Help Designers Create an Environmentally-Conscious Design. *13th Conference of International Building Performance Simulation Association*, pp. 3129–3135. Available at: [http://www.ibpsa.org/proceedings/bs2013/p\\_2499.pdf](http://www.ibpsa.org/proceedings/bs2013/p_2499.pdf).
- Ruben, B., Bjørn Petter, J. and Arild, G. 2010. Properties, requirements and possibilities of smart windows for

## REFERENCES

dynamic daylight and solar energy control in buildings: A state-of-the-art review. *Solar Energy Materials and Solar Cells* 94(2), pp. 87–105. Available at: <http://www.sciencedirect.com/science/article/pii/S0927024809002992>.

- Sabry, H., Sherif, A., Gadelhak, M. and Aly, M. 2014. Balancing the daylighting and energy performance of solar screens in residential desert buildings: Examination of screen axial rotation and opening aspect ratio. *Solar Energy* 103, pp. 364–377. Available at: <http://dx.doi.org/10.1016/j.solener.2014.02.025>.
- Sadeghi, S.A., Karava, P., Konstantzos, I. and Tzempelikos, A. 2016. Occupant interactions with shading and lighting systems using different control interfaces: A pilot field study. *Building and Environment* 97, pp. 177–195. Available at: <http://dx.doi.org/10.1016/j.buildenv.2015.12.008>.
- Sadek, A.H. and Mahrous, R. 2018. Adaptive glazing technologies: Balancing the benefits of outdoor views in healthcare environments. *Solar Energy* 174(September), pp. 719–727. doi: 10.1016/j.solener.2018.09.032.
- Sadineni, S.B., Madala, S. and Boehm, R.F. 2011. Passive building energy savings: A review of building envelope components. *Renewable and Sustainable Energy Reviews* 15(8), pp. 3617–3631. Available at: <http://dx.doi.org/10.1016/j.rser.2011.07.014>.
- Safa, M. 2011. *Determination and Modelling of Energy Consumption in Wheat Production Using Neural Networks*.
- Salles, R., Belloze, K., Porto, F., Gonzalez, P.H. and Ogasawara, E. 2019. Nonstationary time series transformation methods: An experimental review. *Knowledge-Based Systems* 164, pp. 274–291. Available at: <https://doi.org/10.1016/j.knosys.2018.10.041>.
- Samarasinghe, S. 2007. *Neuronal networks for applied sciences and engineering*. New York: Auerbach Publications.
- Sargent, R.G. 2010. Verification and validation of simulation models. In: *Proceedings - Winter Simulation Conference.*, pp. 166–183. doi: 10.1109/WSC.2010.5679166.
- Sauerbruch, M., Hutton, L. and Hinterthan, A. 2011. *CTBUH Interviews – 2011 Awards Symposium*.
- Saunders, M., Lewis, P. and Thornhill, A. 2016. *Research Methods for Business Students*. Available at: [https://www.researchgate.net/publication/330760964\\_Research\\_Methods\\_for\\_Business\\_Students\\_Chapter\\_4\\_Understanding\\_research\\_philosophy\\_and\\_approaches\\_to\\_theory\\_development](https://www.researchgate.net/publication/330760964_Research_Methods_for_Business_Students_Chapter_4_Understanding_research_philosophy_and_approaches_to_theory_development).
- Schleicher, S., Schleicher, S., Lienhard, J., Poppinga, S., Masselter, T. and Speck, T. 2011. Adaptive Façade Shading Systems inspired by Natural Elastic Kinematics. In: *Adaptive Architecture Conference*. London, pp. 1–12.
- Schumacher, M., Schaeffer, O., Marcus Vogt, M. and Müller, A. 2010. *Move: architecture in motion-dynamic components and elements mendeley citation*. Birkhäuser, Basel.
- SEEC 2015. *Saudi Arabia Energy efficiency report*.
- Seeger, C. 2018. An investigation of categorical variable encoding techniques in machine learning: binary versus one-hot and feature hashing. *Degree Project Technology*, p. 41. Available at: <http://www.diva-portal.org/smash/get/diva2:1259073/FULLTEXT01.pdf>.
- Seyedzadeh, S., Rahimian, F.P., Glesk, I. and Roper, M. 2018. Machine learning for estimation of building energy consumption and performance: a review. *Visualization in Engineering* 6(1). doi: 10.1186/s40327-018-0064-7.
- Shakouri, M. and Banihashemi, S. 2012. Developing an empirical predictive saved load-rating model for

## REFERENCES

- windows by using artificial neural network. *International Journal of Green Energy* 16(13), pp. 961–970. Available at: <https://doi.org/10.1080/15435075.2012.738451>.
- Shakouri, M. and Banihashemi, S. 2019. Developing an empirical predictive saved load-rating model for windows by using artificial neural network. *International Journal of Green Energy* 16(13), pp. 961–970. Available at: <https://doi.org/10.1080/15435075.2012.738451>.
- Sharaidin, K., Burry, J. and Salim, F. 2012. Integration of digital simulation tools with parametric designs to evaluate kinetic façades for daylight performance. *Digital Physicality-Proceedings of the 30th eCAADe Conference* 2, pp. 701–709. Available at: [https://cpb-us-e1.wpmucdn.com/blogs.uoregon.edu/dist/9/447/files/2015/06/Sharaidin\\_ecaade2012\\_kineticfacades\\_ltg-oeomx3.pdf](https://cpb-us-e1.wpmucdn.com/blogs.uoregon.edu/dist/9/447/files/2015/06/Sharaidin_ecaade2012_kineticfacades_ltg-oeomx3.pdf).
- Sheikh, W.T. and Asghar, Q. 2019. Adaptive biomimetic facades: Enhancing energy efficiency of highly glazed buildings. *Frontiers of Architectural Research* . doi: 10.1016/j.foar.2019.06.001.
- Shen, E., Hu, J. and Patel, M. 2014. Energy and visual comfort analysis of lighting and daylight control strategies. *Building and Environment* 78, pp. 155–170. Available at: <http://dx.doi.org/10.1016/j.buildenv.2014.04.028>.
- Shi, X., Abel, T. and Wang, L. 2020. Influence of two motion types on solar transmittance and daylight performance of dynamic façades. *Solar Energy* 201(March), pp. 561–580. doi: 10.1016/j.solener.2020.03.017.
- Skarning, G.C.J., Hviid, C.A. and Svendsen, S. 2017. The effect of dynamic solar shading on energy, daylighting and thermal comfort in a nearly zero-energy loft room in Rome and Copenhagen. *Energy and Buildings* 135, pp. 302–311. Available at: <http://dx.doi.org/10.1016/j.enbuild.2016.11.053>.
- van Soomeren, P., Klundert, W. van de, Aquilué, I. and de Kleuver, J. 2016. High-rise in trouble? Learning from Europe. *Journal of Place Management and Development* 9(2), pp. 224–240. doi: 10.1108/JPMD-12-2015-0058.
- Sözen, A., Arcaklioglu, E. and Özalp, M. 2004. Estimation of solar potential in Turkey by artificial neural networks using meteorological and geographical data. *Energy Conversion and Management* 45(18–19), pp. 3033–3052. doi: 10.1016/j.enconman.2003.12.020.
- Srivastava, N., Hinton, G., Krizhevsky, A., Sutskever, I. and Salakhutdinov, R. 2016. Dropout: A Simple Way to Prevent Neural Networks from Overfittin. *2016 International Conference on Advances in Electrical, Electronic and Systems Engineering, ICAEES 2016* 15, pp. 520–525. doi: 10.1109/ICAEEES.2016.7888100.
- Svetnik, V., Liaw, A., Tong, C., Christopher Culberson, J., Sheridan, R.P. and Feuston, B.P. 2003. Random Forest: A Classification and Regression Tool for Compound Classification and QSAR Modeling. *Journal of Chemical Information and Computer Sciences* 43(6), pp. 1947–1958. doi: 10.1021/ci034160g.
- Tabadkani, A., Banihashemi, S. and Hosseini, M.R. 2018. Daylighting and visual comfort of oriental sun responsive skins : A parametric analysis., pp. 663–676.
- Tabadkani, A., Roetzel, A., Li, H.X. and Tsangrassoulis, A. 2020a. A review of automatic control strategies based on simulations for adaptive facades. *Building and Environment* 175(March). doi: 10.1016/j.buildenv.2020.106801.
- Tabadkani, A., Roetzel, A., Li, H.X. and Tsangrassoulis, A. 2020b. A review of automatic control strategies based on simulations for adaptive facades. *Building and Environment* 175(January), p. 106801. Available at: <https://doi.org/10.1016/j.buildenv.2020.106801>.
- Tabadkani, A., Roetzel, A., Li, H.X. and Tsangrassoulis, A. 2021a. Design approaches and typologies of adaptive

## **REFERENCES**

- facades: A review. *Automation in Construction* 121(October 2020), p. 103450. Available at: <https://doi.org/10.1016/j.autcon.2020.103450>.
- Tabadkani, A., Roetzel, A., Xian Li, H., Tsangrassoulis, A. and Attia, S. 2021b. Analysis of the impact of automatic shading control scenarios on occupant's comfort and energy load. *Applied Energy* 294(January), p. 116904. Available at: <https://doi.org/10.1016/j.apenergy.2021.116904>.
- Tabadkani, A., Valinejad Shoubi, M., Soflaei, F. and Banihashemi, S. 2019a. Integrated parametric design of adaptive facades for user's visual comfort. *Automation in Construction* 106(June), p. 102857. Available at: <https://doi.org/10.1016/j.autcon.2019.102857>.
- Tabadkani, A., Valinejad Shoubi, M., Soflaei, F. and Banihashemi, S. 2019b. Integrated parametric design of adaptive facades for user's visual comfort. *Automation in Construction* 106(May), p. 102857. Available at: <https://doi.org/10.1016/j.autcon.2019.102857>.
- Thomas M. Mitchell 1997a. *Machine Learning Book*. McGraw-Hill, Inc. New York, NY, USA ©1997. Available at: <http://www-stat.stanford.edu/~tibs/book/preface.ps>.
- Thomas M. Mitchell 1997b. *Machine Learning Book*. McGraw-Hill, Inc. New York, NY, USA ©1997. doi: 10.1007/978-0-387-84858-7.
- Thompson, M., Duda, R.O. and Hart, P.E. 1974. Pattern Classification and Scene Analysis. *Leonardo* 7(4), p. 370. doi: 10.2307/1573081.
- Touma, A. Al and Ouahrani, D. 2017. Shading and day-lighting controls energy savings in offices with fully-Glazed façades in hot climates. *Energy and Buildings* 151, pp. 263–274. Available at: <http://dx.doi.org/10.1016/j.enbuild.2017.06.058>.
- Touma, A. Al and Ouahrani, D. 2018. Quantifying savings in spaces energy demands and CO2 emissions by shading and lighting controls in the Arabian Gulf. *Journal of Building Engineering* 18(April), pp. 429–437. Available at: <https://doi.org/10.1016/j.jobbe.2018.04.005>.
- Trigaux, D. and De Troyer, F. 2015. A design tool to optimize solar gains and energy use in neighbourhoods. *PLEA 2015 book of proceedings* (September)
- Tsanas, A. and Xifara, A. 2012. Accurate quantitative estimation of energy performance of residential buildings using statistical machine learning tools. *Energy and Buildings* 49, pp. 560–567. Available at: <http://dx.doi.org/10.1016/j.enbuild.2012.03.003>.
- Tso, G.K.F. and Yau, K.K.W. 2007. Predicting electricity energy consumption: A comparison of regression analysis, decision tree and neural networks. *Energy* 32(9), pp. 1761–1768. doi: 10.1016/j.energy.2006.11.010.
- Tung, K.Y., Huang, I.C., Chen, S.L. and Shih, C.T. 2005. Mining the Generation Xers' job attitudes by artificial neural network and decision tree - Empirical evidence in Taiwan. *Expert Systems with Applications* 29(4), pp. 783–794. doi: 10.1016/j.eswa.2005.06.012.
- Turhan, C., Kazanasmaz, T., Uygun, I.E., Ekmen, K.E. and Akkurt, G.G. 2014. Comparative study of a building energy performance software (KEP-IYTE-ESS) and ANN-based building heat load estimation. *Energy and Buildings* 85, pp. 115–125. Available at: <http://dx.doi.org/10.1016/j.enbuild.2014.09.026>.
- Tzempelikos, A. and Athienitis, A.K. 2007. The impact of shading design and control on building cooling and lighting demand. *Solar Energy* 81(3), pp. 369–382. doi: 10.1016/j.solener.2006.06.015.
- Vattam, S., Helms, M. and Goel, A.K. 2007. Biologically-Inspired Innovation in Engineering Design: A Cognitive Study. *Technical Report, Graphics, Visualization and Usability Center* , p. 41. Available at: <https://smartech.gatech.edu/handle/1853/14346>.

## **REFERENCES**

- Vattam, S.S., Helms, M.E. and Goel, A.K. 2009. Nature of creative analogies in biologically inspired innovative design. (January 2009), p. 255. doi: 10.1145/1640233.1640273.
- Velasco, R., Brakke, A.P. and Chavarro, D. 2015. Computer-Aided Architectural Design Futures. *The Next City - New Technologies and the Future of the Built Environment*. 527, pp. 172–191. Available at: <http://link.springer.com/10.1007/978-3-662-47386-3>.
- Vincent, J.F.V. 2009. Biomimetics - A review. *Proceedings of the Institution of Mechanical Engineers, Part H: Journal of Engineering in Medicine* 223(8), pp. 919–939. doi: 10.1243/09544119JEIM561.
- Wang, J., Beltrán, L.O. and Kim, J. 2012. From Static to Kinetic: A Review of Acclimated Kinetic Building Envelopes. *World Renewable Energy Forum, WREF 2012* 5, pp. 4022–4029. Available at: <http://www.scopus.com/inward/record.url?eid=2-s2.0-84871549544&partnerID=tZOtx3y1>.
- Wang, Z. and Srinivasan, R.S. 2017. A review of artificial intelligence based building energy use prediction: Contrasting the capabilities of single and ensemble prediction models. *Renewable and Sustainable Energy Reviews* 75(October 2016), pp. 796–808. Available at: <http://dx.doi.org/10.1016/j.rser.2016.10.079>.
- Wankanapon, P. and Mistrick, R.G. 2011. Roller Shades and Automatic Lighting Control with Solar Radiation Control Strategies. *Built* 1(1), pp. 35–42. doi: 10.14456/built.2011.2.
- Wei, C.C. 2017. Predictions of surface solar radiation on tilted solar panels using machine learning models: A case study of Tainan City, Taiwan. *Energies* 10(10). doi: 10.3390/en10101660.
- Wells, M. 2005. *Skyscrapers: Structure and Design*. London: Laurence King.
- Westermann, P. and Evins, R. 2019a. Adaptive sampling for building simulation surrogate model derivation using the LOLA-voronoi algorithm. *Building Simulation Conference Proceedings* 3, pp. 1559–1563. doi: 10.26868/25222708.2019.211232.
- Westermann, P. and Evins, R. 2019b. Surrogate modelling for sustainable building design – A review. *Energy and Buildings* 198, pp. 170–186. Available at: <https://doi.org/10.1016/j.enbuild.2019.05.057>.
- Westermann, P. and Evins, R. 2019c. Surrogate modelling for sustainable building design – A review. *Energy and Buildings* 198, pp. 170–186. Available at: <https://doi.org/10.1016/j.enbuild.2019.05.057>.
- Wienold, J., Frontini, F., Herkel, S. and Mende, S. 2011. Climate based simulation of different shading device systems for comfort and energy demand. *Proceedings of Building Simulation 2011: 12th Conference of International Building Performance Simulation Association*, pp. 2680–2687.
- Wigginton, M. and Harris, J. 2002. *Intelligent Skins*. Architectural Press.
- William, Z. and Clark, R. 1970. *Kinetic Architecture*. 1st editio. New York: Van Nostrand Reinhold.
- Wisker, G. 2007. *The Postgraduate Research Handbook: Succeed with your MA, MPhil, EdD and PhD*. Palgrave.
- Wong, S.L., Wan, K.K.W. and Lam, T.N.T. 2010. Artificial neural networks for energy analysis of office buildings with daylighting. *Applied Energy* 87(2), pp. 551–557. Available at: <http://dx.doi.org/10.1016/j.apenergy.2009.06.028>.
- Yadav, A.K. and Chandel, S.S. 2014. Solar radiation prediction using Artificial Neural Network techniques: A review. *Renewable and Sustainable Energy Reviews* 33, pp. 772–781. doi: 10.1016/j.rser.2013.08.055.
- Yu, Z., Haghighat, F., Fung, B.C.M. and Yoshino, H. 2010a. A decision tree method for building energy demand modeling. *Energy and Buildings* 42(10), pp. 1637–1646. Available at: <http://dx.doi.org/10.1016/j.enbuild.2010.04.006>.



## **REFERENCES**

- Yu, Z., Haghghat, F., Fung, B.C.M. and Yoshino, H. 2010b. A decision tree method for building energy demand modeling. *Energy and Buildings* 42(10), pp. 1637–1646. Available at: <http://dx.doi.org/10.1016/j.enbuild.2010.04.006>.
- Yun, G., Park, D.Y. and Kim, K.S. 2017. Appropriate activation threshold of the external blind for visual comfort and lighting energy saving in different climate conditions. *Building and Environment* 113, pp. 247–266. Available at: <http://dx.doi.org/10.1016/j.buildenv.2016.11.021>.
- Yun, G., Yoon, K.C. and Kim, K.S. 2014. The influence of shading control strategies on the visual comfort and energy demand of office buildings. *Energy and Buildings* 84, pp. 70–85. Available at: <http://dx.doi.org/10.1016/j.enbuild.2014.07.040>.
- Zeigler, B.P. and Nutaro, J.J. 2016. Towards a framework for more robust validation and verification of simulation models for systems of systems. *The Journal of Defense Modeling and Simulation: Applications, Methodology, Technology*
- Zell, E. et al. 2015. Assessment of solar radiation resources in Saudi Arabia. *Solar Energy* 119, pp. 422–438. Available at: <http://dx.doi.org/10.1016/j.solener.2015.06.031>.
- Zhang, G., Eddy Patuwo, B. and Y. Hu, M. 1998. Forecasting with artificial neural networks: The state of the art. *International Journal of Forecasting* 14(1), pp. 35–62. doi: 10.1016/S0169-2070(97)00044-7.
- Zhang, L., Wen, J., Li, Y., Chen, J., Ye, Y., Fu, Y. and Livingood, W. 2021. A review of machine learning in building load prediction. *Applied Energy* 285(January), p. 116452. Available at: <https://doi.org/10.1016/j.apenergy.2021.116452>.
- Zhang, Y., O'Neill, Z., Dong, B. and Augenbroe, G. 2015. Comparisons of inverse modeling approaches for predicting building energy performance. *Building and Environment* 86, pp. 177–190. Available at: <http://dx.doi.org/10.1016/j.buildenv.2014.12.023>.
- Zhao, H.X. and Magoulès, F. 2012a. A review on the prediction of building energy consumption. *Renewable and Sustainable Energy Reviews* 16(6), pp. 3586–3592. Available at: <http://dx.doi.org/10.1016/j.rser.2012.02.049>.
- Zhao, H.X. and Magoulès, F. 2012b. A review on the prediction of building energy consumption. *Renewable and Sustainable Energy Reviews* 16(6), pp. 3586–3592. doi: 10.1016/j.rser.2012.02.049.

## **APPENDIX**

## **Appendix A: Validation**

APPENDIX

29/05/1440 H      **TRANSACTION PROCESSED**      04-02-2019 02:29:07 PM # 188513 - 040219 - 157

Ref.No: 157BSF11621\189513\44963305  
 Payment By: Account  
 Debit Account: 50757000171      Account Hold. name: A/O OMRANIA AND ASSOCIATES  
 Debit Currency: SAR      Debit Amount: 4,746.42  
 Biller Name: 002 Saudi Electric Company      Sell Rate: 1.000000  
 Biller No. 10036342131  
 Biller Amt. (SAR): 4,746.42

---

**فوترة استهلاك الطاقة الكهربائية**

الشركة السعودية للكهرباء  
Saudi Electricity Company  
جول باندان من املحبر

القطاع الأوسط      إدارة كهرباء      مدينة الرياض      مكتب خدمات العملاء

رقم الفاتورة: ٢١٨٠٠٨٠٧٤٣٠٦  
 بداية الفترة: ٢٠١٨/١١/٢٦  
 نهاية الفترة: ٢٠١٨/١٢/٢٥

المشترك: باسم صبحي الشهابي  
 العنوان: المالك باسم صبحي الشهابي

|                           |                                |
|---------------------------|--------------------------------|
| رقم الحساب: ١٠٠٣٦٣٤٢١٣١   | تاريخ الفاتورة: ٢٠١٩/٠١/٢٠     |
| المبلغ المستحق: ٤,٧٤٦,٤٢  | تاريخ بداية احتساب: ٢٠١٩/٠١/٢٨ |
| للمرور بتاريخ: ٢٠١٩/٠٢/٢٤ | تاريخ إصدار الفاتورة:          |

|                          |                                |
|--------------------------|--------------------------------|
| رقم الاشتراك: ١١١٤٩٣٦٠٤٠ | رقم العداد: ٦٥٩٦               |
| معدلة التامع: ١٥٠        | الحدود المتعددة: ٦١٤٧٤٨        |
| معدلة التسليم: ٥٩٧٧٣٠    | معدلة التسليم: ١,٠٠            |
| كثافة الاستهلاك: ١٧٠١٨   | المبلغ المطلوب: ١٧٠١٨,٠٠       |
| رقم المنطقة: ١١١٠٠٣      | رقم الفاتورة: R١٠٠١٤٩٣٦ ٠٠٠٠٤٠ |

|                          |                            |                         |
|--------------------------|----------------------------|-------------------------|
| رقم الفاتورة: ٢٠١٩/٠١/٢٨ | رقم الفاتورة: ٢١٨٠٠٨٠٧٤٣٠٦ | رقم الحساب: ١٠٠٣٦٣٤٢١٣١ |
| المبلغ المطلوب: ٤,٧٤٦,٤٢ | المبلغ المطلوب: ٤,٧٤٦,٤٢   | رقم الحساب: ١٠٠٣٦٣٤٢١٣١ |

السادة بنك .....  
 أرجو حسم قيمة هذه الفاتورة من حسابي لديكم رقم .....  
 التوقيع  
 الرقم الضريبي للمورد: ٣٠٠٠٠٣٦١٣١٠٠٠٣

100363421312450699947300000004746420

Sample of the monthly electricity bills for the examined office building.

## فاتورة إستهلاك الطاقة الكهربائية

### ملخص الفاتورة

رقم الحساب: ١٠٠٢٦٣٤٣٠٧٧ تاريخ الفاتورة: ٢٠١٩/٠٦/٠٣  
 اخر موعد للسداد: ٢٠١٩/٠٧/٢٥ تاريخ بداية الاستحقاق: ٢٠١٩/٠٦/٢٨  
 المبلغ المطلوب سداداً: **٧,٧٦٥.٨٠** ريال

اسم المشترك: باسم صبحي الشهابي  
 رقم المشترك: ١٠٣٦٨٣٤٤٢  
 العنوان: السليمانية العمرانية ٣  
 رقم الموقع: ٤٠٠٣٦٢٣٠١٨  
 مكتب خدمات الشمال / كهرباء مدينة الرياض

### بيانات مالية (ريال)

|                   |          |                        |          |
|-------------------|----------|------------------------|----------|
| * قيمة الاستهلاك: | ٧,٣٧٤.٠٠ | المبلغ الخاضع للضريبة: | ٧,٣٩٦.٠٠ |
| * خدمة العداد:    | ٢٢.٠٠    | الضريبة %:             | ٣٦٩.٨٠   |
|                   |          | المبلغ شامل الضريبة:   | ٧,٧٦٥.٨٠ |
|                   |          | الرصيد السابق:         | ٠.٠٠     |
|                   |          | إجمالي الفاتورة:       | ٧,٧٦٥.٨٠ |

(\*)مبالغ خاضعة لضريبة القيمة المضافة

### شراخ الاستهلاك

| شركة                   | استهلاك | قيمة (مسا) | المبلغ (مسا) |
|------------------------|---------|------------|--------------|
| الشركة الاولى          | ٦٠٠٠    | ٢٠         | ١,٢٠٠.٠٠     |
| استهلاك الشركة الثانية | ٢٠٨٠    | ٣٠         | ٦,١٧٤.٠٠     |

يتم احتساب الاستهلاك على اساس ٣٠ يوم

### بيانات فنية

رقم الاشتراك: ١١١٤٩٣٦٠٤٧  
 رقم العداد: ١٤٠١٢٩٠  
 سعة القاطع: ٣٠٠  
 معامل الضرب: ٦٠.٠٠  
 كمية الاستهلاك: ٢٦٥٨٠ وحدة كمية الاستهلاك هي (ك.و.س)

### A/O OMRANIA AND ASSOCIATES

Debit Amount : 7,765.80  
 Unit Rate : 0.000000  
 \$ / 1 Rate : 1.600000

ريخ بلك بالاشتراك بخدمة الفاتورة الثابتة بمبلغ ٧٤٥٠٠٠ ريال شهريا

6/10/1440 H      **TRANSACTION PROCESSED**      19-06-2019 01:36:03 PM # 716507 - 190619 - 157 #

Ref. No: 157BSF760371880747444763      Account Hold. name: A/O OMRANIA AND ASSOCIATES  
 Agent By: Account 50757000171      Debit Account: 50757000171      Account No.: 10036343077  
 Debit Currency: SAR      Debit Amount: 7,765.80  
 Biller Name: 002 Saudi Electric Company      Biller No.: 10036343077  
 Biller Amt. (SAR): 7,765.80

رقم الفاتورة: ٢٢٠٠٠٨٩٤٦٢٠  
 الرقم الضريبي للمورد: ٣٠٠٠٠٠٢١٦١٠٠٣  
 عنوان الشركة: المملكة العربية السعودية  
 المركز الرئيسي- حي العارض ص ب ٢٢٩٥٥ الرياض ١١٤١٦

هاتف: 920000222 الطوارئ: 933  
 مركز خدمة المشتركين: 920001100

الشركة السعودية للكهرباء  
Saudi Electricity Company  
نعمل بانفاق من الخلف

1003634307723750834467600000007765800

www.se.com.sa  
٩٣٥

الصفحة ١ من ١

Sample of the monthly electricity bills for the examined office building.

## **Appendix B: High Rise Buildings (Case Studies)**

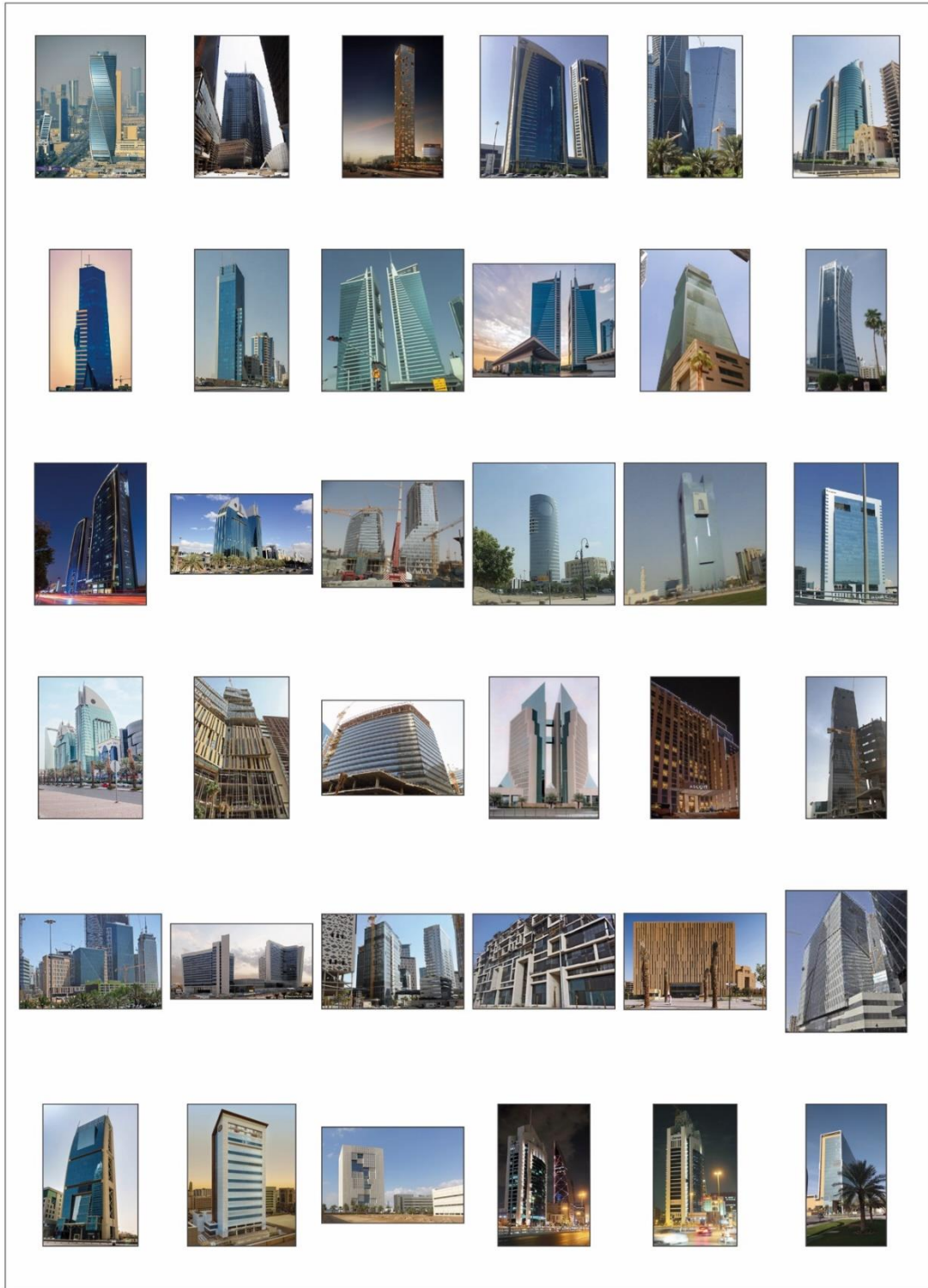
**APPENDIX**



High rise buildings case studies



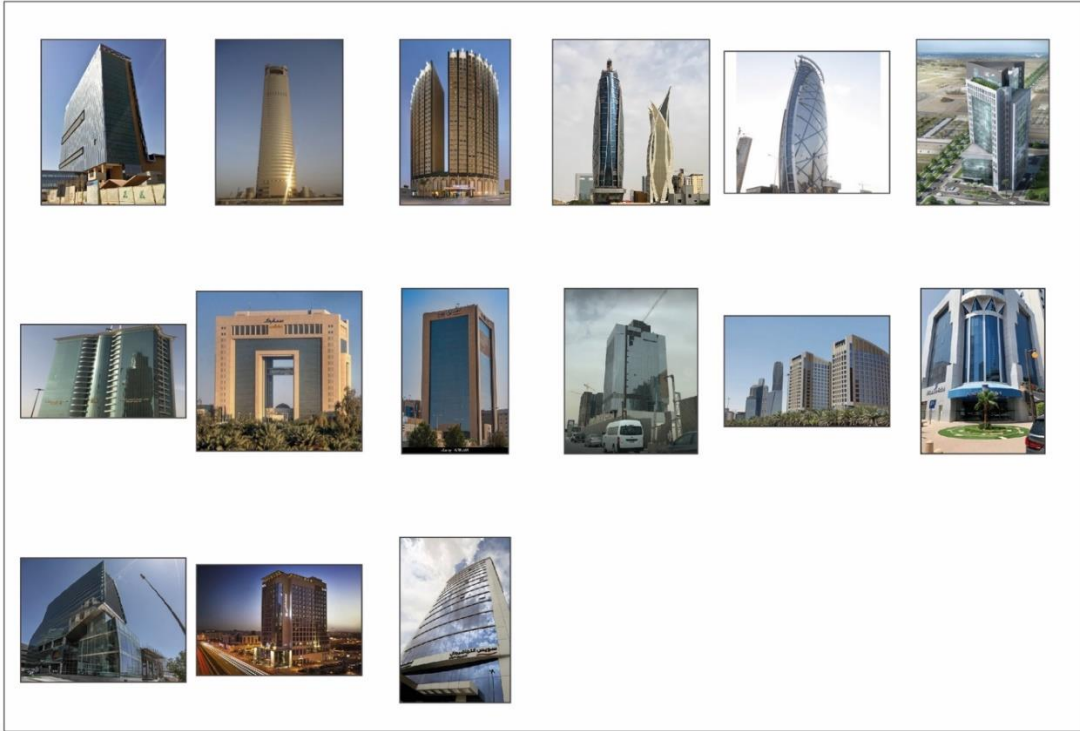
**APPENDIX**



High rise buildings case studies



**APPENDIX**



High rise buildings case studies

**APPENDIX**

*Office building Case studies.*

| Case No | Name                               | Total NLA | Total GFA | Tower Height | Floor to ceiling Height | Number of Floors | Core Dimensions | Core Configurations | Floor efficiency | Leasing Depth | Façade Glazing Orientation |   |   |   |      | Shading System Existence |       |
|---------|------------------------------------|-----------|-----------|--------------|-------------------------|------------------|-----------------|---------------------|------------------|---------------|----------------------------|---|---|---|------|--------------------------|-------|
|         |                                    |           |           |              |                         |                  |                 |                     |                  |               | E                          | W | S | N | No n | Poor                     | Exist |
| Case 1  | Public Investment Fund (PIF) Tower | 1800m2    | 2400m2    | 385 m        | 4 m                     | 77               | 600m2           | Central core        | 78%              | 12m to 14m    | ✓                          | ✓ | ✓ | ✓ | -    | -                        | ✓     |
| Case 2  | Al Faisaliah Tower                 | 1300m2    | 1700m2    | 267 m        | 4 m                     | 44               | 400m2           | Central core        | 80%              | 10m           | ✓                          | ✓ | ✓ | ✓ | -    | -                        | ✓     |
| Case 3  | Samba Bank HQ Tower                | 1640 m2   | 2050 m2   | 231.2 m      | 4.0 m                   | 40               | 410 m2          | Central core        | 80%              | 10m to 13m    | ✓                          | ✓ | ✓ | ✓ | -    | -                        | ✓     |
| Case 4  | KAFD Parcel 1.18                   | 1880 m2   | 2350 m2   | 150 m        | 3.8 m                   | 32               | 470 m2          | Central core        | 82%              | 11m           | ✓                          | ✓ | ✓ | ✓ | ✓    | -                        | -     |
| Case 5  | PPA 30 Parcel 5.03                 | 1390 m2   | 1780 m2   | 105 m        | 4 m                     | 26               | 390m2           | Central core        | 78%              | 10m           | ✓                          | - | ✓ | ✓ | ✓    | -                        | -     |
| Case 6  | KAFD World Trade Center            | 1815 m2   | 2270 m2   | 304 m        | 4 m                     | 67               | 455m2           | Central core        | 77%              | 10m to 14m    | ✓                          | ✓ | ✓ | ✓ | -    | -                        | ✓     |
| Case 7  | KAFD Parcel 3.05                   | 960 m2    | 1200 m2   | 84 m         | 4.20 m                  | 19               | 240 m2          | Central core        | 80%              | 10m           | ✓                          | ✓ | ✓ | ✓ | ✓    | -                        | -     |
| Case 8  | KAFD Parcel 5.08                   | 1208 m2   | 1510 m2   | 107.96 m     | 4.20 m                  | 24               | 302 m2          | Central core        | 80%              | 10m           | ✓                          | ✓ | ✓ | ✓ | -    | -                        | ✓     |
| Case 9  | PP 10 Parcel 3.04                  | 665 m2    | 950 m2    | 144.60 m     | 4 m                     | 34               | 285 m2          | Side core           | 70%              | 10m           | ✓                          | ✓ | ✓ | ✓ | -    | -                        | ✓     |
| Case 10 | Kingdom Tower                      | 1950 m2   | 2450 m2   | 302.3 m      | 4 m                     | 41               | 500 m2          | Central core        | 80%              | 13m           | ✓                          | ✓ | ✓ | ✓ | ✓    | -                        | -     |
| Case 11 | KAFD Parcel 4.01                   | 1000 m2   | 1250 m2   | 71.98 m      | 4.20 m                  | 16               | 250 m2          | Central core        | 80%              | 9m to 10m     | ✓                          | ✓ | ✓ | ✓ | -    | -                        | ✓     |
| Case 12 | KAFD Parcel 4.04 -waterfall tower  | 880 m2    | 1160 m2   | 107.96 m     | 4 m                     | 20               | 280 m2          | Central core        | 80%              | 11m           | ✓                          | ✓ | ✓ | ✓ | -    | ✓                        | -     |
| Case 13 | KAFD Muqarnas Tower                | 1274 m2   | 1820 m2   | 138 m        | 4 m                     | 30               | 546 m2          | Side core           | 70%              | 9 m           | ✓                          | ✓ | - | ✓ | -    | -                        | ✓     |
| Case 14 | KAFD Parcel 2.12                   | 1108 m2   | 1438 m2   | 105 m        | 4 m                     | 23               | 330 m2          | Central core        | 77%              | 10m to 12m    | ✓                          | ✓ | ✓ | ✓ | -    | -                        | ✓     |
| Case 15 | PPA 30 Parcel 4.09                 | 765 m2    | 980 m2    | 182 m        | 4.0 m                   | 46               | 215 m2          | Central core        | 78%              | 10m           | ✓                          | ✓ | ✓ | ✓ | -    | ✓                        | -     |
| Case 16 | KAFD Parcel 3.09                   | 1615 m2   | 1900 m2   | 138 m        | 4.20 m                  | 33               | 285 m2          | Central core        | 85%              | 11m           | ✓                          | ✓ | ✓ | ✓ | ✓    | -                        | -     |
| Case 17 | KAFD Parcel 2.13                   | 710 m2    | 900 m2    | 160.7 m      | 4 m                     | 34               | 190 m2          | Central core        | 79%              | 9 m           | ✓                          | ✓ | ✓ | ✓ | -    | -                        | ✓     |
| Case 18 | KAFD PPA 30 Parcel 2.11            | 1008 m2   | 1260 m2   | 55 m         | 4 m                     | 13               | 252 m2          | Side core           | 80%              | 10m           | ✓                          | - | ✓ | ✓ | ✓    | -                        | -     |

**APPENDIX**

| Case No | Name                                     | Total NLA | Total GFA | Tower Height | Floor to ceiling Height | Number of Floors | Core Dimensions | Core Configurations | Floor efficiency | Leasing Depth | Façade Glazing Orientation |   |   |   |      | Shading System Existence |       |
|---------|--|-----------|-----------|--------------|-------------------------|------------------|-----------------|---------------------|------------------|---------------|----------------------------|---|---|---|------|--------------------------|-------|
|         |  |           |           |              |                         |                  |                 |                     |                  |               | E                          | W | S | N | No n | Poor                     | Exist |
| Case 19 | Olaya Tower 1                            | 1320 m2   | 1650 m2   | 166 m        | 4.0 m                   | 34               | 330 m2          | Central core        | 80%              | 10m to 14m    | ✓                          | ✓ | ✓ | ✓ | ✓    | -                        | -     |
| Case 20 | Crystal Tower 2 (PPA 30 Parcel 1.10)     | 960 m2    | 1200 m2   | 80 m         | 4.00 m                  | 18               | 240 m2          | Central core        | 80%              | 10m           | ✓                          | ✓ | ✓ | ✓ | -    | -                        | ✓     |
| Case 21 | Crystal Tower 1 (PPA 30 Parcel 1.10)     | 858 m2    | 1100 m2   | 135 m        | 4.00 m                  | 26               | 242 m2          | Central core        | 78%              | 10m           | ✓                          | ✓ | ✓ | ✓ | -    | -                        | ✓     |
| Case 22 | GCC Bank Headquarters (KAFD Parcel 1.14) | 1515 m2   | 2020 m2   | 264 m        | 4 m                     | 53               | 505 m2          | Central core        | 75%              | 10m           | ✓                          | ✓ | ✓ | ✓ | -    | ✓                        | -     |
| Case 23 | KAFD Parcel 2.11                         | 840 m2    | 1050 m2   | 77 m         | 4.0 m                   | 17               | 210 m2          | Central core        | 80%              | 9m to 10m     | ✓                          | - | ✓ | ✓ | -    | ✓                        | -     |
| Case 24 | KAFD Parcel 4.06                         | 1264 m2   | 1580 m2   | 122 m        | 4.00 m                  | 33               | 316 m2          | Central core        | 80%              | 11m to 13m    | ✓                          | ✓ | ✓ | ✓ | -    | -                        | ✓     |

**APPENDIX**

*High-rise buildings in the studied context.*

| #  | Building                           | Height | Floors | Building type      | Year | Glazing Orientation |   |   |   | Shading System Existence |      |       | Building Geometry |
|----|------------------------------------|--------|--------|--------------------|------|---------------------|---|---|---|--------------------------|------|-------|-------------------|
|    |                                    |        |        |                    |      | E                   | W | S | N | Non                      | Poor | Exist |                   |
| 1  | Kingdom Trade Center Tower III     | 148    | 33     | high-rise building | -    | N                   | N | N | N | N                        | N    | N     | N                 |
| 2  | Kingdom Trade Center Tower II      | 148    | 33     | high-rise building | -    | N                   | N | N | N | N                        | N    | N     | N                 |
| 3  | King Fahd Twin Towers 2            | 144    | 32     | high-rise building | 2021 | ✓                   | ✓ | - | - | ✓                        | -    | -     | Tringle           |
| 4  | KAFD Tower 4.06                    | 135    | 30     | high-rise building | 2020 | ✓                   | ✓ | - | ✓ | -                        | -    | ✓     | Irregular Form    |
| 5  | SABB Bank Tower                    | 135    | 30     | high-rise building | 2021 | ✓                   | - | ✓ | ✓ | -                        | ✓    | -     | Square            |
| 6  | Muqarnas Tower                     | 135    | 30     | high-rise building | 2014 | ✓                   | ✓ | ✓ | ✓ | -                        | -    | ✓     | Irregular Form    |
| 7  | Al Khozama Towers I                | 135    | 30     | high-rise building | -    | ✓                   | ✓ | ✓ | ✓ | ✓                        | -    | -     | Rectangle         |
| 8  | Rafal Residence Tower              | 126    | 28     | high-rise building | 2016 | ✓                   | ✓ | ✓ | ✓ | ✓                        | -    | -     | Circle            |
| 9  | Riyadh Bank                        | 126    | 28     | high-rise building | -    | N                   | N | N | N | N                        | N    | N     | N                 |
| 10 | KAFD Tower 4.12                    | 121    | 27     | high-rise building | 2020 | ✓                   | - | ✓ | ✓ | -                        | -    | ✓     | Square            |
| 11 | KAFD Tower 4.10                    | 117    | 26     | high-rise building | 2020 | ✓                   | ✓ | ✓ | ✓ | -                        | -    | ✓     | Rectangle         |
| 12 | Malthak                            | 117    | 26     | high-rise building | 2018 | N                   | N | N | N | N                        | N    | N     | N                 |
| 13 | Al-Birr Foundation Office Tower    | 117    | 26     | high-rise building | -    | ✓                   | ✓ | ✓ | ✓ | -                        | -    | ✓     | Square            |
| 14 | Riyadh Sofitel                     | 112    | 25     | high-rise building | 2021 | ✓                   | ✓ | ✓ | ✓ | -                        | -    | ✓     | Irregular Form    |
| 15 | Alyaaah Hospital                   | 112    | 25     | high-rise building | 2020 | ✓                   | ✓ | ✓ | ✓ | ✓                        | -    | -     | Square            |
| 16 | Al Fawaz Tower                     | 112    | 25     | high-rise building | 2018 | ✓                   | ✓ | - | ✓ | ✓                        | -    | -     | Rectangle         |
| 17 | Al Khozama Towers III              | 112    | 25     | high-rise building | -    | N                   | N | N | N | N                        | N    | N     | N                 |
| 18 | Kingdom Trade Center Tower IX      | 112    | 25     | high-rise building | -    | N                   | N | N | N | N                        | N    | N     | N                 |
| 19 | Kingdom Trade Center Tower VIII    | 112    | 25     | high-rise building | -    | N                   | N | N | N | N                        | N    | N     | N                 |
| 20 | Kingdom Trade Center Tower IV      | 112    | 25     | high-rise building | -    | N                   | N | N | N | N                        | N    | N     | N                 |
| 21 | KAFD Parcel 3.04 Residential Tower | 98     | 26     | high-rise building | 2014 | ✓                   | ✓ | ✓ | ✓ | -                        | -    | ✓     | Irregular Form    |
| 22 | Crystal Towers 2                   | 95     | 18     | high-rise building | 2019 | ✓                   | ✓ | ✓ | ✓ | -                        | -    | ✓     | Irregular Form    |
| 23 | Hilton Riyadh Hotel                | 93     | 23     | high-rise building | 2016 | ✓                   | ✓ | ✓ | ✓ | ✓                        | -    | -     | Rectangle         |
| 24 | Wyndham Grand Hotel                | 92     | 20     | high-rise building | 2020 | ✓                   | ✓ | ✓ | ✓ | -                        | ✓    | -     | Rectangle         |
| 25 | KAFD Parcel 4.07                   | 88     | 18     | high-rise building | 2016 | ✓                   | ✓ | ✓ | ✓ | -                        | -    | ✓     | Irregular Form    |
| 26 | KAFD Parcel 3.05 Office Tower      | 83     | 19     | high-rise building | 2014 | ✓                   | ✓ | ✓ | ✓ | ✓                        | -    | -     | Square            |
| 27 | KAFD Parcel 5.01                   | 83     | 19     | high-rise building | 2020 | ✓                   | ✓ | ✓ | ✓ | ✓                        | -    | -     | Rectangle         |
| 28 | KAFD Parcel 1.11                   | 83     | 18     | high-rise building | 2020 | ✓                   | ✓ | ✓ | ✓ | -                        | -    | ✓     | Irregular Form    |
| 29 | KAFD Parcel 5.03, Tower 2          | 76     | 16     | high-rise building | 2019 | ✓                   | - | ✓ | ✓ | -                        | ✓    | -     | Square            |
| 30 | Hilton Riyadh Residence            | 71     | 16     | high-rise building | 2016 | ✓                   | ✓ | ✓ | ✓ | ✓                        | -    | -     | Irregular Form    |
| 31 | KAFD Tower 4.11                    | 70     | 12     | high-rise building | 2020 | ✓                   | ✓ | ✓ | ✓ | -                        | -    | ✓     | Irregular Form    |

**APPENDIX**

| #  | Building   | Height | Floors | Building type      | Year | Glazing Orientation |   |   |   | Shading System Existence |      |       | Building Geometry |
|----|--|--------|--------|--------------------|------|---------------------|---|---|---|--------------------------|------|-------|-------------------|
|    |  |        |        |                    |      | E                   | W | S | N | Non                      | Poor | Exist |                   |
| 32 | KAFD Parcel 3.05 Residential Tower                       | 67     | 17     | high-rise building | 2014 | ✓                   | ✓ | ✓ | ✓ | –                        | –    | ✓     | Irregular Form    |
| 33 | Vertical Medina  | 66     | 16     | high-rise building | 2020 | ✓                   | ✓ | ✓ | ✓ | ✓                        | –    | –     | Rectangle         |
| 34 | The Butterfly  | 66     | 15     | high-rise building | 2020 | ✓                   | ✓ | ✓ | ✓ | –                        | –    | ✓     | Irregular Form    |
| 35 | King Faisal Foundation North Building                    | 65     | 15     | high-rise building | 1984 | –                   | – | ✓ | ✓ | ✓                        | –    | –     | Tringle           |
| 36 | King Faisal Foundation South Building                    | 65     | 15     | high-rise building | 1984 | –                   | – | ✓ | ✓ | ✓                        | –    | –     | Tringle           |
| 37 | Cascading Condos   | 60     | 13     | high-rise building | 2017 | ✓                   | ✓ | ✓ | ✓ | –                        | –    | ✓     | Irregular Form    |
| 38 | KAFD Parcel 2.12   | 55     | 13     | high-rise building | 2020 | ✓                   | ✓ | ✓ | ✓ | –                        | –    | ✓     | Irregular Form    |
| 39 | Criminal Court   | 45     | -      | high-rise building | 2007 | ✓                   | ✓ | ✓ | ✓ | –                        | –    | ✓     | Square            |
| 40 | King Faisal Foundation Phase II                          | 36     | 8      | high-rise building | 1985 | ✓                   | – | – | ✓ | ✓                        | –    | –     | Tringle           |
| 41 | Kingdom Trade Center Tower XI                            | 112    | 25     | high-rise building | -    | N                   | N | N | N | N                        | N    | N     | N                 |
| 42 | KAFD Tower 5.08  | 108    | 24     | high-rise building | 2016 | ✓                   | ✓ | ✓ | ✓ | –                        | –    | ✓     | Square            |
| 43 | Al-Jomaiah Tower   | 108    | 24     | high-rise building | -    | ✓                   | ✓ | ✓ | ✓ | ✓                        | –    | –     | Square            |
| 44 | Hital Tower  | 108    | 24     | high-rise building | 2015 | ✓                   | ✓ | ✓ | ✓ | –                        | –    | ✓     | Square            |
| 45 | Al Munaje Tower  | 103    | 23     | high-rise building | 2012 | ✓                   | ✓ | – | – | ✓                        | –    | –     | Rectangle         |
| 46 | Marriott Courtyard                                       | 103    | 23     | high-rise building | -    | ✓                   | ✓ | ✓ | ✓ | ✓                        | –    | –     | Square            |
| 47 | KACST Tower  | 103    | 23     | high-rise building | 2019 | ✓                   | ✓ | ✓ | ✓ | –                        | –    | ✓     | Square            |
| 48 | Kingdom Trade Center Tower VI                            | 103    | 23     | high-rise building | -    | N                   | N | N | N | N                        | N    | N     | N                 |
| 49 | Kingdom Trade Center Tower V                             | 103    | 23     | high-rise building | -    | N                   | N | N | N | N                        | N    | N     | N                 |
| 50 | Waterfall Tower  | 99     | 22     | high-rise building | 2020 | ✓                   | ✓ | ✓ | ✓ | –                        | –    | ✓     | Rectangle         |
| 51 | Al Khozaa Towers II                                      | 99     | 22     | high-rise building | -    | N                   | N | N | N | N                        | N    | N     | N                 |
| 52 | Al Waseel Tower  | 94     | 21     | high-rise building | 2011 | ✓                   | ✓ | ✓ | ✓ | ✓                        | –    | –     | Rectangle         |
| 53 | 4250 King Fahd Rd  | 94     | 21     | high-rise building | 2012 | N                   | N | N | N | N                        | N    | N     | N                 |
| 54 | King Abdullah Center for Tumors and Liver Disease        | 94     | 21     | high-rise building | 2015 | ✓                   | ✓ | ✓ | ✓ | –                        | –    | ✓     | Rectangle         |
| 55 | TAM Tower  | 90     | 20     | high-rise building | 2021 | ✓                   | – | – | ✓ | ✓                        | –    | –     | Square            |
| 56 | Khaldia Tower 4  | 90     | 20     | high-rise building | -    | ✓                   | – | – | ✓ | ✓                        | –    | –     | Circle            |
| 57 | Spiasco Addwaeih Tower                                   | 90     | 20     | high-rise building | 2018 | ✓                   | ✓ | ✓ | ✓ | ✓                        | –    | –     | Ellipse           |
| 58 | InterContinental Riyadh King Abdullah Financial District | 90     | 20     | high-rise building | 2019 | N                   | N | N | N | N                        | N    | N     | N                 |
| 59 | Haven Towers   | 81     | 18     | high-rise building | 2018 | ✓                   | ✓ | ✓ | ✓ | ✓                        | –    | –     | Square            |
| 60 | 5565 King Fahd Branch Rd                                 | 81     | 18     | high-rise building | 2016 | N                   | N | N | N | N                        | N    | N     | N                 |
| 61 | Clemenceau Center  | 81     | 18     | high-rise building | 2019 | ✓                   | ✓ | ✓ | ✓ | ✓                        | –    | –     | Tringle           |
| 62 | Al-Sahab Tower   | 76     | 17     | high-rise building | 2021 | ✓                   | – | – | ✓ | ✓                        | –    | –     | Rectangle         |
| 63 | Al-Suwaile Tower   | 76     | 17     | high-rise building | 2018 | ✓                   | ✓ | ✓ | ✓ | –                        | ✓    | –     | Square            |
| 64 | The Council of Cooperative Health Insurance              | 76     | 17     | high-rise building | 2015 | ✓                   | ✓ | ✓ | ✓ | ✓                        | –    | –     | Rectangle         |

**APPENDIX**

| #  | Building   | Height | Floors | Building type      | Year | Glazing Orientation |   |   |   | Shading System Existence |      |       | Building Geometry |
|----|--|--------|--------|--------------------|------|---------------------|---|---|---|--------------------------|------|-------|-------------------|
|    |  |        |        |                    |      | E                   | W | S | N | Non                      | Poor | Exist |                   |
| 65 | Indigo Hotel Riyadh King Abdullah Financial District | 76     | 17     | high-rise building | 2020 | ✓                   | ✓ | ✓ | ✓ | -                        | -    | ✓     | Irregular Form    |
| 66 | SABIC Headquarters                                   | 76     | 17     | high-rise building | 2002 | ✓                   | ✓ | ✓ | ✓ | ✓                        | -    | -     | Square            |
| 67 | Arab National Bank Building                          | 76     | 17     | high-rise building | -    | ✓                   | ✓ | ✓ | ✓ | ✓                        | -    | -     | Square            |
| 68 | Verona Tower 2                                       | 72     | 16     | high-rise building | -    | N                   | N | N | N | N                        | N    | N     | N                 |
| 69 | Movepick A   | 72     | 16     | high-rise building | 2020 | ✓                   | ✓ | ✓ | ✓ | ✓                        | -    | -     | Square            |
| 70 | Al Moosa Hotel                                       | 72     | 16     | high-rise building | 2020 | ✓                   | ✓ | ✓ | ✓ | ✓                        | -    | -     | Square            |
| 71 | KAFD Parcel 4.01                                     | 72     | 16     | high-rise building | 2019 | ✓                   | ✓ | ✓ | ✓ | -                        | ✓    | -     | Irregular Form    |
| 72 | Marriott Executive Suites                            | 67     | 15     | high-rise building | 2012 | ✓                   | ✓ | ✓ | ✓ | ✓                        | -    | -     | Square            |
| 73 | Waha Centre  | 67     | 15     | high-rise building | 2018 | ✓                   | ✓ | ✓ | ✓ | -                        | -    | ✓     | Rectangle         |
| 74 | Hilton Garden Inn                                    | 67     | 15     | high-rise building | 2020 | ✓                   | ✓ | ✓ | ✓ | -                        | -    | ✓     | Square            |
| 75 | Swiss Spirit Hotel                                   | 67     | 15     | high-rise building | 2017 | ✓                   | - | - | ✓ | ✓                        | -    | -     | Square            |
| 76 | Swiss International Royal Hotel                      | 67     | 15     | high-rise building | 2017 | ✓                   | ✓ | - | ✓ | ✓                        | -    | -     | Square            |
| 77 | Ion Suites   | 67     | 15     | high-rise building | 2015 | ✓                   | - | - | ✓ | ✓                        | -    | -     | Square            |
| 78 | KAFD Tower 4.03                                      | 67     | 15     | high-rise building | 2020 | ✓                   | ✓ | ✓ | ✓ | ✓                        | -    | -     | Irregular Form    |
| 79 | Le Meridien Riyadh                                   | 67     | 15     | high-rise building | 2019 | ✓                   | ✓ | ✓ | ✓ | ✓                        | -    | -     | Ellipse           |
| 80 | Ministry of Communication and IT                     | 67     | 15     | high-rise building | -    | ✓                   | ✓ | ✓ | ✓ | -                        | -    | ✓     | Rectangle         |
| 81 | Morena Tower   | 63     | 14     | high-rise building | 2021 | ✓                   | ✓ | ✓ | ✓ | ✓                        | -    | -     | Square            |
| 82 | Movepick B   | 63     | 14     | high-rise building | 2020 | ✓                   | ✓ | ✓ | ✓ | -                        | ✓    | -     | Square            |
| 83 | Al alqa Elite Hotel                                  | 63     | 14     | high-rise building | 2017 | ✓                   | ✓ | ✓ | ✓ | ✓                        | -    | -     | Square            |
| 84 | Rose Continental Hotel                               | 63     | 14     | high-rise building | 2015 | ✓                   | - | - | ✓ | ✓                        | -    | -     | Square            |
| 85 | Safwa Complex  | 63     | 14     | high-rise building | -    | ✓                   | ✓ | ✓ | ✓ | ✓                        | -    | -     | Circle            |
| 86 | Corp Inn Deira                                       | 58     | 13     | high-rise building | -    | ✓                   | ✓ | ✓ | ✓ | ✓                        | -    | -     | Rectangle         |
| 87 | Cayan Office Building                                | 58     | 13     | high-rise building | 2018 | ✓                   | - | ✓ | ✓ | ✓                        | -    | -     | Square            |
| 88 | Al Rossais Commercial Center                         | 58     | 13     | high-rise building | -    | ✓                   | ✓ | ✓ | ✓ | ✓                        | -    | -     | Irregular Form    |
| 89 | Futuro Tower   | 54     | 12     | high-rise building | 2009 | ✓                   | ✓ | ✓ | ✓ | ✓                        | -    | -     | Square            |
| 90 | The Capital Market Authority Tower                   | 385    | 77     | skyscraper         | 2017 | ✓                   | ✓ | ✓ | ✓ | -                        | -    | ✓     | Irregular Form    |
| 91 | Burj Rafal   | 308    | 68     | skyscraper         | 2014 | ✓                   | ✓ | ✓ | ✓ | ✓                        | -    | -     | Ellipse           |
| 92 | KAFD World Trade Center                              | 304    | 67     | skyscraper         | 2020 | ✓                   | ✓ | ✓ | ✓ | -                        | -    | ✓     | Irregular Form    |
| 93 | Kingdom Centre Tower                                 | 302    | 32     | skyscraper         | 2002 | ✓                   | ✓ | ✓ | ✓ | ✓                        | -    | -     | Ellipse           |
| 94 | Al Faisaliyah Center                                 | 267    | 30     | skyscraper         | 2000 | ✓                   | ✓ | ✓ | ✓ | -                        | -    | ✓     | Square            |
| 95 | Takeen Tower   | 258    | 58     | skyscraper         | 2012 | ✓                   | ✓ | ✓ | ✓ | ✓                        | -    | -     | Ellipse           |
| 96 | GCC Bank Headquarters                                | 254    | 53     | skyscraper         | 2020 | ✓                   | ✓ | ✓ | ✓ | -                        | -    | ✓     | Irregular Form    |
| 97 | Al Rajhi Tower                                       | 250    | 33     | skyscraper         | 2017 | ✓                   | ✓ | ✓ | ✓ | ✓                        | -    | -     | Square            |

**APPENDIX**

| #   | Building                                 | Height | Floors | Building type | Year | Glazing Orientation |   |   |   | Shading System Existence |      |       | Building Geometry |
|-----|--|--------|--------|---------------|------|---------------------|---|---|---|--------------------------|------|-------|-------------------|
|     |  |        |        |               |      | E                   | W | S | N | Non                      | Poor | Exist |                   |
| 98  | Al ajdou Tower                           | 244    | 54     | skyscraper    | 2019 | ✓                   | ✓ | ✓ | ✓ | -                        | ✓    | -     | Irregular Form    |
| 99  | Saba Bank HQ Tower                       | 231    | 40     | skyscraper    | 2020 | ✓                   | ✓ | ✓ | ✓ | -                        | -    | ✓     | Irregular Form    |
| 100 | Rafal Living Tower                       | 213    | 62     | skyscraper    | 2020 | ✓                   | ✓ | ✓ | ✓ | -                        | -    | ✓     | Square            |
| 101 | Al Rajhi Bank Headquarters               | 205    | 37     | skyscraper    | 2017 | ✓                   | ✓ | ✓ | ✓ | ✓                        | -    | -     | Square            |
| 102 | DAAC Tower by Paramount Hotels & Resorts | 200    | 45     | skyscraper    | 2016 | ✓                   | - | - | ✓ | ✓                        | -    | -     | Rectangle         |
| 103 | Tadawul Tower                            | 200    | 41     | skyscraper    | 2020 | ✓                   | ✓ | ✓ | ✓ | -                        | ✓    | -     | Irregular Form    |
| 104 | Al-Obeikan Hilton Tower Hotel            | 200    | 35     | skyscraper    | 2017 | ✓                   | ✓ | ✓ | ✓ | ✓                        | -    | -     | Circle            |
| 105 | Nakheel Tower                            | 200    | 26     | skyscraper    | 2011 | ✓                   | - | ✓ | ✓ | ✓                        | -    | -     | Square            |
| 106 | KAFD Tower 4.09                          | 182    | 46     | skyscraper    | 2015 | ✓                   | ✓ | ✓ | ✓ | -                        | -    | ✓     | Irregular Form    |
| 107 | Olaya Tower 2                            | 180    | 38     | skyscraper    | 2013 | ✓                   | ✓ | ✓ | ✓ | ✓                        | -    | -     | Square            |
| 108 | Olaya Tower 1                            | 166    | 36     | skyscraper    | 2013 | ✓                   | ✓ | ✓ | ✓ | ✓                        | -    | -     | Square            |
| 109 | ETLAL Residence                          | 165    | 40     | skyscraper    | 2021 | N                   | N | N | N | N                        | N    | N     | N                 |
| 110 | Villas In the Sky                        | 165    | 34     | skyscraper    | 2016 | ✓                   | ✓ | ✓ | ✓ | ✓                        | -    | -     | Square            |
| 111 | Hamad Tower                              | 163    | 39     | skyscraper    | 2016 | ✓                   | ✓ | ✓ | ✓ | -                        | ✓    | -     | Rectangle         |
| 112 | Boudl-Narcissus Classic Tower            | 155    | 28     | skyscraper    | 2017 | ✓                   | ✓ | ✓ | ✓ | ✓                        | -    | -     | Square            |
| 113 | Burj Al-Swaile                           | 151    | 28     | skyscraper    | 2017 | ✓                   | ✓ | ✓ | ✓ | ✓                        | -    | -     | Square            |
| 114 | Burj Rala                                | 150    | 37     | skyscraper    | 2020 | N                   | N | N | N | N                        | N    | N     | N                 |
| 115 | DAAC Exclusiva                           | 150    | 30     | skyscraper    | 2016 | ✓                   | - | ✓ | ✓ | -                        | ✓    | -     | Rectangle         |
| 116 | KAFD Parcel 5.05 Residential Tower       | 149    | 38     | skyscraper    | 2020 | ✓                   | ✓ | ✓ | ✓ | -                        | -    | ✓     | Irregular Form    |
| 117 | Burj Al Anoud                            | 145    | 20     | skyscraper    | 2005 | ✓                   | ✓ | ✓ | ✓ | ✓                        | -    | -     | Rectangle         |
| 118 | KAFD Parcel 3.04 Office Tower            | 145    | 34     | skyscraper    | 2014 | ✓                   | ✓ | ✓ | ✓ | -                        | -    | ✓     | Irregular Form    |
| 119 | KAFD Parcel 5.09                         | 138    | 33     | skyscraper    | 2017 | N                   | N | N | N | N                        | N    | N     | N                 |
| 120 | KAFD Parcel 3.10                         | 138    | 30     | skyscraper    | 2020 | N                   | N | N | N | N                        | N    | N     | N                 |
| 121 | Crystal Towers 1                         | 135    | 26     | skyscraper    | 2020 | ✓                   | ✓ | ✓ | ✓ | -                        | -    | ✓     | Irregular Form    |
| 122 | KAFD Parcel 4.08                         | 133    | 32     | skyscraper    | -    | ✓                   | ✓ | ✓ | ✓ | -                        | -    | ✓     | Irregular Form    |
| 123 | Moon Tower                               | 133    | 27     | skyscraper    | 2013 | ✓                   | ✓ | ✓ | ✓ | ✓                        | -    | -     | Circle            |
| 124 | Elegance Tower                           | 130    | 27     | skyscraper    | 2016 | ✓                   | ✓ | ✓ | ✓ | ✓                        | -    | -     | Square            |
| 125 | Palm Tower                               | 130    | 27     | skyscraper    | 2017 | ✓                   | ✓ | ✓ | ✓ | ✓                        | -    | -     | Rectangle         |
| 126 | Alnood Tower 2                           | 125    | 25     | skyscraper    | 2012 | ✓                   | ✓ | ✓ | ✓ | ✓                        | -    | -     | Rectangle         |
| 127 | KAFD Parcel 5.05 Office Tower            | 125    | 23     | skyscraper    | 2020 | ✓                   | ✓ | ✓ | ✓ | -                        | -    | ✓     | Irregular Form    |
| 128 | KAFD Parcel 5.03                         | 105    | 26     | skyscraper    | 2020 | ✓                   | - | ✓ | ✓ | ✓                        | -    | -     | Irregular Form    |
| 129 | KAFD Parcel 2.12                         | 105    | 23     | skyscraper    | 2020 | ✓                   | ✓ | ✓ | ✓ | -                        | -    | ✓     | Irregular Form    |
| 130 | KAFD Parcel 2.14                         | 105    | 19     | skyscraper    | 2018 | ✓                   | ✓ | ✓ | ✓ | -                        | -    | ✓     | Irregular Form    |

**APPENDIX**

| #   | Building                       | Height | Floors | Building type | Year | Glazing Orientation |   |   |   | Shading System Existence |      |       | Building Geometry |
|-----|--------------------------------|--------|--------|---------------|------|---------------------|---|---|---|--------------------------|------|-------|-------------------|
|     |                                |        |        |               |      | E                   | W | S | N | Non                      | Poor | Exist |                   |
| 131 | KAFD Parcel 1.12               | 102    | 21     | skyscraper    | 2020 | ✓                   | ✓ | ✓ | ✓ | ✓                        | –    | –     | Rectangle         |
| 132 | Abraj Atta'Awuneya South Tower | 101    | 21     | skyscraper    | 1999 | ✓                   | ✓ | – | – | ✓                        | –    | –     | Tringle           |
| 133 | Abraj Atta'Awuneya North Tower | 101    | 21     | skyscraper    | 1999 | ✓                   | ✓ | – | – | ✓                        | –    | –     | Tringle           |
| 134 | Alriyadh Tower                 | 288    | 64     | skyscraper    | -    | N                   | N | N | N | N                        | N    | N     | N                 |
| 135 | Riyadh Commercial Tower        | 243    | 54     | skyscraper    | -    | N                   | N | N | N | N                        | N    | N     | N                 |
| 136 | King Fahd Twin Towers 1        | 216    | 48     | skyscraper    | 2021 | N                   | N | N | N | N                        | N    | N     | N                 |
| 137 | Kingdom Trade Centre Tower VII | 180    | 40     | skyscraper    | -    | N                   | N | N | N | N                        | N    | N     | N                 |
| 138 | Average                        | 121.8  |        |               |      |                     |   |   |   |                          |      |       |                   |

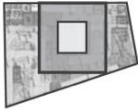



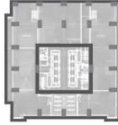


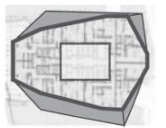


**APPENDIX**

| HIGH RISE OFFICE BUILDING CASES |                    |  | HIGH RISE OFFICE BUILDING CASES |                    |   |
|---------------------------------|--------------------|--|---------------------------------|--------------------|---|
| CASE                            | TYPICAL FLOOR PLAN | CASE DESCRIPTIONS  | CASE                            | TYPICAL FLOOR PLAN | CASE DESCRIPTIONS   |
| CASE 1                          |                    | <p>Name: Public Investment Fund PIF Tower</p> <p>Architect: HOK, Omrania and Associates</p> <p>Total NLA: 1800m<sup>2</sup></p> <p>Total GFA: 2400m<sup>2</sup></p> <p>Tower Height: 385 m</p> <p>Floor to ceiling Height: 4 m</p> <p>Number of Floors: 77</p> <p>Core Dimensions: 60m<sup>2</sup></p> <p>Core Configurations: Central core</p> <p>Floor efficiency: 78%</p> <p>Leasing Depth: Range form 12m to 14m</p> | CASE 5                          |                    | <p>Name: PPA 30 Parcel 5.03</p> <p>Architect: Adrian Smith + Gordon Gill Architecture</p> <p>Total NLA: 1390 m<sup>2</sup></p> <p>Total GFA: 1780 m<sup>2</sup></p> <p>Tower Height: 105 m</p> <p>Floor to ceiling Height: 4 m</p> <p>Number of Floors: 26</p> <p>Core Dimensions: 390m<sup>2</sup></p> <p>Core Configurations: Central core</p> <p>Floor efficiency: 78%</p> <p>Leasing Depth: 10m</p> |
| CASE 2                          |                    | <p>Name: Al Faisaliah Tower</p> <p>Architect: Foster + Partners</p> <p>Total NLA: 1300m<sup>2</sup></p> <p>Total GFA: 1700m<sup>2</sup></p> <p>Tower Height: 267 m</p> <p>Floor to ceiling Height: 4 m</p> <p>Number of Floors: 44</p> <p>Core Dimensions: 40m<sup>2</sup></p> <p>Core Configurations: Central core</p> <p>Floor efficiency: 80%</p> <p>Leasing Depth: 10m</p>   | CASE 6                          |                    | <p>Name: KAFD World Trade Center</p> <p>Architect: GenSLer</p> <p>Total NLA: 1815 m<sup>2</sup></p> <p>Total GFA: 2270 m<sup>2</sup></p> <p>Tower Height: 304 m</p> <p>Floor to ceiling Height: 4 m</p> <p>Number of Floors: 67</p> <p>Core Dimensions: 455m<sup>2</sup></p> <p>Core Configurations: Central core</p> <p>Floor efficiency: 77%</p> <p>Leasing Depth: 10m to 14m</p>                     |
| CASE 3                          |                    | <p>Name: Samba Bank HQ Tower</p> <p>Architect: Foster + Partners</p> <p>Total NLA: 1640 m<sup>2</sup></p> <p>Total GFA: 2050 m<sup>2</sup></p> <p>Tower Height: 231.2 m</p> <p>Floor to ceiling Height: 4.0 m</p> <p>Number of Floors: 40</p> <p>Core Dimensions: 410 m<sup>2</sup></p> <p>Core Configurations: Central core</p> <p>Floor efficiency: 80%</p> <p>Leasing Depth: range from 10m to 13m</p>                | CASE 7                          |                    | <p>Name: KAFD Parcel 3.05</p> <p>Architect: Callison Architects</p> <p>Total NLA: 960 m<sup>2</sup></p> <p>Total GFA: 1200 m<sup>2</sup></p> <p>Tower Height: 84 m</p> <p>Floor to ceiling Height: 4.20 m</p> <p>Number of Floors: 19</p> <p>Core Dimensions: 240 m<sup>2</sup></p> <p>Core Configurations: Central core</p> <p>Floor efficiency: 80%</p> <p>Leasing Depth: 10m</p>                     |
| CASE 4                          |                    | <p>Name: KAFD Parcel 1.18</p> <p>Architect: SOM</p> <p>Total NLA: 1880 m<sup>2</sup></p> <p>Total GFA: 2350 m<sup>2</sup></p> <p>Tower Height: 150 m</p> <p>Floor to ceiling Height: 3.9 m</p> <p>Number of Floors:</p> <p>Core Dimensions: 470 m<sup>2</sup></p> <p>Core Configurations: Central core</p> <p>Floor efficiency: 82%</p> <p>Leasing Depth: 11m</p>  | CASE 8                          |                    | <p>Name: KAFD Parcel 5.08</p> <p>Architect: LAB Architects</p> <p>Total NLA: 1208 m<sup>2</sup></p> <p>Total GFA: 1510 m<sup>2</sup></p> <p>Tower Height: 107.96 m</p> <p>Floor to ceiling Height: 4.20 m</p> <p>Number of Floors: 24</p> <p>Core Dimensions: 302 m<sup>2</sup></p> <p>Core Configurations: Central core</p> <p>Floor efficiency: 80%</p> <p>Leasing Depth: 10m</p>                     |

| HIGH RISE OFFICE BUILDING CASES |                    |  | HIGH RISE OFFICE BUILDING CASES |                    |  |
|---------------------------------|--------------------|--|---------------------------------|--------------------|--|
| CASE                            | TYPICAL FLOOR PLAN | CASE DESCRIPTIONS  | CASE                            | TYPICAL FLOOR PLAN | CASE DESCRIPTIONS  |
| CASE 9                          |                    | <p>Name: PP 10 Parcel 3.04</p> <p>Architect: Callison Architects</p> <p>Total NLA: 665 m<sup>2</sup></p> <p>Total GFA: 930 m<sup>2</sup></p> <p>Tower Height: 144.60 m</p> <p>Floor to ceiling Height: 4 m</p> <p>Number of Floors: 34</p> <p>Core Dimensions: 285 m<sup>2</sup></p> <p>Core Configurations: Side core</p> <p>Floor efficiency: 70%</p> <p>Leasing Depth: 10m</p>                      | CASE 13                         |                    | <p>Name: KAFD Muqarnas Tower</p> <p>Architect: Skidmore, Owings &amp; Merrill</p> <p>Total NLA: 1274 m<sup>2</sup></p> <p>Total GFA: 1820 m<sup>2</sup></p> <p>Tower Height: 138 m</p> <p>Floor to ceiling Height: 4 m</p> <p>Number of Floors: 30</p> <p>Core Dimensions: 546 m<sup>2</sup></p> <p>Core Configurations: Side core</p> <p>Floor efficiency: 70%</p> <p>Leasing Depth: 9 m</p>    |
| CASE 10                         |                    | <p>Name: Kingdom Tower</p> <p>Architect: Elberbe Becket, Omrania &amp; Associates</p> <p>Total NLA: 1950 m<sup>2</sup></p> <p>Total GFA: 2450 m<sup>2</sup></p> <p>Tower Height: 302.3 m</p> <p>Floor to ceiling Height: 4 m</p> <p>Number of Floors: 41</p> <p>Core Dimensions: 500 m<sup>2</sup></p> <p>Core Configurations: Central core</p> <p>Floor efficiency: 80%</p> <p>Leasing Depth: 13m</p> | CASE 14                         |                    | <p>Name: KAFD Parcel 2.12</p> <p>Architect: RMJM</p> <p>Total NLA: 1108 m<sup>2</sup></p> <p>Total GFA: 1438 m<sup>2</sup></p> <p>Tower Height: 105 m</p> <p>Floor to ceiling Height: 4 m</p> <p>Number of Floors: 23</p> <p>Core Dimensions: 330 m<sup>2</sup></p> <p>Core Configurations: Central core</p> <p>Floor efficiency: 77%</p> <p>Leasing Depth: 10m to 12m</p>                       |
| CASE 11                         |                    | <p>Name: KAFD Parcel 4.01</p> <p>Architect: Perkins+Will</p> <p>Total NLA: 1000 m<sup>2</sup></p> <p>Total GFA: 1250 m<sup>2</sup></p> <p>Tower Height: 71.98 m</p> <p>Floor to ceiling Height: 4.20 m</p> <p>Number of Floors: 16</p> <p>Core Dimensions: 250 m<sup>2</sup></p> <p>Core Configurations: Central core</p> <p>Floor efficiency: 80%</p> <p>Leasing Depth: 10 to 10m</p>                 | CASE 15                         |                    | <p>Name: PPA 30 Parcel 4.09</p> <p>Architect: RTKL</p> <p>Total NLA: 765 m<sup>2</sup></p> <p>Total GFA: 980 m<sup>2</sup></p> <p>Tower Height: 182 m</p> <p>Floor to ceiling Height: 4.0 m</p> <p>Number of Floors: 46</p> <p>Core Dimensions: 215 m<sup>2</sup></p> <p>Core Configurations: Central core</p> <p>Floor efficiency: 78%</p> <p>Leasing Depth: 10m</p>                            |
| CASE 12                         |                    | <p>Name: KAFD Parcel 4.04</p> <p>Architect: RMJM</p> <p>Total NLA: 880 m<sup>2</sup></p> <p>Total GFA: 1160 m<sup>2</sup></p> <p>Tower Height: 107.96 m</p> <p>Floor to ceiling Height: 4 m</p> <p>Number of Floors: 27</p> <p>Core Dimensions: 280 m<sup>2</sup></p> <p>Core Configurations: Central core</p> <p>Floor efficiency: 80%</p> <p>Leasing Depth: 11m</p>                                  | CASE 16                         |                    | <p>Name: KAFD Parcel 5.09</p> <p>Architect: Omrania &amp; Associates; RTKL</p> <p>Total NLA: 1615 m<sup>2</sup></p> <p>Total GFA: 1980 m<sup>2</sup></p> <p>Tower Height: 138 m</p> <p>Floor to ceiling Height: 4.20 m</p> <p>Number of Floors: 33</p> <p>Core Dimensions: 285 m<sup>2</sup></p> <p>Core Configurations: Central core</p> <p>Floor efficiency: 85%</p> <p>Leasing Depth: 11m</p> |

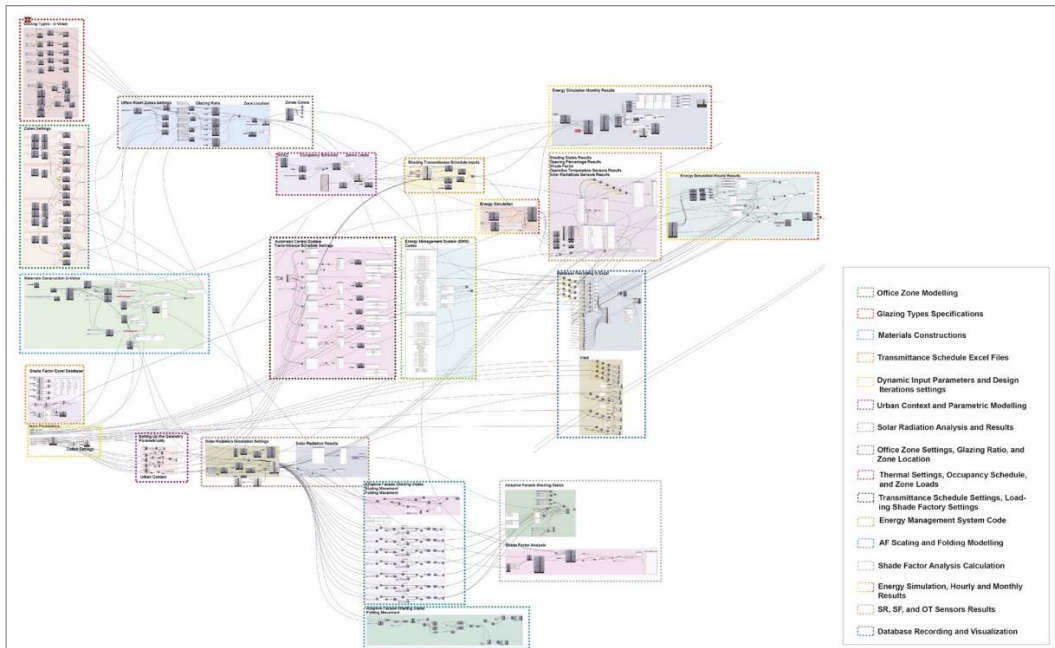
## APPENDIX

| HIGH RISE OFFICE BUILDING CASES |   |   |         |  |  |
|---------------------------------|---|---|---------|--|--|
| CASE                            | TYPICAL FLOOR PLAN  | CASE DESCRIPTIONS   | CASE    | TYPICAL FLOOR PLAN   | CASE DESCRIPTIONS  |
| CASE 17                         |  | <p>Name: KAFD Parcel 2.13</p> <p>Architect: Henning Larsen Architects</p> <p>Total NLA: 710 m<sup>2</sup></p> <p>Total GFA: 900 m<sup>2</sup></p> <p>Tower Height: 160.7 m</p> <p>Floor to ceiling Height: 4 m</p> <p>Number of Floors: 34</p> <p>Core Dimensions: 190 m<sup>2</sup></p> <p>Core Configurations: Central core</p> <p>Floor efficiency: 79%</p> <p>Leasing Depth: 9 m</p>                      | CASE 21 |  | <p>Name: Crystal Tower 1 (PPA 30 Parcel 1.10)</p> <p>Architect: Henning Larsen Architects</p> <p>Total NLA: 858 m<sup>2</sup></p> <p>Total GFA: 1100 m<sup>2</sup></p> <p>Tower Height: 133 m</p> <p>Floor to ceiling Height: 4.00 m</p> <p>Number of Floors: 26</p> <p>Core Dimensions: 242 m<sup>2</sup></p> <p>Core Configurations: Central core</p> <p>Floor efficiency: 78%</p> <p>Leasing Depth: 10m</p> |
| CASE 18                         |  | <p>Name: KAFD PPA 30 Parcel 2.11</p> <p>Architect: Dar Al Handasha, Parkins+Will</p> <p>Total NLA: 1008 m<sup>2</sup></p> <p>Total GFA: 1360 m<sup>2</sup></p> <p>Tower Height: 55 m</p> <p>Floor to ceiling Height: 4 m</p> <p>Number of Floors: 11</p> <p>Core Dimensions: 252 m<sup>2</sup></p> <p>Core Configurations: Side core</p> <p>Floor efficiency: 80%</p> <p>Leasing Depth: 10m</p>               | CASE 22 |  | <p>Name: GGC Bank Headquarters (KAFD Parcel 1.16)</p> <p>Architect: Gensler</p> <p>Total NLA: 1515 m<sup>2</sup></p> <p>Total GFA: 2020 m<sup>2</sup></p> <p>Tower Height: 264 m</p> <p>Floor to ceiling Height: 4 m</p> <p>Number of Floors: 53</p> <p>Core Dimensions: 505 m<sup>2</sup></p> <p>Core Configurations: Central core</p> <p>Floor efficiency: 75%</p>   |
| CASE 19                         |  | <p>Name: Olaya Tower 1</p> <p>Architect: BDPL Gulf</p> <p>Total NLA: 1320 m<sup>2</sup></p> <p>Total GFA: 1630 m<sup>2</sup></p> <p>Tower Height: 166 m</p> <p>Floor to ceiling Height: 4.0 m</p> <p>Number of Floors: 34</p> <p>Core Dimensions: 330 m<sup>2</sup></p> <p>Core Configurations: Central core</p> <p>Floor efficiency: 80%</p> <p>Leasing Depth: 10m to 14m</p>                                | CASE 23 |  | <p>Name: KAFD Parcel 2.11</p> <p>Architect: Gensler</p> <p>Total NLA: 840 m<sup>2</sup></p> <p>Total GFA: 1050 m<sup>2</sup></p> <p>Tower Height: 77 m</p> <p>Floor to ceiling Height: 4.0 m</p> <p>Number of Floors: 17</p> <p>Core Dimensions: 210 m<sup>2</sup></p> <p>Core Configurations: Central core</p> <p>Floor efficiency: 80%</p> <p>Leasing Depth: 9m to 10m</p>                                   |
| CASE 20                         |  | <p>Name: Crystal Tower 2 (PPA 30 Parcel 1.10)</p> <p>Architect: Henning Larsen Architects</p> <p>Total NLA: 960 m<sup>2</sup></p> <p>Total GFA: 1200 m<sup>2</sup></p> <p>Tower Height: 80 m</p> <p>Floor to ceiling Height: 4.00 m</p> <p>Number of Floors: 18</p> <p>Core Dimensions: 240 m<sup>2</sup></p> <p>Core Configurations: Central core</p> <p>Floor efficiency: 80%</p> <p>Leasing Depth: 10m</p> | CASE 24 |  | <p>Name: KAFD Parcel 4.06</p> <p>Architect: Foster</p> <p>Total NLA: 1264 m<sup>2</sup></p> <p>Total GFA: 1580 m<sup>2</sup></p> <p>Tower Height: 122 m</p> <p>Floor to ceiling Height: 4.00 m</p> <p>Number of Floors: 33</p> <p>Core Dimensions: 316 m<sup>2</sup></p> <p>Core Configurations: Central core</p> <p>Floor efficiency: 80%</p> <p>Leasing Depth: 11m to 13m</p>                                |

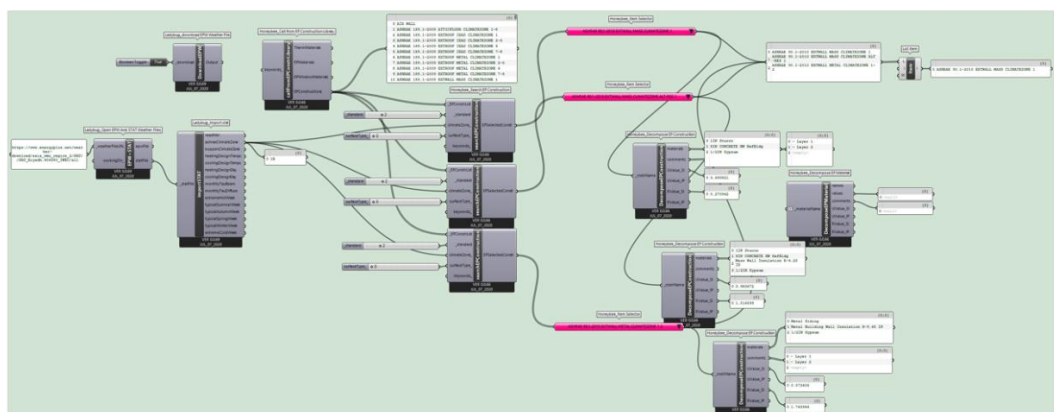
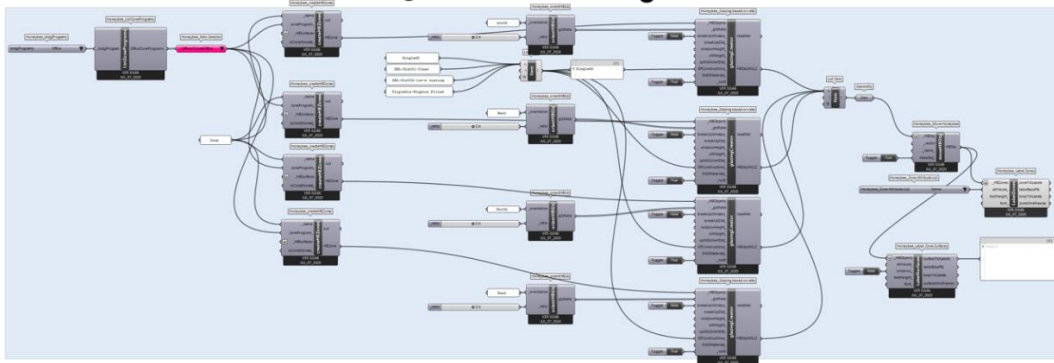
Typical floor office plan of the investigated case studies.

**Appendix C: Modelling and Simulation Workflow  
(Database Generation)**

## APPENDIX

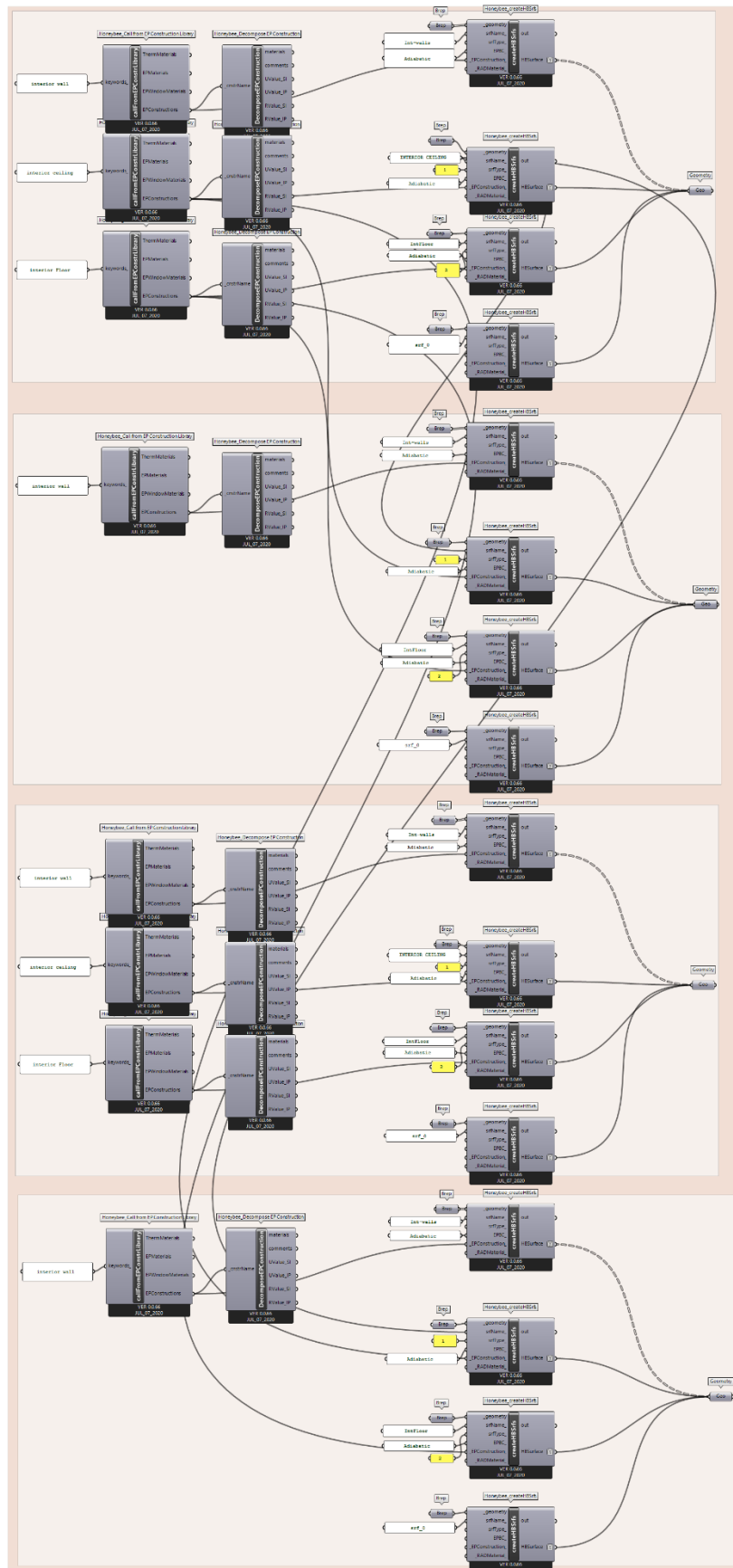


Screenshot showing the workflow of the parametric modelling and simulation in Grasshopper environment



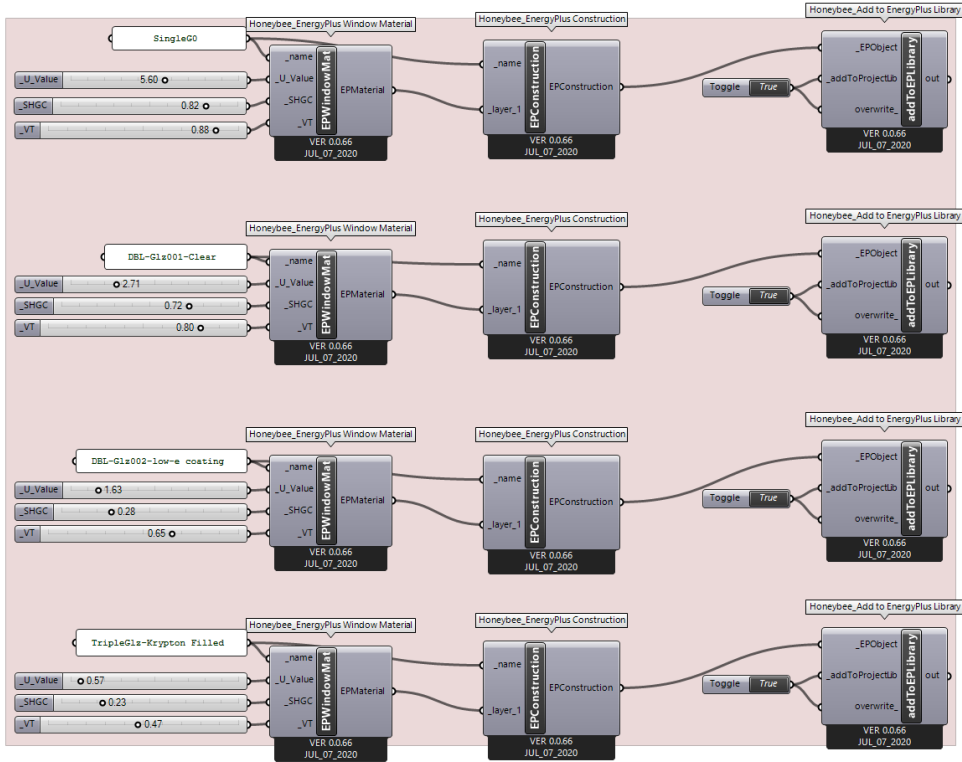
Screenshot showing the zone settings (top), and the construction materials settings (down).

**APPENDIX**

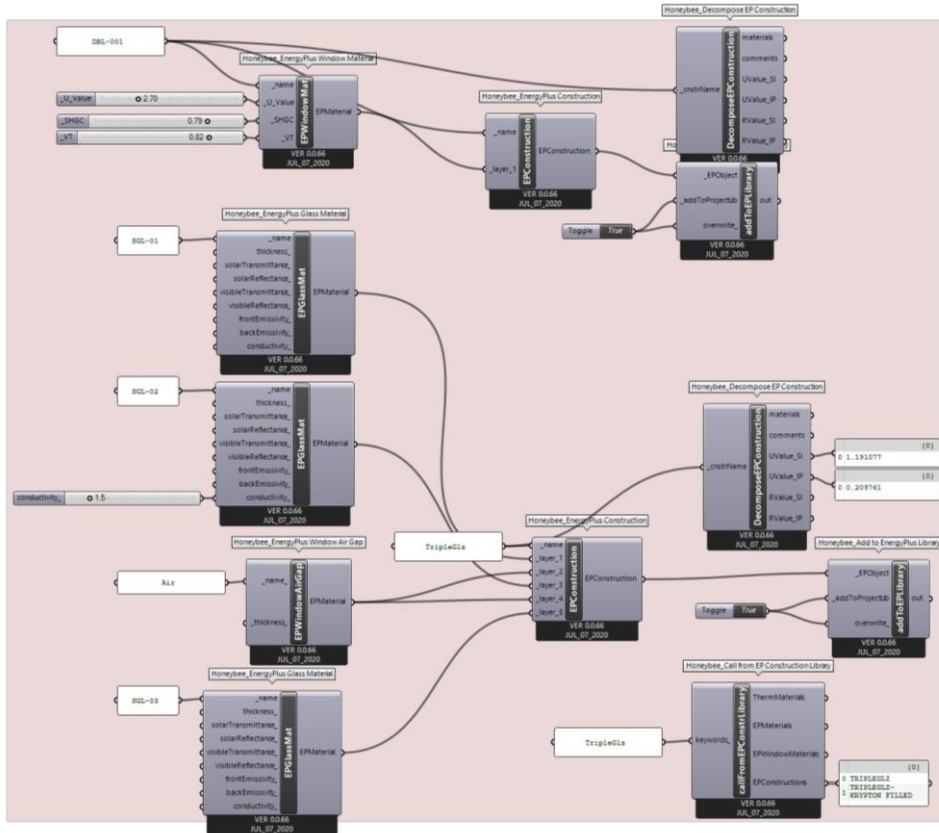


Screenshot showing the office room zones and materials for four orientations.

**APPENDIX**



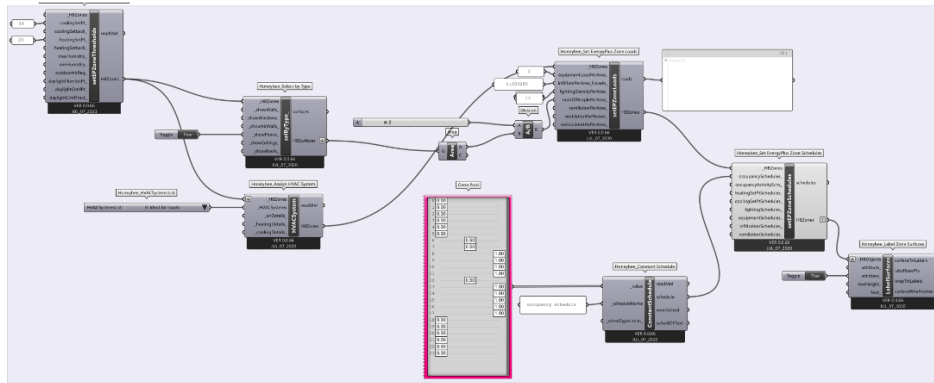
Screenshot showing the window materials and specifications.



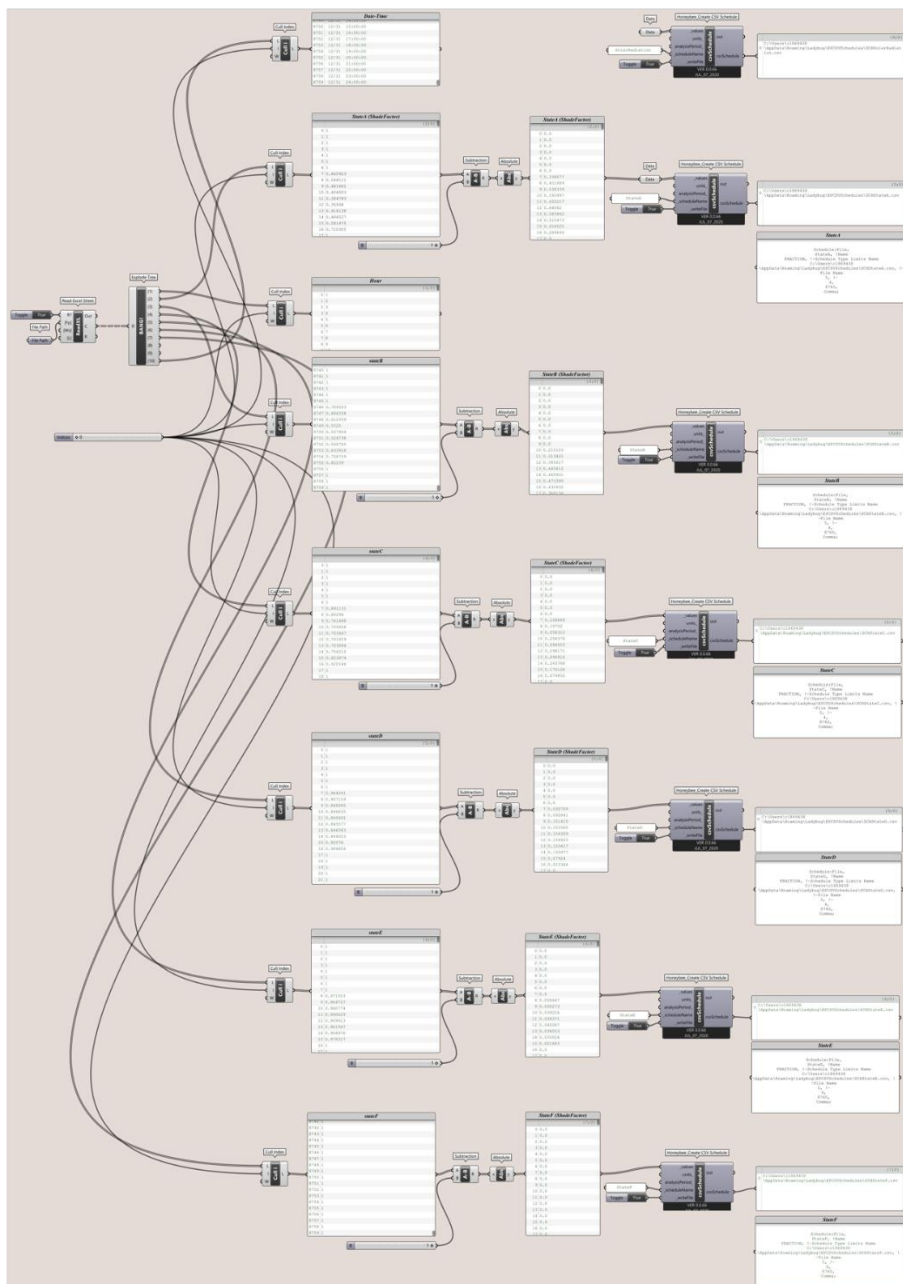
Screenshot showing the window materials and specifications.



## APPENDIX



Screenshot showing the HVAC system, occupancy schedules, and zone loads.



Screenshot showing the shade factor of all shading states loaded from Csv. Files.

**APPENDIX**

**EMS**

```

EnergyManagementSystem:Sensor,
S1,                !- Name
StateA,            !- Output:Variable or Output:Meter Index Key Name
Schedule Value;   !- Output:Variable or Output:Meter Name

EnergyManagementSystem:Sensor,
S2,                !- Name
StateB,            !- Output:Variable or Output:Meter Index Key Name
Schedule Value;   !- Output:Variable or Output:Meter Name

EnergyManagementSystem:Sensor,
S3,                !- Name
StateC,            !- Output:Variable or Output:Meter Index Key Name
Schedule Value;   !- Output:Variable or Output:Meter Name

EnergyManagementSystem:Sensor,
S4,                !- Name
StateD,            !- Output:Variable or Output:Meter Index Key Name
Schedule Value;   !- Output:Variable or Output:Meter Name

EnergyManagementSystem:Sensor,
S5,                !- Name
StateE,            !- Output:Variable or Output:Meter Index Key Name
Schedule Value;   !- Output:Variable or Output:Meter Name

EnergyManagementSystem:Sensor,
S6,                !- Name
StateF,            !- Output:Variable or Output:Meter Index Key Name
Schedule Value;   !- Output:Variable or Output:Meter Name

EnergyManagementSystem:Sensor,
S7,                !- Name
ZZZ,              !- Output:Variable or Output:Meter Index Key Name
Surface Outside Face Incident Solar Radiation Rate per Area; !-
Output:Variable or Output:Meter Name

EnergyManagementSystem:Sensor,
S8,                !- Name
YYY,              !- Output:Variable or Output:Meter Index Key Name
Zone Operative Temperature ; !- Output:Variable or Output:Meter Name

EnergyManagementSystem:Actuator,
myA1,              !- Name
TrNS-SHD,         !- Actuated Component Unique Name
Schedule:Year,    !- Actuated Component Type
Schedule Value;   !- Actuated Component Control Type

EnergyManagementSystem:ProgramCallingManager,
MyComputedTransProg, !- Name
BeginTimestepBeforePredictor, !- EnergyPlus Model Calling Point
MyComputedTransSch; !- Program Name 1

EnergyManagementSystem:Program,
MyComputedTransSch, !- Name
Set StateA = S1, !- Program Line 1
Set StateB = S2, !- Program Line 1
Set StateC = S3, !- Program Line 1
Set StateD = S4, !- Program Line 1
Set StateE = S5, !- Program Line 1
Set StateF = S6, !- Program Line 1
SET SOL = S7, !- Program Line 2,
    SET OT = S8,
    IF (SOL <= 50) && (OT < 21),
        SET myA1 = StateA,
    ELSEIF (SOL <= 50) && (OT > 24),
        SET myA1 = StateB,
    ELSEIF (SOL <= 50) && (OT < 24) && (OT > 21),
        SET myA1 = StateA,
    ELSEIF (SOL > 50) && (SOL <= 100) && (OT < 21),
        SET myA1 = StateB,
    ELSEIF (SOL > 50) && (SOL <= 100) && (OT > 24),
        SET myA1 = StateC,
    ELSEIF (SOL > 50) && (SOL <= 100) && (OT < 24) && (OT > 21),
        SET myA1 = StateB,
    ELSEIF (SOL > 100) && (SOL <= 200) && (OT < 21),
        SET myA1 = StateC,
    ELSEIF (SOL > 100) && (SOL <= 200) && (OT > 24),
        SET myA1 = StateD,
    ELSEIF (SOL > 100) && (SOL <= 200) && (OT < 24) && (OT > 21),
        SET myA1 = StateC,
    ELSEIF (SOL > 200) && (SOL <= 300) && (OT < 21),
        SET myA1 = StateD,
    ELSEIF (SOL > 200) && (SOL <= 300) && (OT > 24),
        SET myA1 = StateE,
    ELSEIF (SOL > 200) && (SOL <= 300) && (OT < 24) && (OT > 21),
        SET myA1 = StateD,
    ELSEIF (SOL > 300) && (SOL <= 350) && (OT < 21),
        SET myA1 = StateE,
    ELSEIF (SOL > 300) && (SOL <= 350) && (OT > 24),
        SET myA1 = StateF,
    ELSEIF (SOL > 300) && (SOL <= 350) && (OT < 24) && (OT > 21),
        SET myA1 = StateE,
    ELSEIF (SOL > 350) && (SOL <= 400) && (OT < 21),
        SET myA1 = StateF,
    ELSEIF (SOL > 350) && (SOL <= 400) && (OT > 24),
        SET myA1 = StateF,
    ELSEIF (SOL > 350) && (SOL <= 400) && (OT < 24) && (OT > 21),
        SET myA1 = StateF,
    ELSEIF (SOL > 450),
        SET myA1 = StateF,
    ENDIF;

EnergyManagementSystem:GlobalVariable,
myglobeA1; !- Eri Variable 1 Name

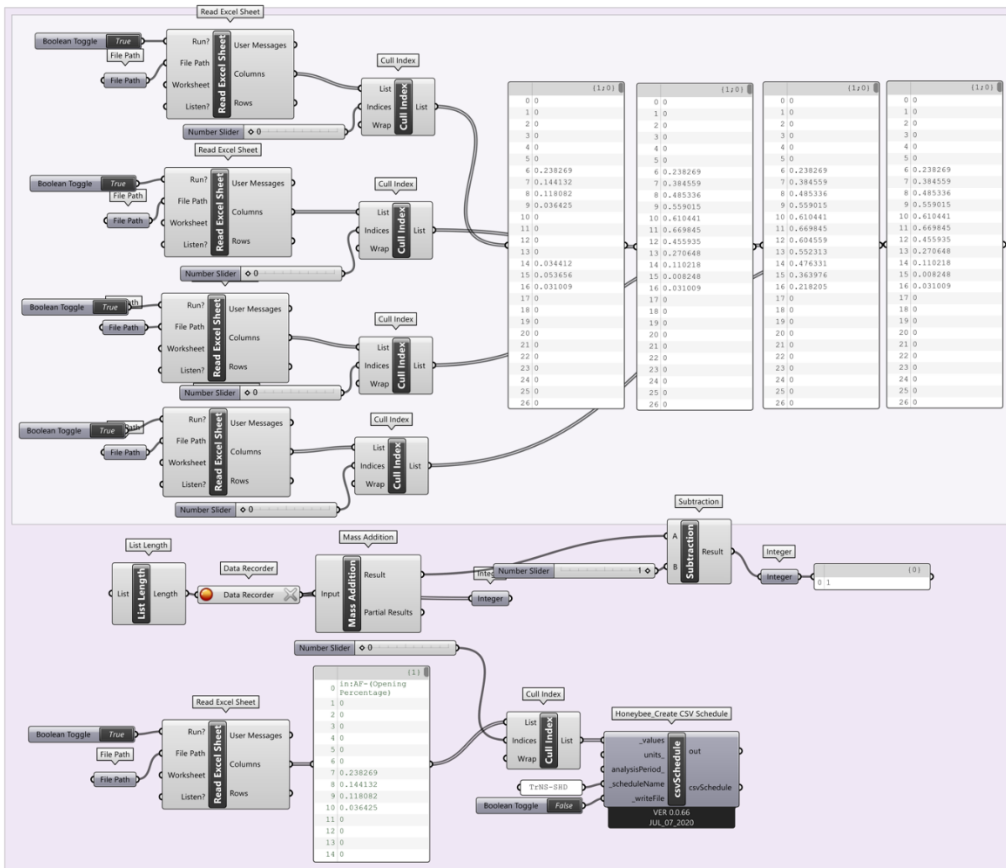
EnergyManagementSystem:OutputVariable,
myglobeA1, !- EMS Variable Name
Averaged, !- Type of Data in Variable
SystemTimestep; !- Update Frequency
    
```

|   | {0}                        |
|---|----------------------------|
| 0 | 0to100 fully open 100%     |
| 1 | 100to200 80% open          |
| 2 | 200 to 300 60% semi closed |
| 3 | 300 to 400 40% semi closed |
| 4 | 400 to 500 20% semi closed |
| 5 | 500 and above 0 closed     |

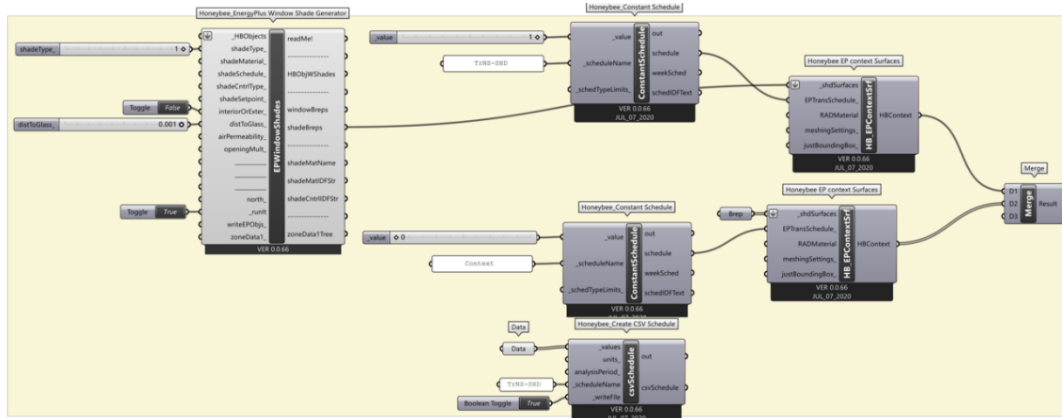
Screenshot showing the conditional statement to actuate the AFs shading system.



# APPENDIX

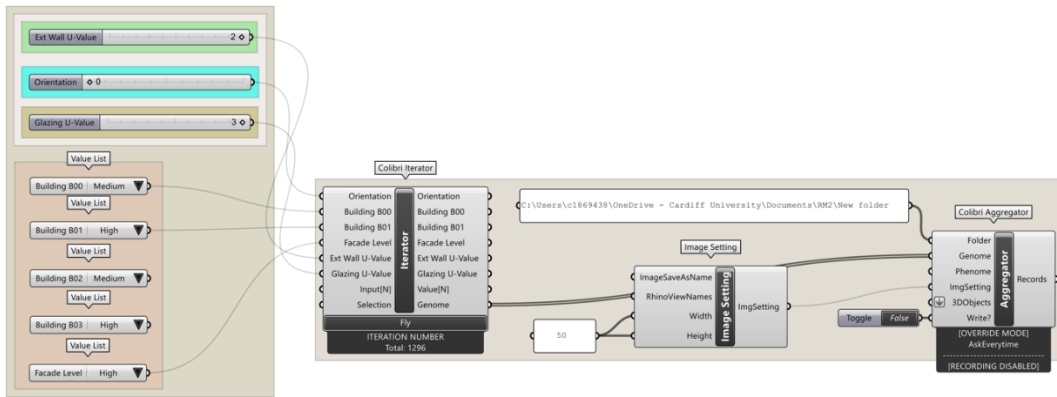


Screenshot showing the transmittance schedules of the AFs shading systems loaded from a CSV. File.

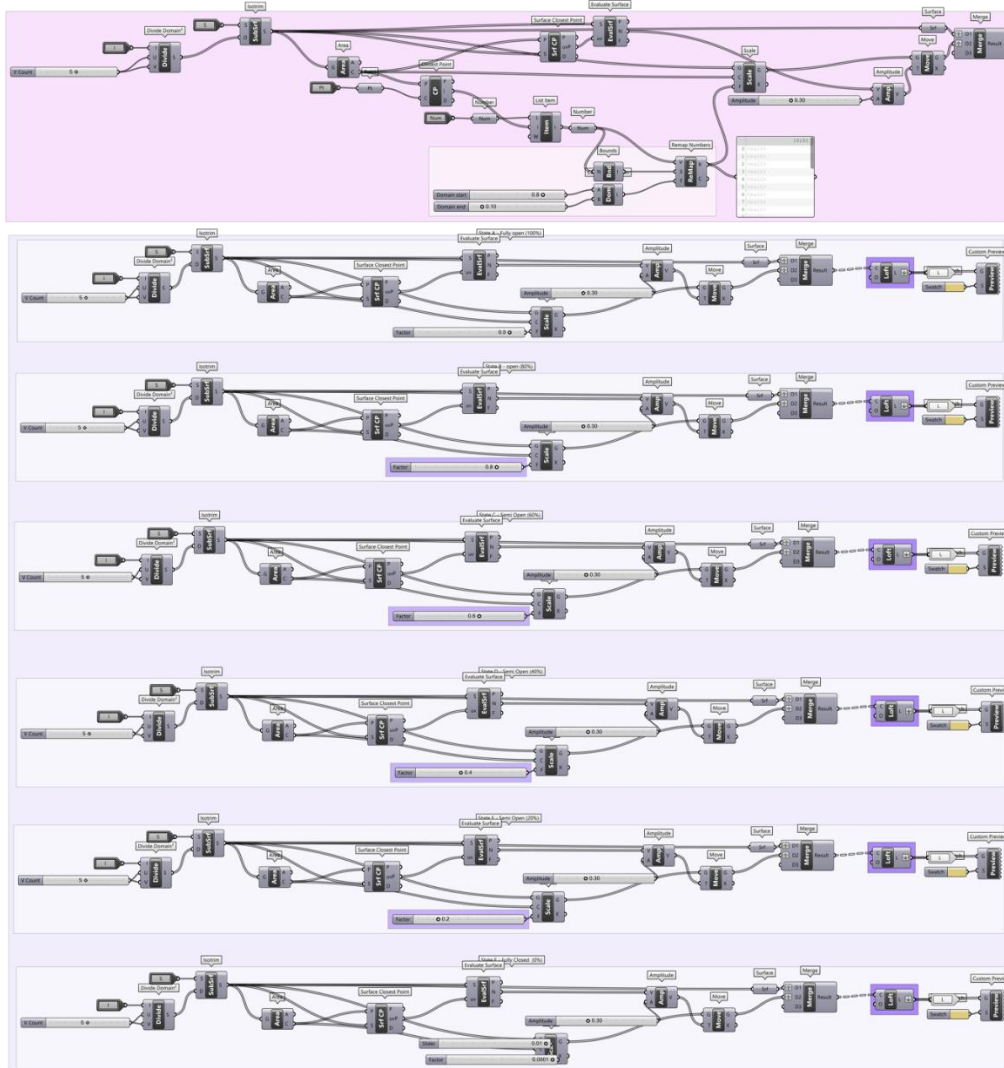


Screenshot showing the transmittance schedules processed within the Honeybee schedule component.

## APPENDIX

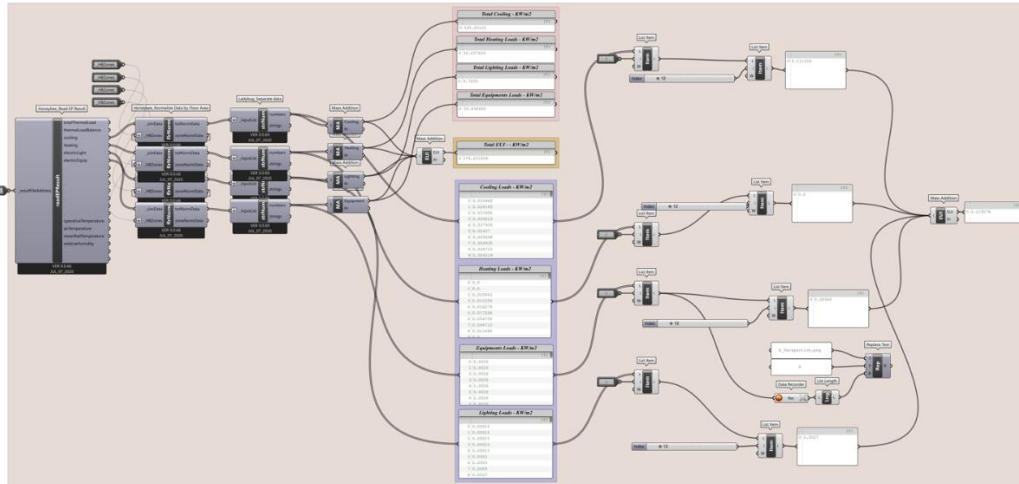
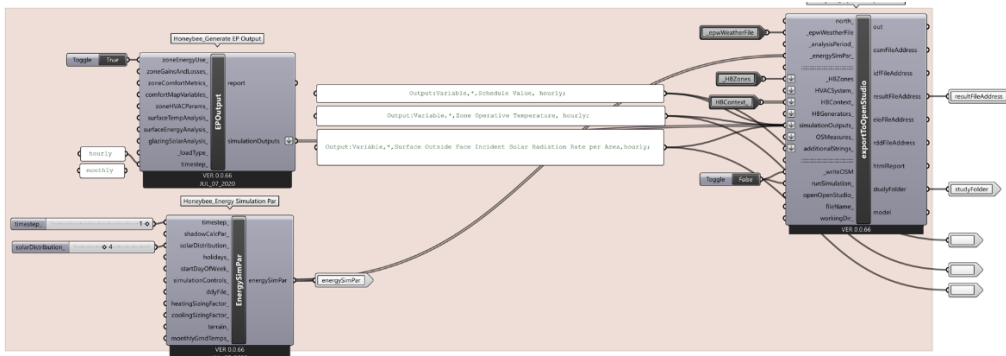


Screenshot showing the iterative workflow of all variable inputs.

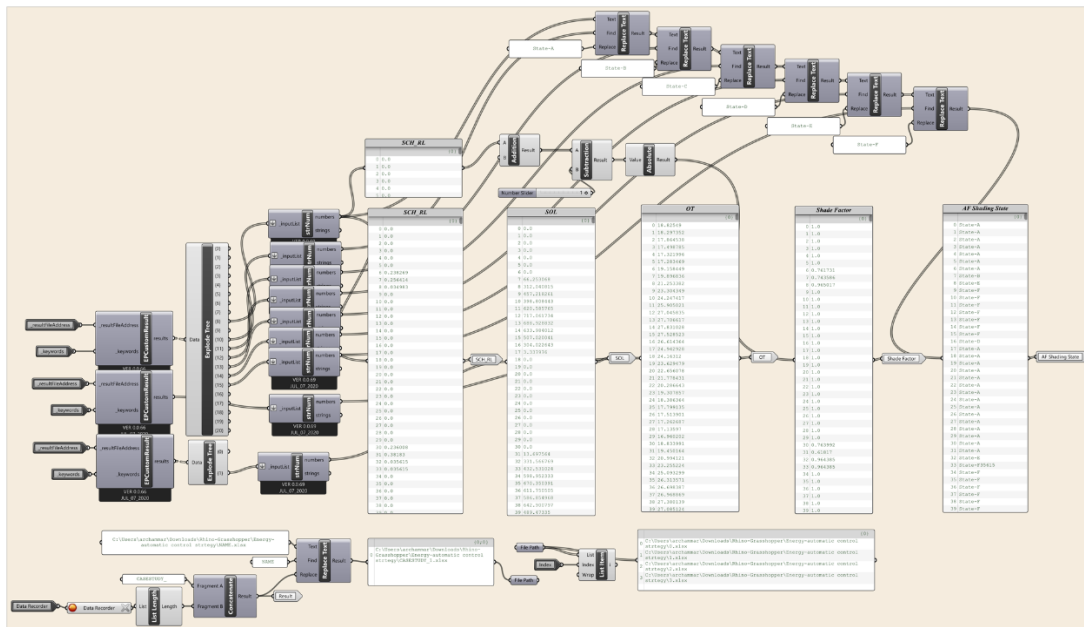


Screenshot showing the AFs shading states modelling.

**APPENDIX**

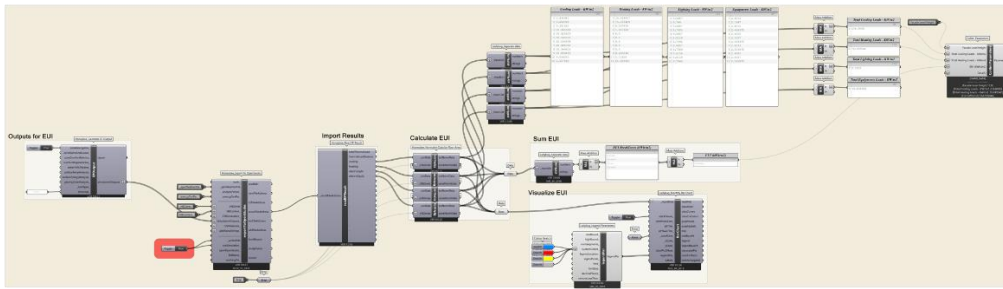


Screenshot showing the energy simulation settings, and energy results processing.

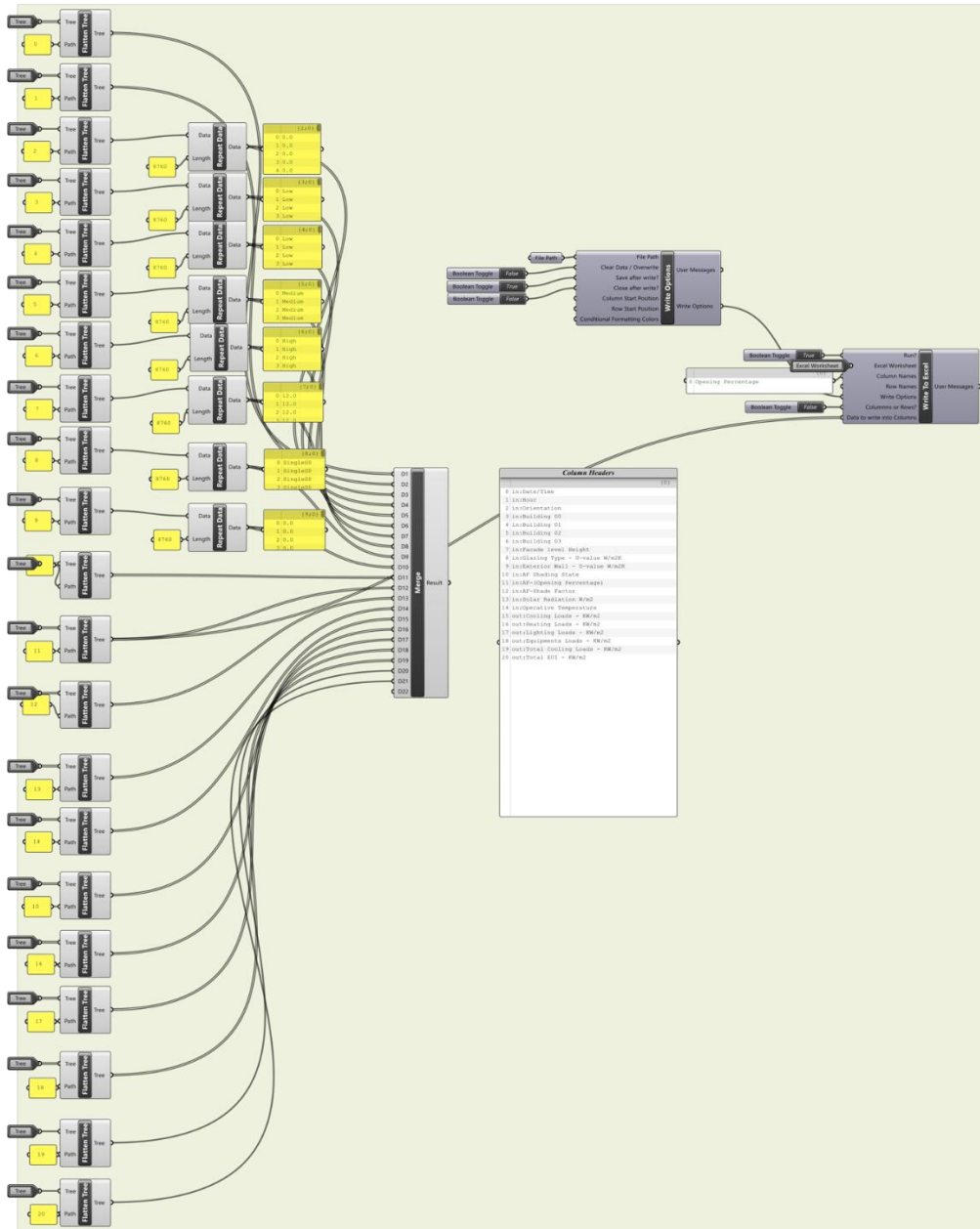


Screenshot showing the environmental control results processing.

**APPENDIX**



Screenshot showing the energy results processing.

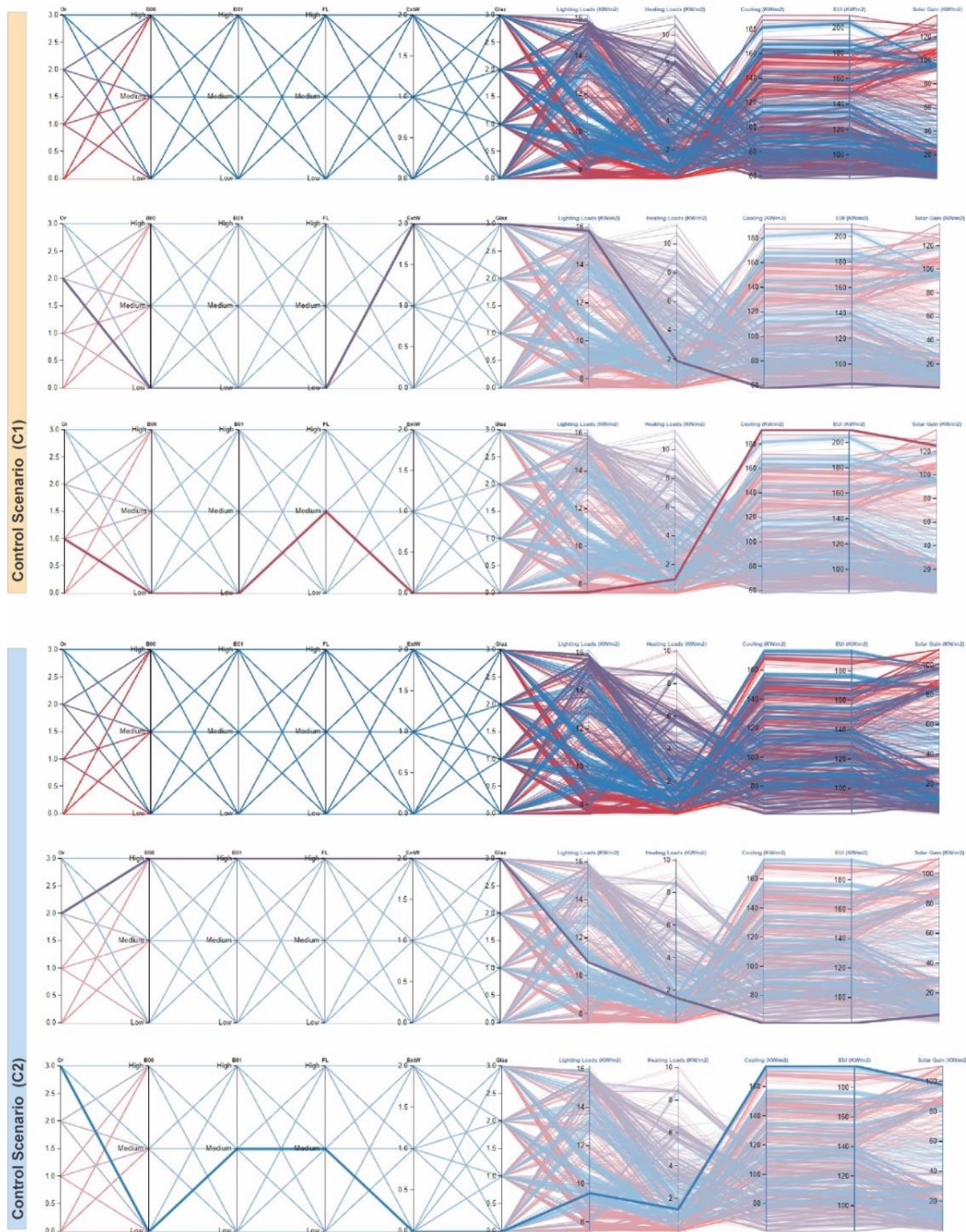


Screenshot showing the database recording.

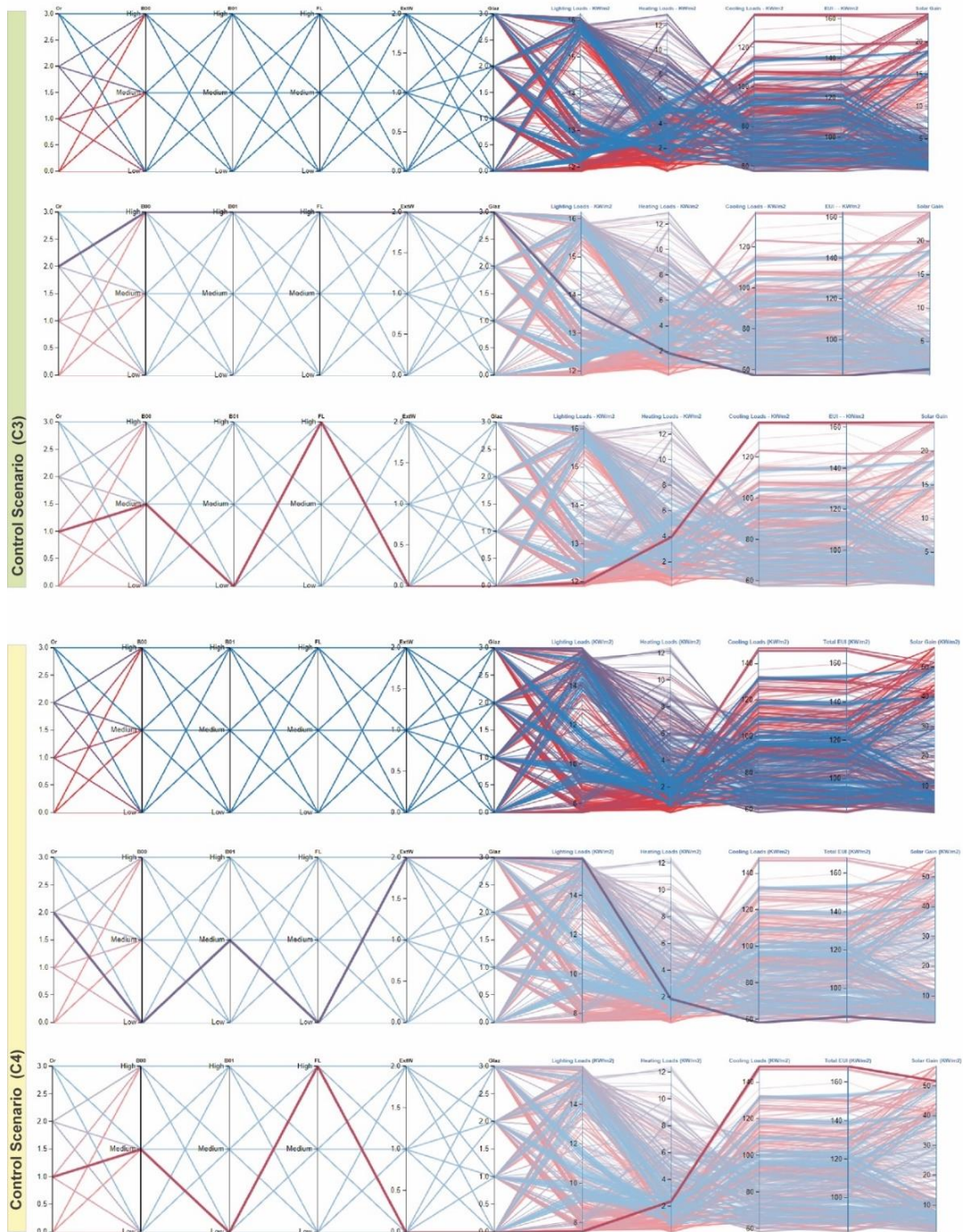




# APPENDIX

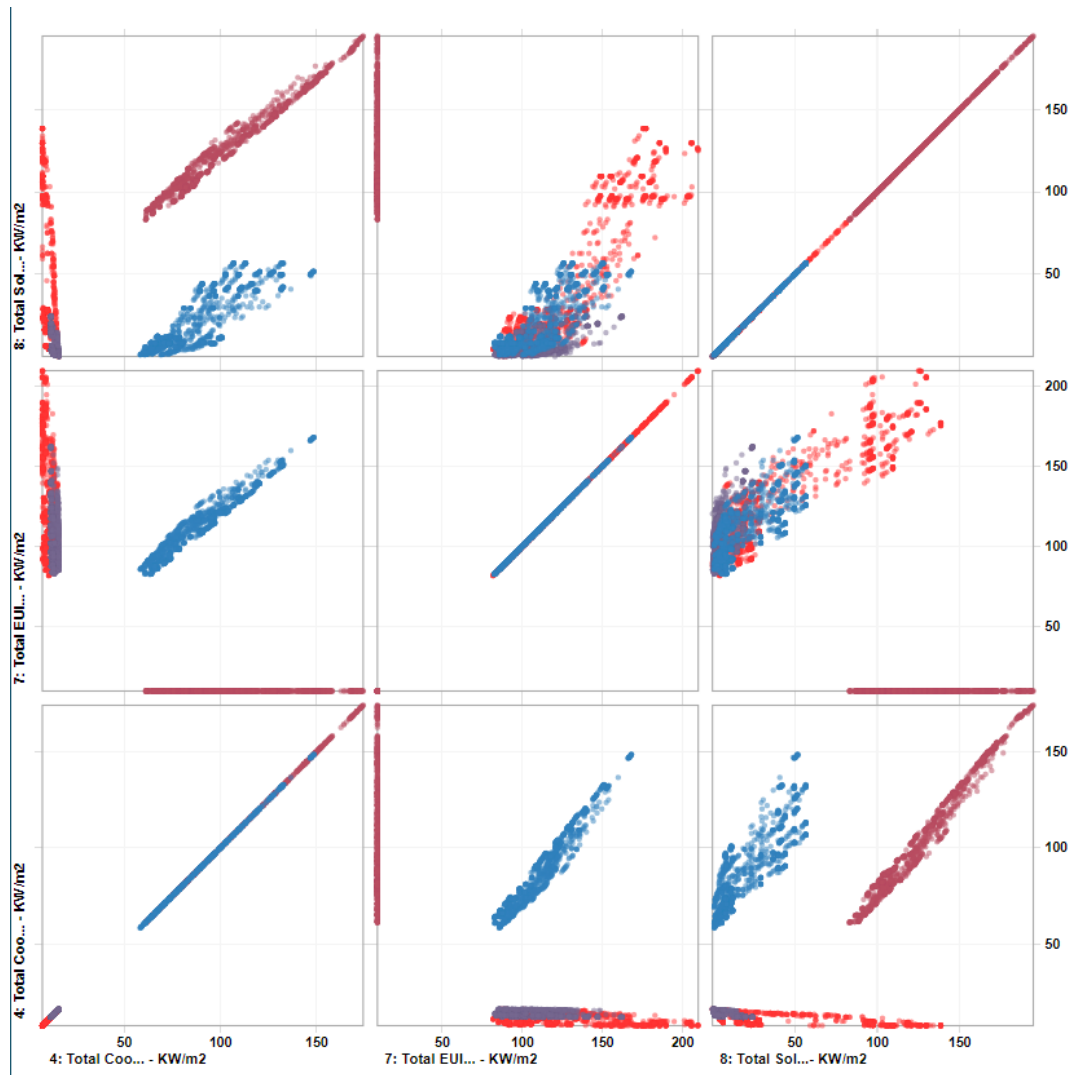


**APPENDIX**



*Web-based comparison of energy performance for control scenario (C1), (C2), (C3) and (C4) showing optimum and worst cases.*

**APPENDIX**



*Scatter plot of all design cases in relation to cooling loads and annual energy consumption.*

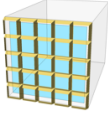
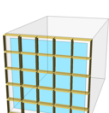
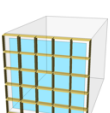
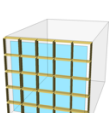
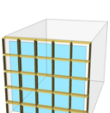
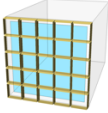
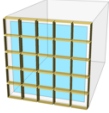
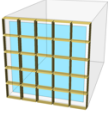
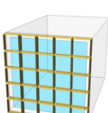
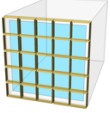
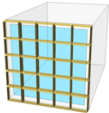
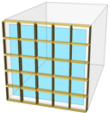
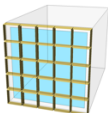
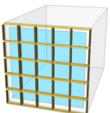


**APPENDIX**

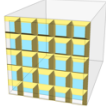
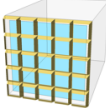
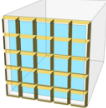
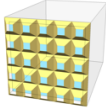
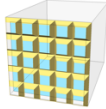
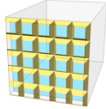
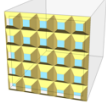
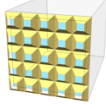
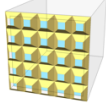
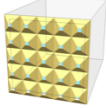
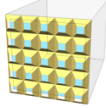
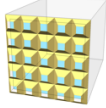
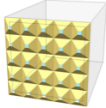
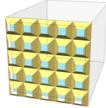
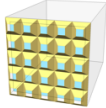
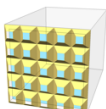
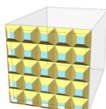
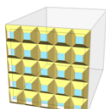
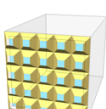
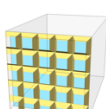
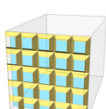
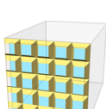
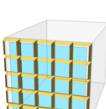
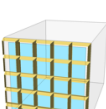
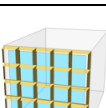
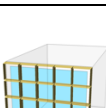
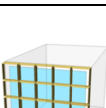
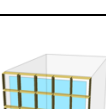
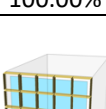
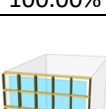
Shading states for two different days of the year (21 March, and 21 September) in different contexts.

| Or. | 21-Mar         | <p>P-AF-SCM<br/>C4_Or_B00Low_<br/>B01Low<br/>_FLLow_ExtW2_Glaz<br/>3</p>  | <p>P-AF-SCM-<br/>C4_Or_B00High_B01Mediu<br/>m<br/>_FLLow_ExtW2_Glaz3</p>  | <p>P-AF-SCM-<br/>C4_Or_B00High_B01High<br/>_FLLow_ExtW2_Glaz3</p>  |
|-----|----------------|--|--|---|
| S   | 03/21<br>06:00 |  <p>100.00%</p>   |  <p>100.00%</p>   |  <p>100.00%</p>  |
|     | 03/21<br>07:00 |  <p>100.00%</p>  |  <p>100.00%</p>  |  <p>100.00%</p>   |
|     | 03/21<br>08:00 |  <p>100.00%</p>   |  <p>100.00%</p>   |  <p>100.00%</p>  |
|     | 03/21<br>09:00 |  <p>100.00%</p>   |  <p>100.00%</p>   |  <p>100.00%</p>  |
|     | 03/21<br>10:00 |  <p>100.00%</p>   |  <p>100.00%</p>   |  <p>100.00%</p>  |
|     | 03/21<br>11:00 |  <p>100.00%</p>   |  <p>100.00%</p>   |  <p>100.00%</p>  |
|     | 03/21<br>12:00 |  <p>90.00%</p>  |  <p>100.00%</p>   |  <p>100.00%</p>  |

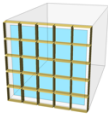
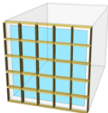
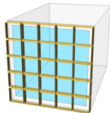
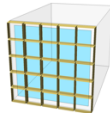
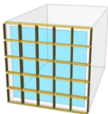
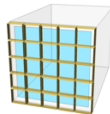
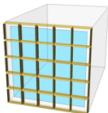
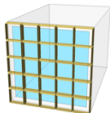
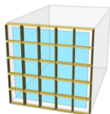
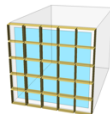
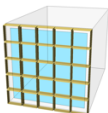
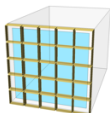
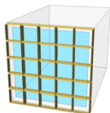
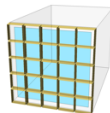
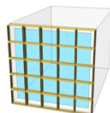
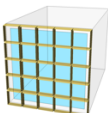
**APPENDIX**

|   |                |  |  |  |
|---|----------------|--|--|--|
|   | 03/21<br>13:00 | <br>100.00%   | <br>100.00%   | <br>100.00%   |
|   | 03/21<br>14:00 | <br>90.00%    | <br>100.00%   | <br>100.00%   |
|   | 03/21<br>15:00 | <br>80.00%    | <br>100.00%   | <br>100.00%   |
|   | 03/21<br>16:00 | <br>100.00%   | <br>100.00%   | <br>100.00%   |
|   | 03/21<br>17:00 | <br>100.00%  | <br>100.00%  | <br>100.00%  |
|   | 03/21<br>18:00 | <br>100.00% | <br>100.00% | <br>100.00% |
|   | Or.            | 21-Sep   |  |  |
| S | 09/21<br>06:00 | <br>100.00% | <br>100.00% | <br>100.00% |
|   | 09/21<br>07:00 | <br>100.00% | <br>100.00% | <br>100.00% |
|   | 09/21<br>08:00 | <br>80.00%  | <br>100.00% | <br>100.00% |

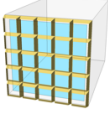
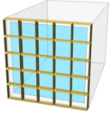
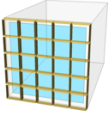
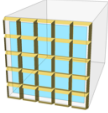
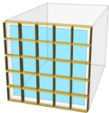
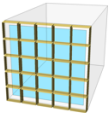
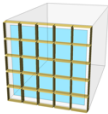
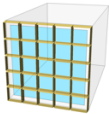
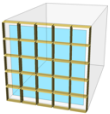
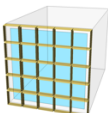
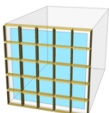
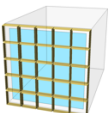
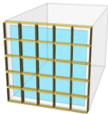
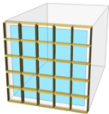
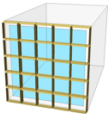
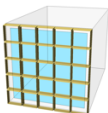
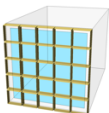
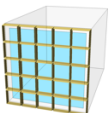
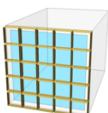
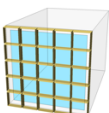
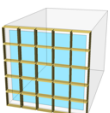
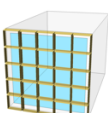
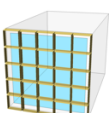
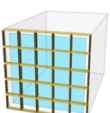
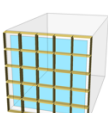
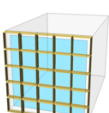
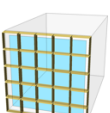
**APPENDIX**

|                |  |  |  |
|----------------|--|--|--|
| 09/21<br>09:00 | <br>60.00%    | <br>80.00%    | <br>90.00%    |
| 09/21<br>10:00 | <br>40.00%    | <br>56.67%    | <br>60.00%    |
| 09/21<br>11:00 | <br>40.00%    | <br>40.00%    | <br>40.00%    |
| 09/21<br>12:00 | <br>20.00%    | <br>40.00%    | <br>40.00%    |
| 09/21<br>13:00 | <br>30.00%   | <br>40.00%   | <br>40.00%   |
| 09/21<br>14:00 | <br>40.00%  | <br>46.67%  | <br>50.00%  |
| 09/21<br>15:00 | <br>50.00%  | <br>60.00%  | <br>60.00%  |
| 09/21<br>16:00 | <br>70.00%  | <br>90.00%  | <br>90.00%  |
| 09/21<br>17:00 | <br>90.00%  | <br>100.00% | <br>100.00% |
| 09/21<br>18:00 | <br>100.00% | <br>100.00% | <br>100.00% |

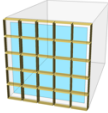
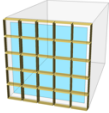
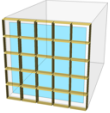
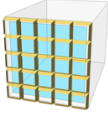
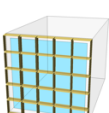
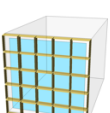
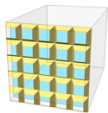
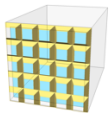
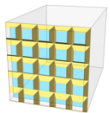
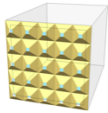
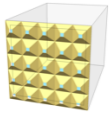
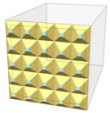
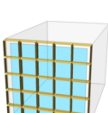
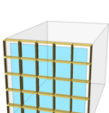
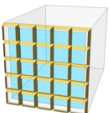
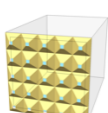
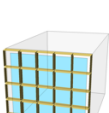
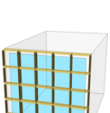
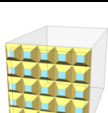
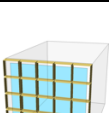
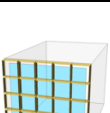
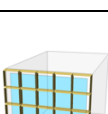
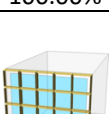
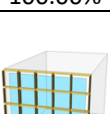
**APPENDIX**

| Or. | 21-Mar         |  |  |  |
|-----|----------------|--|--|--|
| W   | 03/21<br>06:00 | <br>100.00%   | <br>100.00%   | <br>100.00%   |
|     | 03/21<br>07:00 | <br>100.00%   | <br>100.00%   | <br>100.00%   |
|     | 03/21<br>08:00 | <br>100.00%   | <br>100.00%   | <br>100.00%   |
|     | 03/21<br>09:00 | <br>100.00%   | <br>100.00%   | <br>100.00%   |
|     | 03/21<br>10:00 | <br>100.00% | <br>100.00% | <br>100.00% |
|     | 03/21<br>11:00 | <br>100.00% | <br>100.00% | <br>100.00% |
|     | 03/21<br>12:00 | <br>100.00% | <br>100.00% | <br>100.00% |
|     | 03/21<br>13:00 | <br>100.00% | <br>100.00% | <br>100.00% |
|     | 03/21<br>14:00 | <br>100.00% | <br>100.00% | <br>100.00% |

**APPENDIX**

|     |                |  |  |  |
|-----|----------------|--|--|--|
|     | 03/21<br>15:00 | <br>80.00%    | <br>100.00%   | <br>100.00%   |
|     | 03/21<br>16:00 | <br>90.00%    | <br>100.00%   | <br>100.00%   |
|     | 03/21<br>17:00 | <br>100.00%   | <br>100.00%   | <br>100.00%   |
|     | 03/21<br>18:00 | <br>100.00%   | <br>100.00%   | <br>100.00%   |
| Or. | 21-Sep         |  |  |  |
| W   | 09/21<br>06:00 | <br>100.00% | <br>100.00% | <br>100.00% |
|     | 09/21<br>07:00 | <br>100.00% | <br>100.00% | <br>100.00% |
|     | 09/21<br>08:00 | <br>100.00% | <br>100.00% | <br>100.00% |
|     | 09/21<br>09:00 | <br>100.00% | <br>100.00% | <br>100.00% |
|     | 09/21<br>10:00 | <br>100.00% | <br>100.00% | <br>100.00% |

**APPENDIX**

|  |                |  |  |  |
|--|----------------|--|--|--|
|  | 09/21<br>11:00 | <br>100.00%   | <br>100.00%   | <br>100.00%   |
|  | 09/21<br>12:00 | <br>90.00%    | <br>100.00%   | <br>100.00%   |
|  | 09/21<br>13:00 | <br>60.00%    | <br>70.00%    | <br>70.00%    |
|  | 09/21<br>14:00 | <br>20.00%    | <br>30.00%    | <br>20.00%    |
|  | 09/21<br>15:00 | <br>100.00%  | <br>100.00%  | <br>80.00%   |
|  | 09/21<br>16:00 | <br>10.00%  | <br>100.00% | <br>100.00% |
|  | 09/21<br>17:00 | <br>40.00%  | <br>100.00% | <br>100.00% |
|  | 09/21<br>18:00 | <br>100.00% | <br>100.00% | <br>100.00% |

## **Appendix D: Synthetic Database**

## APPENDIX

The database is loaded into the web-based data visualization tool (Design Explorer):

Adaptive Façades Control Scenario (C1).

[https://tt-acm.github.io/DesignExplorer/?ID=BL\\_3SEYQbY](https://tt-acm.github.io/DesignExplorer/?ID=BL_3SEYQbY)

Adaptive Façades Control Scenario (C2).

[https://tt-acm.github.io/DesignExplorer/?ID=BL\\_3BSZP1I](https://tt-acm.github.io/DesignExplorer/?ID=BL_3BSZP1I)

Adaptive Façades Control Scenario (C3).

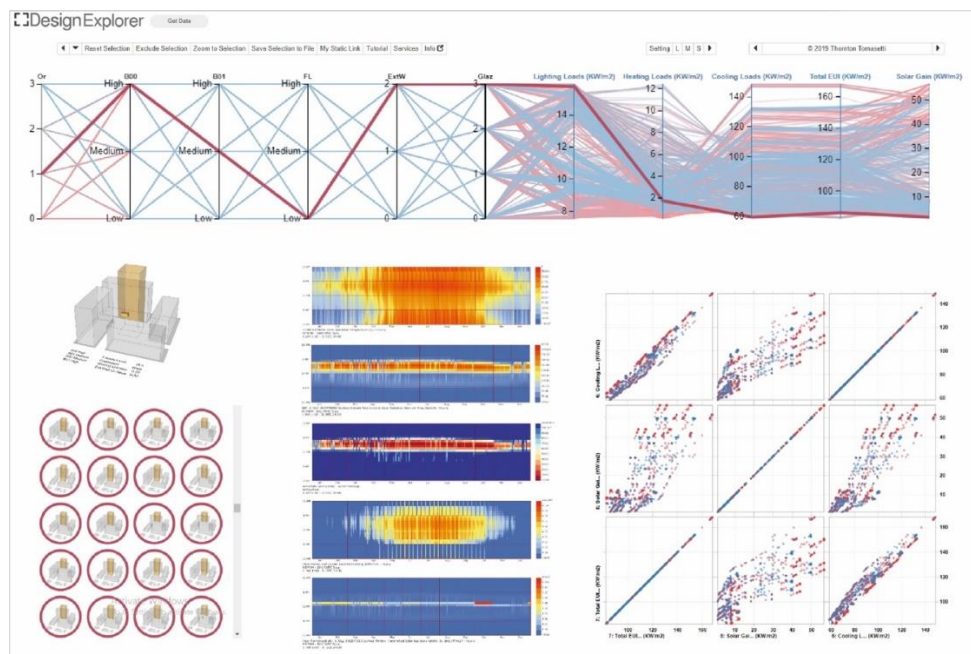
[https://tt-acm.github.io/DesignExplorer/?ID=BL\\_3ULMJeZ](https://tt-acm.github.io/DesignExplorer/?ID=BL_3ULMJeZ)

Adaptive Façades Control Scenario (C4).

[https://tt-acm.github.io/DesignExplorer/?ID=BL\\_3eJReGq](https://tt-acm.github.io/DesignExplorer/?ID=BL_3eJReGq)

Adaptive Façades All Control Scenarios.

[https://tt-acm.github.io/DesignExplorer/?ID=BL\\_3E7vqPE](https://tt-acm.github.io/DesignExplorer/?ID=BL_3E7vqPE)



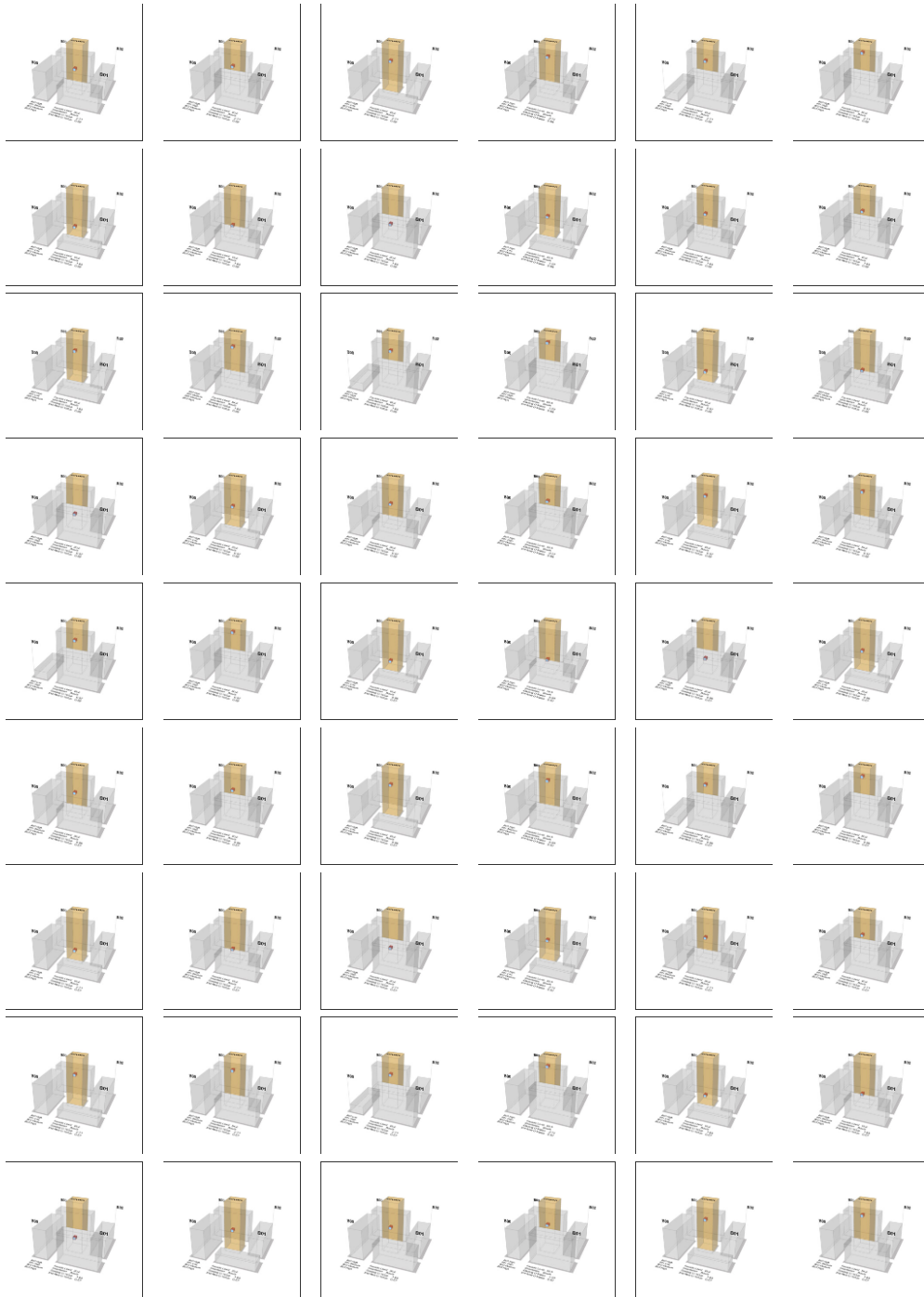


**APPENDIX**



Sample of the parametric generation database for cooling loads using simulation approach.

## APPENDIX



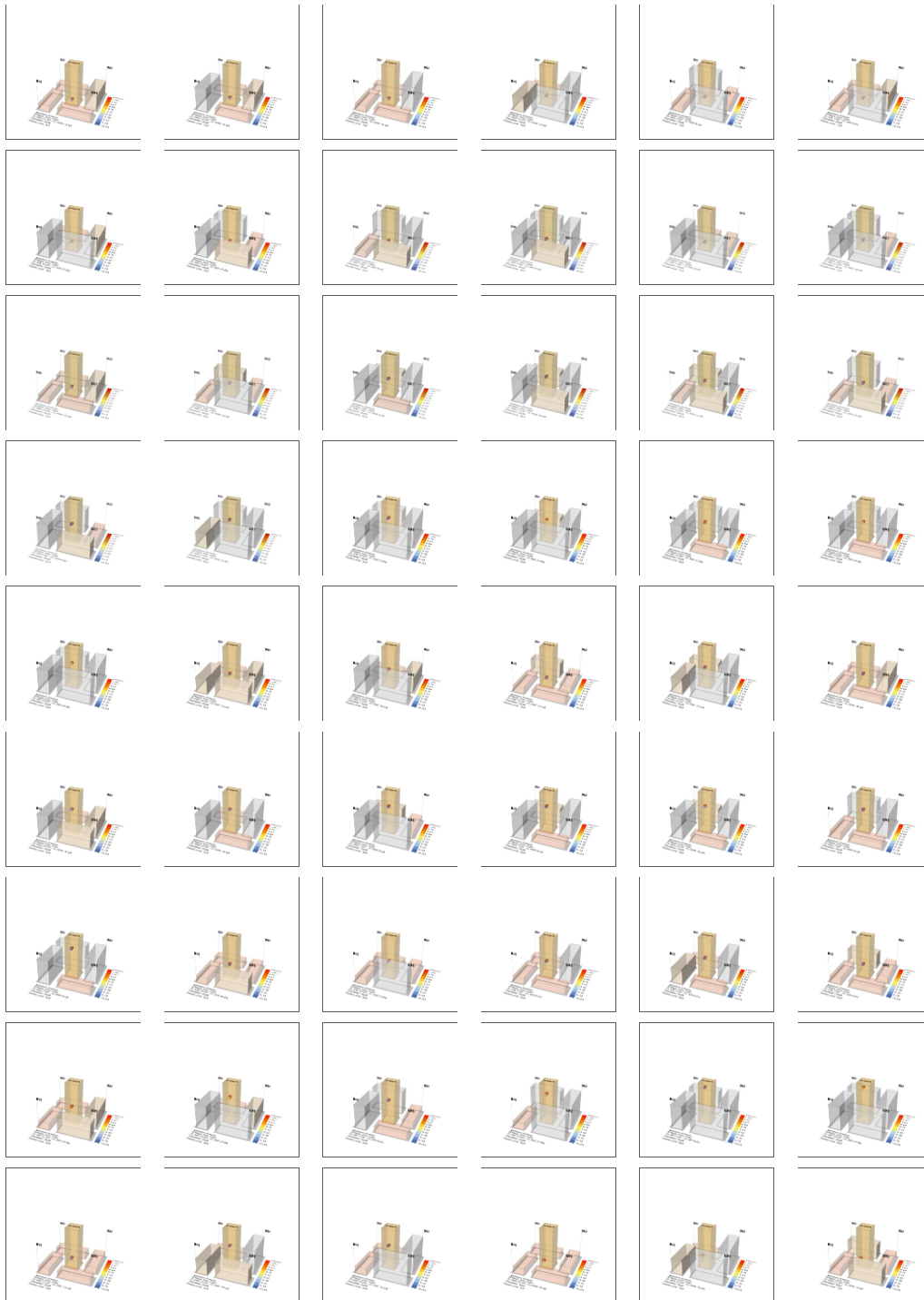
Sample of the parametric generation database for cooling loads using simulation approach.

**APPENDIX**



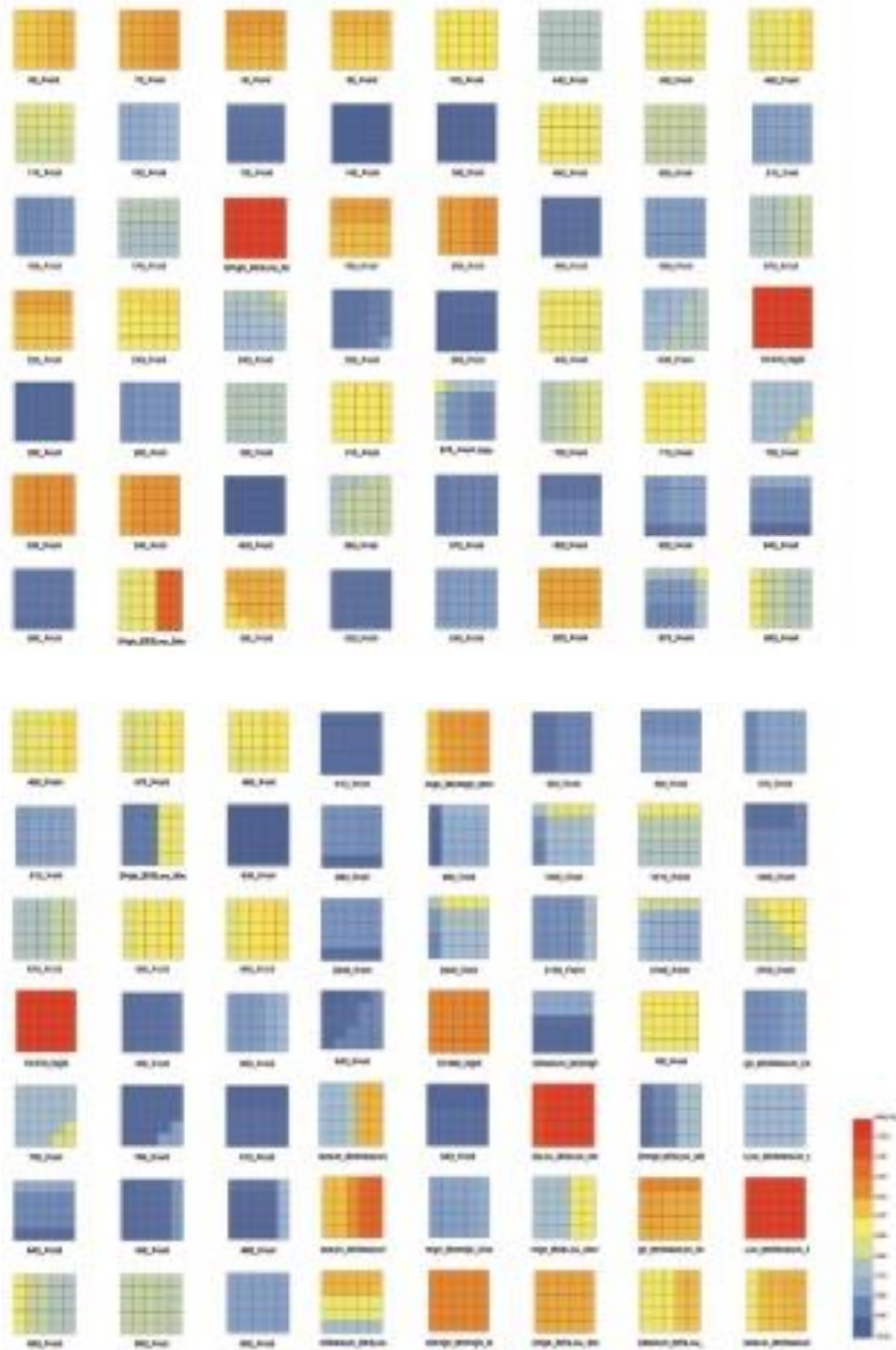
Sample of the parametric generation database for solar radiation using simulation approach.

**APPENDIX**



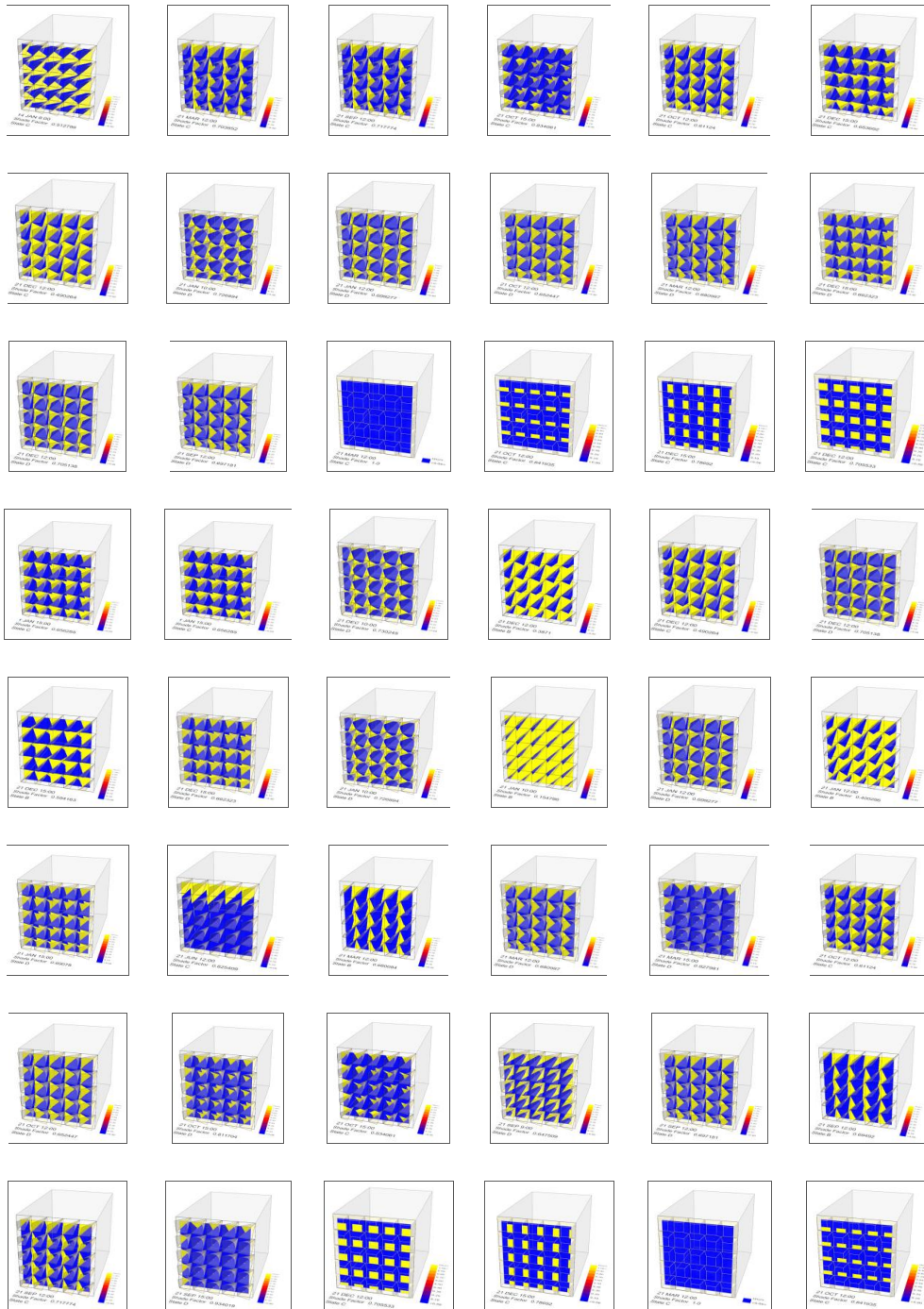
Sample of the parametric generation database for solar radiation using simulation approach.

**APPENDIX**



Sample of the parametric generation database for solar radiation using simulation approach.

## APPENDIX



Sample of the parametric generation database for shade factor using simulation approach.

**APPENDIX**



Sample of the parametric generation database for shade factor using simulation approach.







**APPENDIX**

| L19     |                  |          |                  |          |                  |          |                  |            |                  |         |                  |         |                     |    |    |            |
|---------|------------------|----------|------------------|----------|------------------|----------|------------------|------------|------------------|---------|------------------|---------|---------------------|----|----|------------|
| A       | B                | C        | D                | E        | F                | G        | H                | I          | J                | K       |                  |         |                     |    |    |            |
| in:Hour | out:Shade Factor | State A  | out:Shade Factor | State B  | out:Shade Factor | State C  | out:Shade Factor | State D    | out:Shade Factor | State E | out:Shade Factor | State F | out:Solar Radiation | SR | RA | Date/Time  |
| 1       | 1                | 1        | 1                | 1        | 1                | 1        | 1                | 1          | 1                | 1       | 1                | 1       | 0                   | 0  | 0  | 01/01 01:0 |
| 2       | 1                | 1        | 1                | 1        | 1                | 1        | 1                | 1          | 1                | 1       | 1                | 1       | 0                   | 0  | 0  | 01/01 02:0 |
| 3       | 1                | 1        | 1                | 1        | 1                | 1        | 1                | 1          | 1                | 1       | 1                | 1       | 0                   | 0  | 0  | 01/01 03:0 |
| 4       | 1                | 1        | 1                | 1        | 1                | 1        | 1                | 1          | 1                | 1       | 1                | 1       | 0                   | 0  | 0  | 01/01 04:0 |
| 5       | 1                | 1        | 1                | 1        | 1                | 1        | 1                | 1          | 1                | 1       | 1                | 1       | 0                   | 0  | 0  | 01/01 05:0 |
| 6       | 1                | 1        | 1                | 1        | 1                | 1        | 1                | 1          | 1                | 1       | 1                | 1       | 0                   | 0  | 0  | 01/01 06:0 |
| 7       | 1                | 1        | 1                | 1        | 1                | 1        | 1                | 1          | 1                | 1       | 1                | 1       | 0                   | 0  | 0  | 01/01 07:0 |
| 8       | 0.761731         | 0.867498 | 0.954487         | 0.855868 | 0.93877          | 0.987623 | 261.705          | 303.36     | 01/01 08:0       |         |                  |         |                     |    |    |            |
| 9       | 0.615441         | 0.743586 | 0.65807          | 0.77638  | 0.881918         | 0.965017 | 490.995          | 556.09     | 01/01 09:0       |         |                  |         |                     |    |    |            |
| 10      | 0.440985         | 0.595419 | 0.726354         | 0.84872  | 0.963575         | 643.573  | 735.09           | 01/01 10:0 |                  |         |                  |         |                     |    |    |            |
| 11      | 0.389559         | 0.539314 | 0.711654         | 0.851584 | 0.959913         | 721.593  | 805.46           | 01/01 11:0 |                  |         |                  |         |                     |    |    |            |
| 12      | 0.390155         | 0.535372 | 0.708189         | 0.848139 | 0.960629         | 705.153  | 774.3            | 01/01 12:0 |                  |         |                  |         |                     |    |    |            |
| 13      | 0.395441         | 0.544065 | 0.711332         | 0.851241 | 0.959965         | 751.203  | 816.03           | 01/01 13:0 |                  |         |                  |         |                     |    |    |            |
| 14      | 0.447687         | 0.601135 | 0.729352         | 0.847558 | 0.964219         | 731.165  | 773.42           | 01/01 14:0 |                  |         |                  |         |                     |    |    |            |
| 15      | 0.523669         | 0.667925 | 0.784679         | 0.889782 | 0.965588         | 633.507  | 659.32           | 01/01 15:0 |                  |         |                  |         |                     |    |    |            |
| 16      | 0.636024         | 0.758951 | 0.867021         | 0.946344 | 0.991752         | 487.857  | 478.41           | 01/01 16:0 |                  |         |                  |         |                     |    |    |            |
| 17      | 0.781795         | 0.888683 | 0.968991         | 1        | 1                | 1        | 189.592          | 167.07     | 01/01 17:0       |         |                  |         |                     |    |    |            |
| 18      | 1                | 1        | 1                | 1        | 1                | 1        | 0.904            | 0          | 01/01 18:0       |         |                  |         |                     |    |    |            |
| 19      | 1                | 1        | 1                | 1        | 1                | 1        | 0                | 0          | 01/01 19:0       |         |                  |         |                     |    |    |            |
| 20      | 1                | 1        | 1                | 1        | 1                | 1        | 0                | 0          | 01/01 20:0       |         |                  |         |                     |    |    |            |
| 21      | 1                | 1        | 1                | 1        | 1                | 1        | 0                | 0          | 01/01 21:0       |         |                  |         |                     |    |    |            |
| 22      | 1                | 1        | 1                | 1        | 1                | 1        | 0                | 0          | 01/01 22:0       |         |                  |         |                     |    |    |            |
| 23      | 1                | 1        | 1                | 1        | 1                | 1        | 0                | 0          | 01/01 23:0       |         |                  |         |                     |    |    |            |
| 24      | 1                | 1        | 1                | 1        | 1                | 1        | 0                | -999       | 01/01 24:0       |         |                  |         |                     |    |    |            |
| 25      | 1                | 1        | 1                | 1        | 1                | 1        | 0                | 0          | 01/02 01:0       |         |                  |         |                     |    |    |            |
| 26      | 1                | 1        | 1                | 1        | 1                | 1        | 0                | 0          | 01/02 02:0       |         |                  |         |                     |    |    |            |
| 27      | 1                | 1        | 1                | 1        | 1                | 1        | 0                | 0          | 01/02 03:0       |         |                  |         |                     |    |    |            |
| 28      | 1                | 1        | 1                | 1        | 1                | 1        | 0                | 0          | 01/02 04:0       |         |                  |         |                     |    |    |            |
| 29      | 1                | 1        | 1                | 1        | 1                | 1        | 0                | 0          | 01/02 05:0       |         |                  |         |                     |    |    |            |
| 30      | 1                | 1        | 1                | 1        | 1                | 1        | 0                | 0          | 01/02 06:0       |         |                  |         |                     |    |    |            |
| 31      | 1                | 1        | 1                | 1        | 1                | 1        | 0                | 0          | 01/02 07:0       |         |                  |         |                     |    |    |            |

| HB764 |      |          |          |          |          |          |   |         |        |             |
|-------|------|----------|----------|----------|----------|----------|---|---------|--------|-------------|
| A     | B    | C        | D        | E        | F        | G        | H | I       | J      | K           |
| 8722  | 8721 | 0.509799 | 0.653816 | 0.773288 | 0.880622 | 0.964955 | 1 | 495.815 | 562.64 | 12/30 09:00 |
| 8723  | 8722 | 0.438692 | 0.593489 | 0.722962 | 0.849893 | 0.962963 | 1 | 649.117 | 735.68 | 12/30 10:00 |
| 8724  | 8723 | 0.384424 | 0.537405 | 0.70961  | 0.848834 | 0.960629 | 1 | 739.549 | 825.53 | 12/30 11:00 |
| 8725  | 8724 | 0.329149 | 0.537177 | 0.70962  | 0.846708 | 0.960059 | 1 | 800.37  | 858.23 | 12/30 12:00 |
| 8726  | 8725 | 0.394798 | 0.541503 | 0.707815 | 0.848751 | 0.959883 | 1 | 767.395 | 837.87 | 12/30 13:00 |
| 8727  | 8726 | 0.445809 | 0.59905  | 0.727475 | 0.847527 | 0.963638 | 1 | 731.399 | 770.05 | 12/30 14:00 |
| 8728  | 8727 | 0.523659 | 0.667925 | 0.786443 | 0.889782 | 0.964385 | 1 | 630.174 | 647.31 | 12/30 15:00 |
| 8729  | 8728 | 0.636044 | 0.757934 | 0.866326 | 0.946344 | 0.991628 | 1 | 477.876 | 488.17 | 12/30 16:00 |
| 8730  | 8729 | 0.77723  | 0.886058 | 0.96897  | 1        | 1        | 1 | 200.362 | 175.34 | 12/30 17:00 |
| 8731  | 8730 | 1        | 1        | 1        | 1        | 1        | 1 | 0.448   | 0      | 12/30 18:00 |
| 8732  | 8731 | 1        | 1        | 1        | 1        | 1        | 1 | 0       | 0      | 12/30 19:00 |
| 8733  | 8732 | 1        | 1        | 1        | 1        | 1        | 1 | 0       | 0      | 12/30 20:00 |
| 8734  | 8733 | 1        | 1        | 1        | 1        | 1        | 1 | 0       | 0      | 12/30 21:00 |
| 8735  | 8734 | 1        | 1        | 1        | 1        | 1        | 1 | 0       | 0      | 12/30 22:00 |
| 8736  | 8735 | 1        | 1        | 1        | 1        | 1        | 1 | 0       | 0      | 12/30 23:00 |
| 8737  | 8736 | 1        | 1        | 1        | 1        | 1        | 1 | 0       | 0      | 12/30 24:00 |
| 8738  | 8737 | 1        | 1        | 1        | 1        | 1        | 1 | 0       | 0      | 12/31 01:00 |
| 8739  | 8738 | 1        | 1        | 1        | 1        | 1        | 1 | 0       | 0      | 12/31 02:00 |
| 8740  | 8739 | 1        | 1        | 1        | 1        | 1        | 1 | 0       | 0      | 12/31 03:00 |
| 8741  | 8740 | 1        | 1        | 1        | 1        | 1        | 1 | 0       | 0      | 12/31 04:00 |
| 8742  | 8741 | 1        | 1        | 1        | 1        | 1        | 1 | 0       | 0      | 12/31 05:00 |
| 8743  | 8742 | 1        | 1        | 1        | 1        | 1        | 1 | 0       | 0      | 12/31 06:00 |
| 8744  | 8743 | 0.75865  | 0.864811 | 0.950338 | 1        | 1        | 1 | 2.881   | 3.23   | 12/31 07:00 |
| 8745  | 8744 | 0.612744 | 0.74121  | 0.853908 | 0.93877  | 0.986939 | 1 | 266.744 | 297.35 | 12/31 08:00 |
| 8746  | 8745 | 0.509819 | 0.655933 | 0.776348 | 0.880632 | 0.965007 | 1 | 503.342 | 568.19 | 12/31 09:00 |
| 8747  | 8746 | 0.440975 | 0.595419 | 0.722972 | 0.848689 | 0.964156 | 1 | 652.029 | 739.64 | 12/31 10:00 |
| 8748  | 8747 | 0.386665 | 0.537436 | 0.715633 | 0.851335 | 0.960059 | 1 | 742.039 | 828.2  | 12/31 11:00 |
| 8749  | 8748 | 0.329149 | 0.535372 | 0.70962  | 0.84815  | 0.959332 | 1 | 804.329 | 863.14 | 12/31 12:00 |
| 8750  | 8749 | 0.394798 | 0.541503 | 0.709309 | 0.85011  | 0.95926  | 1 | 775.521 | 846.76 | 12/31 13:00 |
| 8751  | 8750 | 0.448358 | 0.599039 | 0.729197 | 0.847569 | 0.963015 | 1 | 739.479 | 778.28 | 12/31 14:00 |
| 8752  | 8751 | 0.52562  | 0.669523 | 0.786443 | 0.889793 | 0.965017 | 1 | 641.368 | 660.38 | 12/31 15:00 |
| 8753  | 8752 | 0.636024 | 0.757934 | 0.867021 | 0.946344 | 0.991628 | 1 | 490.906 | 478.52 | 12/31 16:00 |
| 8754  | 8753 | 0.781069 | 0.886504 | 0.968991 | 1        | 1        | 1 | 190.111 | 167.95 | 12/31 17:00 |
| 8755  | 8754 | 1        | 1        | 1        | 1        | 1        | 1 | 0.448   | 0      | 12/31 18:00 |
| 8756  | 8755 | 1        | 1        | 1        | 1        | 1        | 1 | 0       | 0      | 12/31 19:00 |
| 8757  | 8756 | 1        | 1        | 1        | 1        | 1        | 1 | 0       | 0      | 12/31 20:00 |
| 8758  | 8757 | 1        | 1        | 1        | 1        | 1        | 1 | 0       | 0      | 12/31 21:00 |
| 8759  | 8758 | 1        | 1        | 1        | 1        | 1        | 1 | 0       | 0      | 12/31 22:00 |
| 8760  | 8759 | 1        | 1        | 1        | 1        | 1        | 1 | 0       | 0      | 12/31 23:00 |
| 8761  | 8760 | 1        | 1        | 1        | 1        | 1        | 1 | 0       | 0      | 12/31 24:00 |

Shade factor database for scaling movements prototype stored in Excel.

**APPENDIX**

The image displays two screenshots of an Excel spreadsheet titled "Shade Factor-Rotation".

The top spreadsheet (sheet K27) contains the following data:

|    | A       | B                        | C                          | D                        | E                        | F                        | G                        | H                            | I      | J              |
|----|---------|--------------------------|----------------------------|--------------------------|--------------------------|--------------------------|--------------------------|------------------------------|--------|----------------|
| 1  | In:Hour | out:Shade Factor State A | out:Shade Factor - State B | out:Shade Factor State C | out:Shade Factor State D | out:Shade Factor State E | out:Shade Factor State F | out:Solar Radiation W/out:SR | SR     | RAD Date/Time  |
| 2  | 1       | 1                        | 1                          | 1                        | 1                        | 1                        | 1                        | 0                            | 0      | 01/01 01:00:00 |
| 3  | 2       | 1                        | 1                          | 1                        | 1                        | 1                        | 1                        | 0                            | 0      | 01/01 02:00:00 |
| 4  | 3       | 1                        | 1                          | 1                        | 1                        | 1                        | 1                        | 0                            | 0      | 01/01 03:00:00 |
| 5  | 4       | 1                        | 1                          | 1                        | 1                        | 1                        | 1                        | 0                            | 0      | 01/01 04:00:00 |
| 6  | 5       | 1                        | 1                          | 1                        | 1                        | 1                        | 1                        | 0                            | 0      | 01/01 05:00:00 |
| 7  | 6       | 1                        | 1                          | 1                        | 1                        | 1                        | 1                        | 0                            | 0      | 01/01 06:00:00 |
| 8  | 7       | 0.57441                  | 0.607899                   | 0.644177                 | 0.625878                 | 0.835244                 | 1                        | 2.879                        | 3.22   | 01/01 07:00:00 |
| 9  | 8       | 0.309655                 | 0.374869                   | 0.473776                 | 0.654035                 | 0.868214                 | 1                        | 261.705                      | 303.36 | 01/01 08:00:00 |
| 10 | 9       | 0.104636                 | 0.176261                   | 0.444243                 | 0.691247                 | 0.882489                 | 1                        | 490.995                      | 556.09 | 01/01 09:00:00 |
| 11 | 10      | 0.058844                 | 0.153821                   | 0.45441                  | 0.700439                 | 0.884958                 | 1                        | 643.573                      | 735.09 | 01/01 10:00:00 |
| 12 | 11      | 0.199541                 | 0.260263                   | 0.459203                 | 0.69548                  | 0.883661                 | 1                        | 721.593                      | 805.46 | 01/01 11:00:00 |
| 13 | 12      | 0.321576                 | 0.370201                   | 0.483344                 | 0.683446                 | 0.878412                 | 1                        | 705.153                      | 774.3  | 01/01 12:00:00 |
| 14 | 13      | 0.418203                 | 0.460302                   | 0.548132                 | 0.672916                 | 0.873484                 | 1                        | 751.203                      | 816.03 | 01/01 13:00:00 |
| 15 | 14      | 0.494652                 | 0.534946                   | 0.604932                 | 0.65696                  | 0.86589                  | 1                        | 731.165                      | 773.42 | 01/01 14:00:00 |
| 16 | 15      | 0.559087                 | 0.59158                    | 0.650237                 | 0.648183                 | 0.855785                 | 1                        | 633.507                      | 659.32 | 01/01 15:00:00 |
| 17 | 16      | 0.609051                 | 0.635495                   | 0.66666                  | 0.662966                 | 0.840794                 | 1                        | 487.857                      | 478.41 | 01/01 16:00:00 |
| 18 | 17      | 0.641076                 | 0.672584                   | 0.693675                 | 0.673382                 | 0.820481                 | 1                        | 189.592                      | 167.07 | 01/01 17:00:00 |
| 19 | 18      | 1                        | 1                          | 1                        | 1                        | 1                        | 1                        | 0.904                        | 0      | 01/01 18:00:00 |
| 20 | 19      | 1                        | 1                          | 1                        | 1                        | 1                        | 1                        | 0                            | 0      | 01/01 19:00:00 |
| 21 | 20      | 1                        | 1                          | 1                        | 1                        | 1                        | 1                        | 0                            | 0      | 01/01 20:00:00 |
| 22 | 21      | 1                        | 1                          | 1                        | 1                        | 1                        | 1                        | 0                            | 0      | 01/01 21:00:00 |
| 23 | 22      | 1                        | 1                          | 1                        | 1                        | 1                        | 1                        | 0                            | 0      | 01/01 22:00:00 |
| 24 | 23      | 1                        | 1                          | 1                        | 1                        | 1                        | 1                        | 0                            | 0      | 01/01 23:00:00 |
| 25 | 24      | 1                        | 1                          | 1                        | 1                        | 1                        | 1                        | 0                            | 0      | 01/01 24:00:00 |
| 26 | 25      | 1                        | 1                          | 1                        | 1                        | 1                        | 1                        | 0                            | 0      | 01/02 01:00:00 |
| 27 | 26      | 1                        | 1                          | 1                        | 1                        | 1                        | 1                        | 0                            | 0      | 01/02 02:00:00 |

The bottom spreadsheet (sheet K8761) contains the following data:

|      | A    | B        | C        | D        | E        | F        | G | H       | I      | J              |
|------|------|----------|----------|----------|----------|----------|---|---------|--------|----------------|
| 8735 | 8734 | 1        | 1        | 1        | 1        | 1        | 1 | 0       | 0      | 12/30 22:00:00 |
| 8736 | 8735 | 1        | 1        | 1        | 1        | 1        | 1 | 0       | 0      | 12/30 23:00:00 |
| 8737 | 8736 | 1        | 1        | 1        | 1        | 1        | 1 | 0       | 0      | 12/30 24:00:00 |
| 8738 | 8737 | 1        | 1        | 1        | 1        | 1        | 1 | 0       | 0      | 12/31 01:00:00 |
| 8739 | 8738 | 1        | 1        | 1        | 1        | 1        | 1 | 0       | 0      | 12/31 02:00:00 |
| 8740 | 8739 | 1        | 1        | 1        | 1        | 1        | 1 | 0       | 0      | 12/31 03:00:00 |
| 8741 | 8740 | 1        | 1        | 1        | 1        | 1        | 1 | 0       | 0      | 12/31 04:00:00 |
| 8742 | 8741 | 1        | 1        | 1        | 1        | 1        | 1 | 0       | 0      | 12/31 05:00:00 |
| 8743 | 8742 | 1        | 1        | 1        | 1        | 1        | 1 | 0       | 0      | 12/31 06:00:00 |
| 8744 | 8743 | 0.572004 | 0.606156 | 0.643214 | 0.625753 | 0.836115 | 1 | 2.881   | 3.23   | 12/31 07:00:00 |
| 8745 | 8744 | 0.307954 | 0.373002 | 0.472399 | 0.664626 | 0.868546 | 1 | 266.744 | 297.35 | 12/31 08:00:00 |
| 8746 | 8745 | 0.103028 | 0.174591 | 0.444502 | 0.691496 | 0.882551 | 1 | 503.342 | 568.19 | 12/31 09:00:00 |
| 8747 | 8746 | 0.059912 | 0.153904 | 0.454607 | 0.700615 | 0.885083 | 1 | 652.029 | 739.64 | 12/31 10:00:00 |
| 8748 | 8747 | 0.200195 | 0.260792 | 0.459099 | 0.695304 | 0.883713 | 1 | 742.039 | 828.2  | 12/31 11:00:00 |
| 8749 | 8748 | 0.321628 | 0.370335 | 0.483334 | 0.68356  | 0.878536 | 1 | 804.329 | 863.14 | 12/31 12:00:00 |
| 8750 | 8749 | 0.417892 | 0.460095 | 0.547831 | 0.673082 | 0.873526 | 1 | 775.521 | 846.76 | 12/31 13:00:00 |
| 8751 | 8750 | 0.494019 | 0.534293 | 0.604434 | 0.657115 | 0.866118 | 1 | 739.479 | 778.28 | 12/31 14:00:00 |
| 8752 | 8751 | 0.558143 | 0.590429 | 0.649542 | 0.647519 | 0.855889 | 1 | 641.368 | 660.38 | 12/31 15:00:00 |
| 8753 | 8752 | 0.607816 | 0.634572 | 0.665404 | 0.662095 | 0.840867 | 1 | 490.906 | 478.52 | 12/31 16:00:00 |
| 8754 | 8753 | 0.640433 | 0.6722   | 0.693789 | 0.673642 | 0.821166 | 1 | 190.111 | 167.95 | 12/31 17:00:00 |
| 8755 | 8754 | 1        | 1        | 1        | 1        | 1        | 1 | 0.448   | 0      | 12/31 18:00:00 |
| 8756 | 8755 | 1        | 1        | 1        | 1        | 1        | 1 | 0       | 0      | 12/31 19:00:00 |
| 8757 | 8756 | 1        | 1        | 1        | 1        | 1        | 1 | 0       | 0      | 12/31 20:00:00 |
| 8758 | 8757 | 1        | 1        | 1        | 1        | 1        | 1 | 0       | 0      | 12/31 21:00:00 |
| 8759 | 8758 | 1        | 1        | 1        | 1        | 1        | 1 | 0       | 0      | 12/31 22:00:00 |
| 8760 | 8759 | 1        | 1        | 1        | 1        | 1        | 1 | 0       | 0      | 12/31 23:00:00 |
| 8761 | 8760 | 1        | 1        | 1        | 1        | 1        | 1 | 0       | 0      | 12/31 24:00:00 |

*Shade factor database for folding movements prototype stored in Excel.*

**APPENDIX**

The top screenshot shows an Excel spreadsheet with columns J through V. The data includes energy metrics for different states (State-A to State-F) and a total EU1 - K value. The bottom screenshot shows an Excel spreadsheet with columns A through M. The data includes date, orientation, building type, facade glazing type, and energy metrics.

*Energy simulation database for adaptive façade (scaling movement) which was stored in Excel.*

The screenshot shows an Excel spreadsheet with columns A through Q. The data includes date, orientation, building type, facade glazing type, and energy metrics. The table contains 29 rows of data.

*Energy simulation database for base case model, which was stored in Excel.*

**APPENDIX**

| 1  | In:Date/ | Tin:in:Hour | In:Orientation | In:Buildir | In:Buildir | In:Buildir | In:Facade | In:Glazing | In:Typ | In:Exterior     | In:Opera | out:Cooling | out:Heating | out:Light | out:Equi | Total  | Total   | Total   | Total  | Total  |         |
|----|----------|-------------|----------------|------------|------------|------------|-----------|------------|--------|-----------------|----------|-------------|-------------|-----------|----------|--------|---------|---------|--------|--------|---------|
| 2  | 01/01    | 01:00       | 1              | 1          | High       | High       | Medium    | High       | 60     | TripleGlz-Krypt | 2        | 20.5462     | 0           | 0         | 0.00015  | 0.0008 | 59.2855 | 2.72661 | 9.7059 | 9.4888 | 81.2069 |
| 3  | 01/01    | 02:00       | 2              | 1          | High       | High       | Medium    | High       | 60     | TripleGlz-Krypt | 2        | 20.261      | 0           | 0         | 0.00015  | 0.0008 |         |         |        |        |         |
| 4  | 01/01    | 03:00       | 3              | 1          | High       | High       | Medium    | High       | 60     | TripleGlz-Krypt | 2        | 20.092      | 0           | 0         | 0.00015  | 0.0008 |         |         |        |        |         |
| 5  | 01/01    | 04:00       | 4              | 1          | High       | High       | Medium    | High       | 60     | TripleGlz-Krypt | 2        | 19.7545     | 0           | 0         | 0.00015  | 0.0008 |         |         |        |        |         |
| 6  | 01/01    | 05:00       | 5              | 1          | High       | High       | Medium    | High       | 60     | TripleGlz-Krypt | 2        | 19.5058     | 0           | 0         | 0.00015  | 0.0008 |         |         |        |        |         |
| 7  | 01/01    | 06:00       | 6              | 1          | High       | High       | Medium    | High       | 60     | TripleGlz-Krypt | 2        | 19.2635     | 0           | 0         | 0.0003   | 0.0008 |         |         |        |        |         |
| 8  | 01/01    | 07:00       | 7              | 1          | High       | High       | Medium    | High       | 60     | TripleGlz-Krypt | 2        | 20.8467     | 0           | 0.026088  | 0.0003   | 0.0008 |         |         |        |        |         |
| 9  | 01/01    | 08:00       | 8              | 1          | High       | High       | Medium    | High       | 60     | TripleGlz-Krypt | 2        | 21.1599     | 0           | 0.013654  | 0.0009   | 0.0008 |         |         |        |        |         |
| 10 | 01/01    | 09:00       | 9              | 1          | High       | High       | Medium    | High       | 60     | TripleGlz-Krypt | 2        | 21.3185     | 0           | 0.010974  | 0.0027   | 0.0018 |         |         |        |        |         |
| 11 | 01/01    | 10:00       | 10             | 1          | High       | High       | Medium    | High       | 60     | TripleGlz-Krypt | 2        | 21.4308     | 0           | 0.005606  | 0.0027   | 0.0018 |         |         |        |        |         |
| 12 | 01/01    | 11:00       | 11             | 1          | High       | High       | Medium    | High       | 60     | TripleGlz-Krypt | 2        | 21.513      | 0           | 0.003044  | 0.0027   | 0.0018 |         |         |        |        |         |
| 13 | 01/01    | 12:00       | 12             | 1          | High       | High       | Medium    | High       | 60     | TripleGlz-Krypt | 2        | 21.5851     | 0           | 0.00337   | 0.0027   | 0.0018 |         |         |        |        |         |
| 14 | 01/01    | 13:00       | 13             | 1          | High       | High       | Medium    | High       | 60     | TripleGlz-Krypt | 2        | 21.6412     | 0           | 0.000666  | 0.0027   | 0.0016 |         |         |        |        |         |
| 15 | 01/01    | 14:00       | 14             | 1          | High       | High       | Medium    | High       | 60     | TripleGlz-Krypt | 2        | 21.8222     | 0           | 0         | 0.0027   | 0.0018 |         |         |        |        |         |
| 16 | 01/01    | 15:00       | 15             | 1          | High       | High       | Medium    | High       | 60     | TripleGlz-Krypt | 2        | 22.1538     | 0           | 0         | 0.0027   | 0.0018 |         |         |        |        |         |
| 17 | 01/01    | 16:00       | 16             | 1          | High       | High       | Medium    | High       | 60     | TripleGlz-Krypt | 2        | 22.4926     | 0           | 0         | 0.0027   | 0.0018 |         |         |        |        |         |
| 18 | 01/01    | 17:00       | 17             | 1          | High       | High       | Medium    | High       | 60     | TripleGlz-Krypt | 2        | 22.5611     | 0           | 0         | 0.0027   | 0.0018 |         |         |        |        |         |
| 19 | 01/01    | 18:00       | 18             | 1          | High       | High       | Medium    | High       | 60     | TripleGlz-Krypt | 2        | 22.3809     | 0           | 0         | 0.0021   | 0.0016 |         |         |        |        |         |
| 20 | 01/01    | 19:00       | 19             | 1          | High       | High       | Medium    | High       | 60     | TripleGlz-Krypt | 2        | 22.0882     | 0           | 0.001565  | 0.0015   | 0.0012 |         |         |        |        |         |
| 21 | 01/01    | 20:00       | 20             | 1          | High       | High       | Medium    | High       | 60     | TripleGlz-Krypt | 2        | 21.9893     | 0           | 0.003589  | 0.0015   | 0.0012 |         |         |        |        |         |
| 22 | 01/01    | 21:00       | 21             | 1          | High       | High       | Medium    | High       | 60     | TripleGlz-Krypt | 2        | 21.9391     | 0           | 0.004679  | 0.0009   | 0.001  |         |         |        |        |         |
| 23 | 01/01    | 22:00       | 22             | 1          | High       | High       | Medium    | High       | 60     | TripleGlz-Krypt | 2        | 21.9001     | 0           | 0.005036  | 0.0009   | 0.001  |         |         |        |        |         |
| 24 | 01/01    | 23:00       | 23             | 1          | High       | High       | Medium    | High       | 60     | TripleGlz-Krypt | 2        | 21.1854     | 0           | 0         | 0.0003   | 0.0008 |         |         |        |        |         |
| 25 | 01/01    | 24:00       | 24             | 1          | High       | High       | Medium    | High       | 60     | TripleGlz-Krypt | 2        | 20.913      | 0           | 0         | 0.00015  | 0.0008 |         |         |        |        |         |

Energy simulation database for adaptive façade (folding movement), which was stored in Excel.

## **Appendix E: ML Surrogate Models Codes and Deployments**

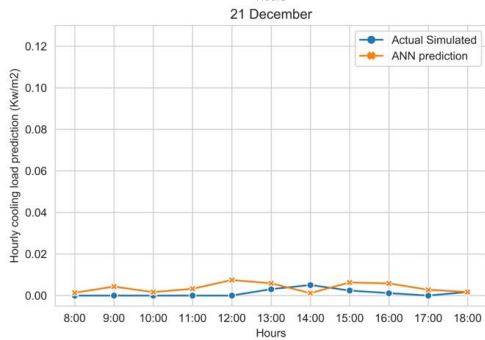
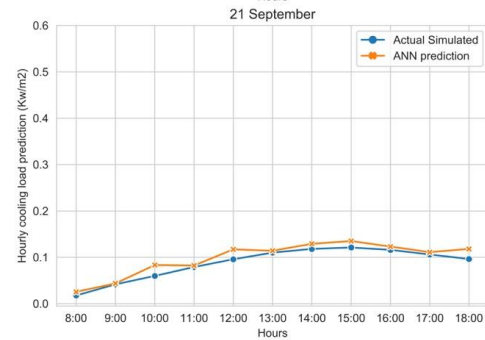
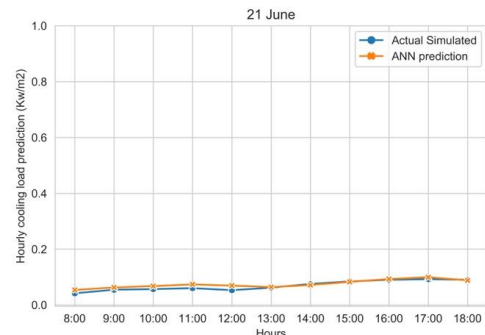
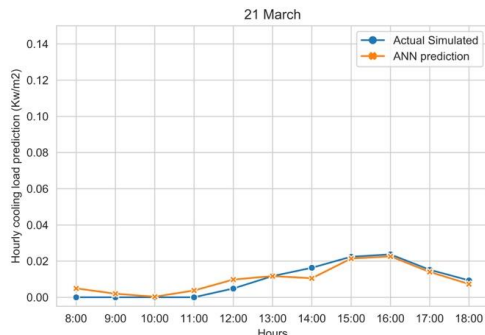
## **APPENDIX**

The codes and files of the surrogate models can be accessed from this link:

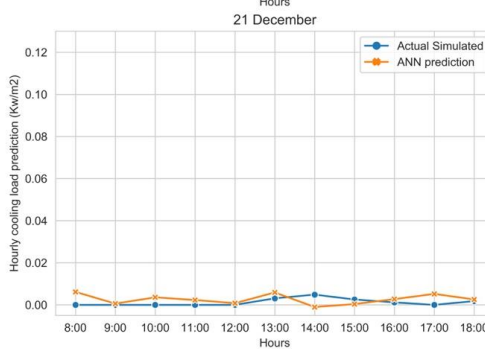
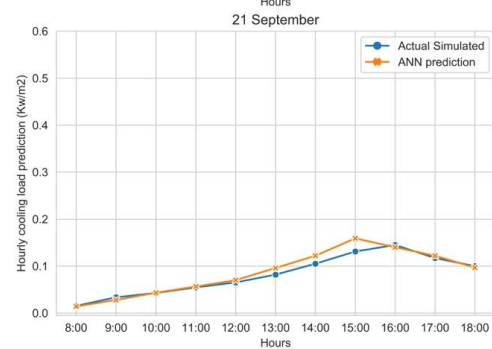
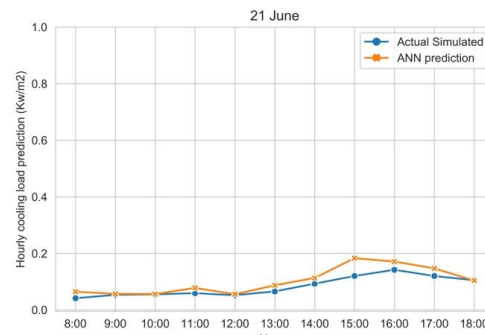
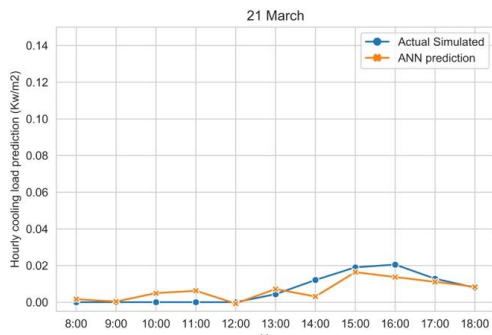
<https://github.com/archammar/Predicting-Hourly-Cooling-Loads-of-Adaptive-Facades-Using-Machine-Learning.git>

<https://github.com/archammar/Solar-radiation-prediction-for-office-tower-using-machine-learning.git>

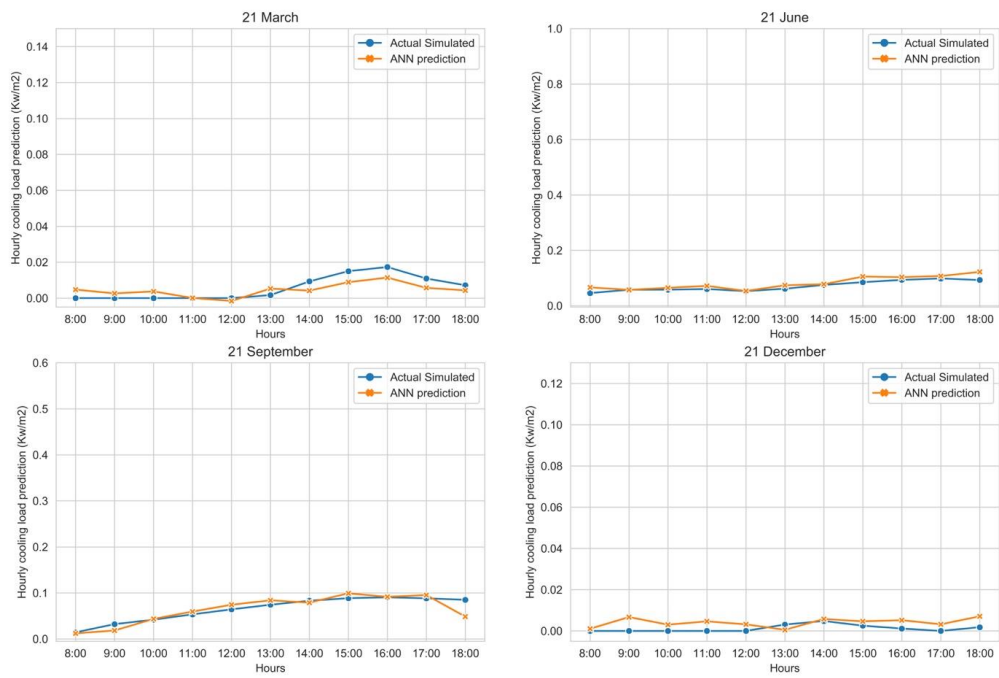
SOUTH



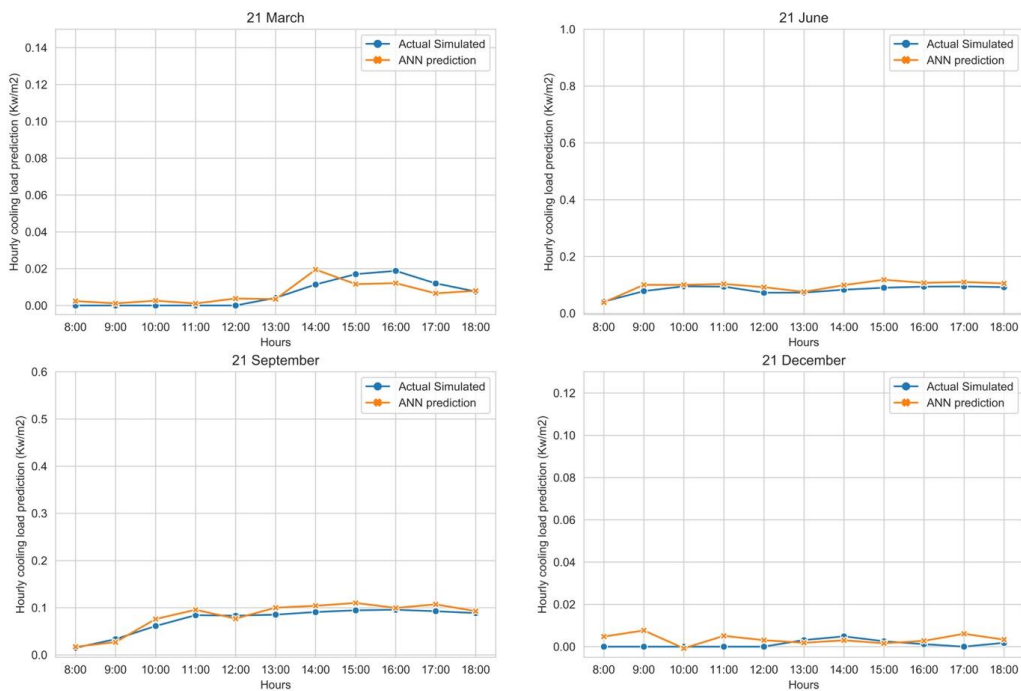
WEST



NORTH



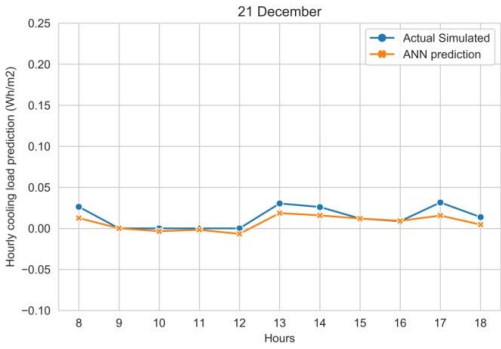
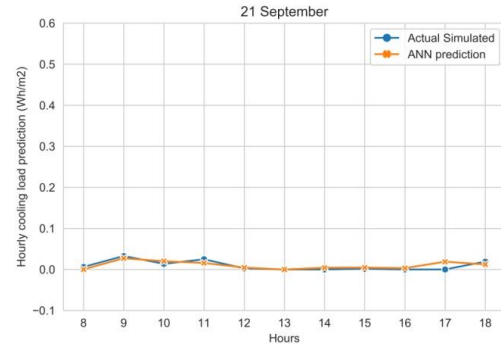
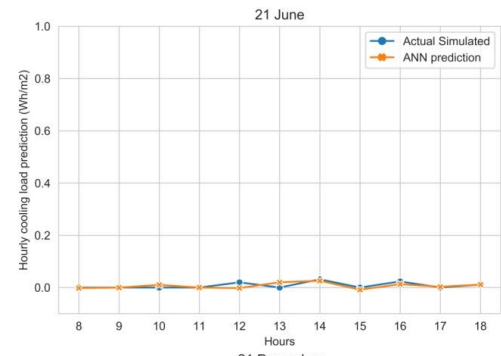
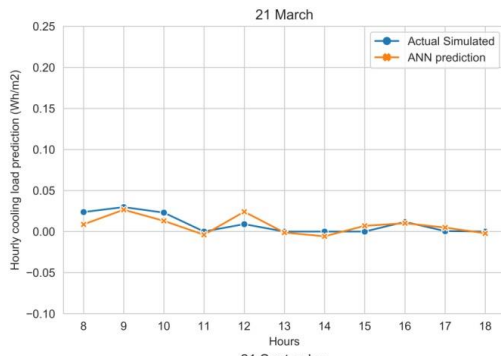
EAST



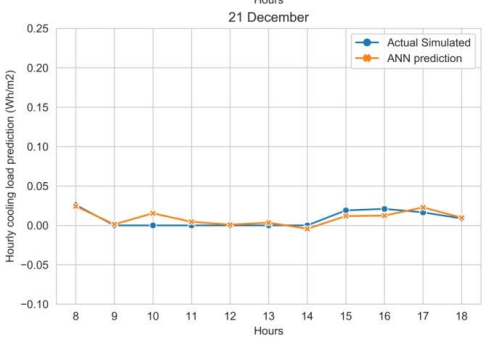
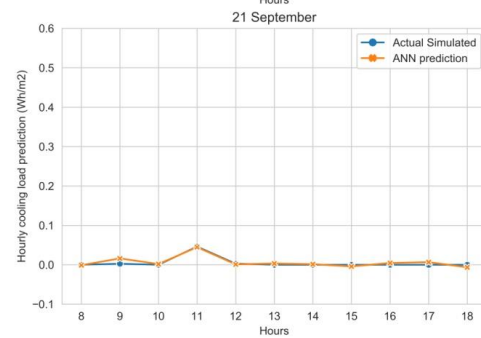
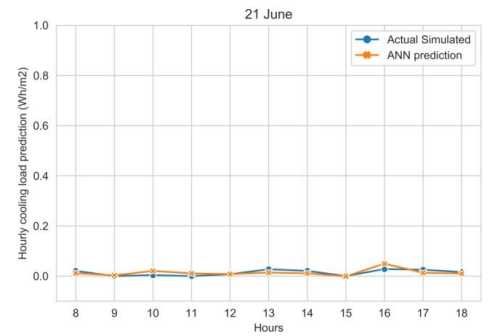
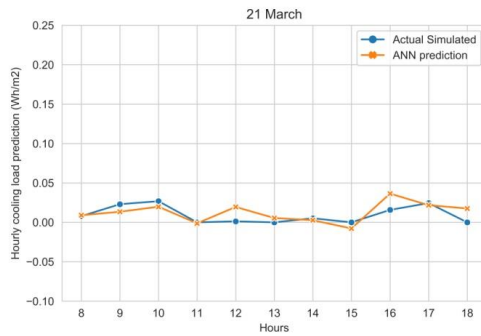
Some selected cases to show actual simulated data vs. predicted data with ANN.



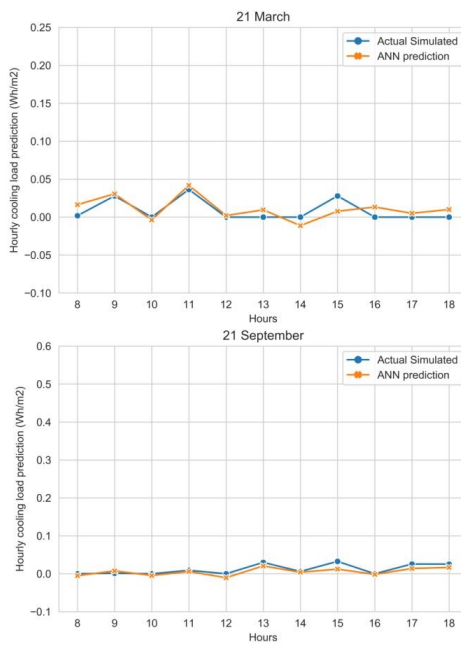
SOUTH



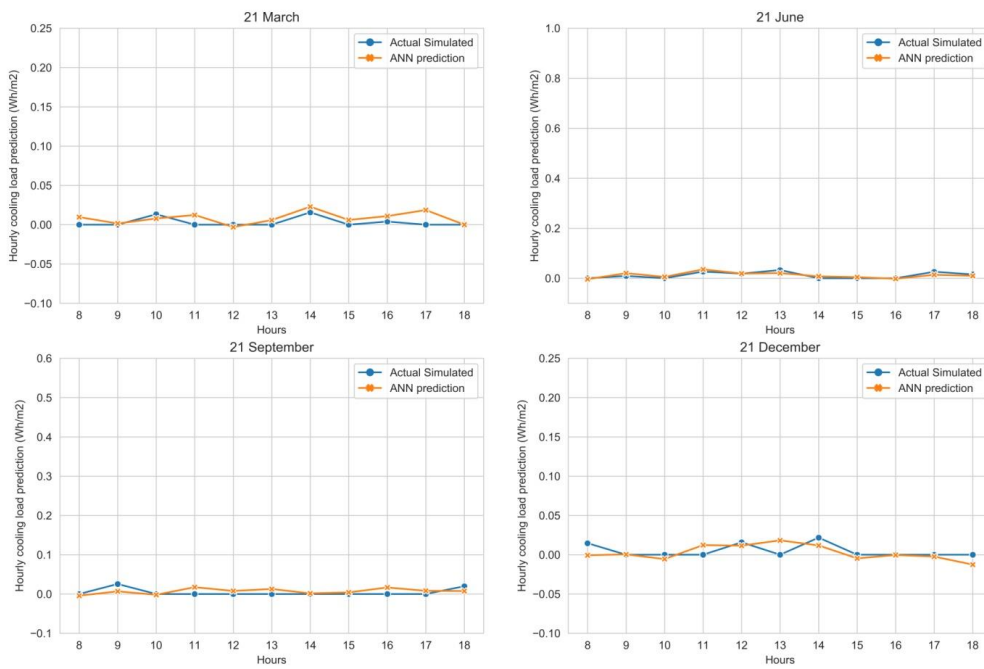
WEST



NORTH



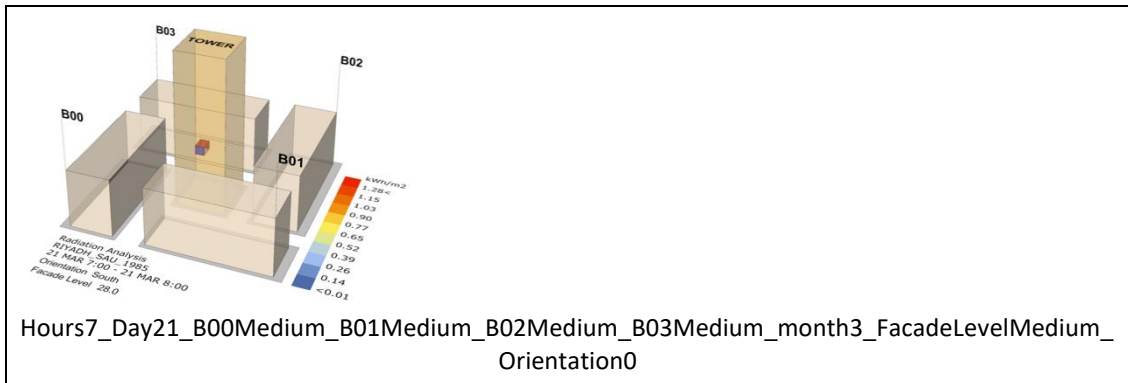
EAST



Some selected cases to show actual simulated data vs. predicted results with ANN surrogate model.

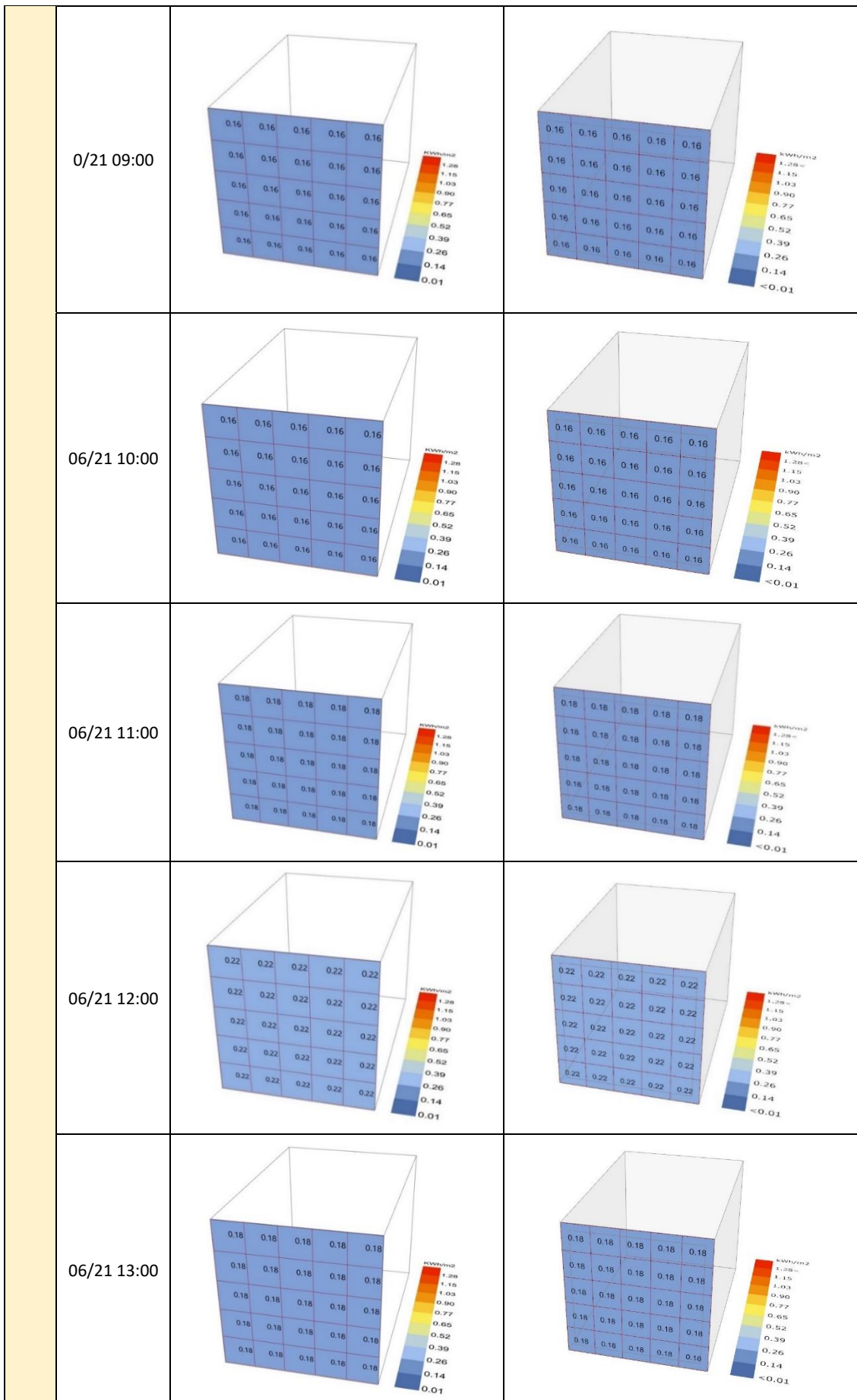
**APPENDIX**

Comparison analysis between DT model prediction and the simulation prediction of hourly solar radiation.

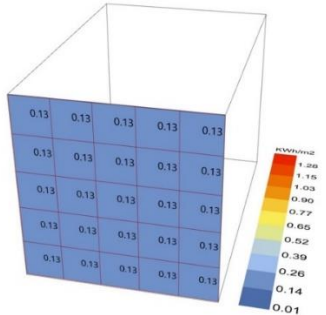
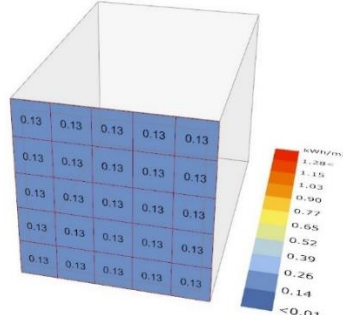
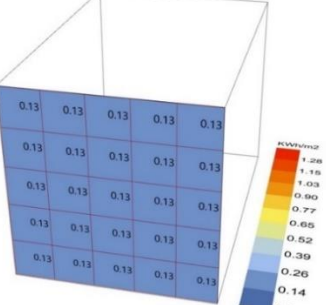
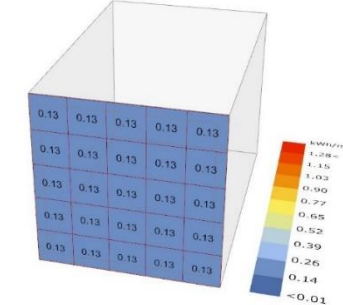
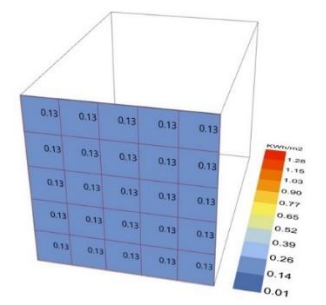
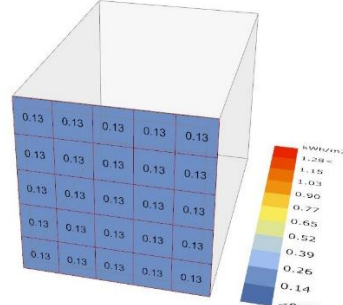
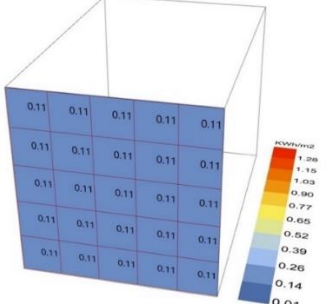
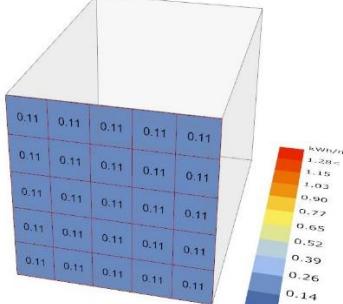
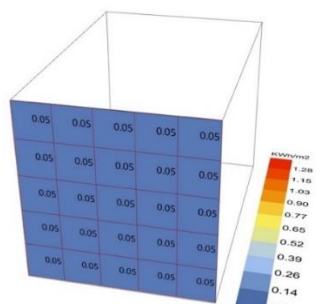
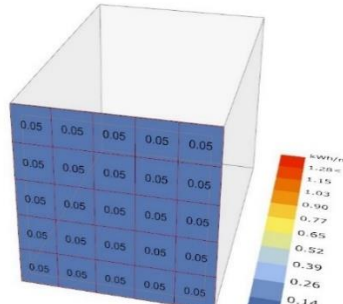


| Or. | Time         | Predicted (DT) | Simulated |
|-----|--------------|----------------|-----------|
| S   | 06 /21 06:00 |                |           |
|     | 06/21 07:00  |                |           |
|     | 06/21 08:00  |                |           |

**APPENDIX**

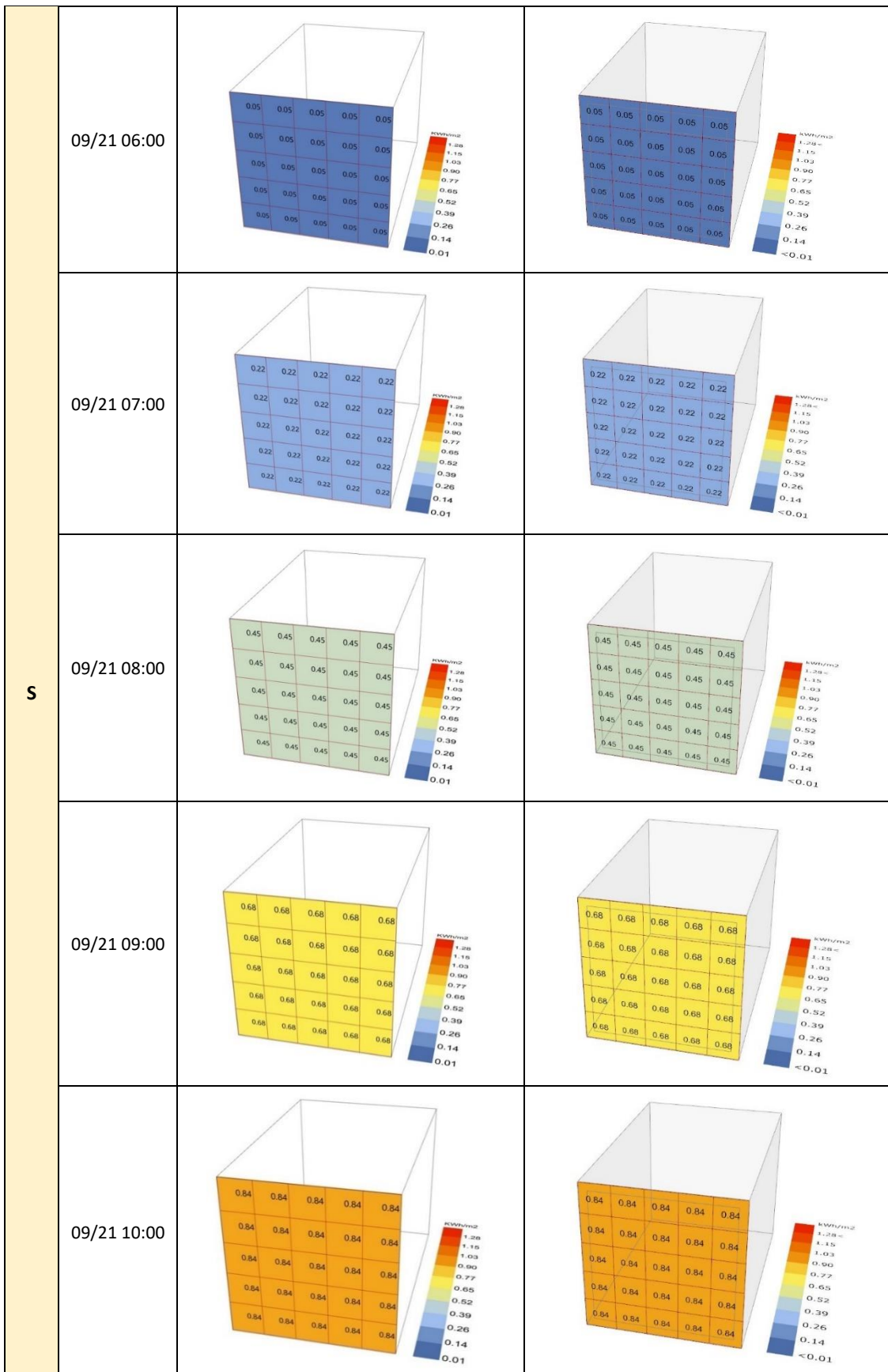


**APPENDIX**

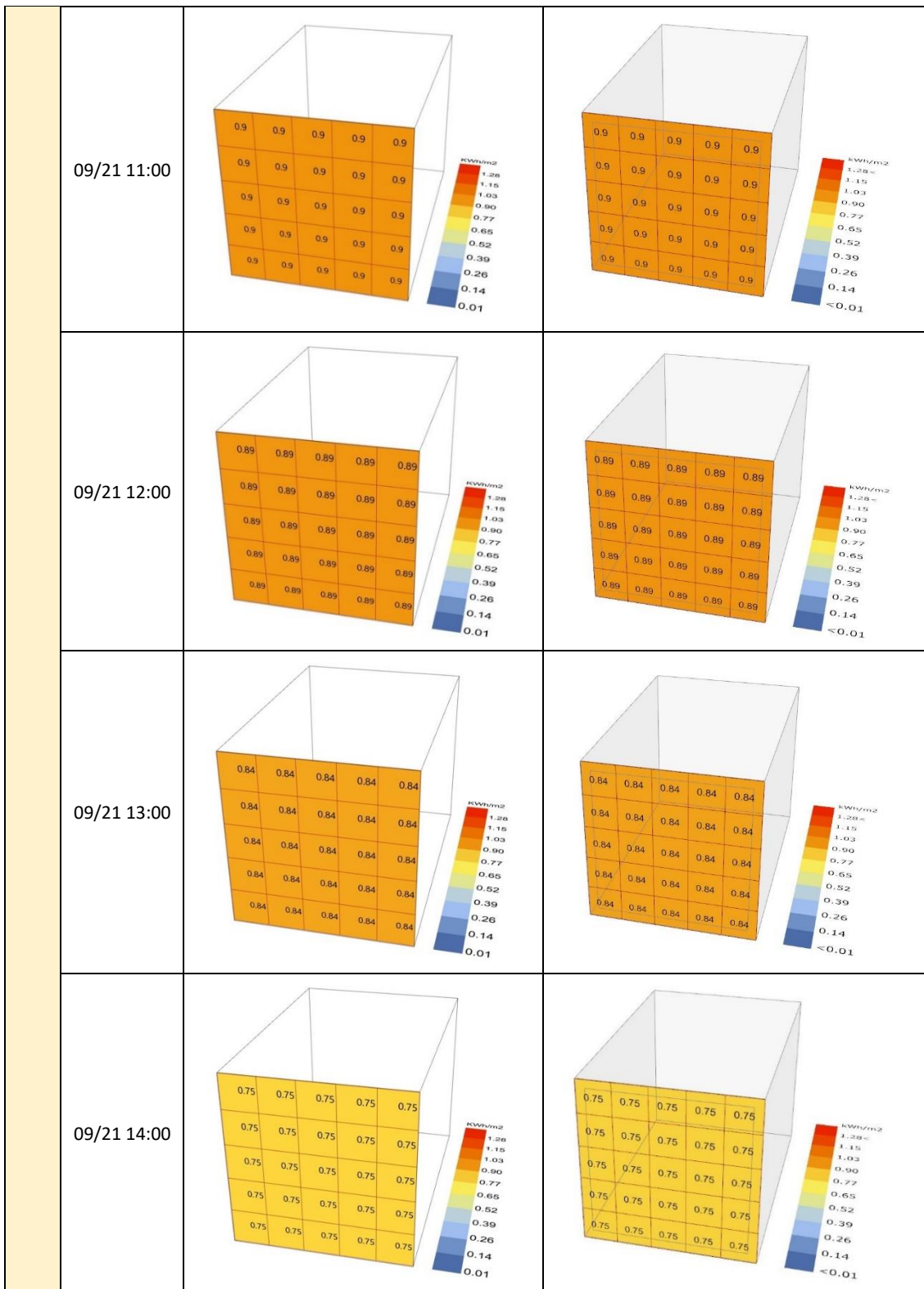
|     |             |   |  |
|-----|-------------|---|--|
|     | 06/21 14:00 |    |    |
|     | 06/21 15:00 |    |    |
|     | 06/21 16:00 |   |   |
|     | 06/21 17:00 |  |  |
|     | 06/21 18:00 |  |  |
| Or. | Sep.        |   |  |



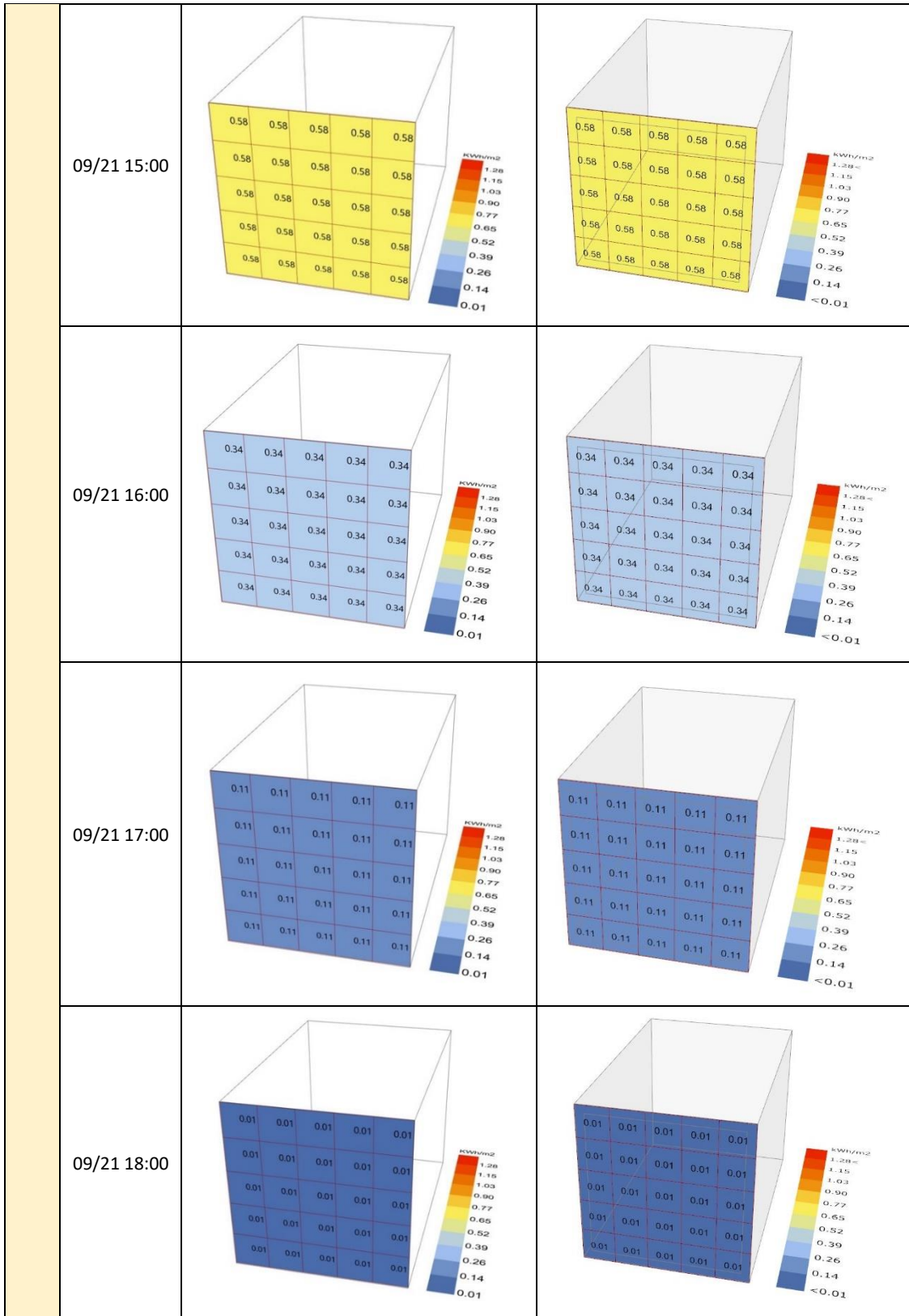
**APPENDIX**



**APPENDIX**

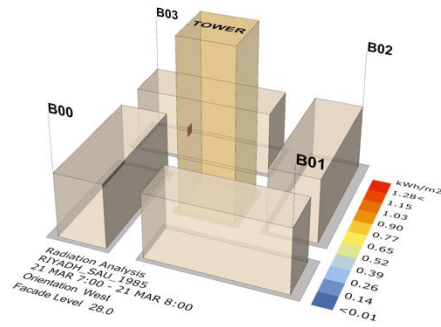


**APPENDIX**





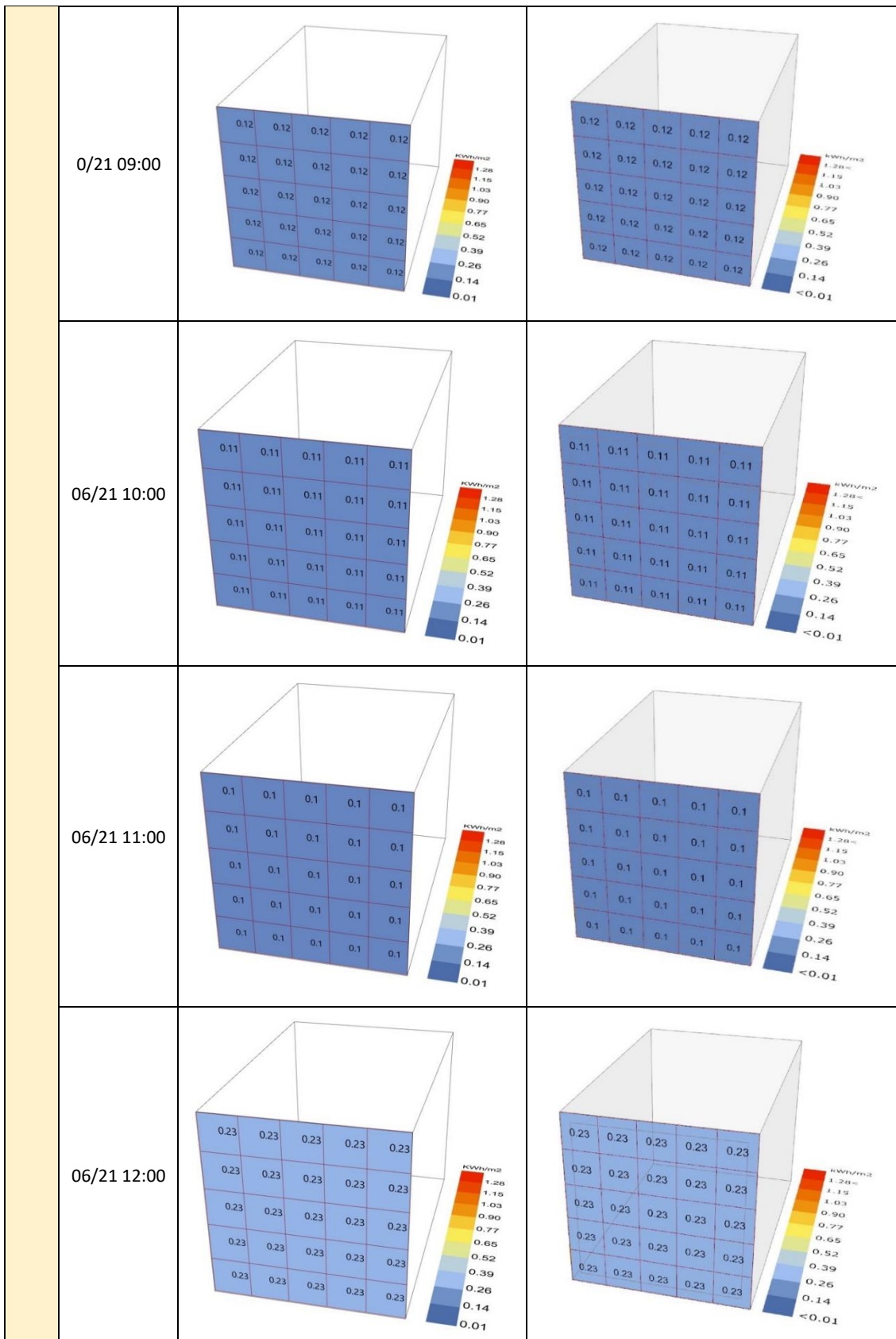
**APPENDIX**



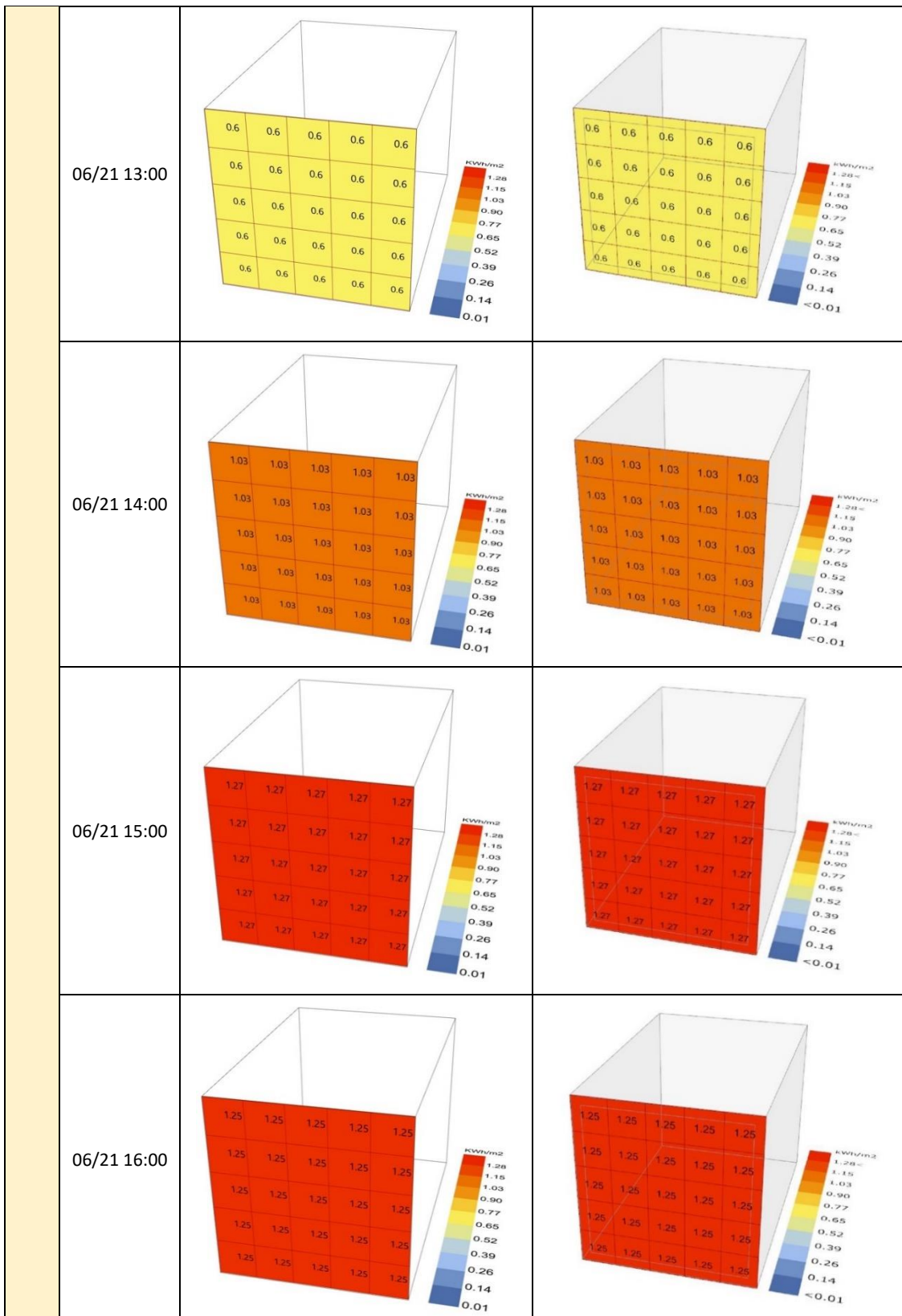
Hours7\_Day21\_B00Medium\_B01Medium\_B02Medium\_B03Medium\_month3\_FacadeLevelMedium\_Orientation1

| Or. | Time         | Predicted (DT) | Simulated |
|-----|--------------|----------------|-----------|
| W   | 06 /21 06:00 |                |           |
|     | 06/21 07:00  |                |           |
|     | 06/21 08:00  |                |           |

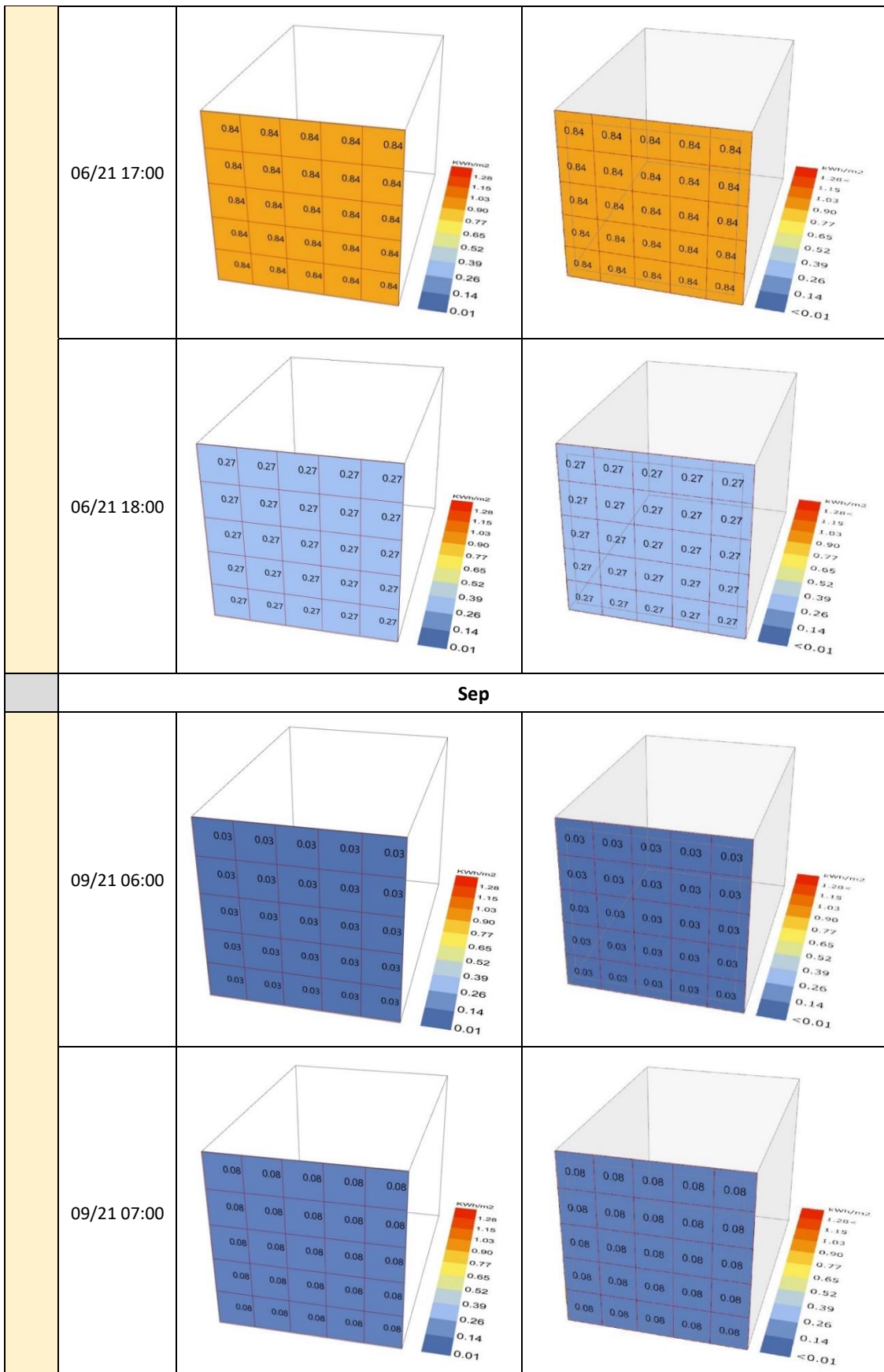
**APPENDIX**



**APPENDIX**

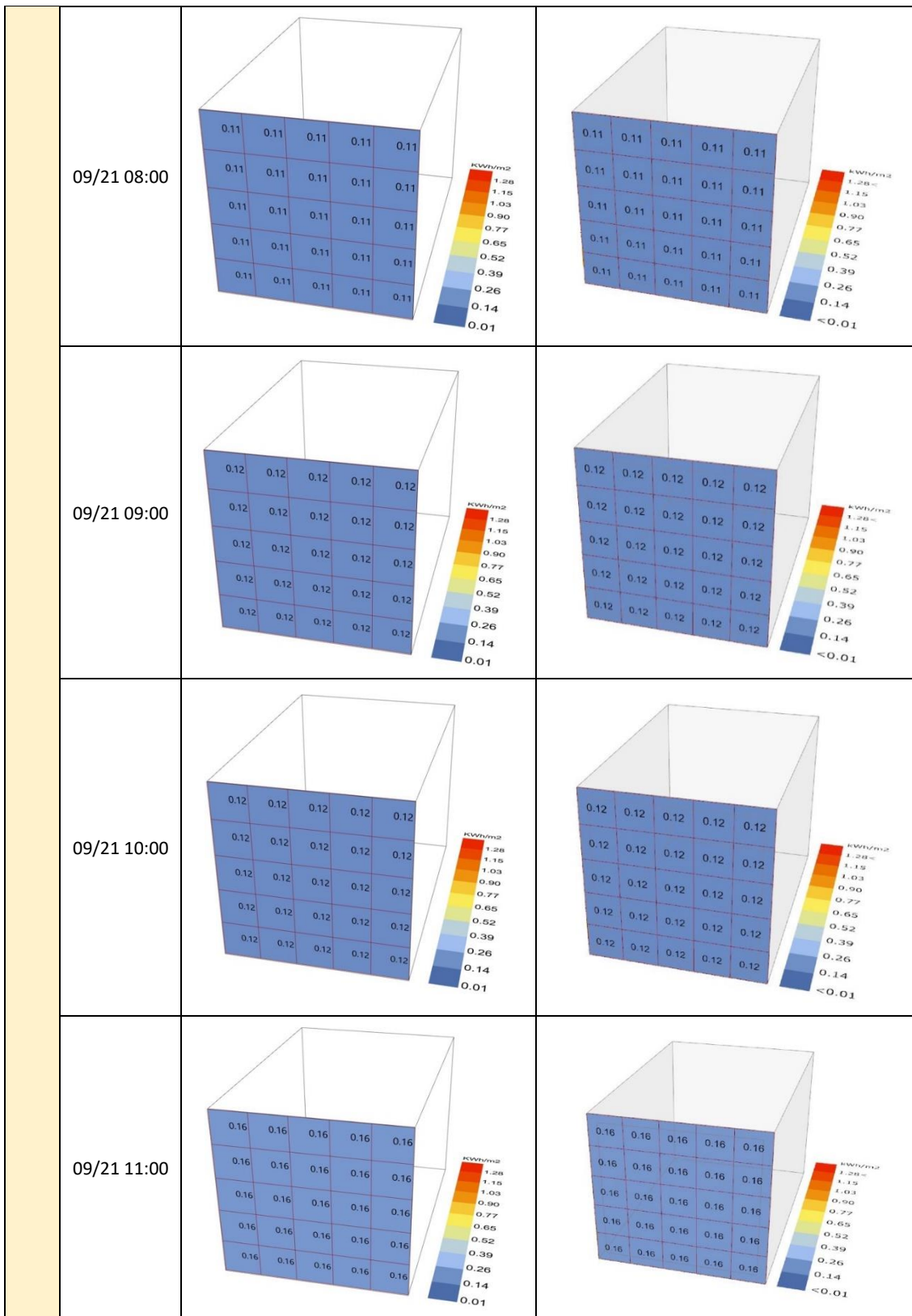


**APPENDIX**

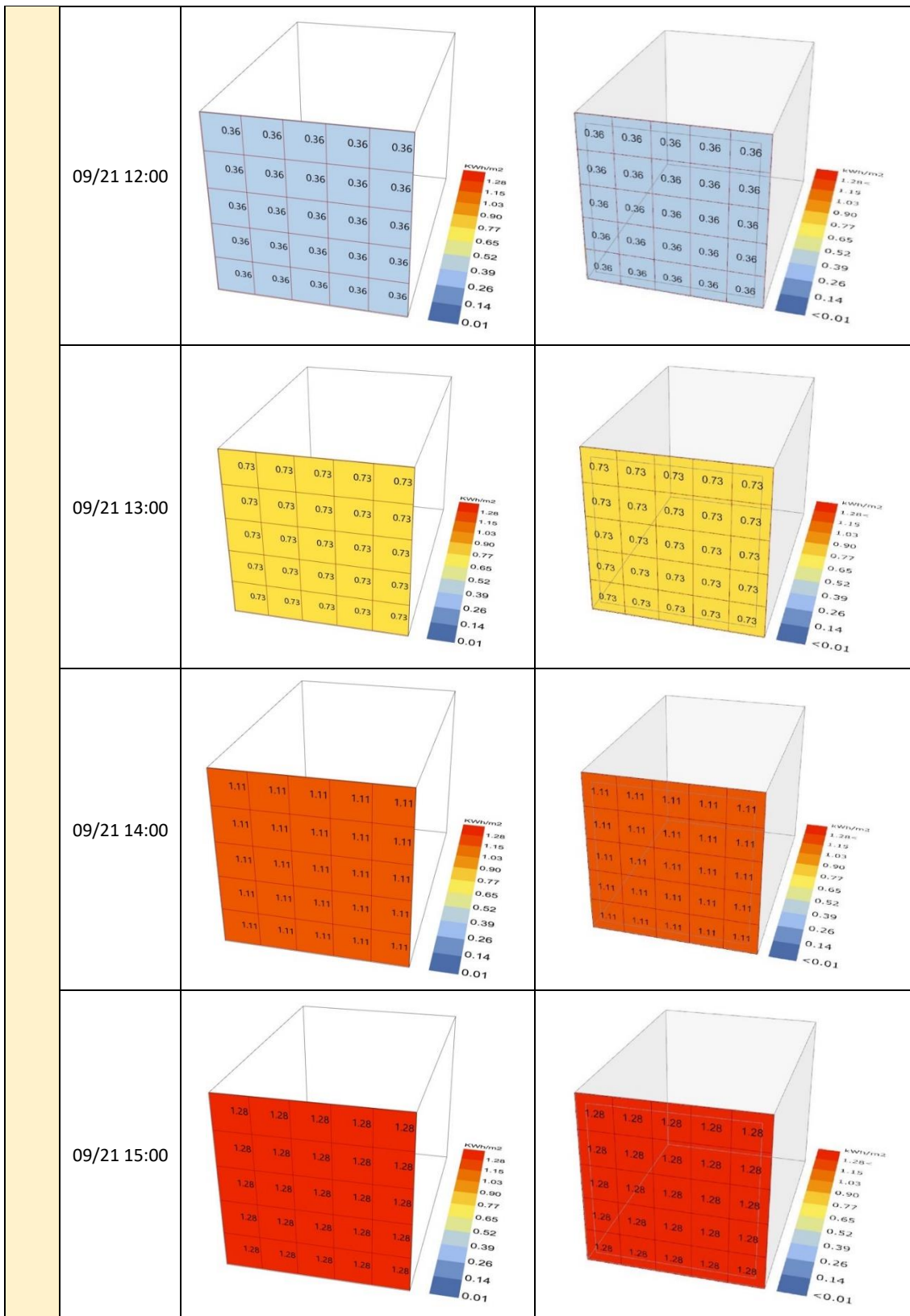




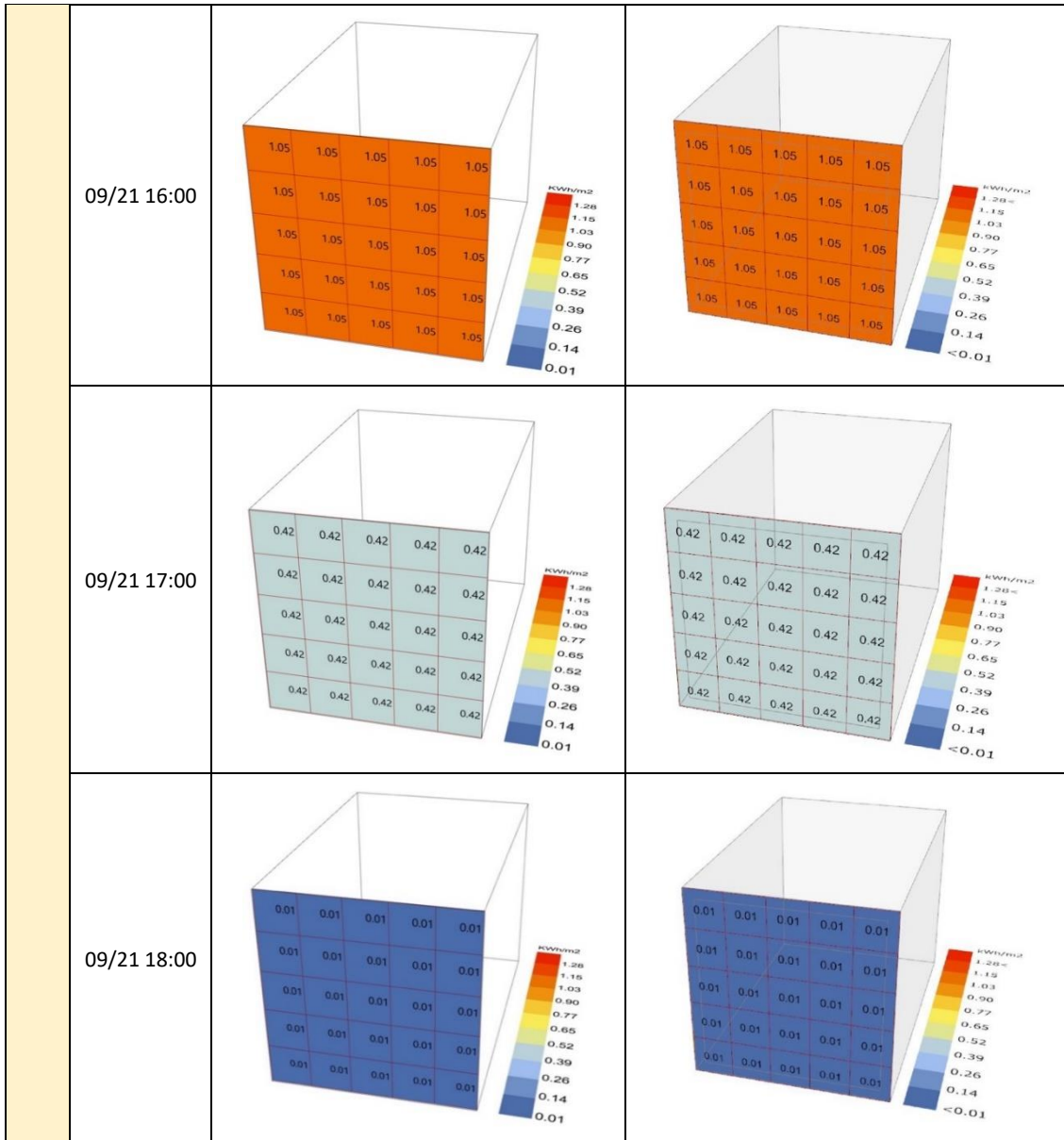
**APPENDIX**



**APPENDIX**

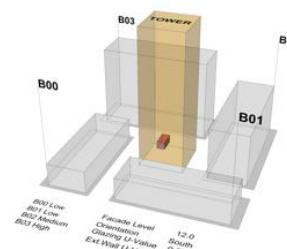
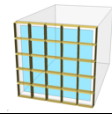
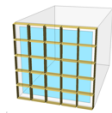
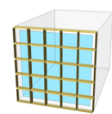
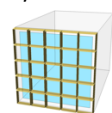
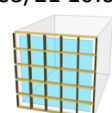
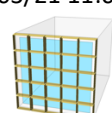
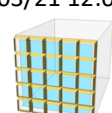




**APPENDIX**



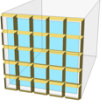
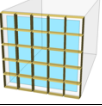
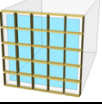
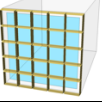
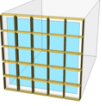
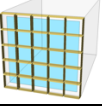
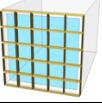
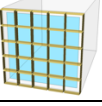
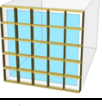
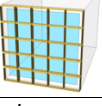
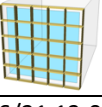
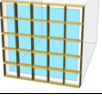
**APPENDIX**

Comparison between RF model predictions, ANN model predictions, and simulation predictions of hourly cooling loads.

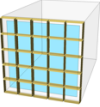
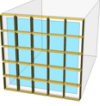
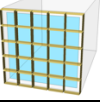
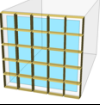
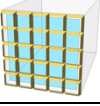
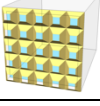
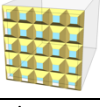
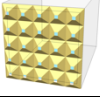
| P-AF-SCM C4_Or0_B00Low_B01Low_FLLow_ExtW0_Glaz0  |           |               |                |                   |                   |
|--|-----------|---------------|----------------|-------------------|-------------------|
|                   |           |               |                |                   |                   |
| Date/Time  | Simulated | DT Prediction | ANN Prediction | Squared Error- DT | Squared Error ANN |
| 03/21 06:00<br>   | 0         | 0             | 0.00063962     | 0                 | 4.09114E-07       |
| 03/21 07:00<br>   | 0         | 0             | 0.0018528      | 0                 | 3.43287E-06       |
| 03/21 08:00<br>  | 0         | 0             | 0.00347372     | 0                 | 1.20667E-05       |
| 03/21 09:00<br> | 0         | 0             | 0.00482053     | 0                 | 2.32375E-05       |
| 03/21 10:00<br> | 0         | 0             | 0.00486856     | 0                 | 2.37029E-05       |
| 03/21 11:00<br> | 0         | 0             | 0.00781538     | 0                 | 6.10802E-05       |
| 03/21 12:00<br> | 0         | 0             | 0.01052411     | 0                 | 0.000110757       |
| 03/21 13:00<br> | 0.002935  | 0.00295205    | 0.00946786     | 2.90702E-10       | 4.24558E-05       |
| 03/21 14:00<br> | 0.006068  | 0.00609395    | 0.00987883     | 6.73403E-10       | 1.43253E-05       |



**APPENDIX**

|  |          |            |            |             |             |
|--|----------|------------|------------|-------------|-------------|
| 03/21 15:00<br>   | 0.008511 | 0.0085772  | 0.01141295 | 4.38244E-09 | 8.04148E-06 |
| 03/21 16:00<br>   | 0.009399 | 0.009405   | 0.01016875 | 3.6E-11     | 5.83314E-07 |
| 03/21 17:00<br>   | 0.005386 | 0.0054682  | 0.00996322 | 6.75684E-09 | 2.02052E-05 |
| 03/21 18:00<br>   | 0.003778 | 0.00372855 | 0.00788688 | 2.4453E-09  | 1.72917E-05 |
| <b>RMSE</b>  |          |            |            | 3.34948E-05 | 0.005095918 |
| 06/21 06:00<br>   | 0        | 0          | 0.01753172 | 0           | 0.000307    |
| 06/21 07:00<br> | 0.01786  | 0.0181679  | 0.01682233 | 9.48024E-08 | 1.81E-06    |
| 06/21 08:00<br> | 0.020488 | 0.0201411  | 0.01704724 | 1.2034E-07  | 9.57E-06    |
| 06/21 09:00<br> | 0.029397 | 0.028008   | 0.0170715  | 1.92932E-06 | 0.00012     |
| 06/21 10:00<br> | 0.031831 | 0.03077335 | 0.01657612 | 1.11862E-06 | 0.000202    |
| 06/21 11:00<br> | 0.033673 | 0.0323202  | 0.01772165 | 1.83007E-06 | 0.000213    |
| 06/21 12:00<br> | 0.035112 | 0.03327895 | 0.01814125 | 3.36007E-06 | 0.000229    |
| 06/21 13:00<br> | 0.03847  | 0.0367129  | 0.01778296 | 3.0874E-06  | 0.000358    |

**APPENDIX**

|  |          |            |            |             |          |
|--|----------|------------|------------|-------------|----------|
| 06/21 14:00<br>   | 0.040883 | 0.0380818  | 0.01898606 | 7.84672E-06 | 0.000365 |
| 06/21 15:00<br>   | 0.040538 | 0.0393877  | 0.01952982 | 1.32319E-06 | 0.000394 |
| 06/21 16:00<br>   | 0.041028 | 0.0399767  | 0.01969586 | 1.10523E-06 | 0.000411 |
| 06/21 17:00<br>   | 0.038693 | 0.0378785  | 0.02080395 | 6.6341E-07  | 0.000292 |
| 06/21 18:00<br>   | 0.03743  | 0.03693465 | 0.01955895 | 2.45372E-07 | 0.000302 |
| <b>RMSE</b>  |          |            |            | 0.001322136 | 0.0157   |
| 09/21 06:00<br> | 0        | 0          | 0.01232615 | 0           | 0.000152 |
| 09/21 07:00<br> | 0.009475 | 0.00938795 | 0.01248029 | 7.58E-09    | 9.56E-06 |
| 09/21 08:00<br> | 0.014123 | 0.0141736  | 0.01475517 | 2.56E-09    | 3.38E-07 |
| 09/21 09:00<br> | 0.024685 | 0.02441    | 0.01660042 | 7.56E-08    | 6.1E-05  |
| 09/21 10:00<br> | 0.026623 | 0.02644025 | 0.01826062 | 3.34E-08    | 6.69E-05 |
| 09/21 11:00<br> | 0.029634 | 0.02942275 | 0.0207883  | 4.46E-08    | 7.46E-05 |
| 09/21 12:00<br> | 0.03161  | 0.03167685 | 0.02130514 | 4.47E-09    | 0.000108 |

**APPENDIX**

|  |          |            |            |          |             |
|--|----------|------------|------------|----------|-------------|
| 09/21 13:00<br>   | 0.034053 | 0.03413245 | 0.02171762 | 6.31E-09 | 0.000154    |
| 09/21 14:00<br>   | 0.036311 | 0.0363179  | 0.02179689 | 4.76E-11 | 0.000211    |
| 09/21 15:00<br>   | 0.037411 | 0.03732795 | 0.02132144 | 6.9E-09  | 0.000256    |
| 09/21 16:00<br>   | 0.037316 | 0.0373728  | 0.01977217 | 3.23E-09 | 0.00031     |
| 09/21 17:00<br>   | 0.035338 | 0.03536515 | 0.01877693 | 7.37E-10 | 0.000275    |
| 09/21 18:00<br>  | 0.034004 | 0.0340319  | 0.01627251 | 7.78E-10 | 0.000315    |
| <b>RMSE</b>  |          |            |            | 0.00012  | 0.012383    |
| 12/21 06:00<br> | 0        | 0          | 1.74E-03   | 0        | 3.02462E-06 |
| 12/21 07:00<br> | 0        | 0          | 1.09E-03   | 0        | 1.19594E-06 |
| 12/21 08:00<br> | 0        | 0          | 8.51E-05   | 0        | 7.24765E-09 |
| 12/21 09:00<br> | 0        | 0          | 4.74E-04   | 0        | 2.24532E-07 |
| 12/21 10:00<br> | 0        | 0          | 3.50E-04   | 0        | 1.22783E-07 |
| 12/21 11:00<br> | 0        | 0          | 8.36E-04   | 0        | 6.98996E-07 |

**APPENDIX**

|  |   |   |          |   |             |
|--|---|---|----------|---|-------------|
| 12/21 12:00<br>   | 0 | 0 | 1.02E-03 | 0 | 1.04557E-06 |
| 12/21 13:00<br>   | 0 | 0 | 8.46E-04 | 0 | 7.1547E-07  |
| 12/21 14:00<br>   | 0 | 0 | 6.32E-04 | 0 | 3.98999E-07 |
| 12/21 15:00<br>   | 0 | 0 | 8.77E-04 | 0 | 7.69061E-07 |
| 12/21 16:00<br>   | 0 | 0 | 7.56E-04 | 0 | 5.7175E-07  |
| 12/21 17:00<br>  | 0 | 0 | 1.89E-03 | 0 | 3.55341E-06 |
| 12/21 18:00<br> | 0 | 0 | 1.35E-03 | 0 | 1.83322E-06 |
| <b>RMSE</b>  |   |   |          | 0 | 0.001043721 |

**APPENDIX**

Comparison between RF model predictions, ANN model predictions, and simulation predictions of hourly cooling loads.

| P-AF-SCM C4_Or1_B00High_B01Low_FLMedium_ExtW1_Glaz3 |           |               |                |                  |                  |
|---|-----------|---------------|----------------|------------------|------------------|
|   |           |               |                |                  |                  |
| Date/Time   | Simulated | DT Prediction | ANN Prediction | Squared Error DT | Squared Error NN |
| 03/21 06:00   | 0         | 0             | 0.00269247     | 0                | 7.25E-06         |
| 03/21 07:00   | 0         | 0             | 0.00024311     | 0                | 5.91E-08         |
| 03/21 08:00   | 0         | 0             | 0.00163205     | 0                | 2.66E-06         |
| 03/21 09:00   | 0.002077  | 0.00205845    | 0.00208605     | 3.44E-10         | 7.62E-10         |
| 03/21 10:00   | 0.005596  | 0.005488      | 0.00128663     | 1.17E-08         | 1.77E-05         |
| 03/21 11:00   | 0.006531  | 0.00652235    | 0.00327451     | 7.48E-11         | 1.05E-05         |
| 03/21 12:00   | 0.006263  | 0.00626365    | 0.00420784     | 4.22E-13         | 4.23E-06         |
| 03/21 13:00   | 0.00825   | 0.00824135    | 0.00491856     | 7.48E-11         | 1.1E-05          |
| 03/21 14:00   | 0.009119  | 0.0090998     | 0.00595564     | 3.69E-10         | 9.89E-06         |
| 03/21 15:00   | 0.009889  | 0.00988845    | 0.00785162     | 3.03E-13         | 4.15E-06         |
| 03/21 16:00   | 0.010042  | 0.010027      | 0.00620709     | 2.25E-10         | 1.46E-05         |
| 03/21 17:00   | 0.006821  | 0.00681345    | 0.00642306     | 5.7E-11          | 1.52E-07         |
| 03/21 18:00   | 0.005477  | 0.00546695    | 0.00491066     | 1.01E-10         | 3.09E-07         |
| <b>RMSE</b>   |           |               |                | 3.15E-05         | 0.00252          |
| 06/21 06:00   | 0         | 0             | 0.01446847     | 0                | 0.000209         |
| 06/21 07:00   | 0.014706  | 0.0144129     | 0.01335956     | 8.59E-08         | 1.11E-06         |
| 06/21 08:00   | 0.014031  | 0.0140291     | 0.01351771     | 3.61E-12         | 2.62E-07         |
| 06/21 09:00   | 0.021098  | 0.0205188     | 0.01325031     | 3.35E-07         | 5.28E-05         |
| 06/21 10:00   | 0.021375  | 0.0205924     | 0.0126246      | 6.12E-07         | 6.35E-05         |
| 06/21 11:00   | 0.021702  | 0.02174935    | 0.0134067      | 2.24E-09         | 6.96E-05         |
| 06/21 12:00   | 0.021103  | 0.02019575    | 0.01333381     | 8.23E-07         | 4.71E-05         |
| 06/21 13:00   | 0.022922  | 0.0220854     | 0.01471085     | 7E-07            | 5.44E-05         |
| 06/21 14:00   | 0.023689  | 0.0223639     | 0.01950239     | 1.76E-06         | 8.19E-06         |
| 06/21 15:00   | 0.023236  | 0.02313125    | 0.02248658     | 1.1E-08          | 4.16E-07         |
| 06/21 16:00   | 0.023413  | 0.02311535    | 0.02369244     | 8.86E-08         | 3.33E-07         |
| 06/21 17:00   | 0.021088  | 0.021134      | 0.02363452     | 2.12E-09         | 6.25E-06         |
| 06/21 18:00   | 0.01999   | 0.01943825    | 0.01826493     | 3.04E-07         | 1.38E-06         |
| <b>RMSE</b>   |           |               |                | 0.000603         | 0.006292         |
| 09/21 06:00   | 0         | 0             | 0.00931766     | 0                | 8.68E-05         |
| 09/21 07:00   | 0.009838  | 0.00984       | 0.00943285     | 3.42E-12         | 1.66E-07         |
| 09/21 08:00   | 0.010496  | 0.010483      | 0.01030559     | 1.73E-10         | 3.14E-08         |
| 09/21 09:00   | 0.018807  | 0.018796      | 0.01014763     | 1.24E-10         | 7.48E-05         |
| 09/21 10:00   | 0.019239  | 0.019234      | 0.00975762     | 2.86E-11         | 8.98E-05         |
| 09/21 11:00   | 0.02023   | 0.02023       | 0.01150014     | 9E-14            | 7.62E-05         |
| 09/21 12:00   | 0.019705  | 0.019701      | 0.01170036     | 1.3E-11          | 6.4E-05          |
| 09/21 13:00   | 0.021256  | 0.021253      | 0.01432112     | 1.23E-11         | 4.8E-05          |
| 09/21 14:00   | 0.021753  | 0.021751      | 0.01805645     | 3.8E-12          | 1.37E-05         |
| 09/21 15:00   | 0.022016  | 0.022013      | 0.02142563     | 1.16E-11         | 3.45E-07         |
| 09/21 16:00   | 0.021545  | 0.021536      | 0.0215202      | 7.57E-11         | 2.59E-10         |
| 09/21 17:00   | 0.019495  | 0.019494      | 0.01917387     | 4.22E-13         | 1.03E-07         |
| 09/21 18:00   | 0.018191  | 0.018185      | 0.01248406     | 3.84E-11         | 3.25E-05         |
| <b>RMSE</b>   |           |               |                | 6.1E-06          | 0.006117         |

**APPENDIX**

|             |   |   |            |   |          |
|-------------|---|---|------------|---|----------|
| 12/21 06:00 | 0 | 0 | 0.00378397 | 0 | 1.43E-05 |
| 12/21 07:00 | 0 | 0 | 0.00257411 | 0 | 6.63E-06 |
| 12/21 08:00 | 0 | 0 | 0.00186988 | 0 | 3.5E-06  |
| 12/21 09:00 | 0 | 0 | 0.00225542 | 0 | 5.09E-06 |
| 12/21 10:00 | 0 | 0 | 0.00287586 | 0 | 8.27E-06 |
| 12/21 11:00 | 0 | 0 | 0.00165981 | 0 | 2.75E-06 |
| 12/21 12:00 | 0 | 0 | 0.00237481 | 0 | 5.64E-06 |
| 12/21 13:00 | 0 | 0 | 0.00213686 | 0 | 4.57E-06 |
| 12/21 14:00 | 0 | 0 | 0.00181599 | 0 | 3.3E-06  |
| 12/21 15:00 | 0 | 0 | 0.00122759 | 0 | 1.51E-06 |
| 12/21 16:00 | 0 | 0 | 0.00145808 | 0 | 2.13E-06 |
| 12/21 17:00 | 0 | 0 | 0.00021952 | 0 | 4.82E-08 |
| 12/21 18:00 | 0 | 0 | 0.00032277 | 0 | 1.04E-07 |
| <b>RMSE</b> |   |   |            | 0 | 0.002109 |

**APPENDIX**

*Comparison between surrogate models' prediction and simulation prediction for four different cities.*

| P-AF-SCM C4_OrO_B00High_B01Low_FLLow_ExtW1_Glaz3 |           |               |                |                   |                  |
|--|-----------|---------------|----------------|-------------------|------------------|
| Location: Jeddah                                 |           |               |                |                   |                  |
| Date/Time  | Simulated | DT Prediction | ANN Prediction | Squared Error- DT | Squared Error NN |
| 09/21 06:00                                      | 0         | 0             | 0.01449259     | 0                 | 0.00021          |
| 09/21 07:00                                      | 0.025571  | 0.02416015    | 0.01286777     | 1.99E-06          | 0.000128         |
| 09/21 08:00                                      | 0.028366  | 0.02588355    | 0.01390472     | 6.16E-06          | 0.000143         |
| 09/21 09:00                                      | 0.040585  | 0.0345987     | 0.0147919      | 3.58E-05          | 0.000392         |
| 09/21 10:00                                      | 0.037648  | 0.0315219     | 0.01643904     | 3.75E-05          | 0.000227         |
| 09/21 11:00                                      | 0.035595  | 0.029368      | 0.01884475     | 3.88E-05          | 0.000111         |
| 09/21 12:00                                      | 0.034336  | 0.02961785    | 0.01935158     | 2.23E-05          | 0.000105         |
| 09/21 13:00                                      | 0.037398  | 0.0354318     | 0.01984899     | 3.87E-06          | 0.000243         |
| 09/21 14:00                                      | 0.034207  | 0.02903395    | 0.01999195     | 2.68E-05          | 8.18E-05         |
| 09/21 15:00                                      | 0.03018   | 0.0284952     | 0.01929807     | 2.84E-06          | 8.46E-05         |
| 09/21 16:00                                      | 0.034228  | 0.0297973     | 0.01829678     | 1.96E-05          | 0.000132         |
| 09/21 17:00                                      | 0.031411  | 0.02663725    | 0.01775941     | 2.28E-05          | 7.88E-05         |
| 09/21 18:00                                      | 0.030042  | 0.0254701     | 0.01522427     | 2.09E-05          | 0.000105         |

| P-AF-SCM C4_OrO_B00High_B01Low_FLLow_ExtW1_Glaz3 |           |               |                |                   |                  |
|--|-----------|---------------|----------------|-------------------|------------------|
| Location: Kuwait                                 |           |               |                |                   |                  |
| Date/Time  | Simulated | DT Prediction | ANN Prediction | Squared Error- DT | Squared Error NN |
| 09/21 06:00                                      | 0         | 0             | 0.01231566     | 0                 | 0.000151675      |
| 09/21 07:00                                      | 0.018542  | 0.01795565    | 0.01191821     | 3.43806E-07       | 3.64507E-05      |
| 09/21 08:00                                      | 0.015749  | 0.0136542     | 0.01360248     | 4.38819E-06       | 2.67496E-09      |
| 09/21 09:00                                      | 0.03054   | 0.0241262     | 0.01517036     | 4.11368E-05       | 8.02071E-05      |
| 09/21 10:00                                      | 0.027721  | 0.02317645    | 0.0168404      | 2.06529E-05       | 4.01455E-05      |
| 09/21 11:00                                      | 0.02825   | 0.0260543     | 0.01969854     | 4.8211E-06        | 4.03957E-05      |
| 09/21 12:00                                      | 0.027265  | 0.0280171     | 0.02020409     | 5.65654E-07       | 6.10431E-05      |
| 09/21 13:00                                      | 0.028858  | 0.03010145    | 0.02083067     | 1.54617E-06       | 8.59474E-05      |
| 09/21 14:00                                      | 0.028802  | 0.0338863     | 0.02152199     | 2.58501E-05       | 0.000152876      |
| 09/21 15:00                                      | 0.034824  | 0.03379085    | 0.02119408     | 1.0674E-06        | 0.000158679      |
| 09/21 16:00                                      | 0.03496   | 0.03210395    | 0.01969337     | 8.15702E-06       | 0.000154022      |
| 09/21 17:00                                      | 0.029383  | 0.0289755     | 0.01872011     | 1.66056E-07       | 0.000105173      |
| 09/21 18:00                                      | 0.026936  | 0.028347      | 0.0157568      | 1.99092E-06       | 0.000158513      |

| P-AF-SCM C4_OrO_B00High_B01Low_FLLow_ExtW1_Glaz3 |           |               |                |                   |                  |
|--|-----------|---------------|----------------|-------------------|------------------|
| Location: Phoenix                                |           |               |                |                   |                  |
| Date/Time  | Simulated | DT Prediction | ANN Prediction | Squared Error- DT | Squared Error NN |
| 09/21 06:00                                      | 0         | 0             | 0.00372739     | 0                 | 1.38934E-05      |
| 09/21 07:00                                      | 0         | 0             | 0.00565509     | 0                 | 3.198E-05        |
| 09/21 08:00                                      | 0         | 0             | 0.00824758     | 0                 | 6.80226E-05      |
| 09/21 09:00                                      | 0.005187  | 0.00016015    | 0.01084305     | 2.52692E-05       | 0.000114124      |
| 09/21 10:00                                      | 0.008298  | 0.0091609     | 0.0145648      | 7.44596E-07       | 2.92021E-05      |
| 09/21 11:00                                      | 0.010004  | 0.01846345    | 0.01877742     | 7.15623E-05       | 9.85772E-08      |
| 09/21 12:00                                      | 0.010381  | 0.0219027     | 0.02018813     | 0.00013275        | 2.93975E-06      |

**APPENDIX**

|             |          |            |            |             |             |
|-------------|----------|------------|------------|-------------|-------------|
| 09/21 13:00 | 0.01255  | 0.0218241  | 0.02113594 | 8.60089E-05 | 4.73564E-07 |
| 09/21 14:00 | 0.014213 | 0.02556085 | 0.02179296 | 0.000128774 | 1.4197E-05  |
| 09/21 15:00 | 0.015357 | 0.0273997  | 0.02163508 | 0.000145027 | 3.32308E-05 |
| 09/21 16:00 | 0.015774 | 0.02944635 | 0.02011921 | 0.000186933 | 8.69955E-05 |
| 09/21 17:00 | 0.014624 | 0.0270655  | 0.01895543 | 0.000154791 | 6.57732E-05 |
| 09/21 18:00 | 0.013121 | 0.0253331  | 0.01544593 | 0.000149135 | 9.77561E-05 |

| P-AF-SCM C4_Or0_B00High_B01Low_FLLow_ExtW1_Glaz3 |           |               |                |                   |                  |
|--|-----------|---------------|----------------|-------------------|------------------|
| Location: Tucson                                 |           |               |                |                   |                  |
| Date/Time  | Simulated | DT Prediction | ANN Prediction | Squared Error- DT | Squared Error NN |
| 09/21 06:00                                      | 0         | 0             | 0.00774492     | 0                 | 5.99838E-05      |
| 09/21 07:00                                      | 0         | 0             | 0.00835961     | 0                 | 6.98831E-05      |
| 09/21 08:00                                      | 0.001833  | 0             | 0.01169577     | 3.35989E-06       | 0.000136791      |
| 09/21 09:00                                      | 0.008994  | 0.0093566     | 0.01478599     | 1.31479E-07       | 2.94783E-05      |
| 09/21 10:00                                      | 0.010813  | 0.01962565    | 0.01751973     | 7.76628E-05       | 4.4349E-06       |
| 09/21 11:00                                      | 0.012827  | 0.02284225    | 0.02085647     | 0.000100305       | 3.94332E-06      |
| 09/21 12:00                                      | 0.012451  | 0.02240855    | 0.02125269     | 9.91528E-05       | 1.33601E-06      |
| 09/21 13:00                                      | 0.015034  | 0.02475925    | 0.02133584     | 9.45805E-05       | 1.17197E-05      |
| 09/21 14:00                                      | 0.016502  | 0.0270583     | 0.02137996     | 0.000111435       | 3.22435E-05      |
| 09/21 15:00                                      | 0.016838  | 0.0285472     | 0.02059869     | 0.000137105       | 6.31788E-05      |
| 09/21 16:00                                      | 0.017034  | 0.02976985    | 0.0186174      | 0.000162202       | 0.000124377      |
| 09/21 17:00                                      | 0.015505  | 0.0277367     | 0.01760292     | 0.000149614       | 0.000102693      |
| 09/21 18:00                                      | 0.012961  | 0.02523125    | 0.01447455     | 0.000150559       | 0.000115707      |